

Versuchsanstalt für Wasserbau  
Hydrologie und Glaziologie  
der Eidgenössischen  
Technischen Hochschule Zürich

---

**Mitteilungen**

**258**

**Fish protection and guidance at water intakes  
with horizontal bar rack bypass systems**

Julian Meister

Zürich, 2020

Herausgeber: Prof. Dr. Robert Boes

**ETH** zürich

*Zitiervorschlag für VAW-Mitteilungen:*

Meister, J. (2020).

Fish protection and guidance at water intakes with horizontal bar rack bypass systems.

*VAW-Mitteilungen* 258, Versuchsanstalt für Wasserbau, Hydrologie und Glaziologie (VAW),  
(R. M. Boes, ed.), ETH Zürich, Schweiz.

Im Eigenverlag der  
Versuchsanstalt für Wasserbau,  
Hydrologie und Glaziologie  
ETH Zürich  
CH-8093 Zürich

Tel.: +41 - 44 - 632 40 91  
Fax: +41 - 44 - 632 40 92  
e-mail: [info@vaw.baug.ethz.ch](mailto:info@vaw.baug.ethz.ch)

Zürich, 2020

ISSN 0374-0056

# Preface

The free fish movement in rivers, both in upstream and downstream directions, is often hampered by transverse structures like hydropower plants, weirs, and dams, leading to a fragmentation of habitats. Whereas much effort was made to allow for upstream passage, the awareness of the need for protection of downstream moving fish is quite recent in Europe. The Swiss Waters Protection Act requires rehabilitation measures at more than 700 obstacles for downstream fish movement to limit fish injury and mortality. The safe downstream passage is particularly important for long distance migrators like diadromous species moving between sea and freshwater systems, e.g. the European eel and Atlantic salmon, who often have to pass a series of hydropower plants, resulting in elevated cumulative effects. Horizontal bar rack bypass systems (HBR-BSs) are a state-of-the-art technology to allow for safe fish downstream passage at small to medium-scale hydropower plants with discharges up to about 100 m<sup>3</sup>/s, while there is currently hardly any proven technology for the protection of the wide variety of indigenous fish fauna at larger run-of-the-river plants. Although HBR-BSs have been widely applied recently, there is a lack of knowledge on their hydraulic losses, fish protection and guidance efficiencies, and operational issues like rack blockage by floating debris and sediments. Mr. Meister's research project is in line with a series of research on effective fish protection measures realized at VAW since 2011. It was conducted in the scope of a large European Horizon 2020 research project on innovative technologies for an environmentally enhanced hydropower use.

Dr. Julian Meister systematically investigated the hydraulics and the fish behavior. Prediction equations are proposed to estimate the head losses of HBR-BSs for a wide parameter range, involving different bar shapes and hydropower plant layouts. Live fish tests were conducted in a large laboratory flume for a diverse assemblage of riverine fish species, namely spirlin, barbel, nase, European eel, brown trout, and Atlantic salmon parr. Large fish, with a width exceeding the clear bar spacing, were physically protected. Smaller fish were protected through a partial behavioral guidance effect caused by hydraulic cues like velocity and pressure gradients at the rack bars. Design recommendations are given and equations are proposed to estimate the fish protection and guidance efficiency at HBR-BSs.

The financial support of the EU Horizon 2020 research and innovation program under grant agreement no. 727830, FIThydro (Fishfriendly Innovative Technologies for hydropower), and the Swiss State Secretariat for Education, Research and Innovation (SERI) (grant number 16.0153) is gratefully acknowledged. The investigation of the electrified HBR was supported by the Swiss Federal Office of Energy (grant number SI/501758-01).

I would like to sincerely thank Prof. Dr. Markus Aufleger, Arbeitsbereich Wasserbau, University of Innsbruck, Prof. Paul Kemp, Chair in Ecological Engineering, Faculty of Engineering and the Physical Sciences, University of Southampton, and Dr. Oliver Selz, Department Fish Biology and Evolution, Eawag, for their co-reviews.





# Acknowledgements

This doctoral thesis was written during my employment at the Laboratory of Hydraulics, Hydrology and Glaciology (VAW) at ETH Zurich. This project has received funding from the European Union's Horizon 2020 research and innovation program under grant agreement no. 727830, FIThydro (Fishfriendly Innovative Technologies for hydropower), the Swiss State Secretariat for Education, Research and Innovation (SERI) (grant number 16.0153), and the Swiss Federal Office of Energy (grant number SI/501758-01). I would like to sincerely thank everyone who supported me and contributed to the success of this work, particularly:

- Prof. Dr. Robert M. Boes, VAW director and examiner, who decisively shaped this doctoral project with his continuous support, enthusiasm, and full commitment to the topic.
- Prof Dr. Paul Kemp and Univ.-Prof. Dr. Markus Aufleger for their valuable inputs as co-examiners.
- Dr. Oliver Selz for his personal commitment during the live fish tests, the invaluable feedback during the final project stages, and the detailed review as a co-examiner.
- Dr. Helge Fuchs for his professional supervision and valuable advice with which he substantially shaped this doctoral project.
- Dr. Claudia Beck for the very pleasant and constructive collaboration throughout the entire project and especially for the enormous support during the live fish tests.
- Dr. Ismail Albayrak for funding acquisition and coordination within the FIThydro project.
- Dr. Armin Peter and Nils Schölzel for electrofishing and their valuable inputs during the live fish tests.
- Martin Detert and Anita Moldenhauer-Roth for their great support with the fish tracking system and the electrification.
- The Master students Michael Ruf, Timon Suter, Michael Ganzmann, Andreas Huwiler, Andrea Bianci, and Caterina Rovati and the Bachelor students Nathalie Flury and Tamara Baumgartner for their conscientious work.
- All technical staff including the workshop, electronics laboratory, photographer, and draftsmen for their professional commitment.
- All experts from various disciplines, including biologists, engineers, operators, and policymakers, who contributed to this thesis by participating in the survey or giving valuable inputs at conferences, on the phone, or via e-mail.

- My family, who made my education possible and supported me in every situation.
- My girlfriend Isa with whom I could always recharge my batteries and start each day with a big smile and full motivation!

Zurich, November 2020

Julian Meister

# Contents

<b>Preface</b>	<b>I</b>
<b>Acknowledgements</b>	<b>III</b>
<b>Abstract</b>	<b>IX</b>
<b>Kurzfassung</b>	<b>XI</b>
<b>1 Introduction</b>	<b>1</b>
1.1 Motivation . . . . .	1
1.2 Objectives . . . . .	2
1.3 Thesis outline . . . . .	3
<b>2 Background and fundamentals</b>	<b>5</b>
2.1 Legal foundation . . . . .	5
2.2 Fish biology . . . . .	5
2.2.1 Riverine fish in Switzerland . . . . .	5
2.2.2 Downstream passage corridors at hydropower plants . . . . .	6
2.2.3 Fish movements and movement trigger . . . . .	7
2.2.4 Decline of fish populations . . . . .	10
2.2.5 Fish response to hydraulic and electric stimuli . . . . .	10
2.2.6 Fish characteristics and size distributions . . . . .	12
2.3 Fish injuries and survival rates . . . . .	17
2.3.1 Monitoring techniques and ethohydraulics . . . . .	19
2.3.2 Turbine mortality and survival rates . . . . .	21
2.3.3 Spillway survival rates . . . . .	26
2.3.4 Indirect mortality . . . . .	26
2.3.5 Total and cumulative survival rates . . . . .	27
2.4 Protection measures for downstream moving fish . . . . .	28
2.4.1 Physical barriers . . . . .	30
2.4.2 Mechanical behavioral barriers . . . . .	32
2.4.3 Sensory behavioral barriers . . . . .	34
2.4.4 Bypass systems . . . . .	35
2.4.5 Collection systems . . . . .	35
2.4.6 Environmentally enhanced turbines . . . . .	37
2.4.7 Fish-friendly operation . . . . .	38
2.5 Hydraulic fundamentals . . . . .	38
2.5.1 Laminar and turbulent flow . . . . .	38

2.5.2	Hydraulic losses . . . . .	41
2.5.3	Flow around obstacles . . . . .	43
<b>3</b>	<b>State-of-the-art and design of horizontal bar rack bypass systems</b>	<b>47</b>
3.1	Milestones in the development . . . . .	47
3.2	State-of-the-art . . . . .	49
3.3	Practical examples . . . . .	51
3.4	Design aspects . . . . .	53
3.4.1	Horizontal bar rack design . . . . .	53
3.4.2	Bypass design . . . . .	56
3.5	Rack cleaning machines and operational aspects . . . . .	59
3.6	Limitations . . . . .	61
3.7	Laboratory studies and monitoring campaigns . . . . .	62
3.7.1	Velocity fields . . . . .	62
3.7.2	Head losses . . . . .	64
3.7.3	Ethohydraulic studies . . . . .	65
3.7.4	Monitoring campaigns . . . . .	71
3.8	Identified research gaps and objectives . . . . .	85
<b>4</b>	<b>Experimental setup and methods</b>	<b>87</b>
4.1	Model flumes . . . . .	87
4.1.1	Detailed model diversion hydropower plant . . . . .	87
4.1.2	Detailed model block-type hydropower plant . . . . .	88
4.1.3	Ethohydraulic flume . . . . .	89
4.1.4	Coordinate system . . . . .	92
4.2	Model racks and parameter definition . . . . .	93
4.2.1	Construction of the horizontal bar rack . . . . .	93
4.2.2	Electrification of the horizontal bar rack . . . . .	95
4.2.3	Parameter definition . . . . .	96
4.3	Instrumentation and measurement systems . . . . .	98
4.4	Methods and experimental program . . . . .	101
4.4.1	Velocity fields . . . . .	101
4.4.2	Hydraulic losses . . . . .	102
4.4.3	Live fish tests . . . . .	105
4.4.4	Live fish tests at electrified racks . . . . .	116
4.4.5	Operational aspects . . . . .	118
<b>5</b>	<b>Velocity fields at horizontal bar racks</b>	<b>121</b>
5.1	Parameter effect on the velocity fields . . . . .	121
5.1.1	Bar shape . . . . .	121
5.1.2	Rack angle . . . . .	122

5.1.3	Bar spacing . . . . .	123
5.1.4	Overlays . . . . .	124
5.2	Fish guidance capacity . . . . .	125
5.3	Rack downstream velocity field . . . . .	126
5.4	Effect of the hydropower plant layout . . . . .	128
5.5	Bypass hydraulics . . . . .	132
5.6	Discussion of selected aspects . . . . .	137
5.6.1	Comparison with literature . . . . .	137
5.6.2	Vertical tie-bars . . . . .	139
5.6.3	Engineering application considerations . . . . .	139
<b>6</b>	<b>Head losses of horizontal bar racks</b>	<b>141</b>
6.1	General observations . . . . .	141
6.2	General equation for head loss prediction . . . . .	142
6.3	Application of equations to larger approach flow angles . . . . .	146
6.4	Hydropower plant layouts . . . . .	147
6.5	Discussion of selected aspects . . . . .	148
6.5.1	Bar depth effect . . . . .	148
6.5.2	Effect of vertical tie-bars . . . . .	149
6.5.3	Comparison of head loss prediction equations with literature data . . .	150
6.5.4	Comparison with other rack types . . . . .	151
6.5.5	Engineering application considerations . . . . .	152
6.5.6	Fish protection . . . . .	153
<b>7</b>	<b>Live fish tests with horizontal bar rack bypass systems</b>	<b>155</b>
7.1	General fish swimming behavior . . . . .	155
7.1.1	Fish swimming capability and general considerations . . . . .	155
7.1.2	Species-specific fish swimming behavior . . . . .	156
7.2	Guidance and protection efficiencies . . . . .	161
7.2.1	Species-specific guidance and protection efficiencies . . . . .	161
7.2.2	Effect of the fish species, size distribution, and clear bar spacing . . . .	166
7.2.3	Overall guidance and protection efficiencies . . . . .	170
7.3	Fish swimming tracks . . . . .	173
7.3.1	Combination with flow velocities . . . . .	173
7.3.2	Sector analysis . . . . .	174
7.4	Rack passages . . . . .	178
7.4.1	Effect of the bypass on rack passages . . . . .	178
7.4.2	Vertical and horizontal location of rack passages . . . . .	179
7.4.3	Rheotaxis during rack passages . . . . .	180
7.4.4	Rotation during rack passages . . . . .	181
7.5	Fish swimming behavior at the bypass inlet . . . . .	183

7.6	Fish activity during live fish tests . . . . .	184
7.7	Limitations and challenges when upscaling to prototype . . . . .	186
7.8	Comparison with ethohydraulic studies and monitoring campaigns . . . . .	188
7.8.1	Ethohydraulic studies . . . . .	188
7.8.2	Monitoring campaigns . . . . .	195
<b>8</b>	<b>Live fish tests with electrified horizontal bar rack bypass systems</b>	<b>201</b>
8.1	Measurements of the electric field . . . . .	201
8.2	Fish behavior, guidance, and protection with the electric field . . . . .	202
8.3	Fish injuries . . . . .	208
8.4	Alternative setup and comparison with other studies . . . . .	210
8.4.1	Alternative electrification setup . . . . .	210
8.4.2	Comparison with other studies . . . . .	211
<b>9</b>	<b>Operational aspects</b>	<b>213</b>
9.1	Operational challenges and general considerations . . . . .	213
9.2	Clogging with floating debris . . . . .	214
9.3	Implications of clogging and remediation measures . . . . .	217
<b>10</b>	<b>Design recommendations and engineering application</b>	<b>219</b>
10.1	Design recommendations . . . . .	219
10.2	Head loss assessment . . . . .	221
10.3	Fish protection, turbine survival rate, and total survival rate . . . . .	223
<b>11</b>	<b>Conclusions and outlook</b>	<b>227</b>
11.1	Conclusions . . . . .	227
11.2	Outlook . . . . .	231
	<b>Abbreviations and list of symbols</b>	<b>233</b>
	<b>References</b>	<b>239</b>
<b>A</b>	<b>Appendix</b>	<b>A-1</b>
A.1	Generalized linear models for the comparison with the curved-bar rack . . . . .	A-1
A.2	Fish injury reports . . . . .	A-3

# Abstract

Fish move up- and downstream within rivers throughout their lives to find suitable habitats. During downstream movements, they can incur severe or even lethal injuries when passing through hydropower plant (HPP) turbines or when they are entrained at other water intakes. Horizontal bar rack bypass systems (HBR-BSs) are a state-of-the-art technology to protect and guide downstream moving fish through a safe corridor around water intakes. They are in operation at multiple HPPs for more than a decade, but technical knowledge about the velocity fields, the head losses, the fish guidance efficiency, and the clogging probability was so far missing. This doctoral thesis encompasses the state of knowledge of HBR-BSs and contributes with novel findings to this topic through hydraulic experiments and live fish tests. The velocity fields of HBR-BSs and hydraulic losses of horizontal bar racks (HBRs) were quantified for a wide parameter range. The fish guidance efficiency was assessed through live fish tests involving a diverse assemblage of riverine fish species, namely spirlin (*Alburnoides bipunctatus*), barbel (*Barbus barbus*), nase (*Chondrostoma nasus*), brown trout (*Salmo trutta*), Atlantic salmon parr (*Salmo salar*), and European eel (*Anguilla anguilla*). Systematic experiments with leaves of different tree species were carried out to determine the clogging probability at HBRs.

The main findings of the present thesis include a detailed analysis of the effect of different parameters on the velocity fields up- and downstream of HBRs. Equations were proposed to predict the head losses at HBRs, which can be applied for a wide parameter range, including rectangular and foil-shaped bars, bottom and top overlays, and different HPP layouts. By applying foil-shaped instead of rectangular bars, the losses were reduced by more than 40%, depending on the rack configuration. The fish swimming behavior was analyzed in detail and equations were proposed to estimate the protection and guidance efficiency of HBR-BSs as a function of the clear bar spacing and the fish dimensions. The fish protection efficiency varied between the factors fish species, size, and clear bar spacing of the HBR. While the laboratory HBR-BS with a clear bar spacing of 20 mm offered hardly any protection for juvenile nase, the average protection efficiency exceeded 90% for spirlin and European eel. The behavioral avoidance effect strongly increased with the application of a low-voltage electric field to the HBR-BS. High protection efficiencies were achieved for spirlin and eel, but their behavior strongly depended on their orientation in the electric field and spirlin often refused to enter the bypass. The probability that a leaf clogged at any bar of an HBR decreased linearly for larger clear bar spacings, while the probability of clogging over multiple bars decayed exponentially.

The present work provides technical knowledge to design HBR-BSs, thereby accounting for fish protection, cost-efficiency, and sustainable operation. The weighting of these aspects has to be defined by involving all stakeholders. The findings of the present study contribute to a better understanding of the hydraulic processes and the fish behavior at HBR-BSs, but they cannot replace extensive monitoring campaigns at prototype sites, which are necessary to verify functional efficiency.





# Kurzfassung

Um geeignete Habitate zu finden, schwimmen Fische in unterschiedlichen Lebensphasen in Flüssen stromauf- und stromabwärts. Wenn sie stromabwärts schwimmen, können sie sich bei den Turbinen von Wasserkraftanlagen oder anderen Wasserfassungen schwer oder sogar tödlich verletzen. Horizontalrechen-Bypass-Systeme (HBR-BS) entsprechen dem Stand der Technik, um stromabwärts schwimmende Fische zu schützen und sie über einen sicheren Korridor an Wasserfassungen vorbei zu leiten. Obwohl HBR-BS schon seit über einem Jahrzehnt an diversen Wasserkraftanlagen in Betrieb sind, fehlten bisher technische Grundlagen, um die Auswirkungen auf die Geschwindigkeitsfelder, die hydraulischen Verluste, die Fischleiteffizienz und die Verlegungswahrscheinlichkeit quantifizieren zu können. Im Rahmen dieser Doktorarbeit wird der Wissensstand von HBR-BS zusammengefasst. Mittels hydraulischer und ethohydraulischer Versuche konnten zudem neue Erkenntnisse gewonnen werden. Die Geschwindigkeitsfelder von HBR-BS und die hydraulischen Verluste von Horizontalrechen (HBR) wurden für ein breites Parameterspektrum messtechnisch ermittelt. Die Fischleiteffizienz wurde mittels Lebendfischversuchen für ein breites Artenspektrum bestimmt, nämlich für Schneider (*Alburnoides bipunctatus*), Barben (*Barbus barbus*), Nasen (*Chondrostoma nasus*), Bachforellen (*Salmo trutta*), atlantische Lachsparrs (*Salmo salar*) und europäische Aale (*Anguilla anguilla*). Mittels systematischer Untersuchungen konnte zudem die Verlegungswahrscheinlichkeit mit Blättern unterschiedlicher Baumarten ermittelt werden.

Zu den Hauptresultaten der vorliegenden Arbeit gehört die detaillierte Analyse der Auswirkungen unterschiedlicher Parameter auf die Geschwindigkeitsfelder ober- und unterstrom von HBR. Die Geschwindigkeitsfelder an Horizontalrechen werden vor allem durch Sohl- und Tauchleitwände und die Kraftwerksanordnung beeinflusst. Im Rahmen dieser Arbeit wurden Gleichungen vorgeschlagen, um die hydraulischen Verluste von HBR für ein breites Parameterspektrum abschätzen zu können, welches Rechteckstäbe und strömungsgünstige Rechenstäbe, Sohl- und Tauchleitwände und unterschiedliche Kraftwerksanordnungen beinhaltet. Durch den Einsatz von strömungsgünstigen Rechenstäben anstelle von Rechteckstäben, konnten die Verluste je nach Konfiguration um mehr als 40% reduziert werden. Das Fischverhalten wurde detailliert analysiert, und es wurden Gleichungen vorgeschlagen, um die Fischschutz- und Fischleiteffizienz von HBR-BS in Abhängigkeit des lichten Stababstands und der Fischgrösse abschätzen zu können. Die Fischschutzeffizienz war stark von der Fischart und -grösse und dem lichten Stababstand des HBR abhängig. Beispielsweise bot das HBR-BS juvenilen Nasen kaum Schutz, während die durchschnittliche Schutzeffizienz für Schneider und europäische Aale über 90% betrug. Die verhaltensbedingten Vermeidungsreaktionen nahmen mit der Kombination des HBR-BS mit einem schwachen elektrischen Feld zu. Es konnten hohe Schutzeffizienzen für Schneider und Aale erreicht werden, das Verhalten war aber stark von der Ausrichtung der Fische im elektrischen Feld abhängig, und viele Schneider verweigerten den Bypasseinstieg. Die Verklauungswahrscheinlichkeit eines Blatts an einem Rechenstab nahm mit zunehmendem

Stababstand linear ab, während die Verklausungswahrscheinlichkeit eines Blatts über mehrere Rechenstäbe exponentiell abnahm.

Die vorliegende Arbeit stellt technisches Wissen zur Verfügung, um HBR-BS unter Berücksichtigung von Fischschutz, Wirtschaftlichkeit und nachhaltigem Betrieb zu dimensionieren. Die Gewichtung dieser Aspekte sollte unter Einbezug aller Interessensgruppen erfolgen. Die Resultate der vorliegenden Untersuchung tragen zu einem besseren Verständnis der hydraulischen Prozesse und des Fischverhaltens an HBR-BS bei, können umfangreiche Monitoringkampagnen an Prototypanlagen jedoch nicht ersetzen.

# 1 Introduction

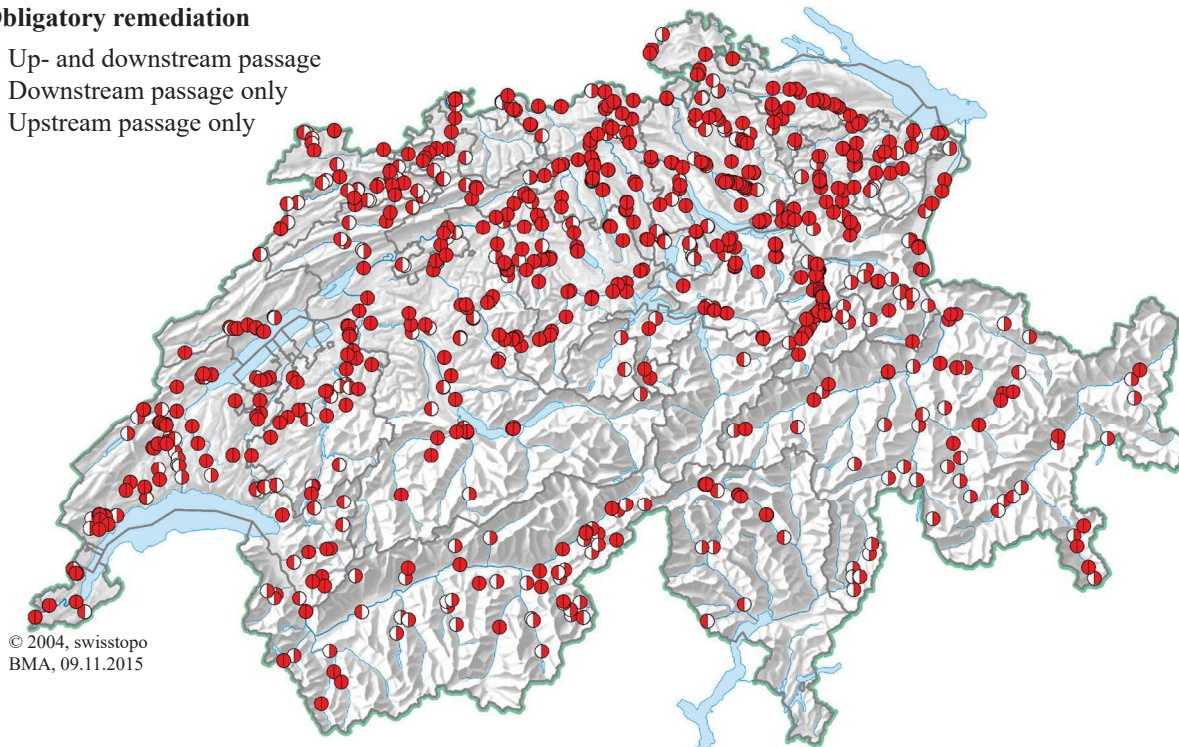
## 1.1 Motivation

In 2019, electricity in Switzerland was produced to 32% by storage hydropower plants, 25% by run-of-river power plants, 35% by nuclear power plants, 4% by renewable and non-renewable conventional thermal power plants, and 4% by other renewables (SFOE, 2020). The latter includes energy production from wood firing, biogas plants, photovoltaic systems, and wind power stations. The Swiss Energy Strategy 2050 aims at further promoting renewables, while demanding a nuclear phase-out. To replace the omitted base load of nuclear power plants, run-of-river power plants are more suitable than other renewables such as photovoltaic systems and wind power stations, which are subject to large fluctuations in electricity production due to changing weather conditions. Hydropower is the most efficient renewable electricity production technology currently available with overall efficiency factors of up to 88% (Giesecke *et al.*, 2014). The energy payback ratio, which is defined as the ratio of the produced energy over the whole life cycle to the energy which is needed for construction, operation, and deconstruction of the power plant, amounts to 78 for storage hydropower plants and 58 for run-of-river power plants, which is significantly larger than for nuclear power (12), photovoltaics (4–8), or wind (18–20) under Swiss conditions (Steffen *et al.*, 2018). In comparison to other energy sources, HPPs cause very limited CO<sub>2</sub> emissions with only 4–5 g CO<sub>2</sub>eq/kWh for run-of-river HPPs and 6–7 g CO<sub>2</sub>eq/kWh for storage hydropower plants (Bauer *et al.*, 2017). A disadvantage of HPPs is their impact on the ecological river system. This includes hydropeaking, the disruption of the sediment transport continuum, and the impairment of fish movements. Fish populations in Switzerland decreased in the last century, which was caused by multiple factors like habitat loss, poor water quality, overfishing, predation by piscivorous fish and birds, and river fragmentation (EAWAG and SAEFL, 2004). As per 2016, about half of the 40 typical riverine fish species in Switzerland are considered as endangered (Dönni *et al.*, 2017). To date, much effort has been made to allow for upstream passage, while little emphasis was put on downstream passage (Silva *et al.*, 2018). Within Switzerland, approx. 700 barriers are subject to obligatory remediation for downstream passage (Fig. 1.1), whereof the vast majority is not yet equipped with a downstream passage facility (Bammatter *et al.*, 2015). Since downstream moving fish often follow the largest flow, many of them end up swimming through the turbines of HPPs, which results in a risk to incur severe or even lethal injuries. Water is also extracted from rivers for other purposes than HPPs, such as for cooling of nuclear and thermal power plants or the extraction of water for irrigation or industry. HBR-BSs are one of the most widely used technologies to allow for safe fish downstream passage at water intakes. Although multiple prototype HPPs with HBR-BSs are successfully in operation in northeast Germany for more than one decade (Ebel, 2016), there is still a lack of systematic studies on the optimization and verification of these state-of-the-art downstream fish passage facilities. Up to now, the effect of different parameters on the velocity fields at HBR-BSs was largely unknown and there was a high uncertainty in

quantifying the hydraulic losses caused by HBRs. Large fish are physically blocked at HBRs, but so far it was difficult to assess their protection effect on small fish. The protection of small fish can be increased with a hybrid barrier, where the HBR is combined with sensory stimuli such as light, sound, or electric fields. The efficiency of most sensory behavioral barriers is limited to certain fish species and environmental conditions (DWA, 2004), whereas recent studies indicate that the protection efficiency of racks can be improved for various fish species, if they are combined with a low-voltage electric field (e.g. Berger, 2018; Tutzer *et al.*, 2019b). However, little was known about the fish behavior at electrified HBRs. Last but not least, HBRs are subject to operational challenges like partial clogging with foliage and floating debris. Studies were missing to quantify the effect of different parameters on the clogging probability. To be able to operate run-of-river power plants in an environmentally sustainable way in the future, the processes at fish downstream passage facilities have to be better understood, such that they can be further optimized.

#### Obligatory remediation

- Up- and downstream passage
- ◐ Downstream passage only
- ◑ Upstream passage only



**Fig. 1.1:** Barriers in Swiss rivers which are subject to obligatory remediation for up- and downstream passage (adapted from Bammatter *et al.*, 2015)

## 1.2 Objectives

The overall goal of this doctoral thesis was to provide technical knowledge, such that HBR-BSs can be designed while accounting for fish protection, cost-efficiency, and sustainable operation. The weighting of these aspects has to be defined by involving all stakeholders. This overall goal was achieved by studying the velocity fields, head losses, fish behavior, and foliage clogging at HBR-BSs. The velocity fields upstream of HBR-BSs are important as they affect the behavior of downstream moving fish, while the downstream velocity field may reduce turbine efficiency. The hydraulic losses of HBR-BSs may significantly decrease the hydraulic head of HPPs, which

reduces the economic efficiency. HBR-BSs are built to protect downstream moving fish, such that the quantification of the fish guidance efficiency is of prime importance. The combination of HBR-BSs with a low-voltage electric field may lead to similar protection efficiencies, while allowing for an increased bar spacing. This would reduce the hydraulic losses and the clogging probability, and thereby increase the economic efficiency. Partial clogging can significantly increase the hydraulic losses, which is one of the major operational challenges at HBR-BSs. In summary, this doctoral thesis aims to

- I) quantify the **velocity fields** up- and downstream of HBRs,
- II) develop an equation to reliably estimate the **hydraulic losses** of HBRs,
- III) determine the **fish protection and guidance efficiencies** of HBR-BSs,
- IV) investigate the fish behavior at HBR-BSs with a **low-voltage electric field**, and
- V) quantify the effect of different parameters on **foliage clogging**.

### 1.3 Thesis outline

This doctoral thesis consists of 11 chapters. The background and fundamentals of fish protection, countermeasures, and related hydraulics are summarized in Chapter 2, while the state-of-the-art of HBR-BSs is assessed in Chapter 3. The experimental setup and methods applied in this thesis are described in Chapter 4. The results and the discussion of the velocity fields, head losses, live fish tests with and without electrification, and operational aspects are presented in Chapters 5–9, respectively. The main findings are then applied to a practical example in Chapter 10. Chapter 11 concludes the most important aspects and gives an outlook by summarizing open research questions.



## 2 Background and fundamentals

### 2.1 Legal foundation

The problem of fish mortality at HPP turbines was identified shortly after the construction of the first industrial HPPs at the end of the 19<sup>th</sup> century and was accordingly mentioned in the particular laws. Article V of the Prussian law from the 30<sup>th</sup> of March 1880, which can be interpreted as the forerunner of today's laws in Germany, mentioned that the minister for commerce and agriculture was able to obligate HPP operators to install apparatuses like lattices on their own costs to protect fish from entering turbines (Gerhard, 1893). Similar requirements were mentioned in Art. 6 of the Swiss Federal Act on Fishing from the 21<sup>st</sup> of December 1888 (Schmassmann, 1928). Because of the limited technical feasibility and the resistance of HPP operators, fish protection measures were only sparsely implemented at that time. Today, Art. 83a and 83b of the revised Swiss Federal Act on the Protection of Waters (WPA/GSchG) obligates all operators of existing hydropower plants in Switzerland to take the appropriate remediation measures according to Art. 9 and 10 of the Swiss Federal Act on Fishing (BGF) within 20 years after the WPA took effect, which was the 1<sup>st</sup> of August 2010. The BGF prescribes that the free up- and downstream fish migration has to be ensured for all new HPPs and also for existing plants if it is economically feasible. According to Art. 34 of the Swiss energy law (EnG), the concessionaire will be entirely refunded by the national network company for all measures in terms of Art. 83a of the WPA and Art. 10 of the BGF. This means that all fish protection measures are economically feasible as their implementation does not lead to any additional costs for the concessionaire (Könitzer *et al.*, 2012). Similarly, the goal of the European Water Framework Directive (WFD) is that “the continuity of the river is not disturbed by anthropogenic activities and allows undisturbed migration of aquatic organisms and sediment transport”. Although it is hardly possible to reestablish undisturbed migration, fish passage can be enhanced with fish passes and fish guidance structures. All regulations mentioned so far demand fish downstream passage facilities, without listing specific numbers for the required fish survival rate. In contrast, the European regulation on eels (EC Regulation No. 1100/2007) emphasizes that the anthropogenic mortality shall be reduced so that at least 40% of the silver eel biomass reaches the sea in comparison to natural conditions without any anthropogenic influences. Summed up, the problem of fish downstream passage has been identified and mentioned in laws already at the end of the 19<sup>th</sup> century, but more recent and stricter laws created new incentives for the implementation of fish downstream passage facilities.

### 2.2 Fish biology

#### 2.2.1 Riverine fish in Switzerland

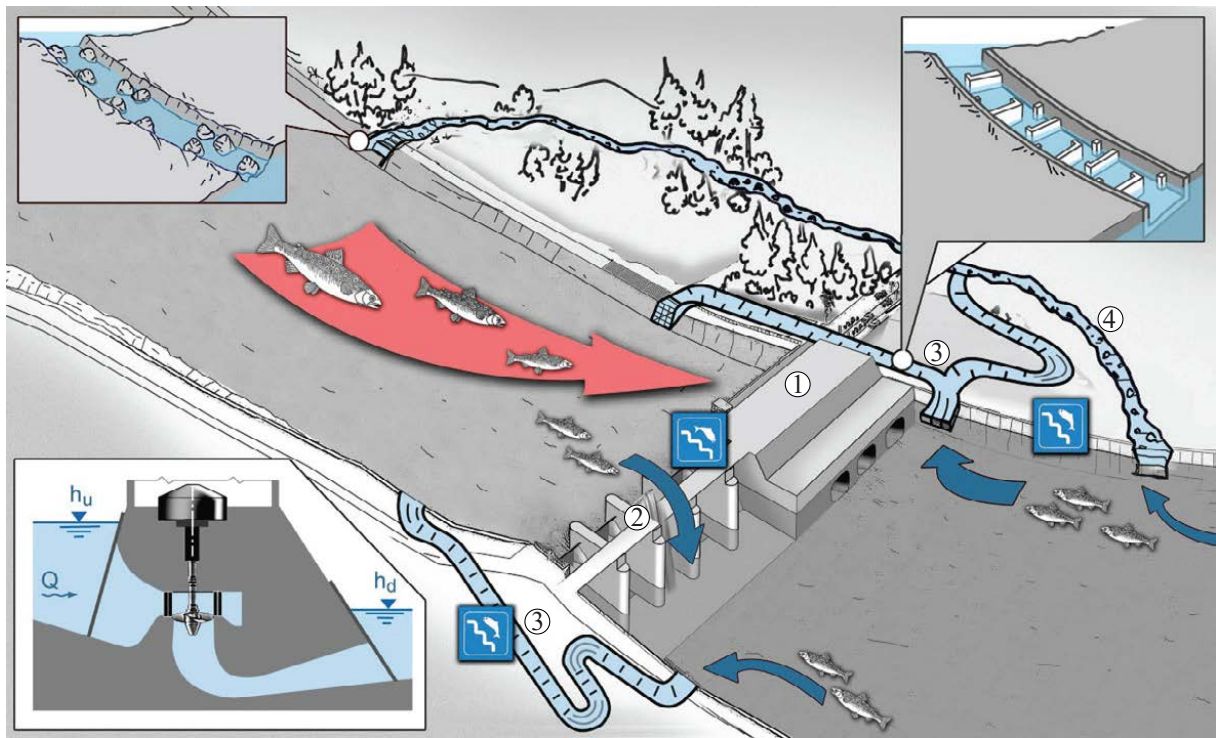
Animal species are classified as not endangered, endangered, highly endangered, in danger of extinction, or already extinct. As per 2016, about half of the 40 typical riverine fish species in Switzerland were considered as endangered (Dönni *et al.*, 2017). To prioritize the protec-

tion of Swiss riverine fish species, Dönni *et al.* (2017) defined the criteria movement distances, state of knowledge, indicator value, flagship character, fishery importance, habitat range, endangered status, and international responsibility. In Switzerland, the most important species regarding migration are several trout species (lake trout (*Salmo trutta*), sea trout (*Salmo trutta*), Rhône trout (*Salmo rhodanensis*), marble trout (*Salmo marmoratus*)), Atlantic salmon (*Salmo salar*), common nase (*Chondrostoma nasus*), zingel asper (*Zingel asper*), European river lamprey (*Lampetra fluviatilis*), European eel (*Anguilla anguilla*), allis shad (*Alosa alosa*), and European sturgeon (*Acipenser sturio*), of which Atlantic salmon, sea trout, European river lamprey, allis shad, and European sturgeon are already absent from the water bodies of Switzerland (Dönni *et al.*, 2017).

### 2.2.2 Downstream passage corridors at hydropower plants

Figure 2.1 gives an overview of corridors for potential up- and downstream movements at typical run-of-river HPPs including ① turbines, ② spillway, ③ fish pass, and ④ natural fishway. Fish often follow the main flow (DWA, 2004), which is typically through the turbines, resulting in swimming through the potentially most harmful corridor. Depending on the river hydrology, modern run-of-river HPPs are typically designed with high design discharges, which are often exceeded less than 20% of the time (Giesecke *et al.*, 2014). The spillways are therefore not accessible for downstream passage at 80% of the days and they may not be suitable for downstream passage of all species. As an example, benthic species are likely to not use an overflow weir for downstream passage. Fish passes and natural fishways were originally built for upstream passage. They can also be used for downstream passage, but due to their low discharge of typically 1–5% of the competing flow (Larinier, 2002), it is difficult for downstream moving fish to find the entrance. Some monitoring campaigns report that fish passes are hardly used for downstream passage (e.g. Agostinho *et al.*, 2011; Pelicice and Agostinho, 2012), whereas in others the fish passes were frequently used which might be due to hydraulically unfavorable conditions at the other corridors (e.g. Schmalz, 2010; Engler and Adam, 2014; details in Section 3.7.4). The usage of different corridors strongly varies with the species, life stage, and site-specific aspects. Some examples from monitoring campaigns are given in Section 3.7.4.



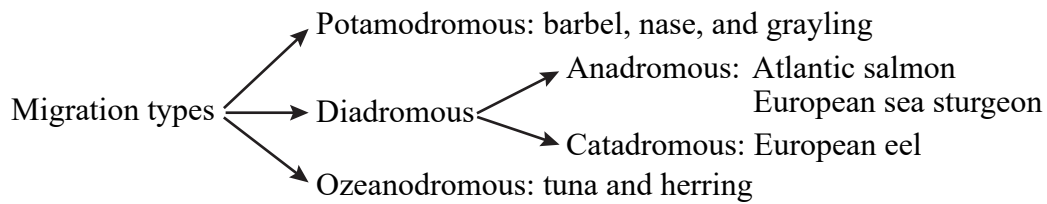


**Fig. 2.1:** Corridors for downstream passage at run-of-river HPPs without a fish downstream passage facility, including ① turbines, ② spillway, ③ fish pass, and ④ natural fishway (adapted from Kriewitz, 2015)

### 2.2.3 Fish movements and movement trigger

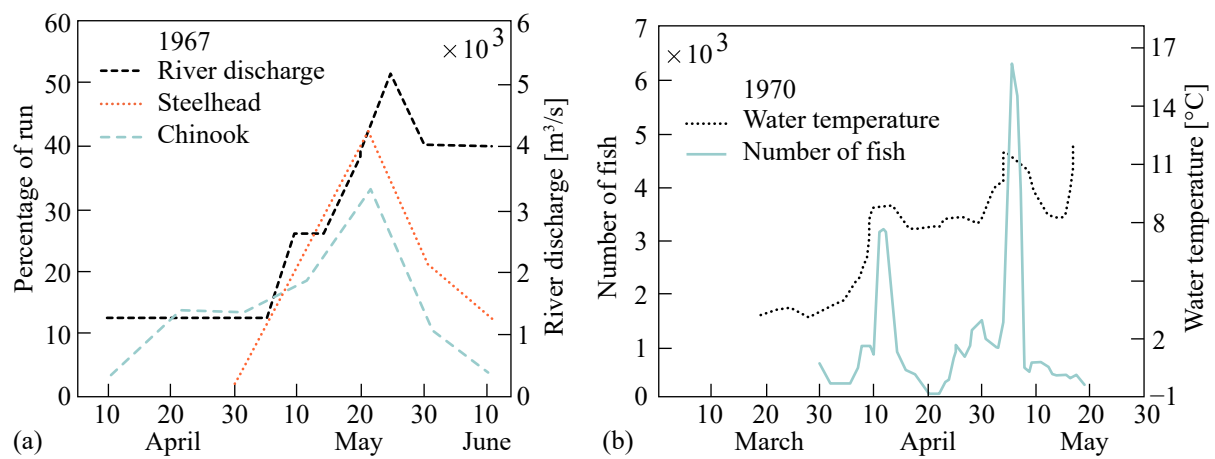
Fish move up- and downstream within river systems throughout their lives for various reasons. Four movement types can be distinguished, namely station-keeping movement, dispersal, nomadism, and migration (Teitelbaum and Mueller, 2019; Schlägel *et al.*, 2020). Station-keeping movements are daily movements within a restricted area (home range; Schlägel *et al.*, 2020). Dispersal is a direct movement from a previously used habitat to a new habitat, which often occurs only once within an individual's lifetime (Teitelbaum and Mueller, 2019). Nomadism includes all movements of individuals and populations, which occur with an irregular timing and causes both within-year and between-year variability (Teitelbaum and Mueller, 2019). Migration can be defined as “movements resulting in an alternation between two or more separate habitats occurring with regular periodicity and involving a large fraction of the population” (Northcote, 1978). Although the frequency and movement distances can vary significantly between and within species (Radinger and Wolter, 2014), all riverine fish move within river systems to find suitable habitats for spawning, nutrition, or hibernation, to find suitable shelter during floods, and to compensate undesired passive drift (DWA, 2014; Ebel, 2016). Fish can be classified according to their migration type (Fig. 2.2). Potamodromous species like barbel, nase, and grayling are characterized by a distinct life cycle, which they spend entirely in fresh water. Some of them, like barbel, are known to regularly move more than 100 km from one habitat to another (Hütte, 2000). Diadromous fish species migrate between fresh and salt water. They are subclassified in anadromous species, living in salt water and migrating into fresh water for spawning (e.g. Atlantic salmon) and catadromous species living in fresh water and migrating into salt water for spawning (e.g. European eel; Lucas and Baras, 2001). Since diadromous

species cover very long migration distances, they are more severely affected by barriers like HPPs. Ozeanodromous species, like tuna and herring, spend their entire life in salt water and are therefore not affected by run-of-river HPPs. Fish passage facilities were historically mainly built for diadromous species, but they are important for all downstream moving fish. From a biological point of view it is important to distinguish between different movement patterns, as for example not all of them lead to gene flow. For practical applications, for example during a monitoring campaign at a fish passage facility, it is often not possible to distinguish between different movement types. Within the present thesis, the word “movement” is therefore used to account for all movement types, whereas the word “migration” is used for diadromous species only.



**Fig. 2.2:** Classification of fish migration types with some examples

The main factors affecting the timing of fish movements are the season, the time of the day, the discharge, the water temperature, and the moon phase (Ebel, 2016). Additional factors, which can be at least partly correlated with the main factors, include the turbidity, salinity and conductivity, oxygen concentration, sky cover, rainfall, air pressure, and wind (Ebel, 2016). While some of these factors can be well correlated with the downstream movement activity, no clear trend could be identified for others. Although numerous studies focused on the prediction of downstream movement behavior, it is up to now not possible to satisfactorily predict the movement behavior of most fish species. This information is of high importance for operational measures like the temporarily operational shutdowns during the main movement period. Raymond (1979) investigated the downstream migration behavior of different salmonids (chinook salmon and steelhead) in the Snake and Columbia Rivers during the period 1966 to 1975. In 1967, the peak of downstream migration activity matched the maximal discharge period (Fig. 2.3a). In addition, a positive correlation of the downstream migration activity and the water temperature was noted in 1970 (Fig. 2.3b). Lowe (1952) observed the highest downstream migration activity of silver eels when floods coincided with moonless phases, while only few eels migrated during full moon. Zaugg and Mendez (2018) found that the downstream movement activity of riverine species in the Limmat River increased in autumn at dawn and night with increasing discharge, resulting in leave transport in slightly turbid water with temperatures of  $T < 13.2^{\circ}\text{C}$  and when the weather was between cloudy and rainy. The reasons why these factors increase the downstream movement activity can be manifold, but it is likely that fish try to avoid moving in low flow periods with clear water to reduce the predation risk (Zaugg and Mendez, 2018).



**Fig. 2.3:** Correlation between downstream migration activity and (a) river discharge and (b) water temperature (adapted from Raymond, 1979)

While there is little information available on the movement behavior of riverine species, multiple studies investigated the distinct day-night migration behavior of European eels (e.g. Adam and Schwevers, 1999; Durif *et al.*, 2003; Schwevers *et al.*, 2011; Schmalz, 2012). Eels generally show only little activity between 6 a.m. and 6 p.m., with the lowest activity between 11 a.m. and 3 p.m. (Adam and Schwevers, 1999). With darkness approaching at around 7 p.m., eel activity starts and peaks between 2 a.m. and 4 a.m. (Adam and Schwevers, 1999). Table 2.1 gives a simplified overview of the main movement periods of selected fish species.

**Table 2.1:** Main movement periods of selected fish species with respect to their growth stage (adapted from Ebel, 2016)

Species	Growth stage	Jan	Feb	Mar	Apr	May	Jun	Jul	Aug	Sep	Oct	Nov	Dec
Eel	4 (Yellow eel)												
	5 (Silver eel)												
Atlantic salmon	4 (Smolt)												
	5 (Kelt)												
Potamodromous	1 + 2 + 3												
	4												
	5												

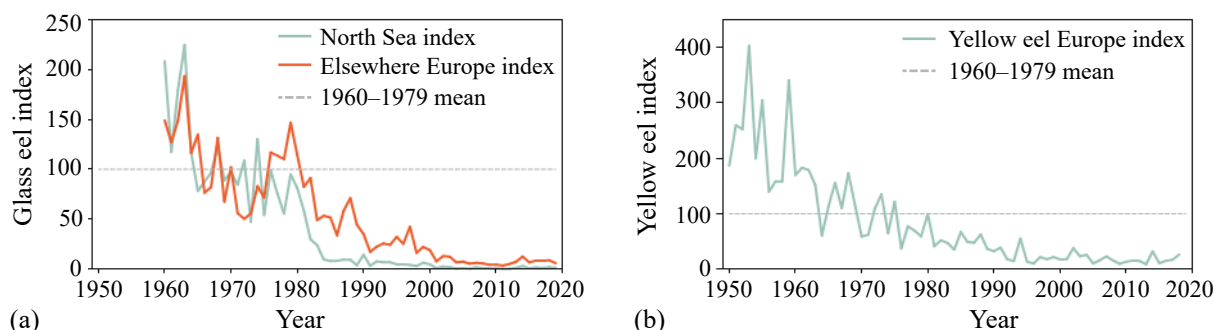
1	Eggs / embryos	Absent from fresh water or small movement and drift activity
2	Yolk-sac larvae	Movements due to different motivation
3	Larvae	Diadromous migration or drift to feeding grounds
4	Juvenile	Diadromous migration or drift to spawning grounds
5	Adult / subadult	

While riverine fish move almost throughout the year (Ebel, 2016; Adam *et al.*, 2018), diadro-

mous species migrate primarily in certain months, which depends on the location, the species, and the life stage. As an example, Atlantic salmon kelts migrate during winter, while Atlantic salmon smolts start their seaward migration in spring (Table 2.1).

### 2.2.4 Decline of fish populations

Most fish populations in Europe declined in the last decades due to various stressors causing habitat loss, poor water quality, overfishing, predation by piscivorous fish and birds, and river fragmentation (EAWAG and SAEFL, 2004). Particularly dramatic is the development of the eel population in Europe (Fig. 2.4). The average glass eel recruitment in the period 2012–2016 was only 1.7% of the recruitment in 1960–1979 (ICES, 2019). Eels are the only remaining diadromous fish species in Switzerland since the populations of Atlantic salmon, sea trout, European river lamprey, allis shad, and European sturgeon became locally extinct (Boller and Dönni, 2011; Dönni *et al.*, 2017). Although it is more difficult to quantify the development of riverine fish populations as the magnitude varies between species and regions, it is undisputed that the catches of brown trout and other species declined within the past 30 years in Switzerland (EAWAG and SAEFL, 2004). Identifying the main stressors causing the decline of fish populations is crucial to efficiently implement conservation measures (Mueller *et al.*, 2020a). Northcote (1998) found that the decline of many threatened freshwater species in Europe is associated with a reduced connectivity due to dams, weirs, and other alterations in river channel features, leaving little doubt that the reduced longitudinal connectivity threatens many European freshwater fish species.



**Fig. 2.4:** Development of (a) glass eel and (b) yellow eel populations in Europe (adapted from ICES, 2019)

### 2.2.5 Fish response to hydraulic and electric stimuli

Fish sense the surrounding flow with their lateral line organ, which consists of velocity and pressure sensitive arrays at their head and sides (Tuhtan and Fuentes-Perez, 2018). With the lateral line organ, fish can orient themselves in the flow and react to pressure gradients and large-scale flow patterns (Tuhtan and Fuentes-Perez, 2018). The orientation of fish in running water is called rheotaxis. A positive rheotaxis means that a fish turns its head against the oncoming current, while a negative rheotaxis means that a fish swims downstream with its head first. When a critical flow velocity of typically 0.1–0.3 m/s is exceeded, most fish species orient themselves with positive rheotaxis (Adam and Lehmann, 2011). Fish reactions to hydraulic stimuli often co-depend on various other factors and will most likely vary among species, popu-

lations, and even individuals. Vowles *et al.* (2014) observed that downstream migrating juvenile salmon showed stronger avoidance reactions to accelerating flow when the experimental channel contained light in comparison to when tested under full darkness. Actively migrating fish often favor corridors with large flow velocities to reduce energy expenditure (Ebel, 2016), but they diverge from flow which exceeds their prolonged speeds (Silva *et al.*, 2020). It is also known that high levels of turbulences and large accelerations may hamper fish orientation and reduce their swimming stability (e.g. Haro *et al.*, 1998; Enders *et al.*, 2012; Vowles *et al.*, 2014; Silva *et al.*, 2016, 2020). Besides the ability to perceive pressure and velocity changes, fish can sense optical, acoustic, smell, temperature, and possibly magnetic field changes (Turnpenny and O’Keeffe, 2005; Adam and Lehmann, 2011). A distinction is made between species which generally show positive and negative phototaxis, meaning that they tend to actively swim towards light or avoid it, respectively. Likewise, fish can show positive or negative thigmotaxis, which means that they seek or avoid physical contact, respectively.

While only few studies investigated reactions of downstream moving fish at hybrid barriers, that is, where a rack is combined with a low-voltage electric field (details in Section 2.4.3 and examples in Section 3.7.3), most knowledge about fish reactions in electric fields comes from electrofishing. In electric fields, current always flows from the anode (positively charged) to the cathode (negatively charged) along the potential gradient (field lines), which are perpendicular to the equipotential lines. At a certain voltage gradient, fish orient themselves towards the anode in electric fields, which is used for decades in electrofishing and is generally known as galvanotaxis (Beaumont, 2016). Fish reactions in electric fields can be related to the “body voltage”, which is the voltage potential over the fish length. This means that if a fish is aligned along an electric field line, it is exposed to a large voltage potential, while the voltage potential is small if a fish is aligned along an equipotential line. The fish behavior in electric fields depends on various factors, such as its orientation, the water conductivity, the fish conductivity, the voltage gradients, and the waveform. The most commonly used waveform for electric barriers are direct current gated bursts (gpDC), where high-frequency pulse groups are repeated in certain intervals. This waveform is hard to produce and the level of injury is variable, but it leads to high catch efficiencies in electrofishing and requires less power than other waveforms (Beaumont, 2016). Fish behavior in electric fields can be classified in the

- **indifference zone**, where the electric field does not affect fish,
- **repulsion zone**, where fish react to the electric stimuli, but it is not strong enough to physiologically attract fish,
- **attraction zone**, where fish are attracted to the anode
- **narcosis zone**, where fish are immobilized but still breathe and recover instantly, and
- **tetanus zone**, where fish are immobilized, potentially harmed, or it requires several minutes for fish to recover (Beaumont, 2016).

The goal of electrofishing is to maximize the attraction zone, while the repulsion zone should be sought for electric barriers. For pulsed direct current (pDC), the attraction and tetanizing thresholds are  $\Delta U_e = 0.1\text{--}0.2\text{ V/cm}$  and  $\Delta U_e = 0.5\text{--}0.6\text{ V/cm}$ , respectively (Beaumont, 2016). In moderate water conductivity ( $250\text{--}1000\text{ }\mu\text{S}$ ), voltage gradients of  $\Delta U_e = 0.1\text{--}1.0\text{ V/cm}$  are considered suitable for electrofishing (Beaumont, 2016). Besides their positive effects, electric fields can cause fish injuries, which are likely a result of powerful convulsions of the body musculature (Snyder, 2003). Potential injuries include spinal fractures and hemorrhages, which are often not externally obvious (Snyder, 2003). However, the frequency and extent of these injuries depends on various factors, such that they can hardly be generalized.

### 2.2.6 Fish characteristics and size distributions

Fish characteristics can be very species-specific. This section briefly describes selected fish species, their preferred movement locations, biometry, and swimming performance.

#### Spirlin

The spirlin (*Alburnoides bipunctatus*) is a small-sized cyprinid, which prefers moderate to fast flowing waters in the barbel and grayling zone (Flügel *et al.*, 2015). It is known for its distinct schooling behavior in the open water and is endangered in Switzerland (Kirchhofer *et al.*, 2007).

#### Barbel

The barbel (*Barbus barbus*) is a rheophilic cyprinid of the barbel zone which is potentially endangered in Switzerland (Kirchhofer *et al.*, 2007). Barbels are known to move over long distances and are bottom-oriented (Eichenberger and Kirchhofer, 2013).

#### Nase

The common nase (*Chondrostoma nasus*) is a cyprinid, which prefers fast flowing rivers in the grayling and barbel zone. It is known for moving over large distances and is in danger of extinction in Switzerland (Kirchhofer *et al.*, 2007).

#### Brown trout

The brown trout (*Salmo trutta fario*) prefers fast flowing rivers in the trout zone, moves over a wide range of distances, and shows a partial migration tendency. The latter means that a part of the population moves downstream as juveniles and returns as large lake trout, while another part of the population spends its entire life in the river system and has a more restricted movement pattern. Brown trout are classified as potentially endangered in Switzerland (Kirchhofer *et al.*, 2007). Adam and Lehmann (2011) described trout as solitary, showing little activity in ethohydraulic experiments.

#### Salmon

The Atlantic salmon (*Salmo salar*) is an anadromous species which became locally extinct in Switzerland in the 1950s (Kirchhofer *et al.*, 2007; Boller and Dönni, 2011). Since then, there are only stocked populations in tributaries of the Rhine River which are not self-sustaining. One reason therefore is that by 2019, four HPPs on the Rhine River were still not equipped

with a fish pass (Baier, 2019) and none of the 21 HPPs had a fish guidance structure for downstream passage. Mature Atlantic salmon spawn in gravel-bed rivers. The hatched salmon are called alevin, which develop to fry and subsequently parr. After smoltification, they start their downstream migration to the Atlantic ocean. Salmon parr and smolts are known to have a very sensitive optical perception in ethohydraulic experiments, which means that they never collide with any obstacles and they also react sensitive to movements outside of the flume (Adam and Lehmann, 2011).

## Eel

The European eel (*Anguilla anguilla*) is a catadromous species with a fascinating life-cycle. Mature eels spawn in the Sargasso sea and the larvae drift with the Gulf stream to European estuaries. The glass eels migrate up the Rhine River to the Swiss plateau rivers. On average, they spend 10 years in fresh water as yellow eels (Adam and Lehmann, 2011), before they start their downstream migration as silver eels. Eels are endangered (Kirchhofer *et al.*, 2007) and populations in Swiss rivers are very likely originating from stocking, since not all HPPs on the Rhine River are equipped with fish passes (Baier, 2019). The undulatory swimming movements enable eels to swim back- and forwards (Adam and Lehmann, 2011). Eels have a limited optical perception but they avoid bright light (negative phototaxis) and are known to act solitary (Adam and Lehmann, 2011), while they seek physical contact (positive thigmotaxis; e.g. Adam *et al.*, 1999; Russon *et al.*, 2010; Russon and Kemp, 2011; Silva *et al.*, 2016).

## Preferred movement locations

Knowing the preferred movement locations in vertical and horizontal direction is very valuable for implementing fish protection measures, but it varies among species, populations, and to a certain extent even individuals. It has to be assumed that fish move downstream across the whole cross section, that is, close to the river banks and midstream. The preferred movement depth is affected by external conditions, such as flow velocities or flow depth. As an example, downstream migrating salmon smolts prefer the mid part of the river channel and follow, to some extent, the main flow (Thorstad *et al.*, 2012; Silva *et al.*, 2020). They are known to mostly migrate downstream near the water surface (Thorstad *et al.*, 2012; Ebel, 2016), which is based on studies at large and deep rivers such as the Connecticut River in the USA (e.g. Normandeau Associates, 1995). In small rivers with flow depth of  $\approx 1$  m, salmon smolts were also observed migrating close to the bottom (e.g. Davidsen *et al.*, 2005; Svendsen *et al.*, 2007) and they also tend to swim towards the bottom on sensing danger (Turnpenny and O’Keeffe, 2005). At multiple monitoring campaigns, eels preferred the bottom to the top bypass opening (e.g. Travade and Larinier, 2006; Hermens and Gubbels, 2017) and are therefore known to generally migrate close to the river bottom (Ebel, 2016). By observing downstream migrating eels at HPP Dettelbach on the Main River (49°47'39.5"N, 10°10'52.5"E) with echo sounders, Fiedler and Göhl (2006) found that 75% of the eels migrated within one meter above the bottom in the five meter deep river. In contrast, by tracking downstream migrating eels, Brown *et al.* (2007) found that most eels entered the power canal of HPP Arapuni in New Zealand



(38°04'16.9"S, 175°38'32.7"E) near the water surface, where dominant flow patterns existed. Most eels searched for a suitable downstream passage corridor across the entire water column, before they ended up in the turbines as the HPP was not equipped with a bypass (Brown *et al.*, 2007). Comparatively little is known about the preferred swimming depth of downstream moving riverine fish. While sturgeon, barbel, bream, and gudgeon prefer to move close to the river bottom, no clear preference is known for roach and bleak (Ebel, 2016). At HPP ECI in Roermond (51°11'23.1"N, 5°58'52.5"E), the Netherlands, most salmon smolts preferred the surface bypass, whereas almost all eels migrated through the bottom bypass opening (Hermens and Gubbels, 2017). The majority of riverine species used the bottom opening, but the share of riverine species using the surface bypass was also considerable (Hermens and Gubbels, 2017). Due to knowledge gaps and species- and site-specific variations in the preferred swimming depth, it has to be assumed that fish move downstream within the entire water column.

### Fish biometry

In the following, the common names spirlin, barbel, nase, trout, salmon, chub, and eel are used as synonyms for the fish species *Alburnoides bipunctatus*, *Barbus barbus*, *Chondrostoma nasus*, *Salmo trutta fario*, *Salmo salar*, *Squalius cephalus*, and *Anguilla anguilla*, respectively. Fish biometry allows to calculate certain proportional metrics, which can be derived from the following characteristic dimensions:  $w_f$  = absolute fish width [m],  $h_f$  = absolute fish height [m], and  $TL$  = total fish length [m], which is measured from the nose to the caudal fin. The relative fish width  $w_{f,rel}$  and the relative fish height  $h_{f,rel}$  are given by Eq. (2.1) and (2.2),

$$w_{f,rel} = \frac{w_f}{TL} \quad (2.1)$$

$$h_{f,rel} = \frac{h_f}{TL}. \quad (2.2)$$

Intuitively, the fish width is decisive for determining the clear bar spacing  $s_b$  of physical barriers with vertical bars, whereas the fish height is limiting for physical barriers with horizontal bars. However, fish are not static and can adjust their body axes and position in the water column. Hence, when approaching a barrier, they can turn to their sides, that is, rotate themselves by 90°, allowing them to pass through HBRs even if  $h_f > s_b$ . There is hardly any literature available, describing to which extent fish adjust their position in the water column and turn to their sides when approaching and eventually passing through barriers. Stewart and Ferrell (2002) tested the efficiency of fish traps with either horizontally or vertically aligned bars and hypothesized that most species can turn on their sides to escape traps with horizontal bars. Although their findings cannot be directly transferred to the application of HBRs, because of the different setup and fish species (salt water species), it indicates that fish can adapt their body position by turning to their sides to pass through barriers with horizontal bars. At multiple monitoring campaigns, fish with  $h_f > s_b$  were caught with stow nets at the turbine outlets of HPPs with HBRs (e.g. Schmalz, 2010; Wagner *et al.*, 2019b; Mueller *et al.*, 2020b; details in Section 3.7.4), which indicates that fish do rotate themselves to pass through HBRs. However, it is hardly known if this behavior is



limited to certain fish species or life stages. Due to this knowledge gap, Ebel (2016) suggested to design  $s_b$  of physical barriers independent of the orientation of the bars. Thereby, the critical total fish length  $TL_{crit}$  is defined as the minimal total fish length, above which fish are physically blocked at barriers. It depends not only on  $w_{f,rel}$  and  $h_{f,rel}$  but also on  $s_b$  and can be calculated with Eq. (2.3). Table 2.2 lists  $w_{f,rel}$  and  $h_{f,rel}$  of selected fish species, which were derived from multiple monitoring campaigns, and the corresponding  $TL_{crit}$  for  $s_b = 10, 20$ , and  $30$  mm calculated with Eq. (2.3). Although the fish biometry can vary between rivers and individuals,  $w_f$  and  $h_f$  can be estimated from  $TL$  with  $w_{f,rel}$  and  $h_{f,rel}$ . At barriers with either horizontally or vertically aligned bars and fish with  $h_f \geq w_f$ , the ratio of  $s_b$  and  $w_f$  is known as the permeability index, that is,  $PI = s_b/w_f$  (Ebel, 2016). Racks are a physical barrier for fish if  $s_b < w_f$  or in other words if  $PI < 1$ .

$$TL_{crit} = s_b / \min\{w_{f,rel}, h_{f,rel}\} \quad (2.3)$$

**Table 2.2:** Relative fish width  $w_{f,rel}$  and height  $h_{f,rel}$  for different species and the corresponding  $TL_{crit}$  for  $s_b = 10, 20$ , and  $30$  mm

Fish species	$w_{f,rel}$ [–]	$h_{f,rel}$ [–]	$TL_{crit}$ [cm]		
			$s_b = 10$ mm	$s_b = 15$ mm	$s_b = 20$ mm
Spirlin	0.09 <sup>1</sup>	0.20 <sup>1</sup>	11.1	16.7	22.2
Barbel	0.11 <sup>2</sup>	0.17 <sup>2</sup>	9.1	13.6	18.2
Nase	0.11 <sup>2</sup>	0.24 <sup>2</sup>	9.1	13.6	18.2
Trout	0.10 <sup>2</sup>	0.19 <sup>2</sup>	10.0	15.0	20.0
Salmon	0.10 <sup>2</sup>	0.18 <sup>2</sup>	10.0	15.0	20.0
Chub	0.12 <sup>2</sup>	0.21 <sup>2</sup>	8.3	12.5	16.7
Eel	0.03 <sup>2,3</sup>	0.03 <sup>2,3</sup>	33.3	50.0	66.7

<sup>1</sup> Data from Wagner *et al.* (2019b)

<sup>2</sup> Data from Ebel (2016)

<sup>3</sup> Accounts for the body flexibility of eels

By measuring more than 200 000 individual from 30 fish species at the two fish passes at the Geesthacht weir on the Elbe River (53°25'35.2"N, 10°20'17.1"E), Schwevers and Adam (2019, 2020) found that  $w_{f,rel}$  and  $h_{f,rel}$  are no species-specific constants, but slightly increase with  $TL$ . They proposed Eq. (2.4)–Eq. (2.8) to calculate  $w_f$  and  $h_f$  for barbel, nase, trout, salmon, and chub, where  $TL$  has to be inserted in centimeters. For fish with  $TL \approx 15$  cm, Eq. (2.4)–Eq. (2.8) lead to similar  $w_f$  and  $h_f$  as Table 2.2, while Eq. (2.4)–Eq. (2.8) lead to smaller  $w_f$  and  $h_f$  for small fish and larger  $w_f$  and  $h_f$  for large fish.

$$w_f = 0.0727TL^{1.1237} [\text{cm}], h_f = 0.1103TL^{1.1313} [\text{cm}] \text{ for barbel} \quad (2.4)$$

$$w_f = 0.0506TL^{1.215} [\text{cm}], h_f = 0.099TL^{1.1964} [\text{cm}] \text{ for nase} \quad (2.5)$$

$$w_f = 0.0501TL^{1.2094} [\text{cm}], h_f = 0.121TL^{1.1378} [\text{cm}] \text{ for trout} \quad (2.6)$$

$$w_f = 0.0672TL^{1.0918} [\text{cm}], h_f = 0.1241TL^{1.077} [\text{cm}] \text{ for salmon} \quad (2.7)$$

$$w_f = 0.0547TL^{1.2429} [\text{cm}], h_f = 0.1109TL^{1.1914} [\text{cm}] \text{ for chub} \quad (2.8)$$

### Fish swimming performance

The fish swimming performance depends not only on the species and fish length, but also the water temperature, the concentration of dissolved oxygen, the level of exercise, and the motivation (Turnpenny *et al.*, 2006). Depending on the considered swimming duration  $t$ , Beamish (1979) introduced the fish swimming categories

- **burst speed**, which can be maintained for  $t \leq 20$  s,
- **prolonged speed**, which can be maintained for  $20 \text{ s} < t \leq 200$  min, and
- **sustained speed**, which can be maintained for  $t > 200$  min.

Much literature is available describing fish swimming performance, which is often based on experiments in enclosed swimming chambers (e.g. Beamish, 1979; Clough and Turnpenny, 2001; Clough *et al.*, 2004; Katopodis and Gervais, 2016). It does therefore not necessarily represent natural conditions, but it is widely applied for designing fishways and fish guidance structures. Ebel (2016) used the data of multiple studies to develop empirical equations to estimate the absolute fish swimming speed  $v_f$  [m/s] as a function of  $TL$  [m], duration  $t$  [s], and water temperature  $T$  [°C]. Ebel (2016) recommends Eq. (2.9) for rheophilic species, Eq. (2.10) for non-rheophilic species, and Eq. (2.11) for eels. If the decisive water temperature is unknown, Ebel (2016) suggests to use  $T = 5$  °C.

$$\log(v_f) = 0.5460 + 0.7937 \log(TL) - 0.0902 \log(t) + 0.2813 \log(T) \quad (2.9)$$

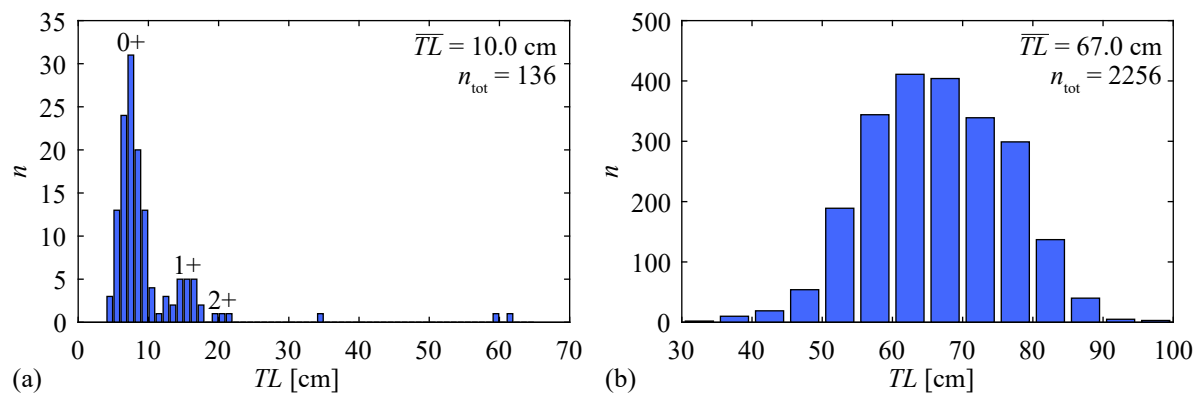
$$\log(v_f) = 0.3674 + 0.7692 \log(TL) - 0.0982 \log(t) + 0.3649 \log(T) \quad (2.10)$$

$$\log(v_f) = 0.4250 + 0.5670 \log(TL) - 0.1330 \log(t) \quad \text{for } T > 10 \text{ °C} \quad (2.11)$$

### Fish size distributions

Fish have a large reproduction rate, which means that most individuals in river systems are typically juveniles. Although the number of large adults is comparably small, they are very important from a population biology perspective and should therefore have a high protection level. There are only few studies quantifying the fish size distribution for different species. However, by conducting quantitative electrofishing campaigns within the “NAWA” and “Progetto fiume” projects, a database containing the fish size distribution of many Swiss rivers is available (details in Spalinger *et al.*, 2017). The fish size or generally the fish size distributions of the relevant species are very important to design physical barriers (cf. Table 2.2). Eichenberger and Kirchhofer (2013) carried out an extensive monitoring campaign to investigate the barbel

population in the Limmat River. Figure 2.5a shows the size distribution of  $n_{\text{tot}} = 136$  individual barbels collected by electrofishing close to the banks in autumn 2011 and additional catches from the fish pass at HPP Aue (47°28'13.4"N, 8°18'39.1"E). Since large barbels were not showing up frequently close to the banks, they might be underrepresented in Fig. 2.5a (Eichenberger and Kirchhofer, 2013). The majority of barbels was younger than one year (0+), but several barbels older than one year (1+) and older than two years (2+) were also observed. The minority of barbels was older than 2 years and accordingly longer than  $TL = 20$  cm (Fig. 2.5a). In a comparable monitoring campaign in 2012 with  $n_{\text{tot}} = 319$  individuals, the 0+ barbels were even smaller, which was caused by the colder spring leading to a later spawning. Although monitoring campaigns are likely to be size-selective, many field studies showed that the vast majority of fish is small with  $TL < 20$  cm (e.g. Schmalz, 2010; Zaugg and Mendez, 2018; Wagner *et al.*, 2019b). In contrast to riverine species like barbel which may move within rivers in all life stages, European eels are typically  $TL = 30$ –90 cm long during downstream migration (Table 2.1). Figure 2.5b shows a typical size distribution of downstream migrating eels, which were caught with stow nets in the season 2008/09 downstream of HPP Drakenburg (52°41'17.6"N, 9°12'37.9"E) on the Weser River, Germany.



**Fig. 2.5:** Size distribution of (a) barbels in Limmat River in 2011 (data from Eichenberger and Kirchhofer, 2013) and (b) eels caught downstream of HPP Drakenburg in the season 2008/09 (data from Schwevers *et al.*, 2011)

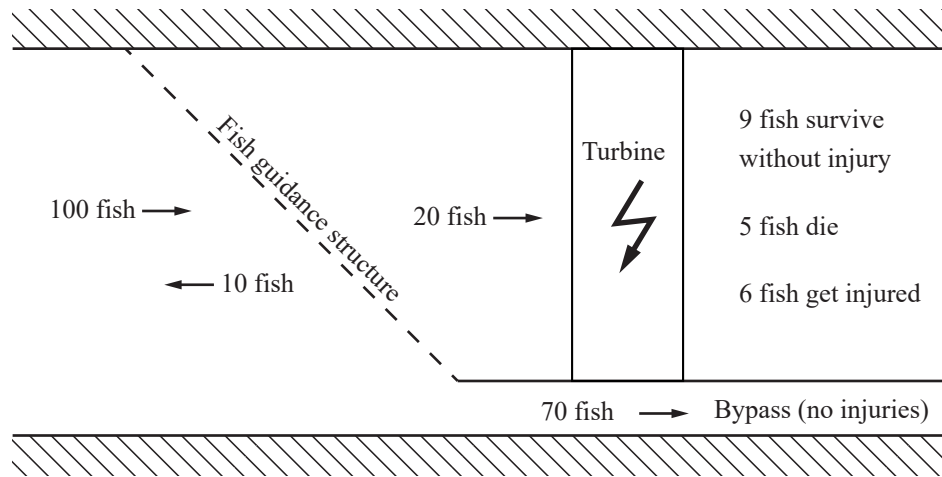
## 2.3 Fish injuries and survival rates

The negative impact of HPPs and other water intakes on downstream moving fish ranges from slight injuries all the way to mortality. Mortality is distinguished into two categories, direct and indirect/delayed mortality. Direct mortality are lethal injuries, which can result from HPP passage (e.g. through racks, turbines, spillways, or bypasses) and lead to death during passage (Nieland *et al.*, 2015). In contrast, indirect mortality can be caused for example by increased predation due to disorientation, increased energy expenditure, or an increased vulnerability to diseases (Čada, 2001). Only few studies consider indirect mortality as it is very difficult to quantify, but an extensive monitoring campaign at HPP Unkelmühle (50°46'03.8"N, 7°30'01.7"E) on the Sieg River revealed that it can be as large as 25% for salmon smolts (details in Section 3.7.4). As mentioned in Section 2.1, no quantitative survival rates are required by law in Europe. Ideally, survival rates should be determined based on population-biological reasoning. This ap-

proach is very challenging in practice, as fish populations are not only affected by HPPs, but many other factors like water quality and habitat availability. Population-biological reasoning is especially difficult for riverine species showing frequent irregular movements (nomadism), as little is known about the movement patterns of most species, which makes it difficult to assess the cumulative effect of multiple HPPs. Additional reasons why no quantitative survival rates are required by law in Europe are that sufficient protection rates can be site-specific (e.g. local fish species and populations) and hard to verify. As a reference, regional goals in the USA comprise that at least 80% of all juveniles should migrate through non-turbine routes and that the overall juvenile survival rate should exceed 95% per HPP (Ferguson *et al.*, 1998). Lucas and Baras (2001) recommended survival rates of 90–100% per HPP for diadromous species and potamodromous migratory species, while the authors stated that lower survival rates are likely acceptable for eurytopic species without specialized habitat requirements. Yet a part of freshwater species are neither classified as potamodromous nor as eurytopic (i.e. generalist regarding ecological requirements) and no survival rate recommendations are given for this large group of species. Dumont *et al.* (2005) proposed to require a minimal survival rate of 75% per river basin for all migratory life stages of diadromous species. In rivers of high ecological importance like the Unstrut and Saale River in Germany, new HPPs typically get only approved if the survival rate exceeds 99% (Ebel *et al.*, 2018). The Federal Columbia River Power System, which comprises multiple hydroelectric projects in the Columbia River Basin, is obligated to ensure survival rates of  $\geq 96\%$  for spring migrants and 93% for summer migrants at each HPP (NOAA Fisheries, 2008).

In literature, terms like survival rate, mortality rate, or protection rate are not always defined identically. For this reason, commonly used terms are defined on the basis of a simple calculation example illustrated in Fig. 2.6. A diversion HPP with negligible spillway mortality is equipped with a fish guidance structure, which is approached by 100 downstream moving fish. A total of 70 individuals is successfully guided downstream through the bypass without injuries. Ten fish are blocked by the rack, but they do not find the bypass and stay on the long term upstream of the rack. The other 20 fish manage to pass the rack. Thereof, nine survive turbine passage without injury, five fish die, and six fish get injured. The fish guidance efficiency (FGE) is defined as the percentage of fish which were successfully guided along the rack, entered the bypass, and subsequently moved downstream ( $FGE = 70/100 = 70\%$ ). The fish protection efficiency (FPE) is the percentage of fish not passing the rack  $FPE = ((100 - 20)/100 = 80\%)$ . The turbine survival rate  $SR_t$  is the ratio of all fish surviving turbine passage (injured or without injury) over the total number of fish entering the turbines ( $SR_t = (9 + 6)/20 = 75\%$ ). The turbine mortality rate is the reverse of the turbine survival rate, thus all fish dying by turbine passage over all fish entering the turbines ( $5/20 = 25\%$ ). The total survival rate  $SR_{tot}$  is defined as the ratio of all downstream moving fish which did not die by trying to pass the HPP ( $SR_{tot} = (100 - 5)/100 = 95\%$ ). The reverse, the overall mortality rate, is determined by all fish which died by trying to pass the HPP over the total amount of approaching fish ( $5/100 = 5\%$ ). If other corridors like fish passes or spillways are present, they have to be taken into account

accordingly with their survival rates. To enhance comparability, mortality rates from literature were converted to survival rates in the following. If not explicitly mentioned, indirect mortality is not considered in the given numbers. At HPPs and other water intakes, it can be very challenging to determine FGE and FPE as it is difficult to distinguish between fish which were willing to move downstream and were blocked by the fish guidance structure and fish which used the headwater as a habitat. Depending on the fish species and site, FGE or FPE can be more meaningful, which has to be decided based on population-biological principles.

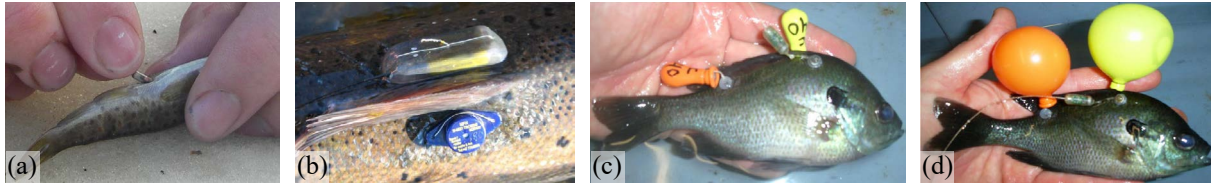


**Fig. 2.6:** Example of fish at a diversion HPP which is used to define survival and mortality rates

### 2.3.1 Monitoring techniques and ethohydraulics

Different monitoring techniques are used to study fish behavior at HPPs and to determine FGE, FPE,  $SR_t$ , and  $SR_{tot}$ . It can be distinguished between monitoring techniques where fish are marked, and monitoring techniques where natural moving fish are studied. The main disadvantages of the latter are that preexisting injuries can hardly be determined and it is difficult to quantify which fish did not pass the HPP. The most common techniques include fish tagging, stow nets, and visual fish observations. Fish tags can be implanted (Fig. 2.7a) or attached outside of free-swimming fish (Fig. 2.7b–d) and can wirelessly record the fish position and movements by using a mobile receiver or stationary loggers (Thorstad *et al.*, 2013). Passive integrative transponder tags (PIT-tags, Fig. 2.7a) do not emit any signal, but they can be detected at antennas, which are typically installed at up- or downstream passage corridors. The advantages of PIT-tags are their small size, allowing for tagging fish with  $TL > 5$  cm, the large number of unique codes, and the long lifetime (Thorstad *et al.*, 2013). Vollset *et al.* (2020) found that the mortality risk of PIT-tagged salmonids increases with the ratio of the tag size to the total fish length  $TL$  and suggested to limit the tag size to 17.5% of  $TL$ . This means that a 12 mm PIT-tag can be used for fish with  $TL > 6.9$  cm. As PIT-tags have no batteries, they can record fish movements over multiple years, but they do not work reliably if multiple tagged fish are in the range of one antenna (Wagner *et al.*, 2019b), the detection distance is limited to  $<1$  m, and no information about the fish movements between antennas can be determined (Thorstad *et al.*, 2013). In contrast, continuous information about fish positions can be retrieved from active electronic tags such as radio (Fig. 2.7b) and acoustic transmitters, data storage tags, and

pop-up satellite archival tags (Thorstad *et al.*, 2013). Depending on the battery size, the lifespan of active transmitters varies between a few weeks and several years (Thorstad *et al.*, 2013). To quantify injury rates at spillways or turbines, fish have to be retrieved after passage which can be achieved with balloon tags (Fig. 2.7c,d). They are attached to the side of fish and inflate themselves after passage, such that fish can be collected at the water surface (Fig. 2.7d).



**Fig. 2.7:** Different monitoring techniques: (a) implantation of a PIT-tag, (b) a radio transmitter and a data storage tag (Thorstad *et al.*, 2013), and two inflatable balloon tags (c) prior and (d) after turbine passage (Normandeau Associates, 2009)

As an alternative to balloon tags, turbine outlets can be monitored with fish-catching units such as stow nets, fyke nets, or fish-catching boxes (Pander *et al.*, 2018). Most fish-catching units are size-selective, which should be considered with mark and recapture experiments (Ebel *et al.*, 2015). When using these fish-catching units, catch-related injuries have to be taken into account which depend on the species, the exposure time in the fish-catching unit, the flow velocity, and the fish and debris biomass (Pander *et al.*, 2018). To reduce catch-related injuries, emptying periods should be as short as possible ( $<0.5\text{--}2\text{ h}$ ; Pander *et al.*, 2018; Zaugg and Mendez, 2018; Mueller *et al.*, 2020b). Stow nets are susceptible to clogging by debris, but they can be applied for discharges up to  $100\text{ m}^3/\text{s}$  (Ebel, 2016). Alternatively, sonars and cameras are used to monitor fish movements along racks and bypasses. Camera-based systems can be a low-cost alternative which allow for proper species identification, but their application is limited to daytime, water with low turbidity, and the observation of fish with  $TL > 15\text{ cm}$  (Egg *et al.*, 2018a). In contrast, sonar-based systems can detect fish during night and in turbid water. The main disadvantages are that species identification is very limited and it is difficult to detect small fish with  $TL < 10\text{ cm}$ , resulting in a clear underestimation of the percentage of small individuals passing the rack, if no stow net is integrated in the monitoring approach (Egg *et al.*, 2018a). Therefore, stow nets are the only reliable technique to monitor the susceptibility of small fish to pass through HBRs. When planning monitoring campaigns, it should be considered that the vast majority of downstream moving fish is very small, such as in the example of Fig. 2.5a. With most monitoring techniques, it is difficult to separate direct from indirect mortality, because the latter can occur strongly delayed or happen outside of the project perimeter. Fish are often kept in holding tanks for 72–96 h after passage to account for delayed mortality (e.g. Mueller *et al.*, 2020b), but it may occur also much later, for example in estuaries or oceans in case of diadromous species (Nieland *et al.*, 2015). To compare fish injuries from different sites, Mueller *et al.* (2017) developed a standard method for evaluating lethal and nonlethal injury patterns due to turbine passage by considering vitality and general health criteria, as well as injury types across 18 body parts.

As monitoring campaigns are demanding, costly, and time-consuming, the fish behavior at hydraulic engineering structures was studied in a recently increased number of live fish tests in laboratories. This field of science, where behavioral biology is combined with the engineering field of hydraulics, is referred to as “ethohydraulics” in the following. It originates from the Greek words “ethos”, “hydro”, and “aulus”, which stand for character, water, and pipe, respectively (Adam and Lehmann, 2011). Selected ethohydraulic studies, that is, laboratory tests involving live fish, are summarized in Section 3.7.3. Ethohydraulics is considered a part of the discipline ecohydraulics, which is “the synthesis of ecology and hydraulics, and as a discipline exists at the interface of the two” (Kemp and Katopodis, 2016).

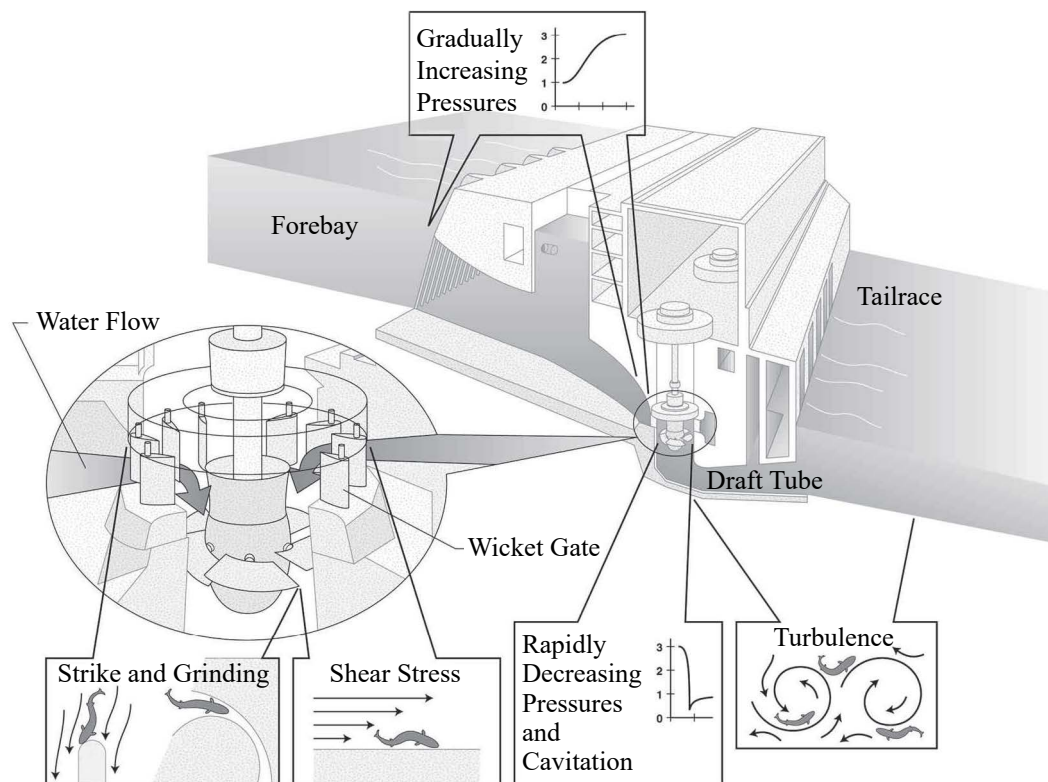
### 2.3.2 Turbine mortality and survival rates

Only shortly after the realization of the first run-of-river HPPs at the end of the 19<sup>th</sup> century, fish injuries from turbines were reported (Gerhard, 1893), and as a consequence, early experiments with live fish were conducted to estimate  $SR_t$ . For instance, Schmassmann (1928) flushed fish of different species with a pipe directly through the turbines of the Swiss HPP Augst on the Rhine River (47°32'12.0"N, 07°42'33.9"E) and monitored the 5 m deep and 8.5 m wide turbine outlet with a stow net with a mesh size of 3 cm. Half of the barbels were so small that they could pass the stow net, while the barbels and nase recovered with the stow net had  $TL \approx 25\text{--}50$  cm (Schmassmann, 1928). From the experiments with barbels, common nase, common chub, trout, common rudd, and common bream, Schmassmann (1928) concluded that the majority of the fish do not incur any injuries during turbine passage. Although he did not conduct experiments with eels, he mentioned that they are an exception and have a higher injury risk than other species. Von Raben (1957) installed a stow net at the turbine outlet of HPP Obernau on the Main River (49°55'58.0"N, 9°07'40.3"E) and caught 250 eels within twelve days, whereof 16.4% were injured and 3.2% disintegrated. From these results and theoretical derivations of the collision probability between eels and turbine blades, von Raben (1957) proposed equations to estimate the injury risk of eels for Kaplan- and Francis turbines. The governing parameters are  $TL$ , and HPP and turbine specific parameters like the angle of the turbine blades to the flow, the number of turbine blades, the rotational speed of the turbine, the discharge, and the outer diameter of Kaplan turbine blades. Qualitatively,  $SR_t$  increases for small fish, small angles between the flow and the turbine blades as they reduce the probability of collision, for a low number of turbine blades, a low rotational speed of the turbine, and for large discharges. One of the findings of von Raben (1957) was that fish have a lower survival rate at Francis turbines compared to Kaplan turbines, which is subjected to the higher number of turbine blades. The main causes of fish injuries during turbine passage are

- **strike** (collision with structures like turbine blades, stay vanes, wicket gates, and draft tube piers) and **grinding** (pinching in gaps between turbine blades and power channel),
- **shear stresses** resulting from regions with different flow velocities,
- **rapid pressure changes and cavitation**,



- and **turbulences** (Fig. 2.8, Čada, 2001; Pracheil *et al.*, 2016).



**Fig. 2.8:** Injury risks during turbine passage at run-of-river HPPs (adapted from Čada, 2001)

To which extent these different injury mechanisms contribute to the total injury rate can be very site- and species-specific (Turnpenny *et al.*, 2000). As an example, pressure and shear can be the main injury cause for small fish, while blade strike is typically dominant for larger fish (Turnpenny, 1998). By combining computational fluid dynamics, biological dose-response relationships, and field test, Turnpenny *et al.* (2000) quantified the contribution of different injury mechanisms. They concluded that if a salmon smolt/parr passes through a small low-head HPP turbine, shear stress accounts for <2% of the injuries, pressure changes account for up to 6.3% of the injuries, and runner-strike-related injuries were 3–4 times larger than hydraulic effects (shear stress, pressure changes). Table 2.3 summarizes the potentially fatal injury rates of a salmon parr with  $TL = 8.2$  cm passing through a very small Kaplan turbine with four turbine blades, a hydraulic head of 7 m, and a rotational speed of 700 rotations per minutes (Turnpenny *et al.*, 2000). The majority of injuries was caused by blade strikes at the runner at this specific, fast-rotating turbine (Table 2.3).



**Table 2.3:** Potentially fatal injury rates at different positions in the turbine of a salmon parr with  $TL = 8.2$  cm, passing through a very small Kaplan turbine (adapted from Turnpenny *et al.*, 2000)

Position in turbine	Percentage of potentially fatal injuries due to			
	Strike	Shear	Pressure	Compound
Intake	0.00	0.00	0.00	0.00
Guide vanes	0.00	0.00	0.00	0.00
Runner	25.10	1.44	1.72	28.26
Draft tube	0.00	0.33	1.41	1.73
Compound	25.10	1.76	3.10	30.00

Within the last decades, a number of studies was conducted using empirical and theoretical approaches to estimate  $SR_t$  (e.g. Bell *et al.*, 1972; Montén, 1985; Larinier and Dartiguelongue, 1989; Turnpenny *et al.*, 2000; Gomes and Larinier, 2008), of which the vast majority focused on juvenile salmonids in the United States (Algera *et al.*, 2020). Ebel (2008) took the results of 40 different studies involving 16 HPPs and proposed the following equation to estimate the site-specific averaged turbine survival rate for eels.

$$SR_t = 144.6 + 13.6s_{\text{abs,max}} - 2.7u_{\text{max}} - 109TL \text{ [%]}, \quad (2.12)$$

where  $s_{\text{abs,max}}$  = blade spacing at the maximal runner diameter [m],  $u_{\text{max}}$  = maximal tangential velocity of the runner [m/s], and  $TL$  = total fish length [m]. One of the most widely used approaches to estimate the species-unspecific  $SR_t$  is Eq. (2.13), which was proposed by Montén (1985) and is based on the theoretical blade strike probability. The equation was validated in field campaigns and can also be applied for partial load as the relative blade spacing at the middle of the runner  $s_{\text{rel,mid}}$  [m] depends on the discharge (details in Montén, 1985 and Ebel, 2016).

$$SR_t = 100 - 50 \frac{TL}{s_{\text{rel,mid}}} \text{ [%]} \quad (2.13)$$

Turbine survival rates are very site-specific and strongly depend on  $TL$ , such that they can hardly be generalized. Whitney *et al.* (1997) summarized multiple studies conducted at large HPPs on the Columbia River and found that turbine survival rates of juvenile salmon and steelhead are in the range of 83.1–97.7%. The survival rate of eels is generally lower as their length increases the blade strike risk. The survival rate of downstream migrating eels was quantified in a major monitoring campaign at HPPs Landesbergen (52°34'37.6"N, 9°06'36.3"E) and Drakenburg on the Weser River, which are both equipped with Kaplan turbines. In total, 4600 downstream migrating silver eels with an average  $TL = 65$  cm were caught, of which 85–86% survived turbine passage and 28–30% were injured (Schwevers *et al.*, 2011). Ebel (2008) compared different studies in which  $SR_t$  of eels was quantified and found that it can vary from 0–100%. Up to now, a comprehensive review of  $SR_t$  of riverine species involving a large number of

studies is missing (Ebel, 2016). The large variations of  $SR_t$  are caused by various factors, which are qualitatively described below following Füllner (1997).

### **Turbine type**

Typical run-of-river HPPs are equipped with Kaplan or Francis turbines. The  $SR_t$  at Kaplan turbines is typically larger than at Francis turbines, which most authors attribute to different applications in terms of discharge and hydraulic head (Montén, 1985; Larinier and Dartiguelongue, 1989; Ebel, 2016). Nevertheless, strike probability and pressure changes can vary significantly between turbine types (Boys *et al.*, 2018), such that their application can lead to different  $SR_t$ . Recently developed turbines try to reduce gaps, abrupt pressure changes, and the blade strike probability and are therefore called “environmentally enhanced turbines”, which are described in Section 2.4.6.

### **Efficiency factor and turbine admission**

The efficiency factor can be characterized as a function of the turbine admission and typically peaks between 60–95% of the maximal discharge for Kaplan and Francis turbines (Giesecke *et al.*, 2014). The highest efficiencies are achieved with reduced turbulences and wide blade openings for Kaplan turbines, such that  $SR_t$  is assumed to be high if turbines are operated with maximal efficiency. At low discharges, Kaplan turbines are typically operated in partial mode, where the rotational speed remains constant but the aperture angle is reduced, which decreases  $SR_t$  (Schwevers *et al.*, 2011). Schwevers *et al.* (2011) tried to quantify this effect for downstream migrating eels, but found only a weak correlation between different aperture angles and  $SR_t$ . By analyzing the data of multiple studies at the Snake and Columbia River including salmonids and nonsalmonids, Skalski *et al.* (2002) found a slightly positive correlation between turbine efficiency and  $SR_t$ . However, the maximal  $SR_t$  did not exactly coincide with the peak turbine efficiency, such that Skalski *et al.* (2002) recommended to operate turbines to maximize  $SR_t$ , instead of focusing on the operating efficiency only.

### **Rotational speed of the turbine**

An increased rotational speed of turbines increases the chance of collision and therefore decreases  $SR_t$  (e.g. Montén, 1985; Ebel, 2016).

### **Number of blades and gaps**

A small number of turbine blades decreases the blade strike risk and therefore leads to higher  $SR_t$ , which is one of the reasons why many modern Kaplan turbines are built with only 3–4 blades. Due to fabrication and installation tolerances, it is not possible to seamlessly fit a turbine into a housing. The resulting gap, which typically ranges between 1–3 mm for Kaplan turbines (Giesecke *et al.*, 2014), should be minimized, because fish can get pinched and injured (grinding in Fig. 2.8; Čada, 2001).

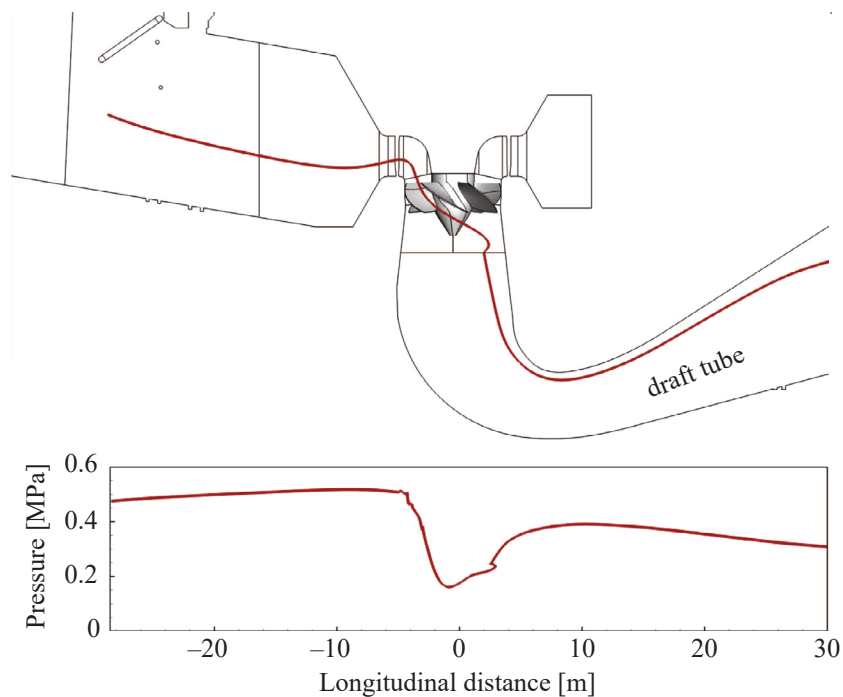
### **Flow velocity**

Flow velocities do not directly affect  $SR_t$  for salmonids, but they may lead to different rotation speeds of the turbines (Füllner, 1997). On the one hand, larger flow velocities may lead to

higher impact velocities with turbine blades, which increases the risk of lethal injuries for eels (Montén, 1985). On the other hand, larger flow velocities may reduce the blade strike risk, if the rotation speed is constant and fish are assumed to swim downstream passively with the flow.

### Pressure difference during turbine passage

Fish can be severely injured due to rapid pressure changes when passing through turbines (Čada, 2001), which is also referred to as barotrauma. Fish injuries due to the rapid decompression arise from two different pathways, which are governed by the Boyle's and Henry's law (Brown *et al.*, 2014). The Boyle's law implies that "the volume of a gas is inversely proportional to the pressure acting on the volume" (Brown *et al.*, 2014), which means that a pressure reduction by 50% doubles the volume of the preexisting gas in the body of a fish. Henry's law states that gas may come out of solution when the surrounding pressure is reduced, which results in gas bubble formation (Brown *et al.*, 2014). To estimate the effect of barotrauma, it is insufficient to simply consider the head difference upstream and downstream of the turbines. Figure 2.9 illustrates the pressure difference along a streamline within a typical large Kaplan turbine, which was obtained from a numerical simulation. At existing turbines, the pressure profiles can also be measured with sensors. In Fig. 2.9, the local pressure reaches its minimum of  $\approx 0.16$  MPa right before the turbine axis due to flow acceleration in the draft tube. Not only the minimal and maximal pressure, but also the temporal pressure gradient affects  $SR_t$ , which can be described as the decompression rate (Boys *et al.*, 2018). The injury risk due the pressure differences is also species-specific, as for example salmon are known to be more robust regarding pressure fluctuations than other species (Turnpenny, 1998).



**Fig. 2.9:** Pressure profile along a streamline within a typical Kaplan turbine (adapted from Richmond *et al.*, 2014)

## Total fish length

Longer fish are more prone to blade strike than smaller fish, which is why  $SR_t$  decreases for larger  $TL$  (e.g. von Raben, 1957; Montén, 1985; Larinier and Dartiguelongue, 1989). In view of physical barriers like HBRs, this is beneficial to maximize  $SR_{tot}$ , as large fish are protected by the physical barrier and small fish have a high  $SR_t$ .

### 2.3.3 Spillway survival rates

The survival rates at spillway passage strongly varies with the hydraulic head of the HPP and the spillway design. Depending on  $SR_t$ , spillways are often considered the safest downstream passage corridor at low head HPPs without fish downstream passage facilities (Whitney *et al.*, 1997). Nevertheless, spillway passage can lead to severe injuries due to

- **impact** on the downstream water surface or the bottom in case of shallow water,
- **collision** with obstacles like baffles or sediments in case of gate flow,
- **shear forces**,
- changes in the **total dissolved gas saturation**, and
- **pressure differences** (adapted from Ebel, 2016).

The spillway survival rate of juvenile salmon and steelhead ranges between 93% and 100% with an average of 98.5%, which is based on multiple studies at HPPs in the Columbia and Snake River with hydraulic heads of  $H < 30$  m (Whitney *et al.*, 1997). The spillway survival rates may be smaller if local conditions, like recirculation zones, favor predation (Whitney *et al.*, 1997). Schoeneman *et al.* (1961) found that salmon smolts passing over the spillway of the McNary Dam (45°56'03.4"N, 119°17'51.1"W) have a survival rate of 98%, which is significantly higher than  $SR_t = 89\%$ . Heisey *et al.* (2008) modified spillways by the installation of a flow deflector, which diverts the flow towards the surface of the tailwater and thereby reduces the total dissolved gas saturation, which can cause gas-bubble disease and mortality. After a four year evaluation period, Heisey *et al.* (2008) concluded that the installation of flow deflectors can increase spillway survival rates. Using live fish and sensor data of the Ice Harbor Dam (46°14'53.5"N, 118°52'46.2"W) on the Snake River, Duncan *et al.* (2018) showed that an adaptation of the spillway slope and deflector radius decreased severe acceleration events and collision with structures from 51% to 35% and from 47% to 27%, respectively. Watene and Boubée (2005) studied the downstream passage of eels over the 82 m high Patea Dam in New Zealand (39°32'48.2"S, 174°34'07.1"E), where most eels survived spillway passage with relatively little injuries. These studies indicate that spillways are not in all cases safe downstream passage corridors, but, if designed appropriately, survival rates are high.

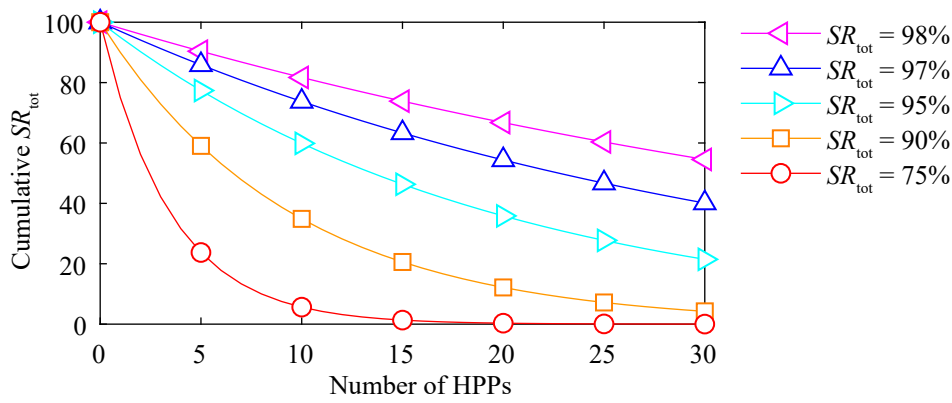
### 2.3.4 Indirect mortality

“Indirect mortality occurs through several mechanisms, such as increased predation risk in modified habitats, increased health risk due to sublethal injuries, and the additive effects of stress

and injury associated with passing one or more dams” (Nieland *et al.*, 2015). It also results from increased energy expenditure (e.g. due to searching for appropriate passage corridors or a reduced downstream swimming speed). An example for the modification of habitats are river impoundments, which likely reduce downstream swimming speeds and increase the population of piscivorous fish species such as pikes (Økland *et al.*, 2016). Sublethal injuries from turbine passage can increase the health risk of fish, as they are then more vulnerable to diseases and parasites. If HPPs delay fish migration significantly, fish may not reach their spawning habitats on time, which impedes reproduction. The indirect mortality is very hard to quantify and highly site-specific. Ferguson *et al.* (2006) used radio- and PIT-tags to quantify the survival of juvenile salmon over a long river reach of the Columbia River, while the direct turbine mortality was estimated with balloon tags. Ferguson *et al.* (2006) estimated that the delayed mortality adds up to 46–70% of the total mortality. At HPP Unkelmühle,  $SR_t$  was reduced to 0% with the installation of a physical barrier with  $s_b = 10$  mm, while the indirect mortality of salmon smolts in the impoundment was  $\approx 10\%$ , which most likely resulted from a denser predator population (Økland *et al.*, 2016; details in Section 3.7.4). In contrast, indirect mortality of downstream migrating salmon smolts in the Diemel River was not larger in the impoundment than in the free-flowing control stretch (Havn *et al.*, 2017).

### 2.3.5 Total and cumulative survival rates

The total survival rate  $SR_{\text{tot}}$  can be calculated from the survival rates and frequency of use of all downstream passage corridors. If these data are not available, they have to be estimated using appropriate assumptions. These estimations are feasible for diadromous and potamodromous species, while they are very challenging for riverine species showing nomadism, as little is known about the movement frequency and the covered distances. It has to be also considered that  $SR_{\text{tot}}$  may vary significantly between years. As an example, spillway mortality can play a minor role in low-flow years, while the prolonged exposure to lethal concentrations of dissolved gas can be the main cause for juvenile fish mortality in high flow years (Raymond, 1979). Especially for diadromous species like eel and salmon, it is important to not only consider  $SR_{\text{tot}}$  at one individual HPP, but to estimate the cumulative survival rate of HPP chains. Assuming equal  $SR_{\text{tot}}$  at each HPP, the cumulative survival rate can be calculated with  $SR_{\text{tot}}^n$ , where  $SR_{\text{tot}}$  is dimensionless and  $n$  corresponds to the number of HPPs. Figure 2.10 illustrates the cumulative survival rates as a function of the number of hydropower plants for different  $SR_{\text{tot}}$ . Eels which migrate from Lake Zurich to the North Sea have to overcome  $\approx 30$  HPPs. Assuming that HPPs are the only cause of anthropogenic mortality,  $SR_{\text{tot}}$  would need to exceed 97% per HPP to reach the target of the European regulation on eels, which requires a cumulative  $SR_{\text{tot}}$  above 40% (Fig. 2.10; cf. Section 2.1). A more detailed analysis requires to consider natural and indirect mortality in the river reaches between HPPs.



**Fig. 2.10:** Cumulative  $SR_{tot}$  as a function of the number of HPPs for different  $SR_{tot}$  at each individual HPP

Norrgård *et al.* (2013) investigated the migration behavior of salmon smolts with acoustic transmitters along a 180 km long reach of Klarälven River, Sweden, including 8 HPPs without fish downstream passage facilities and free flowing river reaches. The signal of 76% of the downstream migrating fish got lost in impounded river reaches and directly at HPPs, whereas this was the case for only 8% in the free-flowing river reaches. Only 16% of the smolts reached the downstream end of the project perimeter and therefore survived passage through all HPPs. As the river discharge hardly exceeded the design discharge during the study period, most salmon must have migrated through the turbines. A cumulative  $SR_{tot} = 100\% - 76\% = 24\%$  at eight HPPs corresponds to an average  $SR_{tot} \approx 84\%$  at each HPP (Fig. 2.10), which is similar to  $SR_t$  discussed in Section 2.3.2. A comparable study was conducted by Nyqvist *et al.* (2017a), in which downstream migrating salmon smolts were monitored at a chain of three HPPs on Winooski River, USA, which were all equipped with rack bypass systems with  $s_b = 25$  mm. Despite high discharges during the study period, only 10% of the tagged smolts reached the downstream lake. The low migration rate was attributed to the poor design of the fish downstream passage facilities (Nyqvist *et al.*, 2017a).

## 2.4 Protection measures for downstream moving fish

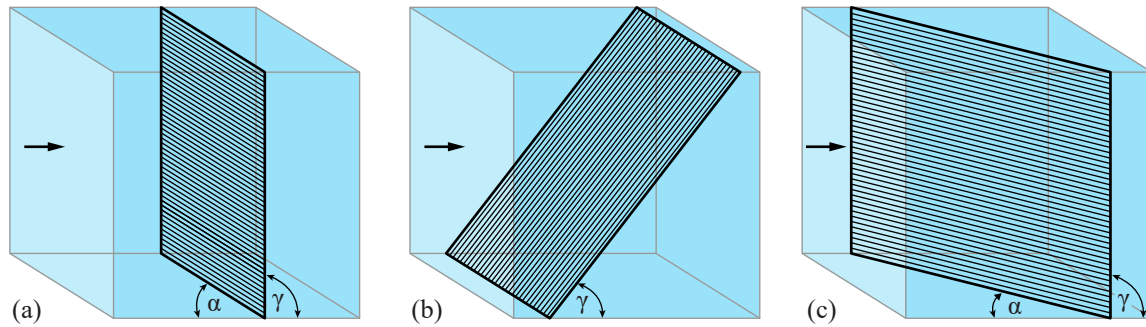
Table 2.4 summarizes existing fish protection measures, following common classification in literature (Larinier and Travade, 2002; DWA, 2004; Turnpenny and O’Keeffe, 2005; USBR, 2006; Ebel, 2016). Their advantages and disadvantages are briefly discussed in the following. Fish protection often focuses on run-of-river HPPs, although the same concepts can be applied to all water intakes, which includes cooling systems of thermal power plants or water extraction for industrial use (e.g. drinking water or irrigation). Table 2.4 is limited to measures which are specifically built or implemented to protect and bypass downstream moving fish. It does not include other potential downstream passage corridors such as fish passes originally built for upstream passage (cf. Section 2.2.2).

**Table 2.4:** Overview of protection measures for downstream moving fish at water intakes (adapted from Kriewitz, 2015)

	Concept	Measure	Examples	
Fish protection measures at water intakes	Protection and bypassing	Physical barriers	Fine screens (e.g. HBRs) Coanda screens Barrier nets Rotating screens (e.g. drum screens) Eicher screens Perforated plate screens	Bypass system
			Guidance structures (Louvers, bar racks) Trash racks Guidance walls (bottom or top)	
		Sensory behavioral barriers	Lights (strobe, mercury-vapor) Low-frequency sounds Air bubble or water-jet curtains Electric screens	
	HPP passage	Collection systems	Collecting channels Trap and truck Submerged traveling screens Fish elevators	
		Environmentally enhanced turbines	Alden turbine Minimum Gap Runner Very Low Head Turbine (VLH) Archimedes screw turbine	
		Fish-friendly HPP operation	Early warning systems Temporary spillway opening No partial load operation	

Most barriers can be either installed over the whole flow depth or only partially submerged. The latter may be favorable for fish which are known to swim close to the water surface such as salmon smolts (Thorstad *et al.*, 2012; Ebel, 2016), whereas they seem to be unsuitable for the protection of a wide variety of riverine species and life stages, like demanded in Switzerland. However, even smolts tend to swim towards the bottom on sensing danger (Turnpenny and O’Keeffe, 2005), which limits the application of partially submerged protection systems. Depending on various factors such as the bar orientation and the clear bar spacing, fish guidance racks can act as physical or mechanical behavioral barriers. Fish guidance racks are rarely installed frontal, non-oblique to the main flow (Fig. 2.11a), due to the high fish impingement risk and the missing guidance effect towards the bypass or collection system. The bars can be arranged horizontally or vertically, where the horizontal approach flow angle  $\alpha$  and the vertical

angle  $\gamma$  can be varied as illustrated in Fig. 2.11b,c. Racks with  $\gamma < 90^\circ$  are typically referred to as inclined racks (Fig. 2.11b), whereas they are called angled racks for  $\alpha < 90^\circ$  (Fig. 2.11c). Most run-of-river HPPs are equipped with traditional trash racks, which were designed to prevent floating debris from entering turbines and for personnel safety. Due to their low inclination of typically  $\gamma = 65\text{--}85^\circ$  and their large  $s_b = 50\text{--}150\text{ mm}$  (Meusburger, 2002), these racks are unsuitable for fish protection.

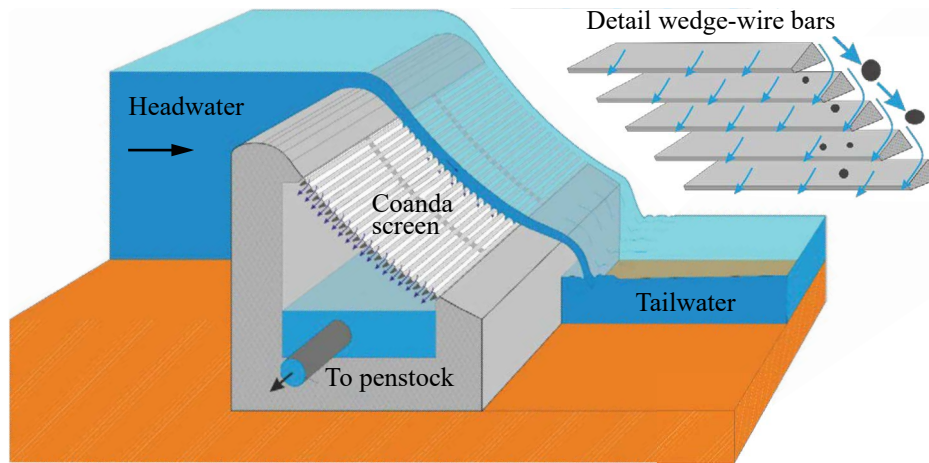


**Fig. 2.11:** Rack layouts: (a) frontal, non-oblique (b) inclined, and (c) angled to the approach flow (adapted from Kriewitz, 2015)

### 2.4.1 Physical barriers

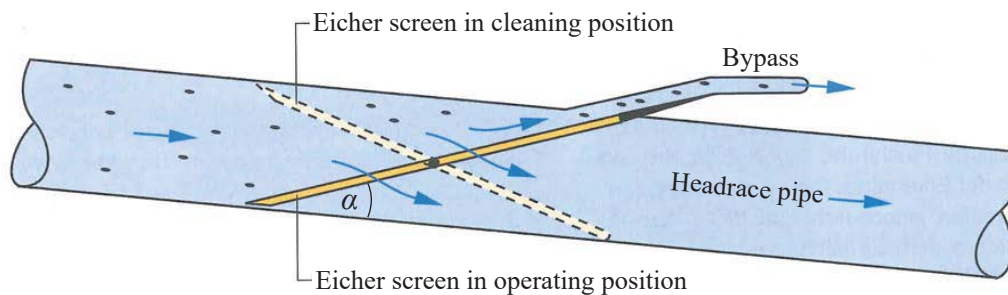
Physical barriers are characterized by small  $s_b$  or narrow openings and are therefore impermeable to many fish. The small  $s_b$  may limit the intake capacity or causes operational challenges at large HPPs, such that most physical barriers are installed primarily at small to medium-sized HPPs. Horizontal bar racks, as studied in the present thesis, are one of the most widely used physical barriers in German-speaking countries (Ebel, 2016), while inclined fine-spaced racks with vertical bars are frequently used for fish protection in France (Raynal *et al.*, 2013b). Physical barriers such as Coanda screens, drum screens, inclined, or angled racks are often made of wedge-wire bars (Fig. 2.12), which are wedge-shaped and are characterized by small dimensions. Depending on the fish species and sizes which should be protected, the clear bar spacing is in the range of  $s_b = 1\text{--}10\text{ mm}$  (DWA, 2004). For Coanda screens, wedge-wire bars with  $s_b = 0.2\text{--}3\text{ mm}$  are aligned to create a concave rack surface (Fig. 2.12; Lifa *et al.*, 2017). Coanda screens physically block even very small fish, thus suggesting that if designed appropriately they are generally fish-friendly. As an example, the tailwater depth should not be smaller than 0.90 m to avoid fish injuries from the impact to the downstream (Odeh and Orvis, 1998; DWA, 2004). Recent live fish tests of the University of Applied Sciences of the Grisons (FHGR) in collaboration with the Laboratory of Hydraulics, Hydrology and Glaciology (VAW) of ETH Zurich with brown trout showed that fish are hardly injured when passing over Coanda screens, with the only incurred injury being scale loss of less than  $<1\%$  under various discharges (Lifa *et al.*, 2020). The main disadvantages of Coanda screens is the small unit intake capacity of 50–250 L/s per meter rack length and the large hydraulic losses, which can be approximated by the difference of the upstream water level and the headrace channel (Fig. 2.12). The hydraulic losses of Coanda screens typically vary from 0.7 to 2.2 m (Lifa *et al.*, 2017), which limits the application to high head HPPs with small design discharges.





**Fig. 2.12:** A Coanda screen with a detailed view on the wedge-wire bars (adapted from Lifa *et al.*, 2017)

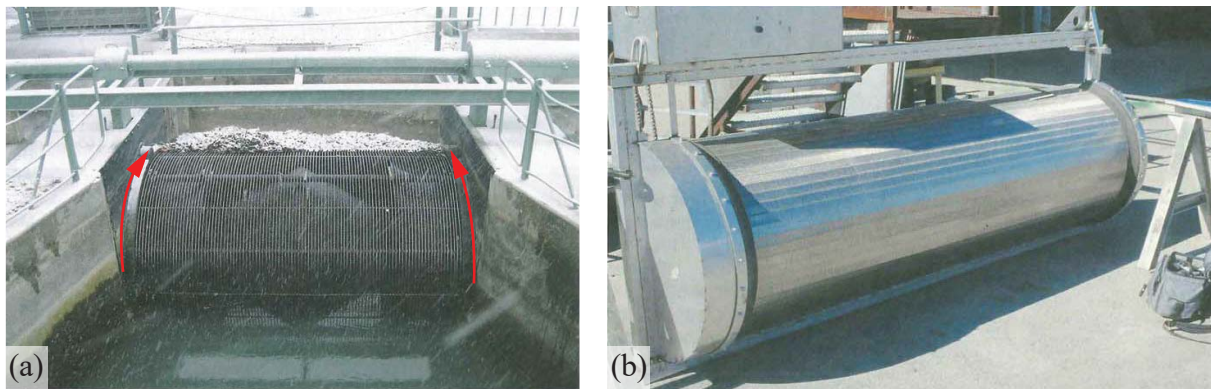
Barrier nets with small mesh sizes ( $<10$  mm) can be used as cheap fish protection measures, but they clog easily and are difficult to clean. Their application is limited to low approach flow velocities ( $U_o = 0.12\text{--}0.15$  m/s), because otherwise they cannot resist the water pressure on the long term when partially clogged (DWA, 2004). Barrier nets can be used to prevent fish from entering turbines, but their guidance efficiency to a bypass is questionable. Thus they are rather used in lakes to block fish from entering pumped storage hydro power stations than as fish protection measures at run-of-river HPPs. Besides static physical barriers, it is possible to install movable screens such as submerged rotating screens, drum screens, and Eicher screens. The latter were developed for HPPs with pressurized pipe flows, where a screen with wedge-wire bars and a clear bar spacing of  $s_b < 2$  mm is installed at an angle of  $\alpha \approx 20^\circ$  in the pipe (Fig. 2.13; Taft, 1986). For pipe flow velocities of 1.5 m/s, survival rates of  $SR_{\text{tot}} \geq 90\%$  were reported for salmon smolts (Taft, 1986).



**Fig. 2.13:** Principle sketch of an Eicher screen indicating cleaning and operating positions (adapted from DWA, 2004)

Rotating screens like drum screens were originally developed to prevent floating debris from entering the turbines, but they can also block fish if  $s_b$  is designed accordingly. Figure 2.14 shows a traditional drum screen, which started its operation in 1953, and a modern drum screen with fine-spaced wedge-wire bars. In general, drum screens are mainly suitable for rivers with small floating debris loads and with little frost risk (DWA, 2004). As drum screens only block fish and have no guidance effect, many of them were replaced in the past years by angled racks (EPRI, 2013). They can still be suitable fish protection measures, if only a small fraction of the

river discharge is extracted at side intakes such that fish bypassing becomes redundant.



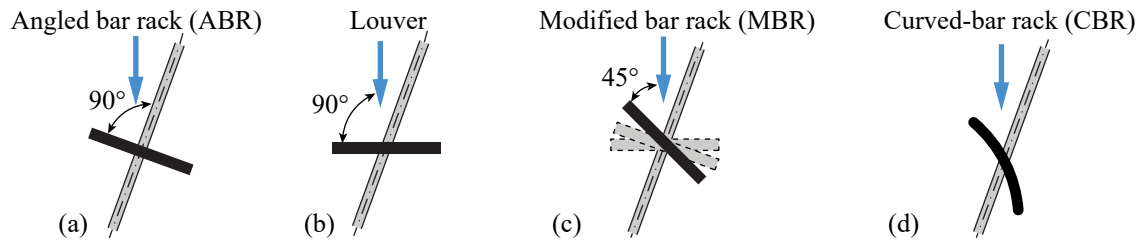
**Fig. 2.14:** (a) Drum screen at HPP Gluringen (46°27'38.8"N, 8°14'08.9"E) in the upper reach of the Rhône River in Switzerland with  $s_b = 25$  mm and (b) a modern drum screen with wedge-wire bars in the USA; the red arrows indicate the direction of rotation (adapted from DWA, 2004)

Perforated plate screens can be angled or inclined and have been used as cheap alternatives to traditional trash racks at small HPPs for several decades (Engel and Weber, 2003). They are typically made of 4–5 mm strong metal sheets with hole diameters of 20–25 mm and were installed as fish protection measures at multiple HPPs in recent years (Engel and Weber, 2003). As perforated plate screens have a large blocking ratio ( $\approx 44$ –50%), they have to be designed  $\approx 20\%$  larger than bar racks (Engel and Weber, 2003). The head loss coefficients of perforated plate screens are in the range of  $\xi_R \approx 0.9$ –1.0 (Engel and Weber, 2003), which is not larger than at most traditional trash racks (Meusburger, 2002). Floating debris at perforated plate screens can be removed by cleaning machines and is then flushed downstream through a bypass (Engel and Weber, 2003).

#### 2.4.2 Mechanical behavioral barriers

Mechanical behavioral barriers are typically racks with larger  $s_b$  than physical barriers, such that they are theoretically permeable for a larger proportion of fish species and size classes. However, they modify the near-structure flow field and induce hydraulic signatures like flow deflections and turbulences in front of the barrier, which aims at triggering avoidance reactions and should guide fish towards the bypass (Kriewitz, 2015; Boes *et al.*, 2016; Albayrak *et al.*, 2020). Although good guidance efficiencies were reported for salmon smolts with a clear bar spacing of up to  $s_b = 30.5$  cm (Ducharme, 1972),  $s_b$  is typically in the range of  $s_b = 25$ –50 mm with  $\alpha \leq 45^\circ$  (Bates and Vinsonhaler, 1957; EPRI and DML, 2001). At angled bar racks (ABR), the individual bars are installed perpendicular to the rack axis, such that the angle between the bars and the approach flow depends on  $\alpha$  (Fig. 2.15a; e.g. Raynal *et al.*, 2013a). In contrast, Louvers are defined by a  $90^\circ$  angle between the bars and the approach flow (Fig. 2.15b; e.g. Bates and Vinsonhaler, 1957). For modified bar racks (MBRs), the angle of the rack construction and the bars can be varied independently (Fig. 2.15c), which leads to smaller hydraulic losses and a more homogeneous downstream flow field (Kriewitz, 2015; Albayrak *et al.*, 2018, 2020). These negative effects are further reduced by the application of curved-bar racks (CBRs) as demonstrated by Beck *et al.* (2019a,b) and Beck (2020). Depending on the application, the

bar shape, the radius of the bars, the angle of the rack axis, and the bar angle can be varied independently (Fig. 2.15d; Beck, 2020).



**Fig. 2.15:** Definition of an (a) angled bar rack (ABR), (b) Louver, (c) modified bar rack (MBR), and (d) curved-bar rack (CBR) (adapted from Beck *et al.*, 2019a; Kriewitz, 2015)

Submerged guidance walls at the bottom or the top of the water column can be used to protect bottom or surface-oriented fish species, respectively. At Bellows Fall HPP on the Connecticut River (43°07'59.8"N, 72°26'30.5"W), a guidance wall, also called fish diversion boom, was installed with an angle to the approach flow of  $\alpha \approx 40^\circ$  to guide salmon smolts to an existing log/ice sluice gate which was used as a bypass (Normandeau Associates, 1995). The guidance wall covered the upper 50% of the 9 m deep water column and led to a guidance efficiency of 84% of the radio tagged smolts, while 16% still passed through the turbines (Normandeau Associates, 1995). The average residence time in front of the guidance wall was only 11 min, indicating that salmon smolts were guided with little delay around the HPP. Riverine species use bypass openings close to the river bottom and surface (Hermens and Gubbels, 2017), such that partially submerged guidance walls are considered unsuitable. On the basis of laboratory experiments and numerical simulations of guidance walls with different submergence depths, approach flow angles, and approach flow velocities, Mulligan *et al.* (2017, 2018) suggested to design partially submerged guidance walls with small approach flow angles of  $\alpha \approx 15^\circ$ , such that the parallel flow component exceeds the vertical (downward) flow component. Guidance walls can be used in combination with fish guidance racks to enhance the overall guidance efficiency for bottom and/or surface-oriented fish. They are referred to as bottom and top overlays in the following. Ethohydraulic studies with eels showed that the fish guidance efficiencies of Louvers and bar racks can be increased with bottom overlays (EPRI and DML, 2001; Kriewitz, 2015). These results cannot be directly transferred to prototype as it is not possible to scale the fish swimming depth, but they show that bottom and top overlays increase the guidance efficiency of racks, if fish are swimming in the corresponding water depth and thereby indicate the potential of the combination of fish guidance racks with overlays. However, without conducting extensive site- and species-specific monitoring campaigns, it should not be assumed that the vast majority of individuals swims at certain flow depth. As an example, Brown *et al.* (2009) demonstrated that eels search for suitable downstream passage corridors in all water depths, although they are generally known to be bottom-oriented. Turnpenny and O'Keeffe (2005) highlighted that surface-oriented smolts tend to swim towards the bottom on sensing danger. Up to now, mechanical behavioral barriers were mostly applied to protect downstream migrating salmon smolts. Field experience about the behavior of a wide range of riverine species and life

stages remains missing.

### 2.4.3 Sensory behavioral barriers

All physical and mechanical behavioral barriers are at least partially submerged in the water column and therefore induce hydraulic losses and may cause operational challenges such as partial clogging. Hence, many different sensory behavioral barriers were tested to prevent fish from entering turbines, including different light, sound, electric field, and air bubble and water-jet barriers (DWA, 2004; Turnpenny and O’Keeffe, 2005). Adam *et al.* (1999) found that neither salmon smolts nor eels can be shoosed in ethohydraulic laboratory tests with strobe lights during day and dawn and mentioned that field tests indicated that the efficiency is strongly affected by water turbidity and flow velocities. Mercury-vapor lamps are used to enhance the attractiveness of bypasses for phototactic positive fish like salmon smolts (Travade and Larinier, 2006). Lowe (1952) conducted laboratory and multi-year field experiments with lights and found that it is possible to guide eels under certain conditions, but the effectiveness was low during floods with turbid water. Richkus and Dixon (2003) summarized multiple investigations and found large variations of the fish guidance efficiency with light, indicating that it is very site- and species-specific and depends on environmental conditions like turbidity and flow velocities. Sand *et al.* (2000) attempted to develop an acoustic fish fence which worked to a certain extent. A submerged infrasound source with a sound frequency of 11.8 Hz and a fish trap with four equally-sized sections were installed in the Imsa River, Norway, to catch downstream migrating silver eels. When the infrasound source was turned on, 57% less eels were caught in the trap closest to the infrasound source and 44% more at the trap at the opposite bank compared to observations when the infrasound source was turned off. Deleau *et al.* (2019) combined an inclined rack with vertical bars and  $s_b = 12$  mm with an acoustic field created by underwater speakers. Although eels were protected well with and without the acoustic field, avoidance reactions were observed, where eels either swam away from the sound source or moved downstream rapidly to the bypass (Deleau *et al.*, 2019). Adam *et al.* (1999) conducted live fish tests in a laboratory flume with air bubble curtains and observed avoidance reactions of eels but they passed the air bubble curtain after they got used to it. Besides the questionable effectiveness of air bubble curtains, their application is limited to small flow velocities and small flow depths, as the air bubbles drift downstream otherwise. A water-jet curtain in the same laboratory flume was completely ignored by salmon smolts and eels (Adam *et al.*, 1999). The first series of patents on electric screens as fish barriers was applied back in 1917 in the United States (Beaumont, 2016). One of the main challenges of electrical screens is that larger fish are exposed to proportionately greater voltage than smaller fish due to the larger body voltage (cf. Section 2.2.5). Pavlov (1989) mentioned that fish down to  $TL = 35\text{--}40$  mm can be protected with electric barriers, but this requires large voltage gradients, which are lethal to large fish. Therefore, graduated electric fields are used, such that fish can react to electric stimuli at different locations, depending on their perception of the voltage gradient. They are widely applied to block upstream movements, which can be useful to avoid dispersal of invasive species or to prevent fish from entering dead ends such as tailrace channels (O’Farrell *et al.*, 2014; Beaumont, 2016). Guiding downstream

moving fish with electricity is far more difficult as the electric field has to be strong enough to trigger avoidance reactions, while injuries, immobilization, and narcosis should be prevented for all species and sizes (Beaumont, 2016). If electric barriers cause immobilization or narcosis to downstream moving fish, they will be swept through the area from which they are meant to be excluded (Beaumont, 2016). To increase the room of reaction of downstream moving fish at electric barriers, O'Farrell *et al.* (2014) recommended to limit approach flow velocities to 0.3 m/s. Downstream moving fish can also be guided with hybrid barriers (Beaumont, 2016), where for example mechanical behavioral barriers are combined with electric fields. Monitoring campaigns at sensory behavioral barriers should not be limited to guidance efficiencies, but should also focus on direct and indirect mortality as sensory behavioral barriers may cause severe injuries (e.g. contact with electrified screen) or increase vulnerability to predation (Ferguson *et al.*, 2006). Summed up, many studies indicate moderate fish guidance efficiencies of different sensory behavioral barriers. Up to now, satisfying fish guidance efficiency could not be proven for any sensory behavioral barrier under a wide range of environmental conditions (e.g. floods) and for different fish species and sizes (DWA, 2004). As fish react differently to most stimuli of sensory behavioral barriers (e.g. negative versus positive phototaxis), it is difficult to use them for the protection of a diverse fish community, but they may be beneficial to guide specific species and life stages at a certain time of the year. When sensory behavioral barriers are applied, it should be verified that fish are not getting used to the stimuli over time, which may diminish the efficiency of the system.

#### **2.4.4 Bypass systems**

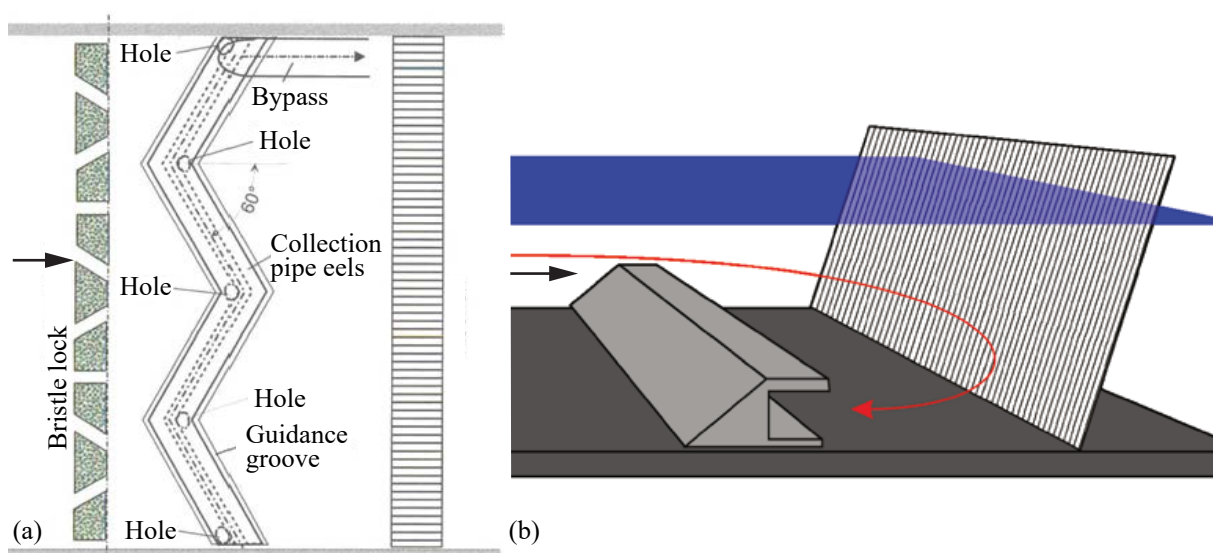
Physical barriers, mechanical behavioral barriers, and sensory behavioral barriers are designed to prevent fish from entering water intakes. To safely guide them around HPPs, additional bypass systems are needed. The location, design, and hydraulics of the bypass are crucial to reach high guidance efficiencies, which is described in more detail in Section 3.4.

#### **2.4.5 Collection systems**

In contrast to bypass systems, fish are usually trapped at collection systems and are then transported safely downstream. Collection systems are often installed in large rivers, where a single bypass entrance is not sufficient. One of the downsides of collection systems is that they often work discontinuously (e.g. fish elevators), which may limit efficiencies. For salmonids, collection channels are typically installed close to the water surface. Fish are then either flushed downstream through a bypass or they are diverted to a fish holding tank, from where they are transported downstream with trucks (trap and truck). A large collection system was installed at the Bonneville Dam on the Columbia River (45°38'53.4"N, 121°56'14.6"W), which was equipped with an attraction flow pump (Turnpenny and O'Keeffe, 2005). The efficiency of the surface collector was expected to be 50–60%, whereas an efficiency of 90% should be achieved in combination with the existing screen (Turnpenny and O'Keeffe, 2005). One of the first collection systems for downstream moving fish in Switzerland was installed at HPP Hagneck (47°03'36.0"N, 7°10'40.4"E) on the Aare-Hagneck canal, where multiple openings were



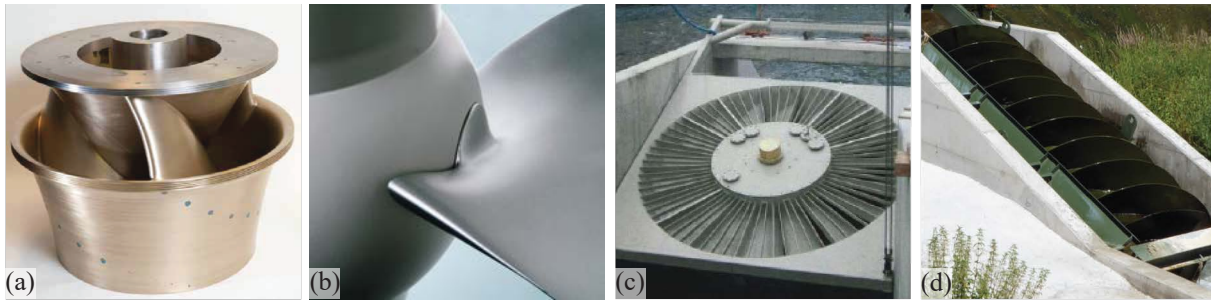
installed in the pier close to the water surface, through which fish are diverted to the natural fish way (Breitenstein *et al.*, 2019). The monitoring campaign was still ongoing in 2019 (Breitenstein *et al.*, 2019). At the Mosel and Saar Rivers, Germany, fishermen systematically catch as many silver eels as possible upstream of all HPPs and transport them with trucks to the Rhine River (Klopries *et al.*, 2016). They are released 40–50 km downstream of Koblenz, from where they can migrate to their spawning habitats without passing any additional HPP (Klopries *et al.*, 2016). Trap and truck is currently not applied in Switzerland, but Baier (2019) evaluated this system to protect downstream migrating eels in the Rhine River. Because of the large efforts, trap and truck is considered as a temporary solution until permanent fish passage facilities are installed (Katopodis and Williams, 2011). With a focus on fish upstream passage at HPPs with limited space or large head differences, multiple fish elevators were constructed in recent years (DWA, 2014). Although fish are collected and may use them for downstream passage, their application is limited due to their discontinuous operating mode and because it is difficult for downstream moving fish to find the entrance. Hassinger and Hübner (2009) introduced a zigzag shaped eel collection system with an adjacent pipe bypass (Fig. 2.16a). Despite good laboratory efficiencies, not a single silver eel was observed using this additional corridor in a monitoring campaign at HPP Lindesmühle in Bad Kissingen (50°11'17.0"N, 10°04'27.9"E), Germany, on the Franconian Saale, which was at least partially attributed to clogging of the entrance holes (Egg *et al.*, 2017; Mueller *et al.*, 2020b). Adam *et al.* (2002) developed a bottom gallery to collect downstream migrating eels (Fig. 2.16b). During catch mode, the bottom gallery is opened, such that eels which collide with the rack and escape upstream close to the river bottom hide in the bottom gallery. The bottom gallery is then closed in certain intervals and eels are flushed downstream through a pipe bypass in transport mode. However, this system was hardly used at HPP Unkelmühle (details in Section 3.7.4).



**Fig. 2.16:** Collection systems for eels: (a) zigzag shaped collection system (adapted from Hassinger and Hübner, 2009) and (b) principle of the bottom gallery where the expected swimming path of eels is indicated in red (adapted from Adam and Lehmann, 2011)

### 2.4.6 Environmentally enhanced turbines

This section gives an overview of environmentally enhanced turbines, which are also known as “fish-friendly turbines”. They are often installed at large HPPs, where other measures like physical barriers are difficult to implement, or in combination with other fish protection measures at small HPPs. Alden turbines are screw-shaped and have no potentially injury-causing gaps, as the blades are directly attached to the housing (Fig. 2.17a). The maximal efficiency in prototype application is expected to be as high as 94% and the turbine survival rate is estimated to be  $SR_t \approx 98\%$  and  $SR_t \approx 100\%$  for fish with  $TL = 20$  cm and  $TL = 10$  cm, respectively (EPRI, 2011), which has yet to be verified in full scale field tests (Hogan *et al.*, 2014). Minimum Gap Runners are modified Kaplan turbines with minimal gaps for all blade positions, which were installed at the Bonneville Dam on the Columbia River (Fig. 2.17b). Turbine survival was higher or equal than for conventional Kaplan turbines with  $SR_t \geq 98\%$  for both turbine types (Hogan *et al.*, 2014). In contrast to Alden turbines and Minimum Gap Runners, the application of Very Low Head turbines (VLH) and Archimedes screw turbines is limited to small HPPs or residual flow turbines (Fig. 2.17c,d). Very Low Head turbines induce small decompression rates (Boys *et al.*, 2018) and are characterized by low rotational speed, but their application is limited to heads between 1.4–3.2 m and discharges of  $Q = 10\text{--}30$  m<sup>3</sup>/s (Yuen *et al.*, 2010). Monitoring campaigns with different fish species indicated high survival rates in the range of  $SR_t = 95\text{--}100\%$  (Hogan *et al.*, 2014). Archimedes screw turbines also induce small decompression rates (Boys *et al.*, 2018) and are known to cause little direct mortality (Piper *et al.*, 2018) as long as the gaps between the turbine blades and the housing are kept minimal (Schmalz, 2010). Schmalz (2010) observed that a reduction of the gaps from 7 mm to 3–4 mm significantly reduced injuries at an Archimedes screw turbine, which could be only achieved with regular maintenance work. Piper *et al.* (2018) found no direct mortality of an Archimedes screw turbine on downstream migrating eels but some individuals got delayed. A standardized monitoring campaign at multiple HPPs with environmentally enhanced turbines (VLH turbines and Archimedes screw turbines) and conventional turbines (Kaplan turbines) revealed that all turbines can lead to high survival rates under certain boundary conditions (Mueller *et al.*, 2020c). However, the high survival rates are not necessarily valid for all fish species and the survival rates at environmentally enhanced turbines are not always larger than at conventional turbines (Mueller *et al.*, 2020c).



**Fig. 2.17:** Environmentally enhanced turbines: (a) model of an Alden turbine (Hogan *et al.*, 2014), (b) detailed view on the connection of a turbine blade with the spherical hub of a Minimum Gap Runner (Voith, 2011), (c) a Very Low Head turbine (Yuen *et al.*, 2010), and (d) an Archimedes screw turbine at HPP Horb-Mühlen (48°27'16.0"N, 8°44'46.4"E; Photo: J. Meister)

### 2.4.7 Fish-friendly operation

Fish-friendly operation of HPPs includes early warning systems to identify periods with increased downstream movement activity, in which  $SR_{\text{tot}}$  can be increased with operational measures like partial spillway openings or temporary turbine shutdowns. Fish-friendly HPP operation also includes the avoidance of partial load at Kaplan turbines, as smaller aperture likely reduces  $SR_t$  (cf. Section 2.3.2). Partial spillway openings are especially effective for diadromous fish species with a distinct migration cycle (Watene and Boubée, 2005). One example for such an early warning system is the Migromat, where wild eels are observed in holding tanks near the HPP. When a certain threshold value of eel activity is exceeded, an alert is triggered, and the HPP switches to fish-friendly operation mode. Until 2018, eleven Migromats were installed in Germany and the Netherlands (Adam, 2018). Becker *et al.* (2009) investigated fish-friendly operation modes as a compromise between HPP efficiency and the protection of downstream migrating eels at a case study at Mosel River, Germany. They pointed out that fish-friendly operation can increase  $SR_{\text{tot}}$ , but the improvement potential significantly varies from year to year, depending mainly on the discharge hydrograph. They also emphasized that reliable and accurate early warning systems are needed, as it is often not reasonable to run HPPs in fish-friendly operation modes permanently (Becker *et al.*, 2009). However, as described in Section 2.2.3, fish movement behavior is complex and depends on many factors. Fish-friendly HPP operation is often used within a restricted time window and therefore requires a good prediction of the fish movement behavior, which limits the application for riverine species.

## 2.5 Hydraulic fundamentals

### 2.5.1 Laminar and turbulent flow

Open channel flow is characterized by a free water surface and is therefore, in contrast to pipe flow, gravity dominated. The state of open channel flow is represented by the ratio of inertial forces to gravity forces, which is also known as the Froude number

$$F = \frac{U}{\sqrt{gL}}, \quad (2.14)$$

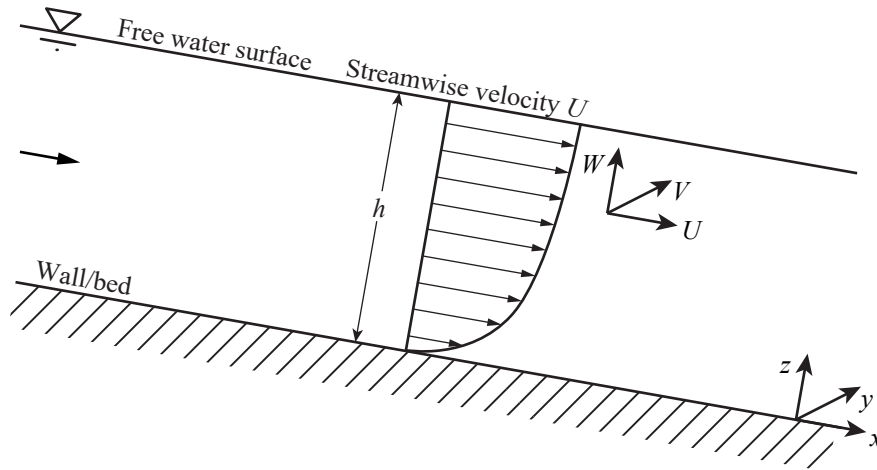
where  $U$  = flow velocity [m/s],  $g$  = gravitational acceleration constant ( $g = 9.81 \text{ m/s}^2$ ), and  $L$  = characteristic length [m]. For open channel flows, the characteristic length corresponds to



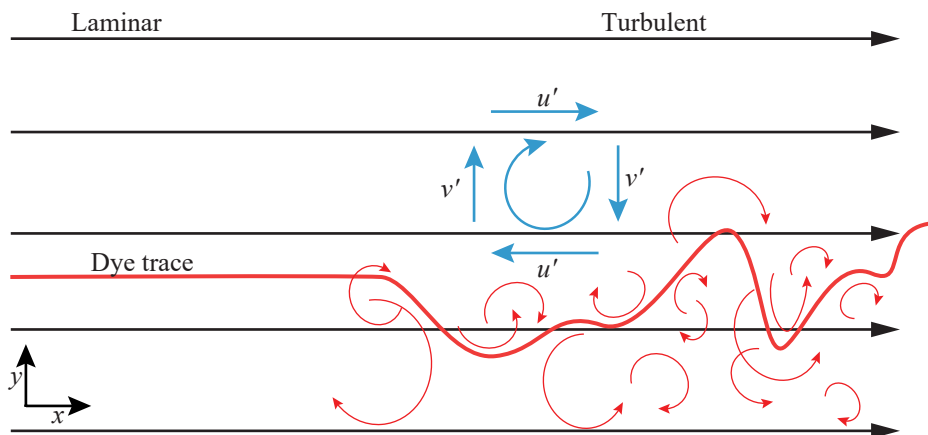
the hydraulic depth, which is defined as the cross-sectional area of water normal to the flow direction divided by the free water surface width (Chow, 1988). The characteristic length of rectangular channels is therefore the flow depth  $h$ , which leads to the Froude number for rectangular channels

$$F = \frac{U}{\sqrt{gh}}. \quad (2.15)$$

The time-averaged flow velocities and their fluctuations are denoted as  $U$ ,  $V$ , and  $W$  and  $u'$ ,  $v'$ , and  $z'$  for the coordinates  $x$ ,  $y$ , and  $z$ , respectively (Fig. 2.18). Open channel flows are typically dominated by the bed roughness, which leads to a logarithmic velocity profile (Fig. 2.18). Open channel flow can be laminar or turbulent. The left side of Fig. 2.19 illustrates laminar flow, where the dye trace is parallel to the horizontal streamlines. In turbulent flow, different-sized eddies superimpose with the main flow, which leads to fluctuations of the flow velocity and thus pressure over time (Fig. 2.19).



**Fig. 2.18:** Visualization of open channel flow with a logarithmic velocity profile and the coordinate definition (adapted from Nezu and Nakagawa, 1993)



**Fig. 2.19:** Plan view on a dye trace in laminar (left) and turbulent (right) flow (adapted from MIT, 2008)

The Reynolds number  $R$  describes the ratio of inertia and viscous friction forces within a flow. It characterizes laminar and turbulent flow and is defined as

$$R = \frac{LU}{\nu}, \quad (2.16)$$

where  $L$  = characteristic length [m] and  $\nu = 1.31 \times 10^{-6}$  and  $1.01 \times 10^{-6}$  m<sup>2</sup>/s, the kinematic viscosity for water temperatures of  $T = 10$  and  $20$  °C, respectively (Bolrich, 2007). The characteristic length has to be chosen to represent flow conditions. For pressurized pipe flow, it is defined as the pipe diameter. For open channel flow, the hydraulic diameter is used, which is defined as four times the hydraulic radius (Bolrich, 2007). In general, the hydraulic radius is defined as the ratio of the cross-sectional area of the flow  $A_{ch}$  and the wetted perimeter  $P_{ch}$ , thus for rectangular open flow channels

$$R_h = \frac{A_{ch}}{P_{ch}} = \frac{hw_{ch}}{2h + w_{ch}}, \quad (2.17)$$

where  $w_{ch}$  = channel width [m]. This leads to the Reynolds number for open channel flow in rectangular cross sections

$$R = \frac{4R_h U}{\nu}. \quad (2.18)$$

The characteristic length of plate flow is the plate length and for flow around bodies, it is the body width. For HPP intake racks, the flow around individual bars is commonly considered as flow around bodies, which leads to the so-called bar Reynolds number

$$R_b = \frac{t_b U_o}{\nu}, \quad (2.19)$$

where  $t_b$  = bar thickness [m]. Pressurized pipe flow changes from laminar to turbulent at Reynolds numbers of  $R \approx 2000$ – $2300$  (Chow, 1988; Bolrich, 2007). For open channel flow, the transition from laminar to turbulent occurs at Reynolds numbers of  $R \approx 500$ , for  $R_h$  as the characteristic length (Chow, 1988). The mean approach flow velocity  $U_o$  can be calculated with the continuity equation for rectangular channels to

$$U_o = \frac{Q}{A} = \frac{Q}{hw_{ch}}. \quad (2.20)$$

The flow velocities in hydraulic laboratory investigations and practical applications related to fish guidance structures are rather large, such that the flow is predominantly turbulent. The instantaneous flow velocities  $u$ ,  $v$ , and  $z$  are composed of the sum of the mean velocity  $U$  and the current fluctuation  $u'$

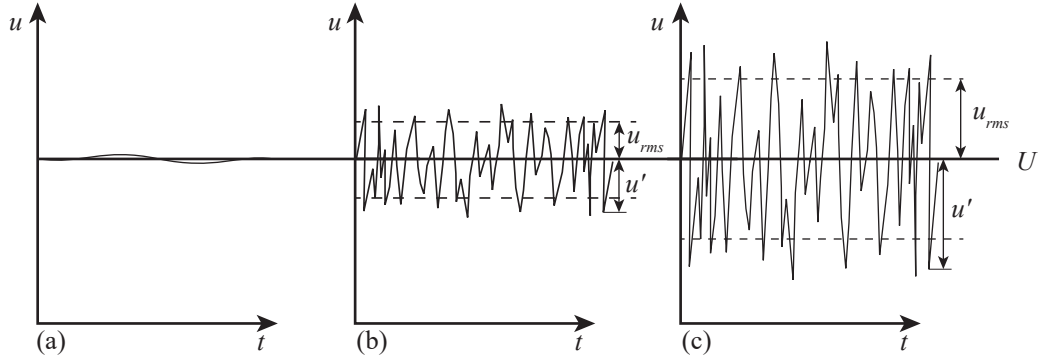
$$u = U + u' \quad (2.21)$$

and analogous  $v = V + v'$  and  $w = W + w'$ . When velocities are measured over time, turbulent intensities can be quantified with statistical dispersion parameters like RMS-values (Root Mean Square) which are defined by

$$u_{rms} = \sqrt{u'^2} \quad (2.22)$$

and analogous  $v_{rms} = \sqrt{v'^2}$  and  $w_{rms} = \sqrt{w'^2}$ . Figure 2.20 illustrates three time series with identical time-averaged streamwise velocities  $U$ , but with different instantaneous velocities  $u$ .

The velocity fluctuations  $u'$  and  $u_{rms}$  increase from laminar flow (Fig. 2.20a), to low turbulent flow (Fig. 2.20b), and highly turbulent flow (Fig. 2.20c).



**Fig. 2.20:** Data series with identical time-averaged streamwise velocities  $U$ , but different instantaneous velocities  $u$  for (a) laminar flow, (b) low turbulent flow, and (c) highly turbulent flow (adapted from MIT, 2008)

The RMS-values can be normalized with  $U$  or the shear velocity  $U^*$  and are then referred to as turbulence intensities. The turbulent kinetic energy (TKE) per unit mass for all three dimensions is defined as

$$\text{TKE} = \frac{1}{2} \left( \overline{u'^2} + \overline{v'^2} + \overline{w'^2} \right). \quad (2.23)$$

The rates of spatial velocity changes of  $U$ ,  $V$ , and  $W$  in  $x$ ,  $y$ , and  $z$ -direction can be described with the spatial velocity gradient tensor with Eq. (2.24) (Nestler *et al.*, 2008). In a straight laboratory flume with small flow deflections,  $V$ ,  $W$ , and velocity variations in  $y$  and  $z$ -direction are small, such that the spatial velocity gradient in  $x$ -direction simplifies to  $\text{SVG}_x = \partial U / \partial x$ .

$$\text{SVG} = \begin{pmatrix} \frac{\partial U}{\partial x} & \frac{\partial U}{\partial y} & \frac{\partial U}{\partial z} \\ \frac{\partial V}{\partial x} & \frac{\partial V}{\partial y} & \frac{\partial V}{\partial z} \\ \frac{\partial W}{\partial x} & \frac{\partial W}{\partial y} & \frac{\partial W}{\partial z} \end{pmatrix} \quad (2.24)$$

## 2.5.2 Hydraulic losses

The total hydraulic losses between two points can be quantified with the Bernoulli equation to

$$\Delta h = z_o + h_o + \frac{U_o^2}{2g} - z_{ds} - h_{ds} - \frac{U_{ds}^2}{2g}, \quad (2.25)$$

where  $z_o, z_{ds}$  = level of the upstream ( $o$ ) and downstream ( $ds$ ) points [m] and  $h_o, h_{ds}$  = upstream and downstream flow depth [m], and  $U_o, U_{ds}$  = upstream and downstream flow velocities [m/s]. The total hydraulic losses  $\Delta h$  compound of the local head losses, such as rack head losses  $\Delta h_R$  or contraction losses  $\Delta h_c$ , and the continuous friction losses  $\Delta h_f$  as

$$\Delta h = \Delta h_R + \Delta h_c + \Delta h_f. \quad (2.26)$$

### Local losses

Local losses can be for example caused by submerged obstacles like racks or by flow contractions. They can be calculated as

$$\Delta h_R = \xi_R \frac{U_o^2}{2g}, \quad \Delta h_c = \xi_c \frac{U_o^2}{2g}, \quad (2.27)$$

where  $\xi_R$  = rack head loss coefficient which is typically determined experimentally and  $\xi_c$  = contraction head loss coefficient. Relating the local losses to  $U_o$  is suitable to describe the hydraulic losses at diversion HPPs with a constant cross section and discharge. If hydraulic losses are to be quantified at various HPP layouts (e.g. block-type HPPs) and operational conditions (e.g. weir and bypass discharge), they can be related to the theoretical average flow velocity

$$U_{th} = \frac{Q_t}{w_{ds} h_o}, \quad (2.28)$$

where  $Q_t$  = turbine discharge [ $\text{m}^3/\text{s}$ ] and  $w_{ds}$  = downstream channel width [m], such that  $\Delta h_R = \xi_R U_{th}^2 / (2g)$ . Independent of the HPP layout,  $U_{th} \approx U_{ds}$  for small head losses. At diversion HPP setups in a straight channel with constant  $w_{ch}$  and without a bypass,  $U_{th} = U_o$ . By using  $U_{th}$  instead of  $U_o$  or  $U_{ds}$ , assessments are independent of potential weir and bypass discharge in case of block-type HPPs, but still account for  $\Delta h_R$ . The contraction losses at a sharp transition, that is, for contraction angles of  $90^\circ$ , can be calculated to

$$\xi_c = \frac{1}{2} \left( 1 - \frac{A_{ds}}{A_o} \right)^{3/4}, \quad (2.29)$$

where  $A_o, A_{ds}$  = cross-sectional area of the upstream and downstream location (Idelchik, 2008).

### Friction losses

The continuous friction losses are calculated with the Darcy-Weisbach equation, which was primarily developed to calculate the continuous losses of pipe flows

$$\Delta h_f = \lambda \frac{l}{d} \frac{U_o^2}{2g}, \quad (2.30)$$

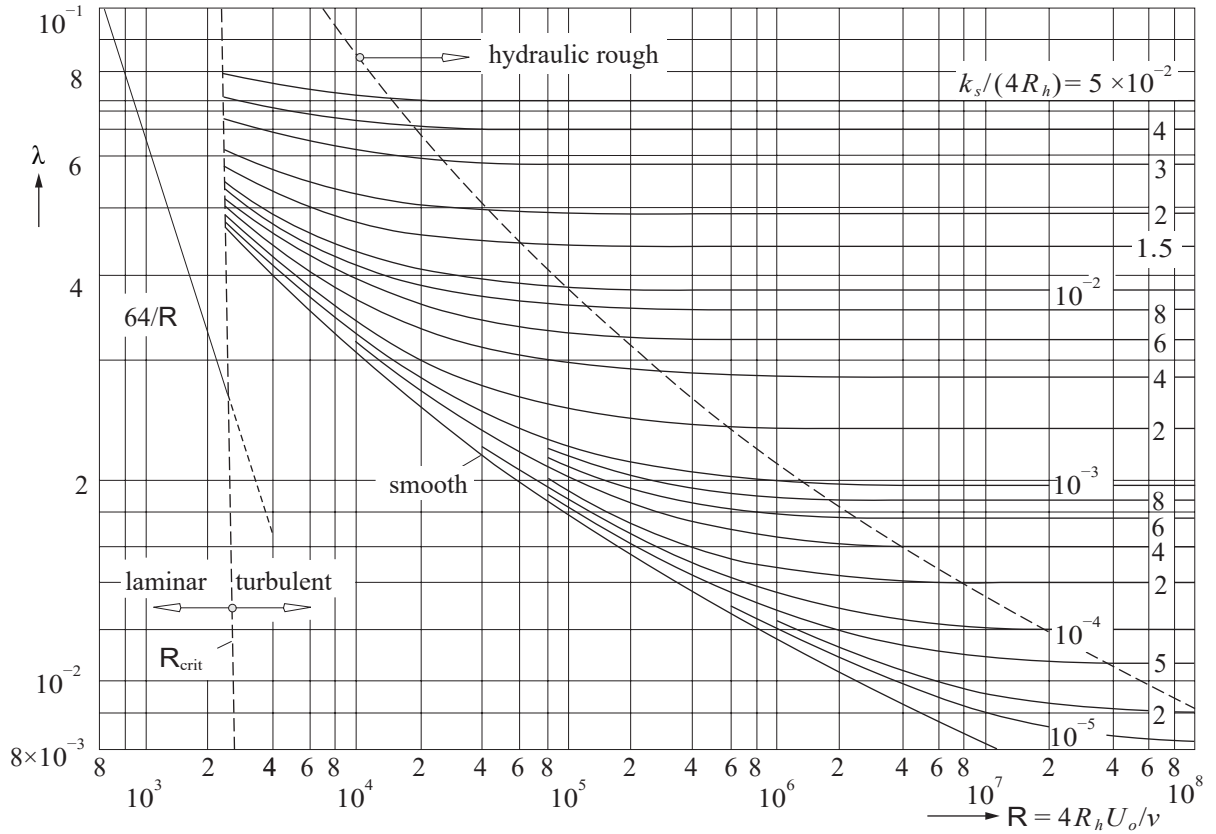
where  $\lambda$  = friction factor [–],  $l$  = pipe length [m], and  $d$  = pipe diameter [m]. The Darcy-Weisbach equation can also be applied for uniform and nearly uniform open channel flow, when the pipe diameter  $d$  is replaced by the hydraulic equivalent diameter  $4R_h$ , which leads to

$$\Delta h_f = \lambda \frac{l_{ch}}{4R_h} \frac{U_o^2}{2g}, \quad (2.31)$$

where  $l_{ch}$  = channel length [m] (Chow, 1988; Bollrich, 2007). The dimensionless friction factor  $\lambda$  can either be calculated with the Colebrook-White equation (Eq. 2.32) or determined graphically with the Moody-diagram (Fig. 2.21).

$$\frac{1}{\sqrt{\lambda}} = -2 \log \left( \frac{2.51}{\text{Re} \sqrt{\lambda}} + \frac{k_s / (4R_h)}{3.71} \right), \quad (2.32)$$

where  $k_s$  = equivalent sand roughness height [m],  $k_{s,\text{glass}} = 1.5 \times 10^{-6}$  m and  $k_{s,\text{PVC}} = 5 \times 10^{-5}$  m (Bollrich, 2007).



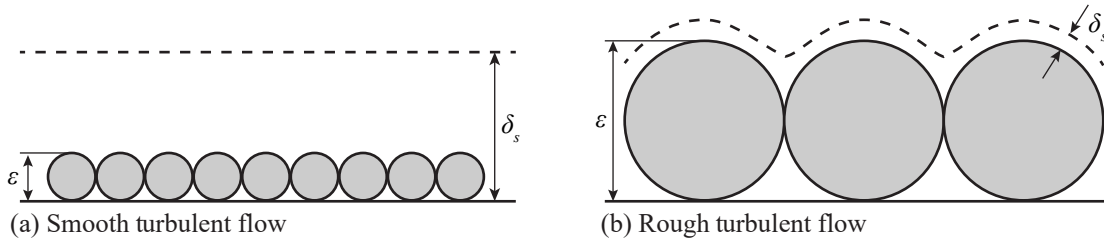
**Fig. 2.21:** Moody-diagram to estimate the dimensionless friction factor  $\lambda$  (adapted from Giesecke *et al.*, 2014)

### 2.5.3 Flow around obstacles

The flow around bodies is independent of the fluid, but it is a function of the Reynolds number and therefore of the flow conditions. This strong similarity allows for comparisons from hydraulic and aerodynamic studies. Flow around a submerged body generates a drag force, which calculates to

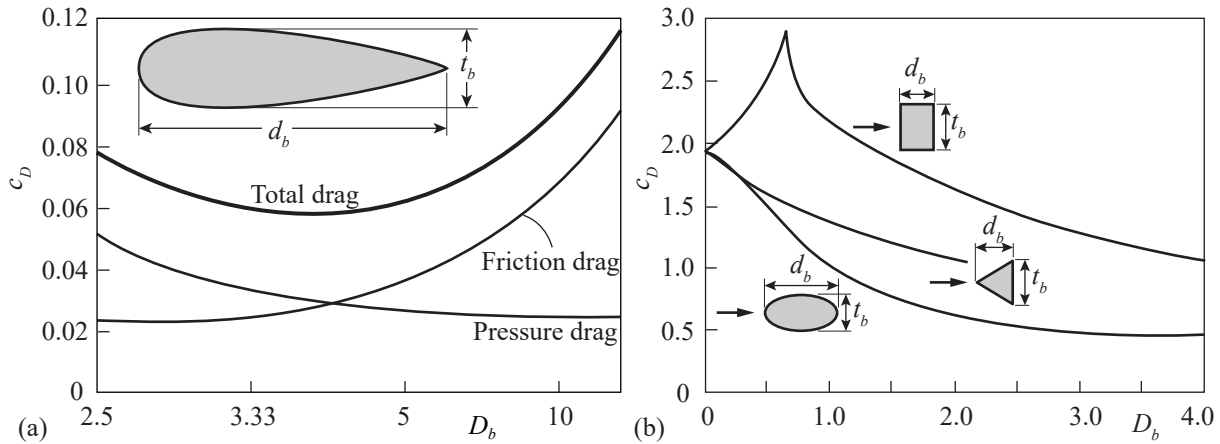
$$F_D = \frac{1}{2} c_D \rho U^2 A, \quad (2.33)$$

where  $c_D$  = drag coefficient [–],  $\rho$  = density of the fluid [kg/m³], and  $A$  = reference area [m²]. The drag force can be split up in a friction and a pressure drag component. The friction drag depends on the surface roughness of the material and on the viscosity of the fluid. A laminar sub-layer with the thickness  $\delta_s$  develops for flow around obstacles. When the equivalent sand roughness  $\varepsilon$  is smaller than the laminar sub-layer, the flow is called smooth turbulent (Fig. 2.22a). In this case, the flow above the laminar sub-layer is not affected by the obstacle roughness. In contrast, the flow above the laminar sub-layer is influenced by the surface of an obstacle, if its roughness is larger than the laminar sub-layer. It is then referred to as rough turbulent flow (Fig. 2.22b).



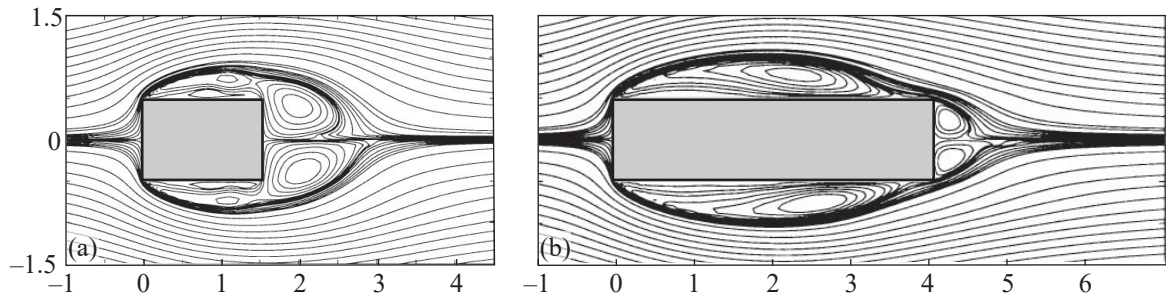
**Fig. 2.22:** Visualization of (a) smooth turbulent flow and (b) rough turbulent flow (adapted from MIT, 2008)

The pressure drag depends on the body shape and is caused by flow separation and pressure differences, which are specifically dominant for very short bodies. The pressure drag is therefore typically predominant for bodies with a small aspect ratio, also called relative bar depth  $D_b = d_b/t_b$  (Fig. 2.23a). Thereby, every body has an optimum  $D_b$  for given flow conditions. Due to its streamlined shape, there are no flow separation zones and only small pressure differences in Fig. 2.23a, which leads to a small overall drag with a minimum of  $D_b \approx 4$ . The interrelation of  $c_D$  and  $D_b$  is discontinuous, depends on  $R_b$ , and may vary significantly between different shapes (Fig. 2.23b). As an example,  $c_D$  increases for  $D_b \leq 0.7$  for rectangles, while it decreases for ellipsoids and triangles (Fig. 2.23b).



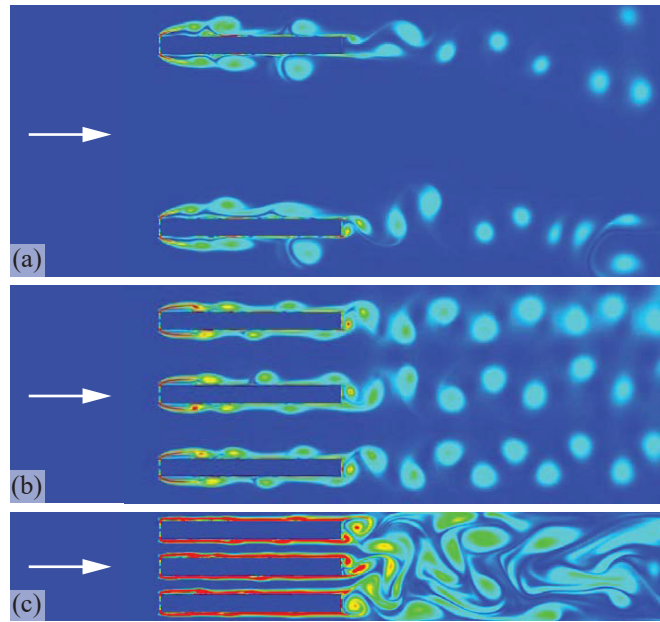
**Fig. 2.23:** (a) Friction, pressure, and total drag of a streamlined body with varying  $D_b$  for  $R_b = 10^4$  (adapted from Flay, 2013) and (b)  $c_D$  as a function of  $D_b$  for different shapes and  $R_b > 10^4$  (adapted from Blevins, 1984)

Blevins (1984) found that the total drag of rectangular bars is minimal for  $D_b \approx 6$  if  $R_b > 10^4$ . Yu and Kareem (1998) investigated the flow around rectangular prisms with different aspect ratios for  $R_b = 10^5$  with a 3D large eddy simulation. They found that the separated flow reattaches to the side face of the prism for aspect ratios  $D_b = 3.0$  and  $D_b = 4.0$ , but not for  $D_b \leq 2.0$  (Fig. 2.24), which was supported by experimental data (Yu and Kareem, 1998). While the mean drag coefficient of obstacles with aspect ratios of  $D_b = 3.0$  and  $D_b = 4.0$  was identical ( $c_D = 1.3$ ), it increased for obstacles with lower aspect ratio ( $c_D = 1.89$  for  $D_b = 1.5$  and  $c_D = 2.14$  for  $D_b = 1.0$ ). Bars of racks should therefore be short to minimize friction losses, but they should have a sufficient depth to allow for the streamlines to reattach to the bars without flow separations, resulting in an optimum of  $D_b \approx 4$ – $6$ . However, stability-related and structural boundary conditions further limit  $D_b$  for practical applications.



**Fig. 2.24:** Streamlines of mean flow around rectangular prisms which do not reattach to the side for (a)  $D_b = 1.5$  in contrast to (b)  $D_b = 4.0$  (adapted from Yu and Kareem, 1998)

If multiple bars are installed close to each other such as at racks, the flow may interact with multiple bars. It is therefore not sufficient to investigate the flow around individual bars. The degree of interaction depends on  $s_b$  and  $t_b$  and can be described with the relative clear bar spacing  $\sigma_b = s_b/t_b$ . Meusburger *et al.* (1999) and Meusburger (2002) numerically investigated a set of rectangular bars with different  $\sigma_b = 1-9$  and  $R_b = 1600-2600$ , which led to the vortex formations in Figure 2.25.



**Fig. 2.25:** Development of the Kármán vortex street at rectangular bars with  $D_b = 10$  for  $\sigma_b =$  (a) 9, (b) 3, and (c) 1 and Reynolds numbers of  $R_b =$  (a) 2600, (b) 1800, and (c) 1600 (adapted from Hermann and Hollenstein, 1998; Meusburger *et al.*, 1999)

For larger bar spacing ( $\sigma_b > 3$ ) a Kármán vortex street developed by vortex shedding (Fig. 2.25a), whereas the vortices of the adjacent bars superimposed for  $\sigma_b \leq 3$  (Fig. 2.25b,c). Very small bar spacing ( $\sigma_b = 1$ ) led to higher pressure gradients and stronger turbulences (Fig. 2.25c). Independent of  $\sigma_b$ , the bars did not affect the upstream flow under the investigated conditions, which means fish are able to sense turbulences only if they are within a few millimeters from the rack. The relative clear bar spacing at traditional trash racks is typically in the range of  $\sigma_b = 5-15$  (Meusburger, 2002), such that the flow around individual bars may be representative, while this is not applicable for physical barriers with typically  $\sigma_b < 3$ .





## 3 State-of-the-art and design of horizontal bar rack bypass systems

### 3.1 Milestones in the development

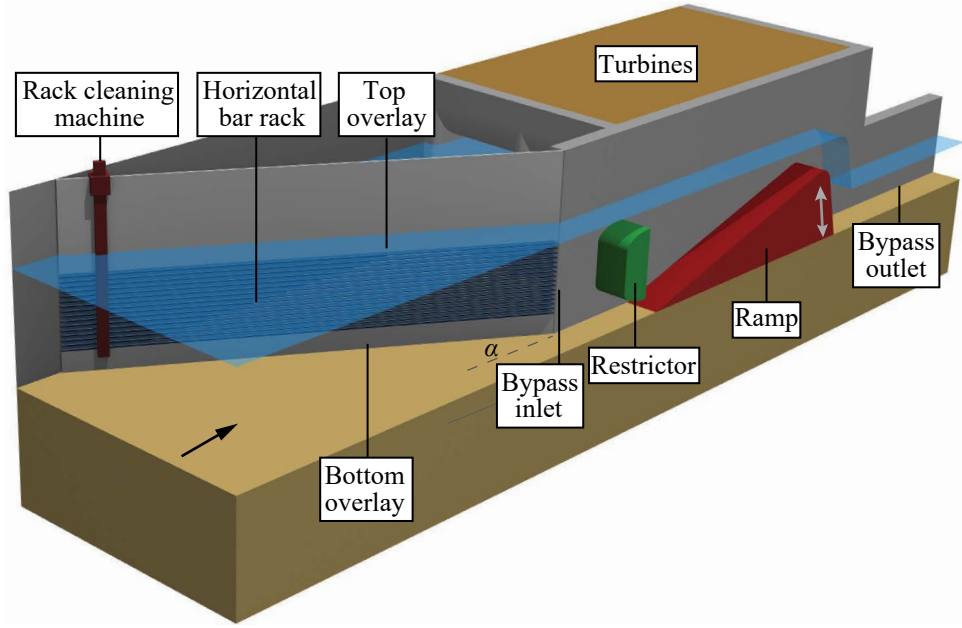
HBRs are built for different purposes, such as for fish protection, blocking of floating debris, or personal safety. Already in 1922, a first HBR was installed at the Hirten weir on the Alz Canal (48°09'14.3"N, 12°39'51.5"E), Burgkirchen, in southern Germany (Fig. 3.1a). The water intake was equipped with nine 5.4 m wide HBR fields with a clear bar spacing of  $s_b = 60$  mm. The red ellipse in Fig. 3.1a highlights one of these rack fields prior to installation. The HBR was installed parallel to the river banks as a side intake and it was equipped with a manually-operated rack cleaning machine (RCM). At that time, the clear bar spacing was mainly determined by personal safety considerations and driftwood dimensions, which were considered problematic for the installed turbines (Sell, 1971). This arrangement enabled to extract water from the Alz River, without interrupting the sediment and floating debris continuum, because solids were flushed over the weir without the need of a bypass. This HBR was successfully in operation for several decades, until it was replaced by a new HBR with an identical layout in 1987. In 1995, the intake was extended with a 4 m wide HBR rack field with  $s_b = 26$  mm for the residual flow turbine.



**Fig. 3.1:** (a) Construction of Hirten weir and an HBR field (encircled in red) in 1922 (courtesy of Wacker Chemie AG) and (b) HBR at the main HPP Dietikon in July 2019, shortly before it started its operation (Photo: H. Fuchs)

One of the first HBRs with an automated RCM was installed at HPP Meinharting on the Mattig River (48°13'28.7"N, 13°04'38.9"E), Austria, which started its regular operation in 1985 (Jank, 2018). The first horizontal bar rack with a bypass system with a specific focus on fish protection was designed in 2001 for HPP Halle-Planena on the Saale River (51°25'00.3"N, 11°57'10.7"E), Germany, and started its operation in 2006 (Gluch, 2007; Ebel, 2016). It combined the concept of behavioral fish guidance racks, which were already installed at multiple HPPs in the USA at that time (e.g. Bates and Vinsonhaler, 1957; Pavlov, 1989), with the concept of horizontal

bars to reduce hydraulic losses and to enhance the transport of floating debris (Ebel, 2016). As HBRs build up a functional unit with the bypass, this system is called horizontal bar rack bypass system (HBR-BS, Fig. 3.2). First design recommendations for this system were published by Ebel (2013), where the system was referred to as “Guidance-rack-bypass-system according to Ebel, Gluch, and Kehl” (Ebel, 2016). The main elements of HBR-BSs are the HBR itself, which can be equipped with bottom and/or top overlays, an automated rack cleaning system to prevent clogging, a bypass inlet with a restrictor, and a ramp to control flow velocities in the bypass (Fig. 3.2). A milestone in terms of upscaling HBR-BSs to larger HPPs was achieved in 2019, when an HBR with  $s_b = 20$  mm was installed at HPP Dietikon on the Limmat River (Fig. 3.1b; 47°24'36.5"N, 8°24'29.4"E), Switzerland, with a design discharge of  $Q_d = 95$  m<sup>3</sup>/s (Balestra and Scherngell, 2019). At that time, the only HBR with a larger design discharge was installed at HPP Danzermühl on the Traun River (47°58'40.2"N, 13°48'43.4"E), Austria, with  $Q_d = 120$  m<sup>3</sup>/s (Gruber, 2019b), but due to its rather large clear bar spacing of  $s_b = 30$  mm in the main section and  $s_b = 45$  mm in the upper section (Gruber, 2018b), it is not a physical barrier for most fish. In recent years in Germany, HBRs have been developed towards smaller  $s_b$ , especially in rivers with diadromous fish species. In 2014 and 2017, the HPPs Freyburg (51°12'31.4"N, 11°46'16.2"E) and Öblitz (51°11'16.0"N, 11°52'20.6"E) with  $Q_d = 25.5$  m<sup>3</sup>/s and  $Q_d = 48.0$  m<sup>3</sup>/s, respectively, were equipped with HBRs with  $s_b = 10$  mm (Ebel *et al.*, 2018). The operational experiences of the first years were promising, as the HBR-induced head losses were small ( $\leq 2$  cm) and no permanent clogging was observed (Ebel *et al.*, 2018). Until recently, most HBR-BSs were built in German-speaking countries (Austria, Germany, and Switzerland), but within the years, HBR-BSs were also installed in other countries, such as Sweden (at least from 2013 on; Nyqvist *et al.*, 2017b), Italy (at least from 2016 on; Gruber, 2018a), and France (at least from 2018 on; Vigne-Lepage, 2020). Despite an extensive literature study, no indications could be found that HBR-BSs were already installed outside of Europe by 2020. It is difficult to estimate how many HPPs were equipped with HBR-BSs all over Europe, but an analysis conducted within the present work revealed that more than 100 HBR-BSs started their operation by 2020. It is possible that the actual number of HBR-BSs is considerably larger, as only one manufacturer installed 230 RCMs for HBRs until 2018 (Jank, 2018). However, not all of these HBRs focus on fish protection and are equipped with bypass systems and many of these HPPs are very small ( $Q_d \leq 10$  m<sup>3</sup>/s), such that little information is available. On the basis of HBR-BSs recently built in Germany, Ebel *et al.* (2018) quantified the specific construction costs, excluding plannings costs, to 14 000–18 000 €/m<sup>3</sup>/s for HBR-BSs with  $s_b = 20$  mm,  $U_o = 0.5$  m/s and 18 000–25 000 €/m<sup>3</sup>/s for  $s_b = 10$  mm,  $U_o = 0.3$  m/s.



**Fig. 3.2:** Principle sketch of an HBR-BS including the HBR itself with bottom and top overlay, RCM, and bypass system with inlet restrictor, ramp, and outlet (adapted from Ebel, 2016)

### 3.2 State-of-the-art

To assess the state-of-the-art, a questionnaire was sent to operators of 50 HPPs with HBR-BSs in Germany, Switzerland, and Austria within the present study in November 2017, where the return rate was 50%. The main results, including characteristics of the HPPs, HBRs, bars, bypasses, and the RCMs are summarized in Table 3.1. The design discharge and the gross head were in the range of  $Q_d = 1.60\text{--}80.00\text{ m}^3/\text{s}$  and  $h_g = 1.40\text{--}364.80\text{ m}$ , respectively. The HBR-BSs were installed at diversion HPPs (60%), bay-type HPPs (25%), and block-type HPPs (15%) and started their operation between 2007 and 2016 (median 2015). The bars of most HBRs were either foil-shaped (30%) or had an ellipsoidal tip and tail (39%), whereas only 4% were rectangular with a circular tip, 4% were rectangular with a reduced width towards the tail (trapezoidal), and 22% were simply rectangular (cf. Fig. 4.14 in Section 4.2.3). While all HBRs which started operation before 2013 were equipped with rectangular bars, this was the case for only 10% of the HBRs which were commissioned after 2013. It was also noticeable that the average clear bar spacing  $\bar{s}_b$  slightly decreased within the years, from an average of  $\bar{s}_b = 19.0\text{ mm}$  in 2007–2012, to  $\bar{s}_b = 17.5\text{ mm}$  in 2013–2016, and it is likely that  $\bar{s}_b < 17.5\text{ mm}$  from 2017 onwards, as some newer HBRs were built with  $s_b = 10\text{ mm}$  (cf. Section 3.1). At 30% of the HPPs, a traditional trash rack was needed in addition to the HBR. This is typically the case if HBRs are installed at the beginning of the headrace channel at diversion HPPs or for safety reasons, if the area between the HBR and the turbines is uncovered. The horizontal approach flow angle  $\alpha$  and the approach flow velocity  $U_o$  could not be systematically analyzed, as their definitions were ambiguous (e.g. side intakes), but the average normal flow velocity from continuity at design discharge was calculated to  $\bar{V}_n = Q_d/A_R$  and was in the range of  $\bar{V}_n = 0.19\text{--}1.0\text{ m/s}$ . The median bar thickness and bar depth were  $\tilde{t}_b = 8\text{ mm}$ , and  $\tilde{d}_b = 60\text{ mm}$ , respectively, leading to a median relative bar depth of  $\tilde{D}_b = 60/8 = 7.5$ , which is close to the

optimal depth of rectangular bars regarding the drag coefficient (cf. Section 2.5.3). Most HBRs were equipped with bottom and top overlays (guidance walls), but a systematic quantification of their heights was difficult as the bottom overlay height was often not constant along the HBR and the submergence depth of the top overlay varied with the water table across the year.

**Table 3.1:** Results of the questionnaire, including the mean  $\bar{x}$ , median  $\tilde{x}$ , minimal value  $\min(x)$ , maximal value  $\max(x)$ , and the standard deviation  $\sigma_x$  of different characteristics regarding the HPP, HBR, bar, bypass, and RCM

		$\bar{x}$	$\tilde{x}$	$\min(x)$	$\max(x)$	$\sigma_x$
HPP	Design discharge $Q_d$ [m <sup>3</sup> /s]	14.4	8.5	1.6	80.0	16.4
	Gross head $h_g$ [m]	23.9	4.3	1.4	364.8	73.5
HBR	Rack length [m]	14.4	12.0	5.5	36.0	7.2
	Rack height <sup>1</sup> [m]	1.9	1.8	0.6	5.2	1.0
	Rack area $A_R$ [m <sup>2</sup> ]	32.7	21.0	4.2	149.8	37.0
	Average normal flow velocity $\bar{V}_n = Q_d/A_R$ [m/s]	0.48	0.44	0.19	1.00	0.20
Bars	Clear bar spacing $s_b$ [mm]	18.0	20.0	15.0	20.0	2.3
	Bar thickness $t_b$ [mm]	10.1	8.0	5.0	20.0	3.5
	Bar depth $d_b$ [mm]	67.8	60.0	40.0	100.0	16.1
	Relative bar depth $D_b = d_b/t_b$	7.2	7.5	3.0	10.0	1.4
Bypass	Absolute bypass discharge <sup>2</sup> $Q_{by}$ [m <sup>3</sup> /s]	0.26	0.16	0.08	0.80	0.21
	Relative bypass discharge <sup>2</sup> $Q_{by,rel} = Q_{by}/Q_d$ [%]	2.9	1.9	0.7	10.0	2.4
RCM and hydraulic losses	Number of rack cleaning cycles per day in spring	7.5	1.8	0.4	48.0	12.3
	Number of rack cleaning cycles per day in summer	5.4	1.0	0.4	48.0	11.3
	Number of rack cleaning cycles per day in autumn	63.4	17.3	0.1	372.0	108.0
	Number of rack cleaning cycles per day in winter	3.1	1.5	0.0	20.0	4.8
	Hydraulic losses after cleaning [m]	0.03	0.02	0.00	0.07	0.02
	Average hydraulic losses [m]	0.04	0.03	0.01	0.08	0.02
	Maximal hydraulic losses (e.g. during flood events) [m]	0.14	0.10	0.04	0.30	0.10

<sup>1</sup> Without considering the bottom and top overlay height

<sup>2</sup> During main fish movement period, but it was almost identical during low fish movement period

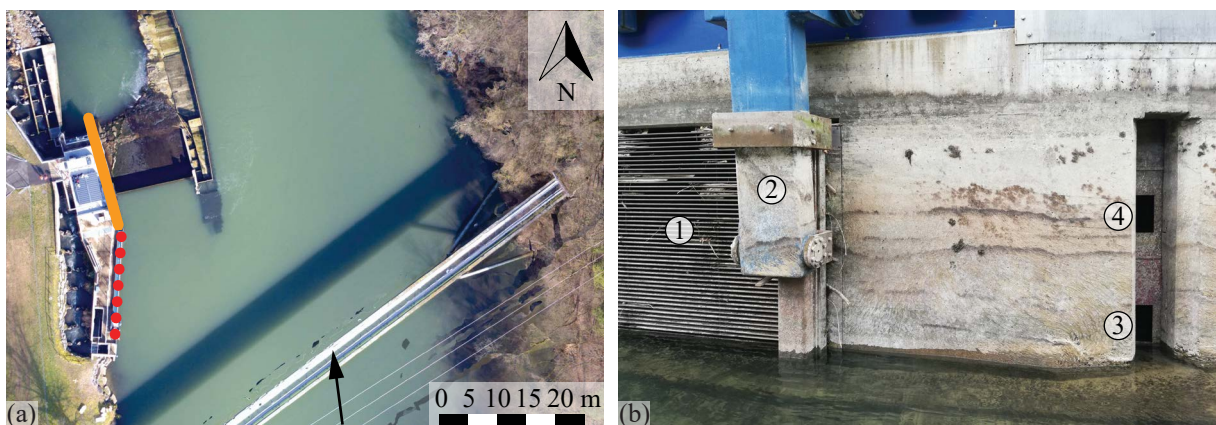
The bypass of 85% of all HBR-BSs was built as an open channel (free water surface), while it was a pressurized pipe bypass at 10%, and a special solution with an intermediate flushing system at 5% of the HBR-BSs. Of all bypasses, 89% had an opening close to the water surface (top opening), 68% close to the bottom (bottom opening), and 76% of the HBR-BSs were equipped with an additional flushing gate. With only one exception, the bypass discharge was constant throughout the year at all HBR-BSs. The absolute bypass discharge varied from  $Q_{by} = 0.08$  m<sup>3</sup>/s to  $Q_{by} = 0.80$  m<sup>3</sup>/s, leading to a relative bypass discharge in the range of  $Q_{by,rel} = 0.7$ –10.0%. While the median number of rack cleaning cycles per day was around 1.5 for summer, winter, and spring, it was 17 in autumn. The standard deviation of the cleaning cycles in autumn was very large ( $\sigma = 108$ ), indicating that clogging of HBRs is very site-specific. The maximal number of cleaning cycles per day at one HBR-BS was 372, which is equivalent to



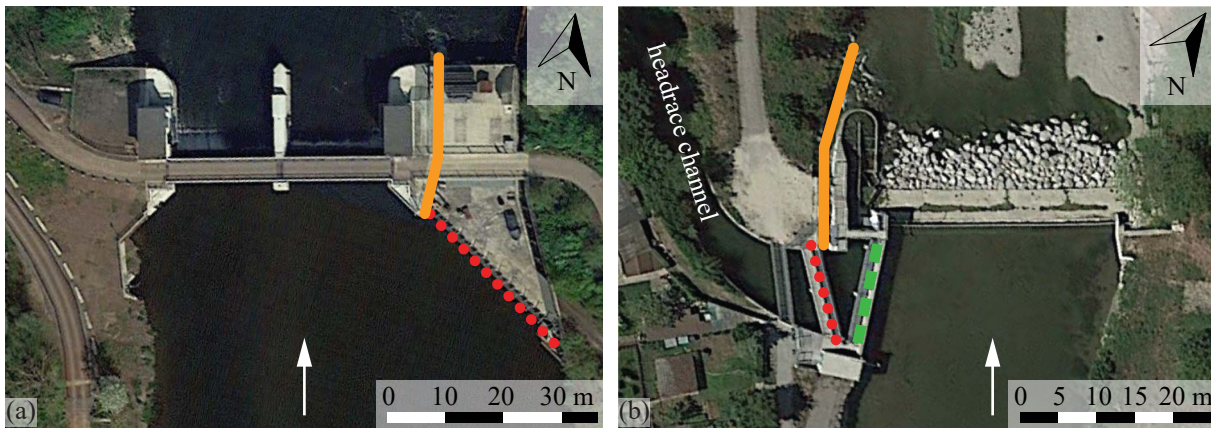
a cleaning cycle every four minutes and means that the RCM was running permanently. The hydraulic losses were continuously monitored at 38% of the HBR-BSs and the majority of operators (90%) reported that clogging of the HBR can be observed at least sometimes visually. The average hydraulic losses were small (median 3 cm), but when clogged, hydraulic losses of up to 30 cm were observed, which required an emergency shutdown of one HPP. The large difference between the maximal hydraulic losses (median 10 cm) and the hydraulic losses after cleaning (median 2 cm) indicates that most RCMs work properly and permanent clogging can usually be prevented. However, at some HBR-BSs, floating debris or sediments disrupted the RCM. This made manual interventions necessary at 11% of the HBR-BSs every 2–4 weeks and at 32% less frequently than every four weeks, while routine inspections were sufficient at 58% of the HBR-BSs. Most HPP operators made good experiences with their HBR-BSs, but operational aspects were very site-specific, which means that the river characteristics (e.g. load of floating debris and sediments) and the structural details of the HBR-BS are very important. Operational challenges reported were clogging of pipe bypasses, foliage clogging primarily in autumn, and clogging between bars by small branches or gravel, which could not be removed by the RCMs. None of the HPP operators reported any problems regarding vibrations of HBRs. A monitoring campaign with respect to fish downstream passage was conducted or planned at 50% of all HBR-BSs.

### 3.3 Practical examples

In this section, three very different HBR-BSs are described and all characteristics are summarized in Table 3.2. These HBR-BSs were chosen for comparison as Halle-Planena was the first HPP with an HBR-BS focusing on fish protection, the residual flow HPP Schiffmühle was part of an extensive research campaign, and HPP Hard with the newest HBR-BS was built according to more recent design recommendations. The layouts of these HBR-BSs differ significantly, which becomes apparent by a comparison of the orthophotos in Fig. 3.3a and Fig. 3.4a,b.



**Fig. 3.3:** (a) Residual flow HPP Schiffmühle with HBR (dotted red line) and pipe bypass (orange line; courtesy of Zabah, E., 2018, Regionalwerke AG Baden) and (b) view on ① downstream rack end with ② RCM and ③ bottom and ④ top bypass openings at residual flow HPP Schiffmühle during reservoir drawdown in July 2018 (Photo: J. Meister)



**Fig. 3.4:** (a) HPP Halle-Planena with HBR (dotted red line) and open channel bypass (orange line) (adapted from Google Earth; date taken: 22.04.2018) and (b) HPP Hard with HBR (dotted red line), open channel bypass (orange line), and automatic sluice gate (dashed green line) (adapted from Google Earth; date taken: 16.08.2018)

While the HBR of the residual flow HPP Schiffmühle was designed as a side intake (Fig. 3.3a), the HBR of HPP Halle-Planena was oriented with an angle of  $\alpha \approx 45^\circ$  to the approach flow (Fig. 3.4a). In contrast to the oldest HBR at HPP Halle-Planena, the newer HBRs at HPPs Schiffmühle and Hard were designed with foil-shaped bars. Other substantial differences are given by the different RCMs (discussed in Section 3.5) and the bypass type. At HPP Schiffmühle, the bottom and top bypass opening are located more than 2 m away from the downstream rack end. They are only 17 cm wide and 24.5 cm high and displaced by an angle of  $\approx 90^\circ$  to the rack (Fig. 3.3b). Fish are supposed to be guided to an adjacent manhole and subsequently to the pressurized pipe bypass with a diameter of 25 cm. The HPP Hard is equipped with an automated sluice gate, which is positioned in front of the HBR (green dashed line in Fig. 3.4b). The sluice gate can be closed to block the full cross section and therefore allow inspections at the HBR-BS and the headrace channel. It can also be partially lowered in case of flood events to divert floating debris, similarly to top overlays.

**Table 3.2:** Specifications of selected HPPs with HBR-BSs (data of Halle-Planena adapted from Ebel, 2016)

		Halle-Planena	Schiffmühle	Hard
HPP	Location	Halle-Planena, Germany	Turgi, Switzerland	Winterthur, Switzerland
	Coordinates	51°25'00.6"N, 11°57'10.6"E	47°29'13.9"N, 8°16'12.0"E	47°30'51.9"N, 8°40'50.7"E
	River	Saale	Limmat	Töss
	HPP design	Bay-type HPP	Residual flow HPP, block unit	Diversion HPP
	Design discharge $Q_d$ [m <sup>3</sup> /s]	50	14	6.5
	Gross head $h_g$ [m]	2.36	2.97	11.60
HBR	Start of operation	2006	2013	2015
	Rack length [m]	29.5	14.6	12.0
	Rack height [m]	3.73	1.82	1.20
	Rack area $A_R$ [m <sup>2</sup> ]	110.0	26.6	14.4
	$\bar{V}_n = Q_d/A_R$ [m/s]	0.45	0.53	0.45
	Approach flow angle $\alpha$ [°]	$\geq 45$	0	65
	Bottom overlay height [m]	0.30	0.35	0.55
	Top overlay height [m]	0	Variable	Rarely submerged
Bars	Bar shape	Rectangular	Foil-shaped	Foil-shaped
	Clear bar spacing $s_b$ [mm]	20	20	20
	Bar thickness $t_b$ [mm]	n/a	12	14
	Bar depth $d_b$ [mm]	n/a	80	90
	Relative bar depth $D_b$	n/a	6.67	6.43
RCM & bypass	RCM type	Rake	Plastic scraper	Rake
	Bypass design	Open channel	Pipe	Open channel
	Bypass inlet openings	Bottom and top	Bottom and top	Bottom and top
	$Q_{by,rel}$ [%]	2.1	1.2	6.1

## 3.4 Design aspects

### 3.4.1 Horizontal bar rack design

#### Bar shape

Most traditional trash racks at large run-of-river HPPs in Switzerland were built with rectangular bars (51%) or with rectangular bars with rounded tips (35%; Meusburger, 2002). Foil-shaped bars were only installed at 14% of the HPPs, typically at HPPs with large approach flow velocities of  $U_o \geq 1$  m/s to reduce hydraulic losses (Meusburger, 2002). The majority of early HBRs, including Hirten weir (Fig. 3.1a) and HPP Halle-Planena, were also equipped with rectangular bars, while foil-shaped bars were more often installed at new HBRs like at HPP Hard (cf. Section 3.2). This is due to the fact that the production costs of foil-shaped bars reduced in recent

years and the bar shape is more important in terms of hydraulic losses for small  $s_b$ . Bars should be deep enough to allow for the streamlines to reattach to the sides, without inducing flow separation zones, which leads to an optimum of  $D_b \approx 4\text{--}6$  from a hydrodynamic point of view (cf. Section 2.5.3). The bar thickness is determined by structural considerations and is typically in the range of  $t_b = 8\text{--}10$  mm (cf. Table 3.1). Besides the economic aspects like the hydraulic losses and production costs, the bar shape affects the operation of HBR-BSs. Kirschmer (1925) emphasized that the smallest gap between two bars should be located at the upstream bar end to improve the cleaning efficiency. Clogged logs can thereby be removed more easily and are either transported downstream through the bypass or the turbines. Up to now, it was unclear if the bar shape affects the foliage clogging probability. It is likely that the bar shape also affects the fish behavior, but studies on this aspects are missing.

### Clear bar spacing

Although HBRs are physical barriers, laboratory studies and monitoring campaigns revealed that they also partially work as mechanical behavioral barriers (examples in Section 3.7.4). As a conservative approach, this behavioral protection effect of HBRs is typically neglected (cf. Section 2.2.6). To properly design physical barriers, it has to be decided which fish species and sizes should be protected. The required clear bar spacing  $s_b$  can then be calculated with Eq. (2.3). The importance of  $s_b$  for fish protection is already known since the 19<sup>th</sup> century. Gerhard (1893) described that downstream moving fish could only be sufficiently protected when  $s_b$  of traditional trash racks was reduced from typically 30–50 mm to 10–15 mm, but he also pointed out that it was not feasible to install racks with such small  $s_b$  at that time. Schmassmann (1928) emphasized that many fish can pass racks with  $s_b = 30$  mm, which was considered the state-of-the-art at that time. Jens (1987) noted that sufficient fish protection is not possible with  $s_b > 20$  mm and referred to the small effect on the hydraulic losses for foil-shaped bars. The same value is mentioned as an upper threshold in the current best practice guideline of the Swiss Federal Office for the Environment of 2012 (Hefti, 2012) and was implemented at many HPPs in the beginning of the 21<sup>st</sup> century (cf. Table 3.2). In general, eels are known to be able to squeeze themselves through very small openings. As an example, Adam *et al.* (1999) observed eels with  $TL = 70$  cm passing through racks with  $s_b = 20$  mm and therefore recommend  $s_b < 20$  mm. This observation is in line with current design recommendations as  $TL_{crit} \approx 67$  cm for eels at HBRs with  $s_b = 20$  mm (cf. Eq. 2.3 and Table 2.2). In recent years, there was a tendency to demand racks with  $s_b < 20$  mm with the argument that fish protection can be significantly improved, while the hydraulic losses are still small for unclogged racks with optimized bar shapes. As an example, if new HPPs are equipped with HBRs in the German state Baden-Württemberg,  $s_b \leq 18$  mm is required in all rivers,  $s_b \leq 15$  mm in rivers with anadromous species, and  $s_b \leq 10$  mm in rivers with eel populations (LUBW, 2016).

### Approach flow angle and velocities at angled racks

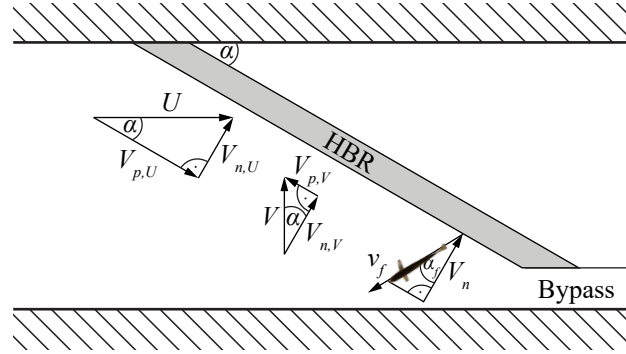
The approach flow velocity of barriers should be designed such that the target species and size classes are able to prevent barrier contact and swim into the bypass, while it has to be ensured



that no fish are impinged (Ebel, 2016). The longitudinal and transversal flow velocities  $U$  and  $V$ , respectively, can be converted to the flow velocity components normal ( $V_n$ , Eq. 3.1) and parallel ( $V_p$ , Eq. 3.2) to the rack (Fig. 3.5). The velocity component  $V_p$  is also referred to as the sweeping velocity and  $V_n$  as the escape velocity (e.g. Turnpenny and O’Keeffe, 2005; Vowles *et al.*, 2013; de Bie *et al.*, 2018).

$$V_n = V_{n,U} + V_{n,V} = U \sin(\alpha) + V \cos(\alpha) \quad (3.1)$$

$$V_p = V_{p,U} - V_{p,V} = U \cos(\alpha) - V \sin(\alpha) \quad (3.2)$$



**Fig. 3.5:** Decomposition of the velocity components  $U$  and  $V$  at angled racks and the typical alignment of downstream moving fish at physical barriers, according to Pavlov (1989)

Bates and Vinsonhaler (1957) assumed that fish align with an angle of  $90^\circ$  to the barrier, such that  $V_n = v_f$ , where  $v_f$  represents the fish swimming velocity and direction. They proposed to design Louvers so that  $v_f$  corresponds to the burst swimming speed. Pavlov (1989) described a similar approach, but observed that fish align with positive rheotaxis and a certain angle  $\alpha_f$  to  $V_n$  at physical barriers (Fig. 3.5). Good guidance efficiencies were achieved for  $V_n < 88\%$  of the critical swimming velocity, which depends on the residence time in front of the barrier and therefore also the rack length, such that  $\alpha_f = \arccos(V_n/v_f) = \arccos(0.88/1.00) \approx 28^\circ$  (details in Pavlov, 1989 and Ebel, 2016). Ruggles and Ryan (1964) described several studies investigating the effect of  $U_o$  on the fish guidance efficiency of Louvers. They found no variations for large  $U_o = 0.60\text{--}1.0$  m/s, but a reduced guidance efficiency of salmon smolts for small  $U_o = 0.30\text{--}0.50$  m/s, which can be explained by smaller turbulences and therefore a reduced behavioral guidance effect. Turnpenny and O’Keeffe (2005) suggested to design angled racks so that  $V_n$  does not exceed the 90<sup>th</sup> percentile of the sustained swimming speed ( $t = 200$  min), based on the smallest fish and the lowest water temperatures, at which fish are likely to encounter the barrier. Thereby, 90% of the downstream moving fish could swim against  $V_n$  for up to 200 min, without getting impinged. For salmonids with  $TL \geq 10$  cm, Turnpenny and O’Keeffe (2005) recommended  $V_n \leq 0.75$  m/s and for cyprinids (except bream) with  $TL \geq 5$  cm  $V_n \leq 0.22$  m/s. The sustained swimming speed of other fish species can be calculated with Eq. (2.9)–(2.11). Turnpenny and O’Keeffe (2005) pointed out that racks should be designed with an over-capacity of at least 20% to account for partial clogging, which increases  $V_n$ . The Environment Agency (2009) recommended to account for partial clogging of 50% for manually cleaned racks and 10% for

racks with automated RCMs. In the following, the approach of Turnpenny and O’Keeffe (2005) is explained on the basis of an example. Assuming that  $TL = 10$  cm and  $T = 5$  °C are decisive, the sustained swimming speed ( $t = 200$  min) of fish is  $v_f = 0.38$  m/s and  $v_f = 0.28$  m/s for rheophilic (Eq. 2.9) and non-rheophilic (Eq. 2.10) species, respectively. At a diversion HPP with  $V \approx 0$  m/s and  $U_o = 0.60$  m/s,  $\alpha = \arcsin(V_n/U_o)$  (Eq. 3.1). Following Turnpenny and O’Keeffe (2005),  $V_n = v_f$  and thereby  $\alpha = \arcsin(v_f/U_o)$ , if partial clogging is neglected. This means that an HBR with  $\alpha = \arcsin(0.38/0.60) \approx 39^\circ$  could be installed in rivers with rheophilic species only and  $\alpha = \arcsin(0.28/0.60) \approx 28^\circ$  in rivers with non-rheophilic species. In contrast, some guidelines in Switzerland and Germany demand  $U_o \leq 0.5$  m/s, without distinguishing between target fish species (e.g. Hefti, 2012; LUBW, 2016). The design flow velocity is therefore independent of  $\alpha$ , which strongly limits the application of HBRs and other fish protection measures as  $U_o > 0.5$  m/s at many existing HPPs. Ebel (2016) pointed out that this approach is not very suitable and it is, from a biological and economic point of view, better to design HBRs as a function of the fish swimming capabilities and  $V_n$ . By comparing different approaches, Ebel (2016) recommended to use the model of Turnpenny and O’Keeffe (2005) to design  $\alpha$  of HBRs as it is most conservative. Adam *et al.* (1999) conducted live fish tests at a rack with vertical bars and  $s_b = 20$  mm, which was installed rectangular to the flow ( $\alpha = \gamma = 90^\circ$ ), such that  $V_n = U_o$ . They observed that eels could free themselves after getting impinged at the rack for water temperatures of 14 °C and  $U_o \leq 0.5$  m/s. For  $U_o > 0.5$  m/s, only physiological active and strong eels managed to free themselves after rack impingement and escaped upstream. In contrast, salmon smolts did not get impinged even for  $U_o = 1.0$  m/s. Another commonly used criterion demands that the ratio of  $V_p$  and  $V_n$ , which is termed Fish Guidance Capacity (FGC) in the following, is larger than 1 ( $V_p/V_n > 1$ ; NMFS, 1997; Courret and Larinier, 2008; Raynal *et al.*, 2013a; Vowles *et al.*, 2013), leading to  $\alpha < 45^\circ$ . Thereby, downstream moving fish which follow the main flow do not get impinged at the rack, but are guided towards the bypass. At HPPs with negligible transversal flow ( $V \approx 0$  m/s), FGC can be calculated as  $V_p/V_n = 1/\tan(\alpha) = \cot(\alpha)$  (Eq. 3.1 and 3.2). Considering these criteria, Ebel (2016) recommended to install HBRs at typical HPPs with a common fish species composition with  $\alpha = 20\text{--}40^\circ$ , which is similar to design guidelines in parts of Germany ( $\alpha \leq 30^\circ$ , LUBW, 2016) and Switzerland ( $\alpha \leq 45^\circ$ , Hefti, 2012).

### 3.4.2 Bypass design

The bypass design is crucial to efficiently guide downstream moving fish around HPPs. Bypasses have to be designed such that fish can find the entrance and move downstream with little delay and a small injury risk, while operational challenges should be reduced. Distinction is made between open channel bypasses and pressurized pipe bypasses. The latter is not recommended for practical application as it is subject to clogging, especially for small pipe diameters and bend radii (Engler and Adam, 2014; Ebel, 2016). Barriers installed frontal, non-oblique to the main flow may hinder fish from entering the turbines, but they do not guide them towards a specific location. Thus, the bypass inlet is only found by time-consuming search movements or by coincidence. In contrast, fish are guided towards the downstream end of angled barriers, such

that bypasses should be installed directly at the downstream rack end (e.g. Bates and Vinsonhaler, 1957; Pavlov, 1989; Odeh and Orvis, 1998; Turnpenny and O’Keeffe, 2005; Ebel, 2016). The displacement of the bypass openings from the downstream rack end, as in the example of the residual flow HPP Schiffmühle in Fig. 3.3, may lead to reduced guidance efficiencies, as it is difficult for fish to find the bypass entrance. Open channel bypasses which extend across the entire flow depth are also referred to as full depth open channel bypasses. They are advantageous, as they are accessible for all downstream moving fish, without requiring a change of their swimming depth (Ebel, 2016). The downside is that they require a large bypass discharge  $Q_{by}$  or lead to very low flow velocities at the bypass entrance, which is considered unfavorable for fish guidance (e.g. Ducharme, 1972). In practical applications, bypass inlets typically consist of openings in different flow depth, such that suitable downstream passage corridors are offered for bottom and surface-oriented fish species, while  $Q_{by}$  is limited to reduce production losses. The minimal relative bypass discharge, defined by Eq. (3.3), should be in the range of  $Q_{by,rel} = 2\text{--}5\%$  for angled racks and  $Q_{by,rel} = 5\text{--}10\%$  for racks installed frontal, non-oblique to the main flow (Larinier, 1998; Odeh and Orvis, 1998; Sheridan *et al.*, 2014; Ebel, 2016). The fish passage engineering design criteria of the U.S. Fish and Wildlife Service, Northeast Region, demand a relative bypass discharge of  $Q_{by,rel} = 5\%$  or an absolute bypass discharge of  $Q_{by} = 0.70 \text{ m}^3/\text{s}$ , whichever is larger (USFWS, 2017).

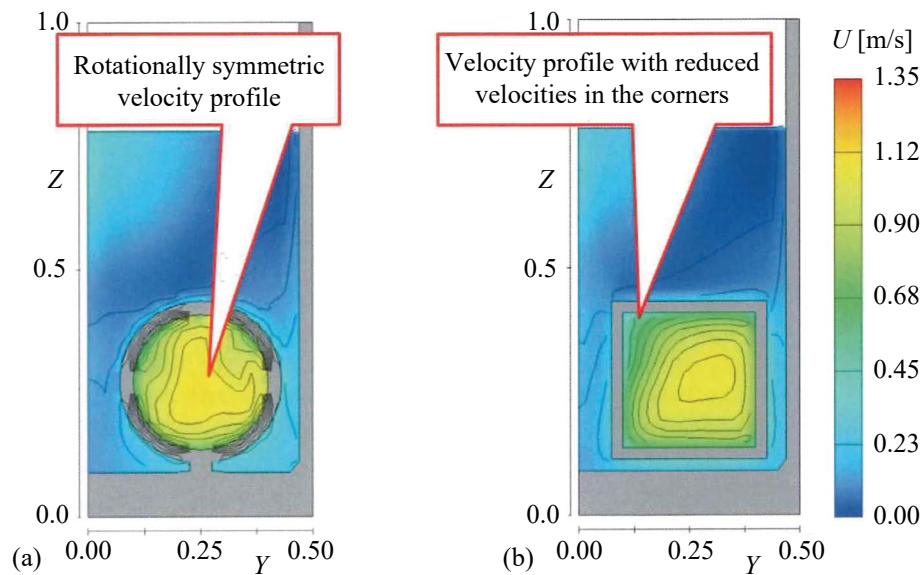
$$Q_{by,rel} = Q_{by}/Q_d \quad (3.3)$$

Fish favor bypass entrances with little turbulences and continuous flow accelerations, while they generally avoid steep velocity gradients (NMFS, 1997; Haro *et al.*, 1998; Turnpenny and O’Keeffe, 2005; Kemp *et al.*, 2006; Ebel, 2016). To minimize turbulences and flow separation zones at the inlet, bypasses are ideally aligned in the extension of the rack axis, which is often difficult to realize at existing HPPs. Bypass designs which require a sharp direction change of downstream moving fish, such as in the example in Fig. 3.3b, should be avoided in any case, as they are less frequently accepted (Lehmann *et al.*, 2016). If the flown-through cross section at the bypass inlet is limited with an installation such as a restrictor (cf. Fig. 3.2), a downstream ramp with an inclination angle of  $\gamma = 10\text{--}30^\circ$  is needed to control the discharge and to ensure gradual flow acceleration (Ebel, 2016). The discharge should not be controlled by reducing the size of the bypass openings, as this would cause steep velocity gradients, especially at HPPs with large hydraulic heads. Instead, the dimensions of the bypass openings have to be designed to account for the largest and most demand fish species and are typically 0.40–0.60 m wide and 0.60–0.90 m high (Ebel, 2016). Larinier and Travade (2002) recommended a minimal width and height of bypass openings of 0.40–0.50 m, which also applies to the weir head of surface openings (cf. Fig. 3.2). If bypass openings are narrower, fish are reluctant to use them for downstream passage (Larinier and Travade, 2002). The absolute mean flow velocities at the bypass inlet should be in the range of  $U_{by,in} = 0.30\text{--}1.50 \text{ m/s}$  (Ebel, 2016). If the bypass inlet does not extend across the whole water column,  $U_{by,in}$  refers to the velocities in the bypass openings and not to the average over the entire cross section. The continuous flow acceleration

towards the bypass can be described as the velocity ratio of the bypass inlet to mean approach flow velocity to

$$VR = U_{by,in}/U_o. \quad (3.4)$$

For salmon smolts at Louvers, Ruggles and Ryan (1964), Ducharme (1972), and Turnpenny and O’Keeffe (2005), recommended  $VR \geq 1.4$ ,  $VR \geq 1.0$ – $1.5$ , and  $VR \approx 1.4$ , respectively. On the basis of multiple studies, USBR (2006) suggested  $VR = 1.0$ – $1.5$  not only for salmon smolts, but also for brown trout and white catfish. NMFS (1997) proposed that  $U_{by,in}$  should be equal to or exceed the maximal flow velocity at the downstream rack end. Turnpenny and O’Keeffe (2005) recommended to install multiple bypasses at long racks. A rack was defined as long, if fish needed more than 60 s to swim from the upstream rack end to the bypass, assuming a swimming velocity along the rack equal to  $V_p$  (Nordlund, 2008). Monitoring campaigns showed that the bypass design is also important to prevent injuries (e.g. Zaugg and Mendez, 2018; Wagner *et al.*, 2019b). To ensure safe bypass passage, Travade and Larinier (1992) recommended not to exceed flow velocities of 12 m/s. Rainey (1985) suggested to limit bypass flow velocities to 3 m/s, because higher velocities can induce stress and mechanical injuries and may increase the predation risk. Ebel (2016) recommended to generally limit flow velocities at the bypass outlet to 4.5 m/s, but 7–8 m/s are acceptable for overflowing water if the downstream flow depth is sufficient. Bypasses should be designed as straight as possible, but if site-specific limitations require curvatures, the radii should be more than five times the bypass width and height (NMFS, 1997; Ebel, 2016), and the radii should not be smaller than 3 m (Turnpenny and O’Keeffe, 2005). The flow velocity in the curvature should not exceed the burst swimming speed of fish, such that they can swim against the flow in case of contact with the bypass walls (Ebel, 2016). To avoid injuries, the minimal downstream depth in the tailwater should be one quarter of the differential head, but at least 0.9 m (Odeh and Orvis, 1998; DWA, 2004). By conducting live fish tests, Lehmann *et al.* (2016) found that especially salmon smolts prefer rectangular over circular bypass openings. However, many fish recovered in the corners of the rectangular bypass with reduced flow velocities (Fig. 3.6b). After resting, some of them swam upstream again and therefore did not successfully pass the bypass. As a result of the rotationally symmetric velocity profile without low flow velocity zones, this behavior was not observed for circular bypasses (Fig. 3.6a). Thus, Lehmann *et al.* (2016) recommended rectangular bypass inlets with a smooth transition to a circular pipe bypass. However, it should be considered that such a bypass is likely to partially clog in prototype application.

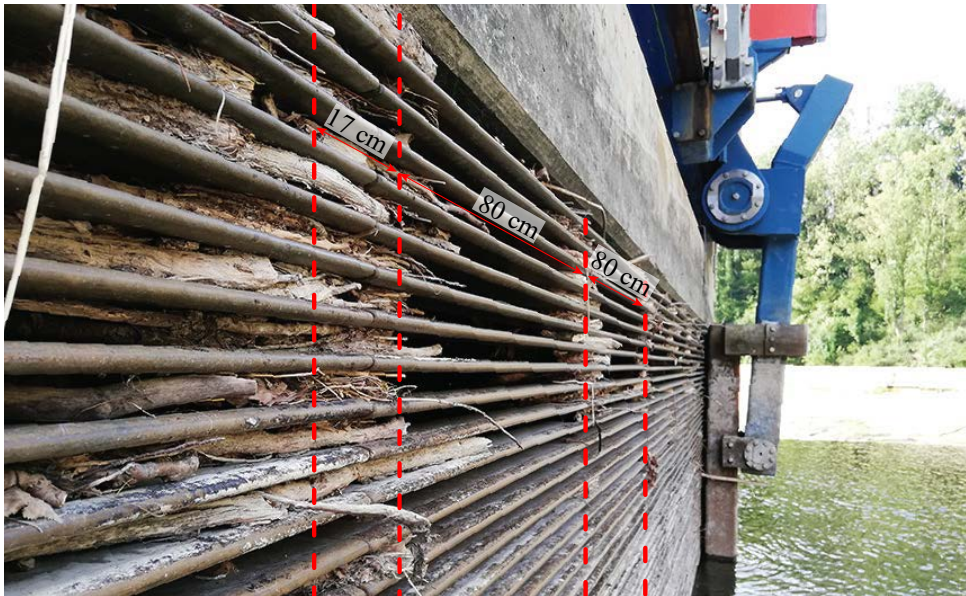


**Fig. 3.6:** Velocity profiles at (a) a circular and (b) a rectangular bypass opening (adapted from Lehmann *et al.*, 2016)

### 3.5 Rack cleaning machines and operational aspects

One of the main challenges at HBR-BSs is to prevent clogging, which requires modern and well-engineered RCMs. Figure 3.7 shows the HBR of the residual flow HPP Schiffmühle after five years of operation during drawdown due to reconstruction works at the weir. The RCM was not able to prevent permanent clogging, such that small branches accumulated particularly at the vertical tie-bars, which were installed every 80 cm. However, at the conjunction of two rack fields, the distance between two vertical tie-bars reduced to 17 cm, which led to large accumulation zones with small branches (Fig. 3.7). RCMs of HBRs can be either equipped with a plastic scraper (Fig. 3.8a), a brush (Fig. 3.8b), or a rake (Fig. 3.8c). The latter is strongly recommended as it increases the cleaning efficiency and prevents permanent clogging (Ebel, 2016). The rakes of RCMs should protrude into the bar gaps for at least 2 cm (Jank, 2018). Modern RCMs are typically controlled by flow depth measurements in front of and behind the HBR. If a certain threshold is exceeded, the RCM automatically starts cleaning the HBR. Most HBR-BSs are equipped with a flushing gate (cf. Section 3.2), which can be combined with the bypass and which opens automatically when the RCM reaches the downstream rack end. If designed adequately, most floating debris can be directly flushed downstream, but a hydraulic loading crane with a lifting capacity >3 tons should be installed to be able to remove large floating debris like tree trunks manually (Ebel, 2016). During flushing, the bypass discharge typically increases by a multiple for a short time, which may also favors fish downstream passage (cf. Section 3.7.4; HPP Widdert).





**Fig. 3.7:** Clogged vertical tie-bars (indicated with red dashed lines) of the HBR at the residual flow HPP Schiffmühle during drawdown in July 2018 (Photo: J. Meister)



**Fig. 3.8:** RCMs of HBRs with (a) a plastic scraper (residual flow HPP Schiffmühle), (b) a brush (residual flow HPP Rühlig, 47°23'56.4"N, 8°03'07.3"E), and (c) a rake (HPP Hard) (Photos: J. Meister; adapted from Meister *et al.*, 2018a)

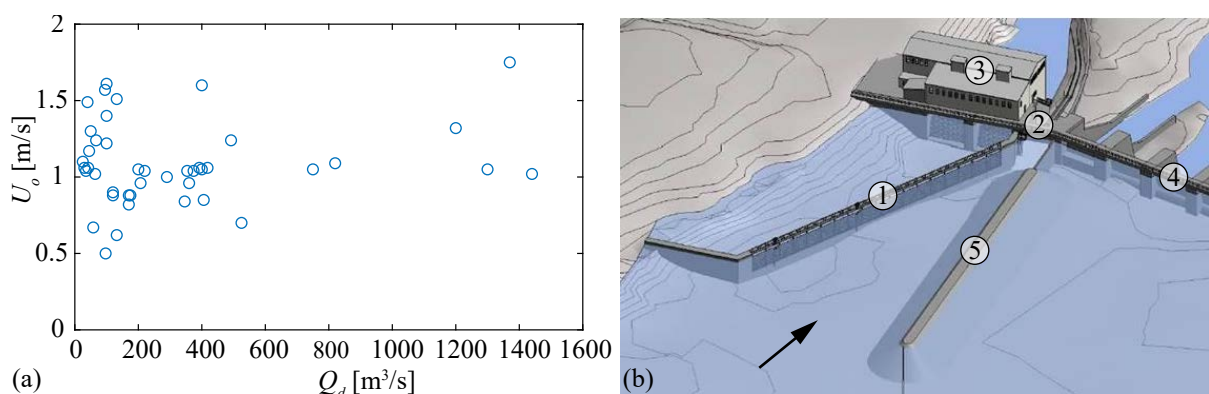
If HBRs are installed in rivers with fine sediments (e.g. sand), sufficiently strong designed RCMs can resuspend sediments, such that they are flushed downstream through the bypass or the turbines. The resuspension process can be enhanced with sediment clearing plates, which should cover the height of the bottom overlay (Ebel *et al.*, 2018). The operating experience of HBR-BSs in gravel bed rivers is very site-specific and therefore hard to generalize. However, an operator of a large HBR-BS installed in the Lech River, Germany, with high gravel transport rates reported that the RCM was designed with a pressure thrust of three tons to remove gravel depositions. The operational experiences are very good and the sediments remain in the river, as the HBR-BS was installed as a side intake. Flushing sediment depositions downstream through

the flushing gate is limited to fine sediments and the area directly in front of the HBR, which was numerically investigated for a small HPP by Scharf (2012). A new concept, which was first installed in 2018 at HPP Schennerpolster on the Ischl River (47°42'56.0"N, 13°32'19.3"E), Austria, includes a separate sediment flushing channel, installed below the HBR to remove gravel depositions, which worked well during its first year of operation (Gruber, 2019a). An echo sounder mounted on the RCM is tested to measure the sediment deposition height, which can be used to automatically operate the flushing gate when necessary (Gruber, 2019a). In mountainous environments, it is also possible that sediments clog between bars. Although only little operational experiences of HBR-BSs in mountainous environments is available, the clogging probability with sediments can likely be reduced by an optimized bar shape (cf. Section 3.4.1), a bottom overlay, a sediment flushing system, and a sufficiently strong designed RCM with a rake, which is able to remove clogged sediments. No operational problems were reported by operators regarding the bypass, if it was designed according to current design recommendations (e.g. no pipe bypass, cf. Sections 3.2 and 3.4.2).

### 3.6 Limitations

While HBR-BSs can be installed at most small to medium-sized newly constructed HPPs, the available space, prevailing flow conditions, and other restrictions such as monument conservation may limit the application of HBR-BSs at existing HPPs. Up to now, most HBR-BSs were installed at small to medium-sized HPPs with design discharges of  $Q_d < 100 \text{ m}^3/\text{s}$  (cf. Section 3.2). Challenges arising by the installation of HBR-BSs at larger HPPs include the increased hydraulic load, the high investment costs, a larger damage in case of fatigue, and potentially larger  $U_o$  which may cause fish impingement. It is also difficult to ensure constant small  $s_b$  due to subsidence and distortions, inspections of the HBR are hardly possible as it cannot be dewatered, multiple bypasses and RCMs may be needed, and the technical feasibility of RCMs is limited to certain flow depth. Despite these challenges, HBRs were realized at HPPs with  $Q_d = 120 \text{ m}^3/\text{s}$ ,  $Q_d = 95 \text{ m}^3/\text{s}$ , and  $Q_d = 48 \text{ m}^3/\text{s}$  with  $s_b \leq 45 \text{ mm}$ ,  $s_b = 20 \text{ mm}$ , and  $s_b = 10 \text{ mm}$ , respectively (cf. Section 3.1). At large HPPs, increased hydraulic load can be diverted into piers between the rack fields. The absolute investment costs increase with  $Q_d$  of the HPP (cf. Section 3.1), but the specific costs per produced electricity are not assumed to be higher than at small HPPs. Large approach flow depths require high HBRs, which are subject to subsidence and distortions, potentially leading to jamming of the RCM rake, especially for  $s_b < 20 \text{ mm}$ . The HBR height is also limited by the driving torque of the RCM. One of the largest RCMs is installed at HPP Dietikon, which prevents the 5.9 m high HBR from clogging (cf. Fig. 3.1b; Balestra and Scherngell, 2019). The approach flow velocity at large HPPs may be larger than at small HPPs, which limits the application of HBR-BSs, especially if  $U_o \leq 0.5 \text{ m/s}$  is demanded (cf. Section 3.4.1). However, a survey conducted by Meusburger (2002) at large Swiss run-of-river HPPs ( $Q_d \geq 10 \text{ m}^3/\text{s}$ ) showed that  $U_o$  hardly increases with  $Q_d$  (Fig. 3.9a). The average approach flow velocity  $U_o$  of 43 HPPs was calculated from  $V_n$  in the unobstructed rack plane of traditional trash racks, that is,  $U_o = V_n/\sin(\gamma)$ . The approach flow

velocities  $U_o$  in Fig. 3.9a cannot directly be compared with  $U_o$  at HBRs, as HBRs are installed further upstream in areas with smaller velocities than traditional trash racks, but the correlation between  $Q_d$  and  $U_o$  is comparable. Despite all limitations and challenges, it is likely that HBR-BSs are installed at larger HPPs in the near future, as well-proven alternatives are missing (cf. Section 2.4). As an example, it is considered to equip HPP Edsforsen on the Klarälven River (60°03'55.3"N, 13°31'34.9"E), Sweden, with  $Q_d = 195 \text{ m}^3/\text{s}$  with a 65 m long and 5.2 m high HBR with  $s_b = 15 \text{ mm}$  and  $\alpha = 30^\circ$  (Fig. 3.9b; Norconsult, 2017; Lindberg and Hagman, 2018). Figure 3.9b visualizes this HBR-BSs, including ① the HBR itself, ② the bypass, ③ the power house, ④ the weir, and ⑤ a dam separating the HBR from the weir. The latter is planned to optimize flow conditions towards the inlet, which was investigated numerically (Norconsult, 2017; Lindberg and Hagman, 2018).



**Fig. 3.9:** (a) Approach flow velocity  $U_o$  as a function of the design discharge  $Q_d$  at large Swiss run-of-river HPPs (data from Meusburger, 2002) and (b) visualization of the HBR-BS at HPP Edsforsen including ① HBR, ② bypass and flushing gate, ③ power house, ④ weir, and ⑤ dam separating the HBR from the weir (adapted from Norconsult, 2017 cited in Lindberg and Hagman, 2018)

## 3.7 Laboratory studies and monitoring campaigns

### 3.7.1 Velocity fields

This paragraph gives an overview of literature about the velocity fields at HBRs. It was first published in a slightly modified form in Meister *et al.* (2020c). The velocity fields upstream of HBRs are important as they affect the guidance of fish, floating debris, and sediments, while the downstream velocity fields may affect the turbine efficiency. Maager (2016) and Albayrak *et al.* (2019) experimentally investigated HBRs in a sectional 1:2 Froude-scaled physical model. The parameter matrix contained two bar shapes (rectangular and one-side rounded bars), two approach flow angles ( $\alpha = 30^\circ$  and  $45^\circ$ ), three blocking ratios ( $BR = 0.33, 0.39, 0.55$ ), and various overlay configurations. Maager (2016) found that the blocking ratio was hardly affecting the velocity field in the range of  $BR = 0.39$ – $0.55$ . Szabo-Meszaros *et al.* (2018) investigated HBRs with  $\alpha = 30^\circ$ ,  $s_b = 15 \text{ mm}$ , and a bar thickness of  $t_b = 8 \text{ mm}$  with rectangular and hydrodynamic bars. Neglecting the effect of the vertical tie-bars, the blocking ratio was  $BR \approx t_b / (s_b + t_b) = 0.35$ . The model included a bypass with a relative width of 10% of the model flume and a fixed,  $30^\circ$ -inclined bypass-ramp. The relative bypass discharge was  $Q_{by,rel} = 4\%$  for rectangular and  $Q_{by,rel} = 3.1\%$  for hydrodynamic bars. The authors did not



find any significant differences in the velocity patterns between the bar shapes. Berger (2018) conducted a laboratory study on HBRs with rectangular bars. A lateral opening next to the rack with a relative width of 12.5% represented a bypass. She focused on live fish tests and measured flow fields for different approach flow velocities. According to her results, HBRs without overlays had no effect on the vertical velocity profile. The transversal velocity components upstream of the rack were small, and the flow slightly accelerated along the rack. De Bie *et al.* (2018) investigated racks with  $\alpha = 30^\circ$  made of horizontally and vertically aligned wedge-wire bars ( $s_b = 6$  mm,  $t_b = 3$  mm,  $BR \approx 0.33$  without accounting for the vertical tie-bars) in a laboratory flume for two different discharges. The bypass was unregulated and extended over 10% of the channel width. However, the bypass discharge was not quantified. The authors found that the streamwise velocity component at racks with horizontal bars was continuously increasing from the rack head to the downstream rack end (measurements 5 cm above bottom;  $U \approx 0.14$  m/s to  $U \approx 0.21$  m/s for an average approach flow velocity from continuity of  $U_o = 0.17$  m/s and  $U \approx 0.32$  m/s to  $U \approx 0.47$  m/s for  $U_o = 0.40$  m/s). Raynal *et al.* (2013b) studied a sectional model of vertically inclined racks with inclination angles in the range of  $\gamma = 15\text{--}90^\circ$ . Cylindrical spacers were used to realize different bar spacings. They reported locally reduced flow velocities downstream of the horizontal tie-bars/spacers. This effect was largest for the most downstream tie-bar/spacer and for shorter racks (large inclination angles). A number of recent laboratory studies involved angled racks with vertical bars with larger bar spacing, including (a) angled bar racks (ABR; Fig. 2.15a; Chatellier *et al.*, 2011; Raynal *et al.*, 2013a), (b) Louvers (Fig. 2.15b; Shepherd *et al.*, 2007), (c) modified bar racks (MBR; Fig. 2.15c; Kriewitz, 2015; Albayrak *et al.*, 2018, 2020), and (d) curved-bar racks (CBR; Fig. 2.15d; Beck *et al.*, 2019a,b; Beck, 2020). Table 3.3 summarizes the studies described above. The total relative overlay height  $H_{Ov}$  is defined in Section 4.2.3.

**Table 3.3:** Overview of laboratory studies investigating velocity fields at fish guidance structures; S: sectional model of the rack without a bypass or weir, B: sectional model of the rack including a bypass, PW: physical model of a hydropower plant including the rack and a weir, and W: sectional model of the rack including a weir

Study	Rack	Angle $\alpha, \gamma$	BR	$H_{Ov}$	Layout
Maager (2016); Albayrak <i>et al.</i> (2019)	HBR	$\alpha = 30^\circ, 45^\circ$	0.33, 0.39, 0.55	0–0.30	S
Szabo-Meszaros <i>et al.</i> (2018)	HBR <sup>1</sup>	$\alpha = 30^\circ$	$\approx 0.35$	0	B
Berger (2018)	HBR	$\alpha = 30^\circ, 45^\circ, 55^\circ, 70^\circ$	0.32–0.57	0	B
De Bie <i>et al.</i> (2018)	HBR <sup>1</sup>	$\alpha = 30^\circ$	$\approx 0.33^2$	0	B
Raynal <i>et al.</i> (2013b)	inclined	$\gamma = 15–90^\circ$	$\approx 0.25–0.50^2$	0	S
Raynal <i>et al.</i> (2013a)	ABR	$\alpha = 30^\circ, 45^\circ, 60^\circ, 90^\circ$	$\approx 0.25–0.50^2$	0	S
Chatellier <i>et al.</i> (2011)	ABR	$\alpha = 30^\circ, 45^\circ, 60^\circ$	$\approx 0.25–0.50^2$	0	S
Kriewitz (2015); Albayrak <i>et al.</i> (2018, 2020)	MBR, Louver	$\alpha = 15^\circ, 30^\circ, 45^\circ$	0.04, 0.08, 0.17	0.11	S, B, PW
Beck <i>et al.</i> (2019a,b); Beck (2020)	CBR	$\alpha = 15^\circ, 30^\circ, 45^\circ$	0.04, 0.08, 0.17	0–0.30	S, W
Present study	HBR	$\alpha = 30^\circ, 45^\circ, 90^\circ$	0.28, 0.35, 0.49	0–0.40	S, W

<sup>1</sup> Other rack types were investigated as well, but only HBRs are relevant for the present study

<sup>2</sup> Blocking ratios estimated as  $BR \approx t_b / (s_b + t_b)$ ; tie-bars were neglected due to lack of information

When analyzing velocity fields upstream of HBRs, it should be considered that they may also be affected by spillway discharge, depending on the exact HPP layout. Overall, the literature review showed that a systematic study was missing, in which the effect of different parameters, such as the bar shape,  $\alpha$ ,  $s_b$ , and overlays on the velocity fields, was systematically investigated for HBRs. Additionally, all laboratory studies mentioned above, except Kriewitz (2015) and Beck (2020), were limited to straight laboratory flumes with constant channel width, thereby typically representing diversion HPPs. However, the HPP layout plays an important role to the approach flow field of HBRs and is very variable in practical applications (cf. Sections 3.2 and 3.3).

### 3.7.2 Head losses

Only a few studies focused on the head losses of HBRs, which are briefly mentioned in the following. This paragraph was first published in a slightly modified form in Meister *et al.* (2020b). The hydraulic losses of different HPP intake rack types have so far mainly been investigated in physical models. Kirschmer (1925) conducted 1:1 scaled laboratory experiments with trash racks oriented frontal, non-oblique and inclined to the approach flow ( $\gamma = 30–90^\circ$ ; cf. Fig. 2.11a,b) with different bar shapes and proposed an equation to estimate the rack head loss coefficient. Other authors such as Zimmermann (1969), Meusburger (2002), and Raynal *et al.* (2013b) built upon the equation of Kirschmer (1925) by including characteristics such as partial clogging, overlays, and angled approach flows. However, up to now, proof is missing that these

equations, developed for traditional trash racks with typically vertical bars, are suitable for head loss estimations of HBRs. Therefore, Maager (2016) and Albayrak *et al.* (2019) experimentally investigated the hydraulics of HBRs in a 1:2 Froude-scaled model for a wide range of basic parameters, including  $\alpha = 30^\circ$  and  $45^\circ$ ,  $s_b = 10, 20$ , and  $30$  mm (prototype dimensions), two different bar depths, and various overlay configurations. Their study was limited to rectangular bars and rectangular bars with a rounded tip (“one-side rounded bars”). The latter were investigated for  $\alpha = 30^\circ$  only. A similar study on a Froude scale of 1:2 was conducted by Lemkecher *et al.* (2020), including  $\alpha = 30^\circ, 45^\circ, 60^\circ$ , and  $90^\circ$ ,  $s_b = 10\text{--}40$  mm (prototype dimensions), and two different bar shapes. Böttcher *et al.* (2019a) studied angled racks with horizontally aligned, cylindrical bars without overlays in a 1:2 Froude-scaled model. Racks with  $\alpha = 30^\circ, 45^\circ$ , and  $90^\circ$  and  $s_b = 10, 20$ , and  $30$  mm (prototype dimensions) were investigated. All laboratory studies presented so far focused on sectional models, where only a section of the rack was investigated. Other associated structures such as a bypass for fish downstream passage or an adjacent weir were not included in these models. Some studies like Berger (2018) and Szabo-Meszaros *et al.* (2018) focused on physical models of HBRs including a bypass, which makes it difficult to compare the head loss coefficients obtained in these studies with the losses of sectional models. Up to now, a study focusing on the head losses of HBRs for a wide parameter range and different HPP layouts was missing. To precisely predict the head losses at HPPs, it is important to account for different bar shapes,  $\alpha$ ,  $s_b$ ,  $D_b$ , bottom and top overlays, and different HPP layouts (cf. Section 3.2).

### 3.7.3 Ethohydraulic studies

Multiple ethohydraulic studies at HBR-BSs were conducted in recent years, which are briefly described in this section. It is not limited to classical HBR-BSs, as investigated in the present thesis, but also includes other barriers equipped with horizontal bars such as the flexible fish fence.

#### Holzner and Blankenburg (2007): racks with horizontal and vertical bars

Holzner and Blankenburg (2007, 2008) studied the behavior of brown trout (*Salmo trutta forma fario*) and grayling (*Thymallus thymallus*) in ethohydraulic experiments at different rack types. The experiments were conducted in a 7.1 m long, 1.25 wide, and  $h_o \approx 0.4$  m deep outdoor flume with a gravel bed at the hydraulic test facility Obernach of the Technical University of Munich. Wooden racks with either horizontal bars (HBRs) or vertical bars with a clear bar spacing of  $s_b = 20$  mm were installed rectangular to the approach flow ( $\alpha = 90^\circ$ ) and no bypass was installed as the goal of the experiments was to judge the protection efficiency only. The approach flow velocity was in the range of  $U_o = 0.2\text{--}0.3$  m/s. Fish could either pass through the rack or stay in the headwater. The total length, width, and height of the tested fish were in the range of  $TL = 6.2\text{--}22.0$  cm,  $w_f = 0.3\text{--}2.4$  cm, and  $h_f = 0.7\text{--}3.8$  cm for trout and  $TL = 11.4\text{--}20.2$  cm,  $w_f = 0.7\text{--}1.4$  cm, and  $h_f = 1.1\text{--}2.6$  cm for grayling. All fish approached the racks with positive rheotaxis and most fish kept a distance of 5–10 cm to the racks. Due to experimental constrictions, the different rack types could not be conclusively evaluated, but the

experiments indicated a better protection of the rack with horizontal bars. Although the number of individuals used per size class were similar, 70% of the brown trout which passed through the HBR had a  $TL < 12.5$  cm, whereas only 30% had a  $TL \geq 12.5$  cm. Nevertheless, several rack passages of trout and grayling with  $TL = 18\text{--}20$  cm were observed, which were too high to pass the rack in a regular swimming position, and must have therefore turned to their sides to pass through the HBR. Holzner and Blankenburg (2008) concluded that HBRs with  $s_b = 20$  mm cause avoidance reactions to fish with  $TL = 12\text{--}14$  cm, but offer full protection only for fish with  $TL > 18\text{--}20$  cm.

### **Berger (2018): horizontal bar rack bypass systems**

Berger (2018) conducted ethohydraulic laboratory experiments with Atlantic salmon smolts and European eels at HBR-BSs with rectangular bars for different approach flow angles ( $\alpha = 30, 45, 55, 70^\circ$ ), clear bar spacings ( $s_b = 10, 18, 30$  mm), and approach flow velocities ( $U_o = 0.4, 0.5, 0.7, 0.8$  m/s). The lowest 5 cm of the HBRs were physically blocked by a beam, which acted as a bottom overlay (cf. Fig. 7.29a,c). The full depth open channel bypass was not separated from the downstream channel with a wall, meaning that the discharge and the flow velocities in the bypass could not be controlled independent of  $U_o$ . The behavior of eels was also studied at a hybrid barrier, where the HBR was combined with a low-voltage electric field (gpDC, Neptun system, company Procom). The HBR acted as the anode and a rack-parallel steel mesh as the cathode. The exact position of the steel mesh was not mentioned in Berger (2018), but it was estimated from a picture that the metal mesh was installed  $\approx 30$  cm downstream of the HBR (measured perpendicular to the HBR). The voltage was specified with 34–35 Volt, but further information about the pulse pattern and the development of the electric field is missing. In general, both salmon smolts and eels were well protected with the HBR for most configurations. Not a single salmon smolt passed through the HBR with  $s_b = 10$  mm and only two rack passages from 610 tested specimens were observed with  $s_b = 18$  mm (Berger, 2018). The salmon smolts were even well protected with  $s_b = 30$  mm, where only nine out of 182 salmon passed through the HBR. Berger (2018) mentioned that most eels had a total length of  $TL = 60\text{--}80$  cm, while some individuals were small with  $TL = 40$  cm. However, the number of individuals per size class remains unknown. Independent of  $\alpha$ ,  $U_o$ , and the electrification, no rack passages were observed for eels with  $s_b = 10$  mm and  $s_b = 18$  mm. Without electrification, 12.5%, 19.7%, and 13.5% of the eels passed through the HBR with  $s_b = 30$  mm for  $\alpha = 30^\circ, 45^\circ$ , and  $55^\circ$ , respectively. The number of rack passages was significantly reduced with the electrification for the same configurations to 0%, 2.0%, and 1.7%. Averaged over all  $\alpha$  with  $s_b = 30$  mm, the percentage of rack passages of eels was reduced from 15% without, to 1% with the electrification. Berger (2018) concluded that HBRs partially work as mechanical behavioral barriers besides their physical barrier effect and that rack passages can be reduced by the application of a low-voltage electric field for large  $s_b$ .

### De Bie (2017): horizontal bar rack bypass systems

De Bie (2017, Chapter 5) investigated the behavior of hatchery-reared, downstream moving juvenile chub (*Squalius cephalus*) and barbel (*Barbus barbus*) at HBR-BSs with  $s_b = 10$  mm, bars with a circular cross section, and  $\alpha = 30, 45^\circ$  in a  $w_o = 1.38$  m wide laboratory flume. The  $w_{by} = 0.14$  m wide full depth open channel bypass was unregulated and approach flow velocities of  $U_o = 0.19$  m/s and  $U_o = 0.36$  m/s were tested. Fish were acclimatized to the flow conditions for a minimum of twenty minutes and experiments lasted for up to one hour. Fish were tested in groups of five individuals and learning effects were precluded by testing each individual only once within the study. The different hydraulic conditions, fish biometry, and the fish response reactions are summarized in Table 3.4.

**Table 3.4:** Tested hydraulic conditions ( $U_o$ ,  $\alpha$ ), fish biometry ( $TL$ ,  $w_f$ ,  $h_f$ ), and the fish response reactions (bypass passage, rack passage, inactive) at an HBR-BS with  $s_b = 10$  mm;  $N$  represents the number of tested individuals (data from de Bie, 2017)

$U_o$ <sup>1</sup> [m/s]	$\alpha$ [°]	Fish species	$\overline{TL} \pm \sigma_{TL}$ [cm]	$\overline{w_f} \pm \sigma_{w_f}$ <sup>2</sup> [cm]	$\overline{h_f} \pm \sigma_{h_f}$ <sup>2</sup> [cm]	$N$ [–]	Bypass [%]	Rack [%]	Inactive [%]	Guidance <sup>3</sup> [%]
0.36	30	Chub	$8.83 \pm 0.75$	$0.82 \pm 0.09$	$1.49 \pm 0.15$	90	54.7	23.3	22.1	70.1
		Barbel	$8.42 \pm 0.71$	$0.80 \pm 0.08$	$1.23 \pm 0.12$	95	32.1	29.5	38.5	52.1
0.36	45	Chub	$8.62 \pm 0.82$	$0.80 \pm 0.10$	$1.44 \pm 0.17$	80	26.2	49.2	24.6	34.7
		Barbel	$8.17 \pm 0.75$	$0.77 \pm 0.08$	$1.19 \pm 0.12$	95	16.7	14.6	68.8	53.4
0.19	45	Chub	$8.53 \pm 0.61$	$0.79 \pm 0.07$	$1.43 \pm 0.12$	50	28.0	66.0	6.0	29.8
		Barbel	$9.31 \pm 0.57$	$0.89 \pm 0.06$	$1.38 \pm 0.10$	50	30.8	30.8	38.5	50.0

<sup>1</sup> Measured at mid-channel and mid-depth

<sup>2</sup> Calculated with Eq. (2.4) and (2.8)

<sup>3</sup> Calculated as the percentage of bypass passages from bypass and rack passages (excluding inactive fish)

Barbel and chub primarily swam close to the flume bottom and mostly approached the rack individually. All tested fish could physically pass through the HBR ( $w_f < s_b$ ) but only if they were turning to their sides as  $h_f > s_b$  (Table 3.4). For chub, the guidance efficiency was larger for  $\alpha = 30^\circ$  than for  $\alpha = 45^\circ$ , while  $\alpha$  did not affect the guidance efficiency of barbel (Table 3.4). Although a non-negligible share of fish of both species was guided by the HBR into the bypass, many fish passed through the rack with  $s_b = 10$  mm, such that de Bie (2017) concluded that HBR-BSs do not sufficiently guide juvenile cyprinids under the tested conditions.

### De Bie (2017) and de Bie et al. (2018): fine-spaced wedge-wire screens

De Bie (2017, Chapter 6) and de Bie et al. (2018) investigated the behavior of downstream moving juvenile chub (*Squalius cephalus*) at angled racks with  $\alpha = 30^\circ$  with vertically and horizontally aligned wedge-wire bars with  $s_b = 6$  mm. Discharges of  $Q_o = 0.09$  m<sup>3</sup>/s and  $Q_o = 0.15$  m<sup>3</sup>/s were tested for approach flow depths of  $h_o = 0.38$  m and  $h_o = 0.27$  m, respectively, leading to  $U_o = 0.17$  m/s and  $U_o = 0.40$  m/s in the  $w_o = 1.38$  m wide flume. The unregulated full depth open channel bypass was  $w_{by} = 0.14$  m wide. The acclimatization time was 20 min and fish were tested in groups of five, but each individual was used only once. An experiment lasted until all fish entered the bypass or after the maximal experimental duration of two hours. Despite

the small size ( $\overline{TL} = 10.8$  cm), fish were not able to physically pass through the rack. This study therefore focused on the guidance efficiency and the bypass acceptance. Total guidance was defined as the percentage of the number of bypass entries to the number of approaches. The rack with horizontal bars with  $U_o = 0.17$  m/s led to the highest total guidance of 25% and the least bypass rejections/refusals. With  $U_o = 0.40$  m/s, the total guidance was only 12%, indicating that juvenile chub avoid abrupt flow accelerations. De Bie *et al.* (2018) concluded that hydraulic conditions at racks provoke avoidance reactions of juvenile chub, but that they were lower for the rack with horizontal bars than with vertical bars for small  $U_o$ .

### **Carlsson (2019): horizontal bar rack bypass systems**

Carlsson (2019) studied the behavior of European eels at HBR-BSs in ethohydraulic experiments at the Vattenfalls laboratorium in Älvkarleby, Sweden. A 6.8 m long HBR with rectangular bars,  $\alpha = 30^\circ$ , and  $s_b = 15$  mm and 30 mm was installed in the 24 m long, 4 m wide, and 2 m deep flume. A 0.60 m wide and 0.50 m high bypass opening was positioned at the downstream rack end and a ramp with an inclination angle of  $\gamma = 30^\circ$  guided the eels from the bottom to the bypass opening. The water temperature was in the range of  $T = 8.5$ – $10.2$  °C and  $U_o = 0.7$  m/s. A PIT-tagging antenna and a trap were installed at the bypass outlet and cameras were used to study the fish behavior. However, some eels were observed escaping the trap, such that the trap catches might have underestimated bypass passages. The eels had an average total length of  $\overline{TL} = 84.5$  cm with  $\sigma_{TL} = 7.4$  cm, each rack configuration was tested four times with five eels per experiment, and learning effects were ruled out by testing each specimen only once. At each experiment, the eels were released from the acclimatization compartment in the flume center between 7 p.m. and 8 p.m, after an acclimatization time of 15 minutes. The experiments went on over night for 13.5 hours under constant low light (2–5 lux), corresponding to lighting conditions in the evening or night time. Eels could either stay upstream, pass through the HBR, enter the bypass, or combinations thereof. Eels were counted as a “successful passage” when they were either located by the PIT-tagging antenna or when they were found in the trap at the end of the experiment, while all other eels were counted as “unsuccessful passage”. No rack passages were observed with the cameras, but one eel was found behind the HBR after an experiment with  $s_b = 30$  mm, whereas there were no signs that any eel passed through the HBR with  $s_b = 15$  mm. However, it cannot be excluded that some eels were counted as “successful passage” after they passed through the HBR, when they swam upstream again and entered the bypass thereafter. A total of 100% and 95% of all tested eels were detected by the PIT-tagging antenna in the bypass for  $s_b = 15$  mm and  $s_b = 30$  mm, respectively, whereas the same percentages were 95% and 30% for counting eel catches in the bypass trap only. From his experiments, Carlsson (2019) concluded that HBR-BSs are suitable for guiding downstream migrating eels and that HBRs act not only as physical barriers, as eels were also well guided at HBRs with  $s_b = 30$  mm.

**Böttcher *et al.* (2019b) and Kammerlander *et al.* (2020): flexible fish fence**

The flexible fish fence consists of steel cables aligned horizontally with small  $s_b$ , similarly to the bars of HBRs. The guidance and protection efficiency of the flexible fish fence was investigated in a series of extensive ethohydraulic studies, which were reported by Böttcher *et al.* (2019b) and Kammerlander *et al.* (2020). The experiments were conducted in a 20 m long and 2 m wide outdoor flume with a gravel bed and constant approach flow depth of  $h_o = 0.5$  m. The flexible fish fence was tested with trout (brown and rainbow trout), chub, and grayling with  $s_b = 10, 20$  mm,  $\alpha = 20, 40^\circ$ , and  $U_o = 0.3, 0.5$ , and  $0.65$  m/s. The  $w_{by} = 0.25$  m wide full depth open channel bypass was controlled with a flap gate, such that the flow velocity in the bypass corresponded to  $U_o$  ( $VR = 1.0$ ). Each experiment was carried out with 25 individuals of the same species and most rack configurations were tested five times. The total length of the fish was in the range of  $TL = 10\text{--}20$  cm and the fish height of three quarters of all individuals was  $h_f \geq 20$  mm, such that they could pass the flexible fish fence only when turning to the side. All fish were PIT-tagged and antennas were installed in the bypass and behind the flexible fish fence. After an acclimatization time of 45 minutes in the acclimatization compartment, fish could swim around freely for the experimental duration of 60 minutes. Fish which were first detected inside the bypass or behind the rack were counted as bypass passages or rack passages, respectively. All other fish were classified as “headwater”, independent of their position within the headwater, which means that it was not distinguished between fish which swam close to the rack and fish which stayed far upstream for the whole experimental duration. The results of the ethohydraulic experiments of Kammerlander *et al.* (2020) are summarized in Table 3.5 for different  $s_b$ , which had a larger effect than  $\alpha$  and  $U_o$ .

**Table 3.5:** Percentage of fish responding with a rack passage, bypass passage, or stayed in the headwater for  $s_b = 10$  mm and  $s_b = 20$  mm, independent of  $\alpha$  and  $U_o$  (data from Kammerlander *et al.*, 2020)

	Response [%] for $s_b = 10$ mm			Response [%] for $s_b = 20$ mm		
	Rack	Bypass	Headwater	Rack	Bypass	Headwater
Chub	0	63	37	17	37	46
Grayling	$\approx 1$	19	81	74	6	20
Trout	0	46	54	41	14	45

With  $s_b = 10$  mm, only five out of 1346 individuals passed through the rack, leading to a fish protection efficiency of  $FPE \approx 100\%$  for all species (Table 3.5). In contrast, only 6%, 14%, and 37% of grayling, trout, and chub, respectively, entered the bypass for  $s_b = 20$  mm (Table 3.5). Especially grayling were poorly protected with  $s_b = 20$  mm, where three quarters of all specimens passed through the flexible fish fence. Larger flow velocities increased fish protection, which might be a result of the increased cable vibrations, presumably triggering avoidance reactions (Kammerlander *et al.*, 2020). Larger  $U_o$  led to increased velocity changes and turbulences in the bypass, which negatively affected the bypass acceptance (Kammerlander *et al.*, 2020). In summary, fish with  $TL = 10\text{--}20$  cm could only be sufficiently protected with the flexible fish

fence for  $s_b = 10$  mm, but not for  $s_b = 20$  mm.

### **Brinkmeier *et al.* (2017) and Tutzer *et al.* (2019b,a): fish protector**

To enhance the protection efficiency of the flexible fish fence for larger  $s_b$ , the steel cables of the flexible fish fence were electrified with 80 Volt pulsed direct current (gpDC, Neptun system, company Procom; Brinkmeier *et al.*, 2017; Tutzer *et al.*, 2019a,b). The setup and methods were very similar to the experiments at the flexible fish fence and are therefore not repeatedly described. The experiments were conducted with  $\alpha = 20, 40^\circ$ ,  $s_b = 30, 60$  mm, without electrification for reference, with a small electric field reaching  $\approx 10$  cm upstream, and a large electric field reaching  $\approx 20$  cm upstream, leading to a total of twelve configurations. These configurations were assessed in terms of the passage rate, which was defined as the percentage of fish passing through the fish protector from all tested fish. Tutzer *et al.* (2019b) described that fish were approaching the fish protector with positive rheotaxis and showed a clear and controlled escape reaction towards the upstream. Although the passage rate did not vary significantly between the smaller and larger electric field, the latter was advantageous because it offered more room for reactions to the electric field and therefore led to less escape reactions towards the rack. The fish size ( $TL = 10\text{--}25$  cm) and  $\alpha$  did not significantly affect the rack passage rate. Without an electric field, the median passage rate was 7% and 20% for  $s_b = 30$  mm and  $s_b = 60$  mm, respectively. In contrast,  $s_b$  had no significant effect with the electric field and only a few rack passages were observed, with a median passage rate in the range of 0–1%. Tutzer *et al.* (2019b) did not report the number of bypass passages as the main goal of the project was to compare the protection efficiency of different configurations. However, Tutzer *et al.* (2019a) published the percentage of bypass passages for  $s_b = 60$  mm and  $\alpha = 20$ , which was in the range of 5–10% and did not significantly differ between the configuration without electrification, and the smaller and larger electric field. The vast majority of fish remained in the headwater, which could have been a result of an electric gradient in the bypass or model limitations. Tutzer *et al.* (2019b) concluded that downstream moving fish can be efficiently protected with the fish protector even for large  $s_b$ . In 2018, a pumping station at the Danube River, Germany, was equipped with a fish protector and the fish behavior was observed with a sonar system for three days (Egg *et al.*, 2018b). The functional efficiency could be proven with a fish returning rate of up to 72%, but a few rack passages were also observed. However, the results cannot be generalized as the study was limited to a small sample size, low water temperatures ( $T = 4.3^\circ\text{C}$ ), and very small approach flow velocities of  $U_o = 0.05$  m/s (Egg *et al.*, 2018b).

### **Conclusions and limitations of ethohydraulic studies**

Ethohydraulic studies showed that HBR-BSs are suitable to guide fish safely downstream, but that their efficiency strongly depends on  $s_b$  and the bypass design. They also indicate that at least some fish turn to their sides to pass through HBRs and that the protection efficiency of HBRs can be significantly increased by the application of an electric field with voltages  $U_e \leq 80$  V. Ethohydraulic studies enable to observe fish behavior in detail under laboratory conditions, that



is, most parameters such as the discharge, light conditions, and turbidity can be kept constant and the effect of single parameter like  $s_b$  on the protection and guidance efficiency can be quantified. However, results from ethohydraulic studies have to be carefully interpreted, as differences to prototype situations like environmental influences, differences in the fish biology, and geometric restrictions (e.g. limited bypass width) may affect fish behavior. Information gained from ethohydraulic studies can be valuable for designing prototype facilities, but they cannot replace extensive monitoring campaigns.

### 3.7.4 Monitoring campaigns

Multiple monitoring campaigns, which focus on fish downstream passage at HPPs with HBR-BSs, were conducted in recent years. They are chronologically summarized in Table 3.6 and briefly described in the following. Additionally, the monitoring campaigns at HPP Rotenfels and Unkelmühle are described, where no HBR-BS was installed, but valuable information about the fish behavior at an electric barrier, the usage of different corridors, and indirect mortality was presented. Some monitoring campaigns only aimed at verifying if the bypass is accepted for downstream passage, while different corridors were simultaneously monitored at a few HPPs to quantify the relative corridor usage. The different monitoring techniques are described in Section 2.3.1.

**Table 3.6:** Chronological overview of monitoring campaigns conducted at HBR-BSs

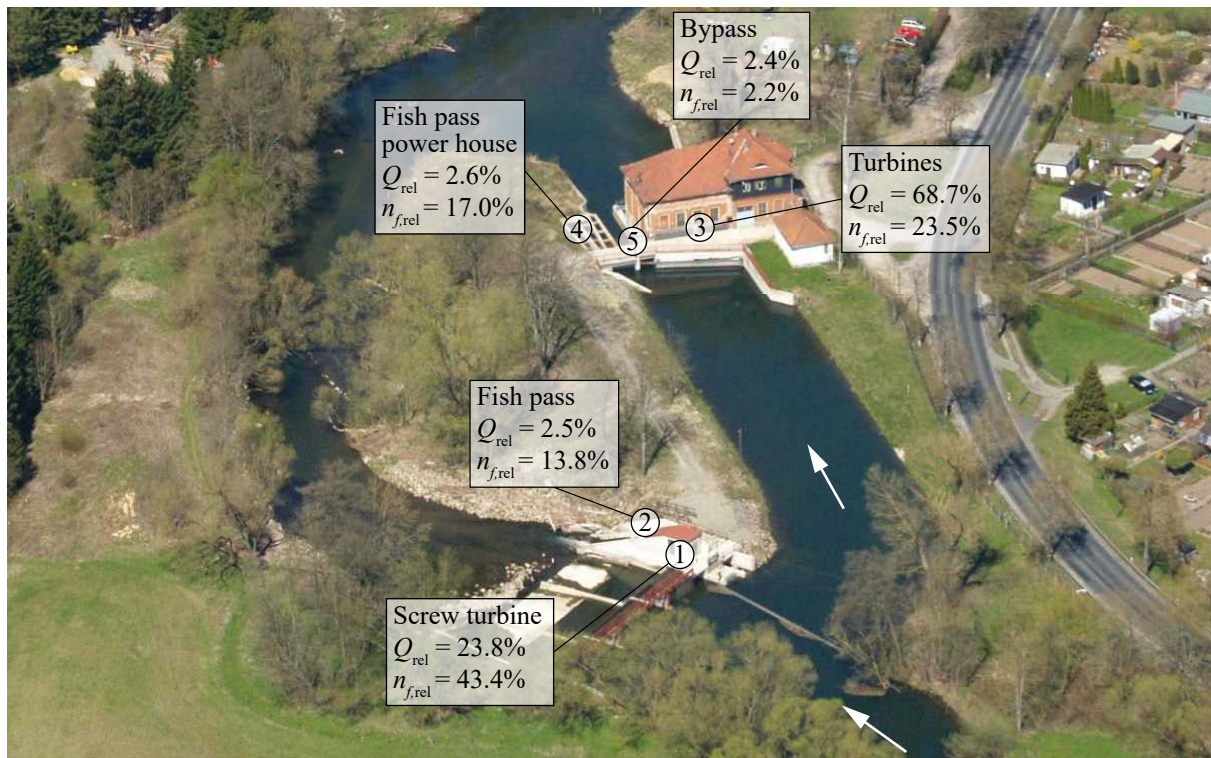
HPP	HPP and HBR-BS					Year		
	Coun-try	$\alpha$ [°]	$s_b$ [mm]	$Q_d$ [m <sup>3</sup> /s]	$Q_{by,rel}$ [%]	Start oper-ation HBR	Monitoring campaign	Publication main results
Walkmühle	DE	75	20	12.0	1.5	2007	2010	2010
Rothenburg	DE	38	20	68.0	2.1	2007	2008/2011	2013
Wehlitz	DE	54	20	8.5	2.0	2013	2013	2013
Herting	SE	30	15	40.0	1.5	2013	2014	2017
Ottenau	DE	44	18	14.5	5.5	2012	2016/2017	2018
Widdert	DE	30	12	14.0	n/a	2014	2013–2018	2018
Stroppel	CH	38	20	33.0	2.1	2014	2015–2017	2018
Rappenberghalde	DE	30	15	22.0	0.7	2013	2017/2018	2019
Lindesmühle	DE	30	15	10.8	n/a	2013	2015	2020
Schiffmühle*	CH	n/a	20	14.0	1.2	2013	2017–2020	2020
Aue*	CH	n/a	20	14.0	1.4	2013	2018–2020	2020

\* Residual flow HPP with the HBR installed as a side intake, which makes the definition of  $\alpha$  ambiguous

#### HPP Walkmühle

Schmalz (2010) conducted an extensive monitoring campaign at the diversion HPP Walkmühle on the Werra River (50°33'05.4"N, 10°24'36.9"E), Germany, where an HBR with  $s_b = 20$  mm and bars with an ellipsoidal tip and tail was installed in 2007. The approach flow angle was  $\alpha \approx 75^\circ$  and did therefore not meet current design recommendations (cf. Section 3.4.1). The bypass

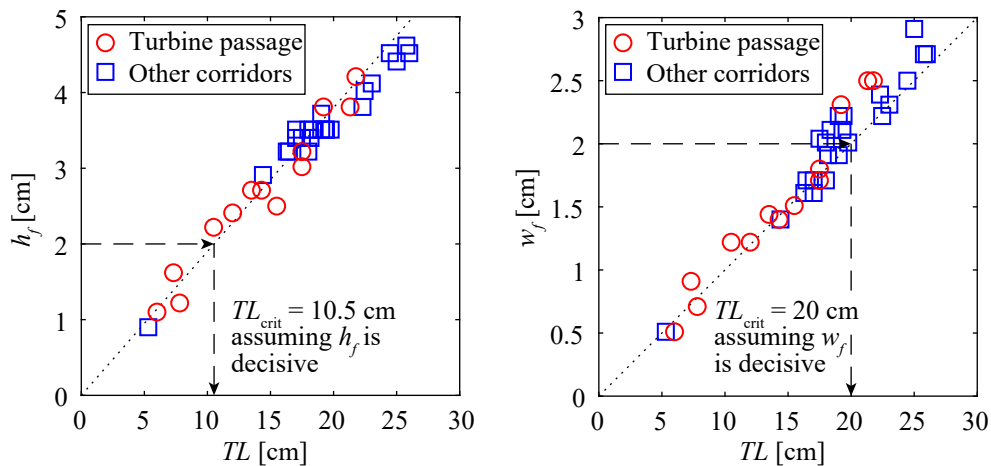
at the downstream rack end was built with a bottom opening ( $22.5 \text{ cm} \times 22.5 \text{ cm}$ ), leading to an intermediate pool and finally to the fish pass near the power house. The design discharge of the HPP is  $Q_d = 12 \text{ m}^3/\text{s}$  and the bypass discharge of  $Q_{by} = 0.18 \text{ m}^3/\text{s}$  leads to flow velocities from continuity at the bypass inlet of  $U_{by,in} = 3.56 \text{ m/s}$ , significantly exceeding  $U_{by,in}$  from design recommendations (Section 3.4.2). Fish could use the following five corridors for downstream passage: ① Archimedes screw turbine for environmental flow with a vertical trash rack ( $s_b = 197\text{--}240 \text{ mm}$ ), ② fish pass at the weir, ③ turbines after passing through the HBR, ④ fish pass at the power house, and ⑤ bypass which was specifically built for downstream passage (Fig. 3.10). All five corridors were monitored between 03.05.–07.05.2010 and 07.06.–11.06.2010 with stow and fyke nets simultaneously, leading to a total of 816 fish catches. All nets, with the exception of the bypass, were emptied every three hours during nighttime and every six hours during daytime, which are long intervals compared to literature data, potentially causing catch-related fish injuries (Section 2.3.1). Figure 3.10 shows the passage corridors and the relative distribution of downstream moving fish and discharges during the study period.



**Fig. 3.10:** Downstream passage corridors at HPP Walkmühle with the relative usage ( $n_{f,rel}$ ) and the corresponding discharge distribution ( $Q_{rel}$ ; Photo: LaNaServ, K. Winter; adapted from Schmalz, 2010)

Although the main discharge was diverted through the headrace channel ( $Q_{rel} = 73.7\%$ ), only 42.7% of the downstream moving fish used one of the adjacent corridors (Fig. 3.10, ③–⑤). Despite the HBR with  $s_b = 20 \text{ mm}$ , 23.5% of all fish passed through the turbines. The bypass was hardly used for downstream passage, which was attributed to the large inlet flow velocities. The screw turbine was the most frequently used corridor, but also both fish passes were well accepted, which might be a result of hydraulically unfavorable conditions at the other corridors (cf. Section 2.2.2). The stow nets were installed for 33 days between June 2009 and June 2010,

in which a total of 952 fish were caught. Schmalz (2010) reported the fish length, width, and height of each individual from 21 species and specified for each fish if it swam downstream through the turbines, and therefore also passed through the HBR, or if it used another corridor. As an example, the length-height and length-width diagram of all brown trout is shown in Fig. 3.11. The dotted lines illustrate the correlation between  $TL$  and the fish height and width, presuming  $h_{f,rel} = 0.19$  and  $w_{f,rel} = 0.10$ , respectively (cf. Table 2.2). If it was assumed that trout do not turn themselves to their sides to pass through barriers with horizontal bars, the HBR with  $s_b = 20$  mm should have protected all trout with  $TL > TL_{crit} = s_b/h_{f,rel} = 10.5$  cm (Eq. 2.2 and Table 2.2), which is indicated with the dashed line in Fig. 3.11a. Only three out of 13 brown trout caught at the turbine outlet were small enough to pass the HBR without turning to their sides (Fig. 3.11a). If it was assumed that trout rotate themselves by  $90^\circ$ , the HBR was a physical barrier for trout with  $TL > TL_{crit} = s_b/w_{f,rel} = 20.0$  cm (Fig. 3.11b, Eq. 2.1, and Table 2.2). Three trout which passed through the HBR were slightly larger than  $TL_{crit} = 20$  cm, which can be explained by body flexibility, measurement inaccuracies, small bar deformations, or these trout entered the stow net from the downstream during recovery. Schmalz (2010) concluded that fish rotate themselves to pass through HBRs, as multiple individuals from different species were caught at the turbine outlet with  $h_f > s_b$ . Fish with  $h_f > s_b$  caught at the turbine outlet were brown trout, grayling, bream, gudgeon, dace, carp, ruffe, roach, rainbow trout, rudd, tench, and zander. Most species, of which individuals with  $h_f < s_b$  were caught at the turbine outlet only, occurred in low numbers or were small-sized species like minnow, which do not exceed  $h_f = 20$  mm even when fully grown. These results indicate that a wide range of species turns sidewise to pass through HBRs, at least to a certain extent. To improve fish downstream passage at HPP Walkmühle, Schmalz (2010) recommended to decrease  $U_{by,in}$  and to reduce the clear bar spacing to  $s_b = 15$  mm and the approach flow angle to  $\alpha = 45^\circ$  to meet current design recommendations (cf. Section 3.4).



**Fig. 3.11:** (a) Length-height and (b) length-width diagram of brown trout which passed through the turbines, and therefore also the HBR with  $s_b = 20$  mm, and which were caught at other downstream passage corridors (data from Schmalz, 2010)

### HPP Rothenburg

One of the first HBR-BSs was installed at the bay-type HPP Rothenburg on the Saale River (51°38'48.6"N, 11°45'06.0"E), Germany, in 2007 (Ebel *et al.*, 2015). It was equipped with rectangular bars with  $s_b = 20$  mm,  $\alpha \leq 38^\circ$ , a  $h_{Bo} = 0.60$  m high bottom overlay and had a bypass discharge of  $Q_{by} = 1.45$  m<sup>3</sup>/s (Ebel, 2016). The bypass acceptance was monitored during 34 days in 2008, where 7657 fish of 29 species with  $TL = 5$ –130 cm were caught at the bypass outlet (Ebel, 2016). In 2011, all three turbine outlets were monitored with stow nets, despite the large design discharge of  $Q_d = 68$  m<sup>3</sup>/s (Ebel *et al.*, 2015). This monitoring campaign focused on downstream migrating silver eels, for which reason the rack passages were not quantified for other species, as this would have required time-consuming species-specific mark and recapture experiments (cf. Section 2.3.1). The majority of eels used the bypass for downstream passage (83.3%), whereas only 16.7% passed through the HBR and migrated through the turbines (Ebel *et al.*, 2015). This led to a total survival rate of  $SR_{tot} = 97.5\%$ , which is significantly higher than the estimated survival rate of 70% without an HBR-BS (Ebel *et al.*, 2015; Ebel, 2016).

### HPP Wehlitz

HPP Wehlitz on the Weiße Elster River (51°23'22.8"N, 12°11'46.4"E), Germany, with  $Q_d = 8.5$  m<sup>3</sup>/s was equipped with an HBR-BS with  $s_b = 20$  mm and  $\alpha = 54^\circ$  in 2013 (Wagner *et al.*, 2013). The monitoring results were reported by Wagner *et al.* (2013) and Wagner (2016). All potential downstream passage corridors were sampled with stow nets. The bypass was equipped with a bottom and top opening, but only one of the openings could be monitored with a stow net at once. Table 3.7 summarizes the normalized relative daily catches and the relative discharges  $Q_{rel}$  during the study period.

**Table 3.7:** Normalized relative daily catches and relative discharge during the study period at different downstream passage corridors (data from Wagner *et al.*, 2013)

Corridor	Normalized relative daily catches [%]	$Q_{rel}$ [%]
Spillway	39	10–23
Fish pass	8	4
Turbines	47	70–85
Bypass	6	2

Most fish passed the HBR and swam downstream through the turbines or they used the spillway, while neither the fish pass nor the bypass were well accepted for downstream passage (Table 3.7). The latter was attributed to the low relative bypass discharge of  $Q_{by,rel} = 2\%$  (Table 3.7). Observations with a sonar indicated that many fish did not find the bypass entrance. The majority of fish (95%) caught at the turbine outlet was small ( $TL \leq 20$  cm) but 50 eels and 18 individuals of other species with  $TL > 20$  cm passed through the HBR. In contrast,  $\approx 20\%$  of the fish caught in the bypass had a  $TL > 20$  cm, indicating a good guidance and protection efficiency for large fish. Nevertheless, most fish caught at the bypass outlet could have physically passed the HBR, which implies a partial behavioral guidance effect.

### HPP Herting

Multiple radio-tagging campaigns were conducted at the diversion HPP Herting 1 on the Ätran River (56°54'01.1"N, 12°31'10.6"E), Sweden, to investigate fish downstream passage (Calles *et al.*, 2012; Nyqvist *et al.*, 2017b, 2018). Until 2013, an inclined trash rack with  $\gamma \approx 60^\circ$  and  $s_b = 90$  mm was installed in front of the two Kaplan turbines with  $Q_d = 40$  m<sup>3</sup>/s (Calles *et al.*, 2012). In the beginning of 2006, a temporary surface bypass with a maximal discharge of 2 m<sup>3</sup>/s and a bottom pipe bypass ( $\varnothing = 200$  mm) with a discharge of 0.25 m<sup>3</sup>/s were installed near the turbine intake (Calles *et al.*, 2012). The bypass improved downstream passage, but it was still insufficient, with the guidance efficiency ranging between no effect for eels and trout smolts, to 17% for salmon smolts, and 58% for trout kelts. In 2013, the inclined trash rack was replaced by a modern HBR with  $\alpha = 30^\circ$ ,  $s_b = 15$  mm, foil-shaped bars, and  $A = 80$  m<sup>2</sup>, leading to an average  $V_n = 0.50$  m/s at design discharge (Nyqvist *et al.*, 2017b). The bypass was arranged to extend the rack axis and had a discharge during regular operation mode of  $Q_{by} = 0.60$  m<sup>3</sup>/s, which was diverted through a bottom (0.20 m × 0.20 m) and a top opening (0.30 m × 0.65 m; width × height; Nyqvist *et al.*, 2017b). Nineteen out of 20 wild downstream migrating radio-tagged salmon smolts which approached the turbine intake channel, were re-detected in the downstream. Fourteen specimens accepted the bypass, whereas the downstream passage corridor of five specimens was unclear, which means they either passed through one of the turbines or escaped the bypass trap (Nyqvist *et al.*, 2018). The guidance efficiency of salmon smolts was therefore between 70–95%. Most salmon smolts passed the HPP fast at their first attempt and it took them a median time of 10.5 h from release to passage, corresponding to a migration speed through the HPP of  $\approx 40$  m/h (Nyqvist *et al.*, 2018). For test purposes, the bypass was also fully opened, such that it was working as a full depth open channel bypass with  $Q_{by} = 3.00$  m<sup>3</sup>/s (Nyqvist *et al.*, 2017b). However, it did not seem to improve guidance, as no radio-tagged smolt passed the bypass four hours before or after such spill events (Nyqvist *et al.*, 2018). Nyqvist *et al.* (2018) concluded that the HBR-BS improved fish downstream passage and that fish are now able to pass the HPP with little delay and reasonably high survival.

### HPP Ottenau

In 2012, HPP Ottenau on the Murg River (48°47'32.0"N, 8°20'09.8"E), Germany, with  $Q_d = 14.5$  m<sup>3</sup>/s was equipped with an HBR-BS with rectangular bars,  $\alpha = 44^\circ$ ,  $s_b = 18$  mm, and a  $h_{Bo} = 0.35$  m high bottom overlay (Berger, 2018). In 2016/2017, the efficiency of the HBR-BS was assessed in a radio-telemetry monitoring campaign reported by Berger (2018). Sixty hatchery-reared Atlantic salmon smolts with an average total length of  $\overline{TL} = 20.7$  cm ( $TL_{\min} = 18.0$  cm) and 124 wild European eels with  $\overline{TL} = 71$  cm ( $TL_{\min} = 50$  cm) were tagged and their behavior at the HBR-BS was studied. The average approach flow velocity was  $U_o = 0.4$  m/s, but it increased locally up to  $U = 0.7$ – $0.8$  m/s. The bypass discharge was constant with  $Q_{by} = 0.8$  m<sup>3</sup>/s, corresponding to  $Q_{by,rel} = 5.5\%$ . The percentage of salmon smolts and eels migrating downstream through the different passage corridors are summarized in Table 3.8.

**Table 3.8:** Relative corridor usage of downstream migrating salmon smolts and eels at HPP Ottenau (data from Berger, 2018)

Corridor	Usage salmon [%]	Usage eels [%]
Corridor undefined	2	7
Bypass	63	33
Rock-ramp fishway	25	19
Side weir	8	41
Rack passage	2	0

The HBR protected all downstream migrating salmon smolts, except one specimen with  $TL = 19.5$  cm, which passed through the HBR. It has to be considered that the tagged salmon smolts were rather large ( $TL \geq 18$  cm) and the critical total length with  $s_b = 18$  mm was  $TL_{crit} = 18$  cm (cf. Eq. 2.3 and Table 2.2). The HBR was therefore a physical barrier for the majority of tagged salmon smolts, even if they were turning themselves to their sides to try to pass through the rack. However, the bypass and the fishway were well accepted for downstream passage (Table 3.8). It is also not surprising that none of the eels passed through the HBR, as only 9% of the tagged eels were smaller than or equal to  $TL_{crit} = 60$  cm (cf. Eq. 2.3 and Table 2.2). At the beginning of the eel experiments in November 2016, there was a flood in the Murg River with a discharge of up to  $Q \approx 50$  m<sup>3</sup>/s, which was used by many eels to pass the HPP over the side weir (Table 3.8). Nevertheless, the eels also used the bypass and the fishway frequently for downstream passage (Table 3.8). Summed up, the monitoring campaign at HPP Ottenau showed that most salmon smolts and eels were protected by the HBR with  $s_b = 18$  mm, which is however limited to the tested fish sizes.

### HPP Rotenfels

HPP Rotenfels (48°48'32.9"N, 8°18'38.8"E) with  $Q_d = 11.80$  m<sup>3</sup>/s, which is located  $\approx 2$  km downstream of HPP Ottenau, was not equipped with a fish protection rack, but an electric barrier was temporally installed between 2014–2017 at the beginning of the headrace channel (Berger, 2018). Fish could therefore either use the fish pass, a bypass, the side weir, or the headrace channel for downstream passage. The setup of the barrier and the results were published by Weibel (2016) and Berger (2018). The electric barrier consisted of three parallel rows of electrodes with a distance of 110 cm between rows and 80 cm between individual electrodes (gpDC, Neptun system, company Procom). The efficiency of the electric barrier was assessed by releasing tagged salmon smolts and by the detection of the downstream migrating silver eels, which were released upstream of HPP Ottenau. A total of 124 silver eels were tagged, of which 73 were detected at HPP Ottenau, 68 successfully passed HPP Ottenau, and 46 were redetected upstream of the electric barrier at HPP Rotenfels.

**Table 3.9:** Relative corridor usage of salmon smolts in 2015 and silver eels in 2016/2017 at HPP Rotenfels, where  $n$  = number of detected fish (data from Berger, 2018)

Corridor	Usage salmon [%], $n = 123$	Usage eels [%], $n = 46$
Detected, but stayed upstream	0	9
Fish pass + bypass	87	17
Side weir	4	33
Headrace channel	9	41

The majority of downstream migrating salmon smolts either used the fish pass or the bypass for downstream passage, while only 9% passed through the electric barrier, leading to a guidance efficiency of 91% (Table 3.9). In contrast, only 50% of the eels were successfully guided downstream, while 41% passed through the electric barrier and 9% were detected at the electric barrier but stayed in the upstream area. When interpreting the results, it has to be considered that no control experiments were conducted, where the electrification was turned off. This makes it difficult to quantify the effect of the electric field, even though the main discharge was diverted through the headrace channel. Berger (2018) concluded that downstream migrating eels could, in contrast to salmon smolts, not be sufficiently protected with the electric barrier at HPP Rotenfels. She recommended to either combine electric barriers with operational measures or to use hybrid barriers consisting of a rack and an electric barrier.

### HPP Widdert/Auer Kotten

Between 2013 and 2018, a PIT-tagging monitoring campaign, described in multiple intermediate reports such as Engler and Adam (2014) and the final report by Adam *et al.* (2018), was conducted at the diversion HPP Widdert with  $Q_d = 14 \text{ m}^3/\text{s}$  on the Wupper River (51°08'08.4"N, 7°05'13.7"E), Germany. This HPP is equipped with an HBR-BS with  $\alpha = 30^\circ$  and  $s_b = 12 \text{ mm}$  and two separate pipe bypasses which are arranged perpendicular to the rack area, one close to the bottom (0.30 m × 0.30 m) and one close to the surface (0.30 m × 0.60 m; width × height). Additionally, a 12 m wide and 0.6 m high opening called “smolt bypass” is located above the rack, which is diverted to the surface bypass. It is equipped with an HBR with  $s_b = 35 \text{ mm}$  to prevent floating debris from entering the bypass, while being permeable for smolts. Alternative downstream passage corridors are a flushing gate at the downstream rack end (1.00 m × 3.50 m; width × height), a vertical-slot pass at the power house, the weir, and a rock-ramp fishway at the weir. Although Lehmann *et al.* (2016) conducted a flow velocity measurement campaign at HPP Widdert, the discharges through the different corridors were neither reported by Lehmann *et al.* (2016) nor Adam *et al.* (2018). A total of 16 PIT-tagging antennas were installed to monitor all corridors. The downstream migration behavior of European silver eels and Atlantic salmon smolts was of main interest, but wild fish caught with electrofishing, including brown trout, grayling, nase, and barbel, were also tagged and registered during downstream passage. Table 3.10 summarizes the usage of the different downstream passage corridors. A PIT-tagging antenna at the turbine outlet was used to confirm that the turbines were not used for down-



stream passage, as the HBR was a physical barrier for all downstream migrating silver eels ( $TL = 49\text{--}110\text{ cm}$ ,  $TL_{\text{crit}} = 40\text{ cm}$ ) and salmon smolts ( $TL = 12\text{--}23\text{ cm}$ ,  $TL_{\text{crit}} = 12\text{ cm}$ ).

**Table 3.10:** Relative corridor usage of downstream moving fish at HPP Widdert, where  $n$  = number of tagged fish (adapted from Adam *et al.*, 2018)

Corridor	Usage silver eels [%]		Usage salmon smolts [%]			Usage wild fish [%]
	2013	2016	2014	2015	2018	
	$n = 212$	$n = 213$	$n = 525$	$n = 212$	$n = 537$	$n = 119$
Undefined	10.8	8.9	9.0	1.9	0.4	24.4
Weir	2.8	5.2	0.2	0	0	4.2
Rock-ramp fishway at the weir	4.2	8.5	2.1	0.5	1.7	5.9
Flushing gate	29.7	27.2	25.7	3.3	90.3	33.6
Bottom bypass	0.5	0	0.2	0	0	0
Surface bypass	7.5	13.6	39.0	62.3	5.2	5.9
Smolt bypass	2.8	6.1	8.8	17.5	1.3	0
Vertical-slot pass power house	41.5	30.5	15.0	14.6	1.1	26.1

The majority of all downstream moving fish ( $\approx 80\%$ ) followed the main flow towards the power house, such that the weir and the rock-ramp fishway at the weir played only a minor role for downstream passage. The bottom bypass clogged very frequently and was therefore hardly used by any fish. The smolt bypass was also not well accepted, which was traced back to the small inlet flow velocities. The much smaller surface bypass was used by  $>60\%$  of the salmon smolts in 2015 (Table 3.10). The vertical-slot pass, located at the upstream end of the HBR, was frequently used by silver eels and wild fish, primarily barbels. The most important corridor was the flushing gate, which was used by approximately one third of all fish for downstream passage. In 2015, the flushing gate was opened only once or twice a day, which led to a low passage rate of 3.3% by salmon smolts (Table 3.10). In contrast, since 2016, the flushing gate was opened at night in intervals of 30 minutes, which led to a passage rate of salmon smolts of over 90% in 2018. However, the new flushing regime did not improve the downstream passage for eels. Adam *et al.* (2018) concluded that downstream migrating salmon smolts and eels were well protected at the HBR with  $s_b = 12\text{ mm}$  and that the flushing gate with emptying intervals of 30 minutes was the most efficient corridor for downstream passage.

### HPP Stroppel

The first extensive monitoring campaign at an HBR-BS in Switzerland was conducted at the diversion HPP Stroppel on the Limmat River ( $47^\circ 30' 09.4''\text{N}$ ,  $8^\circ 14' 23.9''\text{E}$ ) between 2015 and 2017 and was reported in detail by Zaugg and Mendez (2018) and Mendez and Zaugg (2020). The 25 m long and 2.7 m high HBR, which was built in 2013/2014 with  $\alpha = 38^\circ$ , is equipped with foil-shaped bars with  $s_b = 20\text{ mm}$ . The design discharge is  $Q_d = 33\text{ m}^3/\text{s}$ , leading to a maximal approach flow velocity of  $U_o = 0.48\text{ m/s}$ . Instead of a bottom overlay, an  $\approx 30\text{ cm}$  deep concrete channel was built in front of the HBR (estimated from picture in Zaugg and Mendez, 2018). The bypass was supplied with a year-round discharge of  $Q_{by} = 0.69\text{ m}^3/\text{s}$  ( $Q_{by,\text{rel}} =$



2.0%) and was equipped with a bottom ( $0.40\text{ m} \times 0.60\text{ m}$ ; width  $\times$  height) and a top opening ( $0.40\text{ m} \times 0.40\text{ m}$ ). The number of fish passing downstream through the bypass was determined with a stow net, which was installed for a total duration of 304 hours, divided into several periods between two and 72 hours. To reduce catch-related injuries, the stow net was emptied in intervals of 30 minutes. In total, 11 348 fish of 28 species were caught in the bypass, including all frequently occurring species in the Limmat River except benthic species like stone loach (*Barbatula barbatula*), spined loach (*Cobitis taenia*), and burbot (*Lota lota*). Fish were caught in the bypass at all times of the day, but the majority of fish (76%) moved downstream during dawn and the first hours of the night. Most fish were small, that is, 87% of the individuals had a  $TL < 10\text{ cm}$ , 12% of  $10\text{ cm} \leq TL \leq 20\text{ cm}$ , and only 1% had a  $TL > 20\text{ cm}$ . Six cameras were used to observe the fish behavior in front of the HBR. Most fish approached the rack with positive rheotaxis and swam then against the current towards the upstream rack end. After some time, they entered the bypass with positive rheotaxis, while no escape reactions were observed at the bypass entrance. Some fish approached the HBR with negative rheotaxis and swam head-first along the HBR into the bypass. Fish were observed in the entire water column and likely used the bottom and top bypass opening for downstream passage. Some species such as eel, barbel, and common perch were frequently detected in the bottom channel. No stow net was installed behind the turbines to quantify rack passages, but no rack passages were observed with the cameras. A sonar Aris Explorer 3000 was installed for 38 hours between 25.10.–27.10.2016 behind the rack, which allowed for the observation of a thin cone of  $\approx 30^\circ \times 14^\circ$  up to a distance of maximal 15 m. During this period, lots of leafs were transported in the Limmat River, which made it difficult to quantify the number of fish behind the HBR. However, some fish were observed with the sonar, from which it was estimated that 100–200 fish passed through the HBR. Within the same time period, 6239 fish were caught in the stow net at the bypass outlet, from which Zaugg and Mendez (2018) concluded that only 1.6–3.2% of the fish passed through the HBR.

### HPP Rappenberghalde

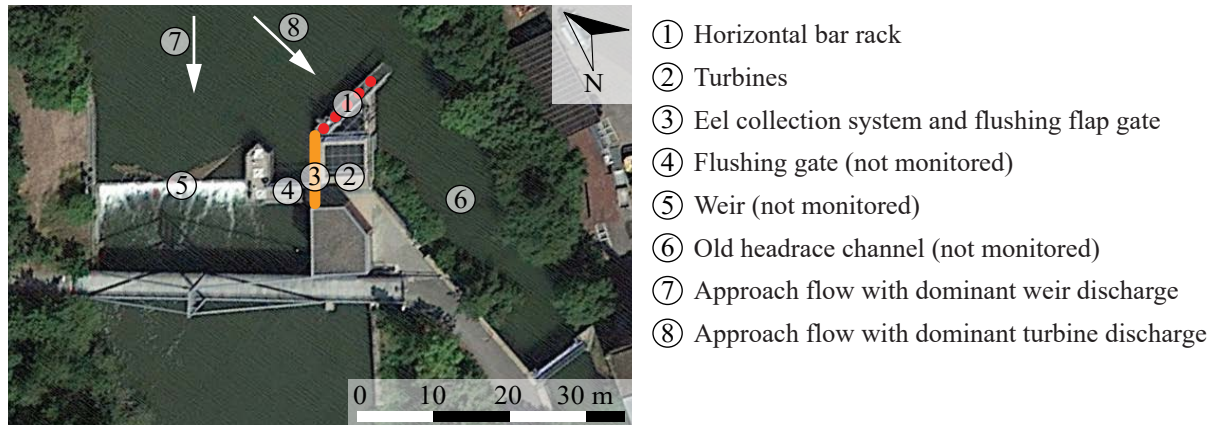
In 2013, the diversion HPP Rappenberghalde on the Neckar River ( $48^\circ 30' 27.5''\text{N}$ ,  $9^\circ 01' 54.7''\text{E}$ ), Germany, with  $Q_d = 22\text{ m}^3/\text{s}$  was equipped with an HBR-BS with  $s_b = 15\text{ mm}$ ,  $\alpha = 30^\circ$ , and an average approach flow velocity at design discharge of  $U_o = 0.3\text{ m/s}$  (Wagner *et al.*, 2019b). A  $h_{Bo} \geq 0.92\text{ m}$  high bottom overlay was installed and the bypass with three openings in different flow depths was operated discontinuously. This means that it was emptied in intervals between one and three hours, while it had a rather low permanent discharge of  $Q_{by} = 0.15\text{ m}^3/\text{s}$  to attract fish (Wagner *et al.*, 2019b). An additional flushing gate at the downstream rack end was opened at each cleaning cycle. Between 2017 and 2018, an extensive monitoring campaign was carried out, including radio telemetry, PIT-tagging, video- and sonar-observations, and stow nets behind all corridors. The first results from 2017 were published in Wagner *et al.* (2019a) and the final results were reported by Wagner *et al.* (2019b). Flow velocities were measured with an acoustic Doppler current profiler. At a turbine discharge of  $Q = 6.5\text{ m}^3/\text{s}$ , the maximal measured normal flow velocity component was  $V_n = 0.22\text{ m/s}$ , whereas the average value from continuity

was  $\overline{V}_n = 0.12$  m/s. A total of 65 locally caught fish with  $TL \geq 28$  cm were equipped with radio-tags and eight antennas were installed at the bypass entrances and along the HBR. The majority of all fish (81%) swam downstream after their first rack contact, indicating a good guidance effect towards the downstream rack end, where they spent most of their time searching for a suitable corridor for downstream passage. Although each fish was detected on average 40 times at the HBR, only eight fish entered the bypass, of which a single individual passed downstream. The low bypass acceptance was attributed to the discontinuous operation mode and the location of the bypass, which was too far away from the downstream rack end. Neither a reduction of the bypass emptying interval from three hours to one hour, nor the installation of a funnel did significantly improve the bypass efficiency. A total of 1394 wild fish were caught with stow nets downstream of the HPP, of which 46% passed the HBR and swam through the turbines and 54% used either the bypass or the flushing gate. This share between rack and bypass passage was very species-specific. As an example, the percentage of fish which used the flushing gate or the bypass instead of passing through the HBR was 79%, 67%, 22%, and 10% for spirlin, brown trout, barbel, and eel, respectively. The majority of fish (98.1%) caught in the bypass and the flushing gate was small and could have physically passed through the HBR, indicating a partial behavioral protection effect. A positive correlation between the fish length and the guidance efficiency was found for fish with  $h_f \leq 15$  mm, corresponding to  $s_b$ . The guidance efficiency for fish which could have passed through the HBR only with turning to their sides ( $h_f > 15$  mm) was in the range of 30–70%. No positive correlation between the guidance efficiency and  $h_f$  was found for these fish, which was explained by the lack of a suitable downstream passage corridor, species-specific differences which were not analyzed due to the rather low number of individuals of the same species but different size classes, and a bias of the results of bottom-oriented fish which were potentially guided along the bottom overlay without rack contact. The survival rates at the turbine, bypass, and flushing gate were 76.3%, 98.4%, and 99.1%, respectively. In summary, the HBR at HPP Rappenberghalde acted not only as a physical barrier, but had also a behavioral barrier effect. Despite the small clear bar spacing of  $s_b = 15$  mm, many fish managed to pass through the HBR. This was at least partially attributed to the uncommon bypass design, which likely increased fish encounters with the HBR.

### HPP Lindesmühle

HPP Lindesmühle on the Franconian Saale (50°11'17.0"N, 10°04'27.9"E), Germany, with  $Q_d = 10.8$  m<sup>3</sup>/s and a Kaplan bulb turbine was equipped with an HBR with  $s_b = 15$  mm and  $\alpha = 30^\circ$  in 2013 (Mueller *et al.*, 2020b). The results of the monitoring campaign were published by Mueller *et al.* (2020b) and are summarized in the following. During 12 days in spring and 22 days in autumn 2015, four downstream passage corridors were monitored with fish traps and stow nets simultaneously, namely the turbines, a nature-like fishway, a zigzag-shaped eel collection system (cf. Section 2.4.5), and a flushing flap gate. The arrangement of the HBR and the adjacent corridors is illustrated in Fig. 3.12. The entrance to the nature-like fishway was located  $\approx 70$  m upstream of the HPP and therefore not within the extract in Fig. 3.12. Fish could also

have temporarily moved downstream through the flushing gate and the weir, but these corridors were not monitored due to site-specific limitations. However, the river discharge during the monitoring period was low, that is,  $Q \approx 8\text{--}10\text{ m}^3/\text{s}$  in spring and  $Q \approx 2\text{--}7\text{ m}^3/\text{s}$  in autumn and therefore  $<Q_d$ . Accordingly, it has to be assumed that the weir discharge was negligible during the study period, making the turbine discharge dominant. The approach flow direction is shown in Fig. 3.12 for a situation with dominant weir discharge and a situation with dominant turbine discharge. The flow velocity measured directly in front of the HBR was only 0.12 m/s during the study period. In total, 690 fish from 23 species were caught, of which most were small-sized species and not long distance migratory species, namely roach (40.4%), gudgeon (14.6%), ruffe (8.3%), dace (7.8%), and perch (7.4%). The relative corridor usage for different size classes and the relative corridor discharge  $Q_{\text{rel}}$ , calculated as an average over the monitoring period, are summarized in Table 3.11. The turbine mortality was assessed by releasing a total of 7859 eels ( $TL = 19.6\text{--}64.5\text{ cm}$ ), nase ( $TL = 4.0\text{--}12.6\text{ cm}$ ), brown trout ( $TL = 9.0\text{--}24.0\text{ cm}$ ), and perch ( $TL = 6.7\text{--}15.0\text{ cm}$ ) with known preexisting injuries upstream of the HPP.



**Fig. 3.12:** HPP Lindesmühle with HBR, downstream passage corridors, and main flow direction, depending on if the turbine or weir discharge is dominant (adapted from Google Earth; date taken: 26.07.2019)

**Table 3.11:** Relative corridor usage of downstream moving fish per size class at HPP Lindesmühle in 2015 and relative corridor discharge  $Q_{\text{rel}}$  (data from diagram in Mueller *et al.*, 2020b)

Corridor	Corridor usage [%] for different size classes $TL$ [cm]						$Q_{\text{rel}}$ [%]
	$\leq 5$	$> 5 \leq 10$	$> 10 \leq 15$	$> 15 \leq 20$	$> 20 \leq 30$	$> 30$	
	$n = 227$	$n = 239$	$n = 169$	$n = 28$	$n = 9$	$n = 7$	
Turbine	87	74	82	79	33	0	93.9
Nature-like fishway	8	15	10	7	33	86	5.9
Eel collection system	5	7	5	0	0	14	0.1
Flushing flap gate	0	5	4	14	33	0	0.1

Despite the HBR with  $s_b = 15\text{ mm}$ , the majority of fish passed downstream through the turbines (Table 3.11). Not only very small fish, but also fish with a total length of  $15\text{ cm} < TL \leq 20\text{ cm}$  were primarily caught at the turbine outlet. Even one fifth of all fish with  $TL > 20\text{ cm}$  passed through the turbines, to which most the HBR should have been a physical barrier. As an ex-

ample, a perch with  $TL = 20$  cm, a tench with  $TL = 20$  cm, and a nase with  $TL = 16.5$  cm were caught at the turbine outlet, which were considerably larger than the critical total lengths for  $s_b = 15$  mm listed by Ebel (2016), which are  $TL_{crit} = 12.5$  cm, 11.5 cm, and 13.6 cm, respectively. However, a suitable alternative corridor was missing, as the entrance to the nature-like fishway was far upstream and the eel collection system and the flushing flap gate had a very small discharge (Table 3.11). Due to the high relative turbine discharge and the arrangement of the HBR, it has to be assumed that the flow approached the HBR with an angle of  $\approx 90^\circ$  (® in Fig. 3.12). A total of 27% of the released fish were recaptured at any of the corridors. Considering the catch-related mortality and the delayed mortality after 96 hours, the total survival rate of these fish after rack and turbine passage was in the range of 57–65%. Only three eels with  $TL \leq 38$  cm were caught at the turbine outlet, indicating that also rather small eels were protected by the HBR. This is in line with the findings of Egg *et al.* (2017), who studied the downstream migration behavior of eels at HPP Lindesmühle with a sonar Aris Explorer 3000 in 2015 and 2016. A total of 1323 eels were detected, but no rack passages were observed and not a single individual used the zigzag-shaped eel collection system for downstream passage. Mueller *et al.* (2020b) concluded that the HBR at HPP Lindesmühle has likely a low guidance effect and acts mainly as a physical barrier for the tested species (with the exception of eel) and has hardly any behavioral protection effect.

### Residual flow HPP Schiffmühle

The residual flow HPP Schiffmühle on the Limmat River (47°29'13.9"N, 8°16'12.0"E) with  $Q_d = 14$  m<sup>3</sup>/s was equipped with an HBR-BS with  $s_b = 20$  mm and a bypass discharge of  $Q_{by} = 0.17$  m<sup>3</sup>/s in 2013 (information from questionnaire). The rack was arranged as a side intake (Fig. 3.3a) and the bypass consisted of two narrow openings, which were located more than two meters away from the downstream rack end (Fig. 3.3b). The discharge of both bypass openings merged in a manhole, from where a pressurized pipe should allow for safe downstream passage. Between 28.09.2017 and 25.02.2020, a monitoring campaign was conducted by Schölzel *et al.* (2020), of which the most important findings regarding fish downstream passage are briefly summarized in the following. The inlet and outlet of the fish pass and the bypass for downstream passage were equipped with PIT-tagging antennas. Fish could have also passed downstream through the HBR and the turbines, the weir, or through the main HPP Schiffmühle, but these corridors were not equipped with PIT-tagging antennas. In total, 3087 wild fish from 17 species were PIT-tagged, of which some were released upstream and some downstream of the residual flow HPP. Within the study period, 178 fish used the fish pass for downstream passage, while only one barbel with  $TL = 15.1$  cm and one spirlin with  $TL = 9.6$  cm very likely used the bypass for downstream passage. Another 265 downstream passages, mainly spirlin, barbel, and chub, were registered, but the corridor could not be identified. This means that they either passed through the HBR and the turbines, the weir, or the main HPP Schiffmühle. Schölzel *et al.* (2020) reported that the pipe bypass clogged often, which is one reason why it was not used more frequently for downstream passage. Nevertheless, it is questionable if the bypass would be well-accepted for downstream passage even if clogging could be prevented, as it does not

meet most common design criteria described in Section 3.4.2.

### Residual flow HPP Aue

The residual flow HPP Aue (47°28'06.0"N, 8°18'29.8"E) with  $Q_d = 14 \text{ m}^3/\text{s}$ , which is located  $\approx 5.5 \text{ km}$  upstream of the residual flow HPP Schiffmühle, was equipped with a very similar HBR-BS as the residual flow HPP Schiffmühle in 2013. It consists of an HBR with  $s_b = 20 \text{ mm}$  and a pipe bypass with  $Q_{by} = 0.19 \text{ m}^3/\text{s}$ . A total of 379 individuals from 15 species were PIT-tagged and released at the residual flow HPP Aue between 05.06.2018 and 25.02.2020. Additionally,  $\approx 770$  tagged fish, which were released at the residual flow HPP Schiffmühle, were redetected at the residual flow HPP Aue (Schölzel *et al.*, 2020). Only 9 downstream passages were registered through the fish pass and 43 through an unknown corridor, while not a single individual used the bypass for downstream passage (Schölzel *et al.*, 2020). Despite the low number of individuals, this monitoring campaign confirmed that such a pipe bypass is hardly used for downstream passage.

### HPP Unkelmühle

HPP Unkelmühle on the Sieg River (50°46'03.8"N, 7°30'01.7"E), Germany, with  $Q_d = 27 \text{ m}^3/\text{s}$  was retrofitted with an inclined fine rack with  $\gamma = 27^\circ$ ,  $s_b = 10 \text{ mm}$ , and vertical bars in 2013 (Wilke *et al.*, 2019). Although no HBR-BS was installed at HPP Unkelmühle, the very extensive monitoring campaign gives valuable information about the usage of different downstream passage corridors of eels and salmon smolts and the magnitude of indirect mortality. The rack fields were 8.10 m long (Wilke *et al.*, 2019), indicating approach flow depths of  $h_o \approx 3.7 \text{ m}$ . The results of Atlantic salmon smolts and European silver eels were reported in Økland *et al.* (2016) and Økland *et al.* (2017), respectively. In total, 256 salmon smolts and 270 silver eels were tagged and their behavior was studied using radio telemetry in 2014 and 2015. Downstream passage was theoretically possibly through eight different corridors, namely the spillway, surface bypass, turbines, vertical slot pass, nature-like fishway, canoe pass, bottom gallery (cf. Fig. 2.16b), or the side bypass. The turbines could not be used for downstream passage, as the rack was a physical barrier for all tagged fish ( $TL > TL_{\text{crit}}$ ; salmon smolts:  $TL = 11\text{--}21 \text{ cm}$  (Økland *et al.*, 2016) with  $TL_{\text{crit}} = 10 \text{ cm}$ ; silver eels:  $TL = 60\text{--}108 \text{ cm}$  (Økland *et al.*, 2017) with  $TL_{\text{crit}} = 33 \text{ cm}$ ). The bottom gallery was opened during catch mode, thereby offering shelter to eels which escaped upstream after rack contact (cf. Section 2.4.5). During transport mode, the bottom gallery was closed to flush eels downstream through a bypass. Similarly to the bottom gallery, the side bypass was especially designed for eels and consisted of three holes in different depths in front of the turbine intake. The relative usage of all corridors is summarized in Table 3.12.

**Table 3.12:** Relative corridor usage of downstream migrating salmon and eels at HPP Unkelmühle in 2014 and 2015 (data from Økland *et al.*, 2016, 2017)

Corridor	Usage salmon [%]		Usage eels [%]	
	2014	2015	2014	2015
Spillway	0	1	59	49
Surface bypass	83	95	24	27
Rack/turbines	0	0	0	0
Vertical slot pass	5	1	12	8
Nature-like fishway or canoe pass	12	3	2	4
Bottom gallery	0	0	5	9
Side bypass	0	0	1	1

The vast majority of downstream migrating smolts used the surface bypass. The vertical slot pass, nature-like fishway, and canoe pass were used by a few smolts, whereas the other corridors were avoided. In contrast, most eels used the spillways for downstream passage and one quarter was successfully guided to the surface bypass. Some eels used the vertical slot pass, nature-like fishway, and canoe pass, but less than 10% passed through the bottom gallery or the side bypass which were specifically designed for eels. Wilke *et al.* (2019) assumed that the bottom gallery at HPP Unkelmühle was not working more efficiently due to the low rack inclination, which guided eels towards the surface bypass. None of the salmon smolts and silver eels passed the fine rack, such that the turbines were not used for downstream passage and no direct mortality was observed. To quantify indirect mortality, the natural losses at a 5.8 km long free-flowing reference stretch were compared with the losses in the 2.3 km impounded river reach and the downstream river reach. The impounded river stretch caused extra losses compared to a free-flowing river reach of 7.2% in 2014 and 17.1% in 2015 of salmon smolts, which was attributed to a denser predator population in the impounded river reach. On the basis of observations 7.5 km downstream of the HPP, it was concluded that the additional extra loss of smolts was at least 12.8%. This corresponded to a total indirect mortality rate of 25.1% in 2015, accounting for the impounded river stretch and delayed mortality due to injuries. Indirect mortality of silver eels was significantly smaller than for salmon smolts. For some eels it could not be certainly clarified if they were dead or alive when detected after HPP passage, but at least 96% of the eels in 2014 and 92% in 2015 likely survived the HPP passage.

### Conclusions and limitations of monitoring campaigns

Monitoring campaigns can provide very valuable information about the fish behavior and the efficiency of HBR-BSs, but it is difficult to generalize findings as they are often site-specific. The results of the presented monitoring campaigns show that HBR-BSs are suitable to reduce mortality and injuries of downstream moving fish, but that their efficiency strongly depends on the design of HBR-BSs, including  $s_b$ ,  $\alpha$ , and the bypass. A large number of small fish, which could have theoretically passed through the HBRs, was caught in the bypass in multiple monitoring

campaigns. This indicates that HBRs do not only act as physical barriers, but that they also have a partial behavioral protection effect. Stow net catches at multiple HPPs indicate that fish turn, to a certain extent, to their sides to pass through HBRs. It is very challenging to quantify the guidance efficiencies at existing HBR-BSs, because this requires simultaneous monitoring of all downstream passage corridors with a large sample size. The protection efficiency is especially difficult to quantify for non-migratory species, as it is difficult to distinguish between fish which use the headwater as a habitat and fish which want to swim downstream but are blocked by the HBR and do not find the bypass entrance. Another limitation of monitoring campaigns is that it is not feasible to vary a single parameter such as  $s_b$  at a specific site and monitor its effect on downstream passage, while all other parameters are kept unchanged. A comparison of the monitoring results from different sites is also challenging, as the monitoring techniques are often different and the data analysis and reporting varies strongly between studies. If fish are tagged, conclusions are valid for the tagged species and size classes only, which often limits findings to silver eels and salmon smolts. Additionally, it is very difficult to study rack passages, as fish which can physically pass through HBRs with  $s_b \leq 20$  mm are typically small with  $TL \leq 20$  cm, which means that they can only be reliably quantified with stow nets (cf. Section 2.3.1). The comparability between studies could be enhanced by defining minimal requirements for monitoring campaigns, the data analysis, and the reporting. It would also be very valuable to collect the data of different monitoring campaigns in a standardized data base. In all monitoring campaigns with stow nets installed at the turbine outlets, a substantial number of fish was caught despite HBRs with  $s_b = 15\text{--}20$  mm. However, these monitoring campaigns did either focus on eels only (HPP Rothenburg) or they were conducted at HBR-BSs not meeting current design recommendations (HPP Walkmühle, HPP Wehlitz, and HPP Rappenberghalde). In case of HPP Lindesmühle, the rack-parallel velocity component was negligible due to the arrangement of the HBR and a suitable bypass was missing. A monitoring campaign at a state-of-the-art HBR-BS, where the number of rack and bypass passages was simultaneously and reliably quantified, is still missing.

### 3.8 Identified research gaps and objectives

In this chapter, an overview of the state-of-the-art and the design of HBR-BSs was given. It was shown that previous studies at HBR-BSs focused on a limited parameter range, such that little was known about the velocity fields up- and downstream of HBRs. Up to now, it was also difficult to precisely estimate hydraulic losses for a wide range of rack parameters and different HPP layouts. Although a reasonable number of ethohydraulic studies and monitoring campaigns was conducted at HBR-BSs, it remains difficult to estimate the fish guidance and protection efficiency. Studies indicate that the combination of HBRs with a low-voltage electric field allows for increasing the clear bar spacing, while enabling fish protection, but the fish behavior in the electric field has hardly been analyzed. The available information on operational aspects of HBRs is site-specific and based on few observations at prototype HPPs. A systematic investigation with floating debris like leaves and branches was missing. The identified research

gaps have led to the following objectives of this doctoral thesis:

- I) Quantify the **velocity fields** up- and downstream of HBRs,
- II) develop an equation to reliably estimate the **hydraulic losses** of HBRs,
- III) determine the **fish guidance efficiency** of HBR-BSs,
- IV) investigate the fish behavior at HBR-BSs with a **low-voltage electric field**, and
- V) quantify the effect of different parameters on **foliage clogging**.



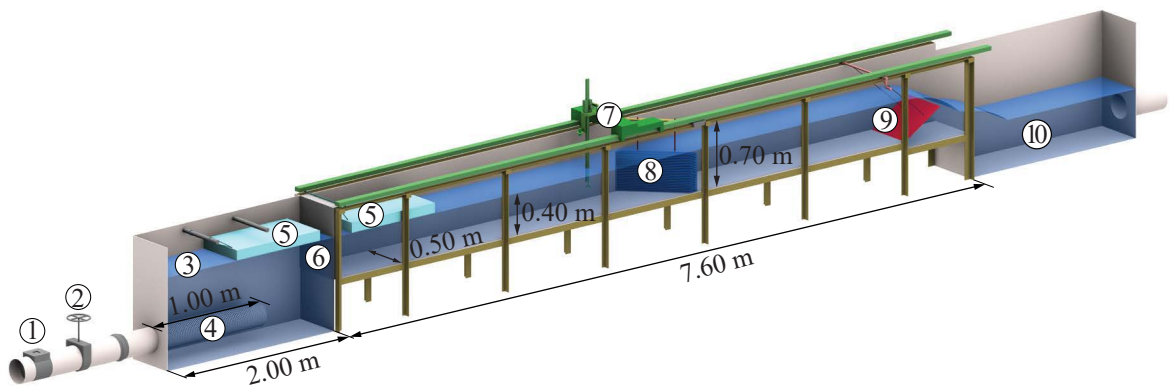
## 4 Experimental setup and methods

### 4.1 Model flumes

To address different research questions, the experiments of the present thesis were conducted in three different laboratory flumes. A detailed section of an HBR on a scale of 1:1 was investigated in all experiments, but the bypass was only modeled in the largest flume, called ethohydraulic flume in the following. A detailed hydraulic model investigation was conducted with a diversion HPP setup, meaning that the channel width was constant up- and downstream of the rack. In addition, experiments were carried out in a flume with an adjustable upstream channel width, allowing for the investigation of a block-type HPP, where the powerhouse is smaller than the approach flow width. The live fish tests were conducted in the ethohydraulic flume.

#### 4.1.1 Detailed model diversion hydropower plant

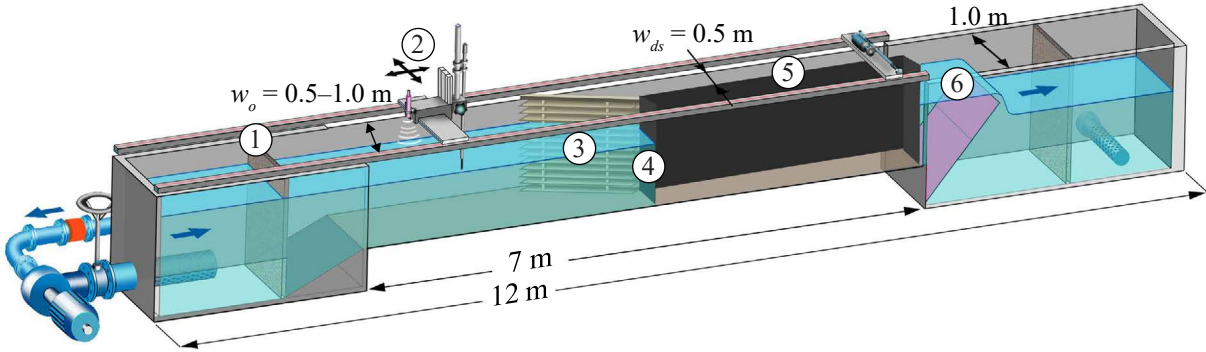
This laboratory flume had a horizontal bed, was 7.60 m long,  $w_{ch} = 0.50$  m wide, and 0.70 m deep (Fig. 4.1). The channel bottom and back wall were made of PVC (polyvinyl chloride), whereas the front wall was made of glass to allow for visual observations. The discharge of the closed water circulation system was controlled with a gate valve and measured with a magnetic-inductive flow meter (MID). To achieve symmetric approach flow conditions, a honeycomb flow straightener was placed at the channel inlet. The rack end was positioned 4.2 m downstream of the honeycomb flow straightener. Two 1 m long hard foam floaters were used to reduce surface waves. The water level was controlled with a downstream flap gate, creating a free overfall into the outlet basin. The measurement traverse carried an ultrasonic distance sensor (UDS) and an acoustic Doppler velocimeter (ADV).



**Fig. 4.1:** Schematic 3D view of the experimental flume for the detailed model investigation of the diversion HPP setup including the following elements: ① MID, ② gate valve, ③ inlet tank, ④ perforated inlet pipe, ⑤ floater, ⑥ honeycomb-shaped flow straightener, ⑦ traverse system and measurement cart carrying an ADV and an UDS, ⑧ HBR, ⑨ flap gate, and ⑩ outlet tank

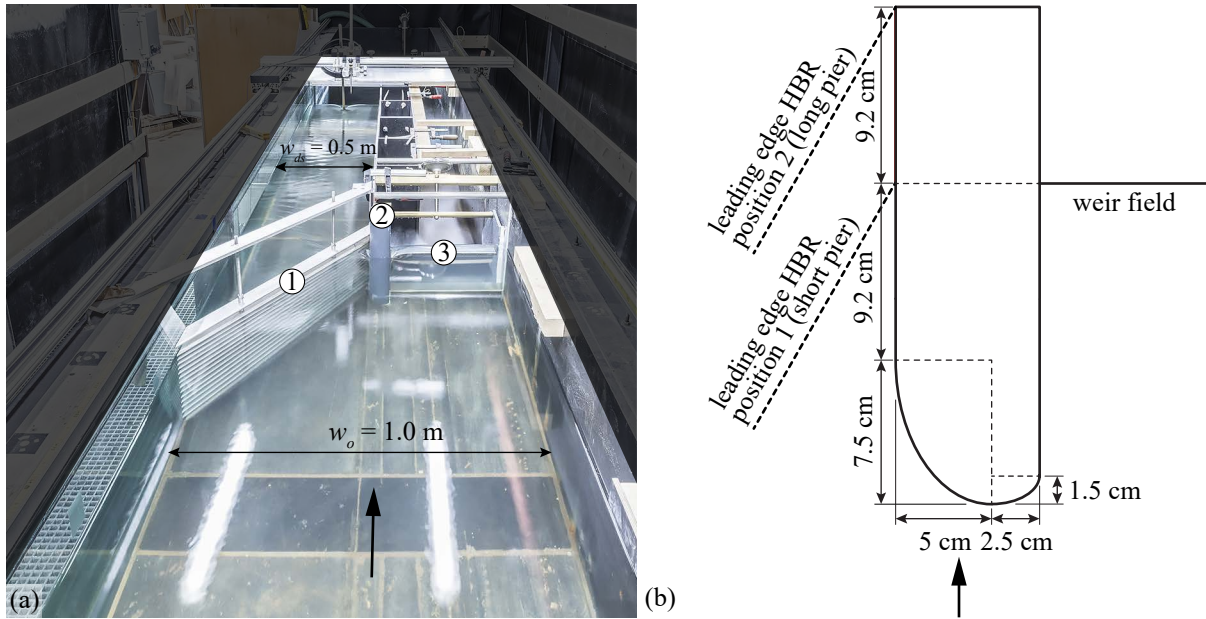
#### 4.1.2 Detailed model block-type hydropower plant

The block-type HPP was investigated in a similar flume as the diversion HPP (Fig. 4.2), but it was possible to adapt the upstream channel width. Upstream channel widths of  $w_o = 0.50$ ,  $0.625$ ,  $0.75$ , and  $1.00$  m were investigated, leading to contraction ratios of  $w_o/w_{ds} = 1.0$ ,  $1.25$ ,  $1.5$ , and  $2.0$ , where  $w_{ds}$  = downstream channel width. An under- and overshot gate was installed at the downstream rack end to model the adjacent weir (Fig. 4.3a). When both openings of the gate were closed, the weir corresponded to a vertical wall, leading to a sharp contraction from the upstream to downstream (Fig. 4.2).



**Fig. 4.2:** Schematic 3D view of the experimental flume for the detailed model investigation at the block-type HPP with a contraction ratio of  $w_o/w_{ds} = 2.0$  including ① a honeycomb-shaped flow straightener, ② traverse system and measurement cart carrying an ADV and an UDS, ③ HBR, ④ under- and overshot gate (closed), ⑤ PVC wall to reduce the channel width, and ⑥ flap gate (adapted from Kriewitz, 2015)

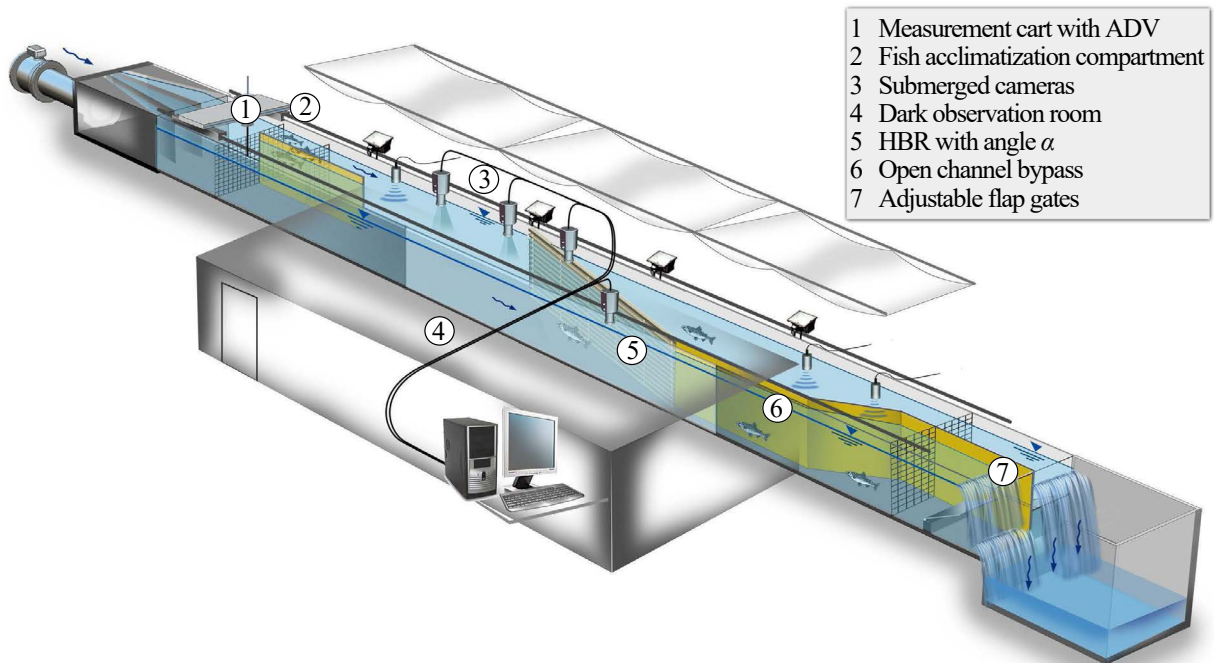
A dividing pier was installed between the HBR and the weir field to reduce detachment zones and improve the HBR approach flow field (Fig. 4.3a). The design of the pier was based on two quarter ellipses with a width of  $0.15w_{ds} = 7.5$  cm, following the guidelines of Rouvé (1958) (Fig. 4.3b). The other dimensions of the pier were selected to represent typical Swiss run-of-river HPPs and are shown in Fig. 4.3b. The position of the HBR was varied to represent different pier lengths. The leading edge of the HBR was installed at  $0.167$  m  $= 0.33w_{ds}$  and  $0.259$  m  $= 0.52w_{ds}$  downstream of the pier nose, representing a short and long pier, respectively (Fig. 4.3b).



**Fig. 4.3:** (a) View in flow direction on the block-type HPP setup with a contraction ratio of  $w_o/w_{ds} = 2.0$  with ① an HBR with foil-shaped bars,  $\alpha = 30^\circ$ ,  $s_b = 20 \text{ mm}$ , ② a short pier, and ③ opened weir field; (b) dimensions of the pier and positioning of the HBR to investigate the short and the long pier

#### 4.1.3 Ethohydraulic flume

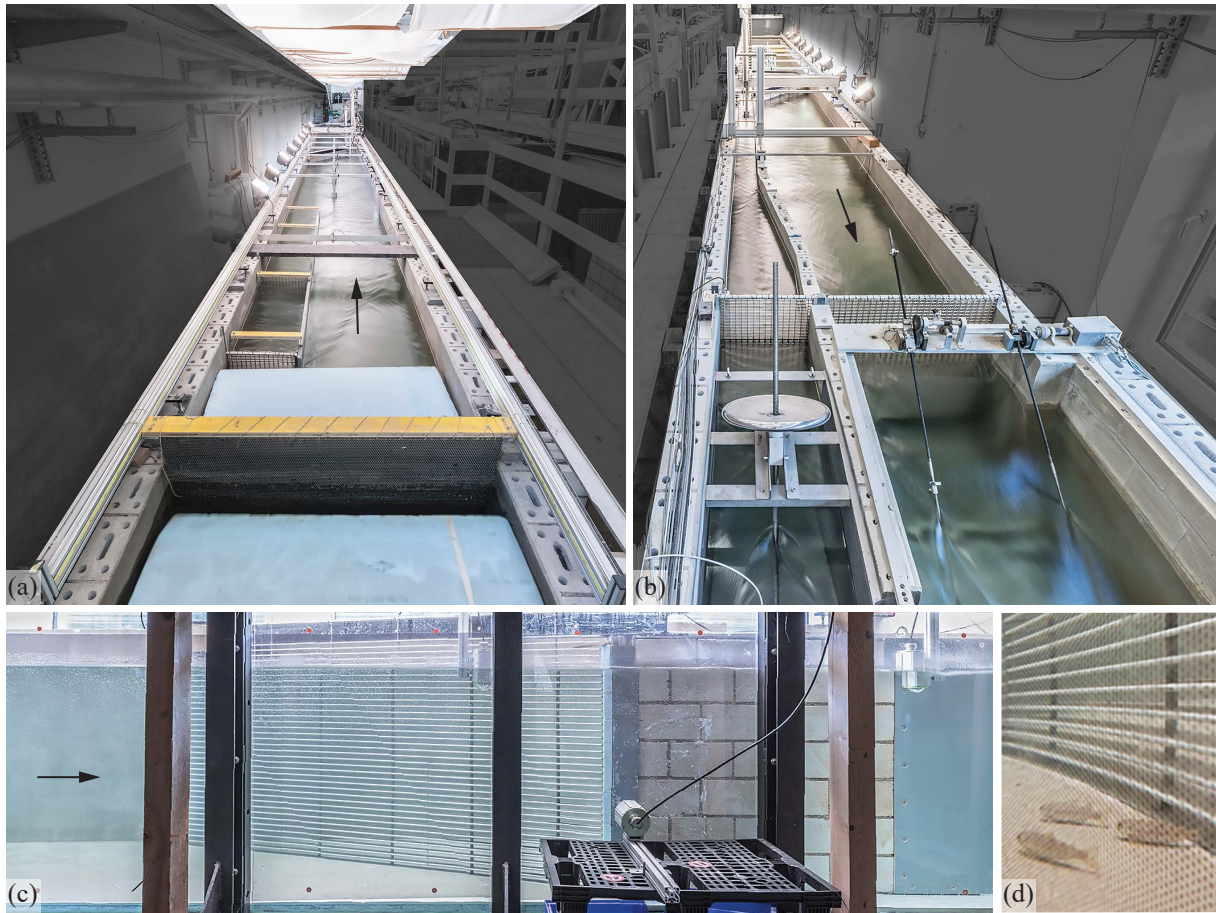
The live fish tests were conducted in a 30 m long,  $w_o = 1.5 \text{ m}$  wide, and 1.4 m deep laboratory flume with a horizontal bed (Fig. 4.4 and 4.5). The water temperature of the closed water circuit was controlled with a cooling system, such that all live fish tests were carried out with water temperatures in the range of  $T = 12\text{--}16^\circ\text{C}$ , which is important as it affects the fish swimming capabilities (cf. Eq. 2.9, 2.10). The discharge could be continuously regulated in the range of  $0.2\text{--}1.2 \text{ m}^3/\text{s}$ , leading to average approach flow velocities from continuity of  $U_o = 0.15\text{--}0.89 \text{ m/s}$  for an approach flow depth of  $h_o = 0.90 \text{ m}$ . A symmetric approach flow was achieved with a honeycomb flow straightener and two hard foam floaters (Fig. 4.5a). An ADV-probe was used to measure flow velocities (Fig. 4.4). A 1.5 m long acclimatization compartment was installed 12–10.5 m upstream of the bypass inlet (Fig. 4.4 and 4.5a) on the left side (opposite of bypass entrance). The fish movements were tracked with five submerged cameras upstream of the rack and their behavior was simultaneously studied from the observation room (Fig. 4.4 and 4.5c,d).



**Fig. 4.4:** Sketch of ethohydraulic flume illustrating ① measurement cart with an ADV, ② fish acclimatization compartment, ③ submerged cameras, ④ dark observation room, ⑤ HBR with angle  $\alpha$ , ⑥ open channel bypass, and ⑦ adjustable flap gates at the downstream end of the bypass and the main flume (adapted from Kriewitz, 2015)

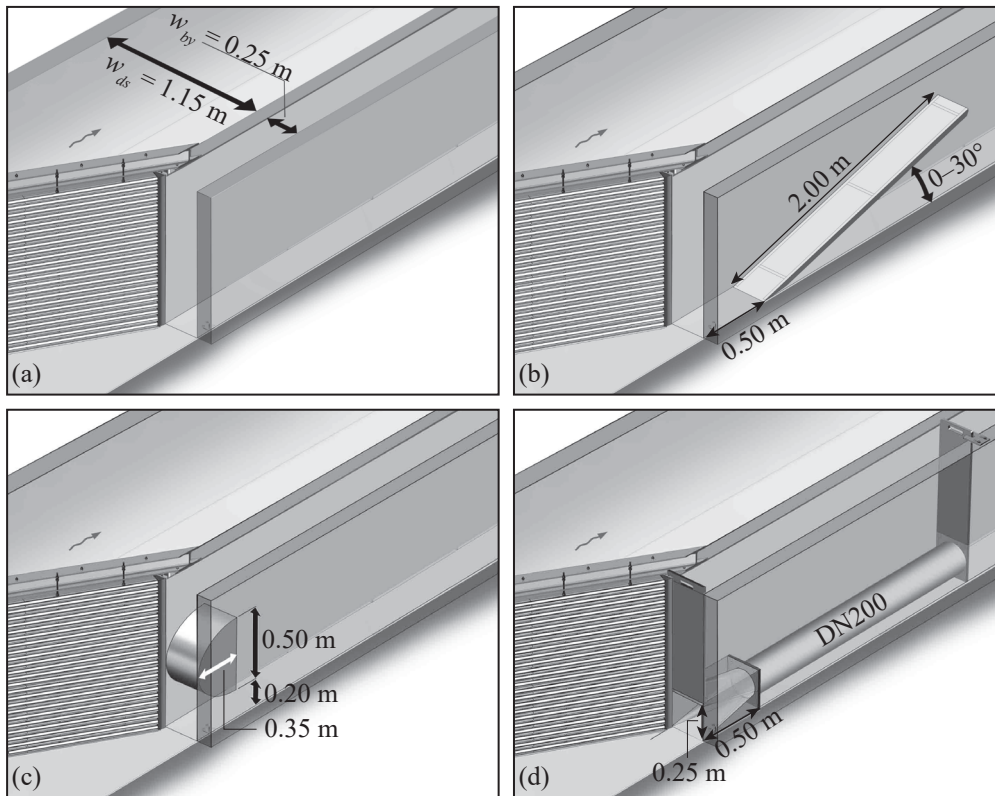
The left channel wall (in flow direction) and the bottom were made of concrete, whereas the right channel wall was made of glass to allow for visual observations from the dark observation room (Fig. 4.4). Figure 4.5c shows a picture from the observation room through the glass wall on the HBR and the bypass during the first live fish tests. After the first two experimental weeks with live fish, a perforated foil was attached to the glass wall. This foil was imitating a concrete wall, such that fish could not see into the observation room and were not mirrored at the glass wall, while they could still be observed from the side (Fig. 4.5d). To ensure constant light conditions for all experiments, white sheets were installed above the flume and illuminated with eight 1000 Watt halogen spot lights, creating constant indirect light conditions across the entire flume for all experiments. A 10 cm wide concrete wall was installed at the downstream rack end to separate the bypass from the tailwater. The bypass was  $w_{by} = 0.25$  m wide and expanded to 0.50 m in the downstream section, such that fish entering the bypass were not exposed to large flow velocities until the end of the experiment (Fig. 4.5b). The bypass and the tailwater could be regulated with separate flap gates to control the flow depth and the flow velocity in the bypass independently (Fig. 4.4).





**Fig. 4.5:** Ethohydraulic flume (a) in flow direction from the inlet, (b) against the flow direction from the outlet, (c) from the observation room through the glass wall (without perforated foil), and (d) a detailed view from the observation room through the glass wall with the perforated foil on three salmon parr

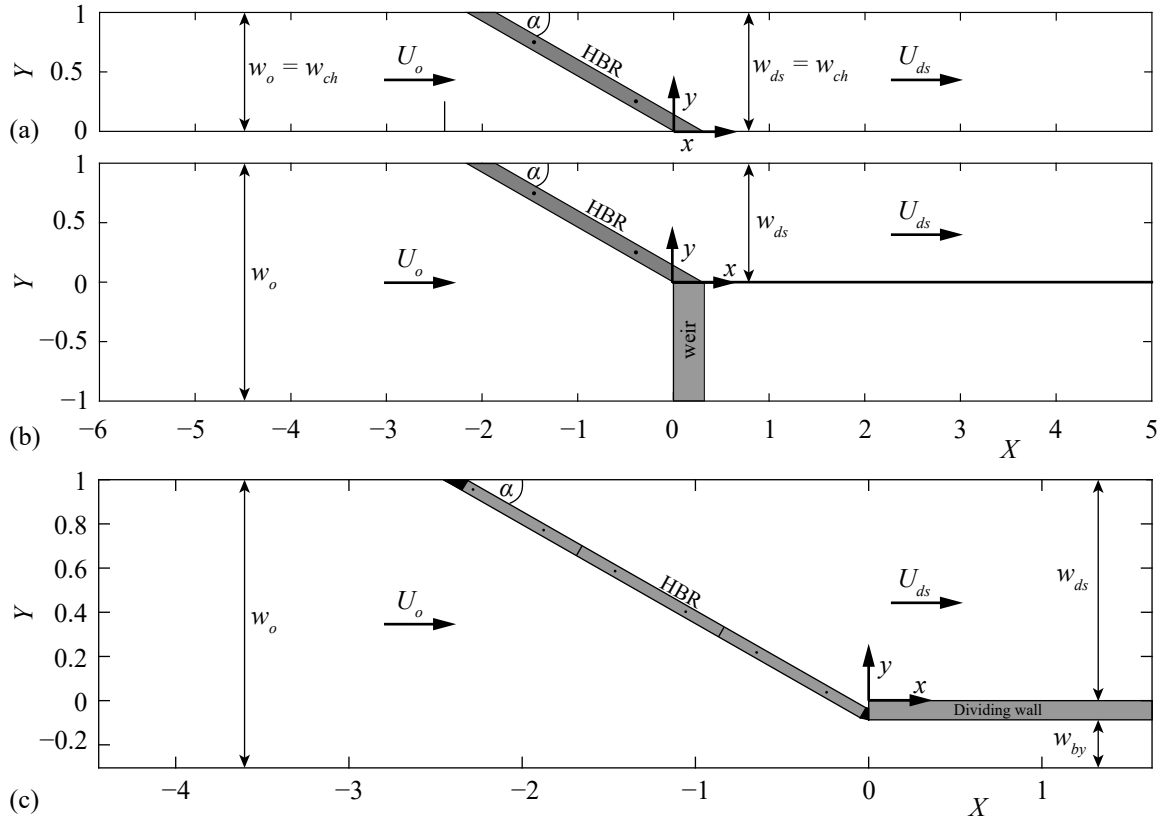
The bypass was designed modular, such that different bypass entrances could be investigated. Figure 4.6a shows the full depth open channel bypass (OC), where fish could enter the bypass in all flow depths. Figure 4.6b illustrates the open channel bypass with a 2 m long flap gate to create continuous flow accelerations. The angle to the horizontal could be varied between  $\gamma = 10\text{--}30^\circ$ . To reduce the bypass discharge while maintaining flow accelerations, a restrictor was installed at the bypass inlet (RE), creating a bottom and top opening for downstream passage (Fig. 4.6c). Figure 4.6d shows a rectangular bypass opening with a subsequent pipe as recommended by Lehmann *et al.* (2016) (cf. Section 3.4.2). The opening was 0.25 m wide and high, followed by a 0.50 m long transition cone to a pipe bypass with a diameter of 0.20 m.



**Fig. 4.6:** Different bypass configurations: (a) full depth open channel bypass (OC), (b) open channel bypass with flap gate, (c) open channel bypass with inlet restrictor (RE), and (d) pipe bypass

#### 4.1.4 Coordinate system

To enhance comparability, the point of origin in all flumes was set to the downstream rack end at the flume bottom (Fig. 4.7). The  $x$ - and  $z$ -axis were normalized with  $h_o$  and the  $y$ -axis with  $w_{ds}$ , such that  $X = x/h_o$ ,  $Y = y/w_{ds}$ , and  $Z = z/h_o$ . The HBRs therefore extended across  $Y = 0-1$ , while negative  $Y$ -coordinates represented the location of the weir (Fig. 4.7b) and the bypass including the dividing wall between the bypass and the downstream in the ethohydraulic flume (Fig. 4.7c).

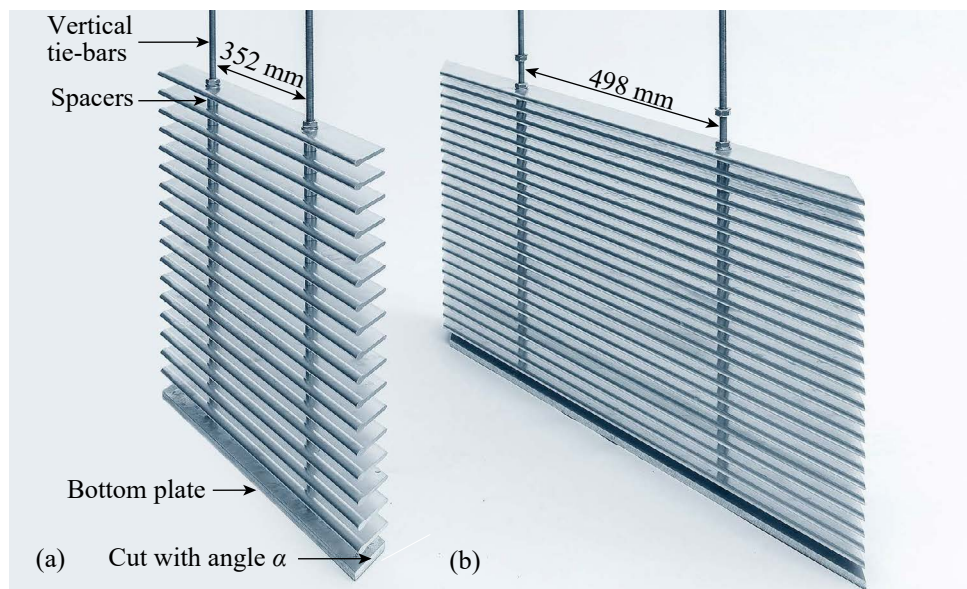


**Fig. 4.7:** Definition of the coordinate system at (a) diversion HPP, (b) block-type HPP, and (c) ethohydraulic flume with the HBR with  $\alpha = 30^\circ$ ; the circles ( $\bullet$ ) indicate the location of the vertical tie-bars

## 4.2 Model racks and parameter definition

### 4.2.1 Construction of the horizontal bar rack

The model racks were constructed on Froude-scale 1:1, which means that the bars were on prototype scale, but only a section of the rack was modeled. The modular construction allowed to build racks with different bar shapes, approach flow angles, clear bar spacing, and overlay configurations (details in Section 4.2.3). For the detailed model investigation at the diversion HPP and the block-type HPP (Section 4.1.1 and 4.1.2), the racks were constructed with a  $t_{bp} = 10$  mm thick bottom plate,  $t_s = 15$  mm thick spacers (outer diameter), and two M10 threaded bars, which are also referred to as vertical tie-bars (Fig. 4.8). The latter were positioned at  $Y = y/w_{ds} = 0.25$  and  $0.75$ , independent of  $\alpha$ , leading to an axial distance between the tie-bars of 498 mm, 352 mm, and 250 mm, for  $\alpha = 30^\circ$ ,  $45^\circ$ , and  $90^\circ$ , respectively. Both ends of all bars and the bottom plate were cut with the horizontal approach flow angle  $\alpha$ .



**Fig. 4.8:** Model racks of the detailed model investigation (a)  $\alpha = 45^\circ$ ,  $s_b = 20$  mm, bars with ellipsoidal tips and tails and (b)  $\alpha = 30^\circ$ ,  $s_b = 10$  mm, foil-shaped bars (adapted from Meister *et al.*, 2018a)

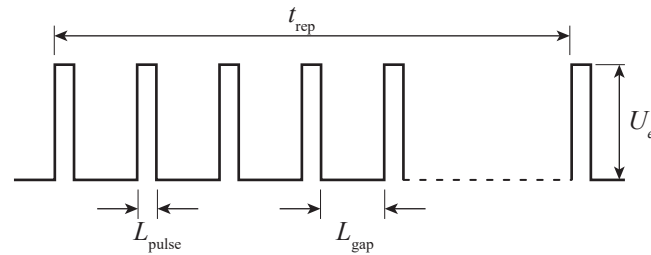
The HBR of the ethohydraulic flume with  $\alpha = 30^\circ$  consisted of two 840 mm and one 683 mm long rack fields, each with two vertical tie-bars with an axial distance of 420 mm. The locations of the rack fields and the vertical tie-bars ( $\cdot$ ) are indicated in Fig. 4.7c. The bars were cut with an  $90^\circ$  angle at both sides and hard foam wedges were used at the up- and downstream end of the rack to get a smooth transition to the flume and bypass wall (Fig. 4.9). A 2 mm thick U-profile was built-in the bottom, such that the 25 mm thick bottom plate was at ground level of the flume (Fig. 4.10). To obtain a constant clear bar spacing of  $s_b = 20$  mm, the spacer height between the bottom plate and the first bar was 21.5 mm, while it was 23 mm between all other bars (Fig. 4.10). At some traditional trash racks, vibrations were observed in the past, which, in some cases, led to deformations of the bars or in the worst case to rack failures (Schleiss, 1985). Due to the generally lower approach flow velocities at HBRs, the vortex-induced vibration risk is lower than at traditional trash racks. The susceptibility of the laboratory HBR to vibrations was estimated following Schleiss (1985) and Schleiss and Fust (1992). The maximal oscillation amplitudes of individual bars in the ethohydraulic flume were less than 0.15 mm and therefore negligible, which was confirmed by the experiments, where no vibrations were observed. However, it is difficult to assess the susceptibility to vibration of entire rack fields (Schleiss and Fust, 1992). The vibration risk at prototype HPPs should therefore be reduced by constructional measures, such as the aggregation of rack fields and force-locking connections to piers (Schleiss and Fust, 1992).





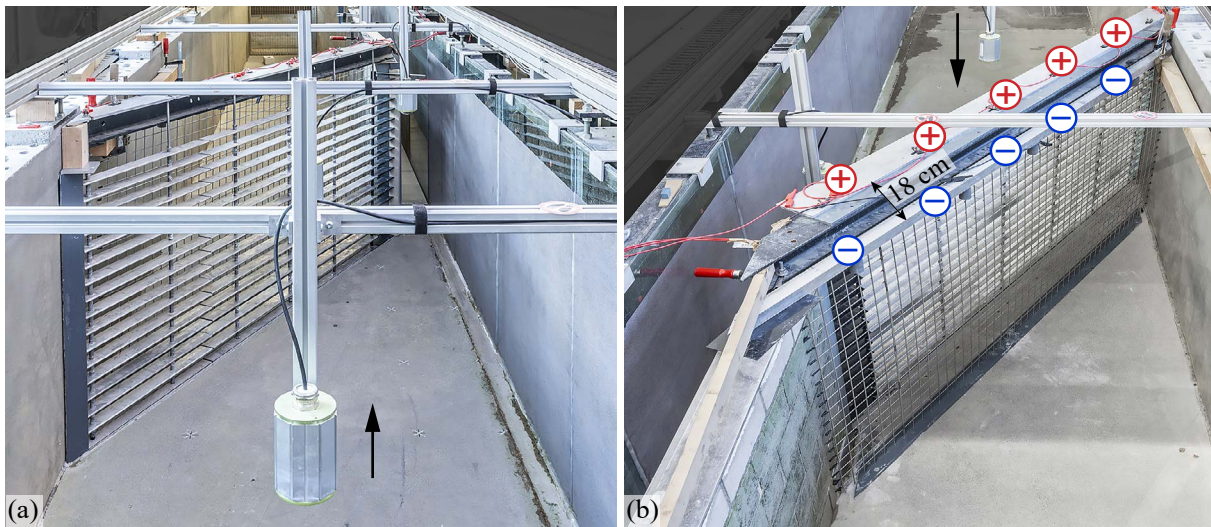
$\approx 0.08 \text{ W}$ .

$$D = \frac{N_{\text{pulse}} L_{\text{pulse}}}{t_{\text{rep}}} \quad (4.1)$$



**Fig. 4.11:** Illustration of the direct current gated bursts (gpDC) generated with Neptun DC fish-guidance system

The model racks consisted of aluminum bars, which were connected with aluminum spacers and tie-bars (cf. Section 4.2.1). Instead of using each bar individually as anode and cathode, a stainless steel metal mesh, which was mounted 18 cm downstream of the HBR (clear distance, measured orthogonal, Fig. 4.12), was used as the cathode  $\ominus$ , while the HBR itself was used as the anode  $\oplus$ . The HBR and the metal mesh were connected with cables and multiple crocodile clips to the control unit. To reduce the electric field in front of the bypass, the most downstream 20 cm of the HBR were isolated with an insulating tape.

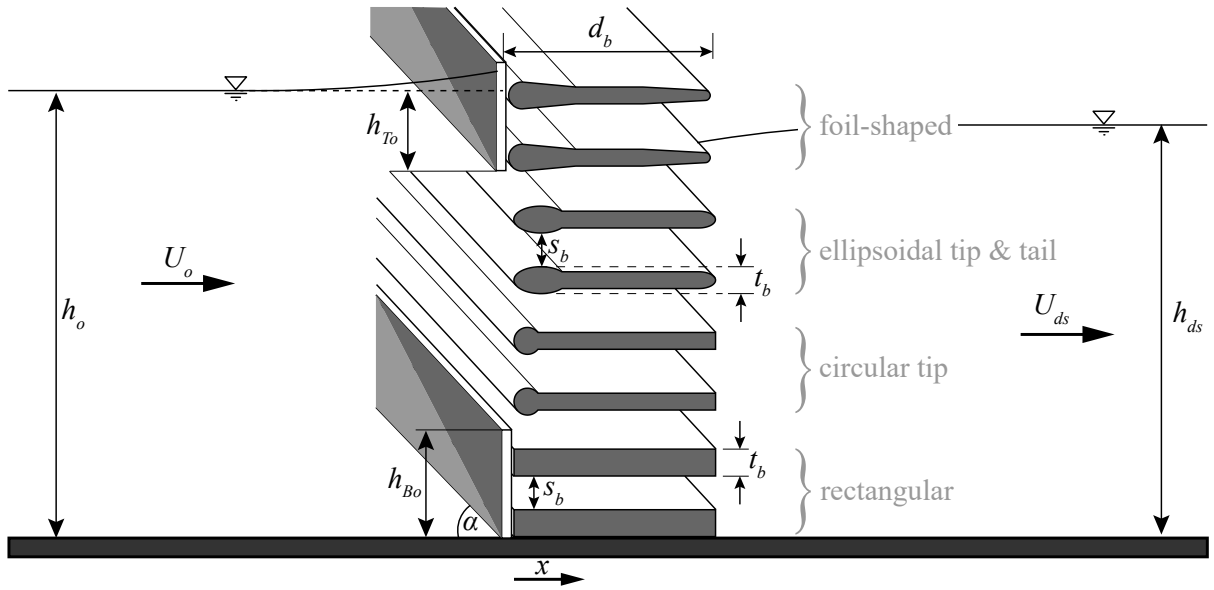


**Fig. 4.12:** Electrification of HBR with  $s_b = 51 \text{ mm}$  (a) in flow direction and (b) against flow direction with HBR as anode  $\oplus$  and metal mesh as cathode  $\ominus$

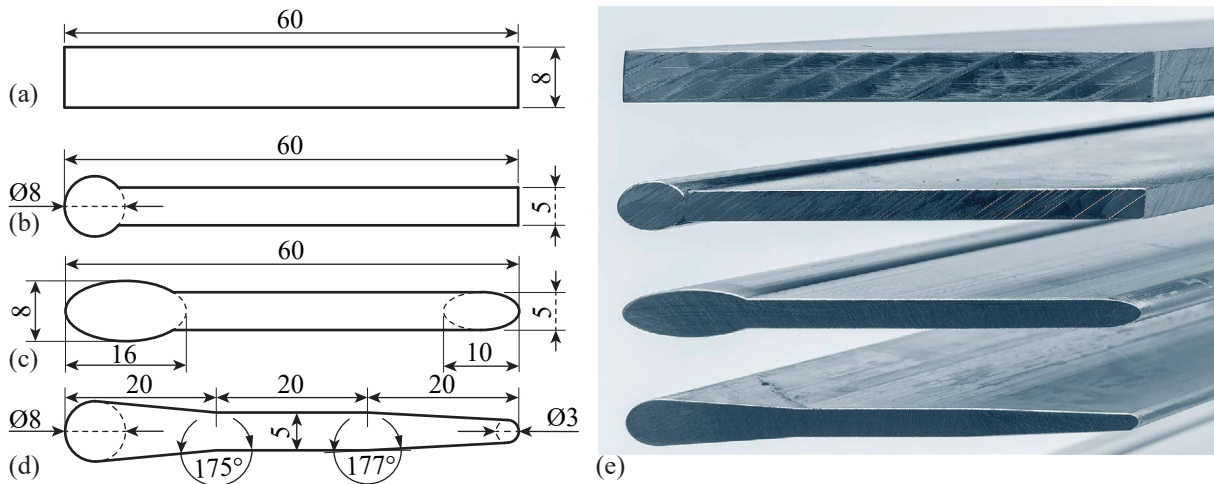
### 4.2.3 Parameter definition

Figure 4.13 gives an overview of the investigated parameters. The approach flow depth upstream of the rack  $h_o$  was controlled with the flap gate at the channel outlets. It was defined as the flow depth far upstream, such that it was unaffected by the backwater rise due to the rack (Fig. 4.13). At that point, the approach flow velocity  $U_o$  was calculated from continuity. Analog, the mean downstream flow velocity  $U_{ds}$  was calculated from continuity using the downstream flow depth. The latter was defined as far downstream, such that it was unaffected by the local

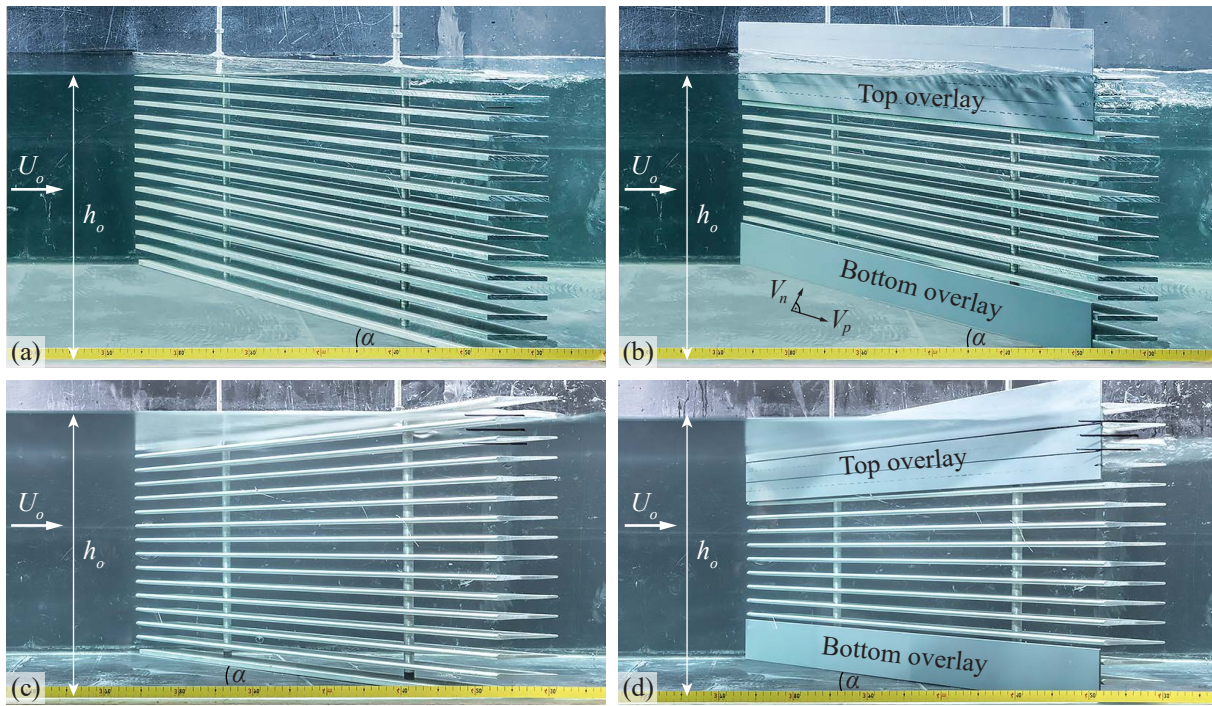
flow depth drop behind the rack (Fig. 4.13). The angle between the rack and the channel walls is denoted as  $\alpha$ . The investigation included rectangular and foil-shaped bars, as well as bars with a circular tip and an ellipsoidal tip and tail (Fig. 4.14). The bar thickness was defined at the thickest point and was constant for all experiments ( $t_b = 8$  mm). The bar thickness at mid cross section (the mounting location) was  $t_{b,m} = 5$  mm, except for the rectangular bars (S1), where  $t_{b,m} = t_b = 8$  mm (Fig. 4.14a–d). In contrast to the rectangular bars (S1), the thickness of the bars S2–S4 reduced from tip to tail, which made them hydrodynamically efficient. These bars (S2–S4) are termed hydrodynamic bars hereafter. The model HBRs consisted of bars on prototype scale and were designed to represent most practically applied shapes and dimensions (cf. Section 3.2). The relative bar depth  $D_b$  was defined as the ratio of the bar depth  $d_b$  and the bar thickness  $t_b$ , that is,  $D_b = d_b/t_b$ . The relative bottom overlay height was calculated from the absolute bottom overlay height  $h_{Bo}$  and the approach flow depth as  $H_{Bo} = h_{Bo}/h_o$ . Accordingly, the relative top overlay height was defined as  $H_{To} = h_{To}/h_o$ , leading to a total relative overlay height of  $H_{Ov} = H_{Bo} + H_{To}$ . The top overlay height  $h_{To}$  was measured from the approach flow depth  $h_o$ , that is, it did not include the backwater rise due to the rack (Fig. 4.13). Figure 4.15 shows laboratory HBRs at the diversion HPP for different bar shapes and overlay configurations. The vector decomposition of  $U$  and  $V$  to  $V_n$  and  $V_p$ , as described in Section 3.4.1, is illustrated in Fig. 4.15b.



**Fig. 4.13:** Definition sketch of the governing rack parameters



**Fig. 4.14:** Detailed view of the investigated bars, which are referred to as (a) S1 rectangular, (b) S2 circular tip, (c) S3 ellipsoidal tip & tail, and (d) S4 foil-shaped in the following; (e) picture of the investigated bar shapes, which were cut with an angle  $\alpha = 45^\circ$



**Fig. 4.15:** Side view of the laboratory HBR at the diversion HPP with  $s_b = 20$  mm and  $\alpha = 45^\circ$  with (a) rectangular bars (S1) without overlays ( $H_{O_v} = 0$ ), (b) rectangular bars with  $H_{Bo} = H_{To} = 0.2$  (adapted from Meister *et al.*, 2018b), (c) foil-shaped bars (S4) without overlays, and (d) foil-shaped bars with  $H_{Bo} = H_{To} = 0.2$

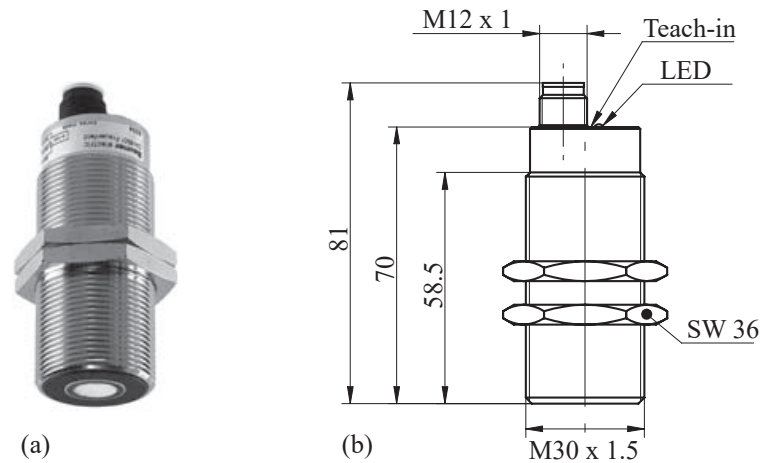
### 4.3 Instrumentation and measurement systems

#### Ultrasonic distance sensors

Distances to water surfaces were measured with ultrasonic distance sensors (UDS) UNAM 30I6103/S14 of the company Baumer (Fig. 4.16). These UDS can be used to measure distances in the range of 100–1000 mm with a sampling rate of 100 Hz. According to the manufacturer, the repeat accuracy is smaller than 0.5 mm and the maximal temperature drift adds up to 2% of the distance between the sensor and the object (Baumer, 2018). The UDS were installed



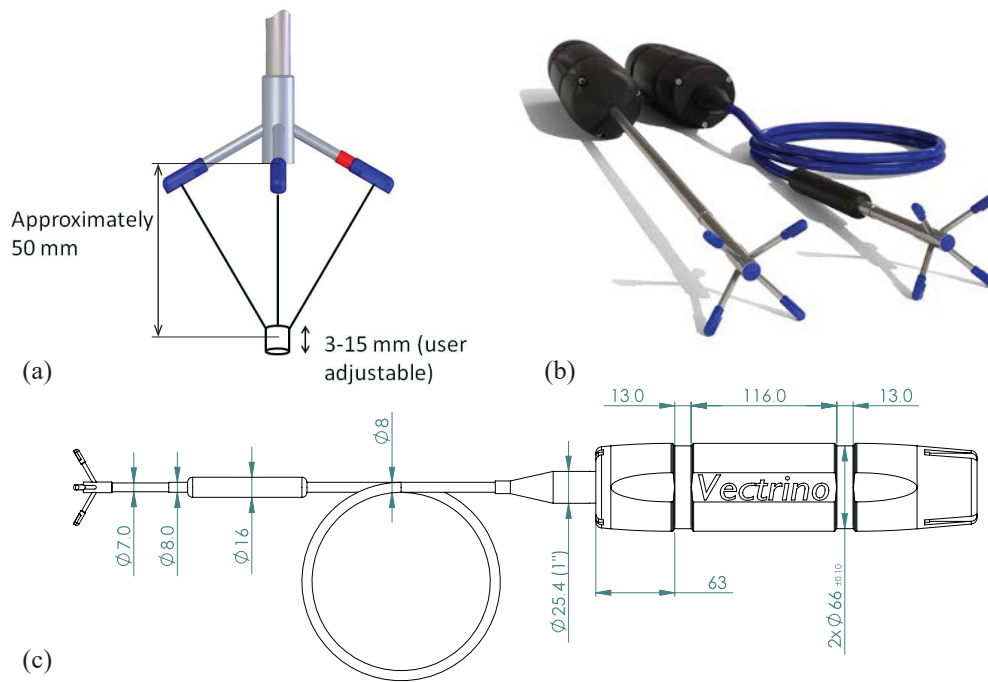
$\approx 350$  mm above the water surface.



**Fig. 4.16:** (a) A picture of the UDS and (b) the corresponding technical illustration (all measures in millimeters) (adapted from Baumer, 2018)

### Acoustic Doppler velocimeter

The flow velocities were measured with down-looking acoustic Doppler velocimeters (ADV) of the company Nortek AS (Fig. 4.17). These acoustic sensors have one transmit transducer and four receive transducers to measure the Doppler shift and therefore quantify 3D velocities and turbulences. The probe volume is situated  $\approx 50$  mm below the transmit transducer (Fig. 4.17a). The velocity measurements for the diversion HPP setup were conducted with the standard firmware, which allowed for a sampling rate of 25 Hz. The Plus firmware was used for the velocities measurements at the block-type HPP setup and in the ethohydraulic flume, allowing for increased sampling rates of 200 Hz. The sampling volume was set to 7.0 mm for all velocity measurements. The accuracy was  $\pm 0.5\%$  of the measured value  $\pm 1$  mm/s (Nortek AS, 2016).



**Fig. 4.17:** Down-looking Nortek ADV: (a) illustration of probe head and measurement volume, (b) picture of two Nortek lab probes, and (c) exact dimensions of the probes in millimeters (adapted from Nortek AS, 2016)

### Magnetic-inductive flow meter

The discharge at all flumes was measured with magnetic-inductive flow meters (MIDs) with an accuracy of approximately  $\pm 0.5\%$  of the measured value. The MID models Aquaflux 010K/D/6 of the company Krohne, Optiflux 2100 of the company Krohne, and Promag 50 of the company Endress+Hauser were installed at the diversion HPP flume (Section 4.1.1), the block-type HPP flume (Section 4.1.2), and the ethohydraulic flume (Section 4.1.3), respectively.

### Fish-tracking

During all live fish tests, fish were observed with a specifically developed camera tracking system. The camera setup, calibration procedure, the tracking algorithm, and the limitations were reported in detail in Harby *et al.* (2020) and are briefly summarized in the following. Five submerged cameras of the type acA2040-35gmNIR (Basler) with a maximal resolution of  $2048 \times 1536$  px<sup>2</sup>, 185° fisheye lenses of type FE185C086HA-1 (Fujifilm), and a waterproof IP67 Orca S dome (autoVimation) were installed upstream of the HBR (cf. Fig. 4.4 and in the foreground of Fig. 4.12a). A GigE Vision 2.0 network with a Precision Time Protocol (PTP) IEEE1588 allowed for synchronous recording of all cameras with 20 frames per second. A checkerboard with  $9 \times 6$  crossing points was recorded from different angles and distances for calibration. The raw images were undistorted to account for the fish eye lens and the refraction due to the glass dome housing. Each pair of cameras with an overlapping view was calibrated with a stereo calibration. Finally, the local stereo camera coordinates were transformed to the global flume coordinates, by using 43 fixed reference points on the flume bottom. Moving objects like fish were then detected on each frame, and a motion-based multiple object tracking algorithm was used to group all detections, corresponding to the same object over time. The

main challenges were to correctly filter out noise, which resulted from moving reflections or fish-shadows and to correctly merge individual tracks. 2D data of the fish center were retrieved for the whole observation area. In regions with an overlapping view of multiple cameras, it was also possible to extract 3D tracks. In the present study, fish were primarily swimming close to the flume bottom and the investigation focused on the swimming behavior in  $x$ - and  $y$ -direction, such that the 2D tracks were used for the analysis. The  $z$ -coordinate was set to 0.02 m above the bottom after calibration. A backward calculation of multiple calibration videos showed that the mean error of the tracking software was  $5\text{--}15 \pm 5\text{--}10$  mm.

## 4.4 Methods and experimental program

### 4.4.1 Velocity fields

This subsection describes the methods and experimental program for the analysis of the velocity fields. It was first published in a slightly modified form in Meister *et al.* (2020c).

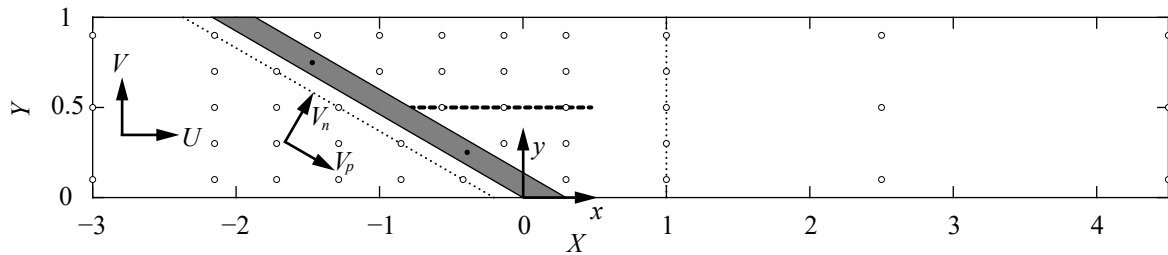
#### Parameter range and test program

Velocity fields were measured up- and downstream of HBRs with rectangular bars (S1), rectangular bars with a circular tip (S2), bars with an ellipsoidal tip and tail (S3), and foil-shaped bars (S4; Fig. 4.13 and 4.14). The bars were  $t_b = 8$  mm thick,  $d_b = 60$  mm deep, and assembled with a clear bar spacing of  $s_b = 10, 20$ , or  $30$  mm. The investigated horizontal approach flow angles were  $\alpha = 30^\circ$  and  $45^\circ$  for all bar shapes. As a reference, HBRs with  $\alpha = 90^\circ$  and S2 bars were studied. Note that such  $90^\circ$ -racks are of small practical relevance for fish protection due to increased fish impingement risk and low guidance effect towards the bypass (cf. Section 2.4). The velocity fields were investigated without overlays ( $H_{Ov} = 0$ ), with either bottom or top overlays ( $H_{Bo} = 0.2, H_{To} = 0$ ;  $H_{Bo} = 0, H_{To} = 0.2$ ), and with combined bottom and top overlays ( $H_{Bo} = H_{To} = 0.2$ ). The approach flow depth and the discharge were kept constant at  $h_o = 0.40$  m and  $Q_o = 0.1$  m<sup>3</sup>/s, respectively, resulting in a mean approach flow velocity of  $U_o = 0.5$  m/s, a Froude number of  $F = U_o / \sqrt{gh_o} = 0.25$ , a bar Reynolds number of  $R_b = t_b U_o / \nu = 4000$ , and a Reynolds number of  $R = 4R_h U_o / \nu = 3 \times 10^5$  for the diversion HPP layout. The hydraulic radius at the diversion HPP was  $R_h = h_o w_o / (2h_o + w_o) = 0.15$  m and the kinematic viscosity  $\nu = 1.01 \times 10^{-6}$  m<sup>2</sup>/s for a water temperature of  $T = 20^\circ\text{C}$ . To allow for a direct comparison of the normalized velocity fields at different HPP layouts and discharge distributions between the power canal and the spillway discharge over the weir, the theoretical flow velocity  $U_{th}$  was used for normalization (cf. Section 2.5.2). To better understand the bypass hydraulics and to analyze the fish behavior, different bypass designs (cf. Fig. 4.6), were investigated in the ethohydraulic flume (cf. Section 4.1.3). All experiments in the ethohydraulic flume were conducted with the hydraulically optimized rack configuration, which was used for most live fish tests, that is, S4-bars,  $\alpha = 30^\circ$ ,  $s_b = 20$  mm, and  $H_{Ov} = 0$ . The velocity field upstream of the HBR and in the bypass was measured in horizontal planes close to the bottom ( $Z = 0.14$ ), at mid flow depth ( $Z = 0.50$ ), and close to the water surface ( $Z = 0.86$ ) in the ethohydraulic flume. Different bypass configurations were compared in terms of  $U/U_o$ , SVG, and TKE at the bypass center line between  $X = -4$  and  $X = 2$ . An additional cross section in the bypass was

measured at  $X = 0.56$  ( $x = 0.50$  m).

### Experimental procedure

The streamwise, transversal, and vertical flow velocities  $U$ ,  $V$ , and  $W$ , respectively, were measured with a down-looking ADV probe. The measurement duration at each location was either 30 s at a sampling rate of 200 Hz or 60 s at a sampling rate of 25 Hz. All ADV-data were de-spiked with the Goring and Nikora (2002) method modified by Mori *et al.* (2007). The minimal correlation and signal-to-noise ratio were set to 70% and 10 db, respectively. The measurements at the diversion HPP and block-type HPP were conducted at three horizontal planes, corresponding to  $Z = 0.1, 0.5, 0.8$  and  $Y = 0.1, 0.3, 0.5, 0.7, 0.9$  (Fig. 4.18). To assess the fish guidance capacity ( $FGC = V_p/V_n$ ; cf. Section 3.4.1), detailed measurements were conducted at a cross section parallel to the rack, at a distance of 40 mm orthogonal to the rack (dotted line in Fig. 4.18). To evaluate the effect of HBRs on the turbine admission flow, the velocities at the cross section  $X = 1$  were measured in detail (dotted line in Fig. 4.18). The filled circles in Fig. 4.18 represent the locations of the vertical tie-bars ( $\bullet$ ) and the circle outlines ( $\circ$ ) indicate the ADV measurement locations. The dashed line shows the location of an 8 mm thick and 50 cm long vertical PVC flow-straightening wall. It was installed in the channel center line, directly connected to a selected HBR configuration, to investigate its effect on the downstream flow field. The bypass discharge in the ethohydraulic flume was calculated for the different configurations at the end overfall of the bypass (Fig. 4.4). Following Bollrich (2007), the Poleni equation for sharp-crested weirs was used and a correction factor was applied to account for the inclination angle  $\gamma$  of the flap gate.



**Fig. 4.18:** Channel top view of the diversion HPP with the ADV measurement locations ( $\circ$ ), the flow-straightening wall (dashed-line), and the cross section along and downstream of the HBR (dotted lines)

### 4.4.2 Hydraulic losses

This subsection describes the methods and experimental program for the head loss assessment and was first published in a slightly modified form in Meister *et al.* (2020b).

#### Parameter range and test program

Head losses were determined for a range of rack and bar parameters representing the geometric characteristics of HBRs, including the four bar shapes introduced in Section 4.2.3. The approach flow angles  $\alpha = 30^\circ$  and  $45^\circ$  were investigated for all bar shapes and bar spacings. For the head loss measurements, the clear bar spacing was varied between  $s_b = 10, 20$ , and 30 mm. Each rack configuration was tested without overlays, and with six different overlay setups: (1)  $H_{Bo} = 0.1, H_{To} = 0$ , (2)  $H_{Bo} = 0, H_{To} = 0.1$ , (3)  $H_{Bo} = 0.2, H_{To} = 0$ , (4)  $H_{Bo} = 0, H_{To} = 0.2$ ,



(5)  $H_{Bo} = H_{To} = 0.1$  ( $H_{Ov} = 0.2$ ), and (6)  $H_{Bo} = H_{To} = 0.2$  ( $H_{Ov} = 0.4$ ). In an additional set of experiments, an approach flow angle of  $\alpha = 90^\circ$  and the effect of the relative bar depth  $D_b$  were investigated. Measurements were conducted for (a) S1-bars with  $s_b = 10, 20$ , and  $30$  mm and (b) S2-bars with  $s_b = 20$  mm. The effect of the relative bar depth  $D_b = 3.5, 5.5, 7.5, 9.5, 12, 15$  was investigated with S2-bars for (a)  $\alpha = 90^\circ$  and  $s_b = 20$  mm and (b)  $\alpha = 30^\circ$  and  $s_b = 10, 20$ , and  $30$  mm. Contraction ratios of  $w_o/w_{ds} = 1.25, 1.5$ , and  $2.0$  were studied for the bar shape S4,  $s_b = 20$  mm, and  $\alpha = 30^\circ$  and  $45^\circ$  with all overlay configurations listed above. A multiple linear regression was performed to develop head loss prediction equations. These equations were then validated with the data of Maager (2016) and Albayrak *et al.* (2019), Böttcher *et al.* (2019a), and Lemkecher *et al.* (2020). The total blocking ratio  $BR$  of the model rack was calculated as the sum of the blocking ratio due to the horizontal bars ( $BR_b$ ), the spacers ( $BR_s$ ), and the bottom plate ( $BR_{bp}$ ) with Eq. (4.2) to

$$BR = BR_b + BR_s + BR_{bp} = \left[ n_b \frac{t_b}{h_o} \right] + \left[ n_s \frac{(s_b + t_b - t_{b,m}) n_v t_s}{h_o w_{ds}} \right] + \left[ \frac{t_{bp}}{h_o} \right], \quad (4.2)$$

where  $n_b$  = number of horizontal bars [–],  $n_s$  = number of spacers per vertical tie-bar [–],  $n_v$  = number of vertical tie-bars [–], and  $t_s$  = spacer thickness (outer diameter). Depending on the rack configuration, the uppermost horizontal bar or spacer was only partially submerged, such that  $n_b$  or  $n_s$  were not whole numbers. The exact values of  $BR$  are listed in Table 4.1. Since the bar thickness reduces from tip to tail for the hydrodynamic bars (S2–S4), a larger proportion of the vertical-tie bars (spacers) was exposed to the flow, thus leading to slightly larger  $BR$  for S2–S4 in comparison to S1 (Table 4.1). For a preliminary design, the blocking ratio of the bottom plate  $BR_{bp}$  can be neglected and a constant bar thickness can be assumed, leading to the approximate blocking ratio  $BR^*$  in Eq. (4.3). The deviation to the exact blocking ratio is then 0.8–6.5%, depending on the configuration.

$$BR^* \approx \frac{t_b + s_b n_v t_s / w_{ds}}{s_b + t_b} \quad (4.3)$$

**Table 4.1:** Exact blocking ratios  $BR$  of the model racks and approximate blocking ratios  $BR^*$  for a preliminary design of racks with different clear bar spacing  $s_b$  and bar shapes S1–S4 (cf. Fig. 4.14)

$s_b$ [mm]	$BR$ of S1	$BR$ of S2–S4	$BR^*$ of S1–S4
10	0.482	0.492	0.478
20	0.342	0.348	0.329
30	0.272	0.276	0.258

### Experimental procedure

The flow depths were measured using an UDS at three transversal locations upstream (subscript  $o$ ;  $X = -5.6$ ;  $Y = 0.1, 0.5, 0.9$ ) and three transversal locations downstream (subscript  $ds$ ;  $X = 4.9$ ;  $Y = 0.1, 0.5, 0.9$ ) of the rack with a measurement duration of 30 seconds. To account for

measurement inaccuracies due to air temperature variations, the reference distance between the measurement cart and the channel bottom was measured prior to each test series. For each rack configuration, the downstream flap gate was adjusted to obtain  $h_o = 0.40$  m. The corresponding flow velocities  $U_o$  and  $U_{ds}$  were determined from continuity (Eq. 4.4) and the hydraulic head loss  $\Delta h_R$  caused by the rack was calculated with the Bernoulli equation (Eq. 4.5):

$$U_o = \frac{Q}{w_o h_o}, U_{ds} = \frac{Q}{w_{ds} h_{ds}} \quad (4.4)$$

$$\Delta h_R = h_o + \frac{U_o^2}{2g} - h_{ds} - \frac{U_{ds}^2}{2g} - \Delta h_f. \quad (4.5)$$

The friction losses were measured following the same experimental procedure as for the rack head losses, but without a rack installed. The head loss prediction equations presented below were intended to be applicable for various HPP layouts and operational conditions. The head loss was therefore related to the theoretical average flow velocity with Eq. (4.6) as

$$U_{th} = \frac{Q_t}{w_{ds} h_o}, \quad (4.6)$$

where  $Q_t$  = turbine discharge [ $\text{m}^3/\text{s}$ ] (cf. Section 2.5.2). Independent of the HPP layout,  $U_{th} \approx U_{ds}$  for small head losses. At diversion HPP setups in a straight channel with constant  $w_{ch}$  and without a bypass,  $U_{th} = U_o$ . By using  $U_{th}$  instead of  $U_o$  or  $U_{ds}$ , the assessment was independent of potential weir and bypass discharge in case of a block-type HPPs, but still accounted for  $\Delta h_R$ . The resulting rack head loss coefficient  $\xi_R$  was then determined with Eq. (4.7) to

$$\xi_R = \Delta h_R \frac{2g}{U_{th}^2}. \quad (4.7)$$

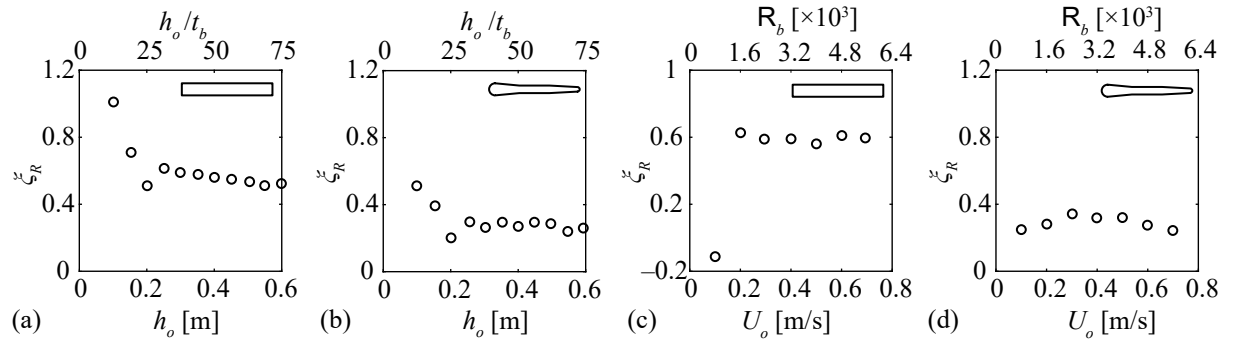
### Measurement uncertainties

Measurement uncertainties were caused by the MID and the UDS, as described above. Their effect on  $\xi_R$  was assessed with a Monte Carlo simulation with  $10^7$  model runs. This uncertainty estimation included the MID measurements, the UDS reference measurements to the bottom, and the water level measurements up- and downstream of the rack. The required input probability density functions were experimentally determined from 480 min of measurement duration. The measured time series was divided into 960 values, each corresponding to a 30 second time average. Finally, a normal distribution was fitted to these data. The probability density function of the ultrasonic distance sensor reference measurements to the channel bottom resulted from 60 min of measurement duration, which was split up into 360 values, corresponding to a 10 second time average. The resulting standard deviations of the UDS and the MID were  $\sigma_{\text{UDS,bottom}} = 1.0$  mm,  $\sigma_{\text{UDS,water}} = 2.7$  mm,  $\sigma_{\text{MID}} = 2.5$  L/s. These measurement uncertainties led to a 95% quantile of  $\xi_R = \pm 0.035$ , independent of the rack configuration.

### Model effects

Potential scale effects were precluded, as the bars were modeled on prototype scale. However, as the physical model corresponded to only a section of a prototype structure, so-called model

effects could have occurred, for instance effects caused by the channel boundaries. The velocity profile created by these boundaries may then differ from a prototype situation. Therefore, the effect of a variation in  $h_o$  and  $U_{th}$  was investigated for racks with S1- and S4-bars,  $\alpha = 45^\circ$ , and  $s_b = 20$  mm ( $BR \approx 0.35$ ) at the diversion HPP setup ( $U_o = U_{th}$ ). Figure 4.19a,b shows the rack head loss coefficient  $\xi_R$  as a function of  $h_o$  for the bar shapes S1 and S4, respectively, with  $U_{th} = 0.50$  m/s. For both bar shapes,  $\xi_R$  was independent of the approach flow depth if  $h_o \geq 0.20$  m ( $h_o \geq 25t_b$ ). Because the channel walls slightly deformed for  $h_o \geq 0.40$  m due to the hydrostatic load,  $h_o = 0.40$  m (corresponding to a flow depth to bar thickness ratio of  $h_o/t_b = 50$ ) was selected as an optimum flow depth in terms of experimental handling. Fig. 4.19c,d shows  $\xi_R$  as a function of  $U_{th}$  for the bar shapes S1 and S4, respectively, for constant  $h_o = 0.40$  m. The coefficient  $\xi_R$  was independent of  $U_{th}$  for  $U_{th} \geq 0.2$  m/s, corresponding to a bar Reynolds number  $R_b = t_b U_{th} / \nu \geq 1600$ , with  $\nu = 1.01 \times 10^{-6}$  m<sup>2</sup>/s as the kinematic viscosity of water at 20 °C. For  $U_{th} > 0.6$  m/s, surface waves reduced the measurement accuracy. Therefore, all further main experiments were conducted at a constant theoretical flow velocity of  $U_{th} = 0.5$  m/s ( $Q_t = 0.1$  m<sup>3</sup>/s, Eq. 4.6) with  $R_b = 4000$ , Froude number  $F = U_{th} / \sqrt{gh_o} = 0.25$ , and Reynolds number  $R = 4R_h U_{th} / \nu = 3 \times 10^5$ , involving the hydraulic radius  $R_h = hw_{ch} / (2h + w_{ch})$ . This flow velocity was an optimum value, thereby representing prototype conditions. Furthermore, the selected parameters were in excess of the threshold values  $h_o/t_b \geq 40$  and  $R_b \geq 1500$  to avoid model effects for different rack types specified in the literature (Zimmermann, 1969; Meusburger, 2002; Albayrak *et al.*, 2018; Beck *et al.*, 2019a).



**Fig. 4.19:** Rack head loss coefficients  $\xi_R$  as a function of the approach flow depth  $h_o$  with a constant theoretical average flow velocity  $U_{th} = 0.50$  m/s for bar shapes (a) S1 and (b) S4, and as a function of the theoretical average flow velocity  $U_{th}$  with constant approach flow depth  $h_o = 0.40$  m for bar shapes (c) S1 and (d) S4

#### 4.4.3 Live fish tests

All live fish tests conducted within the present thesis met the ethical guidelines and legal requirements (Swiss animal welfare act) under permission from the canton of Zurich and the veterinary office (animal experimentation licenses No. 30383 and 31339; laboratory animal husbandry license No. 180).

#### Holding facility and fish handling

Two holding tanks, with a volume of 3.5 m<sup>3</sup> each, were installed close to the flume inlet. Both tanks were separated into two equal-sized compartments, such that different experimental fish

groups could be distinguished. The holding tanks were connected to the cooled water circuit of the ethohydraulic flume (cf. Section 4.1.3), such that the water temperature of the ethohydraulic flume and the holding tanks was identical and always in the range of  $T = 12\text{--}16\text{ }^{\circ}\text{C}$ . Each holding tank was equipped with two filter pumps and an additional air pump. A viewing window was installed in the top cover of the tanks, which allowed to expose the fish to the natural day-night rhythm. Only wild fish were used for the experiments, which were caught with mild DC electrofishing (low voltages (220–250 V), certified devices) in rivers in the cantons of Zurich, Aargau, Thurgau, and Lucerne, from where they were transported in aerated tanks to the laboratory. The river water in the transport tanks was diluted with the water from the holding tanks, such that fish could slowly adapt to laboratory conditions. Water temperature changes were below  $\Delta T \approx 1\text{ }^{\circ}\text{C/h}$  and fish were not released in the holding tanks before the water temperature difference was below  $1\text{ }^{\circ}\text{C}$ . As there are no self-sustaining salmon populations in Switzerland, they were caught from a stocked population in the Möhlinbach. The spirlin, barbels, trout, and nase were kept in the holding tanks for up to four days and the first experiments started the day after they were brought to the laboratory. The salmon parr were kept in the holding tanks for up to five days, because the first experiments started two days after electrofishing. The eels were kept in the laboratory for up to eight days, but the last experiments were conducted not later than seven days after retrieving them from the wild. Throughout the time fish were kept in the laboratory, their condition (physical appearance, natural behavior), the water quality (oxygen concentration, pH), water temperature, and turbidity were monitored daily. Fish were not fed during their stay in the laboratory and different species were not simultaneously kept in the same compartment of the holding tanks. To reduce the number of required fish, individuals were used in several experiments. Learning effects and distress were reduced by not testing individuals more than once per day with a maximum of four experimental rounds per individual and thereby always subjecting them to different rack and/or bypass configurations. After the last experimental round, all fish were set free at the same river reach where they were initially caught.

## Experimental procedure

In previous live fish tests, Flügel *et al.* (2015) found that the group size (number of individuals tested in an experimental round) affected the fish behavior of some species. When tested individually or in small groups, spirlin showed no substantial differences, while barbels were much more active when swimming in groups of three individuals. The experiments of the present study were therefore conducted with groups of three fish of the same species with the exception of two experiments, where eels were tested individually. Limiting the number of fish per experiment to three, allowed for analyzing the fish behavior individually for most experiments. At the beginning of an experiment, three fish were caught with a net from the holding tanks and released into a bucket or cuvette. A picture with a reference scale was taken to measure the total fish length  $TL$ . Afterwards, the fish were released into the acclimatization compartment of the flume. For experiments with  $U_o = 0.7\text{ m/s}$  and all experiments with nase, a brick was positioned in the acclimatization compartment, behind the rack, and in the bypass, offering fish

a zone with reduced flow velocities. After an acclimatization time of 15 minutes in the acclimatization compartment, the brick was removed from the compartment, which was simultaneously opened, enabling the fish to swim within the entire flume. The fish movements were captured with five submerged cameras (Section 4.1.3). Simultaneously, the fish behavior was observed and written down on manual protocols from the observation room. Each experiment was completed when all three fish either passed through the rack or the bypass, or after the maximal experimental duration of 30 minutes. After each experiment, fish were caught with a net and brought back to the holding tanks.

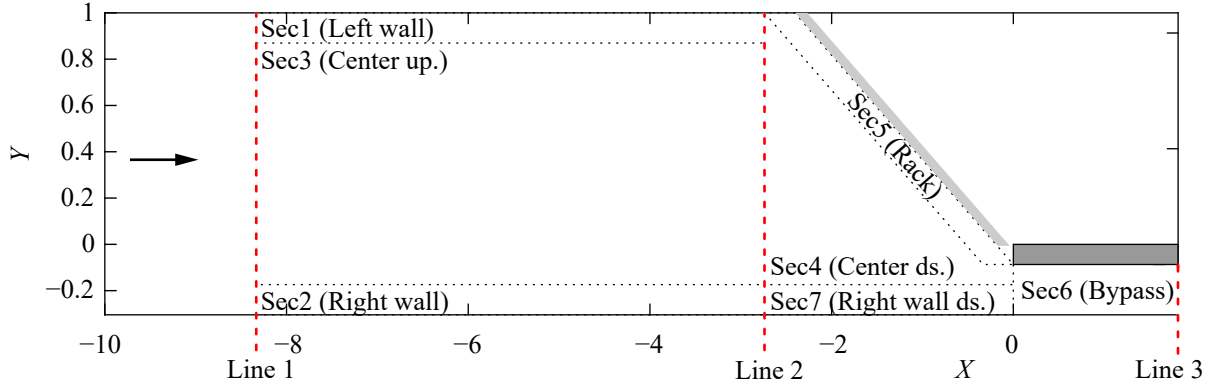
### Fish swimming behavior and sector analysis

The fish swimming behavior was analyzed with the fish swimming tracks. The manually written protocols were used to verify the fish behavior for each experiment. Three main lines were defined, marking different  $x$ -coordinates. Line 1 indicated the upstream end of the relevant experimental area ( $X = -8.3$ ), that is the area which could be studied from the observation room (Fig. 4.20). Line 2 was defined 30 cm upstream of the rack head, that is at  $X = -2.7$  (Fig. 4.20), indicating if fish swam into the area affected by the HBR. Line 3 represents the downstream end of the relevant experimental area at  $X = 1.8$  (Fig. 4.20). On the basis of these lines, the following behaviors were distinguished for each individual, where the number of fish is indicated with the variable  $N$  and the corresponding subscript:

- I) The fish **did not pass line 1** within the maximal experimental duration.
- II) **Time exceedance**: the fish passed line 1, but not line 2 within the maximal experimental duration.
- III) **Bypass passage without rack interaction (RI)**: the fish passed line 3, without crossing sector 5 (Fig. 4.20;  $N_{by,all} - N_{by,RI}$ ).
- IV) **Bypass passage with rack interaction**: the fish passed line 3, with crossing sector 5 (Fig. 4.20;  $N_{by,RI}$ ).
- V) **Rack passage** ( $N_{rack}$ ), the fish passed through the HBR.
- VI) **Refusal**: the fish passed line 2, but neither entered the bypass (did not cross line 3) nor the rack ( $N_{refusal}$ ).

Fish showing the behaviors I and II were likely neither affected by the HBR nor the bypass and were therefore excluded from all analyses regarding the guidance and protection efficiency. Since it is not clear if fish which passed the bypass without rack interaction (behavior III) entered the bypass by chance (e.g. swimming along the glass wall) or were guided by the HBR, they were excluded for assessing the guidance effect of the rack, but used to assess the bypass acceptance. In contrast, fish entering the bypass with rack interaction (behavior IV) were very likely guided by the HBR. Fish classified as “refusals” (behavior VI) were protected by the HBR, but they were either not guided towards the bypass or refused to enter it. For

all analyses, only the first of these six behavioral patterns was considered. To conduct more detailed analyses, the flume was further divided into different sectors (Fig. 4.20). Sector 5 was defined rack-parallel with a rectangular measured distance of 15 cm to the HBR. The sensitivity of this sector definition was assessed by doubling the sector width to 30 cm. The sectors 1, 2, and 7 covered the 15 cm wide boundary area at the walls, while the sectors 3 and 4 represented the main flume area. The bypass was defined as sector 6.



**Fig. 4.20:** Top view of the ethohydraulic flume indicating the lines 1–3 and the definition of the sectors 1–7 (y-axis exaggerated by factor 2)

### Fish guidance and protection efficiency

With the previously defined fish behaviors, the fish guidance efficiency (FGE) and the fish protection efficiency (FPE) were defined with Eq. (4.8) and (4.9), considering bypass passages only if the fish interacted with the rack (RI), which is a conservative approach. Additionally, the fish guidance efficiency  $FGE^*$  and the fish protection efficiency  $FPE^*$  were defined with Eq. (4.10) and (4.11), which include all bypass passages with and without rack interaction. Within the present thesis, FGE and FPE were used for all analyses, while  $FGE^*$  and  $FPE^*$  are additionally shown to enhance comparability with studies not distinguishing between bypass passages with and without rack interaction.

$$FGE = \frac{N_{by,RI}}{N_{by,RI} + N_{rack} + N_{refusal}} \quad (4.8)$$

$$FPE = \frac{N_{by,RI} + N_{refusal}}{N_{by,RI} + N_{rack} + N_{refusal}} \quad (4.9)$$

$$FGE^* = \frac{N_{by,all}}{N_{by,all} + N_{rack} + N_{refusal}} \quad (4.10)$$

$$FPE^* = \frac{N_{by,all} + N_{refusal}}{N_{by,all} + N_{rack} + N_{refusal}} \quad (4.11)$$

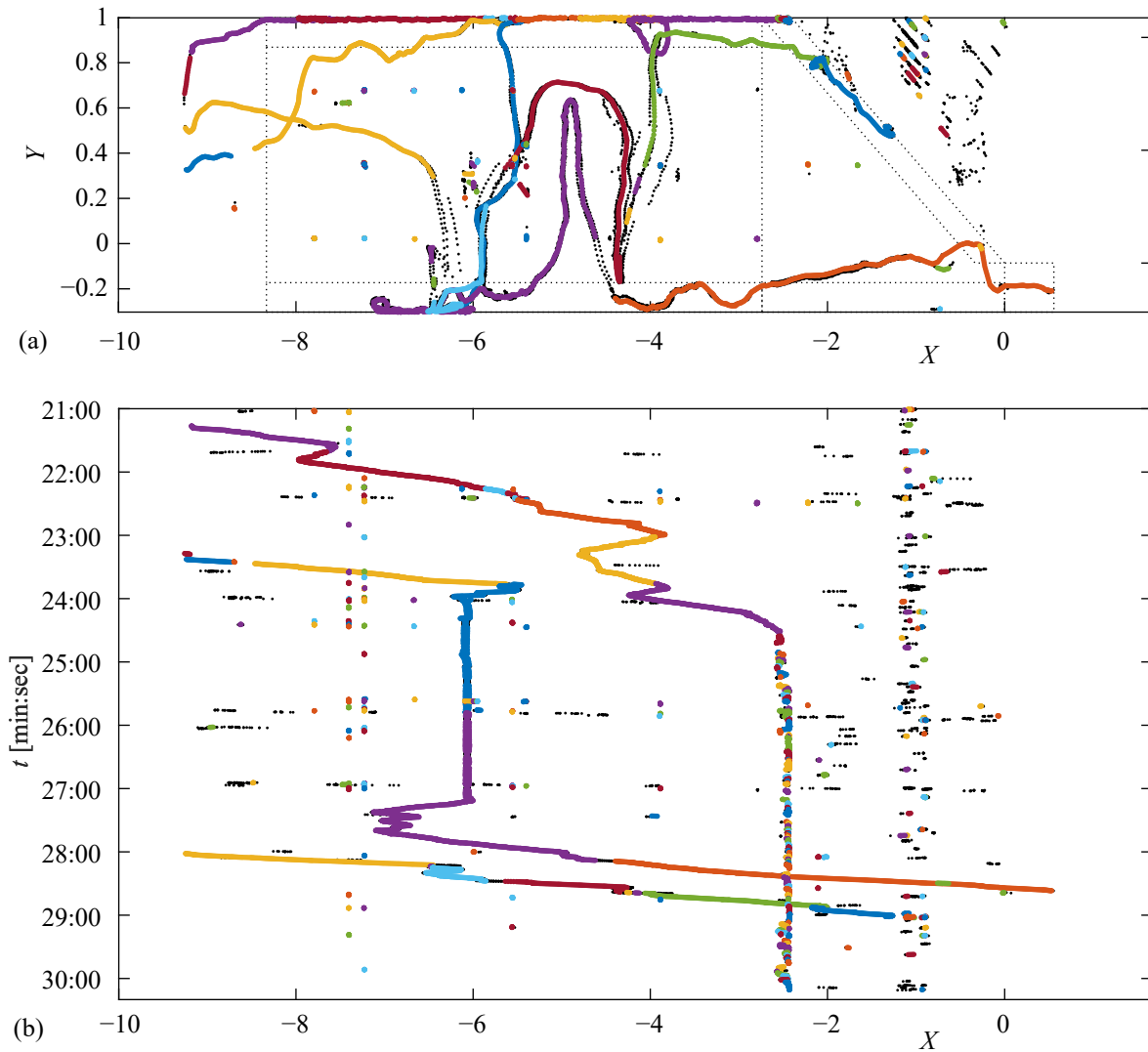
### Post-processing of fish tracks

The output of the fish tracking software, described in Section 4.3, includes the coordinates in x- and y-direction of the fish center, the corresponding time measured from the start of the

experiment, and a track ID. When a fish was detected by the tracking software, a new track ID was created. This ID was assigned to all following data points, until the tracking software lost the fish which happened due to the following reasons:

- the fish swam outside of the tracking area (e.g. back in the acclimatization compartment or behind the rack),
- the contrast between the fish and the background was poor,
- the paths of two fish crossed, they spatially overlapped, or were in close proximity to each other,
- the fish showed little movement and thereby became stationary (e.g. barbels which sometimes used their pectoral fins to keep their position with hardly any movements),
- or the next data point was filtered out because the tracking software thought it was noise and not a fish (e.g. when fish swam very fast with negative rheotaxis, leading to unusual large time steps between data points).

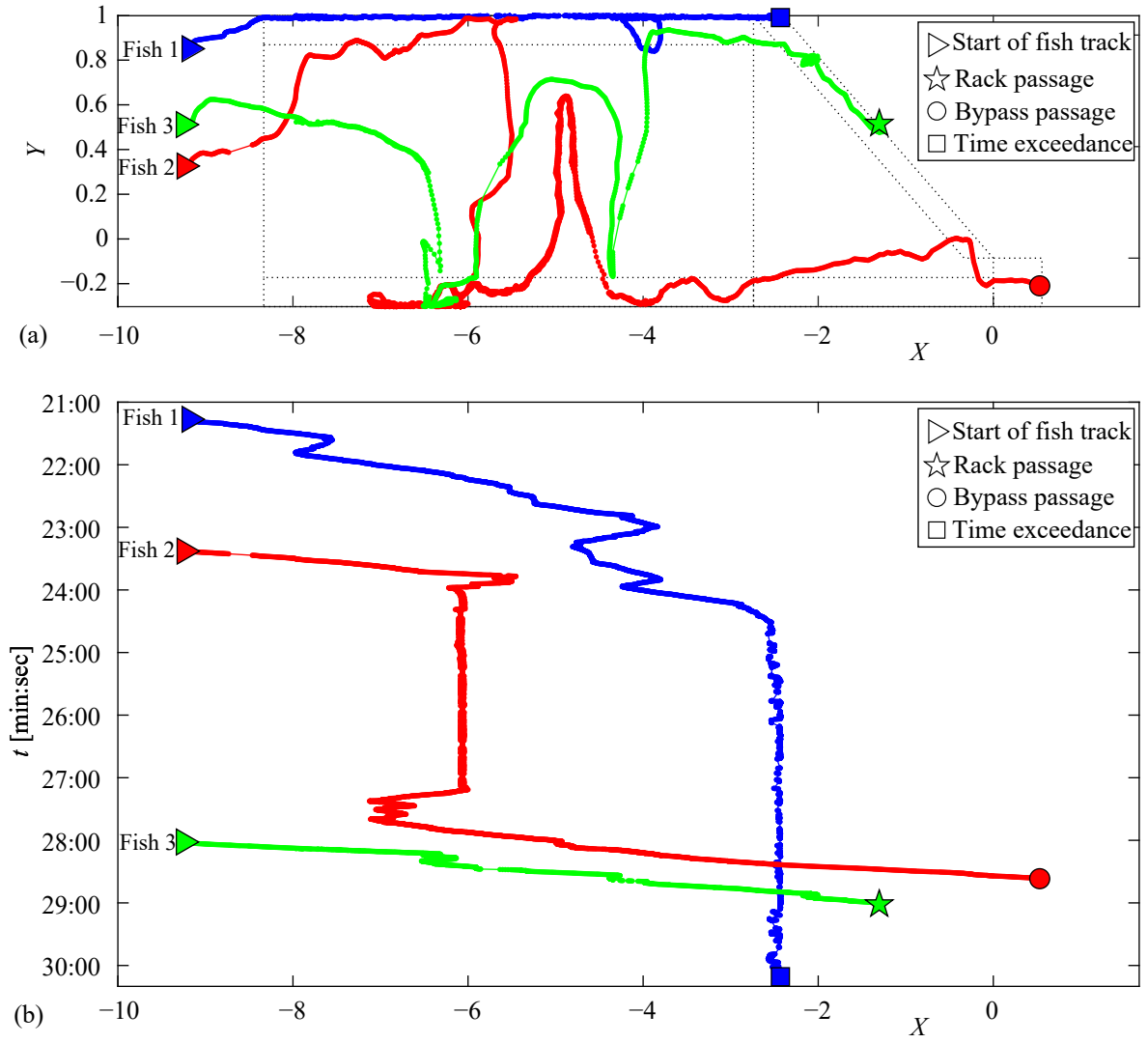
The post-processing of fish tracks is explained below. Figure 4.21a shows the output coordinates of the fish tracking software of one single experiment with three trout, tested with  $U_o = 0.70$  m/s,  $VR = 1.2$ , and the full depth open channel bypass. Different colors were used to illustrate coherent tracks with the same ID. The black dots indicate where a motion was detected, but the data point was filtered out by the tracking software. The dashed lines in Fig. 4.21a indicate the sectors introduced in Fig. 4.20. The data points downstream of the HBR were mainly caused by reflections of the rack, which were only partially filtered out by the tracking software. Figure 4.21b shows the temporal course of  $X$ , where the y-axis of this specific example starts at the time stamp of 21 minutes, because no fish left the acclimatization compartment before.



**Fig. 4.21:** Example of the raw data of the fish tracking software of one experiment with three trout, where (a) shows tracks in  $x$ - and  $y$ -direction ( $y$ -axis exaggerated by factor 2) and (b) the temporal course of the  $X$ -coordinate

The individual tracks, shown in Fig. 4.21, were connected in a semi-automated process and assigned to the individual fish. In some situations, for example when two fish crossed each other, it was difficult to assign each track to the correct fish. In these cases, the tracks were connected manually by means of the video recordings and written protocols. For some experiments, mainly with fish showing a distinct schooling behavior such as spiralin and nase, it was not feasible to create individual tracks for each fish. For these experiments, one track was created to represent the school of fish. The final tracks of the three fish from the previous example are shown in Fig. 4.22. The starting point of each track was marked with a triangle, whereas the end point of the track, representing the first fish reaction, was illustrated with a star for rack passages, a circle for bypass passages, and a square for time exceedance. The final tracks represent the fish swimming path until the fish showed one of the defined reactions. As an example, if a fish passed the rack, swam upstream again, and finally entered the bypass, the final track represents the fish swimming path from the beginning to the rack passage only.





**Fig. 4.22:** Example of the final tracks representing the fish swimming path of three trout in (a)  $x$ - and  $y$ -direction ( $y$ -axis exaggerated by factor 2) and (b) the temporal course of the  $X$ -coordinate

### Residence coefficient

To analyze the fish swimming behavior and to compare different configurations with each other, the so-called residence coefficient  $R_{c,i}$  is introduced with Eq. (4.12). This coefficient is a measure for how much time all fish, tested for a specific HBR-BS configuration, spent in a sector in comparison to the other sectors, while accounting for the different sector sizes. It was calculated for all active fish, that is, fish which crossed line 2 in Fig. 4.20. By normalizing the time a fish  $j$  spent in a sector  $i$  with the total time the fish  $j$  spent in any of the sectors 1–7, each fish was weighted equally, independent of how fast it swam downstream. The normalized residence coefficient  $R_{c,i,\text{norm}}$  is defined with Eq. (4.12). A normalized residence coefficient of  $R_{c,i,\text{norm}} = 1$  means that all fish of the investigated configuration spent the entire time in the sector  $i$ , whereas  $R_{c,i,\text{norm}} = 0$  indicates that none of the fish of the investigated configuration entered the sector  $i$ .

$$R_{c,i} = \frac{1}{n} \sum_{j=1}^n \frac{t_{i,j} A_{\text{tot}}}{t_{j,\text{tot}} A_i} \quad (4.12)$$

$$R_{c,i,\text{norm}} = \frac{R_{c,i}}{\sum_{i=1}^7 R_{c,i}}, \quad (4.13)$$

where  $i$  = sector number [–],  $j$  = fish number [–],  $n$  = number of fish tested for this configuration [–],  $t_{i,j}$  = time the fish  $j$  spent in sector  $i$  [s],  $t_{j,\text{tot}} = \sum_{i=1}^7 t_{i,j}$  = total time the fish  $j$  spent in any of the sectors 1–7 [s],  $A_i$  = area of the sector  $i$  [m<sup>2</sup>],  $A_{\text{tot}} = \sum_{i=1}^7 A_i$  = total area of all sectors 1–7 [m<sup>2</sup>].

### Statistical analyses

Different statistical analyses were conducted to answer different research questions. The effect of the input parameters was assessed with  $\chi^2$ -tests for each fish species individually, while the overall effect was quantified with generalized linear models. The two-sided  $\chi^2$ -tests with a significance level of  $\alpha_{\text{sig}} = 0.05$  were conducted to assess if different parameters, such as  $U_o$  and  $VR$ , significantly affected the fish behavior. To account for species-specific behavior, these tests were conducted for each species separately. The null hypothesis  $H_0$  states that there was no statistically significant difference between the two tested configurations, whereas the alternative hypothesis  $H_1$  applies for significant differences. If two test series with a multinomial output are compared to each other, it is only possible to detect if the output differs significantly. No statements can be made about the individual output categories. Therefore, the multinomial output variable fish reaction (bypass passage, rack passage, and refusal) was converted to binary data (bypass passage: yes/no; rack passage: yes/no; refusal: yes/no) and  $\chi^2$ -test were made for each of these categories. One of the main disadvantages of the  $\chi^2$ -test is that empty cells create zeros in the contingency table, which can lead to implausible results. This problem was mitigated by converting the fish reaction to binary data, as the contingency table of the binary data contained much less zeros.

$\chi^2$ -tests were used to find out if a difference between two configurations was statistically significant or not. It is not possible to detect the most important parameters and to quantify their effect on the results. Therefore, generalized linear models were set up (GLM, logistic logit-regression), where the multinomial output variable fish reaction (bypass passage, rack passage, and refusal) was converted to binary data (bypass passage: yes/no; rack passage: yes/no; refusal: yes/no). Three different GLMs of the general form shown in Eq. (4.14) were used to quantify which parameters affected the bypass passages, rack passages, and refusals.

$$OR = \exp(\beta_0 + \beta_1 X_1 + \dots + \beta_n X_n), \quad (4.14)$$

where  $OR$  = odds ratio,  $\beta_i$  = regression coefficients,  $i$  = parameter number,  $n$  = total number of parameters,  $X_i$  = data of parameter  $i$ . The odds ratio is defined by Eq. (4.15) and can be rewritten as Eq. (4.16) to calculate the probability  $p(X)$  given the independent parameter  $X = (X_1, X_2, \dots, X_n)$ .

$$OR = \frac{p(X)}{1 - p(X)} \quad (4.15)$$

$$p(X) = \frac{OR}{1 + OR} \quad (4.16)$$

The model output includes the regression coefficients  $\beta$  and the standard errors  $\varepsilon$ , which can be used to calculate the confidence intervals (CI) with Eq. (4.17) to

$$CI = \exp \left( \beta \pm \Phi^{-1} \left( 1 - \frac{\alpha_{\text{sig}}}{2} \right) \varepsilon \right), \quad (4.17)$$

where  $\Phi$  = cumulative distribution function of the standard normal distribution and  $\alpha_{\text{sig}}$  = significance level. Equation (4.17) reduces to Eq. (4.18) for the calculation of the 95% CI ( $\alpha_{\text{sig}} = 0.05$ ).

$$CI_{95\%} = \exp(\beta \pm 1.96\varepsilon) \quad (4.18)$$

The first set of GLMs was set up with all HBR data with the full depth open channel bypass and  $s_b = 20$  mm, including the data of spirlin, barbel, nase, trout, salmon parr, and eel. The data set of the GLM included all fish showing one of the following reactions: bypass passage with RI, rack passage, and refusal (behaviors IV–VI). The main regression parameters were  $U_o$  and  $VR$ . Besides, it could not be precluded that the number of times a fish was used for the experiments (usage) and the time of the day (morning/afternoon) affected the results. These parameters were therefore also included in the GLMs. The parameters  $U_o$  (0.5 and 0.7 m/s),  $VR$  (1.2 and 1.4), time (morning: start of experiment until 1 p.m.) and afternoon (start of experiment after 1 p.m.) were modeled as factors, while the parameter usage was defined as a continuous variable. The Akaike information criterion (AIC) and Bayesian information criterion (BIC) were used to test if an interaction term between  $VR$  and  $U_o$  improved the model, where AIC/BIC indicate a better model by considering the trade-off between goodness of fit of the model and model simplicity. To compare the results of the present thesis with the data of Beck (2020) and Beck *et al.* (2020), another set of GLMs was set up with the identical parameters, but the rack type was included as another factor (either HBR or CBR). The HBR was defined as the reference category. In all statistical analyses, each fish was considered as an independent data point, which is a simplification for fish showing schooling behavior and may therefore have led to pseudoreplication. To increase the statistical power of the GLM, a complete randomization of the order of experimental setups prior to the experiments was planned, which could only partially be achieved due to various limitations. As an example, only two different fish species could be kept in the holding tanks at the same time.

### **Fish swimming velocities and combination with flow velocities**

The streamwise and transversal fish ground velocities  $U_g$  and  $V_g$ , respectively, corresponding to the velocities of the swimming tracks, were calculated as the average over five time steps (0.25 seconds) for each track as

$$U_g = \frac{x_{i+5} - x_i}{t_{i+5} - t_i}, \quad V_g = \frac{y_{i+5} - y_i}{t_{i+5} - t_i}. \quad (4.19)$$

A velocity of  $U_g > 0$  m/s means that the fish was moving downstream, and accordingly upstream for  $U_g < 0$  m/s. These ground velocities of the fish swimming tracks were combined with the

flow velocities  $U$  and  $V$  from the ADV measurements, such that the fish swimming velocities in  $x$ - and  $y$ -direction  $U_f$  and  $V_f$ , respectively, could be calculated with Eq. (4.20). The absolute fish swimming speed  $v_f$  was then defined by Eq. (4.21) and (4.22).

$$U_f = U_g - U, \quad V_f = V_g - V \quad (4.20)$$

$$v_f = -\sqrt{U_f^2 + V_f^2} \quad \text{for } U_f < 0 \quad (4.21)$$

$$v_f = \sqrt{U_f^2 + V_f^2} \quad \text{for } U_f \geq 0 \quad (4.22)$$

By combining the fish swimming tracks with the hydraulic measurements, it was possible to draw conclusions on the fish behavior and the rheotaxis. For  $U_g = 0$  m/s,  $U_f = -U$  (Eq. 4.20), which means that the fish kept its position by swimming against the flow with positive rheotaxis. For  $U_g = U$ ,  $U_f = 0$  m/s, indicating that the fish was drifting passively downstream with the flow velocity, which means that the rheotaxis remains unclear. A streamwise ground velocity of  $U_g < 0$  m/s means that the fish actively swam upstream with positive rheotaxis. For  $0 < U_g < U$ , the fish swam slowly downstream with positive rheotaxis, while for  $U_g > U$ , the fish must have had a negative rheotaxis to swim downstream faster than the flow velocity. These behavioral patterns are summarized in Table 4.2.

**Table 4.2:** Possible combinations of the streamwise ground velocity  $U_g$  and the streamwise flow velocity  $U$ , leading to the streamwise fish swimming velocity  $U_f$ , which allowed for drawing conclusions on the rheotaxis and the swimming behavior

$U_g$ [m/s]	$U_f$ [m/s]	Rheotaxis	Swimming behavior
$U_g = 0$	$-U$	Positive	Fish kept its position by swimming against the flow
$U_g = U$	0	Unclear	Fish drifted passively with the flow velocity
$U_g < 0$	$U_g - U$	Positive	Fish swam actively upstream
$0 < U_g < U$	$U_g - U$	Positive	Fish swam slowly downstream
$U_g > U$	$U_g - U$	Negative	Fish swam actively downstream

### Fish swimming behavior at the bypass inlet

Unfavorable flow conditions at the bypass inlet may delay downstream passage and increase the rack passage risk. To assess the effect of different flow conditions at the bypass inlet, the videos were visually analyzed and different behaviors were quantified. The analysis was conducted for spiralin and barbel, as a sufficient number of replicates was available for various flow conditions. A rectangular area was defined, which included the bypass itself and reached 0.5 m upstream from the bypass inlet. Within this area it was counted, how many times fish hesitated before they either accepted the bypass, passed through the rack, or the maximal experimental duration was reached. A hesitation was defined as a small upstream movement, which was likely to be caused by the flow conditions at the bypass. Additionally, the bypass refusals were counted, which were defined as the number of times a fish swam into the bypass area and left it again.

Fish which did not enter the bypass area were excluded from the analysis. The average number of hesitations and bypass refusals per fish is denoted as  $\bar{n}_{\text{hes}}$  and  $\bar{n}_{\text{ref}}$ , respectively. If spirlin were swimming as a school, it could not be distinguished between individuals, such that  $\bar{n}_{\text{hes}}$  and  $\bar{n}_{\text{ref}}$  were counted for all fish of the school and equally distributed between individuals. Differences between bypass acceptance were statistically analyzed with two-tailed t-test with  $\alpha_{\text{sig}} = 0.05$ , where equal variances were assumed.

### Fish activity during live fish tests

It was noted that the fish activity strongly varied between species and experimental days during the live fish tests. A low fish activity means that multiple fish did not swim out of the acclimatization compartment or it took them very long to swim into the rack-affected area. It is very useful to understand the reasons for periods with low fish activity, as this information can be used for optimizing the experimental design of future live fish tests. To systematically analyze the fish activity, a line was defined at  $X = -4$ , which is already close to rack, but where the flow was still independent of the rack configuration (cf. Fig. 4.20). It was thereby possible to include the experiments of Beck (2020) and Beck *et al.* (2020) at CBRs in the analysis of the fish activity, as these experiments were conducted in parallel to the experiments of the present thesis. The fish tracks were used to analyze how long fish needed to cross that line at  $X = -4$ , where fish were excluded if they did not cross the line within the maximal experimental duration of 30 minutes. Two-tailed t-tests assuming equal variances with  $\alpha_{\text{sig}} = 0.05$  were conducted to detect statistically significant differences in the fish activity.

### Test program

The experiments were conducted with a diverse assemblage of riverine fish species to account for species-specific behavior. In the first live fish test phase in autumn 2018 (17.10.–23.11.2018), spirlin (*Alburnoides bipunctatus*), barbel (*Barbus barbus*), nase (*Chondrostoma nasus*), and European eel (*Anguilla anguilla*) were tested. The second test phase was conducted in spring 2019 (14.04.–07.06.2019) with salmonids, namely Atlantic salmon parr (*Salmo salar*) and brown trout (*Salmo trutta fario*). The third test phase in autumn 2019 (08.10.–08.11.2019) focused on electrified HBRs with spirlin (*Alburnoides bipunctatus*) and European eel (*Anguilla anguilla*). The detailed test program is shown in Table 4.3, where the average approach flow velocity from continuity is denoted as  $U_o$ , the mean flow velocity at the bypass inlet  $U_{\text{by,in}}$ , the velocity ratio  $VR = U_{\text{by,in}}/U_o$ , and the clear bar spacing  $s_b$ . The size of the fish used for each configuration is specified with the minimal, maximal, and average total length ( $TL_{\text{min}}$ ,  $TL_{\text{max}}$ , and  $\overline{TL}$ ) and the corresponding standard deviation  $\sigma_{TL}$ . All live fish tests were conducted with a horizontal approach flow angle of  $\alpha = 30^\circ$ . The variable  $N$  represents the total number of fish tested for a specific configuration, whereas  $n$  specifies the number of fish with a valid reaction, that is, a bypass passage, a rack passage, or a refusal. The tests E0 were conducted without the installation of a rack as a reference.

**Table 4.3:** Test program of the live fish tests without electrification

Test	$U_o$ [m/s]	$U_{by,in}$ [m/s]	$VR$ [–]	$s_b$ [mm]	Bypass layout	Fish species	$TL_{min}-TL_{max}$ $(\overline{TL}, \sigma_{TL})$ [cm]	$N$ [–]	$n$ [–]
E0	0.50	0.60	1.2	–	OC <sup>1</sup>	Spirlin	8.5–11.9 (9.9, 1.0)	21	21
E1	0.50	0.60	1.2	15	OC <sup>1</sup>	Trout	11.2–19.6 (15.8, 1.9)	75	30
E2	0.50	0.60	1.2	20	OC <sup>1</sup>	Spirlin	8.1–10.7 (9.6, 0.7)	33	33
E3						Barbel	10.3–20.8 (16.3, 2.8)	45	41
E4						Nase	5.9–9.3 (7.2, 0.9)	18	15
E5						Trout	9.1–18.7 (13.9, 2.3)	36	27
E6						Salmon	9.6–14.9 (11.9, 1.3)	24	24
E7						Eel	47.2–79.6 (66.5, 10.6)	10	8
E8						Spirlin	8.7–12.9 (10.5, 0.8)	27	24
E9						Barbel	11.0–16.3 (13.5, 1.5)	24	19
E10	0.50	0.70	1.4	20	OC <sup>1</sup>	Nase	5.9–8.3 (7.1, 0.6)	21	20
E11						Trout	9.9–21.0 (14.0, 2.7)	42	28
E12						Salmon	9.1–13.4 (11.0, 1.0)	27	24
E13						Eel	41.3–82.8 (64.9, 14.0)	7	7
E14	0.70	0.85	1.2	20	OC <sup>1</sup>	Spirlin	8.0–12.3 (10.1, 1.0)	33	33
E15						Barbel	8.0–20.2 (15.5, 3.5)	24	23
E16						Trout	8.8–20.8 (14.3, 2.6)	51	27
E17	0.70	1.00	1.4	20	OC <sup>1</sup>	Spirlin	7.8–11.3 (9.5, 0.9)	24	22
E18						Barbel	7.5–19.0 (14.3, 3.3)	21	7
E19						Trout	8.6–20.1 (12.7, 2.8)	45	24
E20	0.50	0.75 <sup>3</sup>	1.5	20	RE <sup>2</sup>	Spirlin	8.6–13.4 (10.3, 1.2)	18	18
E21						Barbel	8.2–15.7 (12.7, 2.6)	9	9
E22						Eel	55.2–62.2 (57.6, 4.0)	3	3
E23	0.50	0.90 <sup>3</sup>	1.8	20	RE <sup>2</sup>	Spirlin	8.4–10.8 (9.7, 1.0)	9	9
E24						Barbel	9.1–17.6 (14.6, 4.8)	3	1
E25						Eel	60.4–75.7 (67.2, 5.9)	6	5

<sup>1</sup> Full depth open channel bypass (Fig. 4.6a)<sup>2</sup> Open channel bypass with inlet restrictor (Fig. 4.6c)<sup>3</sup> Measured behind the openings at the downstream restrictor end (narrowest section)

#### 4.4.4 Live fish tests at electrified racks

##### Measuring the electric field

An oscilloscope was used to verify that the pulse pattern in the water, defined by  $N_{pulse}$ ,  $L_{pulse}$ ,  $L_{gap}$ , and  $t_{rep}$  (cf. Section. 4.2.2), was independent of the measurement location and matched

with the settings of the Neptun DC fish-guidance system. The peak voltage  $U_e$  varied across the flume and was measured with a custom-built voltmeter with a measurement range of 1–100 V and an accuracy of  $\pm 0.1$  V. The peak voltage was defined as the difference between the cathode (metal mesh) and measurement points in the flume. The voltmeter was validated with a condenser with a known voltage potential and it was verified that different pulse parameters and different flow velocities did not affect  $U_e$ . All measurements were conducted for output voltages of the control unit of  $U_e = 38$  V and  $U_e = 80$  V with  $U_o = 0.15$  m/s,  $h_o = 0.90$  m,  $N_{\text{pulse}} = 7$ ,  $L_{\text{pulse}} = 0.4$  ms,  $L_{\text{gap}} = 10$  ms,  $t_{\text{rep}} = 300$  ms, and  $D = 0.75\%$ . The voltmeter was mounted on the measurement cart, such that  $U_e$  could be measured at all locations upstream of the HBR and in the bypass with a positioning accuracy of  $\pm 5$  mm. The density of the measurement grid increased towards the HBR (anode) to a minimal distance between measurement points of 3 cm. The measurements and the analyses of the electric field were conducted by Anita Moldenhauer-Roth within her doctorate about electrified fish guidance structures, but they are included in a slightly modified version in the present thesis to analyze the fish reactions in the electric field.

### Test program

The goals of the electrification of the HBR were to assess if the specific protection and guidance efficiencies could be increased with the electric field and if different fish species could be protected sufficiently with larger  $s_b$  to reduce operational challenges for the operators. All live fish tests with the electrified HBR were conducted with  $U_o = 0.5$  m/s,  $U_{\text{by},\text{in}} = 0.6$  m/s,  $\alpha = 30^\circ$ , and the full depth open channel bypass with different pulse patterns with a conductivity of water of  $230 \mu\text{S}/\text{cm}$  (Table 4.4). Scientific literature or reports describing reactions of downstream moving fish to different gpDC pulse patterns at electrified racks are so far missing. Hence, the pulse parameters were chosen on recommendation of the companies Procom and IUS Weibel & Ness GmbH, who have experience with electric deterrent systems for downstream passage and were involved in the experiments of Berger (2018) and Tutzer *et al.* (2019b) (cf. Section 3.7.3). Most experiments were conducted with the following pulse parameters, which were introduced in Section 4.2.2:  $U_e = 38$  V,  $L_{\text{pulse}} = 0.3$  ms,  $L_{\text{gap}} = 7$  ms,  $N_{\text{pulse}} = 5$ ,  $t_{\text{rep}} = 200$  ms (Table 4.4), which is termed “standard pulse pattern” hereafter. The duty cycle of this configuration was  $D = 0.75\%$  (Eq. 4.1). Experiments with  $s_b = 20$  mm were carried out to directly compare the results with and without electrification. The majority of experiments was conducted with  $s_b = 51$  mm, while  $s_b = 100$  mm was tested only twice (Table 4.4). The study focused on eels, because without electrification, they actively tried to move downstream through the rack by trying to squeeze themselves through the narrow bar spacing. Electrification of the rack should prevent this by deterring fish before they get in direct contact with the rack. Spiralin were included in the experiments as a positive control; in previous experiments they were well guided without an electric field and the objective of the electrification was to test if the good guidance is not lost with the electrification of the HBR. The electric field reached far upstream in the flume (details in Section 8.1), such that the behavior of eels and spiralin was affected although they did not swim close to the rack or had direct contact. The distinction between bypass passages with and without rack interaction, as introduced in the beginning of

Section 4.4.3, was therefore not reasonable with the electric field at the HBR. For this reason, all bypass passages were counted with the electric field. No fish injuries were reported in recent studies, where racks were electrified with gpDC with  $U_e \leq 80$  V, such as Berger (2018) and Tutzer *et al.* (2019b), described in Section 3.7.3. Therefore, it was not expected that fish would get injured in the present experiments. However, external injuries were observed for some fish which either had direct contact with the rack or passed through the electrified HBR. Two spirlin were therefore sent to the Centre for Fish and Wildlife Health in Bern, Switzerland, where they were euthanized with an overdose of MS22s and checked for internal injuries.

**Table 4.4:** Test program of the live fish tests with the electrified HBR

Test	$s_b$ [mm]	$U_e$ [V]	$L_{\text{pulse}}$ [ms]	$L_{\text{gap}}$ [ms]	$N_{\text{pulse}}$ [–]	$t_{\text{rep}}$ [ms]	$D$ [%]	Fish species	$TL_{\text{min}}-TL_{\text{max}}$ ( $\overline{TL}$ , $\sigma_{TL}$ ) [cm]	$N$ [–]	$n$ [–]
F1	20	38	0.3	7	5	200	0.75	Spirlin	8.9–13.8 (10.9, 1.0)	36	29
F2	20	38	0.3	7	5	200	0.75	Eel	45.4–84.2 (65.1, 9.2)	15	12
F3	51	38	0.3	7	5	200	0.75	Spirlin	7.4–11.4 (8.9, 0.9)	51	27
F4	51	38	0.3	7	5	200	0.75	Eel	42.9–87.4 (68.1, 8.6)	72	59
F5	51	38	0.2	0	1	100	0.20	Spirlin	7.5–9.9 (9.1, 0.72)	9	8
F6	51	38	0.2	0	1	100	0.20	Eel	45.5–69.8 (59.2, 9.0)	6	5
F7	51	38	0.2	7	3	80	0.75	Eel	57.3–86.3 (69.0, 7.8)	12	8
F8	51	38	0.3	0	1	40	0.75	Eel	57.9–67.8 (62.3, 3.2)	9	7
F9	51	38	0.4	10	7	300	0.93	Eel	67.5–73.2 (69.7, 3.1)	3	3
F10	100	38	0.3	7	5	200	0.75	Eel	57.1–71.5 (63.2, 7.5)	3	3
F11	100	80	0.3	7	5	200	0.75	Eel	65.2–74.0 (68.8, 4.6)	3	2

#### 4.4.5 Operational aspects

Preliminary experiments were conducted with leaves and small branches at the detailed model diversion HPP (Section 4.1.1) in March 2018. The diameter and length of the branches were  $10 \pm 2$  mm ( $\mu \pm \sigma$ ) and  $135 \pm 17$  mm, respectively. The effect of different parameters on the clogging probability of leaves at HBRs was then systematically investigated by Ganzmann (2019) in autumn 2018. The clogging probability  $CP$  was defined as the percentage of leaves which clogged at the bars of the HBR from the total number of leaves added to the flume. The clogging probability  $CP_{2+}$  was defined in the exact same manner, but leaves which clogged at multiple bars were considered only. Leaves which clogged at the vertical tie-bars were not counted as clogged, as the distance between the vertical tie-bars could not be modeled on prototype scale. The experiments were conducted with a set of five or ten almost equal-sized leaves, which means that all leave lengths deviated less than 5% from the mean length of the set. To account for differences in size, shape, and flexibility, the leaves of four different tree species, commonly found in Switzerland, were investigated, namely the common beech (*Fagus sylvatica*), Norway maple (*Acer platanoides*), common hazel (*Corylus avellana*), and common



hornbeam (*Carpinus betulus*). A picture of representative test leaves is shown in Fig. 4.23 and the average dimensions are listed in Table 4.5. The leaf dimensions for the experiments with  $s_b = 10$  mm slightly deviated from the dimensions of all other experiments as shown in Table 4.5.



**Fig. 4.23:** Picture of test leaves from the four different tree species, representing different sizes and shapes; from left to right: beech, maple, hornbeam, and hazel leaf

**Table 4.5:** Dimensions of the leaves used for the foliage clogging experiments (adapted from Ganzmann, 2019)

	Beech	Maple	Hornbeam	Hazel
Leaf length [cm]	7.5; 7.0*	7.4	6.8	11.6; 12.5*
Leaf length incl. the petiole [cm]	8.8	15.5	7.8	12.4
Leaf width [cm]	4.8; 5.0*	10.4	3.3	11.0; 7.0*
Leaf area <sup>1</sup> [cm <sup>2</sup> ]	28; 27*	60	18	100; 69*

\* Dimensions of the leaves used for the experiments with  $s_b = 10$  mm

<sup>1</sup> Approximation, assuming an ellipsoidal shape

All experiments were carried out with an approach flow depth of  $h_o = 0.40$  m and each leaf was released individually with a tongs 15 cm above the bottom ( $Z = 0.375$ ) in the transversal flume center ( $Y = 0.5$ ), 1.5 m upstream of the downstream rack end ( $X = -3.75$ ; cf. Fig. 9.2a). For each configuration, between 60 and 100 replicates were made, where the minimal sample size  $n_{\min}$  was calculated following Henze (2013) with Eq. (4.23), which reduces to Eq. (4.24) for  $\alpha_{\text{sig}} = 0.05$ . The maximal accepted error was set to  $\epsilon_{\max} = \pm 10\%$ . The confidence intervals were calculated with  $CI = CP \pm \epsilon$ , where  $\epsilon$  is the error calculated from the effective sample size.

$$n_{\min} \geq \left( \frac{1 - \frac{\alpha_{\text{sig}}}{2}}{\epsilon_{\max}} \right)^2 CP(1 - CP) \quad (4.23)$$

$$n_{\min} \geq \left( \frac{1.96}{\epsilon_{\max}} \right)^2 CP(1 - CP) \quad (4.24)$$

To achieve realistic densities, all leaves were watered for at least one night prior to the experiment and it was analyzed if the watering time affected  $CP$ . Other parameters investigated were

the clear bar spacing  $s_b = 10\text{--}50$  mm, the average approach flow velocity  $U_o = 0.5\text{--}0.75$  m/s, the approach flow angle  $\alpha = 30\text{--}45^\circ$ , and the bar shape which was varied between rectangular and foil-shaped (cf. Section 4.2.3).

## 5 Velocity fields at horizontal bar racks

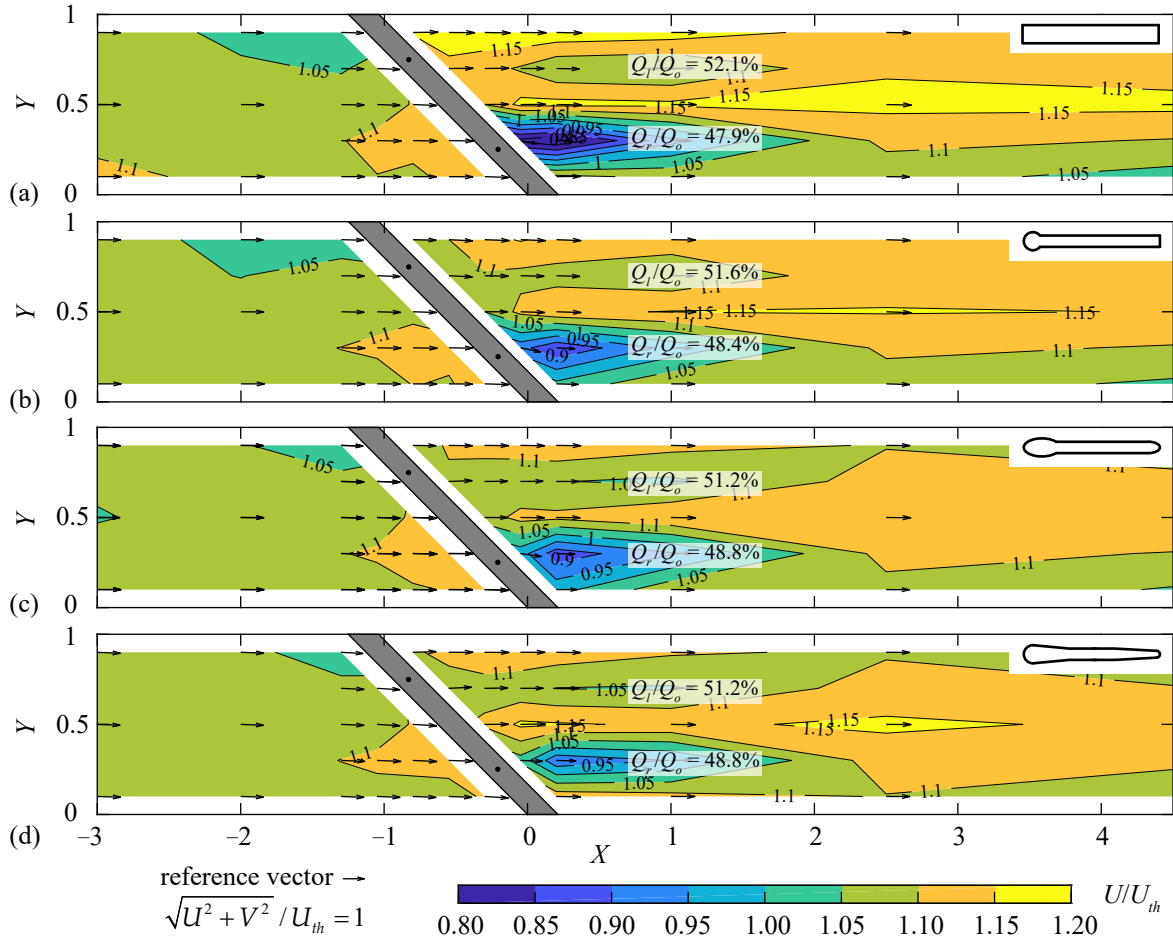
In this chapter, the velocity fields of HBRs and HBR-BSs are presented. Parts of this chapter were first published in a slightly modified form in Meister *et al.* (2020c).

### 5.1 Parameter effect on the velocity fields

In this section, the effect of the bar shape, the rack angle  $\alpha$ , the clear bar spacing  $s_b$ , and the overlays on the up- and downstream velocity fields of HBRs are assessed.

#### 5.1.1 Bar shape

The velocity fields were measured at mid depth ( $Z = 0.5$ ) for all bar shapes (S1–S4), with  $\alpha = 45^\circ$ ,  $s_b = 20$  mm, and  $H_{Ov} = 0$  (Fig. 5.1). The rack is indicated in gray, where the black dots ( $\bullet$ ) mark the location of the vertical tie-bars. The contours illustrate the normalized stream-wise flow velocities  $U/U_{th}$ . The vectors indicate the direction and magnitude of  $U$  and  $V$  at the corresponding ADV measurement locations. The approach flow upstream of the rack at  $X = -3$  was identical for all configurations (Fig. 5.1). Resulting from the bottom boundary layer, the velocities measured at mid depth were slightly higher than the average velocity from continuity ( $U \approx (1.05\text{--}1.11)U_{th}$ ). For all bar shapes,  $U$  slightly decreased at the rack head ( $U \approx (1.02\text{--}1.03)U_{th}$ ), whereas the flow accelerated towards the downstream rack end ( $U \approx (1.11\text{--}1.13)U_{th}$ ). This acceleration from the rack head to the downstream rack end ranged from 9.0% for S4-bars to 9.8% for S1-bars. This rack effect was observed up to  $X \approx -2$  and was slightly more pronounced for rectangular bars compared to the hydrodynamic bars. The effect of the HBR on the downstream velocity field was limited to the wake generated by the vertical tie-bars. A significant velocity reduction was observed downstream of the right tie-bar, which was larger for rectangular bars ( $U_{\min} \approx 0.76U_{th}$ , Fig. 5.1a) in comparison to the hydrodynamic bars ( $U_{\min} \approx (0.86\text{--}0.91)U_{th}$ , Fig. 5.1b–d). At  $X = 1$ , the flow was nearly symmetrical for S4 (Fig. 5.1d), whereas it slightly concentrated at the left channel wall for S1 (Fig. 5.1a). The transversal and vertical flow velocities  $V$  and  $W$ , respectively, were very small for the described configurations without overlays and were hardly affected by the rack. The effect of the different rack configurations on the velocity field was also quantified by the comparison of the relative discharges through the left and right channel halves  $Q_l$  and  $Q_r$ , respectively. The discharges denoted in Fig. 5.1 were derived from ADV measurements at  $X = 1$  in different flow depths. While  $\Delta Q/Q_o = |Q_l - Q_r|/Q_o = 4.2\%$  for rectangular bars (Fig. 5.1a), it ranged from 2.4% to 3.2% for hydrodynamic bars (Fig. 5.1b–d). The larger disturbance of the velocity field of HBRs with rectangular bars in comparison to hydrodynamic bars led to larger head loss coefficients. For the bar shapes S1–S4, the measured head loss coefficients were  $\xi_R = 2g\Delta h_R/U_{th}^2 = 0.50, 0.33, 0.23, \text{ and } 0.26$ , respectively, with  $\Delta h_R$  as the experimentally determined head loss (details in Chapter 6). Overall, the bar shape had a small effect on the velocity field.

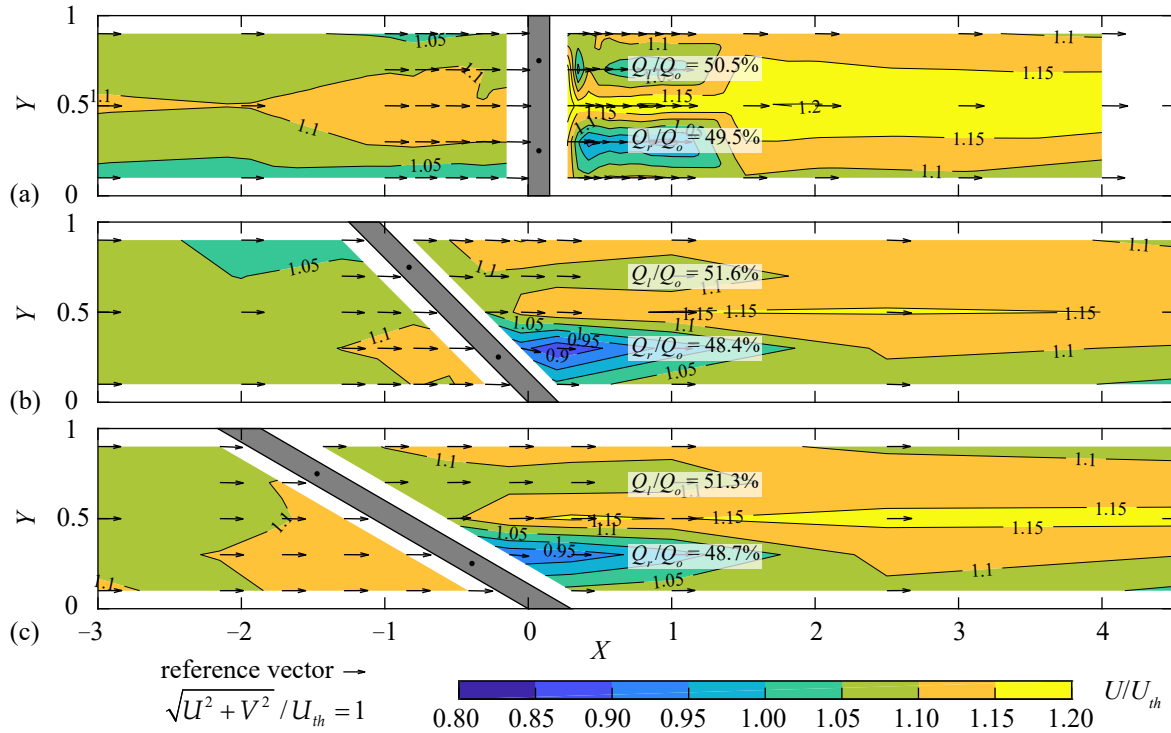


**Fig. 5.1:** Velocity field at  $Z = 0.5$  for  $s_b = 20$  mm,  $\alpha = 45^\circ$ ,  $H_{Ov} = 0$  with bar shape (a) S1 ( $\xi_R = 0.50$ ), (b) S2 ( $\xi_R = 0.33$ ), (c) S3 ( $\xi_R = 0.23$ ), and (d) S4 ( $\xi_R = 0.26$ )

### 5.1.2 Rack angle

For the rack configuration with S2-bars,  $s_b = 20$  mm, and  $H_{Ov} = 0$ , the velocity fields were measured for  $\alpha = 90^\circ$  in addition to  $\alpha = 45^\circ$  and  $\alpha = 30^\circ$  (Fig. 5.2). The HBR with  $\alpha = 90^\circ$  led to a symmetrical velocity field with reduced flow velocities behind the vertical tie-bars and a flow concentration towards the channel center (Fig. 5.2a). The flow upstream of the HBR with  $\alpha = 90^\circ$  concentrated to the center of the channel, with reduced velocities close to the channel walls. In contrast, the upstream flow velocities slightly increased along the rack as described above for the HBR with  $\alpha = 45^\circ$ . Thereby, the vertical tie-bar at the downstream rack end had a larger effect on the downstream velocity field than the upstream vertical tie-bar (Fig. 5.2b). However, this wake effect was observed mainly locally at  $X \leq 1$  and diminished further downstream. The velocity field for  $\alpha = 30^\circ$  was similar to the velocity field for  $\alpha = 45^\circ$ . The flow velocity increased along the HBR from the rack head to the downstream end from  $U = 1.03U_{th}$  to  $U = 1.13U_{th}$  for  $\alpha = 45^\circ$  (increase of 9.4%) and from  $U = 1.05U_{th}$  to  $U = 1.13U_{th}$  for  $\alpha = 30^\circ$  (increase of 7.5%). The transversal flow velocities upstream of the racks were very small for all  $\alpha$  ( $V \leq 0.04U_{th}$ ). Due to symmetry, the discharge through the left and right channel half were almost identical for  $\alpha = 90^\circ$  ( $\Delta Q/Q_o = 1\%$ , Fig. 5.2a). The flow concentration to the left channel half, as described above for  $\alpha = 45^\circ$ , was slightly larger

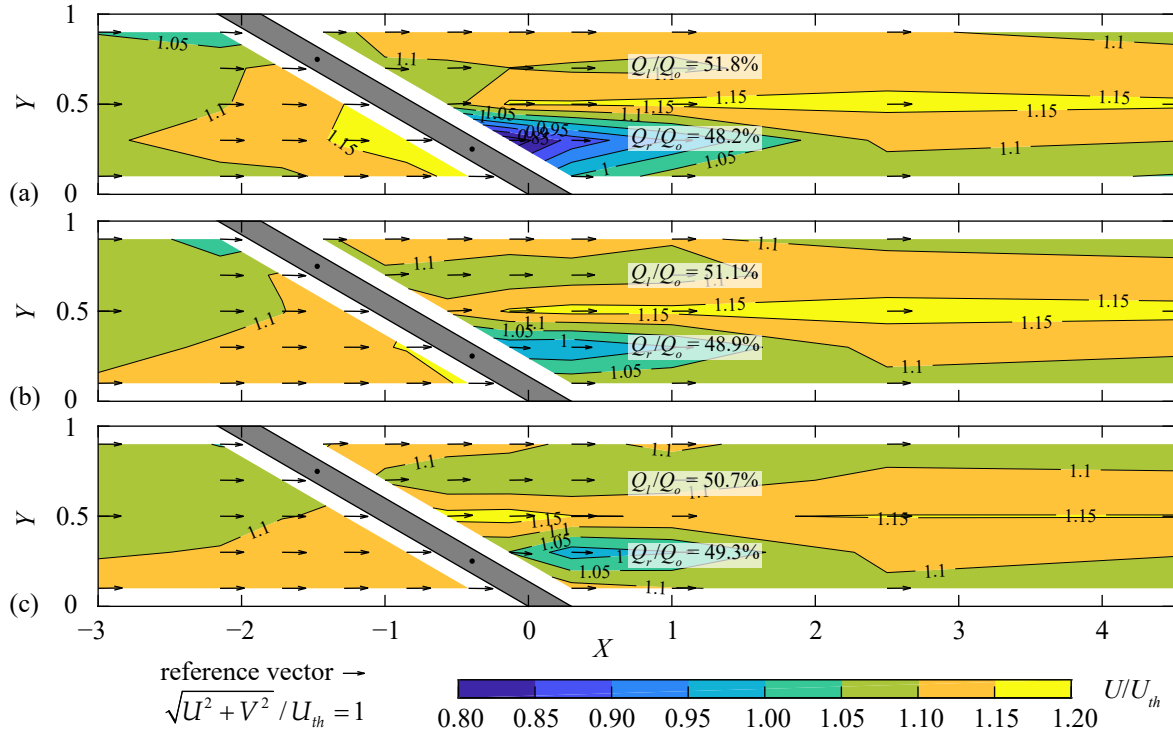
than for  $\alpha = 30^\circ$  ( $\Delta Q/Q_o = 3.2\%$  vs.  $\Delta Q/Q_o = 2.6\%$ , Fig. 5.2b,c). A larger rack angle  $\alpha$  reduced the rack length and thus the hydraulically active rack area, leading to larger normal flow velocities and larger disturbances of the flow field. Consequently, the head loss coefficient decreased from  $\xi_R = 0.43$  for  $\alpha = 90^\circ$  to  $\xi_R = 0.33$  for  $\alpha = 45^\circ$ , and  $\xi_R = 0.29$  for  $\alpha = 30^\circ$ . Overall, HBRs with  $\alpha = 45^\circ$  and  $\alpha = 30^\circ$  led to similar velocity fields, whereas HBRs with  $\alpha = 90^\circ$  concentrated the flow to the channel center.



**Fig. 5.2:** Velocity field at  $Z = 0.5$  for S2,  $s_b = 20$  mm, and  $H_{O_v} = 0$  for (a)  $\alpha = 90^\circ$  ( $\xi_R = 0.43$ ), (b)  $\alpha = 45^\circ$  ( $\xi_R = 0.33$ ), and (c)  $\alpha = 30^\circ$  ( $\xi_R = 0.29$ )

### 5.1.3 Bar spacing

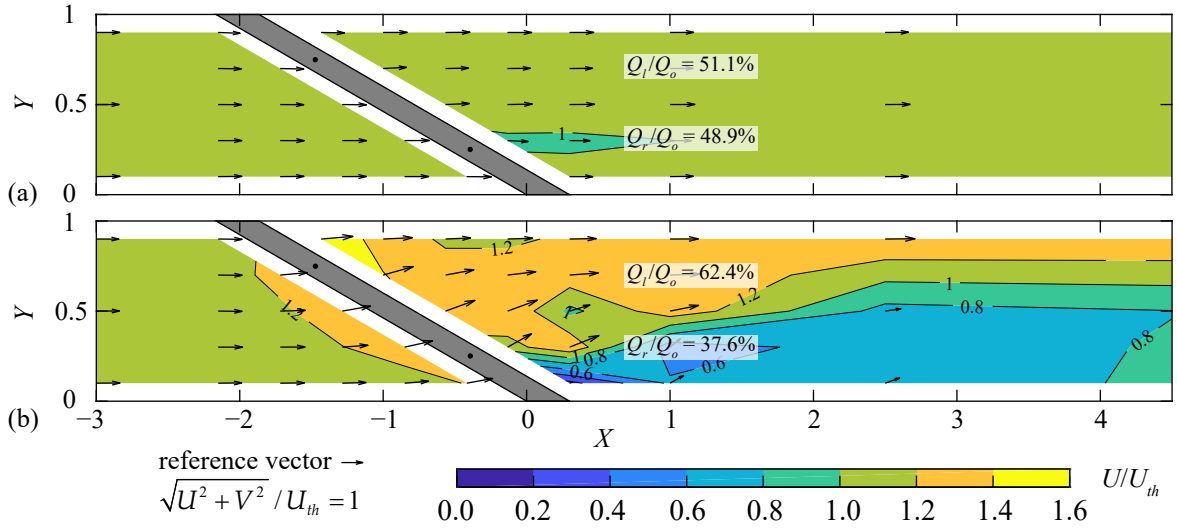
The effect of the clear bar spacing was investigated for  $s_b = 10, 20$ , and  $30$  mm (Fig. 5.3), corresponding to blocking ratios of  $BR \approx 0.49, 0.35$ , and  $0.28$  for S4 (cf. Table 4.1 in Section 4.4.2). With increasing blocking ratios, both the up- and downstream effects as described above became more pronounced. The streamwise velocities increased along the rack from  $U = 1.02U_{th}$  to  $U = 1.17U_{th}$  for  $s_b = 10$  mm (increase of 14.9%; Fig. 5.3a) and from  $U = 1.05U_{th}$  to  $U = 1.13U_{th}$  for  $s_b = 30$  mm (increase of 8.1%; Fig. 5.3c). Accordingly, the formation of the tie-bar wake was more pronounced for  $s_b = 10$  mm ( $U_{\min} \approx 0.76U_{th}$ ) than for  $s_b = 20, 30$  mm with  $U_{\min} \approx (0.95\text{--}0.97)U_{th}$ . The downstream flow field at  $X = 1$  was almost symmetrical for  $s_b = 20, 30$  mm ( $\Delta Q/Q_o = 2.2, 1.4\%$ , Fig. 5.3b,c), whereas the flow was concentrated to the left channel half for  $s_b = 10$  mm ( $\Delta Q/Q_o = 3.6\%$ , Fig. 5.3a). The loss coefficient of the HBR with  $s_b = 10$  mm ( $\xi_R = 0.38$ ) was thus significantly larger than the one of the configurations with  $s_b = 20, 30$  mm ( $\xi_R = 0.23, 0.18$ ). Overall, HBRs with  $s_b = 20, 30$  mm had a small effect on the up- and downstream velocity fields, while HBRs with  $s_b = 10$  mm led to larger flow accelerations along the upstream rack side and a slightly more asymmetric downstream velocity field.



**Fig. 5.3:** Velocity field at  $Z = 0.5$  for S4,  $\alpha = 30^\circ$ , and  $H_{Ov} = 0$  for (a)  $s_b = 10$  mm ( $\xi_R = 0.38$ ), (b)  $s_b = 20$  mm ( $\xi_R = 0.23$ ), and (c)  $s_b = 30$  mm ( $\xi_R = 0.18$ )

### 5.1.4 Overlays

In Fig. 5.4, the velocity field of the rack configuration with S4-bars,  $\alpha = 30^\circ$ , and  $s_b = 20$  mm at mid depth ( $Z = 0.5$ ) is shown (a) without overlays ( $H_{Ov} = 0$ ) and (b) with  $H_{Bo} = H_{To} = 0.2$ . Note that Fig. 5.4a presents the same data as Fig. 5.3b but with a different contour map scaling. HBR configurations without overlays had a small effect on the velocity field with small transversal and vertical velocity components  $V$  and  $W$ , and a homogeneous velocity distribution across the rack area. In contrast, overlays block a part of the hydraulically active area and lead to flow deflections towards the bypass, and thus, significant transversal and vertical flow velocities. As a result of the reduced hydraulically active rack area, the flow passing the remaining open rack area accelerated to  $\sqrt{U^2 + V^2} \approx 1.33U_{th}$ , as compared to the maximum of  $\sqrt{U^2 + V^2} \approx 1.16U_{th}$  for the HBR without overlays. In addition, the overlays directed the flow at mid depth normal to the rack (thus increasing  $V_n$ ) and in the direction of the left channel wall downstream of the rack. The downstream flow field was therefore asymmetric with a flow concentration at the left channel wall and a deceleration zone at the right channel wall ( $\Delta Q/Q_o = 24.8\%$ , Fig. 5.4b). Overlays therefore had a governing effect on the velocity field as compared to the minor effects of the bar shape,  $\alpha$ , and  $s_b$ . The governing effect of the overlays can also be illustrated by the resulting head loss coefficients (details in Chapter 6). In comparison to the configuration without overlays (Fig. 5.4a), the head loss coefficient increased by a factor of 4.4 for the corresponding rack configuration with  $H_{Bo} = H_{To} = 0.2$  (Fig. 5.4b).

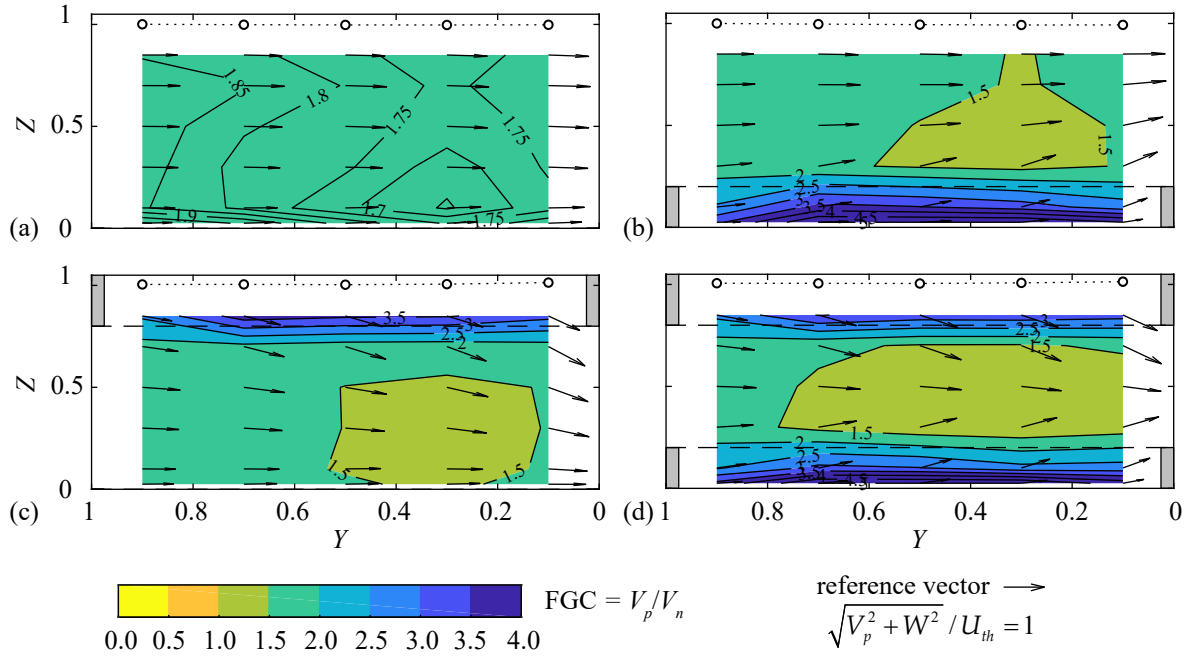


**Fig. 5.4:** Velocity field at  $Z = 0.5$  for S4,  $\alpha = 30^\circ$ ,  $s_b = 20$  mm for (a)  $H_{Bo} = H_{To} = 0$  ( $\xi_R = 0.23$ ) and (b)  $H_{Bo} = H_{To} = 0.2$  ( $\xi_R = 1.01$ ); note the changed contour map scaling in comparison to Fig. 5.1–5.3

## 5.2 Fish guidance capacity

Figure 5.5 shows the fish guidance capacity,  $FGC = V_p/V_n$ , at the rack-parallel section 40 mm upstream of the rack for the configuration with S4-bars,  $\alpha = 30^\circ$ , and  $s_b = 20$  mm and four different overlay configurations: (a)  $H_{Bo} = H_{To} = 0$ , (b)  $H_{Bo} = 0.2$ ,  $H_{To} = 0$ , (c)  $H_{Bo} = 0$ ,  $H_{To} = 0.2$ , and (d)  $H_{Bo} = H_{To} = 0.2$ . The circle outlines (o) indicate the flow depth measurement locations and the dotted lines show the free water surface. The overlay locations are indicated by gray bars and dashed lines. The vectors show the direction and magnitude of the rack-parallel velocities  $V_p$  and the vertical velocities  $W$ . The flow depth along all rack configurations was almost constant, but a small backwater rise was observed for the configurations with top overlays (Fig. 5.5c,d). Without overlays, the FGC was homogeneous across the rack area and ranged between 1.6–2.0 with an average value of 1.80 (Fig. 5.5a). In comparison, the theoretical FGC from vector decomposition of  $U_o = 0.5$  m/s is  $V_p/V_n = \cot(30^\circ) = 1.73$ . The small difference to the measured values indicates that HBRs without overlays induce only negligible transversal velocity components, which are uniformly distributed over the cross section. Overlays block a part of the rack area, leading to small  $V_n$  directly in front of the overlays and thereby large FGCs of  $\geq 4.0$ . Since the flow is then forced to pass the remaining hydraulically active rack area,  $V_n$  increased at the rack center area, thereby decreasing the FGC to values  $\leq 1.5$  for  $\alpha = 30^\circ$  (Fig. 5.5b–d) and  $FGC \leq 0.75$  for  $\alpha = 45^\circ$  (details in Meister *et al.*, 2019). Additionally, a positive vertical flow velocity component was induced by bottom overlays (Fig. 5.5b) and a negative vertical flow velocity component by top overlays (Fig. 5.5c). For configurations with both, bottom and top overlays (Fig. 5.5d), the resulting velocity field was similar to a superposition of the individual velocity fields with bottom and top overlays only. Larger FGCs close to the bottom and the water surface are assumed to be beneficial to guide sediments and floating debris to the bypass, respectively. However, it has to be considered that the overlays reduce the FGC in the remaining hydraulically active area.





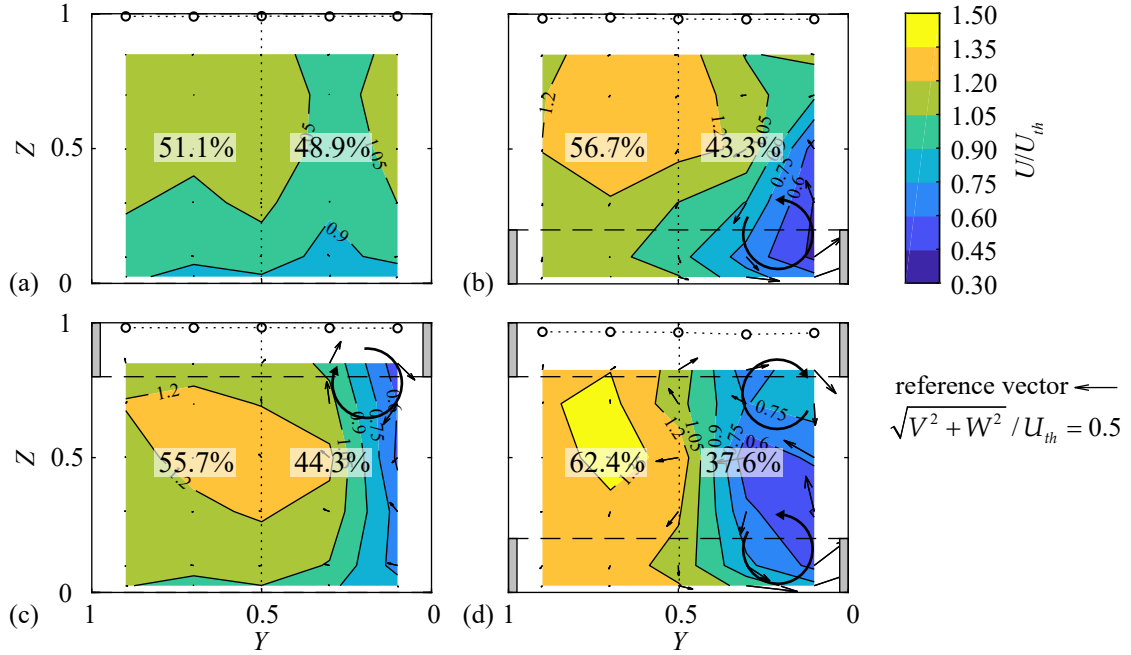
**Fig. 5.5:** Values of rack-parallel fish guidance capacity (FGC) upstream of the rack S4,  $\alpha = 30^\circ$ ,  $s_b = 20$  mm for the overlay configurations (a)  $H_{Bo} = H_{To} = 0$  ( $\xi_R = 0.23$ ), (b)  $H_{Bo} = 0.2$ ,  $H_{To} = 0$  ( $\xi_R = 0.48$ ), (c)  $H_{Bo} = 0$ ,  $H_{To} = 0.2$  ( $\xi_R = 0.50$ ), and (d)  $H_{Bo} = H_{To} = 0.2$  ( $\xi_R = 1.01$ )

### 5.3 Rack downstream velocity field

In Fig. 5.6, the normalized velocities are shown at the cross sections  $X = 1$  for the rack configuration with S4-bars,  $\alpha = 30^\circ$ ,  $s_b = 20$  mm, and four different overlay configurations: (a)  $H_{Bo} = H_{To} = 0$ , (b)  $H_{Bo} = 0.2$ ,  $H_{To} = 0$ , (c)  $H_{Bo} = 0$ ,  $H_{To} = 0.2$ , and (d)  $H_{Bo} = H_{To} = 0.2$ . The vectors show the direction and magnitude of the velocities  $V$  and  $W$  and the circular arrows illustrate vortex formations. The velocity field downstream of HBRs without overlays was homogeneous and symmetrical; only slightly reduced flow velocities were observed in the wake of the vertical tie-bars (Fig. 5.6a). This effect was more pronounced for the right vertical tie-bar as it was located closer to the considered cross section (cf. Fig. 4.18 in Section 4.4.1). As described above, overlays induce transversal and vertical velocity components, leading to asymmetrical downstream flow conditions with a discharge concentration to the left channel wall and a deceleration zone at the right channel wall. The turbine admission flow should be symmetrical to maintain high turbine efficiency. According to Godde (1994), the difference between the relative discharges in the left and right channel half should be below 5% ( $\Delta Q/Q_o = |Q_l - Q_r|/Q_o \leq 5\%$ ). This criterion is fulfilled at  $X = 1$  for the HBR configuration without overlays ( $\Delta Q/Q_o = 2.2\%$ ; Fig. 5.6a), but for none of the HBR configurations with overlays ( $\Delta Q/Q_o = 13.4, 11.4, 24.8\%$ , Fig. 5.6b–d). Resulting from the transversal and vertical flow deflection induced by overlays, a counter-clockwise rotating vortex was generated by the bottom overlay (Fig. 5.6b) and a clockwise rotating vortex by the top overlay (Fig. 5.6c). Both vortices superposed for combined bottom and top overlays, leading to a pronounced transversal flow velocity component at mid depth  $Z = 0.5$  of the right channel half, where both vortices met (Fig. 5.6d). In contrast, the transversal and vertical flow velocities were small at the left channel half. While the water surface was horizontal for the HBR without overlays (Fig. 5.6a), the flow

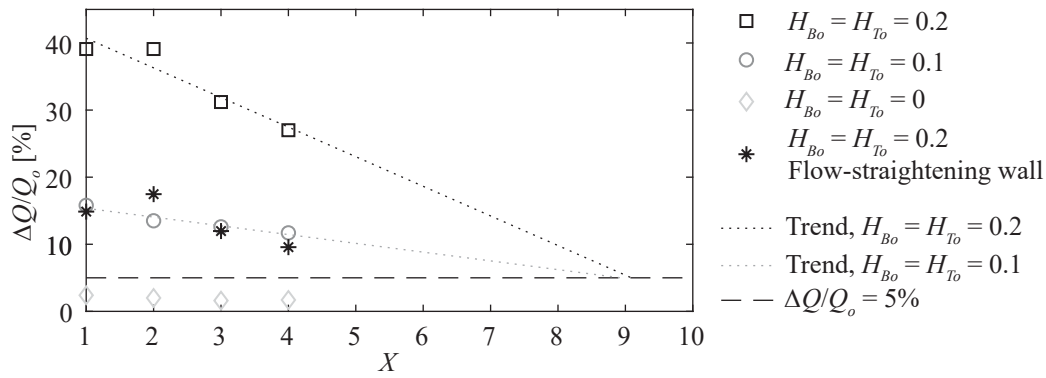


concentration due to the overlays led to slightly increased flow depths at the left channel half (Fig. 5.6d).



**Fig. 5.6:** Normalized velocities at the cross section  $X = 1$  downstream of the rack S4,  $\alpha = 30^\circ$ , and  $s_b = 20$  mm for the overlay configurations (a)  $H_{Bo} = H_{To} = 0$  ( $\xi_R = 0.23$ ), (b)  $H_{Bo} = 0.2, H_{To} = 0$  ( $\xi_R = 0.48$ ), (c)  $H_{Bo} = 0, H_{To} = 0.2$  ( $\xi_R = 0.50$ ), and (d)  $H_{Bo} = H_{To} = 0.2$  ( $\xi_R = 1.01$ ); vortex formation is indicated with circular arrows

The asymmetrical rack outflow homogenized with increasing flow distance. If an HBR was installed at the beginning of a long headrace channel, the effect on the turbine efficiency would become negligible. However, if the rack was installed close to the turbines, the generated velocity field is of prime importance. Due to the limited length of the laboratory channel, the discharge distribution could only be measured to a maximal distance of  $X = 4$ . Figure 5.7 shows  $\Delta Q/Q_o = |Q_l - Q_r|/Q_o$  for the rack configuration with S4-bars,  $\alpha = 45^\circ$ ,  $s_b = 20$  mm without overlays,  $H_{Bo} = H_{To} = 0.1$ , and  $H_{Bo} = H_{To} = 0.2$ . While the criterion of  $\Delta Q/Q_o \leq 5\%$  was fulfilled at all measurement locations without overlays,  $\Delta Q/Q_o = 12\%$  and  $\Delta Q/Q_o = 27\%$  at  $X = 4$  for  $H_{Bo} = H_{To} = 0.1$  and  $H_{Bo} = H_{To} = 0.2$ , respectively. The linear decrease of  $\Delta Q/Q_o$  tends to  $\Delta Q/Q_o = 5\%$  at  $X \approx 9$  for both overlay configurations (Fig. 5.7). Additionally, the measurements of the configuration S4,  $\alpha = 45^\circ$ ,  $s_b = 20$  mm,  $H_{Bo} = H_{To} = 0.2$  with the flow-straightening wall (cf. Fig. 4.18 in Section 4.4.1) were included in Fig. 5.7. Thereby, the discharge distribution for the configuration  $H_{Bo} = H_{To} = 0.2$  was significantly improved from  $\Delta Q/Q_o = 39.0\%$  to  $\Delta Q/Q_o = 14.8\%$  at  $X = 1$  and from  $\Delta Q/Q_o = 27.0\%$  to  $\Delta Q/Q_o = 9.6\%$  at  $X = 4$ . These results indicate that even a simple flow-straightening wall improves the downstream velocity field significantly. For practical application, it is recommended to optimize the design of the flow-straightening wall with numerical simulations or in a physical model by considering site-specific conditions.

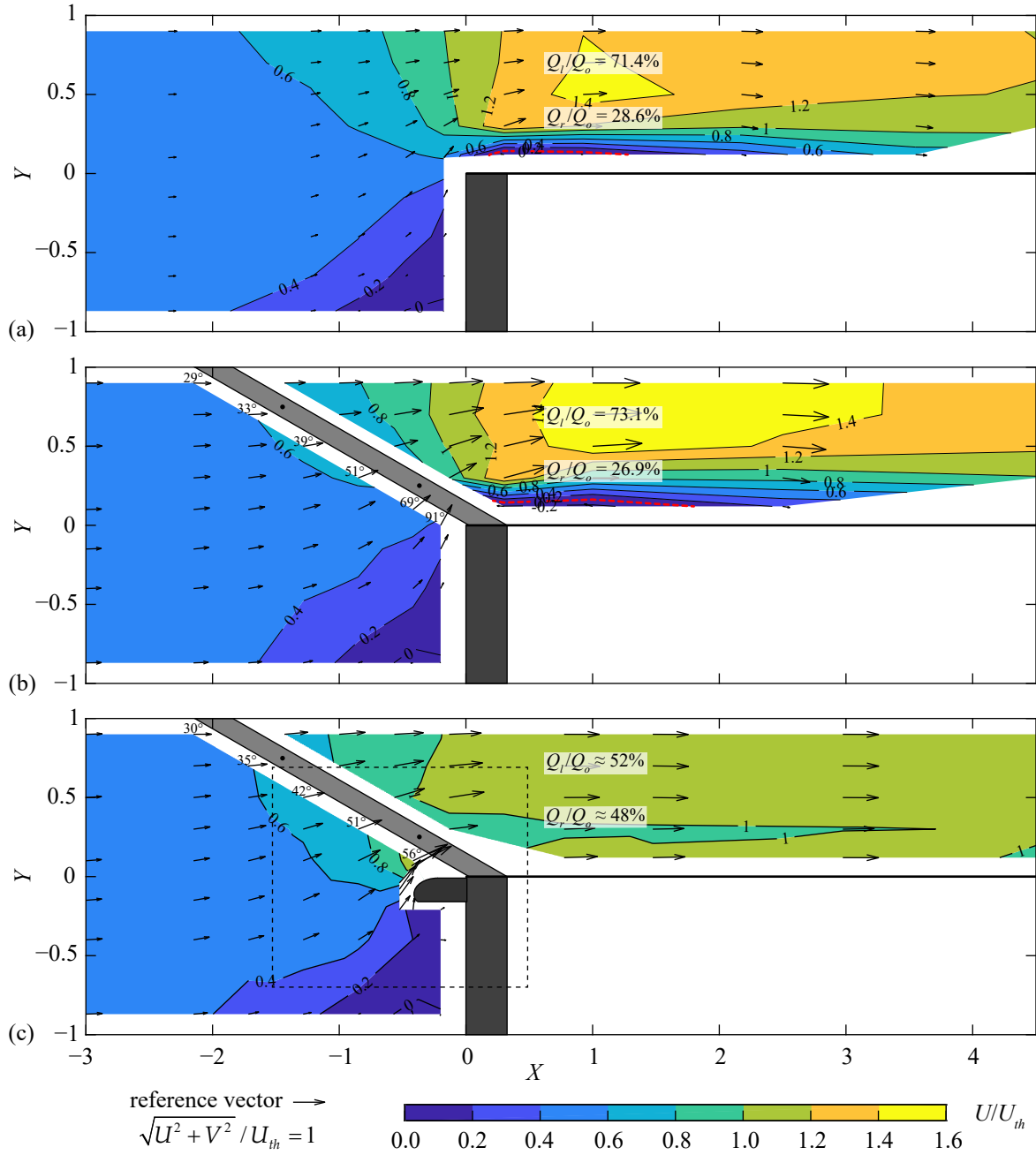


**Fig. 5.7:** Development of  $\Delta Q/Q_o$  along the  $x$ -axis of the configuration S4,  $\alpha = 45^\circ$ ,  $s_b = 20$  mm for different overlay configurations

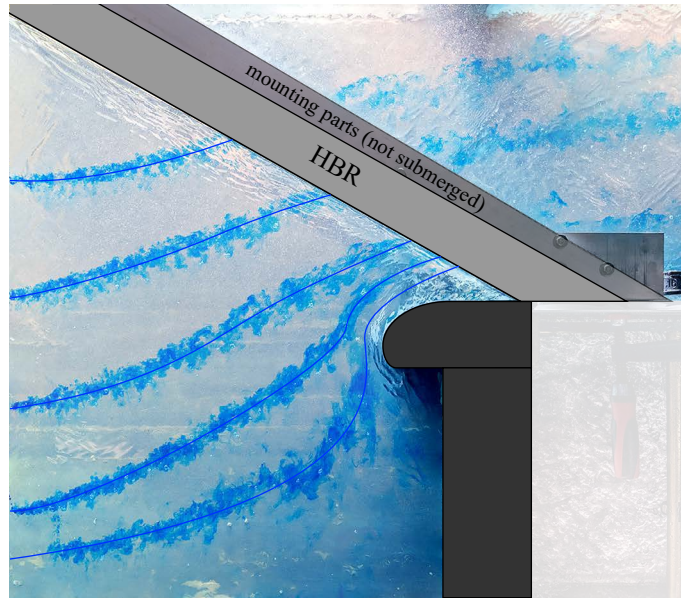
## 5.4 Effect of the hydropower plant layout

All velocity fields presented above relate to diversion HPPs. To investigate the velocity field at block-type HPPs, physical model experiments were conducted in a widened upstream channel, such that  $w_o/w_{ds} = 2$  (cf. Section 4.1.2). The whole discharge was diverted through the HBRs (no spillway discharge), which is the most conservative load case with regard to fish protection. In a first step, the velocity field at mid depth was measured without a rack to investigate the hydraulic effect of the channel contraction (Fig. 5.8a). Starting at  $X \approx -2$ , the flow accelerated towards the contraction and was deflected to the left channel wall. Flow separation at the sharp edge at  $X = 0$  created a recirculation zone, which is indicated by red dashed streamlines in Fig. 5.8a,b. The separation zone was slightly wider for the configuration with the HBR installed (Fig. 5.8b;  $Y = 0-0.16$ ), as compared to the sharp contraction without the HBR (Fig. 5.8a;  $Y = 0-0.14$ ). Resulting from the flow deflection and recirculation zone, the flow concentrated to the left channel wall with a maximal flow velocity of  $U_{\max} = 1.48U_{th}$  without and  $U_{\max} = 1.56U_{th}$  with the HBR installed. At the most downstream measurement location ( $X \approx 4.5$ ), the flow distribution was still asymmetric for both cases (Fig. 5.8a,b). Similar to the diversion HPP setup, the upstream velocity field was hardly affected by a standard rack configuration with S4-bars,  $\alpha = 30^\circ$ ,  $s_b = 20$  mm without overlays (Fig. 5.8a,b). As indicated by the velocity vectors, the flow deflection at the contraction led to increased  $V_n$  at the downstream rack end. The slightly negative  $V_p$  at that location led to negative FGCs, such that fish are expected to have difficulties in finding the bypass entrance. Flow guidance structures, such as a rounded pier extending upstream, are an effective countermeasure to reduce the transversal velocities and therefore increase the FGC at the downstream rack end (Fig. 5.8c). While the angle between the velocity vectors and the rack was  $\approx 30^\circ$  at the rack head with and without the dividing pier, it consistently increased along the rack to  $\approx 91^\circ$  without and  $\approx 56^\circ$  with the pier (Fig. 5.8b,c). Following from the criterion of  $FGC > 1$ , good guidance efficiencies are expected for small angles  $\alpha \leq 45^\circ$ . Since flow velocity measurements with down-looking ADV probes require a minimal distance of 40 mm to solid surfaces, the velocity field directly upstream of the HBR and the pier was visualized by dye injection (Fig. 5.9). The streamlines follow the shape of the pier without any detachment and intersect the HBR with an angle of  $\approx 50^\circ$ , which

is smaller than the  $\approx 56^\circ$  mentioned above, determined from the ADV measurements 40 mm upstream of the HBR (Fig. 5.8c). Between the pier and the HBR, the longitudinal velocities were larger than the transversal velocities, which led to larger  $V_p$  and smaller  $V_n$  as compared to the configuration without a pier. Prevention of flow separation at the rounded pier also led to a symmetrical downstream velocity field with  $U \approx (0.75\text{--}1.15)U_{th}$ , thereby maintaining high turbine efficiencies. The sharp contraction without an HBR led to very asymmetric flow at  $X = 1.0$  ( $\Delta Q/Q_o = 42.8\%$ , Fig. 5.8a). The installation of an HBR had a comparably small effect on the downstream discharge distribution ( $\Delta Q/Q_o = 46.2\%$ , Fig. 5.8b). The relative discharges  $Q_l/Q_o$  and  $Q_r/Q_o$ , shown in Fig. 5.8a,b, were calculated from measurements across different flow depths. In contrast,  $Q_l/Q_o$  and  $Q_r/Q_o$  in Fig. 5.8c were calculated from velocity measurements at mid depth only and therefore have a reduced accuracy. The installation of a pier very positively affected the downstream velocity field ( $\Delta Q/Q_o \approx 4\%$ , Fig. 5.8c), such that the criterion of Godde (1994), that is,  $\Delta Q/Q_o < 5\%$ , was fulfilled. Furthermore, it improved the FGC along the rack.

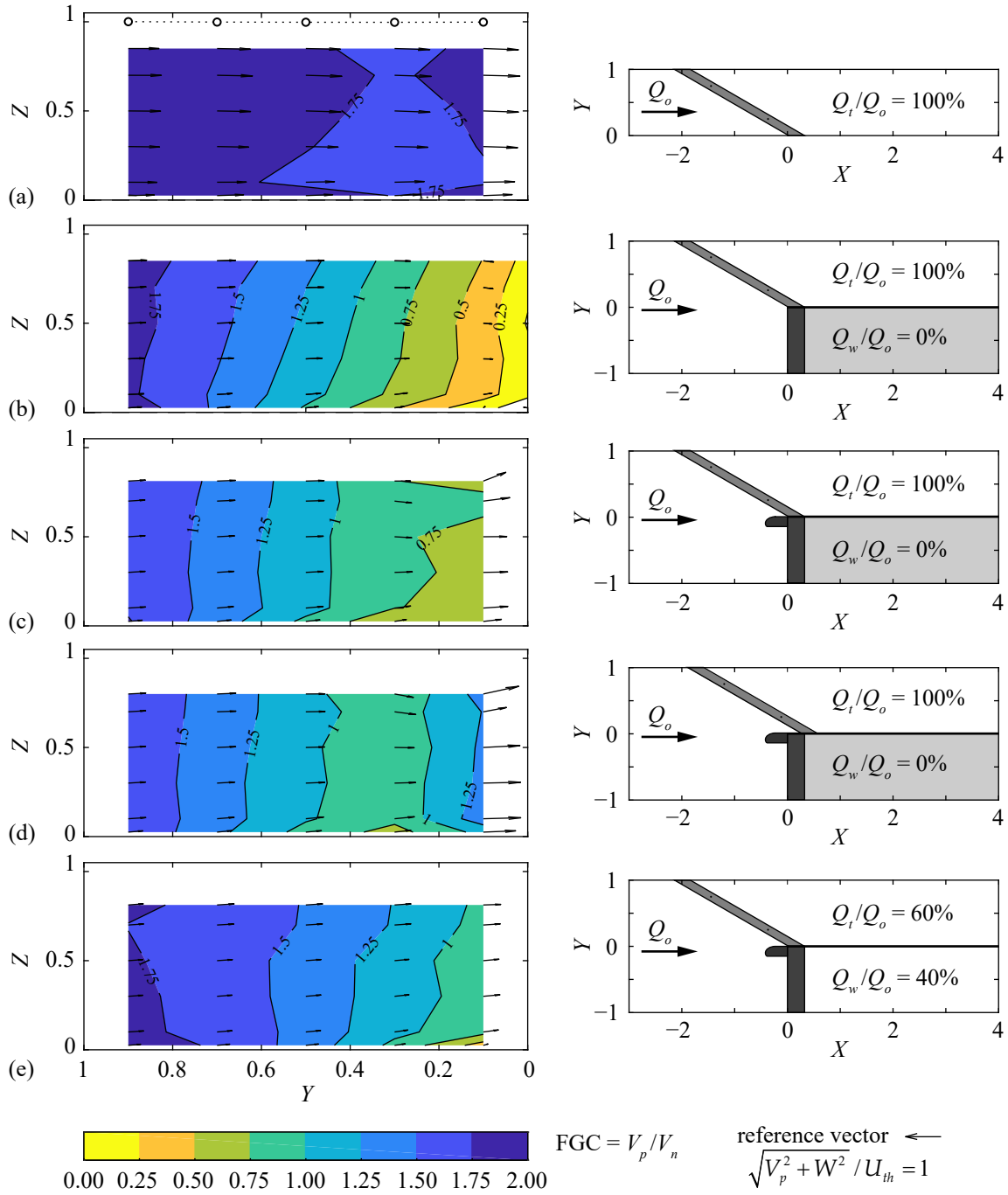


**Fig. 5.8:** Normalized velocity field at block-type hydropower plant configurations (a) without rack (contraction head loss coefficient  $\xi_c = 0.29$ ), (b) S4,  $\alpha = 30^\circ$ ,  $s_b = 20$  mm,  $H_{Ov} = 0$  ( $\xi_c + \xi_R = 0.64$ ), and (c) S4,  $\alpha = 30^\circ$ ,  $s_b = 20$  mm,  $H_{Ov} = 0$  with a dividing pier (for reference:  $\xi_R = 0.23$  for this rack configuration at the diversion HPP); dashed rectangle corresponds to field of view of Fig. 5.9; the red dashed streamlines indicate the separation to the recirculation zone



**Fig. 5.9:** Visualization of the flow around the dividing pier at the downstream rack end with the configuration S4,  $\alpha = 30^\circ$ ,  $s_b = 20$  mm,  $H_{Ov} = 0$ , without spillway flow; field of view corresponds to dashed rectangle in Fig. 5.8c

Figure 5.10 shows the FGC at the rack-parallel section 40 mm upstream of the rack, for the configuration with S4-bars,  $\alpha = 30^\circ$ , and  $s_b = 20$  mm and different HPP layouts: (a) diversion HPP, (b) block-type HPP, (c) block-type HPP with a short dividing pier, (d) block-type HPP with a long dividing pier, and (e) block-type HPP with short pier and 40% relative weir discharge. Note that Fig. 5.10a presents the same data as in Fig. 5.5a but with a different contour map scaling. As described above for the diversion HPP, FGCs between  $\approx 1.6$  and 2.0 are considered good (Fig. 5.10a). For a block-type HPP without weir discharge, the FGC was comparable at the upstream rack end. However, it continuously decreased along the rack to  $\text{FGC} < 0.25$  due to the changing streamline angle (Fig. 5.10b). With a short pier installed, a similar decrease of the FGC was observed at rack locations  $Y \approx 1-0.3$  (Fig. 5.10c). However, the reduction of the FGC between  $Y \approx 0.3$  and 0 was much smaller with the short pier. The minimal value of  $\text{FGC} < 0.75$  remained nearly constant from  $Y \approx 0.35$  up to the bypass entrance at  $Y = 0$ , which is still considered dissatisfactory with regard to fish guidance (Fig. 5.10c). Given a longer pier was installed, the FGC reduction, starting at the upstream rack end up to  $Y \approx 0.3$  with  $\text{FGC} \approx 0.8$ , was similar to the two HPP layouts described above. However, the FGC then again increased to a value of  $\approx 1.3$  at the bypass entrance (Fig. 5.10d). A relative weir discharge of  $Q_w/Q_o = 40\%$  led to a more streamwise directed approach flow field, such that in combination with a short pier,  $\text{FGC} \geq 1$  was maintained at almost all measurement locations along the rack (Fig. 5.10e). A picture of this load case is shown in Fig. 4.3 in Section 4.1.2. Both, the installation of a dividing pier and additional weir discharge can help to improve the FGC at HBRs at block-type HPPs.

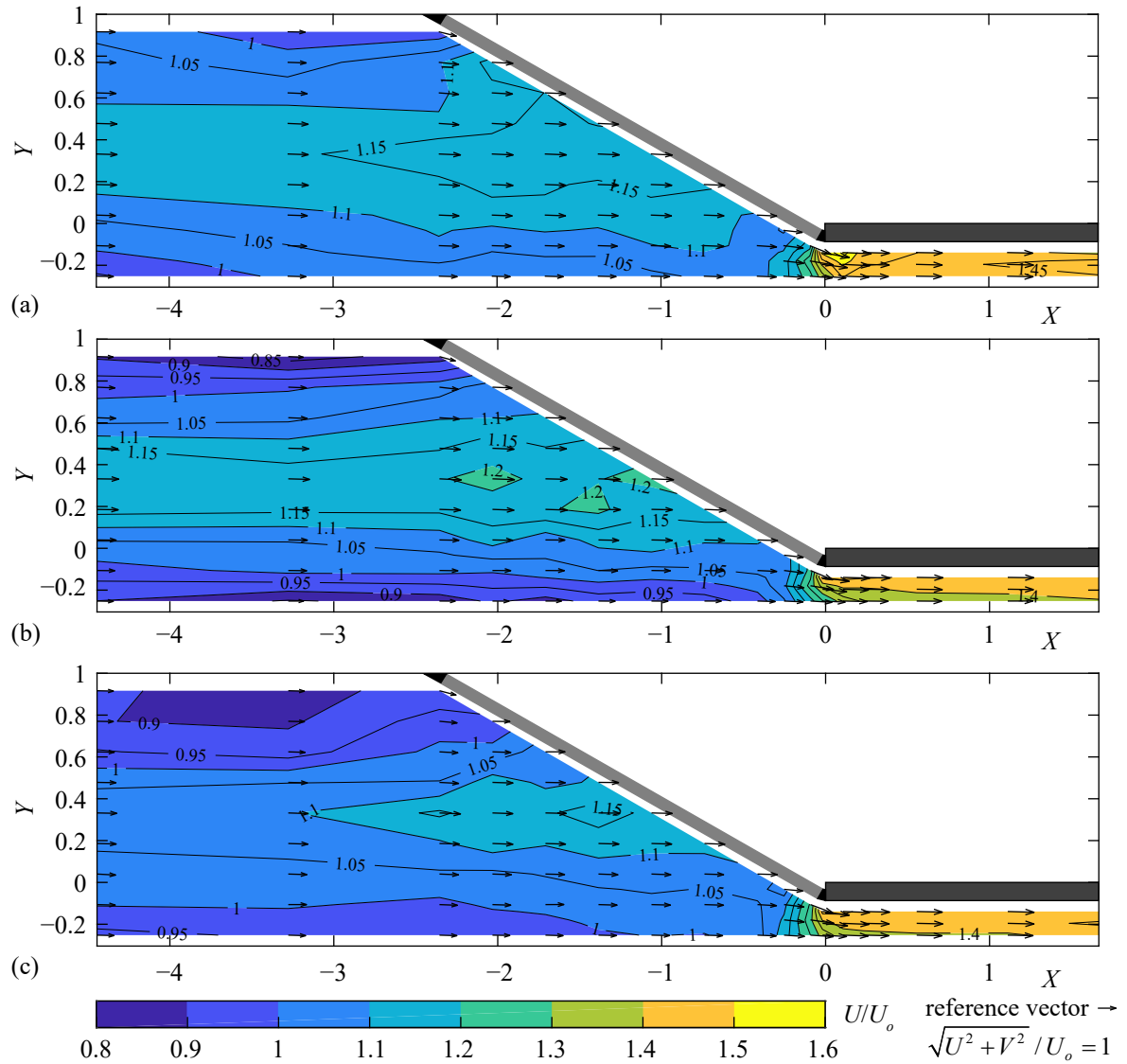


**Fig. 5.10:** Rack-parallel fish guidance capacities (FGCs) of the configuration S4,  $\alpha = 30^\circ$ ,  $s_b = 20$  mm,  $H_{Ov} = 0$  for (a) diversion hydropower plant, (b) block-type, (c) block-type with short pier, (d) block-type with long pier, and (e) block-type with short pier and  $Q_w/Q_o = 40\%$

## 5.5 Bypass hydraulics

As the relative bypass discharge  $Q_{by,rel}$  is typically small at HBR-BSs (cf. Section 3.4.2), it affects the velocity field only locally. All velocity fields shown up to now were therefore conducted without a bypass (cf. Section 4.1). Depending on the bypass design, the flow is accelerated and diverted at the bypass inlet, leading to more turbulent kinetic energy TKE and larger spatial velocity gradients SVG. Fish can perceive these flow characteristics with their lateral line organs and react correspondingly (cf. Section 2.2.5), which is why it is important to study flow characteristics in a model including a bypass. These flow characteristics can then

be used to predict fish behavior (Adam and Lehmann, 2011). All measurements in this section were conducted in the ethohydraulic flume (Section 4.1.3) with the hydraulically optimized rack configuration, which was used for most live fish tests, that is, S4-bars,  $\alpha = 30^\circ$ ,  $s_b = 20$  mm, and  $H_{Ov} = 0$  (cf. Section 4.4.1). Figure 5.11 shows the normalized streamwise flow velocities  $U/U_o$  in three horizontal planes at different flow depths for  $U_o = 0.5$  m/s with the full depth open channel bypass (OC). For this configuration, the ratio of the bypass inlet to mean approach flow velocity was  $VR = U_{by,in}/U_o = 1.4$  and the relative bypass discharge  $Q_{by,rel} = Q_{by}/Q_o = 16.9\%$ . The arrows, shown at each measurement location, indicate the direction and magnitude of the longitudinal and transversal flow velocities  $U$  and  $V$ , respectively.

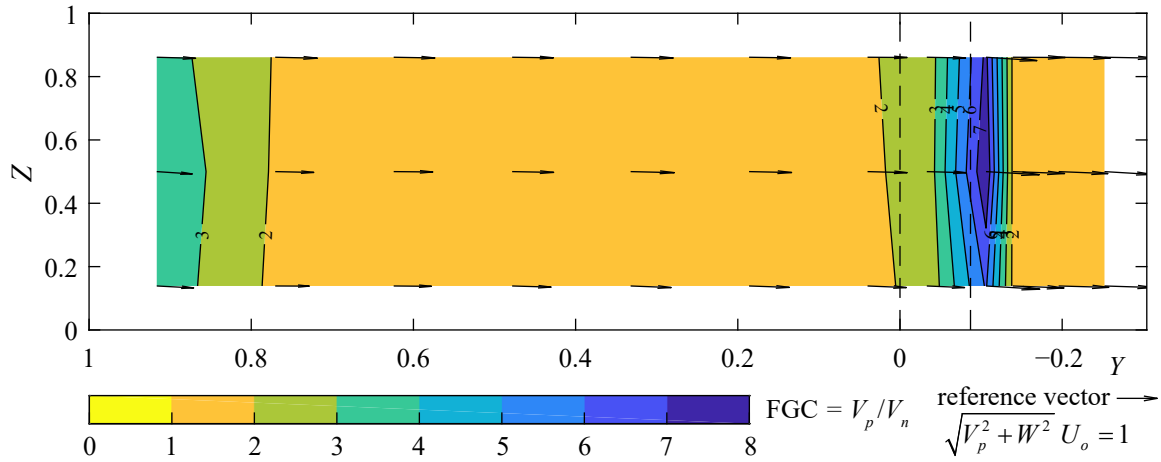


**Fig. 5.11:** Velocity field of the HBR-BS with the OC-bypass,  $U_o = 0.5$  m/s,  $VR = 1.4$  (a) close to the water surface ( $Z = 0.86$ ), (b) at mid flow depth ( $Z = 0.50$ ), and (c) close to the bottom ( $Z = 0.14$ ) with  $Q_{by,rel} = 16.9\%$

As for the measurements without overlays presented up to now, the HBR hardly affected the upstream velocity field. As a result of the logarithmic velocity profile, flow velocities were smallest close to the bottom (Fig. 5.11c). Due to the smooth side walls, the flow velocities were only slightly larger in the flume center than close to the walls. The bypass affected the



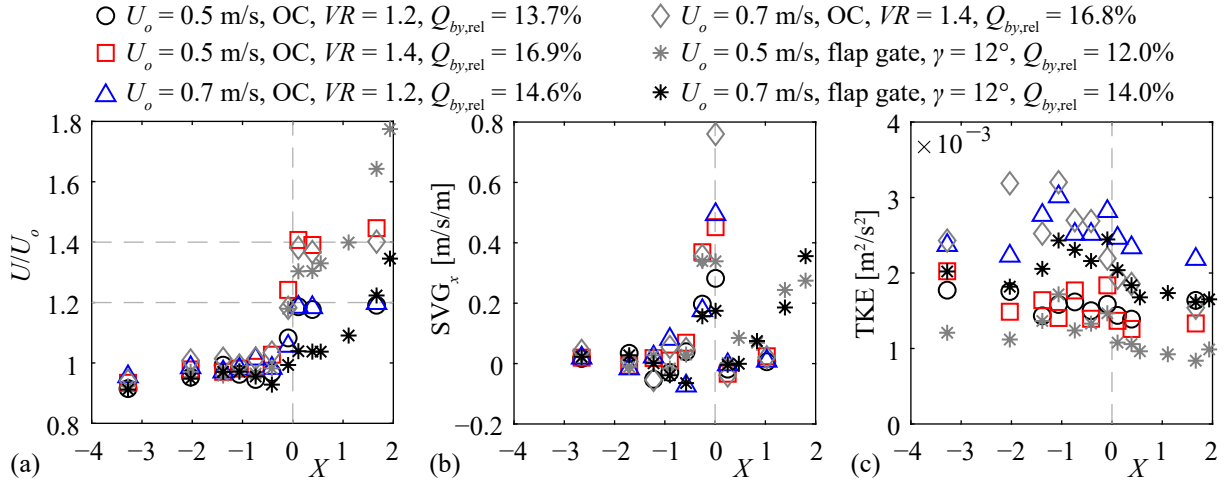
velocity field only locally, where the normalized streamwise velocity increased to  $U/U_o \approx 1.4$ , which corresponds to  $VR = 1.4$  at the bypass inlet. For the same HBR-BS configuration, the fish guidance capacity FGC is shown in a rack-parallel cross section, at a distance of 40 mm orthogonal to the rack in Fig. 5.12. The arrows represent the rack-parallel and vertical flow velocity components at the measurement locations and the vertical dashed lines indicate the 10 cm wide concrete wall, which separated the bypass from the main channel.



**Fig. 5.12:** Cross section of FGC 40 mm upstream of the HBR-BS with the OC-bypass,  $U_o = 0.5$  m/s,  $VR = 1.4$ , and  $Q_{by,rel} = 16.9\%$ ; the vertical dashed lines indicate the wall separating the bypass from the main channel

Between  $Y = 0-0.8$ , the fish guidance capacity was in the range of  $FGC = 1.7-1.9$ , which almost corresponds to the theoretical FGC from vector decomposition neglecting transversal flow components ( $V = 0$  m/s),  $V_p/V_n = \cot(30^\circ) = 1.73$ , which indicates small  $V$  (cf. Section 5.2). As a result of the hard foam wedge installed at the upstream rack end (cf. Fig. 4.9), which is illustrated as a black triangle in Fig. 5.11,  $FGC \geq 2.0$  for  $Y = 0.8-1.0$ . Close to the bypass wall,  $V_n$  was very small, which led, in combination with slightly increased  $V_p$  due to the accelerating flow towards the bypass, to very large fish guidance capacities of up to  $FGC \approx 8$ . As the bypass affected the velocity field only locally, the hydraulic characteristics of different bypass configurations were compared to each other with measurements at the center line of the bypass ( $Y = -0.2$ ) at mid flow depth ( $Z = 0.5$ ). In Fig. 5.13, the measurements of the full depth open channel bypass (Fig. 4.6a) are illustrated with marker outlines, while the measurements at the open channel bypass with a flap gate with an inclination angle of  $\gamma = 12^\circ$  (Fig. 4.6b) are marked with asterisk-symbols. The bypass configuration illustrated in Fig. 5.11 and 5.12 is represented with red rectangles in Fig. 5.13.



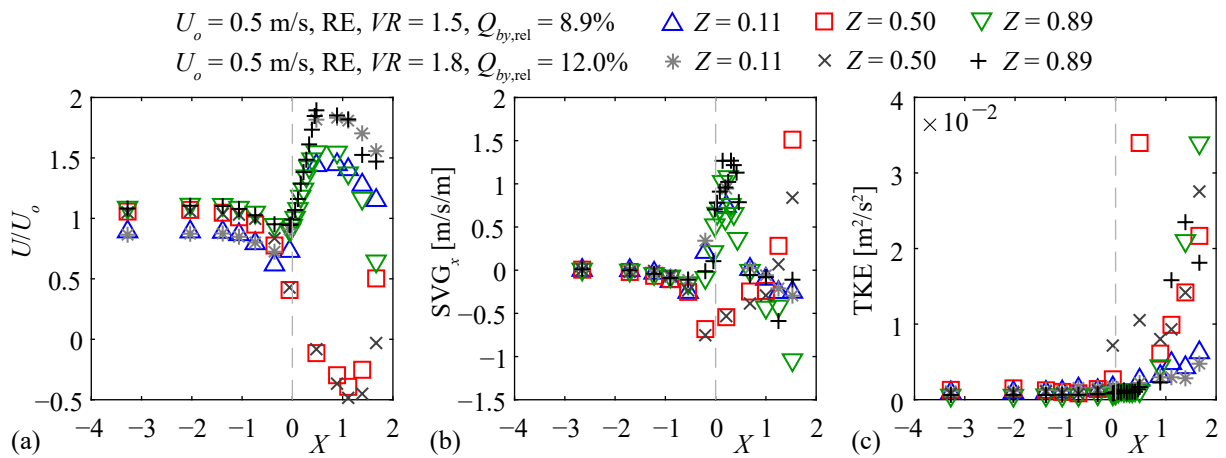


**Fig. 5.13:** Characterization of the hydraulics at the bypass center line ( $Y = -0.2, Z = 0.5$ ) for different bypass configurations with (a) the normalized streamwise flow velocity  $U/U_o$ , (b) the spatial velocity gradient in  $x$ -direction  $SVG_x$ , and (c) the turbulent kinetic energy TKE; the horizontal dashed lines in (a) highlight  $U/U_o = 1.2$  and  $U/U_o = 1.4$ , while the vertical dashed lines indicate the bypass entrance at  $X = 0$

The relative bypass discharge was  $Q_{by,rel} \approx 14\%$  for the OC-bypass with  $VR = 1.2$  and  $Q_{by,rel} \approx 17\%$  for the OC-bypass with  $VR = 1.4$ , while it was slightly smaller with the flap gate ( $Q_{by,rel} \approx 12\text{--}14\%$ ; Fig. 5.13). Independent of the bypass configuration,  $U$  deviated only marginally from  $U_o$  between  $X = -4$  and  $X = -0.5$  (Fig. 5.13a). For all configurations with the OC-bypass,  $U/U_o$  increased almost linearly between  $X = -0.5$  and the bypass entrance ( $X = 0$ ) to  $VR = 1.2$  and  $VR = 1.4$ . The streamwise velocities  $U/U_o$  were almost constant between the bypass entrance and  $X = 2$ . With the flap gate,  $U/U_o$  increased moderately up to  $X = 0.56$ , which is equivalent to  $x = 0.50$  m and corresponded to the beginning of the flap gate (cf. Fig. 4.6b), from where the flow accelerated continuously. Note that the flap gate did not end at  $X = 2$ , but due to the inclination, no measurements could be conducted further downstream at  $Z = 0.5$  (cf. Fig. 4.6b). For the OC-bypass,  $SVG_x$  was almost constant between  $X \approx -3$  and  $X = -1$ , but it strongly increased from  $X = -1$  up to the bypass entrance at  $X = 0$  (Fig. 5.13b). In contrast to  $U/U_o$ , where the increase was independent of  $U_o$  (Fig. 5.13a),  $SVG_x$  increased disproportionately for  $U_o = 0.7$  m/s (Fig. 5.13b) and decreased to  $SVG_x \approx 0$  right behind the bypass inlet. While  $SVG_x$  remained low downstream of the bypass entrance for the OC-bypass, it increased again with the flap gate (Fig. 5.13b). TKE was small for all configurations in Fig. 5.13c and only slightly changed from upstream ( $X \approx -3$ ) to the bypass inlet ( $X = 0$ ). For the OC-bypass and the flap gate bypass, TKE even slightly decreased downstream of the bypass inlet ( $X > 0$ ; Fig. 5.13c). For the OC-bypass, larger  $VR$  did not increase TKE. For the flap gate bypass, TKE was slightly larger for  $U_o = 0.7$  m/s than for  $U_o = 0.5$  m/s (Fig. 5.13c).

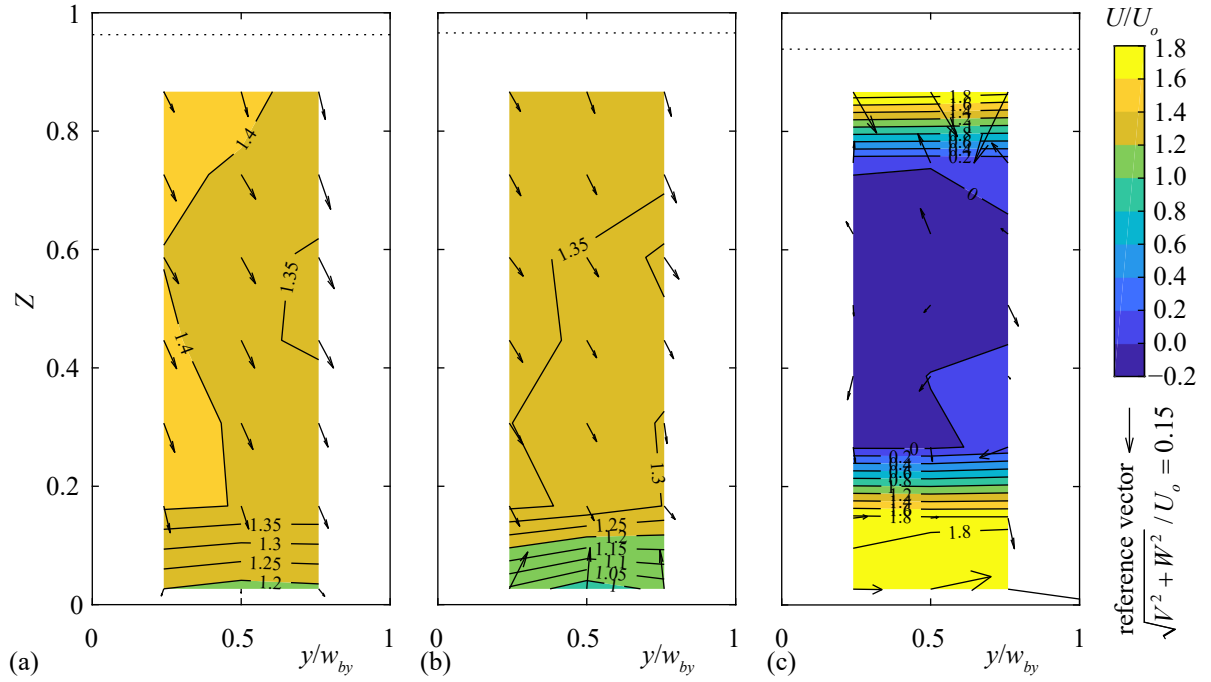
In contrast to the OC-bypass, the hydraulic characteristics strongly varied with the flow depth at the open channel bypass with the inlet restrictor (RE) and were therefore quantified in  $Z = 0.11$ ,  $Z = 0.50$ , and  $Z = 0.89$ , corresponding to the center of the bypass openings and the area in front of the restrictor (cf. Fig. 4.6 in Section 4.1.3). The two different relative bypass discharges  $Q_{by,rel} = 8.9\%$  and  $Q_{by,rel} = 12.0\%$  were tested, which led to overflow depths at the top opening of 16 cm and 15 cm, respectively (Fig. 5.14). For both bypass discharges,  $U/U_o$

hardly varied between  $X = -4$  and  $X = -1$ , but it slightly decreased directly in front of the bypass inlet (Fig. 5.14a). It then increased to maximal values of  $U_{by,in}/U_o = VR \approx 1.5$  and  $U_{by,in}/U_o = VR \approx 1.8$  at  $X \approx 0.4$ , which corresponded to the narrowest section of the restrictor (cf. Fig. 4.6 in Section 4.1.3), before it decreased again. In contrast, flow velocities reduced to  $U/U_o \approx 0.4$  in front of the RE-bypass at mid flow depth. Flow velocities behind the restrictor were slightly negative due to backwater flow. The  $SVG_x$  increased in front of the bottom and top opening ( $Z = 0.11$  and  $Z = 0.89$ ), while it was negative behind the bypass (Fig. 5.14b). For the configuration with  $VR = 1.5$ , the maximal spatial velocity gradient was  $SVG_x \approx 1$  m/s/m, which corresponds to the  $SVG_x$  at an optimized surface bypass (NU–Alden weir; Haro *et al.*, 1998) and above which Enders *et al.* (2012) observed avoidance reactions of salmon smolts. At mid flow depth ( $Z = 0.5$ ),  $SVG_x$  decreased in front of the restrictor and continuously increased downstream of the restrictor again. TKE was small up to the bypass inlet at  $X = 0$ , but it then rapidly increased to  $TKE \approx 3 \times 10^{-2} \text{ m}^2/\text{s}^2$  in front of the top opening and at mid flow depth at  $X \approx 2$  (Fig. 5.14c). For both  $VR$ , TKE was comparably small in front of the bottom opening, that is,  $TKE \leq 0.6 \times 10^{-2} \text{ m}^2/\text{s}^2$ . Note that the scaling of the y-axis in Fig. 5.14c differs by a factor of 10 from the scaling in Fig. 5.13c, which means that even in front of the bottom opening at the RE-bypass, TKE was significantly larger than at the OC-bypass and with the flap gate. However, the maximal measured TKE at the RE-bypass was still in the range of natural rivers and is therefore considered as suitable for fish navigation and stabilization, while  $TKE > 3 \times 10^{-2} \text{ m}^2/\text{s}^2$  may hamper fish swimming performance (Silva *et al.*, 2020). Nevertheless it is likely that the TKE at the RE-bypass triggered avoidance reactions of some fish, as for example Li *et al.* (2020) demonstrated that juvenile cyprinids with  $TL \approx 11$  cm reacted to very small  $TKE < 5 \times 10^{-3} \text{ m}^2/\text{s}^2$ . It would have been possible to further lower  $SVG_x$  and TKE at the RE-bypass by increasing the backwater with the flap gate at the bypass outlet. However, this would reduce  $Q_{by,rel}$  and lead to a larger velocity drop in front of the bypass, which is considered unfavorable for fish guidance. This effect was even more pronounced with the pipe-bypass (Fig. 4.6d; Beck, 2020), such that it was not further investigated.



**Fig. 5.14:** Characterization of the hydraulics at the bypass center line ( $Y = -0.2$ ) with the RE-bypass for different  $VR$  at  $Z = 0.11$ ,  $0.50$ , and  $0.89$  with (a) the normalized streamwise flow velocity  $U/U_o$ , (b) the spatial velocity gradient  $SVG_x$ , and (c) the turbulent kinetic energy TKE; the vertical dashed line indicates the bypass entrance at  $X = 0$

Figure 5.15 compares the velocity fields in the bypass for different configurations at  $X = 0.56$  ( $x = 0.50$  m) with  $U_o = 0.5$  m/s. The  $y$ -axis shows the local bypass coordinates from the left to the right wall, normalized with the bypass width  $w_{by}$ , such that  $y/w_{by} = 0.5$  in Fig. 5.15 corresponds to  $Y = -0.2$  in the global coordinate system in Fig. 5.12 and 5.13. The arrows indicate the direction and magnitude of the transversal and vertical velocity components  $V$  and  $W$ , respectively, and the dotted lines show the flow depth measured in the bypass center ( $y/w_{by} = 0.5$ ).



**Fig. 5.15:** Cross section of  $U/U_o$  in the bypass at  $X = 0.56$  ( $x = 0.50$  m) for different bypass configurations with  $U_o = 0.5$  m/s: (a) OC-bypass,  $VR = 1.4$ ,  $Q_{by,rel} = 16.9\%$ , (b) flap gate,  $\gamma = 12^\circ$ ,  $Q_{by,rel} = 12.0\%$ , and (c) RE-bypass,  $VR = 1.8$ , and  $Q_{by,rel} = 12.0\%$  ( $x$ -axis exaggerated by factor 2)

With the OC-bypass, flow velocities hardly varied with the flow depth, but they were slightly smaller close to the bottom and the right flume wall (Fig. 5.15a). As discussed on the basis of Fig. 5.12, the bypass wall increased  $V_p$ , which led to transversal velocities  $V$  in the bypass (Fig. 5.15a,b). The vertical velocity component is a result of the reduced flow depth in the bypass compared to the approach flow depth  $h_o$  (Fig. 5.15a,b). At  $X = 0.56$ , the velocities with the flap gate bypass were similar to the OC-bypass, but the velocity reduction towards the flume bottom was more pronounced (Fig. 5.15b). The RE-bypass caused very large velocities behind the bottom and top opening ( $U/U_o \approx 1.8$ ), while a recirculation zone behind the restrictor led to negative velocities at mid flow depth. The restrictor also induced large transversal and vertical flow velocity components (Fig. 5.15c).

## 5.6 Discussion of selected aspects

### 5.6.1 Comparison with literature

Szabo-Meszaros *et al.* (2018) investigated HBRs with rectangular and hydrodynamic bars. The velocity patterns caused by the two different bar shapes were similar. By considering four differ-

ent bar shapes, the present study identified small differences between the flow fields, depending on the bar shape. However, the overall effect on the flow field was minor (Fig. 5.1). The small effect of the blocking ratio  $BR$ , the negligible transversal and vertical velocities caused by HBRs without overlays, and the slight increase of  $U$  along the rack of diversion HPPs are in line with previous studies on HBRs (Maager, 2016; Berger, 2018). Chatellier *et al.* (2011) investigated angled bar racks with vertical rectangular and hydrodynamic bars installed normal to the rack axis (angled bar racks). Despite the different rack types, they found that the clear bar spacing and the bar shape had only a small effect on the velocity field. Raynal *et al.* (2013a) observed large flow accelerations along classical angled bar racks with vertical bars, especially for small  $\alpha$ . This can be explained by the stronger flow deflections, as the bars were installed with a  $90^\circ$  angle to the rack axis. For HBRs as investigated in the present study, flow deflections are almost independent of  $\alpha$ . At prototype HPPs with varying approach flow directions (e.g. during periods with and without spillway discharge), HBRs will lead to similar downstream velocity fields, whereas they can significantly change for angled bar racks with vertical bars. De Bie *et al.* (2018) investigated HBRs with wedge-wire bars for  $\alpha = 30^\circ$ . The velocity measured 5 cm above the channel bottom increased by  $\approx 50\%$  from the rack head to the rack end for approach flow velocities of  $U_o = 0.17$  and  $0.40$  m/s. In contrast, in the present investigation, the velocity increase along the rack, measured at mid flow depth, ranged from 7.5% to 14.9% for all configurations presented above. The large difference between these studies is unlikely caused by the different measurement locations in vertical direction, as the effect of HBRs without overlays on the upstream velocity field was similar at all flow depths, except within the boundary layer (Fig. 5.5a). It is also unlikely that these large differences were primarily caused by the different rack parameters such as the blocking ratios and bar shapes. In the study of de Bie *et al.* (2018), an unregulated bypass, covering 10% of the channel width, was included in the physical model. They did not quantify the bypass discharge, but it can be assumed to be considerably above 10% due to the flow resistance of the fine-spaced HBR. The velocity fields shown by de Bie *et al.* (2018) are therefore likely governed by the bypass discharge, which makes it difficult to observe the effect of the HBR itself and to compare it with the velocity fields of the present study. It should be noted that the relative bypass discharge (bypass discharge over design discharge) is recommended to range from 2% to 5% at prototype HPPs (Ebel, 2016), which results in a negligible effect of the bypass flow on the overall flow fields of HBRs. The same challenges occur when the velocity fields of Berger (2018) are analyzed, where the relative bypass width was 12.5%.

Kriewitz (2015) investigated a run-of-river block-type HPP with two turbine inlets. Without a fish guidance structure installed, the difference between the discharge of the left and right half of one turbine inlet was  $\Delta Q/Q_o = 9.4\%$ . The installation of a Louver without overlays with  $\alpha = 30^\circ$  led to very asymmetrical turbine admission flows of  $\Delta Q/Q_o = 78.8\%$ . For a smaller approach flow angle of  $\alpha = 15^\circ$ , the discharge difference was reduced to  $\Delta Q/Q_o = 38.6\%$ . Similarly, the  $\Delta Q/Q_o$  values reduced from  $\Delta Q/Q_o = 13\%$  to  $8\%$  at a modified bar rack, when the approach flow angle was reduced from  $\alpha = 30^\circ$  to  $\alpha = 15^\circ$  (Kriewitz, 2015). This trend

is in line with the present study, where smaller  $\Delta Q/Q_o$  values were determined for smaller  $\alpha$  in the range of  $30^\circ \leq \alpha \leq 45^\circ$  for both, the diversion HPP and the block-type HPP setup. At the diversion HPP, the discharge differences were  $\Delta Q/Q_o = 3.2\%$  and  $\Delta Q/Q_o = 2.6\%$  for the rack configuration with S4-bars,  $s_b = 20$  mm,  $H_{Ov} = 0$  with  $\alpha = 45^\circ$  and  $\alpha = 30^\circ$ , respectively (Fig. 5.26b,c). For the same rack configurations at the block-type HPP without a pier, the discharge differences were  $\Delta Q/Q_o = 50.5\%$  and  $\Delta Q/Q_o = 46.2\%$  (Fig. 5.8b) for  $\alpha = 45^\circ$  and  $\alpha = 30^\circ$ , respectively. Beck *et al.* (2019b) demonstrated that curved-bar racks lead to much more symmetrical downstream flow fields than Louvers. Due to the flow-straightening effect of the curved bars, the criterion of  $\Delta Q/Q_o \leq 5\%$  could be fulfilled for the overlay configurations  $H_{Bo} = 0.15$ ,  $H_{To} = 0$  and  $H_{Bo} = 0$ ,  $H_{To} = 0.15$  at  $X = 3.5$ . In contrast, the present study showed that HBRs with overlays lead to asymmetrical downstream flow fields (Fig. 5.6b–d). The criterion  $\Delta Q/Q_o \leq 5\%$  was not fulfilled for any of the overlay configurations of the HBR with S4-bars,  $s_b = 20$  mm,  $\alpha = 30^\circ$  at  $X = 1$  (Fig. 5.6b–d).

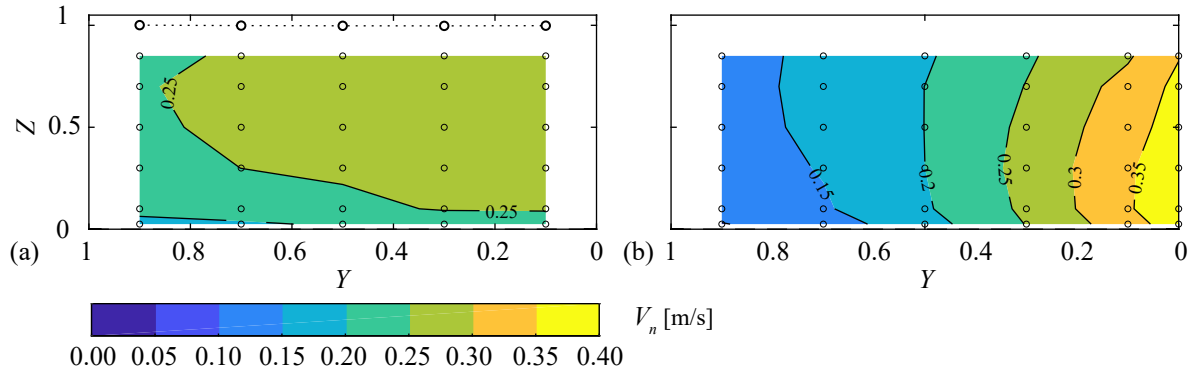
### 5.6.2 Vertical tie-bars

The vertical tie-bars of the model racks of the present investigation were cylindrical (cf. Section 4.2.1). Their effect on the velocity field is independent of the approach flow direction and the HPP layout. However, at prototype HPPs, these vertical tie-bars are often rectangular, leading to larger wake formation for angled approach flows. At block-type HPPs, the approach flow field changes with varying discharge distribution between the turbines and the spillway. Thus, rectangular vertical tie-bars cannot be arranged in flow direction for all operating conditions. It is therefore recommended to use either cylindrical vertical tie-bars or short rectangular bars with rounded tips to avoid flow deflection and separation. At diversion HPPs, the vertical tie-bars should be arranged in flow direction and not orthogonal to the rack axis. Raynal *et al.* (2013b) studied inclined racks with cylindrical spacers. They also observed locally reduced velocities in the wake of the tie-bars, being most pronounced for the most downstream spacer of racks with large inclination angles  $\gamma$  (definition in Section 2.4).

### 5.6.3 Engineering application considerations

Most modern HBRs are equipped with hydrodynamic bars (cf. Section 3.2). On the one hand, they induce significantly smaller head losses than rectangular bars (details in Chapter 6); on the other hand, they are easier to clean, as the narrowest section between two bars is located at the bar tip and can therefore be easily reached by a rack cleaning machine (cf. Section 3.5). The present work showed that foil-shaped bars also lead to a slightly more symmetrical turbine admission flow as compared to rectangular bars. According to common literature, it is recommended to select the approach flow angle  $\alpha$  such that  $V_n$  does not exceed the sustained swimming speed of the target fish species (cf. Section 3.4.1). As recommended by Turnpenny and O’Keeffe (2005), racks should be designed with an over-capacity to compensate for partial clogging. For diversion HPPs,  $V_n$  can be calculated from continuity, whereas it is not equally distributed over the whole rack cross section for block-type HPPs. The distribution of  $V_n$  strongly depends on the HPP layout, including the layout of the dividing pier, the bypass,

and the spillway operation. Therefore, a numerical simulation of the velocity field is suggested to select the appropriate HBR position. Because of the small flow deflections of HBRs without overlays, the rack does not necessarily need to be implemented in the numerical model (e.g. Feigenwinter *et al.*, 2019). The results of the numerical simulation can also be used to analyze the FGC, which should exceed a value of 1 directly in front of the HBR (cf. Section 3.4.1). The clear bar spacing  $s_b$  has only a small effect on the velocity field. It has to be selected in order to be a physical barrier for the target fish species and size (cf. Section 3.4.1). Besides increased head losses (details in Section 6), the main disadvantage of small  $s_b$  is the larger clogging probability of floating debris such as leaves and small branches (details in Section 9). For practical engineering applications, the cross-sectional averaged  $V_n$  at the rack is usually calculated from continuity equation as  $V_n = Q_d / (h_o l_R)$ , where the rack length  $l_R = w_{ds} / \sin(\alpha)$ . For a laboratory flume with a diversion HPP layout and  $Q_d = 0.1 \text{ m}^3/\text{s}$ ,  $h_o = 0.4 \text{ m}$ ,  $w_{ds} = 0.5 \text{ m}$ , and  $\alpha = 30^\circ$  this results in  $V_n = 0.25 \text{ m/s}$ , which agrees well with the measured values of  $V_n = 0.22\text{--}0.29 \text{ m/s}$  (Fig. 5.16a). In contrast,  $V_n$  continuously increased to  $0.40 \text{ m/s}$  at the downstream rack end of the block-type HPP layout without a pier and without spillway discharge (Fig. 5.16b; HPP layout from Fig. 5.10b). The sustained swimming speeds of rheophilic and non-rheophilic fish species with  $TL = 0.10 \text{ m}$  are  $v_f = 0.38 \text{ m/s}$  and  $v_f = 0.28 \text{ m/s}$ , respectively (Eq. 2.9 and 2.10 with  $t = 12\,000 \text{ s}$  and  $T = 5^\circ\text{C}$ ). These velocities are not exceeded at the diversion HPP with  $\alpha = 30^\circ$  (Fig. 5.16a), but at the block-type HPP without a pier and without weir discharge (Fig. 5.16b), potentially leading to rack passage for small fish or impingement for larger fish.



**Fig. 5.16:** Values of  $V_n$  measured in the rack-parallel cross section directly in front of the rack S4,  $\alpha = 30^\circ$ ,  $s_b = 20 \text{ mm}$ ,  $H_{O_v} = 0$  at (a) a diversion hydropower plant layout and (b) a block-type hydropower plant layout without weir discharge

In the past, HBR-BSs and other fish guidance structures were installed at all kinds of HPP layouts (cf. Section 3.2). By analyzing velocity fields at HBRs for different HPP layouts, it was shown that a diversion HPP layout is considered optimal for fish guidance, as the maximal  $V_n$  is smaller and FGC does not decrease towards the downstream rack end (Fig. 5.10 and 5.16). At large block-type HPPs, where it might not be economically reasonable to install a long pier for improving FGC, it is also possible to build a dam separating the HBR from the weir fields, such as planned at HPP Edsforsen (cf. Fig. 3.9b in Section 3.6). Depending on the length and the design of the dam, flow conditions would then be comparable to diversion HPPs.

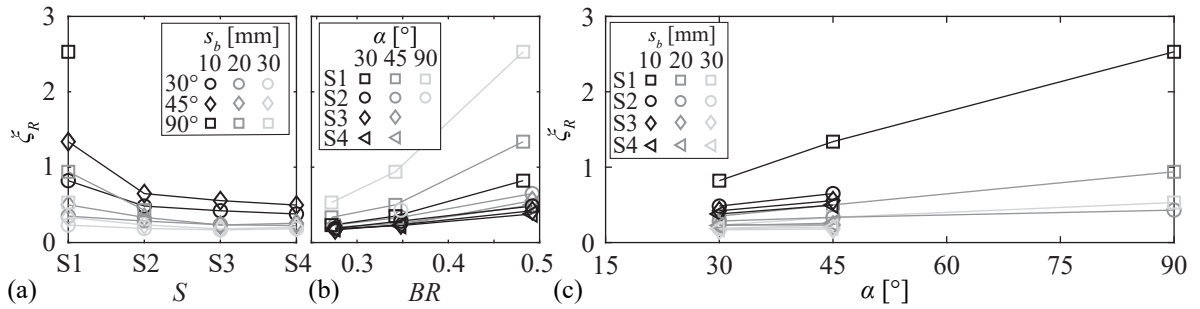
## 6 Head losses of horizontal bar racks

In this chapter, the results of the head loss assessment are presented and discussed. It was first published in a slightly modified form in Meister *et al.* (2020b).

### 6.1 General observations

Figure 6.1 shows the rack head loss coefficient  $\xi_R$  as a function of (a) the bar shape  $S$ , (b) the blocking ratio ( $BR$ ), and (c) the approach flow angle  $\alpha$  for all tested rack configurations without overlays and  $D_b = 7.5$ . Depending on the individual rack configuration, the determined values ranged from  $\xi_R = 0.17$ – $2.53$  without overlays (Fig. 6.1) and up to  $\xi_R = 8.57$  with overlays (not shown in Fig. 6.1). Three governing effects were observed:

- I)  $\xi_R$  reduced from rectangular to hydrodynamic bars for all  $s_b$  (Fig. 6.1a). The difference between S1 and S2 was large, whereas S3 and S4 led to similar  $\xi_R$  as for S2.
- II)  $\xi_R$  increased with increasing  $BR$ , corresponding to smaller  $s_b$ , for all bar shapes and approach flow angles (Fig. 6.1b). This effect was larger for S1 as compared to S2, S3, and S4.
- III)  $\xi_R$  increased with increasing  $\alpha$  (Fig. 6.1c). The angle effect was most pronounced for S1 with  $s_b = 10$  mm ( $BR \approx 0.49$ ) and almost negligible for S4 with  $s_b = 30$  mm ( $BR \approx 0.28$ ). The effect of overlays is not included in Fig. 6.1, because there were superposed effects of the overlay layout, the bar shape,  $BR$ , and  $\alpha$ . The overlay effect is therefore individually described in detail below.

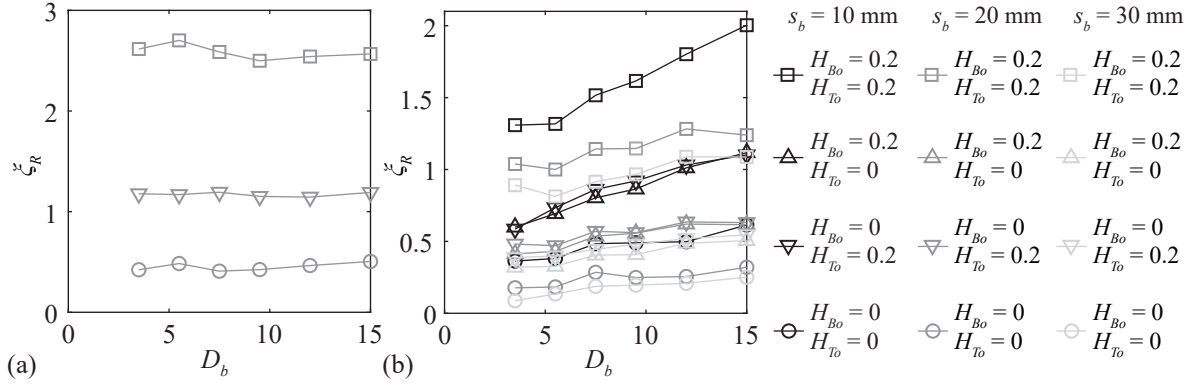


**Fig. 6.1:** Rack head loss coefficients  $\xi_R$  as a function of (a) bar shape S1–S4, (b) blocking ratio  $BR$ , and (c) horizontal approach flow angle  $\alpha$  for all tested rack configurations without overlays and a relative bar depth of  $D_b = 7.5$

Figure 6.2 shows  $\xi_R$  as a function of the relative bar depth  $D_b$  with S2-bars for (a)  $\alpha = 90^\circ$  and (b)  $\alpha = 30^\circ$ . For  $\alpha = 90^\circ$ ,  $D_b$  had no significant effect on  $\xi_R$  (Fig. 6.2a). In contrast, for  $\alpha = 30^\circ$ , shorter bars led to smaller  $\xi_R$  (Fig. 6.2b). This effect was more pronounced for  $s_b = 10$  mm than for  $s_b = 20$  and  $30$  mm. Although the  $\xi_R$  values were almost identical for short bars with  $D_b = 3.5$  and  $D_b = 5.5$ , they increased linearly between  $D_b = 5.5$  and  $D_b = 15$  (Fig. 6.2b). Figure 6.2 also shows that the effect of  $D_b$  on  $\xi_R$  was similar for all overlay configurations.



Overall, within the typical application range of HBRs ( $\alpha = 30^\circ$ ,  $D_b = 5\text{--}10$ ,  $H_{Ov} < 0.4$ ), the effect of  $D_b$  on  $\xi_R$  was small, that is,  $\leq \pm 10\%$ .



**Fig. 6.2:** Rack head loss coefficients  $\xi_R$  as a function of the relative bar depth  $D_b$  for S2-bars with approach flow angle of (a)  $\alpha = 90^\circ$  and (b)  $\alpha = 30^\circ$  and different overlay configurations

## 6.2 General equation for head loss prediction

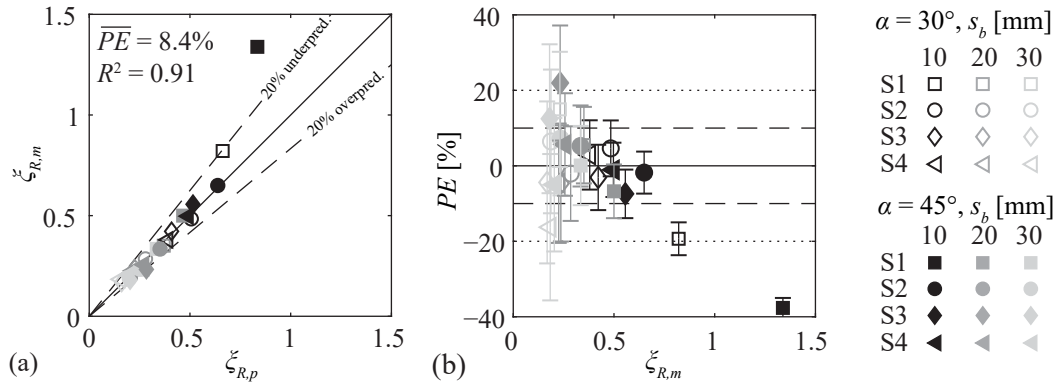
To account for the governing basic parameters, the rack head loss coefficient  $\xi_R$  was defined as the product of five individual coefficients: blocking ratio coefficient  $C_{BR}$ , approach flow angle coefficient  $C_\alpha$ , bar shape coefficient  $C_S$ , bar depth coefficient  $C_{Db}$ , and overlay coefficient  $C_{Ov}$ . On the basis of a curve fitting analysis for the hydrodynamic bars, Eq. (6.1) was proposed to predict the head losses of HBRs with hydrodynamic bars. The computation of the individual coefficients is described in the following sections. The experimentally determined rack head loss coefficients  $\xi_{R,m}$  (subscript  $m$  = measured) were in good agreement with the predicted (subscript  $p$ ) values  $\xi_{R,p}$  on the basis of Eq. (6.1) for S2–S4 without overlays (Fig. 6.3a). The mean prediction error ( $\overline{PE}$ , Eq. 6.2) was less than 22% for all measurement data with S2–S4 (Fig. 6.3b). The error bars show the 95% quantile of the measurement uncertainty as described in Section 4.4.2. For  $\xi_{R,m} > 0.5$ , the measurement uncertainties were small ( $< \pm 7\%$ ), whereas they were relatively large for  $\xi_{R,m} < 0.2$  ( $> \pm 17.5\%$ ; Fig. 6.3b). However, with HPP approach flow velocities in the range of  $U_o = 0.3\text{--}1.0$  m/s, the resulting total losses are small ( $\Delta h_R = \xi_R U_o^2 / (2g) \approx 1.0$  cm; with  $U_o = 1$  m/s and  $\xi_R = 0.2$ ) and this uncertainty becomes negligible for energy production. Equation (6.1) can also be applied for rectangular bars (S1) but then leads to a significant deviation for higher  $\xi_{R,p}$  (Fig. 6.3). Therefore, an alternative equation for rectangular bars is presented below, which is proposed to predict  $\xi_R$  more accurately for S1-bars, accounting for the different hydraulic behavior of rectangular and hydrodynamic bars.

$$\xi_R = C_{BR} C_\alpha C_S C_{Db} C_{Ov} \quad (6.1)$$

$$PE = \frac{\xi_{R,p} - \xi_{R,m}}{\xi_{R,m}} \times 100 [\%]; \quad \overline{PE} = 1/n \sum |PE|, \quad (6.2)$$

where  $n$  is the number of data points.





**Fig. 6.3:** Rack head loss coefficients for configurations with S1–S4-bars without overlays with (a) comparison of predicted (Eq. 6.1;  $\xi_{R,p}$ ) and measured values ( $\xi_{R,m}$ ) and (b) prediction errors  $PE$  as a function of the measured rack head loss coefficients  $\xi_{R,m}$

### Blocking ratio coefficient $C_{BR}$

An increasing blocking ratio decreases the hydraulically active area, whereas it increases the local flow velocity and thus head losses. The blocking ratio coefficient was calculated with Eq. (6.3) as

$$C_{BR} = \frac{BR}{(1 - BR)}. \quad (6.3)$$

On the basis of the investigated parameter range of  $BR$  (cf. Table 4.1 in Section 4.4.2), the application limit is  $0.25 \leq BR \leq 0.50$ , covering the significant range at prototype HPPs. Given a small bar spacing of  $s_b = 10$  mm, the corresponding high  $BR \approx 0.5$  results in  $C_{BR} = 1.0$ . This value reduces to  $C_{BR} = 0.33$  for low  $BR = 0.25$ .

### Approach flow angle coefficient $C_\alpha$

The approach flow angle  $\alpha$  is a measure of the rack length and thus the hydraulically active area. A small  $\alpha$  represents a longer rack and thus a large hydraulically active area, therefore reducing flow velocity and head losses. The approach flow angle coefficient was calculated with Eq. (6.4) as


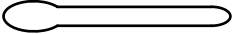
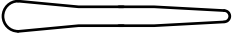
$$C_\alpha = \sin(\alpha)^{2/3}. \quad (6.4)$$

For hydrodynamic bars,  $C_\alpha$  was determined on the basis of experiments with  $\alpha = 30^\circ$  and  $45^\circ$  and validated with  $\alpha = 90^\circ$  for S2 and  $s_b = 20$  mm ( $BR \approx 0.35$ ). The validation for  $\alpha > 45^\circ$ , shown in Section 6.3, indicates an application range of Eq. (6.4) of  $\alpha = 30\text{--}90^\circ$ . For  $\alpha = 90^\circ$ ,  $C_\alpha = 1.0$ , whereas for  $\alpha = 30^\circ$ , it reduces to  $C_\alpha = 0.63$ .

### Bar shape coefficient $C_S$

Hydrodynamic bars minimize flow separation zones and therefore reduce energy dissipation due to vortex shedding and turbulences. The experimentally determined bar shape coefficients are presented in Table 6.1 for the four investigated bar shapes. These shape coefficients indicate that  $\xi_R$  reduces on average by  $\approx 27\%$  from S1 to S2 and by  $\approx 42\%$  from S1 to S3/S4.

**Table 6.1:** Investigated bar shapes S1–S4 and the corresponding bar shape coefficients  $C_S$  (cf. Fig. 4.14 in Section 4.2.3).

Denotation	S1	S2	S3	S4
Shape				
$C_S$	1.13	0.83	0.67	0.64

**Bar depth coefficient  $C_{Db}$** 

Shorter bars lead to reduced friction losses and therefore smaller  $\xi_R$ , as long as the bars are deep enough for the separated flow to reattach to the side face of the bars (cf. Section 2.5.3). The bar depth effect is accounted for with Eq. (6.5). For the standard relative bar depth  $D_b = 7.5$ ,  $C_{Db} = 1$ . Bars with  $D_b < 7.5$  lead to  $C_{Db} < 1$ , whereas  $D_b > 7.5$  leads to  $C_{Db} > 1$ . For an HBR with  $\alpha = 30^\circ$ ,  $C_{Db} = 0.90$  for  $D_b = 5$ , and  $C_{Db} = 1.10$  for  $D_b = 10$ . For  $\alpha = 90^\circ$ , no significant effect of  $D_b$  on  $\xi_R$  was observed in the range of  $D_b = 3.5$ – $15$  (Fig. 6.2a). Therefore,  $C_{Db} = 1$  for  $\alpha = 90^\circ$  (Eq. 6.5). The coefficient  $C_{Db}$  linearly increases from  $\alpha = 90^\circ$  to  $\alpha = 30^\circ$ . The recommended application limit of Eq. (6.5) is  $5 \leq D_b \leq 15$ , which covers the typical range of HBRs at prototype HPPs (cf. Section 3.2).

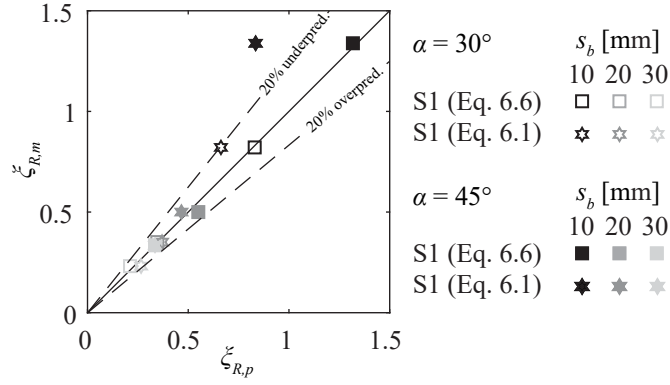
$$C_{Db} = 0.04 (D_b - 7.5) \left( \frac{90^\circ - \alpha}{60^\circ} \right) + 1 \quad (6.5)$$

**Application of general head loss equation to rectangular bars**

Equations (6.1) and (6.3)–(6.5) were developed for hydrodynamic bars. Additionally, a shape factor for S1-bars was determined by minimizing  $(\overline{PE})$ ; Table 6.1), allowing for the application of the above equations for rectangular bars. However, the hydraulic processes at racks with rectangular bars significantly differ from those at racks with hydrodynamic bars. Because flow separations at the tip of rectangular bars additionally decrease the hydraulically active area between two bars, the  $BR$  effect is more pronounced for S1-bars. Therefore,  $\xi_R$  increases disproportionately for rectangular bars for larger  $\alpha$  and smaller  $s_b$  (Fig. 6.1b,c). The loss coefficient  $\xi_{R,p}$  is underestimated by Eq. (6.1) for S1, large  $\alpha$ , and small  $s_b$  (Fig. 6.3). Hence, Eq. (6.5) is proposed to estimate  $\xi_R$  for rectangular bars, where the larger effects of  $\alpha$  and  $s_b$  are taken into account with larger exponents.

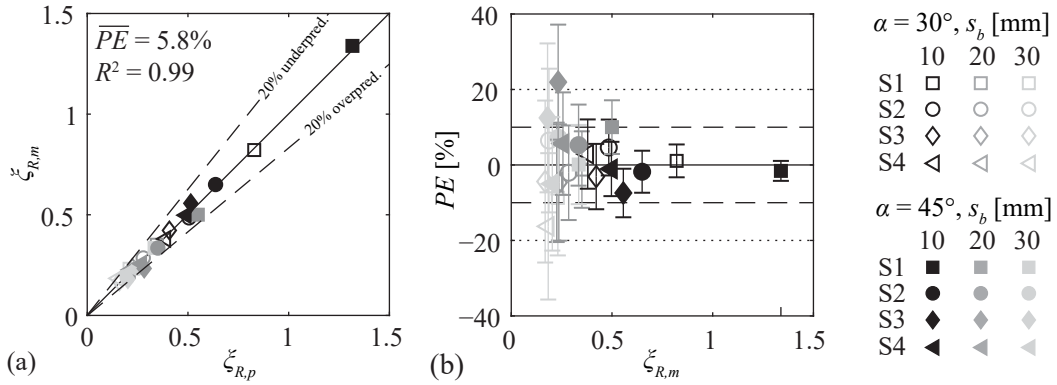
$$\xi_R = 2.33 \left( \frac{BR}{1 - BR} \right)^{3/2} \sin(\alpha)^{4/3} C_{Ov} C_{Db} \quad (6.6)$$

In Fig. 6.4,  $\xi_{R,m}$  is compared to the predictions on the basis of Eq. (6.1) (star-shaped symbols) and Eq. (6.6) (square symbols). For small head loss coefficients ( $\xi_R \leq 0.5$ ), Eq. (6.1) and (6.6) lead to similar  $\xi_{R,p}$ , whereas for  $\xi_R > 0.5$ , Eq. (6.1) underestimates  $\xi_R$  for the S1-bars. Therefore, Eq. (6.1) is recommended for racks with rectangular bars only if  $s_b \geq 20$  mm.



**Fig. 6.4:** Comparison of measured rack head loss coefficients  $\xi_{R,m}$  and predicted rack head loss coefficients  $\xi_{R,p}$  with Eq. (6.1) and (6.6) for racks with rectangular bars (S1)

A very good agreement of  $\xi_{R,m}$  and  $\xi_{R,p}$  results if Eq. (6.1) is applied to hydrodynamic bars and in parallel Eq. (6.6) for rectangular bars (Fig. 6.5). Including all measurement data with  $\alpha = 30^\circ$  and  $45^\circ$ ,  $\overline{PE}$  was only 5.8% with individual maximal deviations of 22%.



**Fig. 6.5:** Rack head loss coefficients  $\xi_R$  for configurations without overlays with (a) comparison of measured ( $\xi_{R,m}$ ) and predicted values ( $\xi_{R,p}$ ; Eq. (6.1) for hydrodynamic bars and Eq. (6.6) for rectangular bars) and (b) prediction error  $PE$  as a function of measured rack head loss coefficients  $\xi_{R,m}$

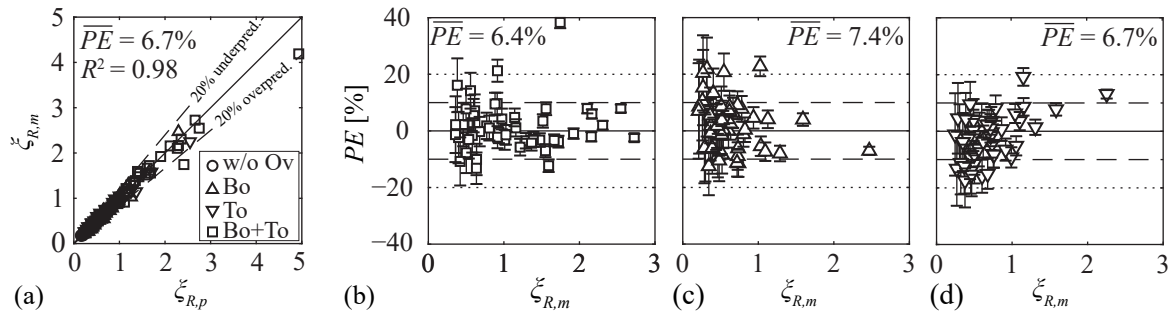
### Overlay coefficient $C_{Ov}$

Overlays block a part of the cross section and thereby reduce the hydraulically active rack area. In addition, overlays create a strong flow deflection (cf. Section 5.1.4), which leads to additional losses. These effects are superposed with additional effects of the overlay layout,  $BR$ ,  $\alpha$ , the bar shape, and the relative overlay height. The overlay coefficient therefore is  $C_{Ov} = f(C_{OL}, BR, \alpha, C_S, H_{Ov})$ , where  $C_{OL}$  is the overlay layout coefficient with  $C_{OL} = 1$  if either bottom or top overlays are applied and  $C_{OL} = 0.9$  for combined bottom and top overlays (Eq. 6.7). Equation (6.7) can be applied to calculate  $C_{Ov}$  in both Eq. (6.1) and (6.6).

$$C_{Ov} = 1 + C_{OL} \left( \frac{1}{2} BR^{-2} + 7.4 \sin(\alpha)^2 C_S^{-0.8} \right) \left( \frac{H_{Ov}}{1 - H_{Ov}} \right)^{4/3} \quad (6.7)$$

For racks without overlays,  $C_{Ov} = 1.0$ . On the basis of the investigated rack configurations with overlays and  $\alpha = 30^\circ$  and  $45^\circ$ ,  $C_{Ov}$  is minimal for S1,  $\alpha = 30^\circ$ ,  $s_b = 10$  mm ( $BR \approx 0.49$ ), and  $H_{Ov} = 0.1$  ( $C_{Ov} = 1.2$ ). It is maximal for S3/S4,  $\alpha = 45^\circ$ ,  $s_b = 30$  mm ( $BR \approx 0.28$ ), and

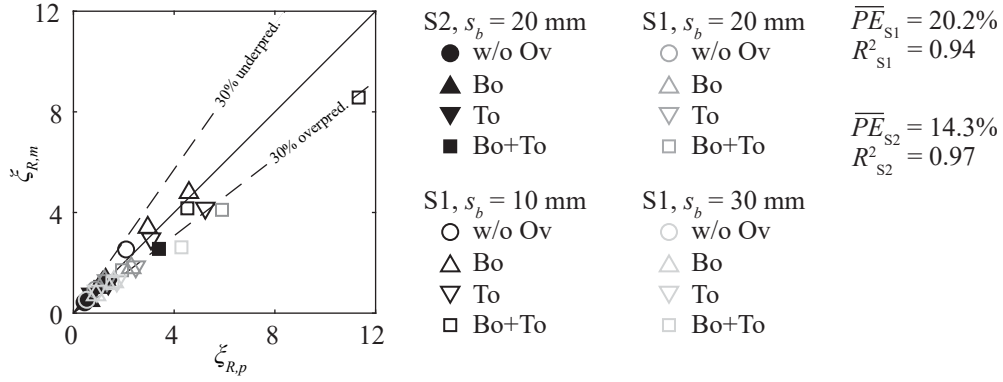
$H_{Bo} = H_{To} = 0.2$  ( $H_{Ov} = 0.4$ ;  $C_{Ov} = 7.2$ ). In other words, overlays increase the head losses by 20%–620%, depending on the bar shape and rack configuration. The predicted  $\xi_{R,p}$  values are in good agreement with the experimentally determined loss coefficients  $\xi_{R,m}$  using Eq. (6.1) for S2–S4 and Eq. (6.6) for S1 (Fig. 6.6a). For the vast majority of data,  $PE$  is within  $\pm 20\%$  for the configurations with combined bottom and top overlays (Fig. 6.6b), bottom overlays only (Fig. 6.6c), and top overlays only (Fig. 6.6d). The outlier in Fig. 6.6b with the largest error of  $PE \approx 40\%$  resulted for a worst case combination of rectangular bars (S1) with  $\alpha = 30^\circ$ , small bar spacing  $s_b = 10$  mm, and a very large overlay blocking  $H_{Bo} = H_{To} = 0.2$ . However, this deviation has little practical relevance, as HBRs with  $s_b = 10$  mm ( $BR \approx 0.49$ ) and  $H_{Ov} = 0.4$  are typically equipped with hydrodynamic bars.



**Fig. 6.6:** Rack head loss coefficients  $\xi_R$  for configurations with and without overlays with (a) comparison of measured ( $\xi_{R,m}$ ) and predicted values ( $\xi_{R,p}$ ; Eq. (6.1) for hydrodynamic bars and Eq. (6.6) for rectangular bars) for all tested configurations, and prediction errors  $PE$  as a function of measured rack head loss coefficients  $\xi_{R,m}$  for (b) combined bottom and top overlays (Bo + To), (c) bottom overlays only (Bo), and (d) top overlays only (To); w/o Ov: racks without overlays

### 6.3 Application of equations to larger approach flow angles

The equations presented above are based on measurements for rack configurations with  $\alpha = 30^\circ$  and  $\alpha = 45^\circ$ . To verify the applicability of Eq. (6.1) and (6.6) for  $\alpha > 45^\circ$ , validation measurements were conducted with  $\alpha = 90^\circ$  for the rack configuration S2,  $s_b = 20$  mm ( $BR = 0.35$ ), and S1,  $s_b = 10, 20, 30$  mm ( $BR = 0.483, 0.342, 0.272$ ) for all overlay combinations listed in Section 4.4.2 (Fig. 6.7). Without overlays, the mean prediction errors are small ( $\overline{PE}_{S1} = 8\%$ ,  $\overline{PE}_{S2} = 3\%$ ). With overlays, the predicted  $\xi_{R,p}$  values also agree well with  $\xi_{R,m}$ . The individual  $PE$  was below 35% for all configurations, except for S1,  $\alpha = 90^\circ$ ,  $H_{Bo} = H_{To} = 0.2$  with  $s_b = 20$  mm and  $s_b = 30$  mm ( $PE = 44\%$ ,  $PE = 64\%$ ). This overprediction of  $\xi_R$  for rack configurations with rectangular bars (S1),  $\alpha = 90^\circ$ , and large overlay blockage is of low importance, because of the low practical relevance of that configuration. The mean prediction errors of all rack configurations with  $\alpha = 90^\circ$  are  $\overline{PE}_{S1} = 20.2\%$  and  $\overline{PE}_{S2} = 14.3\%$ , indicating an application range of  $\alpha = 30$ – $90^\circ$  for the proposed equations.



**Fig. 6.7:** Comparison of measured and predicted rack head loss coefficients  $\xi_{R,m}$  and  $\xi_{R,p}$  (Eq. (6.1) for hydrodynamic bars and Eq. (6.6) for rectangular bars) for rack configurations with S1- and S2-bars and approach flow angle  $\alpha = 90^\circ$ ; w/o Ov: racks without overlays

## 6.4 Hydropower plant layouts

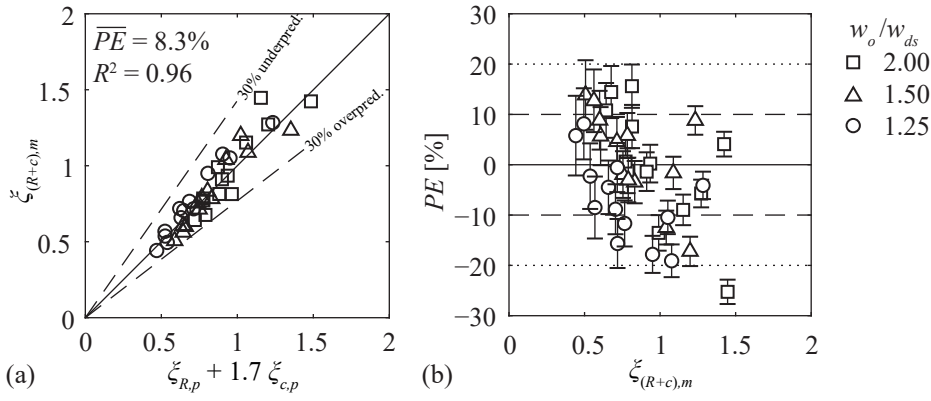
The data presented above corresponded to a straight channel with constant channel width, typically representing diversion HPPs (cf. Fig. 4.7a). At block-type HPPs with turbines and weir adjacent to each other, additional losses are created by flow contractions (cf. Fig. 4.7b). According to Idelchik (2008), the resulting contraction head loss coefficient related to  $U_{ds}$  determines with Eq. (6.8) as

$$\xi_{c,p} = \frac{1}{2} \left( 1 - \frac{A_{ds}}{A_o} \right)^{3/4}, \quad (6.8)$$

where  $A_o$  is the approach flow cross-sectional area and  $A_{ds}$  is the cross-sectional area downstream of the contraction. The predicted losses of a sharp contraction without an HBR installed are in good agreement ( $PE \leq 25\%$ ) with the measurements ( $\xi_{c,p} = 0.15, 0.22, 0.30$  vs.  $\xi_{c,m} = 0.12, 0.20, 0.29$  for  $w_o/w_{ds} = 1.25, 1.5$ , and  $2$ , respectively). The head loss coefficients derived from the measurements at the block-type HPP setup with an HBR ( $\xi_{(R+c),m}$ ) were consistently larger than the sum of the predicted rack head losses ( $\xi_{R,p}$ , Eq. 6.1) and the predicted contraction losses ( $\xi_{c,p}$ , Eq. 6.8). The measurements indicate that HBRs at block-type HPPs do not only induce rack head losses, but they also increase the contraction losses by a factor of 1.7. Therefore, with the contraction head loss, Eq. (4.5) is expanded to determine the rack head losses in general form to

$$\Delta h_R = h_o + \frac{U_o^2}{2g} - h_{ds} - \frac{U_{ds}^2}{2g} - \Delta h_f - 1.7 \Delta h_c. \quad (6.9)$$

With only one outlier, head losses of HBRs at block-type HPPs can be predicted with Eq. (6.9) with a maximal  $PE$  of  $\pm 20\%$  for all investigated contraction ratios (Fig. 6.8a,b). Using Eq. (6.1) and (6.6) combined with Eq. (6.8) is recommended not only for block-type HPPs, but also for diversion HPPs with flushing gates or any other hydraulic structures causing flow contractions. The factor of 1.7 will reduce if a dividing pier is installed between the HBR and the spillway. However, using a factor of 1.7 is conservative.



**Fig. 6.8:** (a) Comparison of predicted and measured head loss coefficients at block-type hydropower plants with horizontal bar racks and (b) corresponding prediction errors  $PE$ ;  $\xi_{(R+c),m}$ : measured rack head loss coefficient at block-type hydropower plants;  $\xi_{R,p}$ : predicted head loss coefficient of the horizontal bar rack;  $\xi_{c,p}$ : predicted contraction head loss coefficient (Eq. 6.8)

If an HPP setup differs from a diversion HPP (e.g. block-type setup, side intakes), the streamline pattern is usually complex and the definition of the horizontal approach flow angle is ambiguous. For such situations, the approach flow angle is determined by trigonometry with Eq. (6.10) as

$$\alpha = \arcsin(w_{ds}/l_R). \quad (6.10)$$

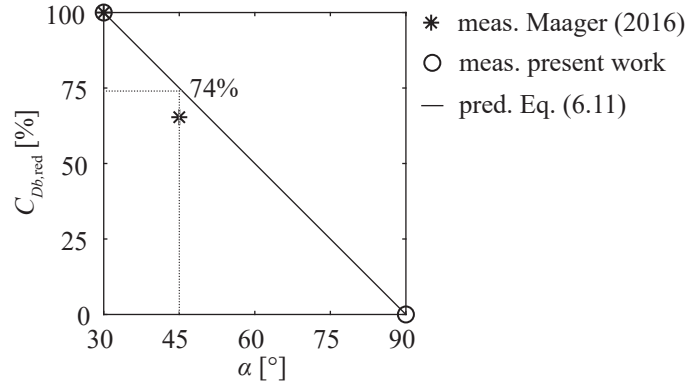
## 6.5 Discussion of selected aspects

### 6.5.1 Bar depth effect

Prototype HBRs are built with bars of  $t_b = 5\text{--}20$  mm and  $d_b = 40\text{--}100$  mm, typically leading to relative bar depths of  $D_b = d_b/t_b = 5\text{--}10$  (cf. Section 3.2). On the one hand, bars with large  $D_b$  implicate a large surface area and thus higher friction losses. On the other hand, longer bars may improve the flow-straightening effect and therefore reduce losses caused by vortex shedding. The coefficient 0.04 in Eq. (6.5) was determined by a multiple linear regression for bar depths  $D_b = 5.5, 7.5, 9.5, 12$ , and  $15$ , as a linear trend was observed within this range (Fig. 6.2b). In the present study, the bar depth was investigated for  $\alpha = 30^\circ$  and  $\alpha = 90^\circ$ . In addition to  $\alpha = 30^\circ$ , a rack angle of  $\alpha = 45^\circ$  was investigated by Maager (2016) and Albayrak *et al.* (2019) for  $D_b = 5$  and  $10$ , and  $BR = 0.55, 0.39$ , and  $0.33$  ( $s_b = 10, 20$ , and  $30$  mm; prototype dimensions) for rectangular bars with various overlay configurations. On the basis of 38 measurements with S1-bars,  $H_{Ov} \leq 0.4$  and  $\alpha = 30^\circ$ , the rack head loss coefficient  $\xi_R$  reduced on average by 15% if the bar depth was halved from  $D_b = 10$  to  $D_b = 5$ . For  $\alpha = 45^\circ$ , this reduction was only 10%. The bar depth effect observed for  $\alpha = 45^\circ$  therefore reduces to  $C_{Db,red} \approx 10$  of the bar depth effect observed for  $\alpha = 30^\circ$  (Fig. 6.9, asterisk symbols). This effect of the rack angle  $\alpha$  on the bar depth effect, where  $C_{Db}$  is calculated with Eq. (6.5), results in Eq. (6.11).

$$C_{Db,red} = \frac{(C_{Db}|D_b, \alpha = 45^\circ) - (C_{Db}|0.5D_b, \alpha = 45^\circ)}{(C_{Db}|D_b, \alpha = 30^\circ) - (C_{Db}|0.5D_b, \alpha = 30^\circ)} \times 100\% = 74\% \quad (6.11)$$

The measurements of Maager (2016), the present work, and the prediction with Eq. (6.5) are shown in Fig. 6.9. The good agreement of  $C_{Db,red}$  for  $\alpha = 45^\circ$  and Eq. (6.5) supports the linear relation between  $\alpha$  and  $C_{Db}$ .



**Fig. 6.9:** Effect of approach flow angle  $\alpha$  on bar depth coefficient  $C_{Db}$  for a reduction of relative bar depth  $D_b$  by 50%

Kirschmer (1925) experimentally investigated the effect of the bar depth ( $D_b = 2.5, 5, 10$ ) on the rack head loss coefficient for traditional trash racks with rectangular vertically oriented bars ( $\gamma = 90^\circ$ ,  $BR = 0.37$ ). He found no significant effect of  $D_b$  on  $\xi_R$ . This can be explained by the small blocking ratios and the perpendicular orientation of the bars to the main flow. In the present work,  $D_b$  had an effect on  $\xi_R$  for  $\alpha = 30^\circ$  but not for  $\alpha = 90^\circ$ . Similarly, it is possible that the effect of  $D_b$  on  $\xi_R$  was not negligible for  $\gamma \neq 90$  (cf. Fig. 2.11). However, it is still feasible to apply the equation of Kirschmer (1925) for the head loss prediction of traditional trash racks, as  $\gamma$  is typically close to  $\gamma = 90^\circ$ , that is, in the range of  $\gamma = 70\text{--}80^\circ$  (Meusburger, 2002). However, if the equation of Kirschmer (1925) is applied for racks with small  $\alpha$  or  $\gamma$ ,  $\xi_R$  is expected to be overpredicted for short bars ( $D_b \ll 5$ ) and underpredicted for deep bars ( $D_b \gg 5$ ). Although the effect of  $D_b$  on  $\xi_R$  was investigated for S2-bars only, due to the similar head loss behavior of S2–S4 bars, it is assumed that the trend can be transferred to all hydrodynamic bar shapes. The measurements of Maager (2016) and Albayrak *et al.* (2019) further indicate that Eq. (6.5) can also be used for rectangular bars. Therefore,  $C_{Db}$  is also included in Eq. (6.6). The measurements in Fig. 6.2b show that the effect of  $D_b$  on  $\xi_R$  is most pronounced for  $s_b = 10$  mm ( $BR \approx 0.49$ ). However, the bar depth effect was similar for  $s_b = 20$  mm ( $BR \approx 0.35$ ) and  $s_b = 30$  mm ( $BR \approx 0.28$ ), which is supported by other studies (Maager, 2016; Albayrak *et al.*, 2019). Therefore, the effect of  $s_b$  on  $C_{Db}$  is neglected in Eq. (6.5). For practical application at a typical HBR with  $\alpha = 30^\circ$  and  $D_b = 5\text{--}10$ , the effect of  $D_b$  on  $\xi_R$  is small ( $\pm 10\%$ ). However, if the bars are very short ( $D_b = 3.5$ ) or very deep ( $D_b = 15$ ),  $\xi_R$  can reduce by 16% or increase by 30%, respectively, in comparison to  $D_b = 7.5$ .

### 6.5.2 Effect of vertical tie-bars

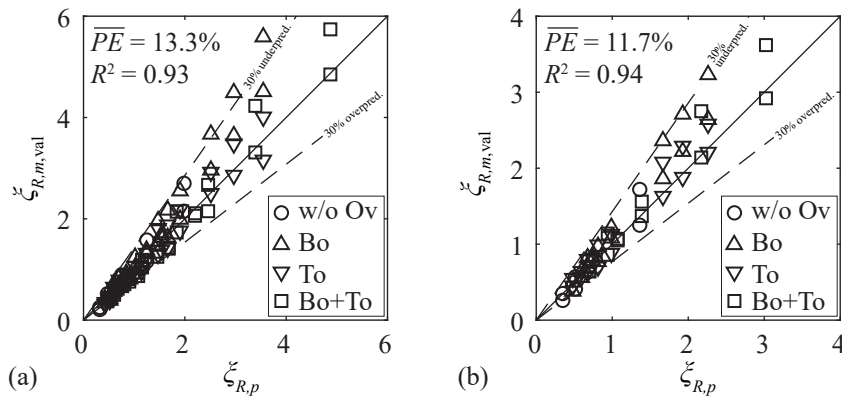
Prototype HBRs are usually assembled using a number of vertical tie-bars installed with a horizontal spacing of 0.4–0.8 m, whereas for the model rack two tie-bars ( $Y = 0.25, 0.75$ ) with a spacing of 0.25, 0.35, and 0.50 m were used for  $\alpha = 90^\circ, 45^\circ$ , and  $30^\circ$ , respectively (cf. Section 4.2.1). These tie-bars can be of different shapes, such as cylindrical or rectangular. Given identical dimensions, cylindrical obstacles generate smaller head losses as compared to rectangular objects with sharp edges. For rectangular objects, an oblique approach flow further increases the flow separation and thus head losses. To minimize losses and the effect on the flow



field, rectangular tie-bars should be aligned with the main flow direction. Within the present work, the head losses of the used mounting parts (cylindrical vertical tie-bars and bottom plate) were individually measured without horizontal bars installed. For rack configurations with large  $\xi_R$  (S1,  $\alpha = 45^\circ$ ,  $s_b = 10$  mm) these mounting parts accounted for only 3% of the overall losses. However, for a hydrodynamically optimized rack configuration (S4,  $\alpha = 30^\circ$ ,  $s_b = 30$  mm) with small overall losses, they accounted for up to 25% of  $\xi_R$ . The effect of the mounting parts is included in Eq. (6.1) and (6.6) by calculating the  $BR$  of racks with cylindrical tie-bars.

### 6.5.3 Comparison of head loss prediction equations with literature data

Many different layouts of fish guidance structures are described in literature (cf. Section 2.4), but only sparse data are available on the head losses of angled HBRs as investigated in the present study (cf. Section 3.7.2). In the studies of Maager (2016) and Albayrak *et al.* (2019), the head losses of HBRs were measured for overlays with  $H_{Ov}$  up to 0.5, creating a large flow diversion and corresponding loss coefficients up to  $\xi_{R,m} = 28$ . Herein, only the head loss measurements of rack configurations with  $H_{Bo} \leq 0.2$  and  $H_{To} \leq 0.2$  were used to validate (subscript val) the proposed equations of the present investigation. Figure 6.10a compares the head loss coefficients of racks with rectangular bars measured by Maager (2016)  $\xi_{R,m, val}$  with the corresponding  $\xi_{R,p}$  values predicted using Eq. (6.5). The majority of data points were predicted with an accuracy of  $\pm 30\%$  with  $\overline{PE} = 13.3\%$  (Fig. 6.10a). If the proposed equation for hydrodynamic bars (Eq. 6.1) was used for the one-side rounded bars of Maager (2016), significant deviations result, indicating that the hydraulic processes at the latter were more similar to rectangular bars. A good agreement with  $\overline{PE} = 11.7\%$  was found for the one-side rounded bars if the proposed equation for rectangular bars (Eq. 6.6) was used with a prefactor reduction from 2.33 to 1.60 (Fig. 6.10b). This means that the predicted hydraulic losses of one-side rounded bars were 31% smaller than the hydraulic losses of rectangular bars. The loss reduction implied by the shape factors of Kirschmer (1925) is 24%.

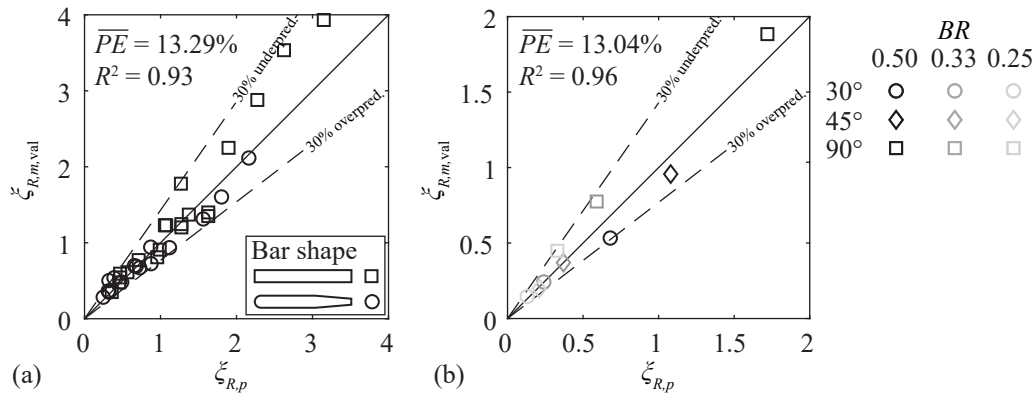


**Fig. 6.10:** Validation of predicted rack head loss coefficients  $\xi_{R,p}$ , on the basis of Eq. (6.6), with rack head loss coefficients measured by Maager (2016)  $\xi_{R,m, val}$  for (a) rectangular bars and (b) one-side rounded bars (with prefactor of 1.60 instead of 2.33 in Eq. 6.6); w/o Ov: racks without overlays

Lemkecher *et al.* (2020) studied HBRs at a diversion HPP layout without overlays for rectangular bars and bars with a rounded tip and a thickness reduction at the tail (Fig. 6.11a). All



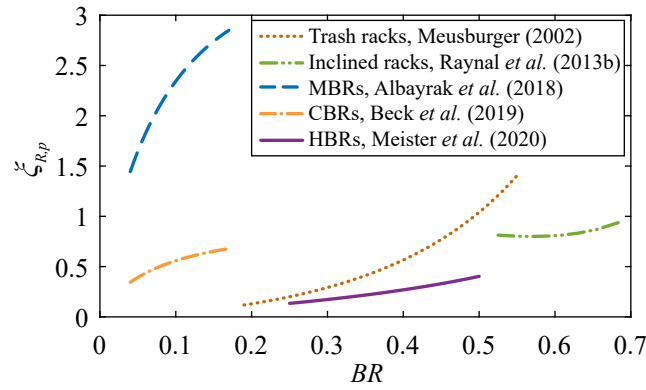
measurements could be reproduced with  $PE \leq 36\%$  with Eq. (6.6), where the prefactor 2.33 was used for rectangular bars and 1.60 for the bars with the rounded tip, as the shape is similar to the one investigated by Maager (2016). Böttcher *et al.* (2019a) investigated HBRs with cylindrical bars without overlays. Their data can be well predicted with Eq. (6.6) if the prefactor is reduced from 2.33 to 1.72 according to the ratio of the shape factors of cylindrical (1.79) and rectangular bars (2.42) given by Kirschmer (1925) (i.e.  $2.33 \times 1.79/2.42 = 1.72$ ).  $PE \leq 30\%$  for all  $\alpha$  and  $BR$  (Fig. 6.11b), indicating that the proposed equations can be applied for various bar shapes. It is recommended that Eq. (6.1) is used for hydrodynamic bars and Eq. (6.6) for non-hydrodynamic bars such as rectangular bars, one-side rounded bars, and cylindrical bars.



**Fig. 6.11:** Validation of the rack head loss coefficients  $\xi_{R,p}$  predicted with Eq. (6.6) with the measured rack head loss coefficients  $\xi_{R,m, val}$  (a) by Lemkecher *et al.* (2020) and (b) by Böttcher *et al.* (2019a); the prefactors 2.33 and 1.60 were used for the comparison with the data of Lemkecher *et al.* (2020) for rectangular and rounded bars, respectively, and 1.72 for the cylindrical bars in the study of Böttcher *et al.* (2019a)

### 6.5.4 Comparison with other rack types

In this section, the head losses of HBRs are compared to other rack types, namely modified bar racks (MBRs; Fig. 2.15c), curved-bar racks (CBRs; Fig. 2.15d), inclined racks (Fig. 2.11b), and traditional trash racks. The comparison is made for unclogged racks without overlays at diversion HPP layouts. The head losses of MBRs and CBRs were calculated following Kriewitz (2015) and Albayrak *et al.* (2018), and Beck *et al.* (2019a), respectively, where  $\alpha = 30^\circ$  and a bar angle to the flow direction of  $45^\circ$  was assumed. The head losses of inclined racks were calculated according to Raynal *et al.* (2013b) for hydrodynamic bars and an inclination angle of  $\gamma = 25^\circ$  as recommended by Courret and Larinier (2008). The head losses of HBRs were calculated with Eq. (6.1) for  $\alpha = 30^\circ$  and foil-shaped bars. The head losses of these fish guidance structures are compared to the head losses of traditional trash racks calculated with the equations of Meusburger (2002) for hydrodynamic bars and an inclination angle of  $\gamma = 90^\circ$ . It should be noted that the equations for the head loss predictions of MBRs and CBRs consider the vertical bars only, which means they do not account for head losses caused by tie-bars, which are included in the other equations in Fig. 6.12.



**Fig. 6.12:** Predicted head loss coefficients  $\xi_{R,p}$  for different rack types as a function of the blocking ratio  $BR$ , where the range of  $BR$  corresponds to the application limit of the equations

HBRs and traditional trash racks with small  $BR$  (large clear bar spacing  $s_b$ ) cause the least head losses. The head losses of inclined racks are significantly larger than for HBRs (Fig. 6.12), which is caused by the low inclination angle and the large number of support bars which increase  $BR$ . The head loss prediction equations for CBRs and MBRs, which are classified as mechanical behavioral barriers (cf. Section 2.4), were developed for smaller  $BR$  than inclined racks and HBRs, which primarily function as physical barriers. While the head losses of CBRs are on average 4.2 times lower than the ones of MBRs (Beck *et al.*, 2019a; Beck, 2020), they are still larger than the head losses of HBRs for most configurations. The head losses of inclined racks are smaller than for MBRs, but larger than for CBRs and HBRs (Fig. 6.12). Depending on  $BR$ , the head losses of traditional trash racks are in the same range as the losses of HBRs, CBRs, and inclined racks, while they are smaller than the losses of MBRs.

### 6.5.5 Engineering application considerations

The predicted head loss coefficient of a typical modern diversion HPP with an HBR with  $\alpha = 30^\circ$ ,  $s_b = 20$  mm ( $BR \approx 0.35$ ),  $t_b = 8$  mm,  $D_b = 7.5$ , and S4-bars without overlays is as low as  $\xi_R = 0.22$  (Eq. 6.1), assuming no blockage by floating debris. For  $U_o = 0.8$  m/s, this results in head losses of  $\Delta h_R = 7$  mm. The predicted head loss increases by a factor of 4.5 if bottom and top overlays of  $H_{Bo} = H_{To} = 0.2$  are installed ( $\xi_R = 0.98$ ,  $\Delta h_R = 32$  mm). For rectangular bars (S1), the head losses increase by  $\approx 70\%$  ( $\xi_R = 0.37$  and  $\Delta h_R = 12$  mm) without overlays, and by  $\approx 50\%$  ( $\xi_R = 1.47$  and  $\Delta h_R = 48$  mm) with overlays, relative to the S4 configuration (Eq. 6.6). For the S1-bars, the overlays thus result in an increase of  $\xi_R$  by a factor of 4. If constructional considerations are not limiting (e.g. mounting of tie-bars), bars with a relative depth of  $D_b = 5.5$  are recommended to reduce costs and hydraulic losses. For practical applications, the effect of  $D_b$  on  $\xi_R$  can be larger than described in Section 6.5.1 if algae growth increases the surface roughness. Meusburger (2002) analyzed the operational data of 43 Swiss run-of-river HPPs with  $Q_d \geq 25$  m<sup>3</sup>/s. The head loss coefficients with respect to  $U_{th}$  of traditional trash racks were  $\xi_R = 0.10$ – $5.04$  with an average of 1.67 and a standard deviation of  $\sigma = 1.20$ . The head losses of clean, unclogged HBRs are therefore of comparable order. No pronounced increase of head losses is expected if these traditional trash racks were replaced by HBRs, provided that substantial clogging can be prevented by an automated rack cleaning machine. Meusburger

(2002) also showed that the head losses of traditional trash racks at existing HPPs are significantly higher than predicted by the equation proposed by Kirschmer (1925), who conducted his measurements in a straight laboratory flume representing diversion HPPs. However, his empirical equation is often applied to block-type HPPs without considering the oblique approach flow and the effect of increased contraction losses due to the rack, as described in Section 6.4. It is important to consider not only the rack itself, but also the HPP layout when head losses are estimated for engineering applications. The higher losses might also be caused by partial clogging of racks at prototype HPPs, which was not considered by Kirschmer (1925). During high flows or even flood events in autumn, some HPP operators report head losses at HBRs caused by foliage clogging of up to  $\Delta h_R = 30$  cm, requiring HPP shutdowns as a safety measure (cf. Section 3.2). In addition, the equation of Kirschmer (1925) does not include the effects of further support bars or intermediate piers, which are typically needed for large flow depths to distribute the substantial additional load in case of rack clogging. When the equations of the present work are used for practical applications, further support bars can be considered with an increased  $BR$ . Potential foliage clogging can be accounted for by substituting the clogged areas with overlays (Eq. 6.7). If no site-specific information is available, Turnpenny and O’Keeffe (2005) suggest assuming that at least 20% of the rack area gets clogged (cf. Section 3.4.1).

### 6.5.6 Fish protection

The findings presented above do not justify statements or predictions on the individual fish behavior at HBRs or their overall fish protection suitability at HPPs. A rack configuration, which is favorable with respect to head losses, is not necessarily favorable for fish protection. As an example, HBRs with foil-shaped bars induce smaller head losses than HBRs with rectangular bars due to the smaller flow separation zones between the bars. Assuming avoidance reactions of fish to these flow separation zones, rectangular bars might be beneficial for fish protection. The goal of the head loss assessment was limited to describing the head losses generated by HBRs, and to propose head loss equations, covering a wide parameter range and different HPP layouts. The selected parameter range covers the typical application range of HBRs (e.g.  $\alpha = 30^\circ$  and  $45^\circ$ ), but it also includes measurements for untypical HBR configurations to validate the proposed equations. For instance, HBR configurations with  $\alpha = 90^\circ$  are unsuitable for fish protection because of the missing guidance effect due to the missing sweeping flow component parallel to the rack to guide fish towards the bypass. For such large  $\alpha$ , the velocity component normal to the rack  $V_n$  is often larger than the sustained fish swimming speed, increasing the risk of fish impingements (Turnpenny and O’Keeffe, 2005; Ebel, 2016). Top and bottom overlays are part of an HBR design, which can significantly increase head losses. Despite this, laboratory studies indicate higher guidance for bottom- and surface-oriented fish (EPRI and DML, 2001; Albayrak *et al.*, 2020). Additionally, overlays improve the routing of driftwood and sediments towards the bypass (Ebel, 2016). Overall, the selection of geometric parameters for an optimum HBR design with regard to high fish guidance and protection depends not only on head loss but also on the resulting velocity field, which affects the fish behavior. Therefore, velocity fields of a range of HBR configurations for different HPP layouts are described in Chapter 5

and Meister *et al.* (2020b). The fish swimming behavior at HBRs is discussed in detail in Chapter 7, which provides information for designing fish guidance structures. Feigenwinter *et al.* (2019) presented a conceptual approach for the evaluation of potential locations of fish guidance structures combining traditional design principles with computational fluid dynamics and novel findings from ethohydraulic research. The approach is based on the three key aspects fish fauna, structural conditions, and hydraulic conditions such as velocity fields and head losses. Nevertheless, to reliably assess the fish behavior at HBRs, extensive field monitoring campaigns at HPPs equipped with HBRs are indispensable.

## 7 Live fish tests with horizontal bar rack bypass systems

### 7.1 General fish swimming behavior

#### 7.1.1 Fish swimming capability and general considerations

The fish swimming capability depends on the prevailing water temperature, the fish species, and fish size. Independent of the rack configuration, Table 7.1 gives an overview of the total length  $TL$  of the fish used for the experiments. The minimal, maximal, and average fish swimming speeds  $v_{f,\min}$ ,  $v_{f,\max}$ , and  $\overline{v_f}$ , respectively, with the corresponding standard deviation  $\sigma_{v_f}$  were calculated with Eq. (2.11) for eel and Eq. (2.9) for all other species with the average water temperature of  $T = 14^\circ\text{C}$  (cf. Section 4.1.3). The swimming velocities were calculated for a swimming duration of  $t = 20\text{ s}$ , corresponding to the minimal burst speed (cf. Section 2.2.6), and for  $t = 45\text{ min} = 2700\text{ s}$ , which is equivalent to the maximal time fish were exposed to the flow in the present study, that is, the acclimatization time plus the maximal experimental duration (cf. Section 4.4.3).

**Table 7.1:** The minimal, maximal, and average fish swimming speeds with its standard deviation for different durations of all tested fish (without electrification)

	$N$ [–]	$TL_{\min}-TL_{\max}$ ( $\overline{TL}$ , $\sigma_{TL}$ ) [cm]	$t = 20\text{ s}$	$t = 2700\text{ s}$
			$v_{f,\min}-v_{f,\max}$ ( $\overline{v_f}$ , $\sigma_{v_f}$ ) [m/s]	$v_{f,\min}-v_{f,\max}$ ( $\overline{v_f}$ , $\sigma_{v_f}$ ) [m/s]
Spiralin	165*	7.8–13.4 (9.9, 1.0)	0.75–1.14 (0.90, 0.07)	0.48–0.73 (0.58, 0.04)
Barbel	126	7.5–20.8 (15.0, 3.1)	0.72–1.62 (1.25, 0.21)	0.47–1.04 (0.80, 0.13)
Nase	39	5.9–9.3 (7.1, 0.7)	0.59–0.86 (0.69, 0.06)	0.38–0.55 (0.44, 0.04)
Trout	249	8.6–21.0 (14.3, 2.6)	0.80–1.64 (1.20, 0.18)	0.52–1.05 (0.77, 0.11)
Salmon	51	9.1–14.9 (11.4, 1.2)	0.84–1.24 (1.00, 0.09)	0.54–0.80 (0.65, 0.06)
Eel	26	41.3–82.8 (65.2, 10.2)	1.08–1.60 (1.40, 0.13)	0.56–0.84 (0.73, 0.07)

\* Includes also the spiralin tested without an HBR installed (E0 in Table 4.3)

When  $v_f$  for  $t = 2700\text{ s}$  in Table 7.1 is compared to the average approach flow velocities of  $U_o = 0.5\text{ m/s}$  and  $U_o = 0.7\text{ m/s}$ , it has to be considered that most experiments were completed in less than 30 minutes, that a brick in the acclimatization compartment offered zones with reduced flow velocities during the acclimatization time (cf. Section 4.4.4), and that fish swam often close to the bottom and the walls with reduced flow velocities. Neglecting the bypass discharge and the transversal flow component, the average normal flow velocities were  $V_n = U_o \sin(\alpha) = 0.25\text{ m/s}$  (Eq. 3.1) for  $U_o = 0.5\text{ m/s}$  and  $V_n = 0.35\text{ m/s}$  for  $U_o = 0.7\text{ m/s}$  and therefore smaller than  $v_{f,\min}$  with  $t = 2700\text{ s}$  for all tested fish. During all experiments without electrification, no impingements or injuries were observed at the rack. The streamwise flow velocities at the

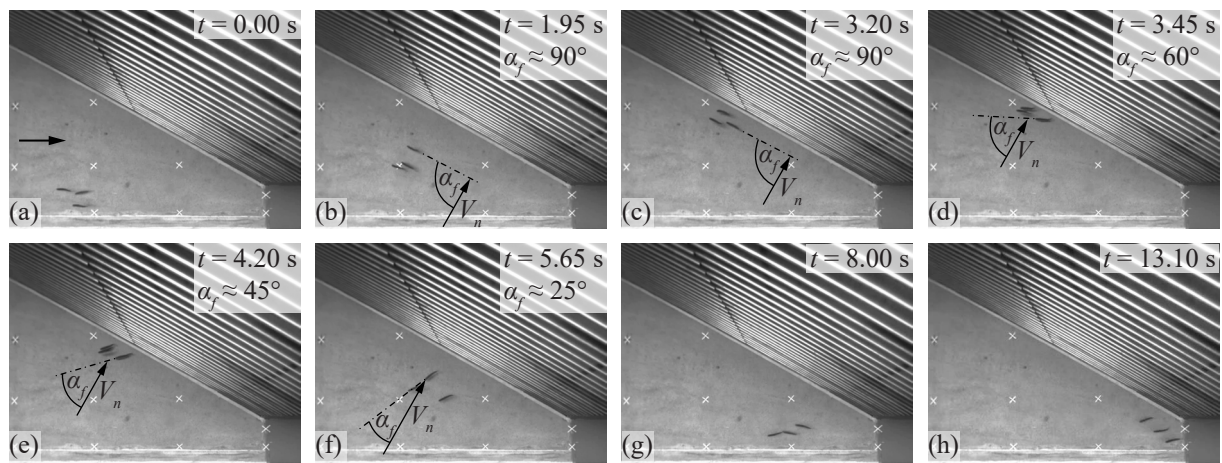
bypass inlet were in the range of  $U_{by,in} = 0.60\text{--}0.98$  m/s for the open channel bypass and  $U_{by,in} = 0.75\text{--}0.90$  m/s for the restrictor bypass (measured at the narrowest section; cf. Section 5.5) and therefore below the minimal burst swimming speed of most fish, except for nase. To prevent exhaustion, nase were therefore tested with  $U_o = 0.5$  m/s only.

### 7.1.2 Species-specific fish swimming behavior

In this section, the typically observed fish swimming behavior of each species is described and illustrated with a picture series, showing the downstream rack end and the bypass inlet (Fig. 7.1–7.6). The relative time, starting at the first frame, is always shown in the top right corner. For selected frames, the fish axis is highlighted with a dashdotted line and the angle to the flow velocity component normal to the rack,  $V_n$ , is shown (cf. Section 3.4.1). The corresponding videos of all screenshot series shown within the present thesis were published and can be downloaded with the link in the figure captions.

#### Spirlin

Spirlin showed a distinct schooling behavior in the experiments and rarely swam individually. The school of spirlin was organized non-hierarchical, meaning that each fish could lead and follow the group, which is characteristic for fish schools (Keenleyside, 1955). With only a few exceptions, most spirlin swam downstream with positive rheotaxis, typically in zigzag movements from one to the other wall using the whole channel width. They mostly swam close to the bottom and approached the water surface almost solely next to the flume wall or, very typically, when they hesitated to enter the bottom opening of the restrictor bypass and searched for an alternative downstream passage corridor. The movements of spirlin seemed very cautious and controlled and they reacted very sensitively to flow accelerations at the bypass inlet. Spirlin swam very close to the HBR and sometimes gently touched the rack with their caudal fins, but they hardly sensed in between the bars. Spirlin passing in between the bars and thus through the rack, did so fast without hesitation. Figure 7.1 shows the typical swimming behavior of spirlin, which approached the HBR with positive rheotaxis (Fig. 7.1a), changed their orientation to swim towards the rack such that they were aligned almost rack-parallel (Fig. 7.1b,c), stopped a curtly in front of the HBR (Fig. 7.1d), changed their direction and swam away from the HBR such that their body was oriented almost perpendicular to the rack (Fig. 7.1e,f), before they entered the bypass (Fig. 7.1g,h). The orientation of the spirlin in Fig. 7.1b–f varied between  $\alpha_f = 90^\circ$  when they approached the HBR (Fig. 7.1b,c) and  $\alpha_f = 25\text{--}45^\circ$  when they swam away from the HBR (Fig. 7.1e,f). Spirlin never faced directly against the flow in front of the HBR ( $\alpha_f = 90^\circ - \alpha = 60^\circ$ ), except for very short moments when they changed their swimming direction (e.g. Fig. 7.1d).

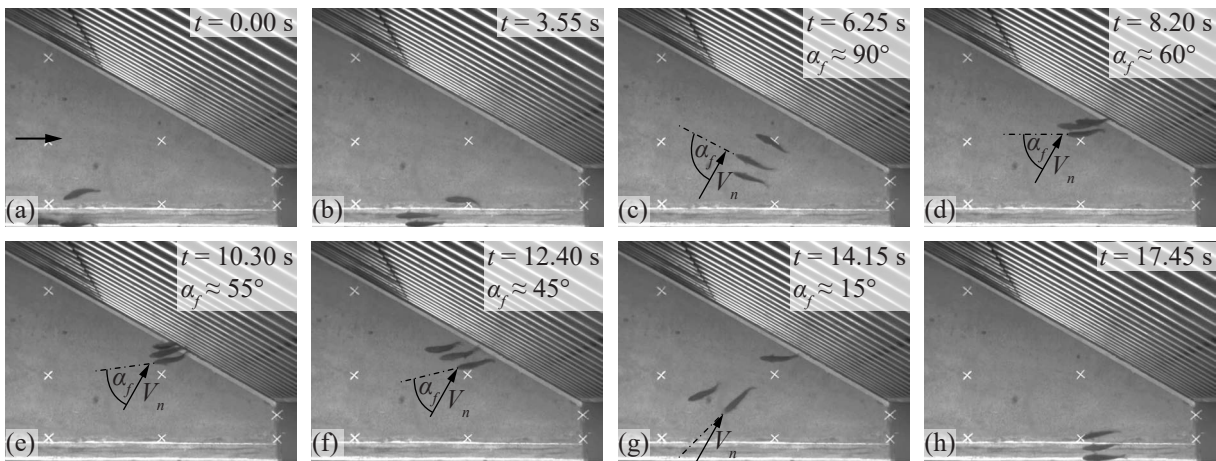


**Fig. 7.1:** Typical swimming behavior of spiralin, which mostly swam downstream as a school in zigzag movements between the rack and the flume wall; the dashdotted line extends a fish axis to indicate the angle  $\alpha_f$  (Video: <http://dx.doi.org/10.3929/ethz-b-000450740>)

## Barbel

The most distinct behavior of barbels was that they were very frequently swimming close to the flume walls. Often, barbels swam towards the glass wall right after they left the acclimatization compartment. They were then slowly moving downstream with positive rheotaxis and many of them entered the bypass without rack interaction. The barbels swam almost exclusively very close to the bottom, while only a few times barbels were observed swimming towards the water surface along the glass wall. Barbels used their pectoral fins to become pressed towards the bottom, which allowed them to passively keep their position for minutes with little effort. In some experiments, barbels showed a schooling behavior, whereas each specimen acted individually in other experiments. When barbels swam towards the HBR, they often touched it only briefly and moved then back to the glass wall. It was observed only a few times that barbels were guided perfectly from the upstream rack end along the rack to the bypass. Barbels did not only seek contact with the flume walls, but also with the bars of the HBR. It seemed that they sensed the flow between the bars with their caudal fins, so that it was not uncommon that half of their body was between the bottom and the lowest bar of the HBR. Barbels which passed through the rack did so very actively, primarily with positive rheotaxis, but sometimes they needed multiple attempts, especially if they were so large that they were hardly fitting through the HBR. Figure 7.2 shows three barbels which swam downstream along the glass wall (Fig. 7.2a,b). In front of the bypass, they swam towards the HBR, such that they were aligned rack-parallel (Fig. 7.2c), before they realigned in flow direction in front of the HBR (Fig. 7.2d). They used their caudal fins to sense the flow at the HBR (Fig. 7.2e), before they swam back to the glass wall into the bypass (Fig. 7.2f–h). Barbels aligned themselves with angles  $\alpha_f = 0\text{--}90^\circ$  to  $V_n$  (Fig. 7.2c–g). In contrast to spiralin, they sometimes persisted for minutes with  $\alpha_f = 60^\circ$  (Fig. 7.2d), that is, directly facing the flow.



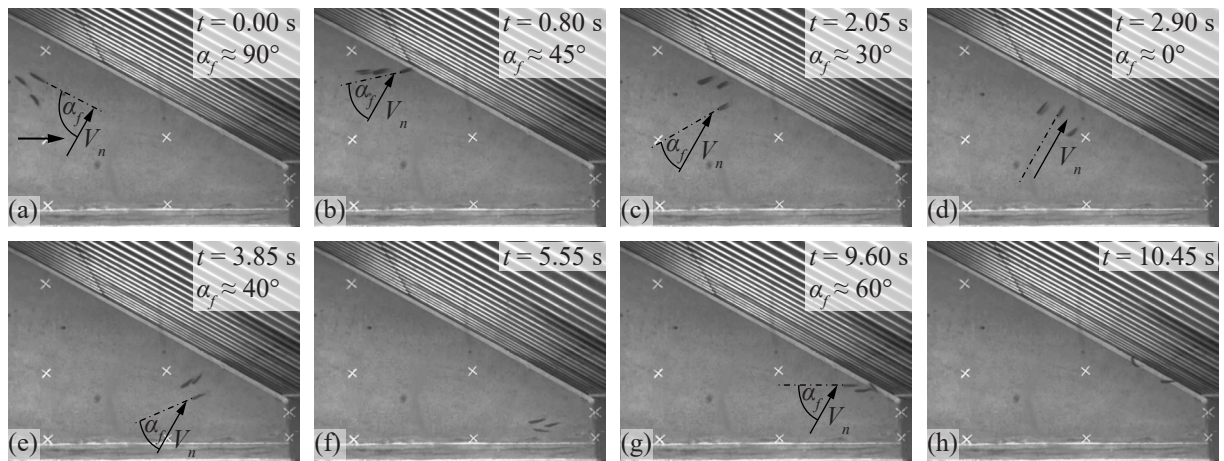


**Fig. 7.2:** Typical swimming behavior of barbels which favored the glass wall and did not avoid rack contact; the dashdotted line extends a fish axis to indicate the angle  $\alpha_f$  (Video: <http://dx.doi.org/10.3929/ethz-b-000450740>)

## Nase

Similarly to spirlin, most nase swam downstream in zigzag movements, making use of the full channel width. Most of the juvenile nase swam primarily together as a school, while only a few specimens acted individually. Nase preferred to swim close to the bottom, were rarely guided by the HBR, and often passed through the rack the first time they approached it. If they were protected at their first approach, they swam another zigzag movement and passed the rack at another attempt. Nase always kept a minimal distance to the rack and never touched it. A negative rheotaxis was observed in one experiment only, where a school of three nase seemed to visually perceive the HBR and changed to positive rheotaxis right in front of it. They were then guided along the rack before they passed through it. Figure 7.3 shows the typical behavior of nase, which were oriented almost rack-parallel when they approached the HBR (Fig. 7.3a), aligned themselves almost in flow direction in front of the rack (Fig. 7.3b), before they swam towards the glass wall (Fig. 7.3d–f), and passed through the HBR at their second attempt (Fig. 7.3g,h). The orientation of nase to  $V_n$  ranged from  $\alpha_f \approx 90^\circ$  when they approached the rack (Fig. 7.3a), to  $\alpha_f \approx 0^\circ$  when swam away from the rack (Fig. 7.3d). Similarly to spirlin, nase directly faced the flow only for short moments at the HBR ( $\alpha_f \approx 60^\circ$ ; Fig. 7.3g).

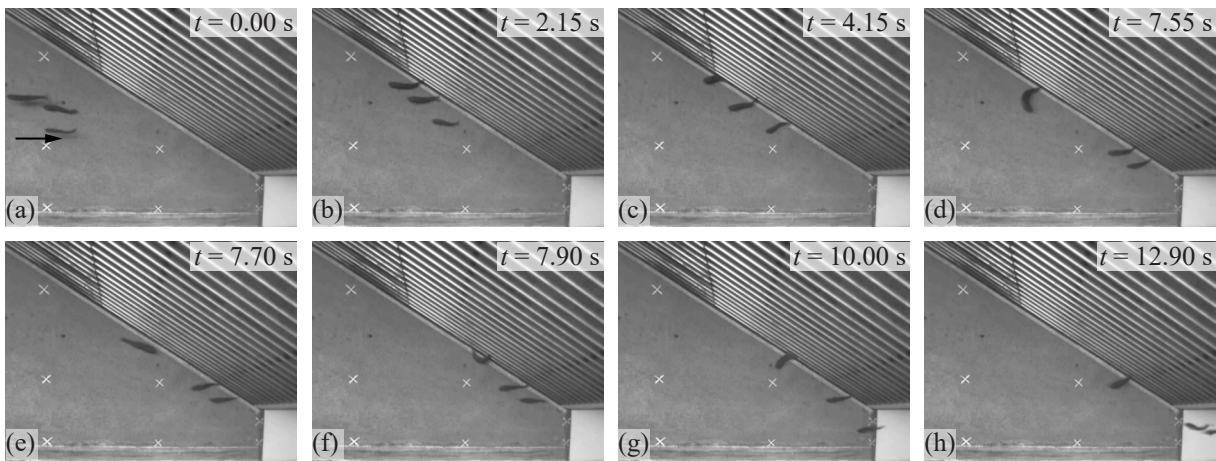




**Fig. 7.3:** Typical swimming behavior of nase, which swam downstream in zigzag movements as a school; in this example they were protected by the HBR at their first approach, but passed through it at the second attempt; the dashdotted line extends a fish axis to indicate the angle  $\alpha_f$  (Video: <http://dx.doi.org/10.3929/ethz-b-000450740>)

## Trout

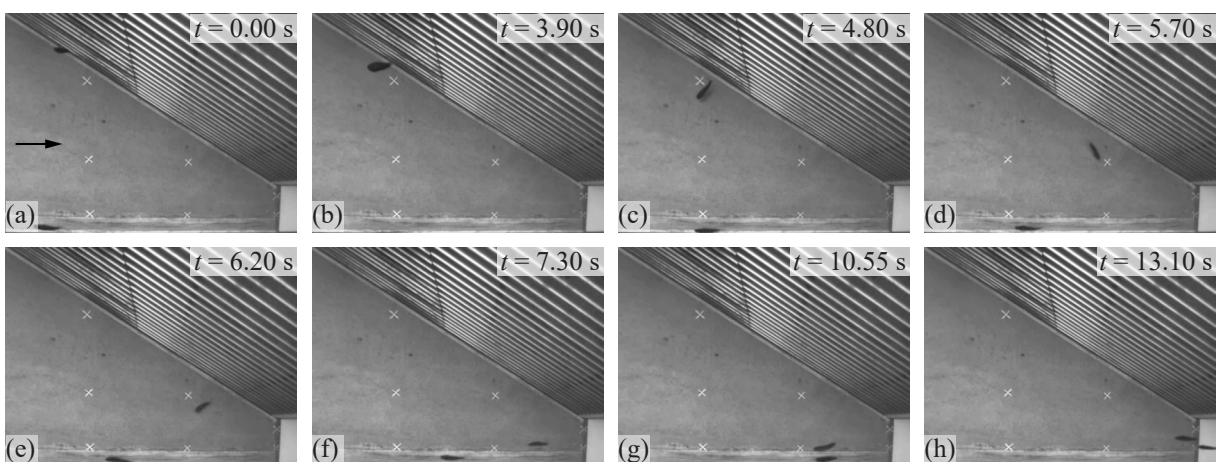
In comparison to most other tested species, trout changed their rheotaxis very frequently. They were generally passive, which means that many specimens did not swim out of the acclimatization compartment or it took them long to do so. In the flume, they sometimes kept their position for several minutes, which was often followed by very fast movements. Trout preferred to swim close to the bottom, but it was observed several times that they quickly swam up to the water surface, before diving down to the bottom again. Trout did not show a tendency to swim along the walls. They sometimes kept their position in the flume center for several minutes, even for  $U_o = 0.7$  m/s, indicating a strong swimming performance. Most trout swam individually, while a schooling behavior was observed in a few experiments only. Trout used their caudal fins to sense the velocities between the bars and sometimes kept their position in front of the rack for several minutes. When they attempted to pass through the HBR they did not hesitate, but especially the larger specimens needed multiple attempts to squeeze through it. Figure 7.4 shows three trout, which were aligned in flow direction when they approached the HBR (Fig. 7.4a). They sensed the flow in front of the rack and between the bars with their caudal fins (Fig. 7.4b,c), before one trout changed its rheotaxis and swam downstream rack-parallel (Fig. 7.4d,e). It tried to pass through the HBR head-first (Fig. 7.4f), before it changed to positive rheotaxis again and swam into the bypass with the other trout (Fig. 7.4g,h). Trout aligned themselves with all possible angles  $\alpha_f$ . Similarly to barbels, they sometimes persisted for minutes with  $\alpha_f \approx 60^\circ$ .



**Fig. 7.4:** Three trout approaching the HBR, of which two were directly guided into the bypass and one specimen showed two rheotaxis changes and tried to pass the HBR head-first before it entered the bypass (Video: <http://dx.doi.org/10.3929/ethz-b-000450740>)

### Salmon parr

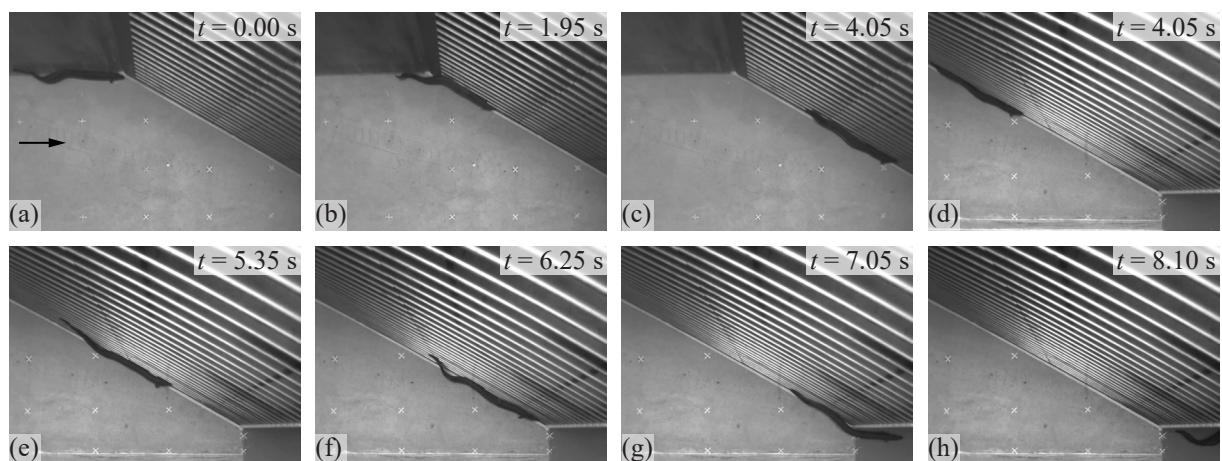
Similarly to trout, most salmon parr swam individually and showed frequent rheotaxis changes. Salmon parr also preferred to swim close to the bottom and did not favor the flume walls. Almost all salmon parr swam out of the acclimatization compartment within the experimental duration, which means they were more active than trout. When salmon parr touched the HBR with their caudal fins, they responded with fast but short avoidance reactions, before touching the rack again. When they used their caudal fins to sense the flow between the bars, it took them usually only a moment to pass through the rack. Figure 7.5 shows a salmon parr approaching the HBR along the glass wall, while another salmon parr persisted halfway behind the HBR for several minutes (Fig. 7.5a), before it suddenly swam out of the HBR (Fig. 7.5b,c), changed to negative rheotaxis for a short moment (Fig. 7.5d), before it realigned itself with positive rheotaxis in flow direction (Fig. 7.5e,f), and entered the bypass tail-first with the other salmon parr (Fig. 7.5g,h). Similarly to trout, no preferences of  $\alpha_f$  were detected for salmon parr.



**Fig. 7.5:** Two salmon parr of which one directly entered the bypass and the other individual was halfway behind the HBR and showed two rheotaxis changes before it entered the bypass (Video: <http://dx.doi.org/10.3929/ethz-b-000450740>)

## Eel

Most eels swam downstream with negative rheotaxis, collided with the HBR, and tried to squeeze themselves head-first through the rack. During these active rack passage attempts, most eels were guided along the HBR and entered the bypass. As has been noted in other studies (e.g. Adam *et al.*, 1999; Russon *et al.*, 2010; Russon and Kemp, 2011), a strong thigmotactic positive behavior was observed, which means that eels sought direct rack contact. Only a few individuals approached the rack either with positive rheotaxis or in passive drift. Eels which swam actively with negative rheotaxis acted insensitive to velocity gradients at the bypass inlet. All eels acted solitary and seemed to be curious, which was expressed by their exploratory behavior in the whole flume. The majority of eels swam close to the bottom and had contact with either a flume wall or the HBR most of the time. Similar observations were noted in other live fish tests (e.g. Russon *et al.*, 2010). Figure 7.6 shows the typical behavior of eels, where one individual approached the HBR with negative rheotaxis and active swimming movements along the left flume wall at the upstream rack end (Fig. 7.6a). At the HBR, the eel kept constant rack contact with its head until it entered the bypass (Fig. 7.6b–h).



**Fig. 7.6:** A typical guidance of an eel along the HBR into the bypass, where (a)–(c) show the upstream rack section and (d)–(h) the downstream rack section including the bypass inlet (Video: <http://dx.doi.org/10.3929/ethz-b-000450740>)

## 7.2 Guidance and protection efficiencies

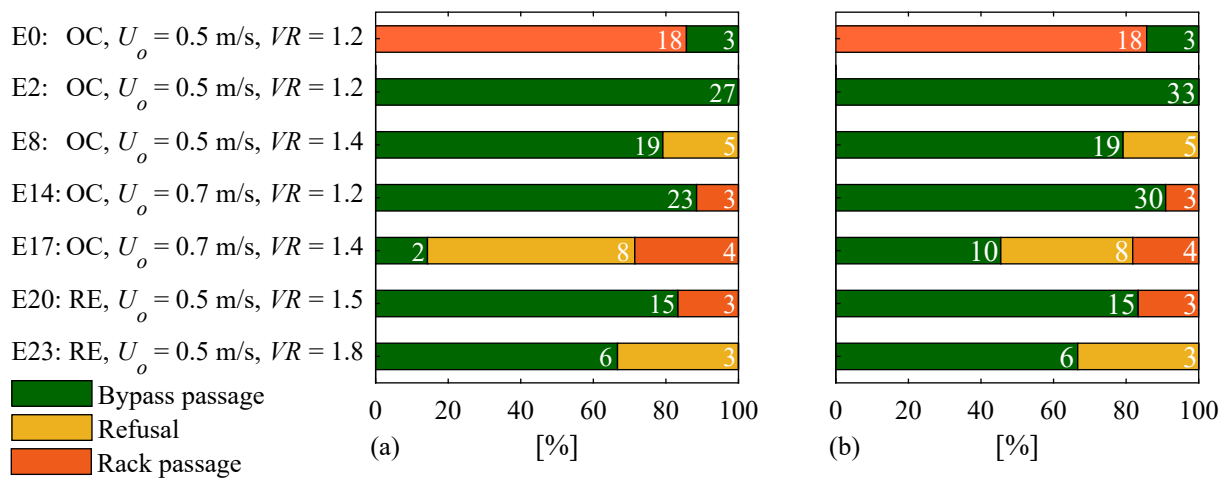
### 7.2.1 Species-specific guidance and protection efficiencies

In this section, the species-specific results of all live fish tests without electrification are shown. All configurations (E0–E25) were introduced in Table 4.3. The guidance and protection efficiencies  $FGE$ ,  $FPE$ ,  $FGE^*$ , and  $FPE^*$ , defined in Section 4.4.3, can be directly read from the  $x$ -axis of the following plots, whereas the absolute number of active fish used for the analysis is indicated with white numbers. The results with the inlet restrictor (RE) are shown for the sake of completeness, but no statistical analyses were conducted due to the low number of replicates. Most tested fish were small, such that they could physically pass through the HBR with  $s_b = 20$  mm (details in Table 7.6).



## Spirlin

Spirlin were tested with seven different configurations without electrification (Fig. 7.7). Figure 7.7a includes bypass passages with rack interaction only, whereas all bypass passages are included in Fig. 7.7b. The configuration E0 was tested for reference without any rack installed, where the behavior was counted as a rack passage if fish crossed the axis, where the HBR was installed for the other experiments (cf. Table 4.3). With the exception of three spirlin which swam into the bypass by chance, all other specimens passed the rack axis without an HBR installed (E0 in Fig. 7.7). The difference to the corresponding configuration with an HBR installed is, as expected, statistically significant (Table 7.2). All spirlin entered the bypass with the full depth open channel bypass (OC),  $U_o = 0.5$  m/s, and  $VR = 1.2$  (E2, Fig. 7.7). An increased approach flow velocity led to significantly more rack passages and significantly less bypass passages (Table 7.2). For some spirlin,  $U_o = 0.7$  m/s was close to the swimming speed they could keep for the maximal experimental duration (cf. Table 7.1). It is possible that some individuals struggled to search for a suitable corridor for long with  $U_o = 0.7$  m/s, causing multiple rack passages. Larger  $VR$  significantly reduced the number of bypass passages, while the number of refusals increased, indicating that spirlin react sensitive to flow accelerations (Table 7.2). Although FGE and FPE varied significantly between configurations, the average guidance and protection efficiency were calculated for OC and  $s_b = 20$  mm to  $\overline{FGE}_{\text{spirlin}} = 78\%$  and  $\overline{FPE}_{\text{spirlin}} = 92\%$ .



**Fig. 7.7:** Results of the live fish tests with spirlin by counting (a) bypass passages with rack interaction only and (b) all bypass passages; note that no rack was installed at the configuration E0 (definition of configurations in Table 4.3)

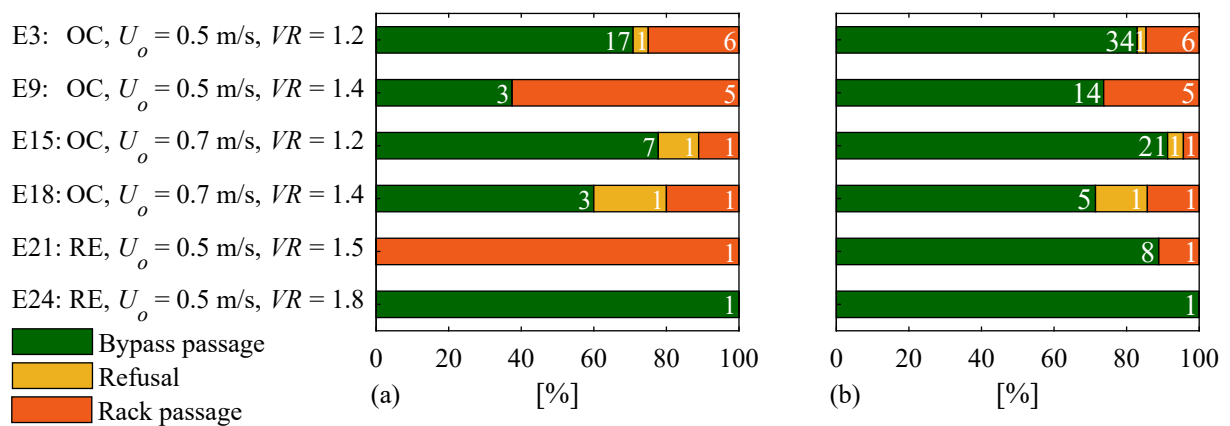
**Table 7.2:** Output of the  $\chi^2$ -tests for the spiralin results with OC shown in Fig. 7.7a

	$U_o$		$VR$		With vs. without HBR	
	E2+E8 vs. E14+E17		E2+E14 vs. E8+E17		E0 vs. E2	
	$p$ -value	$\chi^2$	$p$ -value	$\chi^2$	$p$ -value	$\chi^2$
Bypass	0.004*	8.478	<0.001*	17.495	<0.001*	33.462
Refusal	0.281	1.162	<0.001*	18.452	—	—
Rack	0.007*	7.361	0.645	0.212	<0.001*	33.462

\* significant with a significance level of  $\alpha_{\text{sig}} = 0.05$

### Barbel

Summed up over all test configurations, 83 barbels swam into the bypass, of which only 31 specimens interacted with the rack, corresponding to  $31/83 \approx 37\%$  (Table 4.3). This small rack interaction rate led to large differences between FGE and FPE in Fig. 7.8a, and  $\text{FGE}^*$  and  $\text{FPE}^*$  in Fig. 7.8b. Neither  $U_o$  nor  $VR$  affected the results significantly (Table 7.3). To assess if the outcome of the  $\chi^2$ -tests were affected by omitting the large number of barbels entering the bypass without rack interaction, the same analyses were made for the data of Fig. 7.8b. Although the  $p$ -values differ between these two analyses, they come to the same conclusions, that is, neither  $U_o$  nor  $VR$  affected the reaction of barbels significantly. The results in Fig. 7.8 indicate that an increased  $VR$  led to less bypass passages and more rack passages, but there is a probability of  $\approx 18\%$  that this difference occurred by chance (Table 7.3). The average guidance and protection efficiencies for OC and  $s_b = 20$  mm were  $\overline{\text{FGE}}_{\text{barbel}} = 65\%$  and  $\overline{\text{FPE}}_{\text{barbel}} = 72\%$ .



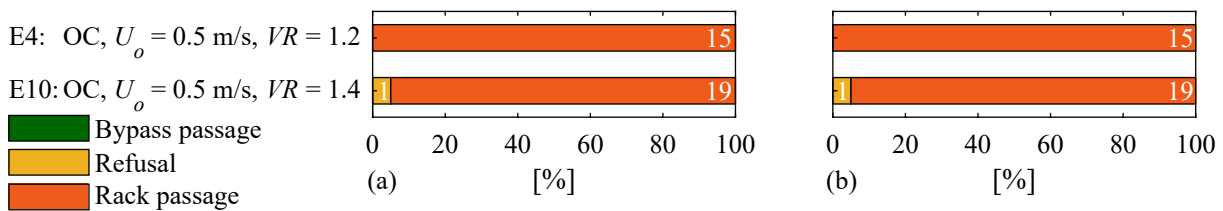
**Fig. 7.8:** Results of the live fish tests with barbels by counting (a) bypass passages with rack interaction only and (b) all bypass passages (definition of configurations in Table 4.3)

**Table 7.3:** Output of the  $\chi^2$ -tests for the barbel results shown in Fig. 7.8a

	$U_o$		$VR$	
	E3+E9 vs. E15+E18		E3+E15 vs. E9+E18	
	$p$ -value	$\chi^2$	$p$ -value	$\chi^2$
Bypass	0.804	0.062	0.174	1.850
Refusal	0.446	0.580	1.000	0.000
Rack	0.300	1.074	0.184	1.764

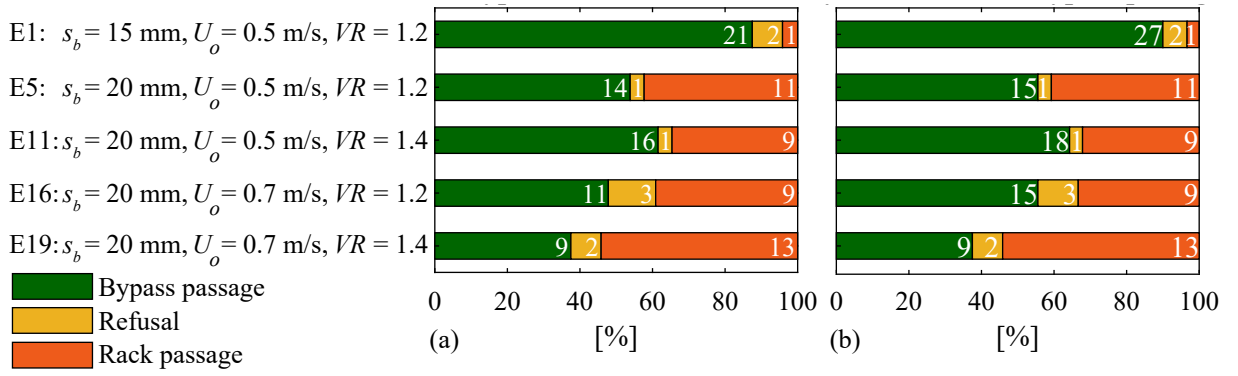
## Nase

In total, 39 nase were tested of which 35 crossed line 2 (Table 4.3). Not a single specimen entered the bypass, neither with nor without rack interaction (Fig. 7.9), while all nase passed the rack with the exception of one individual. Although nase were tested with two different configurations only, it is clear that the HBR with  $s_b = 20$  mm offered no sufficient protection. However, the poor protection of nase might not be a species-specific aspect, but was likely related to the small  $TL$  of the tested specimens ( $\overline{TL} = 7.1$  cm; Table 7.1). The average guidance and protection efficiencies of the tested nase for OC and  $s_b = 20$  mm were  $\overline{FGE}_{\text{nase}} = 0\%$  and  $\overline{FPE}_{\text{nase}} = 3\%$ .

**Fig. 7.9:** Results of the live fish tests with nase by counting (a) bypass passages with rack interaction only and (b) all bypass passages (definition of configurations in Table 4.3)

## Trout

Trout were tested with the full depth open channel bypass only. The FGE and FPE of all trout experiments with  $s_b = 20$  mm (E5, E11, E16, E19) ranged between 38% and 65% (Fig. 7.10a). The difference between FGE (Fig. 7.10a) and  $FGE^*$  (Fig. 7.10b) was very small, indicating that hardly any trout entered the bypass without rack interaction. The results of the  $\chi^2$ -tests, summarized in Table 7.4, show that neither  $U_o$  nor  $VR$  affected any of the fish reactions significantly with a significance level of  $\alpha_{\text{sig}} = 0.05$ . The average guidance and protection efficiencies for trout at the HBR with  $s_b = 20$  mm was calculated by averaging the results of E5, E11, E16, and E19, leading to  $\overline{FGE}_{\text{trout}} = 51\%$  and  $\overline{FPE}_{\text{trout}} = 58\%$ , while  $FGE = 88\%$  and  $FPE = 96\%$  for  $s_b = 15$  mm (E1 in Fig. 7.10a). The effect of  $s_b$  was assessed by comparing the results of E1 with E5. A reduction of the clear bar spacing from  $s_b = 20$  mm to  $s_b = 15$  mm led to significantly more bypass passages and significantly less rack passages (Table 7.4).



**Fig. 7.10:** Results of the live fish tests with trout by counting (a) bypass passages with rack interaction only and (b) all bypass passages (definition of configurations in Table 4.3)

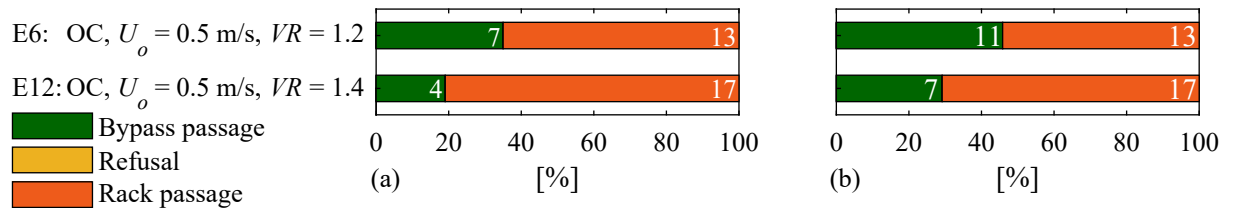
**Table 7.4:** Output of the  $\chi^2$ -tests for the trout results shown in Fig. 7.10a

	$U_o$		$VR$		$s_b$	
	E5+E11 vs. E16+E19		E5+E16 vs. E11+E19		E1 vs. E5	
	$p$ -value	$\chi^2$	$p$ -value	$\chi^2$	$p$ -value	$\chi^2$
Bypass	0.193	1.698	1.000	0.000	0.022*	5.224
Refusal	0.356	0.854	1.000	0.001	0.943	0.005
Rack	0.525	0.404	0.907	0.014	0.005*	7.972

\* significant with a significance level of  $\alpha_{\text{sig}} = 0.05$

### Salmon parr

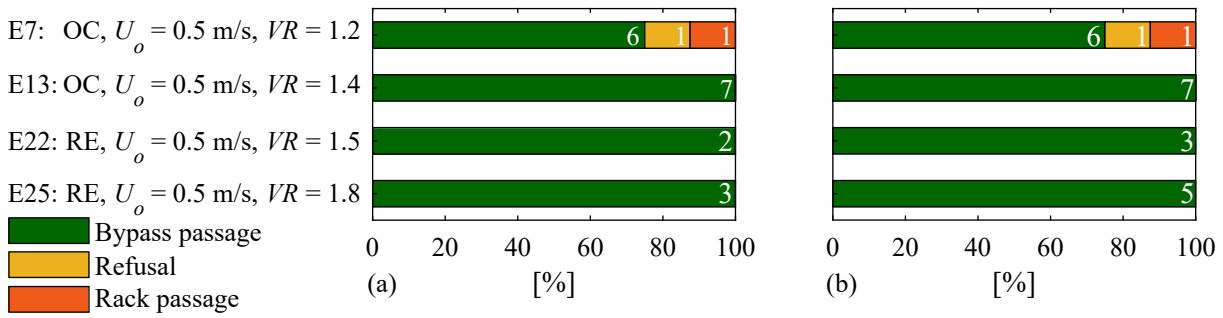
Not a single salmon parr refused the HBR-BS, leading to  $\text{FGE} = \text{FPE}$  (Fig. 7.11). The FGE of the tested configurations ranged between 19% and 35% but the difference was not significant ( $p = 0.424$ ,  $\chi^2 = 0.640$ ). The average guidance and protection efficiency of salmon parr were  $\overline{\text{FGE}}_{\text{salmon}} = \overline{\text{FPE}}_{\text{salmon}} = 27\%$ .



**Fig. 7.11:** Results of the live fish tests with salmon parr by counting (a) bypass passages with rack interaction only and (b) all bypass passages (definition of configurations in Table 4.3)

### Eel

Only a few eels were tested without electrification, of which the majority entered the bypass with rack interaction (Fig. 7.12), while only one rack passage and one refusal were observed. The average guidance and protection efficiencies for OC and  $s_b = 20$  mm were  $\overline{\text{FGE}}_{\text{eel}} = 87\%$  and  $\overline{\text{FPE}}_{\text{eel}} = 93\%$ .



**Fig. 7.12:** Results of the live fish tests with eels by counting (a) bypass passages with rack interaction only and (b) all bypass passages (definition of configurations in Table 4.3)

### Summary of average guidance and protection efficiencies

With the exception of spiralin, no statistically significant differences were detected with OC and  $s_b = 20$  mm. This means that  $U_o$  and  $VR$  either did not affect the fish reactions of barbel, nase, trout, salmon parr, and eel in the range of  $U_o = 0.5$ – $0.7$  m/s and  $VR = 1.2$ – $1.4$ , or that the sample sizes were too small to detect potential differences on a significance level of  $\alpha_{\text{sig}} = 0.05$ . It is therefore reasonable to calculate the species-specific guidance and protection efficiencies averaged over all configurations with OC and  $s_b = 20$  mm to  $\overline{\text{FGE}}$  and  $\overline{\text{FPE}}$  (Table 7.5). As HBRs are typically classified as physical barriers, it is crucial to consider  $TL$  when interpreting the results. The variable  $N$  in Table 7.5 represents the total number of fish per species tested with the HBR installed, the OC-bypass, and  $s_b = 20$  mm.

**Table 7.5:** Species-specific guidance and protection efficiencies averaged over all experiments with an HBR installed, the OC-bypass, and  $s_b = 20$  mm

Fish species	$\overline{\text{FGE}}$ [%]	$\overline{\text{FPE}}$ [%]	$TL_{\min}$ – $TL_{\max}$ [cm]	$\overline{TL}$ [cm]	$\sigma_{TL}$ [cm]	$N$ [–]
Spiralin	78*	92*	7.8–12.9	9.9	0.9	117
Barbel	65	72	7.5–20.8	15.2	3.0	114
Nase	0	3	5.9–9.3	7.1	0.7	39
Trout	51	58	8.6–21.0	13.7	2.7	173
Salmon	27	27	9.1–14.9	11.4	1.2	51
Eel	87	93	41.3–82.8	65.8	11.7	17

\* Has to be interpreted with caution because FGE and FPE varied significantly between configurations

## 7.2.2 Effect of the fish species, size distribution, and clear bar spacing

### Fish size distribution and rack passages

The fish size distribution and therefore also the fish width varied between tested species. As HBRs are classified as physical barriers, it seems likely that the fish size had a crucial effect on the percentage of rack passages. The majority of tested fish could have physically passed through the HBR (Table 7.6). A significant share of small fish was protected and guided towards the bypass, indicating a partial behavioral guidance effect, which was already described by various authors from ethohydraulic studies (e.g. Berger, 2018; Carlsson, 2019; Section 3.7.3)

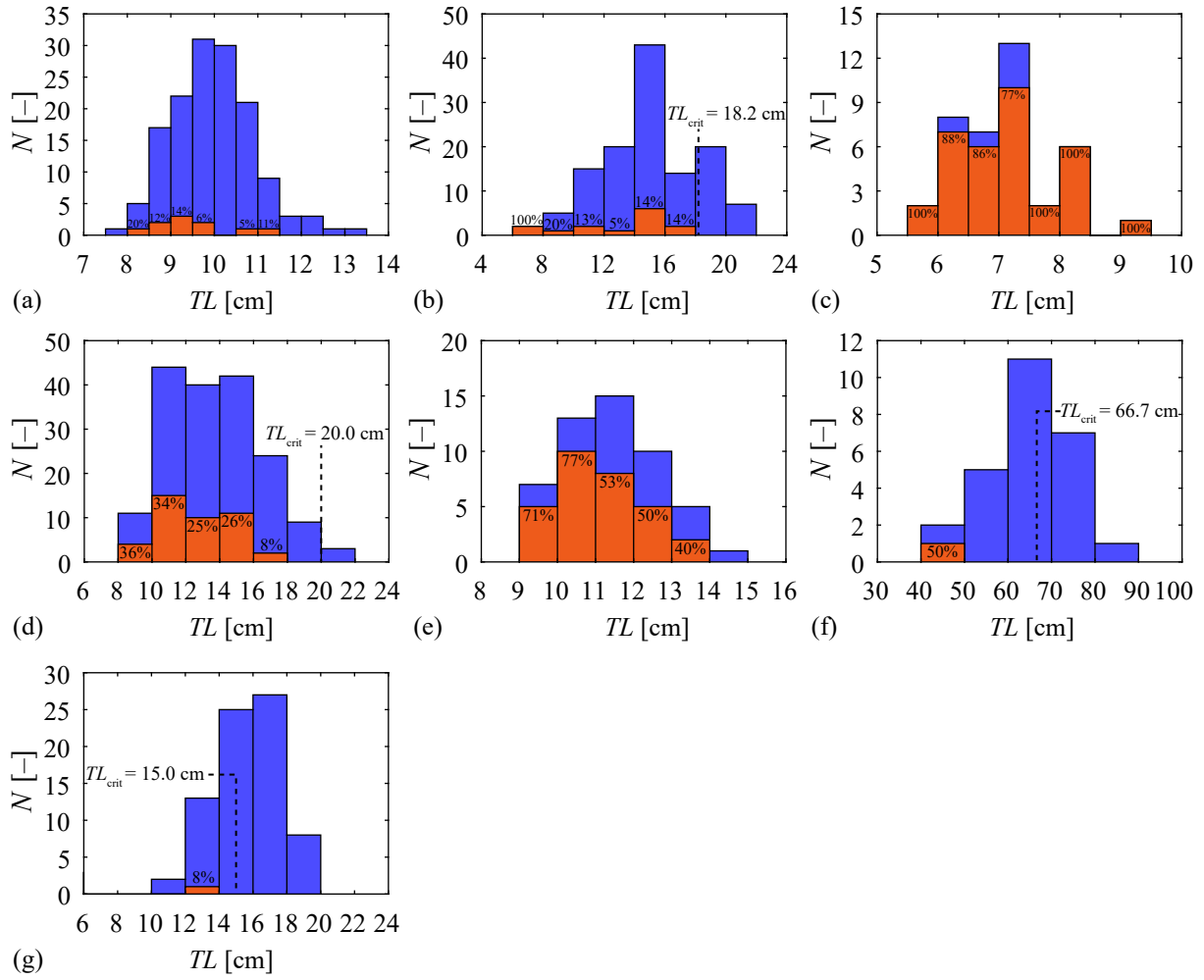


and monitoring campaigns (e.g. Zaugg and Mendez, 2018; Wagner *et al.*, 2019b; Section 3.7.4). Table 7.6 shows that all tested spirlin, nase, and salmon parr could have physically passed the HBR with  $s_b = 20$  mm as  $TL_{\max} = 13.4, 9.3,$  and  $14.9$  cm (Table 7.1) was smaller than  $TL_{\text{crit}} = 22, 18,$  and  $20$  cm (Table 2.2), respectively. The HBR was a physical barrier to only 20% of the barbels, 42% of the eels, and 2% of trout with  $s_b = 20$  mm and to 64% of trout with  $s_b = 15$  mm (Table 7.6).

**Table 7.6:** Number of tested fish  $n$  to which the HBR was a physical barrier ( $TL > TL_{\text{crit}}$ )

	Spirlin	Barbel	Nase	Trout		Salmon	Eel
$s_b$ [mm]	20	20	20	15	20	20	20
$n$ physical barrier [–]	0	25	0	48	3	0	11
$n$ no physical barrier [–]	144	101	39	27	171	51	15
Percentage physical barrier [%]	0	20	0	64	2	0	42

Figure 7.13 shows the size distribution of all fish tested without electrification, where  $TL_{\text{crit}}$  (Eq. 2.3) is indicated with a dashed line if  $TL_{\text{crit}} < TL_{\max}$ . For all fish species, rack passages were observed for fish with  $TL < TL_{\text{crit}}$  only. The percentages in Fig. 7.13 specify how many fish passed through the HBR per size class. For spirlin, barbel, and eel with  $s_b = 20$  mm and trout with  $s_b = 15$  mm, too few rack passages were observed to see a clear trend between the percentage of rack passages and  $TL$  (Fig. 7.13a,b,f,g). For trout and salmon parr, the percentages of rack passages decreased for larger  $TL$  (Fig. 7.13d,e). In other words, larger fish were better protected than smaller fish, which explains the poor protection of the very small tested nase (Fig. 7.13c). It was shown in Section 7.2 that a reduction of  $s_b$  from 20 mm to 15 mm significantly reduced the number of rack passages of trout. Although the size distribution of trout was not identical for different  $s_b$ , Fig. 7.13d,g illustrates that the percentage of rack passages significantly reduced for all size classes. Fish could only be fully protected if  $TL > TL_{\text{crit}}$ .



**Fig. 7.13:** Size distribution of all fish tested without electrification (blue) and all rack passages (red) for  $s_b = 20$  mm (a) spirlin, (b) barbel, (c) nase, (d) trout, (e) salmon parr, (f) eel, and for  $s_b = 15$  mm (g) trout, where the percentages specify the rack passages per size class

### Effect of the fish width on the guidance and protection efficiencies

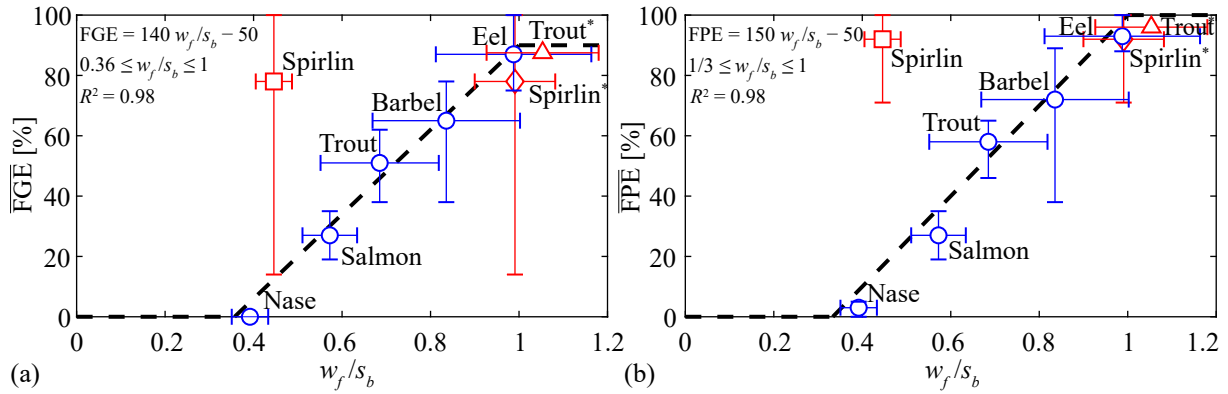
A comparison of  $\overline{FGE}$  and  $\overline{FPE}$  revealed large variations across species (Table 7.5). While the HBR with  $s_b = 20$  mm offered essentially no protection for nase with  $\overline{TL} = 7.1$  cm, more than 90% of the tested spirlin and eels were protected. To assess if these variations resulted from the different species or from the different tested body size distributions and therefore different fish widths,  $\overline{FGE}$  and  $\overline{FPE}$  were plotted as a function of the ratio of the fish width to the clear bar spacing  $w_f/s_b$  (Fig. 7.14), which is the reciprocal of the permeability index  $PI$  (cf. Section 2.2.6). The fish widths  $w_f$  were calculated as an average per species from  $\overline{TL}$  in Table 7.5. A linear trend was observed between nase, salmon parr, trout, barbel, and eel ( $R^2 = 0.98$ , blue circles in Fig. 7.14). A least squares regression analysis led to Eq. (7.1) and (7.2).

$$FGE = 140w_f/s_b - 50 \quad (7.1)$$

$$FPE = 150w_f/s_b - 50 \quad (7.2)$$

The application limits are  $0.36 \leq w_f/s_b \leq 1$  (Eq. 7.1, Fig. 7.14a) and  $1/3 \leq w_f/s_b \leq 1$  (Eq. 7.2, Fig. 7.14b), which means that  $FGE = 0\%$  and  $FPE = 0\%$  for  $w_f/s_b \leq 0.36$  and  $w_f/s_b \leq 1/3$ ,

respectively. As there is no reason to assume a positive correlation between  $w_f/s_b$  and FGE for  $w_f/s_b \geq 1$ , it is proposed to presume constant FGE for  $w_f/s_b \geq 1$ , that is,  $\text{FGE} = 90\%$ . Fish with  $w_f/s_b > 1$  are physically protected by the HBR, such that  $\text{FPE} = 100\%$  for  $w_f/s_b > 1$ . The vertical error bars in Fig. 7.14 mark the minimal and maximal FGE and FPE for the different tested configurations with the full depth open channel bypass and the horizontal error bars  $\overline{TL} \pm \sigma_{TL}$  (cf. Section 7.2.1).



**Fig. 7.14:** (a)  $\overline{\text{FGE}}$  and (b)  $\overline{\text{FPE}}$  as a function of  $w_f/s_b$  for all tested fish species with  $s_b = 20$  mm and additionally with  $s_b = 15$  mm for trout (Trout\*, red triangle); Spirlin\* was calculated with  $h_f/s_b$  instead of  $w_f/s_b$  (red diamond-shaped symbol); the dashed line in (a) shows Eq. (7.1) and in (b) Eq. (7.2)

Spirlin were not considered for determining Eq. (7.1) and (7.2), because FGE and FPE were considerably larger than for all other species (red squares in Fig. 7.14). In contrast to all other species, the reactions of spirlin significantly varied between configurations (cf. Section 7.2.1), which led to the large vertical error bars in Fig. 7.14. It is very likely that the better protection of spirlin is a species-specific result, which is supported by the monitoring campaign at HPP Rappenberghalde, where the protection rate of spirlin was larger than for all other fish species (cf. Sections 3.7.4 and 7.8.2). Figure 7.14 is based on the assumption that the fish width  $w_f$  and not the fish height  $h_f$  limits rack passages (cf. Section 2.2.6). A detailed analysis of the videos of all rack passages revealed that spirlin hardly rotated themselves to pass through the HBR (details in Section 7.4.4). When  $w_f/s_b$  was replaced by  $h_f/s_b$  for spirlin in Fig. 7.14 (red diamond-symbol),  $\overline{\text{FGE}}$  and  $\overline{\text{FPE}}$  corresponded very well with the prediction equations of the other fish species, which indicates that the fish height  $h_f$  might limit rack passages for most spirlin. The FGE and FPE of trout with  $s_b = 15$  mm is shown with red triangles in Fig. 7.14, which also fits well to the proposed equations. The correlation between  $w_f/s_b$  and FGE, FPE in Fig. 7.14 indicates that it is possible that the differences in  $\overline{\text{FGE}}$  and  $\overline{\text{FPE}}$  between all tested species, except spirlin, is mainly a result of the different tested size distributions. However, additional experiments with individuals from the same species but different size ranges are necessary to validate this assumption. In general, the proposed equations have to be used with caution as they are based on data of one size range per species only, but they can give an indication of the correlation between  $w_f/s_b$  and FGE, FPE. These equations try to quantify the behavioral guidance effect at HBR-BSs. However, they should not be applied if the conditions deviate strongly from the conditions in the present experiments, for example, FGE and FPE

are expected to be significantly lower if no suitable bypass is available. If FGE and FPE are estimated with the presented equations, it is strongly recommended to use  $w_f/s_b$ . However, for some species such as spiralin, it might be permissible to replace  $w_f/s_b$  by  $h_f/s_b$ .

### 7.2.3 Overall guidance and protection efficiencies

Up to now, the effects of  $U_o$  and  $VR$  on FGE and FPE were discussed for each species individually, while the overall effect across species is assessed in this section with GLMs. Table 7.7 compares the AICs and BICs of the main model with the parameters  $U_o$ ,  $VR$ , usage, and time with a model including the interaction between  $VR$  and  $U_o$ . For most categories, the main model led to smaller AICs/BICs (Table 7.7). All further analyses were therefore conducted with the main model, without considering the interaction between  $U_o$  and  $VR$ . The output of the GLMs considering the bypass passages, rack passages, and refusals as the dependent variable are summarized in Tables 7.8, 7.9, and 7.10, respectively, including the regression coefficients  $\beta$ , the standard errors  $\varepsilon$ , the total number of observations  $N$ , the log-likelihood, and the AIC/BIC.

**Table 7.7:** Summary of the AICs and BICs of the main model and the model considering the interaction between  $VR$  and  $U_o$  for the dependent variables bypass passage, rack passage, and refusal; \* indicates the smallest AIC/BIC for each column

Model	Bypass passage		Rack passage		Refusal	
	AIC	BIC	AIC	BIC	AIC	BIC
Main	430.817	449.767*	408.624*	427.574*	146.609*	165.559*
Interaction $VR : U_o$	427.800*	450.540	409.393	432.133	148.022	170.762

**Table 7.8:** Summary of the GLM with all HBR data (OC,  $s_b = 20$  mm) with the **bypass passage** as the dependent variable; the reference categories are  $U_o = 0.5$  m/s,  $VR = 1.2$ , and time = morning; \* denotes  $p < 0.05$ , \*\*  $p < 0.01$ , and \*\*\*  $p < 0.001$

	Intercept	$U_o = 0.7$ m/s	$VR = 1.4$	Usage	Time = afternoon
Coefficient $\beta$	1.797***	-0.210	-0.892***	-0.339***	-0.730**
Exp( $\beta$ )	6.029	0.810	0.410	0.712	0.482
Std. error $\varepsilon$	0.389	0.262	0.235	0.103	0.246
$N$	327				
Log-likelihood	-210.409				
AIC	430.817				
BIC	449.767				

**Table 7.9:** Summary of the GLM with all HBR data (OC,  $s_b = 20$  mm) with the **rack passage** as the dependent variable; the reference categories are  $U_o = 0.5$  m/s,  $VR = 1.2$ , and time = morning; \* denotes  $p < 0.05$ , \*\*  $p < 0.01$ , and \*\*\*  $p < 0.001$

	Intercept	$U_o = 0.7$ m/s	$VR = 1.4$	Usage	Time = afternoon
Coefficient $\beta$	−2.427***	−0.160	0.596*	0.558***	0.566*
Exp( $\beta$ )	0.088	0.852	1.814	1.746	1.761
Std. error $\varepsilon$	0.423	0.275	0.242	0.111	0.256
$N$	327				
Log-likelihood	−199.312				
AIC	408.624				
BIC	427.574				

**Table 7.10:** Summary of the GLM with all HBR data (OC,  $s_b = 20$  mm) with the **refusal** as the dependent variable; the reference categories are  $U_o = 0.5$  m/s,  $VR = 1.2$ , and time = morning; \* denotes  $p < 0.05$ , \*\*  $p < 0.01$ , and \*\*\*  $p < 0.001$

	Intercept	$U_o = 0.7$ m/s	$VR = 1.4$	Usage	Time = afternoon
Coefficient $\beta$	−2.446***	1.286**	1.216*	−0.875***	1.039*
Exp( $\beta$ )	0.087	3.618	3.372	0.417	2.828
Std. error $\varepsilon$	0.717	0.473	0.491	0.251	0.472
$N$	327				
Log-likelihood	−68.304				
AIC	146.609				
BIC	165.559				

Prior to the discussion of the results from Tables 7.8–7.10, their interpretation is explained with an example. The intercept describes the standard configuration, where all independent variables are set to their reference categories, that is,  $U_o = 0.5$  m/s,  $VR = 1.2$ , time = morning for the categorical variables and usage = 1 for the continuous variable. The odds ratio of  $\exp(\beta) = \exp(1.797) = 6.029$  of the intercept in Table 7.8 can be converted to a probability with Eq. (4.16) to  $p(X) = \exp(\beta) / (1 + \exp(\beta)) = 0.858$ . This means that the probability was 86% that a fish entered the bypass with the standard configuration. When all other parameters were kept constant, but  $VR$  increased from  $VR = 1.2$  to  $VR = 1.4$ , the odds ratio changed by a factor of 0.410 to  $\exp(\beta) = 6.029 \times 0.410 = 2.472$ , which can be converted to a probability of  $p(X) = 0.712$ . In other words, the probability of a bypass passages reduced from 86% to 71% when  $VR$  of the standard configuration ( $U_o = 0.5$  m/s,  $VR = 1.2$ , time = morning, usage = 1) was increased to  $VR = 1.4$ . The 95% confidence interval can be calculated with Eq. (4.18) to  $CI_{95\%} = \exp(\beta \pm 1.96\varepsilon) = 2.814, 12.929$ , leading to probabilities of  $p = 74, 93\%$  (Eq. 4.16). This means that with a probability of 95%, 74–93% of the fish entered the bypass with the standard configuration, or in other words, there is only a 5% chance that less than 74% or more

than 93% enter the bypass with the standard configuration. In general, a parameter increases the dependent variable if  $\exp(\beta) > 1$  and it decreases the dependent variable for  $\exp(\beta) < 1$ . As an example, the percentage of refusals increased when  $U_o = 0.5$  m/s was changed to  $U_o = 0.7$  m/s,  $VR = 1.2$  to  $VR = 1.4$ , or time = morning to time = afternoon, while the number of refusals decreased if fish were used more often (larger usage; Table 7.10).

### Effect of the approach flow velocity

The approach flow velocity  $U_o$  did neither affect the bypass passages nor the rack passages significantly (Tables 7.8–7.9), but an increase of the approach flow velocity significantly increased the odds of refusals by 3.618 (Table 7.10). In other words, the rather small probability of a refusal for the standard configuration with  $U_o = 0.5$  m/s of 8% increased to 24% for  $U_o = 0.7$  m/s. This tendency was observed for all species which were tested with  $U_o = 0.5$  m/s and  $U_o = 0.7$  m/s, namely spiralin, barbel, and trout (Fig. 7.7, 7.8, and 7.10). However, the effect was not significant on the species-specific analysis (Table 7.2, 7.3, and 7.4), as the species-specific sample sizes were rather small compared to the overall sample size.

### Effect of the velocity ratio

An increased velocity ratio  $VR$  led to significantly less bypass passages (Table 7.8), but more rack passages and refusals (Tables 7.9, 7.10). For the standard configuration, an increase from  $VR = 1.2$  to  $VR = 1.4$  reduced the probability of a bypass passage from 86% to 71%, while the rack passages increased from 8% to 14% and the refusals from 8% to 23%. This trend was also observed for multiple species, but it was only significant for bypass passages and refusals for spiralin (Table 7.2).

### Usage

In tendency, when fish were used more often, the number of bypass passages and refusals reduced, while the number of rack passages increased (Tables 7.8–7.10). This could be an indication of a learning effect, but these results have to be interpreted with caution, as learning effects were not the main research question of the present study and the experimental matrix was not designed accordingly. As an example, all HBR experiments with nase were conducted with a usage = 2, 3 and almost all of them passed through the HBR (Fig. 7.9). In an ideal experimental matrix, optimized to assess learning effects, the number of tested nase should be equally distributed over all usages. If learning effects are of interest in future experiments, it is recommended to mark fish individually to allow for specimen-specific analyses. Lehmann *et al.* (2016) observed learning effects in their live fish tests after approximately one week, which corresponds to the maximal time fish were kept in the laboratory in the present study (cf. Section 4.4.3). In the experiments of Flügel *et al.* (2015), fish were more likely to enter the bypass when they were used for the second time compared to the first time, which the authors attributed to potential learning effects or reduced energy resources. Compared to different live fish tests, no clear trend was observed between usage and bypass passages, rack passages, and refusals.

## Time

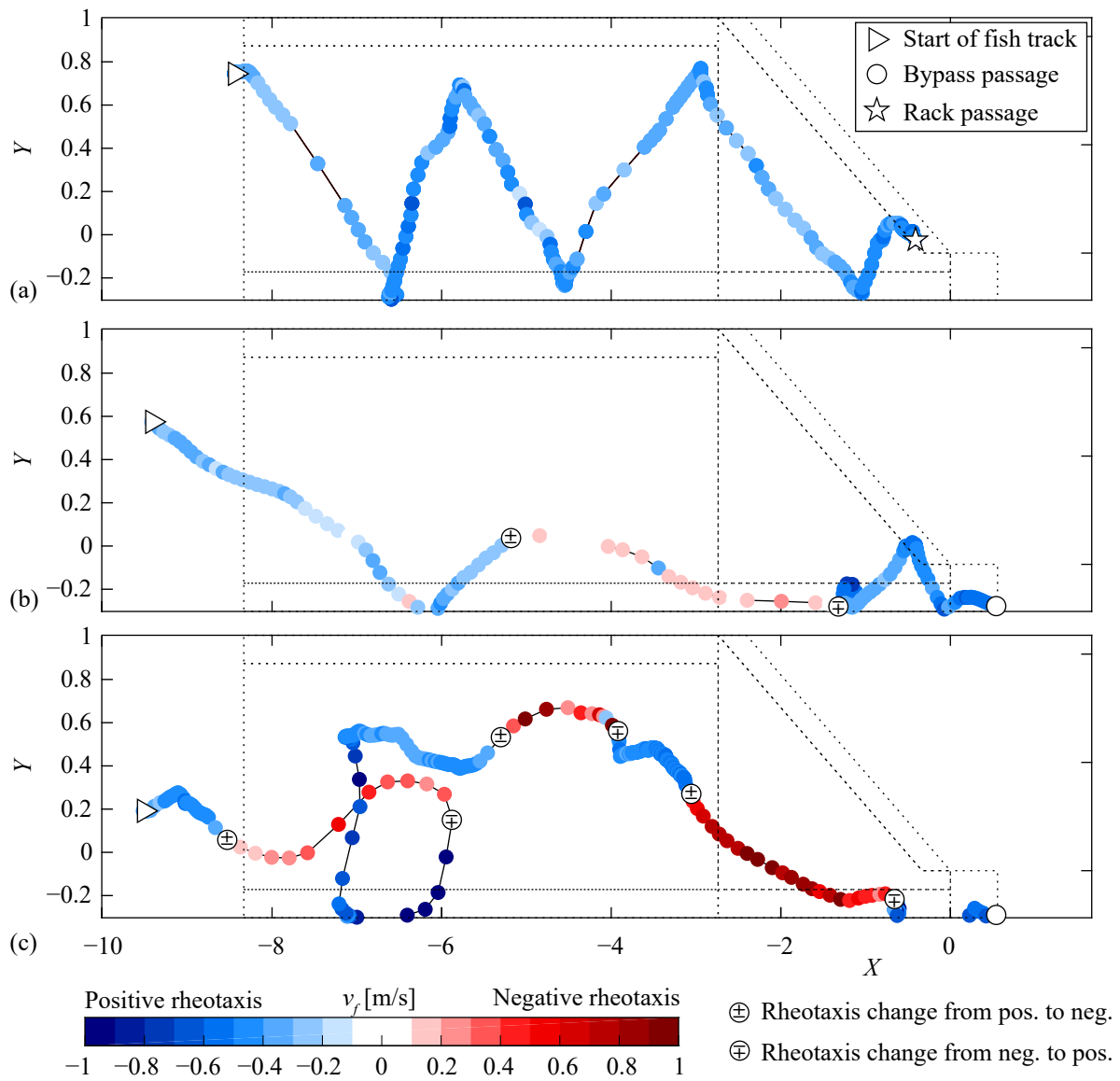
The time of day affected the fish behavior. Testing fish in the afternoon instead of the morning resulted in less bypass passages, more rack passages, and more refusals (Tables 7.8–7.10). However, similar to the usage, it is assumed that this effect is a result of the non-optimized experimental matrix to investigate the effect of the time of the day on the results. It is nevertheless important to consider these variables in the GLM as they also affect the odds ratios of  $U_o$  and  $VR$ , but the odds ratios of the parameters usage and time should not be interpreted further.

## 7.3 Fish swimming tracks

### 7.3.1 Combination with flow velocities

A key element of ethohydraulic studies is to link the fish behavior with the hydraulic conditions. In case of the present investigation, the velocity field upstream of the HBR was very homogeneous and hardly affected by the HBR (cf. Section 5.5). Hydraulic characteristics like the spatial velocity gradient (SVG) or the turbulent kinetic energy (TKE) were therefore, with the exception of the area at the bypass inlet (cf. Section 5.5), very small and hence unsuitable to explain the overall swimming tracks. However, the combination of fish swimming tracks with the velocity fields allowed for analyzing the rheotaxis (cf. Table 4.2 in Section 4.4.3). Figure 7.15 gives three examples of different fish swimming tracks with  $U_o = 0.5$  m/s,  $VR = 1.4$ , and the full depth open channel bypass, which were combined with the corresponding ADV measurements close to the flume bottom (cf. Fig. 5.11c in Section 5.5). Figure 7.15a shows a typical track of three nase, which swam downstream as a school in zigzag movements (cf. Section 7.1.2). They entered the observation area 02:20 [min:sec] after the start of the experiment and passed through the HBR 35 s later. At all times,  $0 < U_g < U$ , meaning that they swam downstream with positive rheotaxis and showed no rheotaxis changes, which was very typical for nase (cf. Table 4.2 in Section 4.4.3). The individual salmon parr in Fig. 7.15b approached the observation area at 23:42 with positive rheotaxis, changed to negative rheotaxis at 23:52 and back to positive rheotaxis at 23:58 with a distance of  $\approx 1$  m to the rack. The salmon parr then swam towards the HBR, slightly touched it with its caudal fin, before it moved further downstream and entered the bypass at 24:18. Figure 7.15c shows the swimming track of an active trout, which swam very fast with the flow and against the flow and performed a total of six rheotaxis changes within  $\approx 1$  minute.





**Fig. 7.15:** Examples of swimming tracks with  $U_o = 0.5$  m/s,  $VR = 1.4$ , and the full depth open channel bypass of (a) three nase, (b) a salmon parr, and (c) a trout; the colors indicate the fish swimming velocity which allowed for determining the rheotaxis and rheotaxis changes

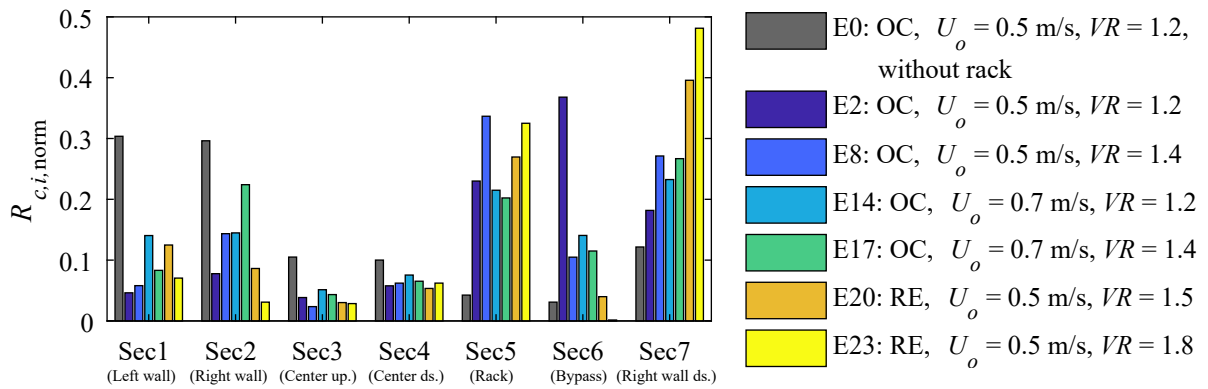
### 7.3.2 Sector analysis

As individual fish swimming tracks can hardly be representative for a test configuration, differences among species and configurations are described with the normalized residence coefficient  $R_{c,i,\text{norm}}$  (Eq. 4.13). The sectors were defined in Fig. 4.20 in Section 4.4.3 and all configurations (E0–E25) were introduced in Table 4.3. Due to the low number of replicates of some configurations with the inlet restrictor, the configurations E22, E24, and E25 were not analyzed in the following (cf. Table 4.3).

#### Spiralin

Without a rack installed (E0),  $R_{c,1,\text{norm}} \approx R_{c,2,\text{norm}}$ , indicating that spiralin were equally distributed between the right (Sec2) and the left flume walls (Sec1; Fig. 7.16). They swam quickly through the rack plane (Sec5) and hardly entered the bypass (Sec6; cf. Fig. 7.7). With the same flow velocities but with an HBR installed (E2), spiralin spent much less time in the upstream

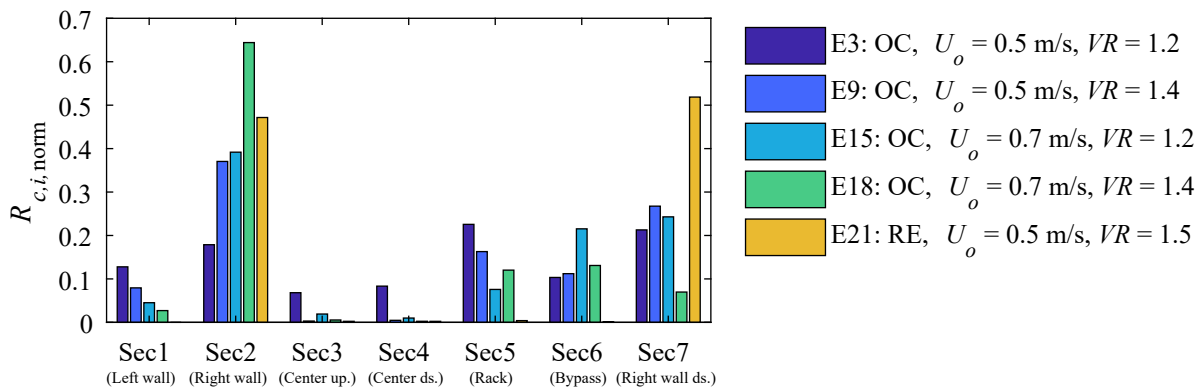
area which was unaffected by the HBR (Sec1–Sec3), while they were swimming much more often in front of the HBR (Sec5) and in the bypass (Sec6). These results point out the excellent guidance efficiency of this configuration (cf. Fig. 7.7). With an increased  $VR$  (E8), spiralin spent more time searching for a downstream passage corridor in front of the rack (Sec5), while they spent less time in the bypass (Sec6). With constant  $U_o$ , an increased  $VR$  led to a larger probability of fish swimming along the right wall upstream of the bypass (E2 vs. E8 and E14 vs. E17; Sec2 and Sec7). With the inlet restrictor (E20, E23), spiralin spent much more time in front of the bypass (Sec7), looking for a suitable downstream passage corridor. They did not avoid the bypass by swimming far upstream (e.g. in Sec2–Sec4), but they often needed several attempts to accept the bypass with the inlet restrictor. This behavior was more pronounced for larger  $VR$  (E20 vs. E23). The results with the inlet restrictor in the bypass (E20 and E23, Sec6) should not be interpreted, because the submerged cameras could not capture movements in front of the bottom opening as the view was obstructed by the restrictor.



**Fig. 7.16:** The normalized residence coefficient  $R_{c,i,norm}$  of spiralin for the sectors Sec1–Sec7 and the configurations defined in Table 4.3

## Barbel

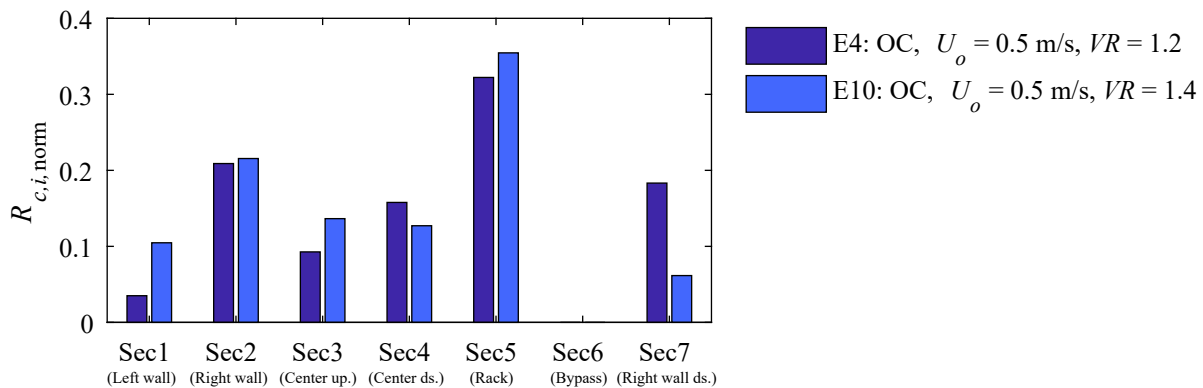
Barbels spent hardly any time in the center of the flume (Sec3, Sec4) and preferred the right wall (Sec2) to the left wall (Sec1) for all configurations (Fig. 7.17). This tendency was small for low  $U_o$  and  $VR$  (E3), while it was most pronounced for large  $U_o$  and  $VR$  (E18). Although barbels preferred to stay close to the right wall in the upstream for large  $U_o$  and  $VR$  (E18, Sec2), they spent less time in the downstream section of the right wall (E18). The sector analysis of barbels with the inlet restrictor has to be interpreted with caution, because it is based on nine specimens only (cf. Table 4.3), but it illustrates the tendency of barbels to swim along the right wall (Sec2 and Sec7). Eight of these nine barbels entered the bypass without rack interaction (cf. Fig. 7.8), which explains why  $R_{c,2,norm} + R_{c,7,norm} \approx 1$  (E21). In contrast to spiralin,  $R_{c,2,norm} \approx R_{c,7,norm}$  for barbels with the inlet restrictor, indicating that they were not hesitating at the bypass inlet.



**Fig. 7.17:** The normalized residence coefficient  $R_{c,i,norm}$  of barbel for the sectors Sec1–Sec7 and the configurations defined in Table 4.3

### Nase

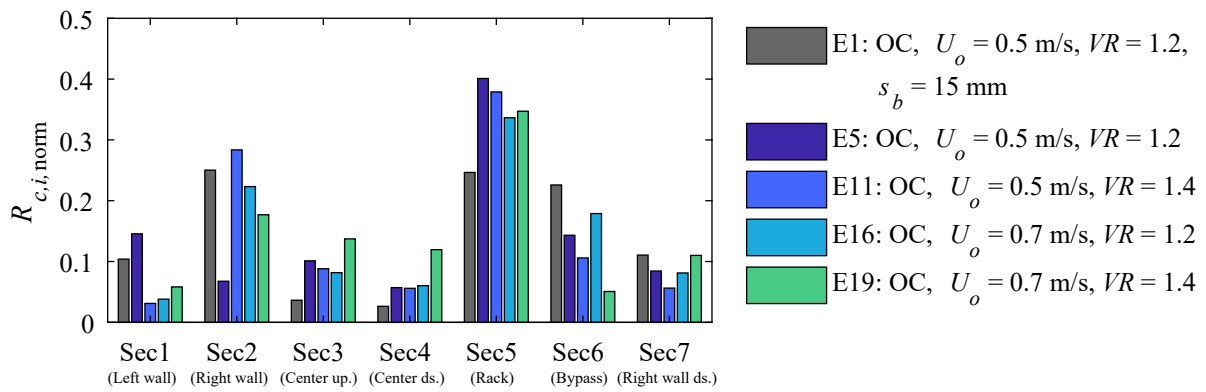
None of the tested nase entered the bypass (cf. Fig. 7.9), that is, Sec6 (Fig. 7.18). Nevertheless, the largest  $R_{c,i,norm}$  were observed for Sec5, which indicates that nase noticed and reacted to the HBR. While many nase passed through the HBR without hesitation, others were guided along the rack for a couple of decimeters prior to the rack passage. No large differences were observed between both tested configurations, but nase spent less time in front of the bypass inlet (Sec7) for larger  $VR$  (E10), indicating avoidance reactions.



**Fig. 7.18:** The normalized residence coefficient  $R_{c,i,norm}$  of nase for the sectors Sec1–Sec7 and the configurations defined in Table 4.3

### Trout

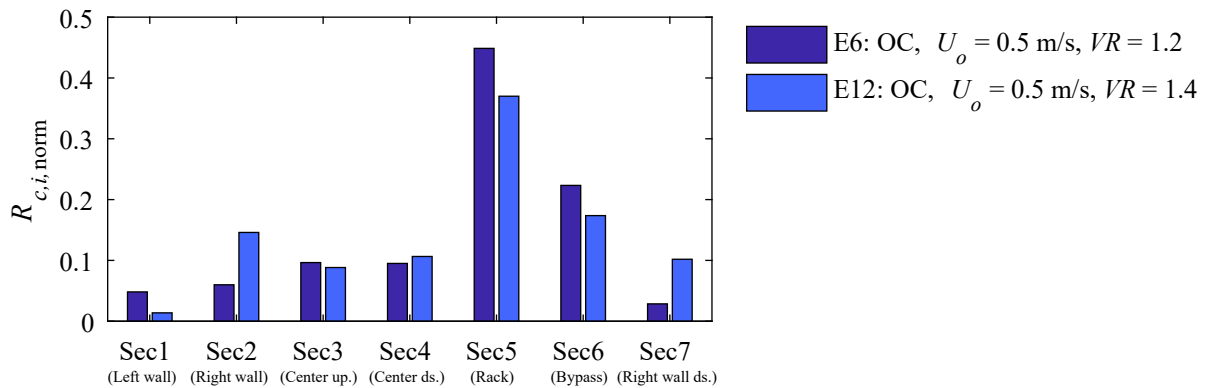
Similarly to FGE and FPE shown in Fig. 7.10, no clear patterns could be detected between the configurations for  $s_b = 20$  mm (E5, E11, E16, E19 in Fig. 7.19). However, with  $s_b = 15$  mm (E1), trout spent more time in the bypass and were guided along the rack more efficiently in terms of spending less time in front of the rack (Sec5).



**Fig. 7.19:** The normalized residence coefficient  $R_{c,i,norm}$  of trout for the sectors Sec1–Sec7 and the configurations defined in Table 4.3

### Salmon parr

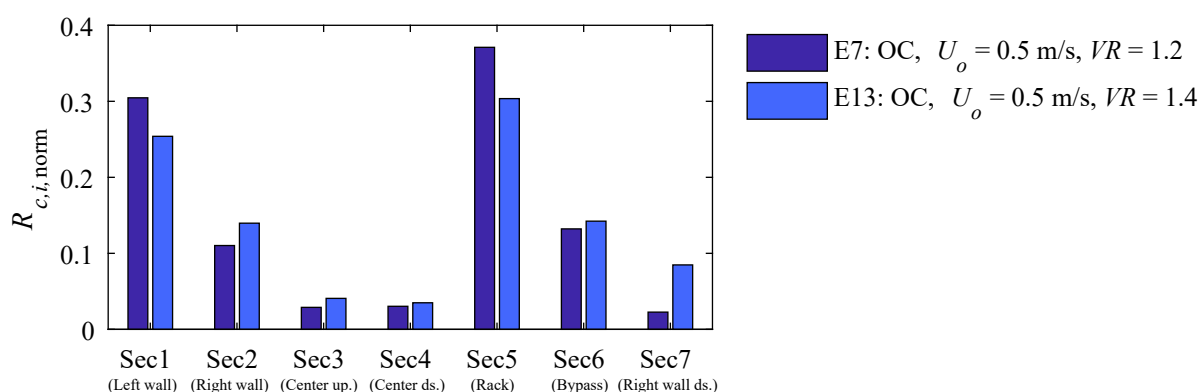
No relevant differences were detected between the configurations of salmon parr (Fig. 7.20). In comparison to most other species, salmon parr spent much time in front of the rack (Sec5) and in front of the bypass inlet (Sec6). They did not prefer the flume walls (Sec1, Sec2, and Sec7) to the flume center (Sec3, Sec4).



**Fig. 7.20:** The normalized residence coefficient  $R_{c,i,norm}$  of salmon parr for the sectors Sec1–Sec7 and the configurations defined in Table 4.3

### Eel

Eels were the only species clearly preferring the left flume wall (Sec1) in comparison to the right flume wall (Sec2; Fig. 7.21). The reason therefore is that many eels left the acclimatization compartment, which was positioned on the left flume side (cf. Fig. 4.4 and 4.5), with negative rheotaxis and were guided along the left flume wall towards the rack. The strong thigmotactic positive behavior of eels becomes very clear with Fig. 7.21, as eels preferred to swim along structures, either the flume walls or the rack (Sec1, Sec2, Sec5, Sec6, and Sec7), while they hardly spent any time in the flume center (Sec3, Sec4).



**Fig. 7.21:** The normalized residence coefficient  $R_{c,i,norm}$  of eel for the sectors Sec1–Sec7 and the configurations defined in Table 4.3

## 7.4 Rack passages

Independent of species identity, 132 rack passages were observed with the HBR without electrification (configurations E1–E25, cf. Table 4.3). In this section, all these rack passages were analyzed in terms of the effect of the bypass, their vertical and horizontal location, the rheotaxis, and fish rotations.

### 7.4.1 Effect of the bypass on rack passages

If the flow conditions at the bypass inlet are unfavorable for fish, they provoke avoidance reactions, which can increase the time fish search along the HBR for a suitable downstream passage corridor and therefore also the rack passage risk. It was thus analyzed, how many fish interacted with the bypass, refused it, and subsequently passed through the HBR. A fish was counted as interacting with the bypass if it swam into the area  $\approx 20$  cm upstream of the bypass inlet, which is where the flow was affected by the bypass (cf. Fig. 5.11). The results are summarized for all species in Table 7.11.

**Table 7.11:** Number of fish which either interacted or did not interact with the bypass prior to passing through the HBR

	Spirlin	Barbel	Nase	Trout	Salmon	Eel	Total
$n$ bypass interaction [–]	6	3	8	6	3	0	26
$n$ no bypass interaction [–]	4	11	26	37	27	1	106
Percentage bypass interaction [%]	60	21	24	14	10	0	20

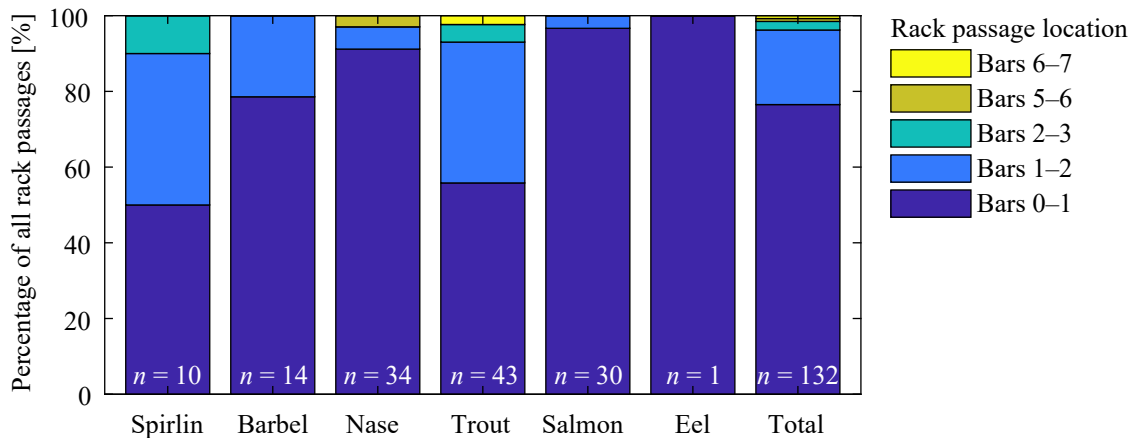
For most species, only  $\approx 10$ – $20\%$  of all individuals which passed through the rack, interacted with the bypass beforehand (cf. Table 7.11). For spirlin and eel, only few rack passages were observed, such that the result has to be interpreted with caution. For spirlin, three out of the six individuals, which interacted with the bypass prior to the rack passage, were tested with the restrictor bypass. However, too few rack passages were observed to conduct the analysis for different bypass configurations. In summary, most fish which passed through the HBR did not

interact with the bypass, which indicates that the bypass was generally well accepted. It can also be concluded that FGE and FPE were not considerably reduced due to potentially unfavorable hydraulic conditions at the bypass inlet.

### 7.4.2 Vertical and horizontal location of rack passages

#### Vertical location

The vertical location of the rack passages was determined visually from the video recordings of the submerged cameras. The horizontal bars were numbered from bottom to top starting with 1, such that “Bars 0–1” in Fig. 7.22 means that fish passed through the HBR between the bottom and the lowermost bar. Figure 7.22 shows the percentage of all rack passages between different bars for each species individually, and in total, which includes all rack passages independent of the species. The number  $n$  indicates the absolute number of fish which were considered for the analysis. No fish passed through the bars 3–5 or >7, while all species showed a strong tendency to pass through the rack very close to the bottom. A total of 77% of all fish passed the rack below the first bar and 97% of the rack passages occurred between the bottom and the second bar, which is equivalent to passing through the rack within 5 cm from the bottom ( $2s_b + t_b$ ; cf. Fig. 4.10 in Section 4.2). Due to different flow depths, the information of the vertical rack passage location cannot be directly transferred to prototype situations (details in Section 7.7). However, this analysis shows that the transition from the flume bottom to the rack is crucial in ethohydraulic experiments to reduce model effects. In the present study, the HBR was connected with a spacer to the flume bottom, which is the most conservative construction in terms of fish guidance (cf. Fig. 4.10 in Section 4.2).

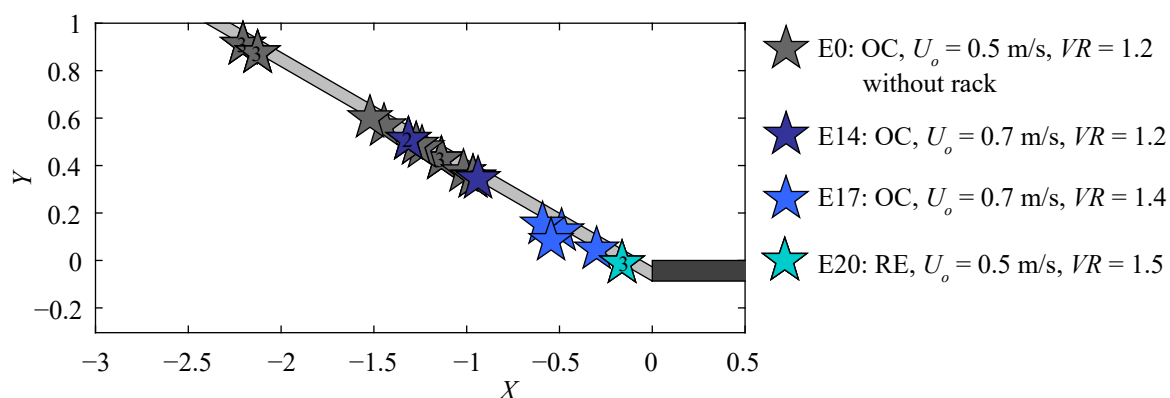


**Fig. 7.22:** Vertical rack passage location, where the bars are numbered from bottom to top (data adapted from Flury, 2019)

#### Horizontal location

The horizontal rack passage locations were extracted from the fish swimming tracks by taking the coordinates of the last data point prior to the rack passage. In contrast to block-type HPPs, FGC and  $V_n$  are very homogeneous along HBRs at diversion HPPs (details in Chapter 5). It is therefore expected that the rack passage location was not primarily affected by the velocity

components  $V_p$  and  $V_n$ . Without a rack installed, most spirlin passed the HBR-axis near the rack center (Fig. 7.23). While no rack passages of spirlin were observed for  $U_o = 0.5$  m/s, and  $VR = 1.2$  (E2, Fig. 7.7), all rack passages occurred close to the rack center for  $U_o = 0.7$  m/s and  $VR = 1.2$  (E14). In contrast, for larger  $VR$ , spirlin passed through the HBR close to the bypass inlet (E17, E20). This indicates that they were partially guided along the HBR and hesitated to enter the bypass, which increased the rack passage risk close to the bypass inlet. No clear pattern of the horizontal rack passage location was found for the other species, as they were passing through the rack at all horizontal locations.



**Fig. 7.23:** Horizontal rack passage location of spirlin for different configurations, where the numbers on the data points indicate that more than one fish passed the HBR at this location

### 7.4.3 Rheotaxis during rack passages

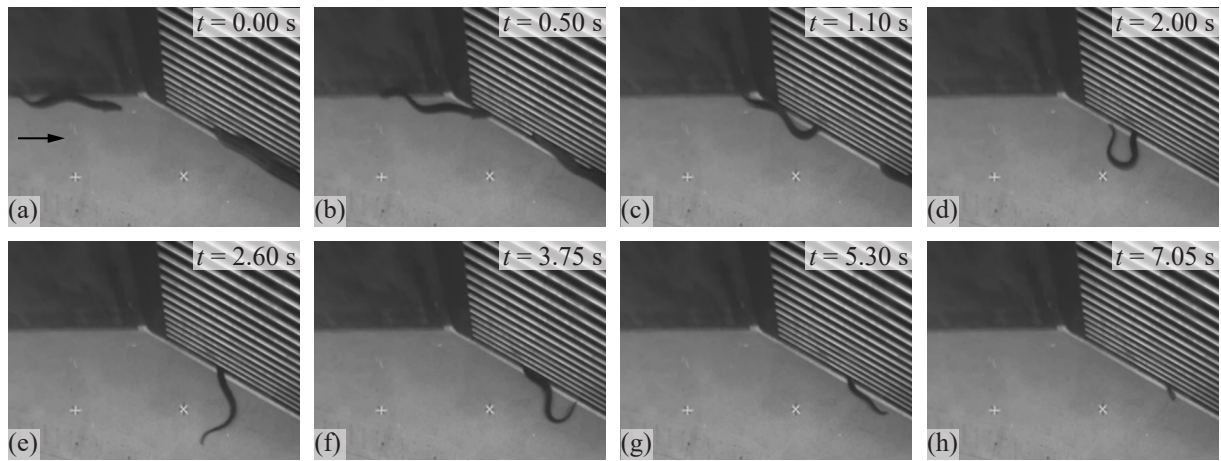
Clear species-specific differences were observed when fish passed through the HBR, which can be expressed by their rheotaxis during rack passage summarized in Table 7.12. All spirlin which passed through the HBR approached it slowly and carefully with positive rheotaxis, which none of them changed during the passage itself (Table 7.12). Some spirlin were oriented in stream-wise direction, while others were swimming towards the rack and were therefore aligned rack-parallel during passage. With the exception of one specimen, all barbels passed through the HBR with positive rheotaxis (Table 7.12). Three other barbels approached the rack from the side with their head-first, but they changed to positive rheotaxis before passing the HBR. All nase approached the HBR with positive rheotaxis and the vast majority of them swam towards the rack and passed it rack-parallel. Five nase turned from positive to negative rheotaxis directly in front of the HBR and actively passed it (Table 7.12). While the individuals of most species passed the HBR predominantly with positive rheotaxis, one third of trout did it with negative rheotaxis. Trout seemed less cautious than other species. Multiple specimens approached the HBR with negative rheotaxis and directly passed it without slowing down or showing any signs of hesitation. In contrast, all salmon parr passed the HBR with positive rheotaxis (Table 7.12). Some of them approached the HBR with negative rheotaxis, but they changed to positive rheotaxis right in front of the rack to pass it. Only one eel with  $TL = 47$  cm passed the HBR without electrification. It swam along the left flume wall with negative rheotaxis (Fig. 7.24a). After passing the rack between the bottom and the first bar with its head (Fig. 7.24b,c), the eel squeezed itself through the HBR by active swimming movements (Fig. 7.24d–h). The rheotaxis



during rack passage can give valuable insights in the species-specific behavior at fish guidance structures. For example, it is expected that fish which approached and passed the HBR with positive rheotaxis, such as spirlin, can be protected easier with behavioral barriers like electric fields. The reason is that fish which passed the HBR frequently with negative rheotaxis, like trout, have a smaller reaction scope at barriers.

**Table 7.12:** Number of fish which passed through the HBR with positive and negative rheotaxis

	Spirlin	Barbel	Nase	Trout	Salmon	Eel	Total
$n$ positive [–]	10	13	29	29	30	0	110
$n$ negative [–]	0	1	5	14	0	1	22
Percentage positive [%]	100	93	85	67	100	0	83



**Fig. 7.24:** An eel with  $TL = 47$  cm which actively passed through the HBR with  $U_o = 0.5$  m/s,  $VR = 1.2$ , and  $s_b = 20$  mm (Video: <http://dx.doi.org/10.3929/ethz-b-000450740>)

#### 7.4.4 Rotation during rack passages

In the present study, only small fish were tested (Table 7.1), such that the vast majority could have physically passed through the HBR with  $s_b = 20$  mm, as  $w_f < s_b$  (cf. Section 2.2.6). However, for many fish the body height should have restricted them from passing through the HBR in a regular swimming position, unless they would turn to their side, that is, rotate themselves over the longitudinal axis. As an example, the average total length of trout was  $\overline{TL} = 14.3$  cm (Table 7.1). The average trout width and height can be calculated with Eq. (2.1) and (2.2) with  $w_{f,rel} = 0.10$  and  $h_{f,rel} = 0.19$  from Table 2.2 to  $w_f = 1.4$  cm and  $h_f = 2.7$  cm, making it impossible for an average-sized trout to pass through the HBR with  $s_b = 20$  mm without turning to its side. In contrast, the smallest fish tested were nase with an average total length of  $\overline{TL} = 7.1$  cm and a maximum of  $TL_{max} = 9.3$  cm (Table 7.1). With Eq. (2.2) and  $h_{f,rel} = 0.24$  (Table 2.2), the average absolute fish height is  $\overline{h_f} = 1.7$  cm with a maximum of  $h_{f,max} = 2.2$  cm. Most nase were therefore able to pass through the rack in a regular swimming position and even the largest nase had to rotate only slightly to fit through the HBR with  $s_b = 20$  mm. Based on a visual analysis of the video recordings, Table 7.13 lists the absolute number of fish  $n$  which

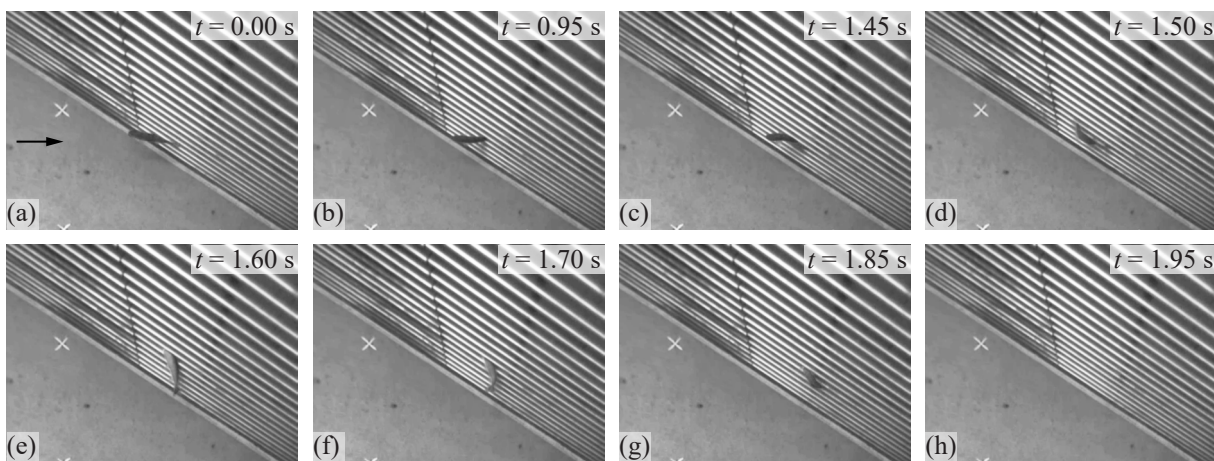


rotated during rack passage and the number of fish which did not rotate during rack passage, that is, the latter passed through the HBR in a regular swimming position. While smaller fish, mainly nase, spirlin, and salmon parr, were mostly turning only slightly to their sides, larger individuals, mainly trout and barbels, sometimes rotated by  $90^\circ$  to pass the HBR. The numbers in Table 7.13 cannot be generalized as they are very size-dependent, but they indicate that a non-negligible percentage of various fish species rotated themselves to pass through the HBR. This is of practical relevance, as it indicates that HBRs work as physical barriers only if  $s_b < w_f$  for fish with  $h_f > w_f$ .

**Table 7.13:** Number of fish which either rotated or did not rotate to pass through the HBR

	Spirlin	Barbel	Nase	Trout	Salmon	Eel	Total
$n$ rotation [–]	2	5	6	16	4	0	34
$n$ no rotation [–]	8	9	28	27	26	1	98
Percentage rotation [%]	20	36	18	37	13	0	26

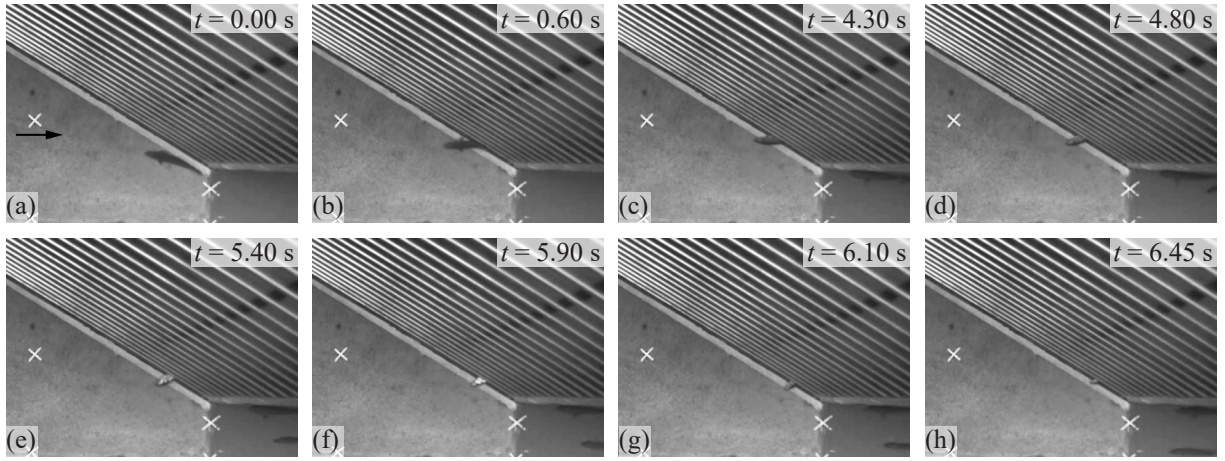
As an example of a rotation during rack passage, Fig. 7.25 shows a trout with  $TL = 15.4$  cm ( $w_f = 1.5$  cm and  $h_f = 2.9$  cm), which was tested with  $U_o = 0.5$  m/s,  $VR = 1.2$ , and  $s_b = 20$  mm. It was therefore impossible for the trout to pass through the HBR in a regular swimming position. After several unsuccessful rack passage attempts, the trout swam in front of the HBR with positive rheotaxis (Fig. 7.25a), before it sensed the flow between the bars 4 and 5 with its caudal fin (Fig. 7.25b). It then started to gain momentum (Fig. 7.25c,d) and actively pushed itself head-first through the bars 6–7 (Fig. 7.25e,f), before disappearing behind the HBR (Fig. 7.25g,h). This rack passage was very active and dynamic. While one and a half seconds passed between Fig. 7.25a and Fig. 7.25c, only half a second elapsed between Fig. 7.25c and Fig. 7.25h.



**Fig. 7.25:** A trout with  $TL = 15.4$  cm,  $w_f = 1.5$  cm, and  $h_f = 2.9$  cm which rotated itself to actively pass through the HBR with  $s_b = 20$  mm (Video: <http://dx.doi.org/10.3929/ethz-b-000450740>)

Another example is shown in Fig. 7.26, where a barbel passed through the HBR with  $U_o = 0.5$  m/s,  $VR = 1.2$ , and  $s_b = 20$  mm. The barbel had a total length of  $TL = 15.1$  cm, leading to  $w_f = 1.7$  cm and  $h_f = 2.6$  cm. It swam downstream along the right flume wall with positive

rheotaxis, before it approached the rack in front of the bypass entrance (Fig. 7.26a). It then aligned itself with the main flow direction and used its caudal fin to sense the flow between the bottom and the first bar (Fig. 7.26b). As soon as its dorsal fin touched the first bar, the barbel started to rotate itself (Fig. 7.26c,d) until it reached a fully lateral position (Fig. 7.26e). Then, the barbel made purposeful movements and actively worked itself through the rack (Fig. 7.26f,g). At last, only the nose was visible in front of the rack (Fig. 7.26h), before the barbel disappeared behind the HBR on the next frame. In contrast to the rack passage of the trout in Fig. 7.25, the barbel in Fig. 7.26 maintained its positive rheotaxis throughout the whole rack passage and it passed the HBR rather slowly. More than six seconds passed between Fig. 7.26a and Fig. 7.26h.

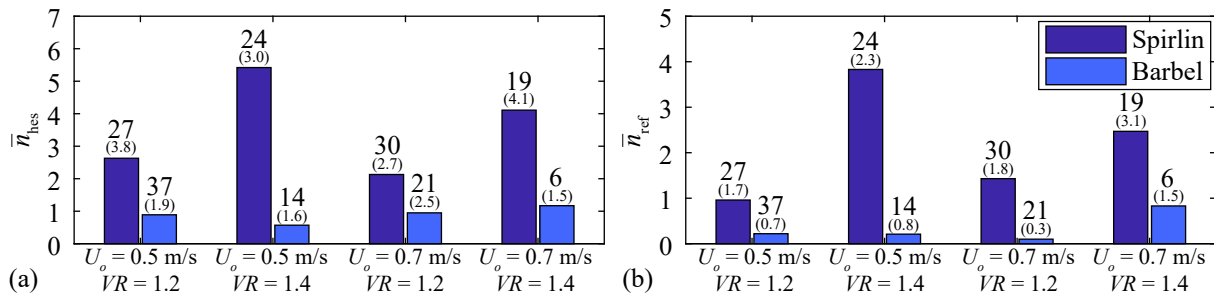


**Fig. 7.26:** A barbel with  $TL = 15.9$  cm,  $w_f = 1.7$  cm, and  $h_f = 2.6$  cm which rotated itself to pass through the HBR with  $s_b = 20$  mm (Video: <http://dx.doi.org/10.3929/ethz-b-000450740>)

The detailed analysis of all rack passages revealed that fish of various species rotate themselves, to a certain extent, to pass through the HBR. This means that the suggestion of Ebel (2016) to design HBRs such that  $s_b < w_f$  for the target fish species and size is appropriate (cf. Section 2.2.6). However, this approach is conservative as it assumes that all fish rotate themselves to pass through HBRs.

## 7.5 Fish swimming behavior at the bypass inlet

The flow conditions at the bypass inlet are very important for the bypass acceptance. If the flow conditions at the bypass inlet are not ideal, fish need several attempts to accept it, which increases the rack passage risk. Figure 7.27 shows the average number of hesitations at the bypass inlet per fish  $\bar{n}_{\text{hes}}$  and the bypass refusals per fish  $\bar{n}_{\text{ref}}$ , defined in Section 4.4.3, for spiralin and barbel for different flow conditions at the full depth open channel bypass without electrification. With the restrictor bypass, a sufficient number of observations was made only for spiralin with  $U_o = 0.5$  m/s and  $VR = 1.5$  (E20 in Table 4.3), where  $\bar{n}_{\text{hes}} = 10.3 \pm 6.1$  ( $\mu \pm \sigma$ ) and  $\bar{n}_{\text{ref}} = 3.6 \pm 2.0$ , based on  $n = 18$  observations.



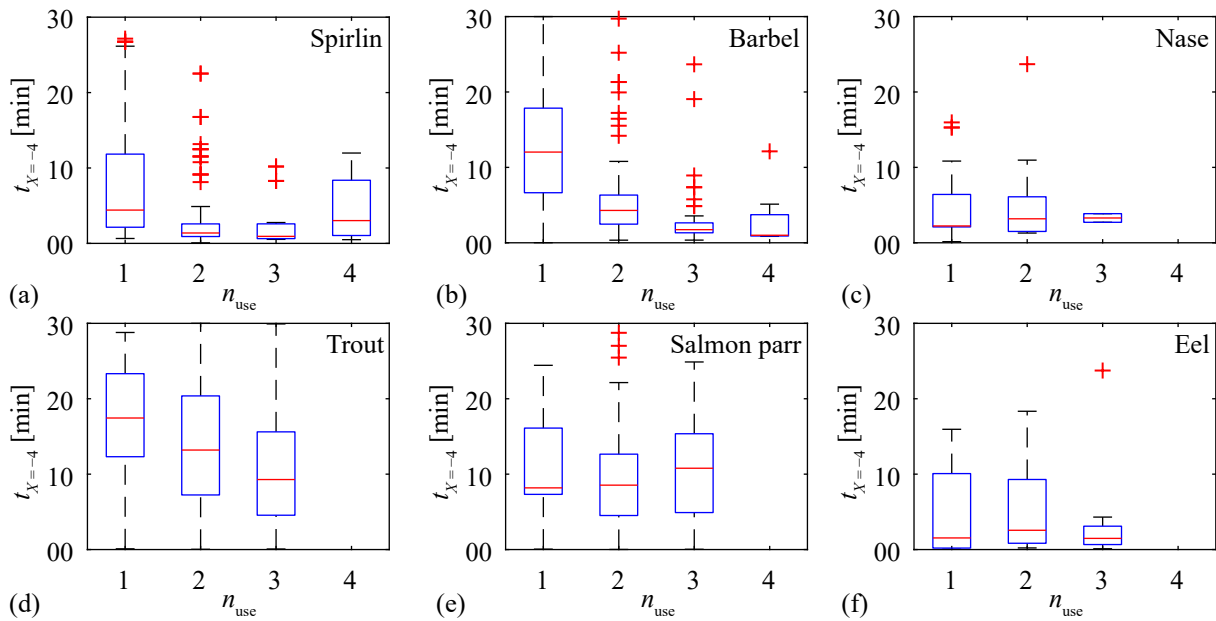
**Fig. 7.27:** The average number of (a) hesitations at the bypass inlet per fish  $\bar{n}_{hes}$  and (b) bypass refusals per fish  $\bar{n}_{ref}$  for spirlin and barbel as a function of  $U_o$  and  $VR$  at the full depth open channel bypass; the numbers above the bars indicate how many fish were considered for the analysis and the standard deviations are shown in parenthesis (data from Baumgartner, 2020)

Averaged over all configurations, spirlin hesitated more often at the bypass inlet ( $\bar{n}_{hes} = 3.4 \pm 3.6$ ) than barbels ( $\bar{n}_{hes} = 0.9 \pm 2.0$ ; t-test,  $t_{176} = 1.97$ ,  $p < 0.0001$ ) and spirlin refused the bypass inlet more often ( $\bar{n}_{ref} = 2.1 \pm 2.5$ ) than barbels ( $\bar{n}_{ref} = 0.2 \pm 0.7$ ; t-test,  $t_{176} = 1.97$ ,  $p < 0.0001$ ). Spirlin hesitated more often at the bypass inlet for  $VR = 1.4$  ( $\bar{n}_{hes} = 4.8 \pm 3.6$ ) than for  $VR = 1.2$  ( $\bar{n}_{hes} = 2.4 \pm 3.3$ ; t-test,  $t_{98} = 1.98$ ,  $p < 0.001$ ) and also refused the bypass inlet more often for  $VR = 1.4$  ( $\bar{n}_{ref} = 3.2 \pm 2.7$ ) than for  $VR = 1.2$  ( $\bar{n}_{ref} = 1.2 \pm 1.8$ ; t-test,  $t_{98} = 1.98$ ,  $p < 0.0001$ ). This is in line with the analysis of FGE and FPE in Section 7.2, where it was shown that an increased  $VR$  led to a statistically reduced number of bypass passages and increased number of refusals (cf. Fig. 7.7 and Table 7.2). No statistically significant effects were observed for differences in  $U_o$  or for the behavior of barbels. Spirlin hesitated more often at the restrictor bypass ( $\bar{n}_{hes} = 10.3 \pm 6.1$ ) than at the full depth open channel bypass ( $\bar{n}_{hes} = 3.9 \pm 3.7$ ; t-test,  $t_{67} = 2.00$ ,  $p < 0.0001$ ), but they did not refuse the restrictor bypass ( $\bar{n}_{ref} = 3.0 \pm 2.0$ ) significantly more often than the full depth open channel bypass ( $\bar{n}_{ref} = 2.3 \pm 2.5$ ; t-test,  $t_{67} = 2.00$ ,  $p > 0.1$ ). This is because spirlin often hesitated to enter the restrictor bypass due to the accelerating flow, but instead of leaving the bypass area to the upstream, they often stayed in front of the restrictor in the area with reduced flow velocities. In summary, spirlin reacted more sensitive to larger velocity ratios at the bypass inlet than barbels and spirlin hesitated more often for larger velocity ratios, while the approach flow velocity did not affect the result in the range of  $U_o = 0.5$ – $0.7$  m/s. This analysis shows that the fish behavior can vary strongly between species and that small velocity ratios at the bypass inlet are beneficial to guide spirlin efficiently without or with little delay into the bypass.

## 7.6 Fish activity during live fish tests

Independent of the test configuration, Fig. 7.28 shows the time fish needed to reach the position  $X = -4$ ,  $t_{X=-4}$ , which is a measure for the fish activity, for all tested species. A small number of  $t_{X=-4}$  means that fish swam out of the acclimatization compartment soon after the start of the experiment and were therefore active. The  $x$ -axis  $n_{use}$  in Fig. 7.28 indicates the usage, that is,  $n_{use} = 1$  means that fish were considered during their first use only, and so forth. In general, spirlin, nase, and eels were more active than salmon parr and trout (Fig. 7.28). Spirlin were significantly less active during their first use ( $t_{X=-4} = 8.06 \text{ min} \pm 7.53 \text{ min}$ ;  $\mu \pm \sigma$ ) compared

to their second use ( $t_{X=-4} = 3.15 \text{ min} \pm 4.37 \text{ min}$ ; t-test,  $t_{255} = 1.97$ ,  $p < 0.0001$ ; Fig. 7.28a), while the differences were not significant between  $n_{\text{use}} = 2, 3$  (t-test,  $t_{144} = 1.98$ ,  $p > 0.1$ ) and  $n_{\text{use}} = 3, 4$  (t-test,  $t_{38} = 2.02$ ,  $p > 0.05$ ). A very similar trend was observed for barbel which were significantly less active for  $n_{\text{use}} = 1$  ( $t_{X=-4} = 12.94 \text{ min} \pm 7.87 \text{ min}$ ) than for  $n_{\text{use}} = 2$  ( $t_{X=-4} = 6.02 \text{ min} \pm 6.23 \text{ min}$ ; t-test,  $t_{122} = 1.98$ ,  $p < 0.0001$ ; Fig. 7.28b). The activity of trout increased significantly from  $n_{\text{use}} = 1$  ( $t_{X=-4} = 17.20 \text{ min} \pm 7.52 \text{ min}$ ) to  $n_{\text{use}} = 2$  ( $t_{X=-4} = 14.43 \text{ min} \pm 8.10 \text{ min}$ ; t-test,  $t_{141} = 1.98$ ,  $p < 0.05$ ), and from  $n_{\text{use}} = 2$  to  $n_{\text{use}} = 3$  ( $t_{X=-4} = 11.07 \text{ min} \pm 7.66 \text{ min}$ ; t-test,  $t_{155} = 1.98$ ,  $p < 0.01$ ; Fig. 7.28d), while no statistically significant differences were observed for nase, salmon parr, and eel (Fig. 7.28c,e,f). Very inactive fish, which did not leave the acclimatization compartment within the maximal experimental duration, were not considered in the analysis in Fig. 7.28. The species-specific activity was therefore also quantified by the share of fish with a valid reaction, that is, a bypass passage, a rack passage, or a refusal of the total number of tested fish, which is equivalent to  $n/N$  in Table 4.3. Without electrification, this share was only 55% for trout, while it was 97%, 94%, 90%, 88%, and 79% for spirlin, salmon parr, nase, eel, and barbel, respectively.



**Fig. 7.28:** The time fish needed to reach position  $X = -4$ ,  $t_{X=-4}$ , as a function of usage  $n_{\text{use}}$  for (a) spirlin, (b) barbel, (c) nase, (d) trout, (e) salmon parr, and (f) eel (adapted from Bianchi and Rovati, 2020)

The reasons for the increased activity of spirlin, barbel, and trout when tested more than once can be manifold. The usage  $n_{\text{use}}$  strongly correlated with the number of days fish were kept in the laboratory. It is not clear if fish were less active for  $n_{\text{use}} = 1$  in the present study, because it was their first experiment or because they had too little time to acclimatize to the laboratory conditions in the holding tanks. Lehmann *et al.* (2016) described that fish species with a distinct schooling behavior normally need between one or two experiments to adapt to the laboratory conditions and then showed their normal behavior for the next three to four days, before the activity decreased in further experiments. Lehmann *et al.* (2016) also found that the eel activity reduced after a couple of days in the laboratory. These findings agree well with the present

study. The decreased fish activity after several days, described by Lehmann *et al.* (2016), could be avoided in the present study by limiting the days fish were kept in the laboratory (cf. Section 4.4.3). From the analysis of the fish activity in the present study, it is recommended to increase the adaption time of spirlin, barbel, and trout in future ethohydraulic experiments. Instead of bringing fish to the laboratory on Mondays and start with the experiments on Tuesdays, they could be caught on Fridays, adapt to the laboratory in the holding tanks over the weekend, before the experiments could be started on Mondays. If experiments are conducted with trout, it must be considered that many individuals will not show any reaction within an experimental duration of 30 minutes.

## 7.7 Limitations and challenges when upscaling to prototype

The present study gives valuable insights in the behavior of various fish species at HBR-BSs under laboratory conditions. However, the results have to be carefully interpreted and some cannot be directly transferred from laboratory to prototype due to abiotic and biotic factors, which could not be mimicked with the current flume setup. This includes variations in environmental conditions, differences in the fish biology, and geometric restrictions. Environmental conditions encompass parameters such as turbidity, floating debris, changes in light conditions, discharge, or water temperature, which are often related to seasonal patterns and were not varied within the present live fish tests. The fish biology includes the natural behavior of fish, which can differ between ethohydraulic experiments due to stress from experimental handling, unnatural environment, small number of individuals affecting the schooling behavior, or the absence of predators. The geometric restrictions include the dimensions of the flume, the HBR, and the bypass. The HBR used for the live fish tests was only 2.3 m long. It is possible that the rack passage risk increases at longer racks, which means that FGE and FPE might be smaller at large HBRs than in the present live fish tests. The upstream channel width was limited to  $w_o = 1.50$  m, which means that the channel walls might had a disproportionately high effect. It was shown that barbels swam primarily along the flume walls and had therefore often no rack contact in the live fish tests conducted within the present thesis, which brings up the question if barbels are a suitable species to test the guidance efficiency of a rack in ethohydraulic experiments. The flow depth was limited to  $h_o = 0.90$  m, which means that fish which swam close to the bottom in the ethohydraulic experiments, do not necessarily swim close to the bottom at HPPs with larger approach flow depths. As an example, it was shown in Section 7.4 that all fish passed through the HBR close to the flume bottom, indicating that the transition from the bottom to the HBR is very important. Although it is likely that the guidance efficiency of HBR-BSs can be increased with bottom overlays, it should not be concluded from the present experiments that fish pass through all HBRs close to the bottom only. The relative bypass discharge varied between  $Q_{by,rel} = 9\text{--}17\%$  in the live fish tests of the present study (Fig. 5.13 and 5.14 in Section 5.5) and was therefore significantly larger than  $Q_{by,rel} = 2\text{--}5\%$ , which is typically recommended for HBR-BSs (Ebel, 2016). Due to size limitations of the flume,  $Q_{by,rel}$  could not be further reduced, without either narrowing the bypass, which would have made it



unsuitable as a downstream passage corridor, or reducing the velocity ratio  $VR$  which is essential for fish guidance. The results can nonetheless be transferred to prototype situations, if the flow conditions are similar. The ratio of the bypass width to the downstream channel width was  $w_{by}/w_{ds} = 0.22$  in the present study and therefore larger than at typical prototype situations. The relative bypass discharge  $Q_{by,rel}$  automatically reduces for smaller  $w_{by}/w_{ds}$ , when  $VR$  is kept constant. Another option to reduce  $Q_{by,rel}$  is to block the flow depth partially in the bypass, which was done with the inlet restrictor in the present study (cf. Fig. 4.6c). However, the fish swimming depth cannot be directly scaled from laboratory to prototype situations, such that the transferability of the results with the inlet restrictor is challenging. In the present experiments, no single fish passed through the top opening, while 38 bypass passages of spirlin, barbel, and eel were observed through the bottom opening. It cannot be certainly said, if fish did not use the top opening in the present live fish tests as they approached the bypass mostly close to the bottom or if they avoided it due to the hydraulic conditions, that is, the small overflow depth and the larger TKE (cf. 5.14 in Section 5.5). The present live fish tests were conducted during daytime, while it is known that eels primarily migrate from dusk till dawn (e.g. Brown *et al.*, 2007; Calles *et al.*, 2012; Egg *et al.*, 2017). Similarly, freshwater species showed higher downstream movement activity at dawn and during the first hours of the night in monitoring campaigns (e.g. Adam *et al.*, 2018; Zaugg and Mendez, 2018; described in Section 3.7.4). Infrared or near-infrared light with typical wavelength of 840–1200 nm, which is considered beyond the visible range of fish (Duncan, 1956; Beach, 1978), was used in multiple experiments to study the fish behavior in the darkness (e.g. Duncan, 1956; Beach, 1978; Kemp and Williams, 2009; Russon *et al.*, 2010; Vowles and Kemp, 2012; Vowles *et al.*, 2014). Water absorbs infrared light stronger than normal light. At least 96% of the incident radiation of infrared light with a wavelength of  $<860$  nm penetrates through each centimeter of pure water (Beach, 1978). This means that only  $\approx 0.96^{90} = 2.5\%$  of the incident infrared radiation reaches the flume bottom with a flow depth of  $h_o = 90$  cm. Studies where the fish behavior is observed with infrared light are therefore often limited to flow depth of  $h_o < 30$  cm. By observing juvenile Pacific salmonids approaching a submerged weir under light and dark (infrared light only) conditions, Kemp and Williams (2009) observed that when light was present, fish formed schools and actively explored the channel. Most fish swam with negative rheotaxis but they changed to positive rheotaxis to pass the weir. In contrast, without light, fish were holding their position with positive rheotaxis and did not form schools, showed less rheotaxis changes, and approached and passed the weir less often. Vowles and Kemp (2012) observed brown trout swimming downstream through a constricted flume section with accelerating flow under light and dark conditions. When light was present, trout were responding to the flow acceleration farther upstream and it took them longer to pass the constricted section (Vowles and Kemp, 2012). Similarly, Vowles *et al.* (2014) showed that juvenile Chinook salmon showed a more distinct avoidance behavior when passing through a small rectangular orifice with accelerating flow with illumination in comparison to without illumination. These studies show that the fish behavior also depends on the light conditions. In the present study with  $h_o = 0.90$  m, it was not feasible to observe fish in detail and track them when

dark. All experiments were therefore conducted during daytime (08:00-18:00) with constant indirect light (cf. Section 4.1.3). Due to the missing visual cues, it is possible that the guidance and protection efficiency of HBR-BSs is smaller when dark, which should be investigated in additional experiments. The present live fish tests give valuable insights in the fish behavior at HBR-BSs, which could have hardly been observed at prototype HPPs. However, due to the discussed limitations, ethohydraulic experiments have to be carefully interpreted and they cannot replace extensive monitoring campaigns.

## 7.8 Comparison with ethohydraulic studies and monitoring campaigns

Multiple ethohydraulic studies and monitoring campaigns were presented in Section 3.7.3 and 3.7.4, of which some are compared to the results of the live fish tests conducted within the present study. Comparing the results with all studies would go beyond the scope of this thesis, but the most important aspects are highlighted and discussed in the following.

### 7.8.1 Ethohydraulic studies

#### Important remarks for comparisons and definition of rack interaction

When the results of different ethohydraulic studies are compared to each other, it is crucial to carefully study the experimental setup, methods, and data analysis. A very important point is to distinguish between fish which interacted with the rack and which did not. Thereby, passive fish which stayed in the headwater throughout the whole experiment can be distinguished from fish actively refusing the rack. This is especially important for inactive species such as trout (cf. Fig. 7.28). Additionally, if fish entered the bypass without rack interaction, it should be acknowledged that they were not guided by the rack. In contrast to the present investigation and the study of Beck (2020) and Beck *et al.* (2020), it was not distinguished between bypass passages with and without rack interaction in the studies of Flügel *et al.* (2015) and Kriewitz (2015), Berger (2018), and Kammerlander *et al.* (2020). This may not be important for some species, while it can strongly affect the results of other species such as barbel, which prefer to swim along flume walls (cf. Section 7.2). This brings up the question on how to define rack interaction. In the present study, it was assumed that a fish interacted with the rack as soon as its track, which corresponded to the center point of a fish, crossed Sec5. This sector was defined as a 15 cm wide, rack-parallel area directly in front of the HBR (cf. Fig. 4.20). The HBR hardly affected the upstream flow field (cf. Section 5). It is therefore unlikely that fish were guided by the HBR without swimming through Sec5, although it is not impossible as fish could have possibly perceived the HBR visually. To assess the sensitivity of the rack interaction definition, the width of Sec5 was increased to 30 cm and the effect on FGE quantified. From all results shown in Section 7.2, the increased width of Sec5 affected the FGE of four configurations only. The effect on FGE was small for three configurations, that is, from FGE = 71% to 74% for E3 (barbel, OC,  $U_o = 0.5$  m/s,  $VR = 1.2$ ), FGE = 35% to 41% for E6 (salmon parr, OC,  $U_o = 0.5$  m/s,  $VR = 1.2$ ), and FGE = 88% to 90% for E14 (spiralin, OC,  $U_o = 0.7$  m/s,  $VR = 1.2$ ).

The percentaged increase of FGE was large for one configuration only, that is, for E17 (spirlin, OC,  $U_o = 0.7$  m/s,  $VR = 1.4$ ) where  $FGE = 14\%$  increased to  $29\%$ . This rather large increase has to be interpreted with caution, as only few specimens showed a valid reaction for this configuration (cf. Fig. 7.7). Summed up, distinguishing between bypass passages with and without rack interaction can play an important role, especially for species such as barbel which prefer to swim along flume walls. In contrast, the overall results were only slightly affected if the width of the rack-parallel sector, Sec5, was doubled from 15 cm to 30 cm, which indicates a robust definition of rack interaction. Using the smaller sector width of 15 cm is more conservative. However, these findings cannot be generalized to other rack types or hybrid barriers, which may provoke avoidance reactions further upstream.

### Curved-bar rack

The live fish tests of the present study were conducted in the same time period, in the same laboratory flume, and with the same fish as the investigation of the curved-bar rack (CBR) by Beck (2020) and Beck *et al.* (2020), allowing for a direct comparison of the results. Therefore, another set of GLMs was set up with the HBR data of the present study and the CBR data of Beck (2020). The model setup was identical to the GLMs described in Section 7.2.3, but the additional independent variable “rack type” was added, where the HBR was used as the reference category. The AICs and BICs of all possible interactions, including the full model with a 3-way interaction between  $VR$ ,  $U_o$ , and the rack type are listed in Table A.1 in Appendix A.1. Depending on the dependent variable and on the information criteria (AIC/BIC), different models were more suitable. However, due to the small differences of AIC/BIC from the main model compared to the models including the interaction terms and for the sake of simplicity, the main model without interactions was used for further analyses. The Tables A.2, A.3, and A.4 summarize the results of the GLMs with bypass passage, rack passage, and refusal as the dependent variables, respectively. The rack type significantly affected the bypass passages, rack passages, and refusals (Tables A.2–A.4, Appendix A.1). The installation of the CBR instead of the HBR with  $s_b = 20$  mm led to more bypass passages and refusals, while it reduced the number of rack passages. Different species reacted very differently to the CBR and the HBR, making it necessary to draw species-specific conclusions.  $\chi^2$ -tests were conducted with all CBR-data from Beck (2020) and all HBR-data from the present thesis with OC,  $U_o = 0.5, 0.7$  m/s,  $VR = 1.2, 1.4$ , and  $s_b = 20$  mm for the HBR. No significant differences in the number of bypass passages, rack passages, and refusals were found for barbels and salmon parr. Spirlin passed through the HBR more frequently ( $p = 0.046$ ,  $\chi^2 = 3.999$ ), although no rack passages were observed for  $U_o = 0.5$  m/s (cf. Fig. 7.7). For trout, significantly more refusals were observed with the CBR ( $p = 0.001$ ,  $\chi^2 = 11.812$ ), but the differences in the number of rack passages and bypass passages were not significant. The most obvious differences were observed for nase, where the installation of the CBR led to less rack passages ( $p < 0.001$ ,  $\chi^2 = 43.392$ ) and more bypass passages ( $p < 0.001$ ,  $\chi^2 = 47.043$ ). This result is very interesting, as the tested nase were small ( $TL < 10$  cm, cf. Table 7.1) and the clear bar spacing at the upstream tip of the bars was  $s_b = 20$  mm for the HBR and  $s_b = 50$  mm for the CBR (details in Beck, 2020). This comparison



shows that the behavioral protection effect of the CBR was larger than for the HBR for juvenile nase. The main difference between the two rack types is that the CBR induces strong hydraulic signatures in between the bars and slightly upstream (details in Beck, 2020), whereas this is not the case for the HBR. Juvenile nase seem to react very sensitively to these different flow regimes. In contrast, the CBR led to significantly more rack passages ( $p = 0.002$ ,  $\chi^2 = 9.492$ ) and less bypass passages ( $p = 0.008$ ,  $\chi^2 = 7.116$ ) for eels. This indicates that most eels were physically protected by the HBR and that eels did hardly react to the hydraulic signatures of the CBR.

### **Berger (2018): horizontal bar rack bypass systems**

The live fish tests of Berger (2018), briefly introduced in Section 3.7.3, addressed very similar research questions with a comparable approach to the present study. However, some findings of these two studies differ starkly and are therefore discussed in this section. While the average FPE of salmon parr was 37% in the present study (Section 7.2), Berger (2018) found  $\text{FPE} = 100\%$ ,  $\text{FPE} \approx 608/610 = 99.7\%$ , and  $\text{FPE} \approx 173/182 = 95\%$  for  $s_b = 10$  mm,  $s_b = 18$  mm, and  $s_b = 30$  mm, respectively (cf. Section 3.7.3). To explain these different findings, the biology and handling, and the hydraulics and the experimental setup of the live fish tests with salmon smolts of Berger (2018) are compared to the present study in Table 7.14. Additional variations were caused by not excluding fish which did not interact with the HBR in the study of Berger (2018), as discussed earlier in this section.

**Table 7.14:** Differences in the biology, handling, hydraulics, and experimental setup of the live fish tests with salmon of Berger (2018) and the present study

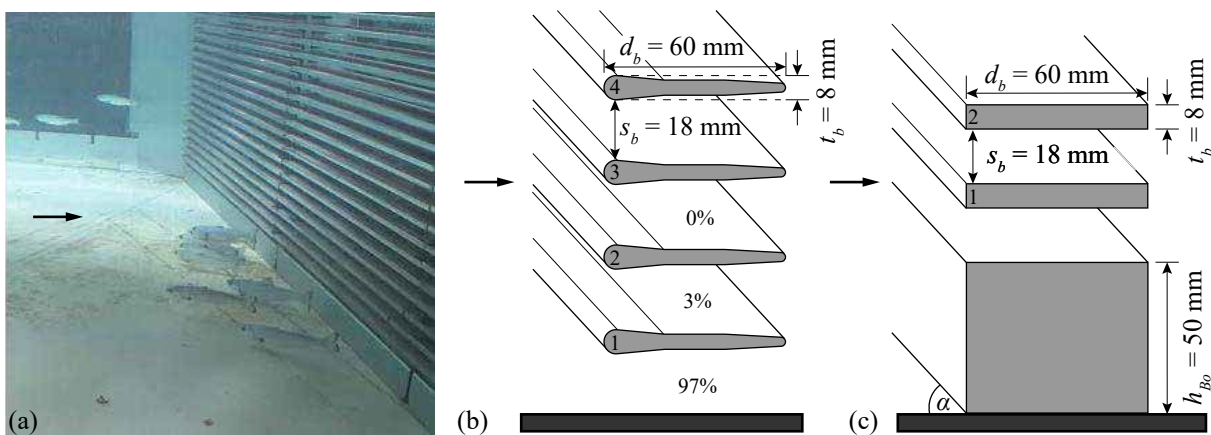
		Berger (2018)	Present study
Biology and handling	Life stage	Smolts	Parr
	Origin	Hatchery-reared	Wild fish
	Average fish length	$\overline{TL} = 16 \text{ cm}$	$\overline{TL} = 11 \text{ cm}$
	Average fish width	$\overline{w_f} = 1.6 \text{ cm}^3$	$\overline{w_f} = 1.1 \text{ cm}^3$
	Average fish height	$\overline{h_f} = 2.9 \text{ cm}^4$	$\overline{h_f} = 2.0 \text{ cm}^4$
	Number of fish per exp.	13	3
	Max. number of usages	4	4
	Max. exp. duration	95 min	30 min
	Water temperature	$T = 18\text{--}20^\circ\text{C}$	$T = 12\text{--}16^\circ\text{C}$
Hydraulics and experimental setup	Upstream channel width	$w_o = 2.0 \text{ m}$	$w_o = 1.5 \text{ m}$
	Bypass width	$w_{by} = 0.20 \text{ m}$	$w_{by} = 0.25 \text{ m}$
	Approach flow velocity	$U_o = 0.4, 0.5, 0.7, 0.8 \text{ m/s}$	$U_o = 0.5, 0.7 \text{ m/s}$
	Approach flow depth	$h_o = 0.60\text{--}0.80 \text{ m}^1$	$h_o = 0.90 \text{ m}$
	Velocity ratio bypass	$VR \approx 1.0^2$	$VR = 1.2, 1.4$
	Transition rack-bypass	Without bypass wall	Bypass wall
	Bar shape	Rectangular	Foil-shaped
	Bar spacing	$s_b = 10, 18, 30 \text{ mm}$	$s_b = 20 \text{ mm}$
	Approach flow angle	$\alpha = 30, 45, 55, 70^\circ$	$\alpha = 30^\circ$
	Bottom overlay	Bottom overlay, $h_{Bo} = 5 \text{ cm}$	Without bottom overlay

<sup>1</sup> Depending on  $U_o$ <sup>2</sup> The flow velocities in the bypass could not be regulated independently of the approach flow velocity<sup>3</sup> Calculated from  $\overline{TL}$  with Eq. (2.1) and  $w_{f,rel} = 0.10$  from Table 2.2<sup>4</sup> Calculated from  $\overline{TL}$  with Eq. (2.2) and  $h_{f,rel} = 0.18$  from Table 2.2

From all differences in the biology and handling in Table 7.14, it is assumed that the size range of the individual fish tested, and thus their body dimensions, had the largest effect on the result. The permeability index (cf. Section 2.2.6) of the present study with salmon parr was  $PI = s_b/w_f = 1.82$ , whereas it was  $PI = 1.13$  and  $PI = 1.88$  in the study of Berger (2018) for  $s_b = 18 \text{ mm}$  and  $s_b = 30 \text{ mm}$ , respectively. Due to the similar  $PI$ , the results of Berger (2018) with  $s_b = 30 \text{ mm}$  should be used for comparisons with the present study.  $FPE \approx 95\%$  in the study of Berger (2018) with  $s_b = 30 \text{ mm}$ , while  $FPE = 37\%$  in the present study, indicating that these variations were not primarily caused by the different fish dimensions. Most parameters in the hydraulics and the experimental setup in Table 7.14 are comparable. It is therefore not assumed that the large differences of the number of rack passages of salmon was primarily caused by variations of  $w_o$ ,  $w_{by}$ ,  $U_o$ ,  $h_o$ ,  $VR$ , the transition between the rack and the bypass,  $s_b$ , or  $\alpha$ . However, it is very difficult to assess the effect of the bar shape, because studies are missing, where the effect of the bar shape on the guidance efficiency was analyzed, while all other parameters were kept constant. Rectangular bars lead to larger flow separation zones, which might trigger avoidance reactions and thereby increase fish protection. Additionally, the sharp edges and the long constricted section of rectangular bars potentially make rack passages more difficult.

From other studies, such as EPRI and DML (2001) and Flügel *et al.* (2015), Kriewitz (2015),

and Albayrak *et al.* (2020), where the exact same Louver and modified bar rack (MBR) configurations were tested with and without bottom overlays, it is known that bottom overlays significantly increase FGE and reduce the number of rack passages in ethohydraulic experiments for various fish species. As an example, FPE of brown trout increased from 83% to 100% for a MBR with  $\alpha = 15^\circ$ ,  $s_b = 50$  mm,  $U_o = 0.6$  m/s, and a bar angle of  $45^\circ$  (cf. Fig. 2.15) with a bottom overlay of  $h_{Bo} = 0.10$  m (Flügel *et al.*, 2015; Kriewitz, 2015; Albayrak *et al.*, 2020). In other words, four out of 23 brown trout passed through the MBR without a bottom overlay, while no rack passages were observed with a bottom overlay. In the experiments of Berger (2018), the lowest 5 cm of the HBR were blocked by a beam, which acted as a bottom overlay (Fig. 7.29a). Berger (2018) highlighted that most salmon smolts preferred to swim close to the bottom or areas with reduced flow velocities, that is, in front of the bottom overlay or at the upstream rack end in front of the wedge, which was installed to create a smooth transition from the channel wall to the HBR (Fig. 7.29a). It is therefore very likely that the bottom overlay in the study of Berger (2018) strongly affected the number of rack passages. Figure 7.29 shows the to-scale transition from the flume bottom to the HBR of the present study (Fig. 7.29b) and the study of Berger (2018) (Fig. 7.29c). The bars are numbered in ascending order from bottom to top and the percentages between the bars in Fig. 7.29b indicate the rack passage location of the salmon parr in the present study (cf. Fig. 7.22). All rack passages occurred in the lowest 5 cm of the flume, which was blocked in the experiments of Berger (2018). It must therefore be assumed that the large guidance efficiencies of salmon smolts in the study of Berger (2018) were at least partly caused by the bottom overlay and not the HBR itself. The argument that HBRs are built with bottom overlays in prototype is not conclusive, because the swimming depth of fish cannot be directly transferred from laboratory studies (cf. Section 7.7). Although some salmon smolts may migrate downstream near the bottom at shallow rivers, most studies indicate that they prefer the upper water column (cf. Section 2.2.6).



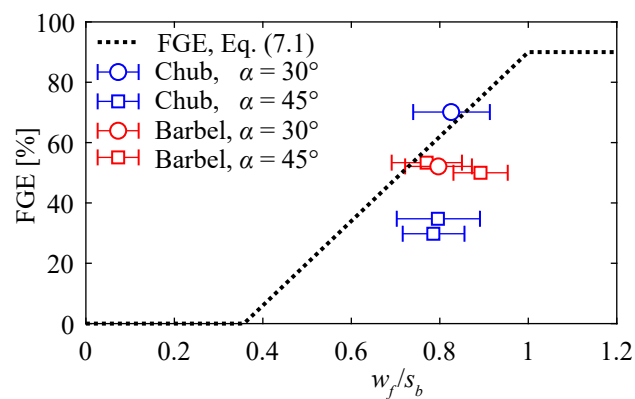
**Fig. 7.29:** (a) Picture of the live fish tests of Berger (2018) with salmon smolts primarily swimming upstream of the bottom overlay at the HBR with  $U_o = 0.7$  m/s,  $s_b = 18$  mm, and  $\alpha = 55^\circ$  (Berger, 2018), (b) the transition from the bottom to the HBR of the present study and (c) the study of Berger (2018) (to scale)

Berger (2018) described that eels often changed their rheotaxis from negative to positive after rack contact and swam upstream instead of towards the bypass, which was independent of  $U_o$

and  $\alpha$ . It was concluded that the HBR guided only 5–10% of all eels. Lehmann *et al.* (2016) made similar observations but pointed out that eels were comparatively well guided for  $\alpha = 30^\circ$  in comparison to  $\alpha = 40^\circ$ . In the present study, 80% of the eels were guided along the HBR with  $\alpha = 30^\circ$  after the first rack contact, similarly to the eel shown in Fig. 7.6, while only 15% showed an avoidance reaction, and 5% passed through the HBR. The eels which showed an avoidance reaction approached the HBR rather passively, while all eels which approached the HBR with active and fast swimming movements were guided into the bypass. Possible reasons for these different findings are variations in  $\alpha$ , the bar shape, and the water temperature (Table 7.14). In contrast to the foil-shaped bars used in the present study, Lehmann *et al.* (2016) and Berger (2018) investigated rectangular bars with sharp edges, which might have caused these avoidance reactions (Fig. 7.29). The comparatively high water temperatures in the study of Berger (2018) might have reduced the eel activity and hence affected their behavior (Table 7.14). As described in Section 3.7.3, no rack passages of eels were observed by Berger (2018) for  $s_b = 10$  mm and  $s_b = 18$  mm. With  $w_{f,rel} = h_{f,rel} = 0.03$  from Table 2.2 and Eq. (2.3),  $TL_{crit} = 33$  cm and 60 cm for  $s_b = 10$  mm and 18 mm, respectively. The good protection of eels was expected, because most specimens had a length of  $TL > 60$  cm and therefore  $TL > TL_{crit}$ . However, the number of eels with  $TL < TL_{crit}$  tested in the study of Berger (2018) remains unknown (cf. Section 3.7.3). Nonetheless, the good eel protection for an HBR with  $s_b \leq 18$  mm is in line with the findings of the present study and observations at HPPs (e.g. Egg *et al.*, 2017). In summary, the large differences in the number of rack passages of salmon between the present study and the study of Berger (2018) is probably mainly a result of the bottom overlay and potentially also the different bar shape. The majority of eels was well protected with  $s_b \leq 18$ –20 mm in both studies.

### De Bie (2017): horizontal bar rack bypass systems

In the following, the live fish tests of de Bie (2017, Chapter 5) with HBR-BSs, which were briefly described in Section 3.7.3, are used to validate Eq. (7.1). The FGE was calculated as the number of bypass passages from all bypass and rack passages, thereby excluding inactive fish like in the present study (last column in Table 3.4). The data points in Fig. 7.30 were calculated for  $\overline{TL}$  and the error bars represent  $\overline{TL} \pm \sigma_{TL}$  (cf. Table 3.4).



**Fig. 7.30:** Validation of Eq. (7.1) with the live fish tests of de Bie (2017)

For  $\alpha = 30^\circ$ , for which Eq. (7.1) was developed, FGE could be very well predicted for chub and barbel (Fig. 7.30; chub:  $FGE = 70\%$ ,  $FGE_{\text{prediction}} = 65\%$ ; barbel:  $FGE = 52\%$ ,  $FGE_{\text{prediction}} = 62\%$ ). For  $\alpha = 45^\circ$ , FGE was overpredicted with Eq. (7.1) for all configurations (Fig. 7.30), but deviations are still small, considering all the uncertainties and differences between the two studies (e.g. different bypass width, fish species, flow velocities, bar shapes). As none of the tested fish could pass through the HBR in regular swimming position as  $h_f > s_b$  (cf. Table 3.4), the investigation of de Bie (2017) supports the findings of the present study, where it was observed that a non-negligible share of fish rotates themselves to pass through HBRs (cf. Section 7.4.4). The validation with the study of de Bie (2017) further confirmed that Eq. (7.1) can be applied to other fish species such as chub, HBRs with smaller  $s_b$ , and fish with smaller  $w_f$ . However, if the setup differs from the setup of the present investigation (e.g.  $\alpha = 45^\circ$  instead of  $\alpha = 30^\circ$ ), prediction accuracy reduces.

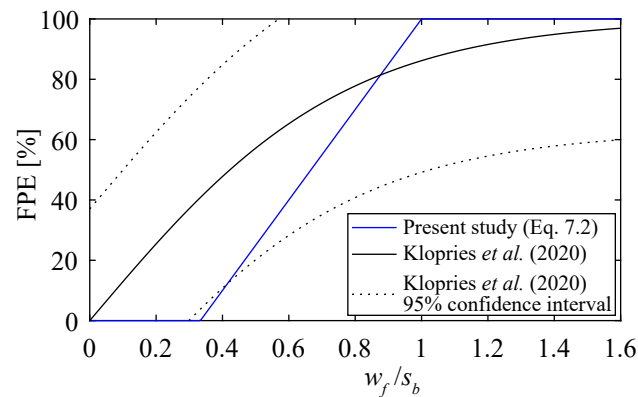
### **Böttcher *et al.* (2019b) and Kammerlander *et al.* (2020): flexible fish fence**

The flexible fish fence with and without electrification was investigated in a series of live fish tests, which were introduced in Section 3.7.3. Although some aspects of the flexible fish fence differ from HBR-BSs investigated in the present study, an interesting comparison can be made. Kammerlander *et al.* (2020) demonstrated that the FPE of the flexible fish fence with  $s_b = 10$  mm is almost 100% for trout, chub, and grayling with  $TL = 10$ –20 cm. Similarly, in the present study,  $FPE = 96\%$  for trout with  $\overline{TL} = 15.8$  cm at the HBR-BS with  $s_b = 15$  mm (Table 4.3 and Fig. 7.10). It is more difficult to compare the results with  $s_b = 20$  mm, because all fish which neither passed through the flexible fish fence nor entered the bypass were classified as “headwater” in the study of Kammerlander *et al.* (2020). It remains unknown how many fish swam in the area which was affected by the rack. Instead of comparing FGE and FPE with different definitions, the percentage of all bypass passages from all bypass and rack passages is compared in the following. For trout with  $s_b = 20$  mm, this percentage was 58% in the present study (cf. Fig. 7.10), while it was 25% in the study of Kammerlander *et al.* (2020) (cf. Table 3.5). The median total length of the trout tested with  $s_b = 20$  mm in the present study was 13.5 cm, compared to the median of 15.4 cm in Kammerlander *et al.* (2020). It cannot be said if these differences are a result of the different rack type or variations in the experimental setup, but both studies found that barriers with horizontal bars with  $s_b = 20$  mm cannot sufficiently protect trout with  $TL \approx 15$  cm. At the flexible fish fence, the probability of a rack passage of grayling was significantly larger than for trout, while it was lower for chub (cf. Table 3.5). Grayling and chub were not tested in the present study, but from the comparison with the results of Kammerlander *et al.* (2020) it can be assumed that HBR-BSs with  $s_b = 20$  mm do not sufficiently protect these species with  $TL = 10$ –20 cm. Similarly to the present study, Kammerlander *et al.* (2020) described that most rack passages occurred close to the flume bottom (cf. Section 7.4). Although not explicitly mentioned in Kammerlander *et al.* (2020), from the fish dimensions and  $s_b$ , multiple fish of all tested species must have turned to their sides to pass the flexible fish fence, which was also observed in the videos of the online supplement of Kammerlander *et al.* (2020).

**Klopries *et al.* (2020): fish protection efficiency of bar racks**

Up to now, an equation was missing to assess FPE of HBR-BSs. However, Klopries *et al.* (2020) published an equation to estimate FPE of adult eels at intake racks, which is based on a literature review including data from live fish tests and monitoring campaigns. A total of 16 data sets from inclined racks, traditional trash racks, angled bar racks, and Louvers were included with  $s_b = 20\text{--}90\text{ mm}$ ,  $\gamma = 35\text{--}90^\circ$ ,  $\alpha = 15\text{--}90^\circ$ , and minimal fish width of  $w_f = 13\text{--}19\text{ mm}$ , leading to Eq. (7.3). In Fig. 7.31, Eq. (7.3) is compared to the FPE prediction equation proposed within the present study (Eq. 7.2) for  $\alpha = 30^\circ$  and  $\gamma = 0^\circ$ .

$$\text{FPE} = \tanh\left(0.6499 \frac{w_f}{s_b \sin(\alpha) \sin(\gamma)}\right) \quad (7.3)$$



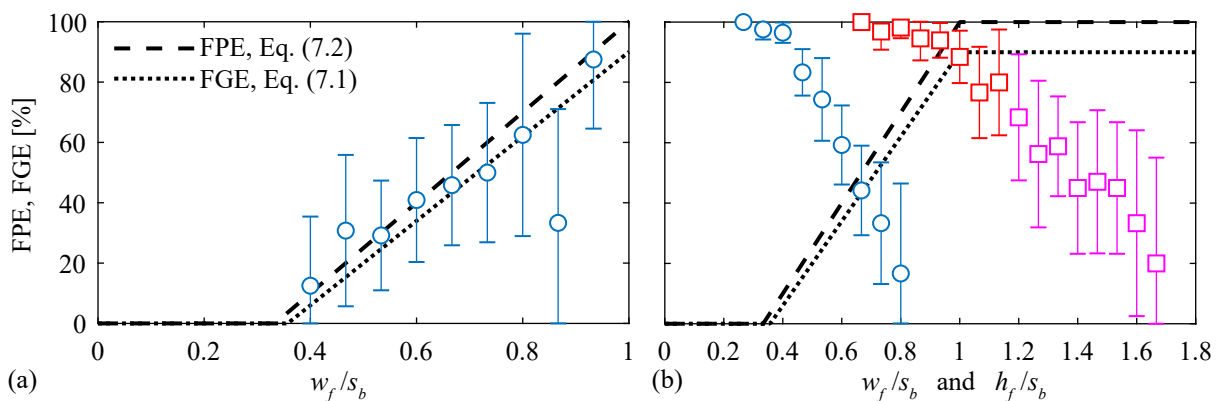
**Fig. 7.31:** Comparison of the FPE prediction equation proposed by Klopries *et al.* (2020) with Eq. (7.2) of the present study

Although the equation proposed within the present study lies almost entirely within the 95% confidence interval of the equation of Klopries *et al.* (2020), the maximal absolute deviation of FPE is up to 40% (for  $w_f/s_b = 0.33$ ). The main reasons are likely the different rack types and fish species. The rather large deviations for small  $w_f/s_b$  can be explained by the larger behavioral barrier effect of bar racks and Louvers as compared to the HBRs in the present study. This comparison shows that when Eq. (7.2) is applied to other rack types with a larger behavioral barrier effect, the estimation of FPE is likely to be conservative, in this case for all fish with  $w_f/s_b < 0.9$  (Fig. 7.31).

**7.8.2 Monitoring campaigns****HPP Rappenberghalde**

The radio-telemetry data from the monitoring campaign at HPP Rappenberghalde indicated a good guidance effect towards the downstream rack end, which was also observed in the present study. The stow net catches revealed that spirlin were better protected than all other species, which also coincides with the results of the present study. A positive correlation between  $TL$  and the protection efficiency was found for fish with  $h_f \leq 15\text{ mm}$ , but not for fish with  $h_f > 15\text{ mm}$ . Due to the low number of individuals per size class of most species, this correlation was not analyzed on a species-specific basis in the final report. However, the raw data were

kindly provided by the Institute of Aquatic Ecology and Fish Biology (IGF Jena) with the permission of the German Environment Agency (UBA), which are compared to the prediction equations of FGE and FPE (Eq. 7.1 and 7.2) in the following. When such comparisons are made, it is important to carefully consider the boundary conditions and differences between the studies. At HPP Rappenberghalde, a high bottom overlay was installed ( $h_{Bo} \geq 0.92$  m,  $H_{Bo} \geq 0.25$ – $0.30$ , depending on  $h_o$ ), which likely affected the protection efficiency of bottom-oriented fish species. The bypass design was not ideal (cf. Section 3.7.4), such that it can be expected that the guidance efficiencies at HPP Rappenberghalde are smaller than at other HBR-BRs with a continuously operating state-of-the-art bypass. Last but not least, the number of refusals of the natural fish population could not be determined at HPP Rappenberghalde, since only the number of individuals which passed through different corridors were compared. The fish guidance efficiency FGE was therefore calculated as the share of fish which were caught at the bypass and flushing gate, from all fish caught either at the bypass and flushing gate or the turbine outlet. As the number of refusals which were considered to develop the prediction equations of FGE and FPE were rather small (cf. Section 7.2.1), they can still be compared to FGE of HPP Rappenberghalde. If the refusals are neglected in Eq. (7.1) and (7.2),  $FGE = FPE$  and the definition of FGE and FPE is identical to the monitoring campaign at HPP Rappenberghalde. In total,  $n = 1394$  individuals of 22 species were caught at the bypass and flushing gate or the turbine outlet. The data were filtered to get species with at least  $n = 5$  individuals per size class and more than five different size classes to allow for a detailed analysis. The size classes were defined in intervals of 1 mm of  $w_f$ . These criteria were fulfilled for three species only, namely spirlin ( $n = 454$ ), chub ( $n = 136$ ), and gudgeon ( $n = 106$ ). The latter is known to be bottom-oriented (Wagner *et al.*, 2019b), which means that its behavior was very likely affected by the bottom overlay, which makes gudgeon unsuitable for a comparison. The data of chub and spirlin are shown in Fig. 7.32, together with the prediction equations for FGE and FPE (Eq. 7.1 and 7.2) with  $s_b = 15$  mm. The circles in Fig. 7.32 represent data with  $w_f/s_b$  and the squares  $h_f/s_b$ . The error bars were calculated with the number of observations per size class, a significance level of  $\alpha_{sig} = 0.05$ , and Eq. (4.24), where  $CP$  was replaced by FGE to calculate the error  $\varepsilon$ .



**Fig. 7.32:** Size-dependent guidance efficiency of the monitoring data from HPP Rappenberghalde with an HBR-BS with  $s_b = 15$  mm for (a) chub ( $n = 136$ ) and (b) spirlin ( $n = 454$ ) and the prediction equations of FPE (Eq. 7.2) and FGE (Eq. 7.1); the circles represent data with  $w_f/s_b$  and the squares  $h_f/s_b$

The data of chub agree very well with the prediction equations of FGE and FPE (Fig. 7.32a). Only the data point of the size class  $w_f = 13$  mm ( $w_f/s_b = 0.87$ ) deviates significantly from the prediction equations. It has to be considered that only  $n = 6$  individuals were caught in this size class, causing large uncertainties. For spirlin, the opposite trend was observed, that is, the guidance efficiency decreased with  $w_f/s_b$  (blue circles in Fig. 7.32b). If  $w_f/s_b$  was replaced by  $h_f/s_b$ , as proposed in Section 7.2.2 for spirlin, they better match with the prediction equations for  $h_f/s_b \leq 1.15$ , which represents  $\approx 70\%$  of all spirlin data (red squares in Fig. 7.32b). Nevertheless, this cannot explain why the guidance efficiency decreased for larger spirlin at HPP Rappenberghalde. It is beyond the scope of the present thesis to assess this correlation in detail, but the live fish tests conducted within the present study revealed that spirlin reacted very sensitive to flow accelerations at the bypass inlet, which significantly increased the number of refusals (cf. Section 7.5 and Fig. 7.7 in Section 7.2.1). One possible explanation for the trend at Rappenberghalde is that small spirlin were less likely to swim through the turbines due to the fast flow accelerations or other stimuli causing avoidance reactions, such as noise or vibrations. Larger spirlin might have shown less distinct avoidance reactions to these behavioral stimuli, such that the correlation between the fish size and the guidance efficiency cannot be attributed to the HBR. However, these are possible explanations only, which are not based on scientific facts and should be investigated in future studies. In summary, many different aspects have to be carefully considered when comparing the results of the present study with monitoring data. Nevertheless, the example of Rappenberghalde showed that the prediction equations proposed within the present thesis match the monitoring data of at least one species very well.

### HPP Stroppel

The general observations of the monitoring campaign at HPP Stroppel by Zaugg and Mendez (2018), which was briefly described in Section 3.7.4, agree well with the observations of the present study. As an example, Zaugg and Mendez (2018) described that most fish approached the HBR and entered the bypass with positive rheotaxis, but they also mentioned that some fish swam with negative rheotaxis along the HBR into the bypass. According to Zaugg and Mendez (2018), only 1.6–3.2% of all fish passed through the HBR with  $s_b = 20$  mm, which was estimated from qualitative sonar observations behind the rack and the stow net catches at the bypass outlet (cf. Section 3.7.4). The problem of comparing the number of small fish caught with a stow net with sonar data was described by Egg *et al.* (2018a), who installed a sonar Aris Explorer 3000 and a stow net simultaneously at a small river. At the experimental location, the river was diverted through a 2.5 m wide sluice gate with a mean discharge of  $Q = 2.36$  m<sup>3</sup>/s during the six day long study period. The sonar data were analyzed with an optimistic approach, where all objects resembling fish shape were counted, and a pessimistic approach where objects were only counted if tail-beat frequencies were observed. While fish with  $TL > 10$  cm were represented well with the sonar, only 40–45% of the fish were detected for  $5 \text{ cm} < TL \leq 10 \text{ cm}$  and only 34–38% for  $TL < 5 \text{ cm}$ . Therefore, Egg *et al.* (2018a) recommended to use sonar data for counting fish movements only if  $TL > 10$  cm. At HPP Stroppel, 87% of the individuals caught in the bypass were  $TL < 10$  cm (Zaugg and Mendez, 2018) and it is likely that this



share is even higher for fish which passed through the HBR. It must therefore be assumed that the effective number of rack passages of small fish at HPP Stroppel is significantly higher than reported by Zaugg and Mendez (2018), also because only a part of the 25 m long and 2.7 m high HBR at HPP Stroppel could be observed with the sonar. This is one explanation why Zaugg and Mendez (2018) concluded that the HBR at HPP Stroppel with  $s_b = 20$  mm protects also very small fish, while the present study indicates hardly any protection for juvenile nase with  $\overline{TL} = 7.1$  cm. However, there are many other differences between the present laboratory study and the monitoring campaign at HPP Stroppel, which most likely also affected the results. Examples are partial clogging with leaves at HPP Stroppel which also affected the velocity field (cf. Fig. 9.1b in Chapter 9), species composition, and the bottom channel in front of the HBR. As an example, most fish caught behind the bypass with the stow net at HPP Stroppel were cyprinids, while salmonids like trout and salmon, which were insufficiently protected in the present study (cf. Section 7.2), were only rarely caught in Stroppel. Barbels, which were only partially protected in the present study, were frequently caught in the bypass of HPP Stroppel. Zaugg and Mendez (2018) described that barbels showed a tendency to swim in the bottom channel and it therefore seems likely that many barbels were guided by this channel. The monitoring campaign at HPP Stroppel provided very valuable information about the fish swimming behavior at an HBR-BS, which matches with observations of the present study on a qualitative basis. However, to reliably quantify the guidance and protection efficiencies, it is indispensable to monitor all downstream passage corridors simultaneously with stow nets, which would have been the bypass and turbine outlet in the case of HPP Stroppel.

### HPP Lindesmühle

In contrast to most ethohydraulic studies and monitoring campaigns, Mueller *et al.* (2020b) concluded that the HBR at HPP Lindesmühle primarily acts as a physical barrier, that the mechanical behavioral protection effect is small, and that the HBR has a low guidance effect. These statements are based on the observation, that not only the majority of very small fish ( $TL \leq 5$  cm) but also the majority of fish with  $5 \text{ cm} < TL \leq 20$  cm passed through the HBR with  $s_b = 15$  mm (cf. Table 3.11 in Section 3.7.4). It has to be considered that almost the entire discharge was diverted through the turbines ( $Q_{by,rel} < 0.2\%$ ) and that the HBR was installed across a small river section without any pier, similarly to a block-type HPP (cf. Fig. 3.12 in Section 3.7.4). The flow therefore approached the HBR with an angle of  $\approx 90^\circ$  and a bypass, which fulfills common design criteria (cf. Section 3.4.2), was missing. It was also conspicuous that multiple fish with  $TL > TL_{crit}$  were caught, to which the HBR should have been a physical barrier. The reasons therefore can be manifold and cannot be assessed within the present thesis. It is possible that  $s_b$  was locally larger than 15 mm, for example due to production or installation inaccuracies or distortions, that some fish were enclosed from the downstream when the stow net was retrieved, that the variations were caused by the accuracy of collecting the fish biometry, or that the fish biometry at HPP Lindesmühle differed from the fish biometry given in literature (e.g. Table 2.2). The low guidance effect can be explained by the large angle between the rack and the approach flow and the lack of a suitable bypass. The findings at HPP Lindesmühle

can therefore not be generalized and a comparison with the data of the present study, where a diversion HPP setup with an optimized bypass was investigated, is not reasonable.

### HPP Widdert

The monitoring campaign at HPP Widdert demonstrated that the HBR with  $s_b = 12$  mm sufficiently protected all downstream migrating silver eels and salmon smolts. The PIT-tagging campaign gave valuable insights in the corridor usage. However, as the fish swimming behavior is not directly observed in PIT-tagging studies, it is challenging to understand why a certain corridor was not well accepted. In case of HPP Widdert, the low usage of the smolt bypass and the bottom bypass was attributed to the small flow velocities at the inlet and the fact that the bottom bypass clogged frequently. A large share of downstream migrating silver eels either used the vertical-slot pass at the power house or the intermittently opened flushing gate. This might lead to the conclusion that eels were not guided along the HBR towards the downstream rack end, but entered the downstream passage corridors by chance or active search movements. On the contrary, eels were guided very efficiently along the HBR towards the bypass in the present study (cf. Fig. 7.6 in Section 7.1.2). It has to be considered that the bottom bypass at the downstream rack end was often clogged and that both bypass inlets were arranged perpendicular to the rack at HPP Widdert. A bypass with a continuous discharge, arranged in the extension of the rack axis or in the main approach flow direction, was missing, which makes it very difficult to judge the guidance efficiency of the HBR itself.

### Concluding remarks and effect of flow velocity

The comparison in this section showed that many observations of the present ethohydraulic study agree well with various monitoring campaigns. However, comparisons have to be done very carefully to not draw wrong conclusions, as small differences between sites or studies may significantly affect the result. It was conspicuous that  $V_n$  was very small at HPPs Rappenberghalde and Lindesmühle during the study periods ( $V_n \approx 0.12$  m/s, cf. Section 3.7.4). For  $\alpha = 30^\circ$  at diversion HPPs, this corresponds to  $U_o = 0.24$  m/s (Eq. 3.1). For such small  $U_o$ , it is not clear if most fish align with positive rheotaxis (cf. Section 2.2.5). Fish which approach HBRs with negative rheotaxis might be more likely to pass through the HBR, as they can actively swim through the rack. The monitoring campaigns at HPPs Rappenberghalde and Lindesmühle have in common, that most fish passed through the HBRs with  $s_b = 15$  mm (cf. Section 3.7.4). This was attributed to various reasons, but it cannot be ruled out that the very small flow velocities were counterproductive for fish guidance. Such small  $U_o$ ,  $V_p$ , and  $V_n$  were not investigated in the present study, but it was shown that the HBR caused a partial behavioral guidance effect. It is known that the guidance efficiency of mechanical behavioral barriers reduces for very small flow velocities as hydraulic signatures are missing. By summarizing multiple studies with Louvers, Ruggles and Ryan (1964) demonstrated that FGE reduces for  $U_o < 0.5$  m/s, which can be explained by less distinct hydraulic signatures such as turbulences (details in Section 3.4.1). Flügel *et al.* (2015) and Kriewitz (2015) observed that larger  $U_o$  did not lead to more rack passages for MBRs in the range of  $U_o = 0.3$ – $0.6$  m/s. Beck (2020) demon-

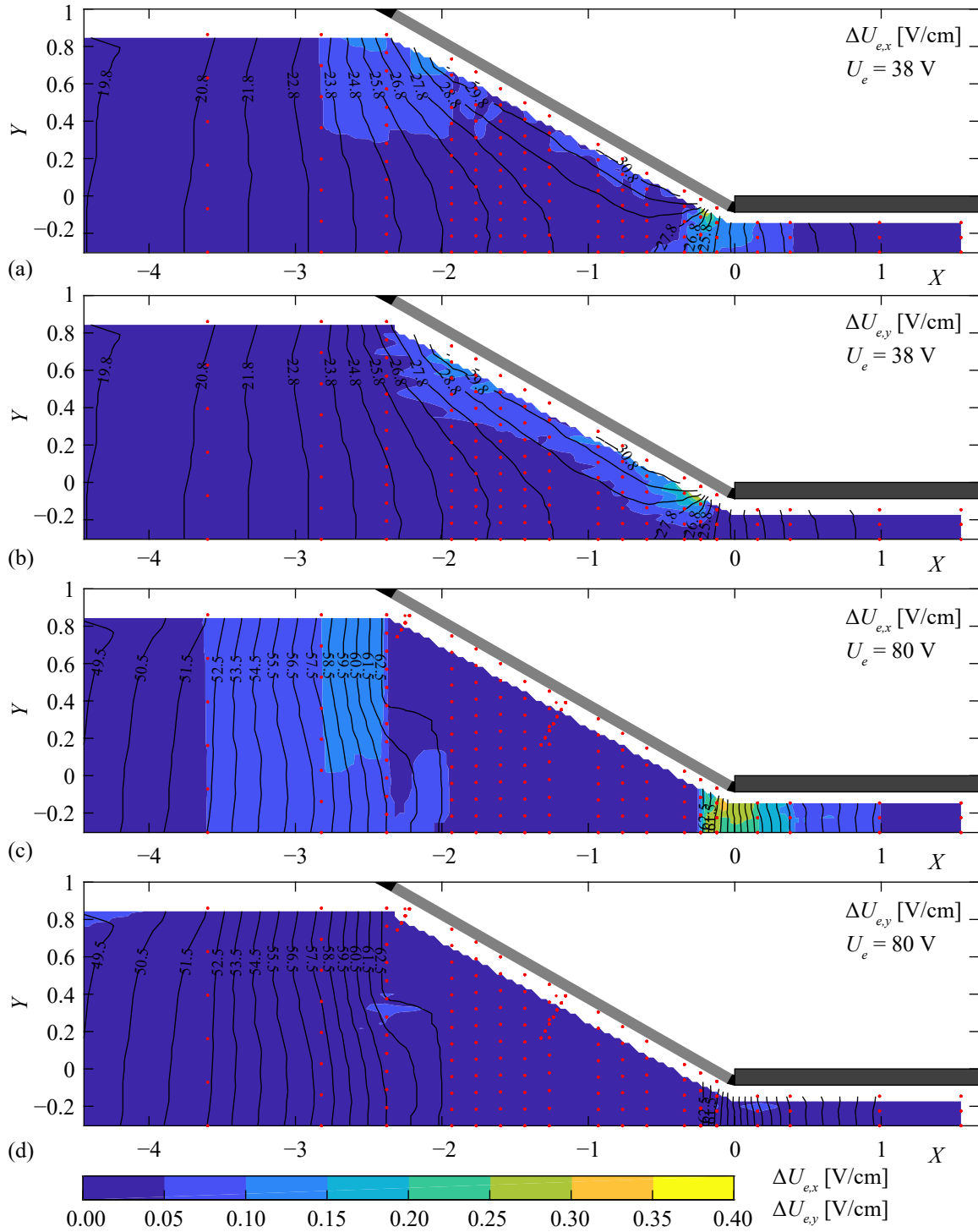
strated that CBRs cause larger FPE with  $U_o = 0.7$  m/s than with  $U_o = 0.5$  m/s. Although not statistically significant on a species-specific basis, FPE for barbels was larger for  $U_o = 0.7$  m/s than for  $U_o = 0.5$  m/s in the present study (cf. Fig. 7.8 in Section 7.2.1). Berger (2018) observed no fish impingements at HBRs with  $U_o = 0.4$ – $0.8$  m/s. To the authors knowledge, no fish impingements were observed in any ethohydraulic study or monitoring campaign at an HBR installed with  $\alpha \approx 30^\circ$  at a diversion HPP. In line with Ebel (2016), it is not suggested to limit the approach flow velocity of HBRs to  $U_o = 0.5$  m/s. Instead, it is recommended to design HBRs such that  $V_n$  does not exceed the sustained swimming speed of the majority of fish, following Turnpenny and O’Keeffe (2005) (details in Section 3.4.1). Especially for mechanical behavioral barriers, for which it is known that FPE can reduce for smaller  $U_o$ , it is important to not only assess the guidance efficiency during design discharge, but to consider the whole flow duration curve throughout the year. It is recommended to conduct further live fish tests with HBRs for very small  $U_o$  to find out if it affects FPE. If feasible, potential fish impingements and the effect of  $U_o$  on the guidance efficiency should also be studied in a monitoring campaign.

## 8 Live fish tests with electrified horizontal bar rack bypass systems

This chapter shows the measurements of the electric field and the results of the live fish tests with the electrified HBR, of which some parts were first published in a slightly modified form in Meister *et al.* (2020a).

### 8.1 Measurements of the electric field

Figure 8.1 shows the measurements of the electric field for different output voltages  $U_e$ . Measurements in different flow depths revealed that the variations of the electric field in vertical direction were marginal, such that the measurements collected close to the bottom are shown in Fig. 8.1 only ( $Z = 0.11$ ). Likewise, it was verified that  $s_b$  did not affect the electric field in the range of  $s_b = 20\text{--}100$  mm. The measurements shown in Fig. 8.1a,b ( $U_e = 38$  V;  $s_b = 51$  mm) and Fig. 8.1c,d ( $U_e = 80$  V;  $s_b = 100$  mm) can therefore be used to explain the fish behavior at all tested configurations with electrified HBRs listed in Table 4.4. The electric field was also measured with inverse polarity, that is, the HBR was used as the cathode and the metal mesh as the anode. The absolute voltages differed from the regular polarity, but the voltage gradients were identical. For voltage outputs of  $U_e = 38$  V and  $U_e = 80$  V from the Neptun system, the largest voltages measured directly upstream of the HBR in the water were 31 V and 63 V, respectively, which means that the output voltage reduced by  $\approx 20\%$  through losses in the cables and the crocodile clips. The equipotential lines in Fig. 8.1a,b were almost rack-parallel close to the HBR, whereas they were almost rectangular to the flume walls further upstream and in the bypass. The largest voltage gradients in  $x$ -direction,  $\Delta U_{e,x}$ , were measured close to the bypass inlet for  $U_e = 38$  V (Fig. 8.1a). The voltage gradient in  $x$ -direction was larger at the upstream rack end than in the rack center and it was also measurable as far upstream as  $X = -4$ , where  $\Delta U_{e,x} \approx 0.02$  V/cm. The electric field in  $y$ -direction for 38 V was larger than  $\Delta U_{e,y} = 0.05$  V/cm within a rack-parallel distance of  $\approx 30$  cm in front of the HBR (Fig. 8.1b) and it was also largest close to the downstream rack end. The electric field completely changed for an output voltage of  $U_e = 80$  V, where a constant absolute voltage of 62.5 V was measured in the whole area between the upstream and downstream rack end, which led to negligible voltage gradients within that region (Fig. 8.1c,d). Further upstream at  $X \approx -2.5$ , the absolute voltages reduced, such that the voltage gradient ranged up to  $\Delta U_{e,x} = 0.16$  V/cm and started to decrease again further upstream (Fig. 8.1c). The absolute voltage strongly decreased at the bypass inlet, which induced large voltage gradients, peaking at around  $\Delta U_{e,x} = 0.30$  V/cm (Fig. 8.1c). For an output voltage of  $U_e = 80$  V, the equipotential lines were almost rectangular to the flume walls, which means that the voltage gradient in  $y$ -direction was small, that is,  $\Delta U_{e,y} \leq 0.05$  V/cm in the whole observation area (Fig. 8.1d).



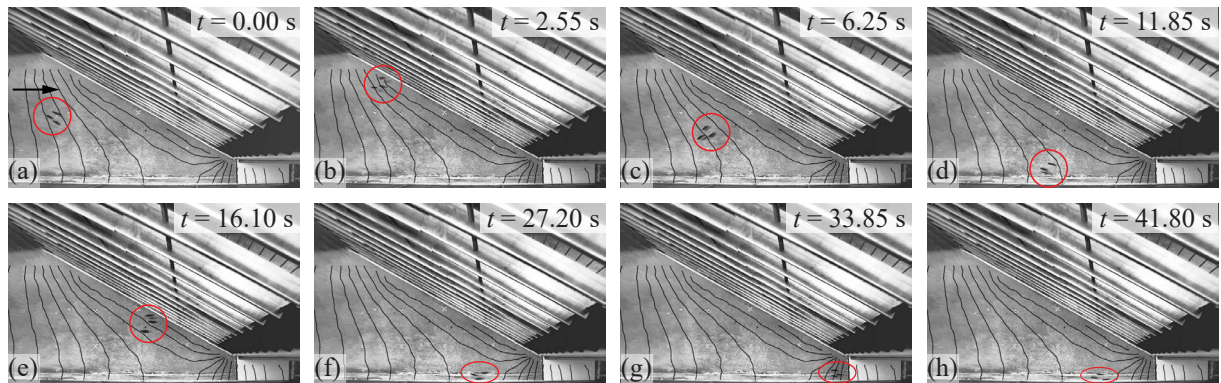
**Fig. 8.1:** Contour maps of the voltage gradients measured at  $Z = 0.11$  for  $U_e = 38 \text{ V}$  and  $s_b = 51 \text{ mm}$  in (a)  $x$ -direction and (b)  $y$ -direction and for  $U_e = 80 \text{ V}$  and  $s_b = 100 \text{ mm}$  in (c)  $x$ -direction and (d)  $y$ -direction; measurement locations are indicated with red dots and the equipotential lines are shown in increments of  $\Delta U_e = 1 \text{ V}$  (data provided by Anita Moldenhauer-Roth)

## 8.2 Fish behavior, guidance, and protection with the electric field

In this section, the results of the electrified HBR are compared to the results without electrification. The analysis refers to the experiments with an output voltage of  $U_e = 38 \text{ V}$  and the standard pulse pattern only (cf. Section 4.4.3), as too few experiments were conducted with other pulse patterns (cf. Table 4.4).

## Spirlin

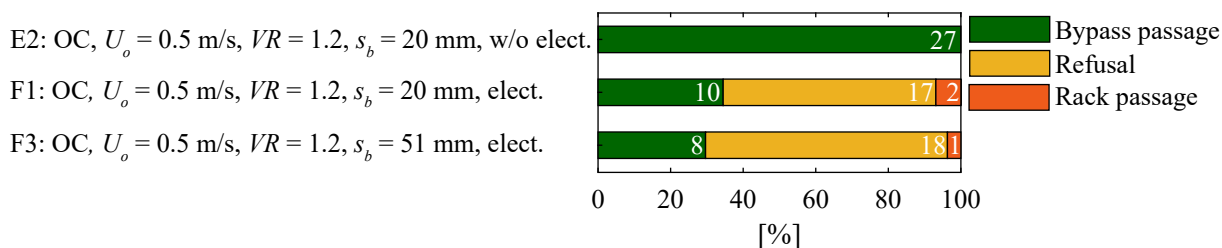
Most spirlin approached the electrified HBR with positive rheotaxis and reacted  $\approx 10\text{--}20\text{ cm}$  upstream of the HBR to the electric field with sudden upstream burst swimming movements. Instead of fleeing to the headwater, spirlin often swam only a couple of centimeters upstream, before they approached the HBR again. After several attempts, they often continued their normally observed swimming behavior in the experiments without electrification, that is, downstream zigzag movements, and were thereby guided towards the bypass, which they often refused to enter until the end of the experiment. However, some spirlin swam very close to the HBR and almost touched it, while others reacted more than 50 cm upstream of the HBR to the electric field. Compared to the configuration without electrification, spirlin did not only swim very close to the flume bottom, but they were frequently using the whole water column searching for an appropriate downstream passage corridor. Figure 8.2 shows the typical behavior of spirlin at the electrified HBR, where three individuals approached the rack with positive rheotaxis. As without electrification, they aligned almost rack-parallel when swimming towards the HBR (Fig. 8.2a), swam close to the rack (Fig. 8.2b), before they changed their swimming direction and moved towards the glass wall (Fig. 8.2c). After another zigzag movement (Fig. 8.2d–f), they tried to swim into the bypass (Fig. 8.2g) but refused to enter it and swam back upstream (Fig. 8.2h). In this experiment, two spirlin entered the bypass  $\approx 14.5\text{ min}$  after they first approach the electrified HBR and only after several attempts of entering the bypass. The sudden upstream burst swimming movements can hardly be visualized with screenshots, but can be best seen on video.



**Fig. 8.2:** Typical behavior of spirlin at the electrified HBR with  $s_b = 51\text{ mm}$  and the standard pulse pattern, which were guided towards the bypass but refused to enter it; the spirlin are encircled in red and the equipotential lines are visualized in black (Video: <http://dx.doi.org/10.3929/ethz-b-000450740>)

The goal of the live fish tests with spirlin at the electrified HBR was to verify if the good guidance, achieved without electrification, could be maintained with the electric field and if it was possible to reach high FGE and FPE with larger  $s_b$ . In Fig. 8.3, the results of the electrified HBR with  $s_b = 20\text{ mm}$  and  $s_b = 51\text{ mm}$  are compared to the results without electrification and  $s_b = 20\text{ mm}$  for the same hydraulic conditions ( $U_o = 0.5\text{ m/s}$ ,  $VR = 1.2$ ). Without an electric field, all spirlin entered the bypass of the HBR-BS with  $s_b = 20\text{ mm}$ , OC,  $U_o = 0.5\text{ m/s}$ , and  $VR = 1.2$  (E2 in Fig. 7.7 and 8.3). While maintaining  $s_b = 20\text{ mm}$ , the application of the electric field led to significantly less bypass passages ( $p < 0.001$ ,  $\chi^2 = 23.931$ ) but more refusals ( $p <$

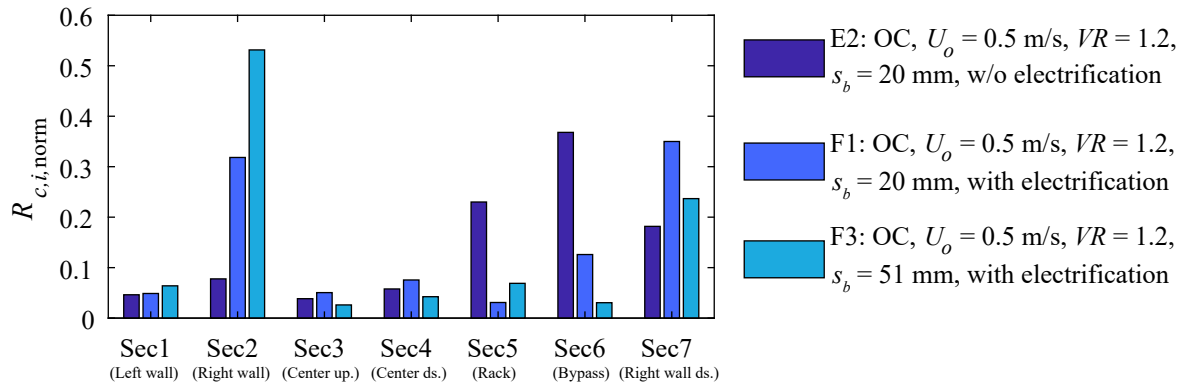
0.001,  $\chi^2 = 20.039$ ; E2 and F1 in Fig. 8.3). The number of rack passages increased too, but due to the low number of observations, this difference was not significant ( $p = 0.503$ ,  $\chi^2 = 0.448$ ). With the electric field, no statistically significant differences were observed between  $s_b = 20$  mm and  $s_b = 51$  mm for bypass passages ( $p = 0.919$ ,  $\chi^2 = 0.010$ ), refusals ( $p = 0.730$ ,  $\chi^2 = 0.119$ ), and rack passages ( $p = 1.000$ ,  $\chi^2 = 0.000$ ). Despite the good protection efficiency of the electrified HBR, two spiralin passed through the HBR with  $s_b = 20$  mm and one spiralin with  $s_b = 51$  mm with the standard pulse pattern (cf. Fig. 8.3). The first spiralin passed through the electrified HBR with  $s_b = 20$  mm at the downstream rack end in the upper water column, 13 minutes after the start of the experiment. It seemed that the electric field impaired the swimming capabilities of the spiralin, resulting in the spiralin being swept downstream through the HBR. Astonishingly, the spiralin still managed to rotate to the side to reduce rack contact. The other spiralin which passed through the electrified HBR with  $s_b = 20$  mm, approached the rack with positive rheotaxis and actively swam towards the rack, such that it was oriented almost rack-parallel during rack passage. After approximately one second, the spiralin swam upstream out of the HBR again and entered the bypass actively with negative rheotaxis. The rack passage of the spiralin at the electrified HBR with  $s_b = 51$  mm is described in detail in Section 8.3.



**Fig. 8.3:** Results of the live fish tests with spiralin with  $U_o = 0.5$  m/s and  $VR = 1.2$ , without and with an electric field for different  $s_b$  (definition of configurations in Tables 4.3 and 4.4)

Figure 8.4 shows the normalized residence coefficients of the electrified HBR with different  $s_b$  and the configuration without electrification,  $U_o = 0.5$  m/s, and  $VR = 1.2$  as a reference. The electrification did not affect the time fish spent near the left flume wall (Sec1) and the flume center (Sec3 and Sec4), but with the electrification spiralin avoided the rack (Sec5) and bypass area (Sec6; Fig. 8.4). With the electrification, spiralin swam more frequently close to the right flume wall upstream of the bypass inlet (Sec2 and Sec7), which indicates that they were guided in the direction of the bypass but they hesitated to enter it. The measurements of the electric field revealed that the electric field reached into the bypass, which is most likely the reason for the bad bypass acceptance. Nevertheless, most spiralin were protected with the electrified HBR.





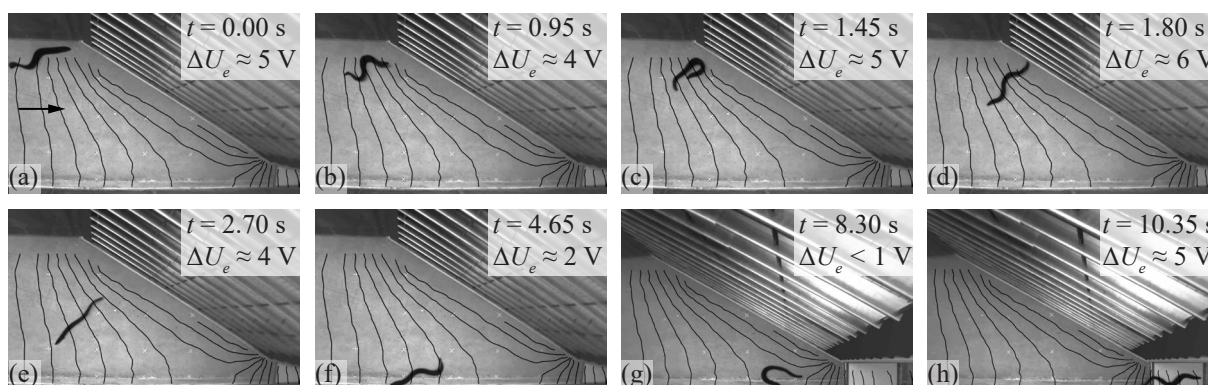
**Fig. 8.4:** The normalized residence coefficient  $R_{c,i,norm}$  of spiralin for the sectors Sec1–Sec7 with the electrification for different  $s_b$  (F1 and F3, Table 4.4) and the reference configuration without electrification (E2, Table 4.3)

With spiralin, only three experiments were conducted with a pulse pattern that differed from the standard pulse pattern (F5 in Table 4.4). The few spiralin tested with the other pulse pattern showed a similar behavior at the electrified HBR, but the configuration was aborted after one spiralin was severely injured (details in Section 8.3).

### Eel

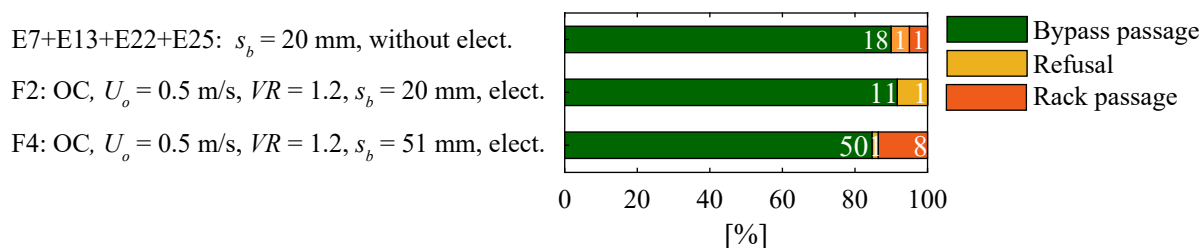
Most eels approached the electrified HBR actively with negative rheotaxis, but some eels swam slowly downstream with positive rheotaxis or let themselves drift passively. The reaction of eels to electric field varied strongly between individuals. A few specimens changed their rheotaxis due to the electric field several meters upstream of the HBR, where the electric gradient was in the range of  $\approx 0.02$  V/cm (cf. Fig. 8.1), while others reacted only after rack contact. In general, eels which swam very actively downstream with negative rheotaxis reacted further downstream to the electric field than eels which approached the HBR slowly or passively. As a reaction to the electric field, eels were typically guided rack-parallel towards the bypass or escaped upstream, either directly in longitudinal direction or rectangular to the rack. While some eels swam upstream to the acclimatization compartment after rack contact, most individuals fled only a couple of meters upstream, before they approached the rack again like the eel in Fig. 8.5, which represents a typical reaction at the electrified HBR. It approached the rack with negative rheotaxis, almost aligned rectangular to the equipotential lines, such that the voltage difference between its nose and tail was  $\Delta U_e \approx 5$  V (Fig. 8.5a). The eel changed its rheotaxis (Fig. 8.5b,c) and fled upstream, such that it was again aligned almost rectangular to the equipotential lines, where it was exposed to  $\Delta U_e \approx 6$  V close to the rack (Fig. 8.5d) and  $\Delta U_e \approx 4$  V further upstream (Fig. 8.5e). The eel then let itself drift downstream along the glass wall where the electric field was rather small (Fig. 8.5f,g), before it changed back to negative rheotaxis to enter the bypass (Fig. 8.5h). Almost all eels flinched during bypass passage, which was most likely a reaction to the comparably large electric gradients at the bypass inlet (cf. Section 8.1). Nevertheless, most eels entered the bypass in contrast to spiralin (Fig. 8.3 and 8.5), indicating that eels react less sensitive to electric fields, despite their length which exposes them to larger body voltages.





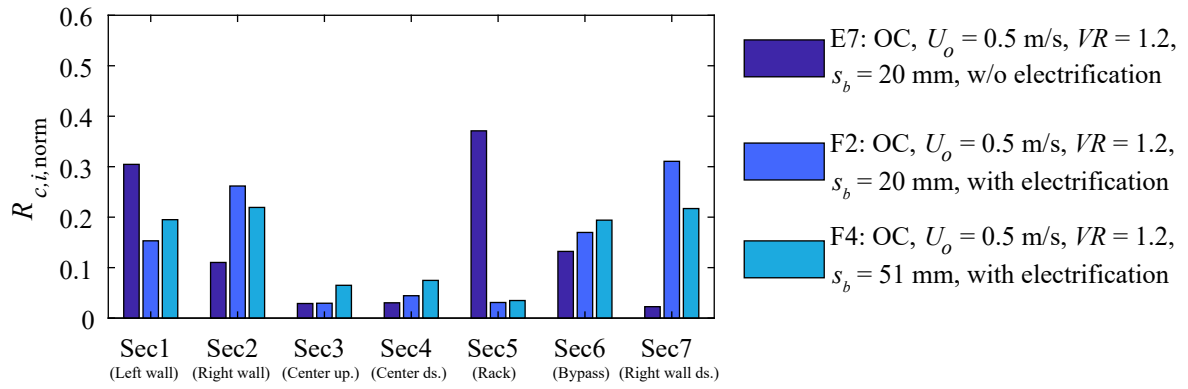
**Fig. 8.5:** Typical behavior of an eel with  $TL = 67$  cm at the electrified HBR with  $s_b = 51$  mm and the standard pulse pattern, which was guided towards the glass wall and subsequently into the bypass; the equipotential lines are visualized in black (Video: <http://dx.doi.org/10.3929/ethz-b-000450740>)

Since eels reacted insensitive to velocity gradients at the bypass inlet, the results of the configurations E7, E13, E22, and E25 with  $U_o = 0.5$  m/s and  $s_b = 20$  mm without electrification, presented in Fig. 7.12, were combined in Fig. 8.6 and compared to the results with the electric field. No rack passages were observed with  $s_b = 20$  mm with the electric field, such that FGE and FPE were similar with and without electrification for  $s_b = 20$  mm (Fig. 8.6). However, as described above, the swimming behavior fundamentally differed due to the electric field. With the electrification and  $s_b = 51$  mm, more rack passages were observed than for  $s_b = 20$  mm with and without electrification, such that  $FGE \approx FPE \approx 85\%$ .



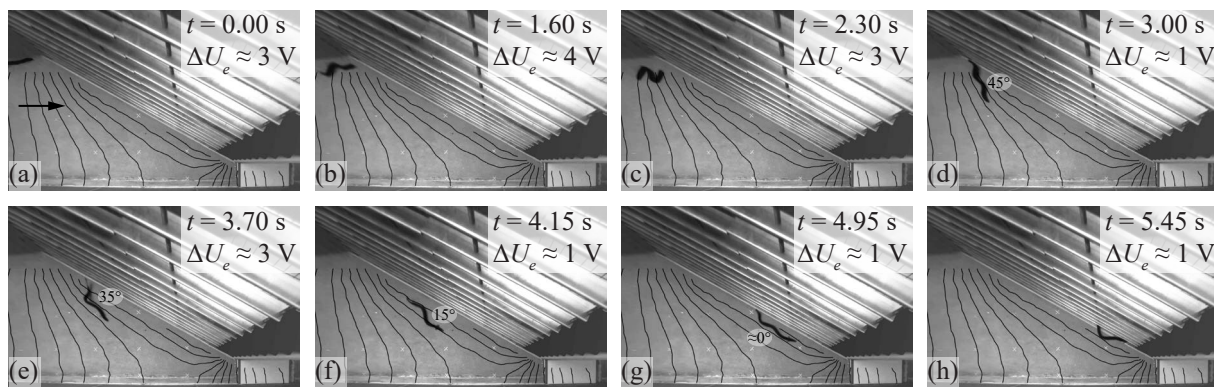
**Fig. 8.6:** Results of the live fish tests with eels with  $U_o = 0.5$  m/s, without and with an electric field for different  $s_b$  (definition of configurations in Table 4.3 and 4.4)

Without electrification, eels were nicely guided along the HBR and hardly hesitated to enter the bypass, which was quantified with the sector analysis in Fig. 8.7. They spent comparatively more time in front of the HBR (Sec5) and only little time in front of the bypass (Sec7; E7 in Fig. 8.7). The behavior was completely different with the electrification, where eels avoided the rack area (Sec5) and hesitated to enter the bypass, which means that they spent more time near the wall upstream of the bypass inlet (Sec2 and Sec7; F2 and F4 in Fig. 8.7).



**Fig. 8.7:** The normalized residence coefficient  $R_{c,i,norm}$  of eel for the sectors Sec1–Sec7 with the electrification for different  $s_b$  (F2 and F4, Table 4.4) and the reference configuration without electrification (E7, Table 4.3)

Although many eels were guided towards the bypass at the electrified HBR with  $s_b = 51$  mm, eight individuals passed through the rack (Fig. 8.6). Such rack passages can be explained by the specific orientation of the eels towards the electric field, which is illustrated with Fig. 8.8. For this specific experiment, the eel approached the HBR with negative rheotaxis at the upstream rack end, resulting in an almost rectangular orientation to the equipotential lines with a voltage difference between its nose and tail of  $\Delta U_e \approx 3$  V (Fig. 8.8a). With backwards swimming movements, the eel changed its orientation at the upstream rack end (Fig. 8.8b,c), and fled with an angle of  $\approx 45^\circ$  to the rack, such that the tail touched the rack, provoking active swimming movements (Fig. 8.8d). As the eel swam along the rack, this angle reduced to  $\approx 35^\circ$  and further to  $\approx 15^\circ$  with  $\Delta U_e \approx 1$  V (Fig. 8.8f). Finally, the eel was almost aligned perfectly rack-parallel along an equipotential line, such that it hardly felt any body voltage and could easily pass through the electrified HBR (Fig. 8.8g,h). In some other experiments, eels showed a very similar behavior as the eel in Fig. 8.8a–e, but instead of aligning rack-parallel, they touched the rack multiple times with their tail and kept an angle of  $\approx 30$ – $45^\circ$  between their body axis and the HBR (like in Fig. 8.8d,e) until they reached the bypass. However, if an eel was approaching a longer HBR with a comparable electrification setup, it is very likely that it would align itself parallel to the equipotential lines sooner or later and would pass through the HBR. It must therefore be assumed that the guidance and protection efficiency at longer racks is lower than determined in the present experiments.



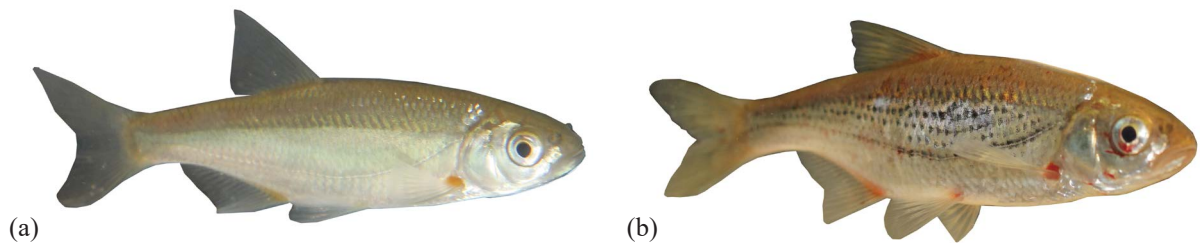
**Fig. 8.8:** Typical rack passage of an eel with  $TL = 57$  cm at the electrified HBR with  $s_b = 51$  mm and the standard pulse pattern, where the eel approached the rack with negative rheotaxis, was guided towards the rack, but passed through the HBR when it was oriented rack-parallel; the equipotential lines are visualized in black (Video: <http://dx.doi.org/10.3929/ethz-b-000450740>)

Five out of the eight eels, which passed the electrified HBR with  $s_b = 51$  mm and the standard pulse pattern (cf. Fig. 8.6), passed it similarly to the eel in Fig. 8.8, that is, they approached the HBR with negative rheotaxis, were guided towards the bypass, and passed through the HBR almost rack-parallel. Two eels directly approached the electrified HBR almost rack-parallel with negative rheotaxis and directly passed through it, whereas one eel swam from the glass wall towards the HBR with positive rheotaxis and passed it also rack-parallel. No eel was aligned rectangular to the equipotential lines when it passed through the electrified HBR, which shows the potential of electrified racks for the guidance of downstream moving eels. However, with the present setup, the guidance and protection effect strongly depended on the orientation of the eels, which led to multiple rack passages. Due to the small number of replicates with different pulse patterns,  $U_e = 80$  V, and  $s_b = 100$  mm (F6–F11 in Table 4.4), the explanatory power of these experiments is small and the results are therefore not shown in detail. However, at least one rack passage was observed for each of these configurations, and the experiments with the electrified HBR with  $s_b = 100$  mm worked out particularly poor, where two out of three eels passed through the rack for both  $U_e = 38$  V and  $U_e = 80$  V (F10, F11).

### 8.3 Fish injuries

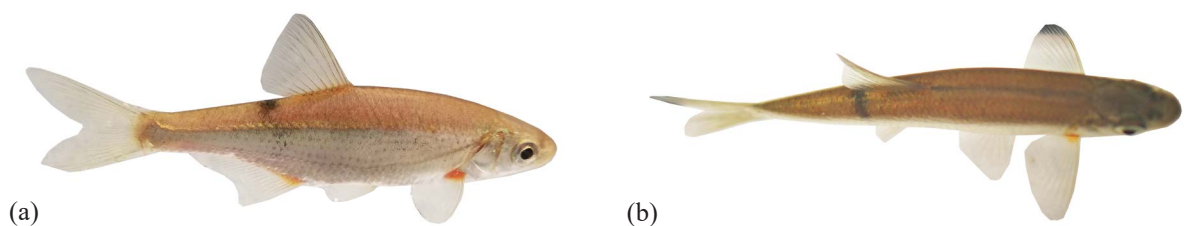
Without electrification, no fish impingements or injuries were observed. At the electrified HBR, local dark melanization of the skin were noticed for some spiralin after the experiments, indicating external injuries. Two spiralin which passed the electrified HBR with  $s_b = 51$  mm were euthanized with an overdose of MS22 and checked for internal injuries by the Centre for Fish and Wildlife Health in Bern, Switzerland. The full German injury reports are in Appendix A.2. The only spiralin, which passed through the electrified HBR with  $s_b = 51$  mm with the standard pulse pattern (cf. Fig. 8.3), actively approached the rack with negative rheotaxis directly after the acclimatization compartment was opened. Figure 8.9 shows this spiralin before the experiment and after rack passage with internal bleeding in the eye and dark melanization of the skin (Fig. 8.9b). However, no internal bleeding were detected in the muscles or along the vertebrae and, although likely, it could not be verified if the dark melanization of the skin resulted from

contact with the electrified rack (details in Fig. A.1 and A.2 in Appendix A.2). This fish passed through the HBR at the beginning of the 30 minute long experiment. It can therefore not be ruled out that the electric field impaired the swimming capabilities of the spirlin and that the injuries resulted from impingement at the downstream net. It is therefore not certain if these injuries resulted directly from the electric field, but the approach flow velocity was only  $U_o = 0.5$  m/s and no such injuries were observed without the electric field. This was the only spirlin which approached the electrified HBR with negative rheotaxis. Also without electrification, spirlin only rarely approached the HBR with negative rheotaxis. However, also Adam and Lehmann (2011) mentioned that spirlin sometimes swim downstream very fast with negative rheotaxis. It is likely that fish which approach electrified racks with negative rheotaxis are less protected and have a higher injury risk because of the limited reaction scope, but further experiments are needed to verify these observations.



**Fig. 8.9:** The spirlin which passed through the electrified HBR with the standard pulse pattern and  $s_b = 51$  mm (a) before and (b) after the experiment

Another spirlin passed through the electrified HBR with  $s_b = 51$  mm but with a different pulse pattern (F5 in Table 4.4). It approached the HBR together with two other spirlin with positive rheotaxis, changed to negative rheotaxis to pass through the rack, before it swam out of the HBR approximately one second later. The school of spirlin then swam towards the bypass. It seemed that all three spirlin wanted to stay away from the bypass inlet, but the one which previously passed through the HBR drifted into the bypass, while the others stayed in front of it. After rack passage, this spirlin had dark melanization of the skin behind the dorsal fin (Fig. 8.10) and its swimming behavior was impaired. The video recordings suggest that the spirlin touched a vertical tie-bar at the location of the dark melanization. The diagnosis of the injury report was a spinal fracture in the area of the spinal canal with associated bleeding in the spinal canal and the surrounding muscles, which was very likely caused by an electric shock (details in Fig. A.3 and A.4 in Appendix A.2).



**Fig. 8.10:** Dark melanization of the skin behind the dorsal fin which were visible on the (a) side and (b) top view, which were caused by the electric field after rack passage



As no fish injuries were expected prior to the present study, they were not systematically analyzed, so that it was not possible to quantify fish injuries at electrified HBRs from the present investigation. However, this study showed that fish can get injured at electric barriers even with low output voltages of  $U_e = 38$  V. The measurements in Fig. 8.1 revealed that  $\Delta U_e \leq 0.40$  V/cm in front of the HBR for  $U_e = 38$  V, which is in the range considered suitable for electrofishing (cf. Section 2.2.5). However, if a fish passed through the HBR, like the spiralin shown in Fig. 8.10, it is exposed to a large voltage gradient between the HBR and the metal mesh. Assuming a linear voltage gradient between the HBR (anode) and the metal mesh (cathode), which was installed 18 cm downstream of the HBR, the voltage gradient in the present study was  $\approx 38 \text{ V}/18 \text{ cm} = 2.1 \text{ V/cm}$ . If the bars of the HBR were electrified alternatively as anode and cathode with  $s_b = 50 \text{ mm}$  and  $U_e = 38 \text{ V}$ , the linear voltage gradient between the bars would be  $\approx 38 \text{ V}/5 \text{ cm} = 7.6 \text{ V/cm}$ , which might have caused even more severe injuries. Although small external eel injuries could not be certainly attributed to the electrified HBR, it was observed on the video recordings several times that eels hemorrhaged a dark fluid after they swam in areas with large voltage gradients. Figure 8.11 shows an eel which slightly touched the HBR at the upstream rack end and subsequently escaped upstream. The dark fluid can hardly be seen on the screenshots, but it is encircled in red in Fig. 8.11c. It can be best seen on the video recordings. The dark fluid was not only observed when eels had contact with the anode, but also when they swam out of the bypass through the area with large voltage gradients (cf. Fig. 8.1). Despite showing multiple videos to several biologists, within the present thesis, it could not be clarified what kind of liquid it was and if it was harmful for the eels. Possible explanations for the observed fluid could be blood that was excreted from the gills or some liquid from the intestine excreted through the pharynx. It should be investigated in detail in future studies involving eels and electrification. In general, it is recommended that fish are systematically investigated regarding external and internal injuries in future experiments when electric fields are applied. It is known from electrofishing that fish can incur severe internal injuries, which are often not externally visible (cf. Section 2.2.5).



**Fig. 8.11:** An eel with  $TL = 61$  cm which approached the HBR with negative rheotaxis and escaped upstream, while it lost a dark fluid (encircled in red) after it was exposed to rather large voltage gradients at the upstream rack end (Video: <http://dx.doi.org/10.3929/ethz-b-000450740>)

## 8.4 Alternative setup and comparison with other studies

### 8.4.1 Alternative electrification setup

Beaumont (2016) highlighted that it is very challenging to guide downstream moving fish with

electric fields, as they approach the electric field with various orientations, causing different reactions. Exactly this problem led to multiple rack passages in the present study, especially for eels where the orientation is particularly important due to their length. It was shown in Section 7.1.2 that multiple other species swam towards the HBR almost rack-parallel. It is expected that they would have aligned themselves almost parallel to the equipotential lines with the present electrification setup, which would likely have led to an insufficient protection. To reduce the variability of the body voltage with the orientation of the fish, it is possible to use each bar alternatively as an anode and cathode. Fish would then sense the body voltage over their height  $h_f$ , independent of their orientation in  $x$ - and  $y$ -direction. Potential downsides of this electrification setup are that the electric field would reach far less upstream, leaving fish less room for reaction, which is especially important for fish swimming downstream with negative rheotaxis. If the same output voltage is applied with this electrification setup, the maximal voltage gradient would be larger due to the smaller distance between the anode and cathode, potentially being more harmful to aquatic organisms, especially to those which actively or passively drift downstream and can physically pass the rack (cf. Section 8.3). It would be ideal to find a setup, which efficiently protects downstream moving fish, while the applied voltage is so small that fish do not get injured, even if they touch the electrodes. If the electrodes are not aligned horizontally but vertically, it has to be ensured that the body voltage does not change rapidly if fish change their orientation.

#### 8.4.2 Comparison with other studies

In the following, the results of the live fish tests with the electrified HBR conducted within the present study are compared to a laboratory study and the monitoring campaign at the temporarily installed electric barrier at HPP Rotenfels.

##### **Berger (2018): electrified horizontal bar rack bypass system**

No rack passages were observed by Berger (2018) at the electrified HBR for  $s_b = 10$  mm and  $s_b = 18$  mm, which corresponds well to the findings of the present study where all eels were protected with the electrification for  $s_b = 20$  mm. However, for such small  $s_b$ , the majority of eels was also protected without electrification. Only  $\approx 1\%$  of all eels passed through the electrified HBR with  $s_b = 30$  mm in the study of Berger (2018), while this was the case for 14% in the present study for  $s_b = 51$  mm. It is possible that electrified HBRs with  $s_b = 30$  mm sufficiently protect eels in contrast to electrified HBRs with  $s_b = 51$  mm, but it is also possible that these variations were caused by differences in the experimental setup, such as the inclusion of a bottom overlay, different bar shapes, pulse patterns, or the size range of the tested fish. As the electrification setup of Berger (2018) was similar to the present study, it has to be assumed that the reaction of the eels also strongly depended on their orientation towards the electric field. No fish injuries due to the electric field were described by Berger (2018). However, no other fish species than eel were tested with the electrification by Berger (2018) and only a few rack passages were observed. In summary, most eels were protected well with  $s_b \leq 18$ –20 mm with and without electrification in both studies, while it cannot be certainly said if eels can be

sufficiently protected with electrified HBRs with  $20 \text{ mm} < s_b < 50 \text{ mm}$ . If electrified HBRs with  $s_b > 20\text{--}30 \text{ mm}$  are planned to be installed for eel protection, it is strongly recommended to conduct additional live fish tests to verify sufficient protection and guidance.

### **HPP Rotenfels**

As described in Section 3.7.4, an electric barrier was installed at HPP Rotenfels and the downstream migration behavior of salmon smolts and silver eels was studied using radio telemetry. Measurements of the electric field were not reported but the electric field was established between parallel rows of anodes and cathodes. It can therefore be assumed that the equipotential lines were also parallel to the barrier, similarly to the present study. Eels could not be sufficiently protected and guided with the electric barrier, which is in line with the findings of the present study. In contrast, 91% of the downstream migrating salmon smolts were successfully guided downstream, which shows that the electric barrier worked efficiently. This finding agrees well with the results of the present study with spiralin. It is likely that the electric field at HPP Rotenfels did not or only hardly reach into the fish pass and bypass at HPP Rotenfels, as the bypass was larger than in the present laboratory study and positioned further away from the barrier. This explains why no refusals of salmon smolts were observed at HPP Rotenfels. Fish were not caught and examined for injuries after they passed through the electric barrier. The maximal voltage gradients were also not reported, such that it cannot be assessed if the electric barrier caused any fish injuries. The example of HPP Rotenfels illustrates that it is very important to collect abiotic and biotic parameters in respect to the setup. In the case of HPP Rotenfels, this would have included for example to measure and report the electric field in detail to adequately interpret the fish behavior. It also shows that it is challenging to assess fish injuries due to the electric field in practical applications, as tagged fish are often not retrieved to check for injuries.

## 9 Operational aspects

### 9.1 Operational challenges and general considerations

The majority of floating debris consists of leaves, which are transported mainly in autumn across the whole flow depth with higher concentrations close to the bottom (Schälchli *et al.*, 1997). Foliage clogging at HBRs can dramatically increase the hydraulic losses and can lead to emergency shutdowns of HPPs (cf. Section 3.2). As an example, Fig. 9.1b shows an underwater picture of foliage clogging at the HBR Stroppel and Fig. 9.1c illustrates the operation of the RCM at HPP Hard during a flood event on 03.12.2018, which followed a dry autumn with low discharges such that many leaves were mobilized. Another problem which was reported by multiple operators of HBR-BSs is that vertical tie-bars clogged with small branches, which could not be removed by the RCM. This was also observed at the HBR of the residual flow HPP Schiffmühle (Fig. 9.1a and Fig. 3.7 in Section 3.5).



**Fig. 9.1:** (a) Permanent clogging at the vertical tie-bars of the residual flow HPP Schiffmühle during drawdown in July 2018 (Photo: J. Meister), (b) underwater picture of foliage clogging at HPP Stroppel in October 2016 (adapted from Zaugg and Mendez, 2018), and (c) operation of RCM at HPP Hard during a flood event on 03.12.2018 (cleaning direction from left to right; Photo: J. Meister); the clear bar spacing of all three HBRs is  $s_b = 20$  mm

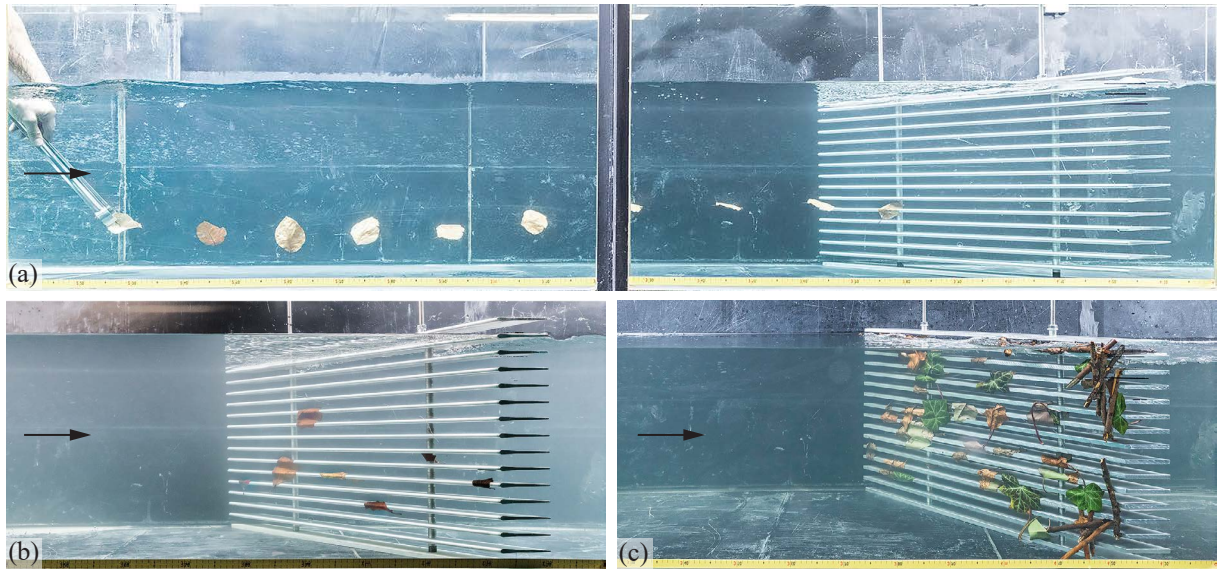
Within the present work, pictures of the whole rack area of the residual flow HPP Schiffmühle were analyzed, where it was observed that permanent clogging with branches occurred mainly within one meter below the water surface at the vertical tie-bars. In total,  $\approx 7\%$  of the upstream rack half and  $\approx 18\%$  of the downstream rack half clogged permanently. However, it has to be mentioned that the RCM at the residual flow HPP Schiffmühle did not meet current design



standards mentioned in Section 3.5, but it was recently replaced with a RCM with a rake (similar to Fig. 3.8c). Other operational challenges of HBR-BSs are sediment depositions and bypass clogging, which were described in Sections 3.2 and 3.5.

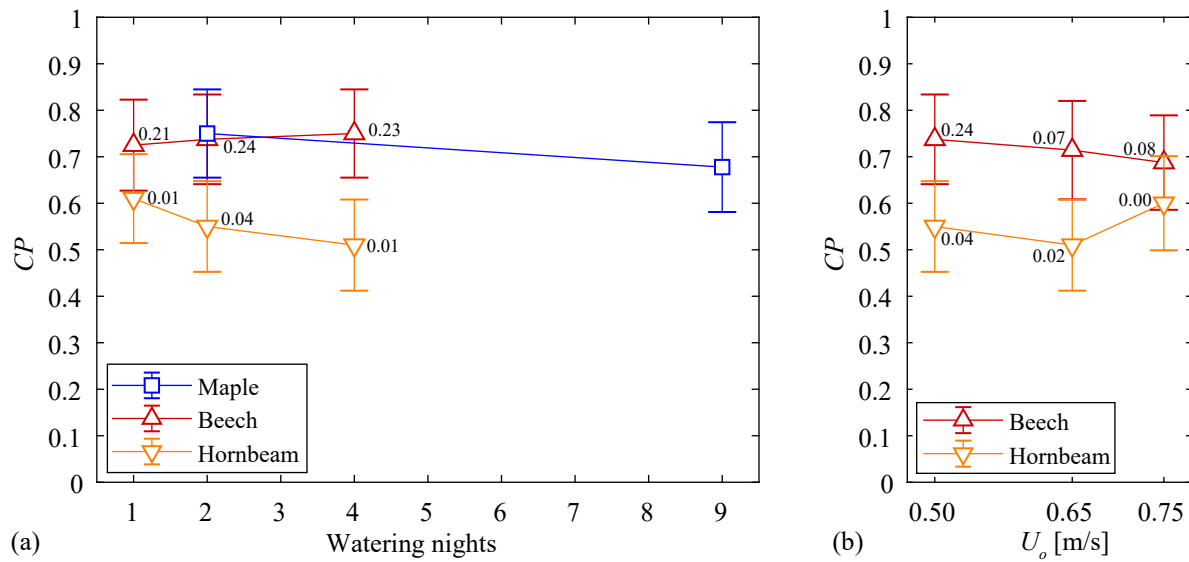
## 9.2 Clogging with floating debris

For practical applications of HBR-BSs, it is not necessary to know the clogged rack area, because RCMs can be operated based on water level measurements in front of and behind HBRs. However, it is useful to know the effect of different parameters on the clogging probability  $CP$  for designing HBRs. In March 2018, preliminary experiments were conducted with leaves and branches. The latter either passed through the HBR, were transported towards the downstream rack end, or clogged at the vertical tie-bars (Fig. 9.2c). As floating debris mainly consists of leaves (Schälchli *et al.*, 1997), small branches are only relevant if they clog permanently and cannot be removed by the RCM, as in the example of Fig. 9.1a. The survey results, presented in Section 3.2, indicate that permanent clogging can be prevented at most modern HBR-BSs, but that the biggest operational challenge is to prevent HBRs from clogging with leaves during flood events in autumn. If RCMs are designed according to common design recommendations, they can remove most leaves from the HBR (cf. Fig. 9.1), but they can reach their capacity limit. The duration of a cleaning cycle depends on the rack length and the RCM speed, but it usually takes a few minutes. The clogging probability of leaves is therefore primarily relevant to reduce hydraulic losses between cleaning cycles and to reduce the overall number of necessary cleaning cycles. The main clogging experiments were therefore conducted with leaves only. Leaves which approached the HBR either passed through the rack or clogged with a certain clogging probability  $CP$ , at the vertical tie-bars, an individual bar, or at multiple bars (Fig. 9.2a,b). Leaves which wrapped around individual bars increased the blocked area only marginally, whereas leaves which clogged at multiple bars blocked a larger rack area and therefore increased the hydraulic losses (Fig. 9.2b).



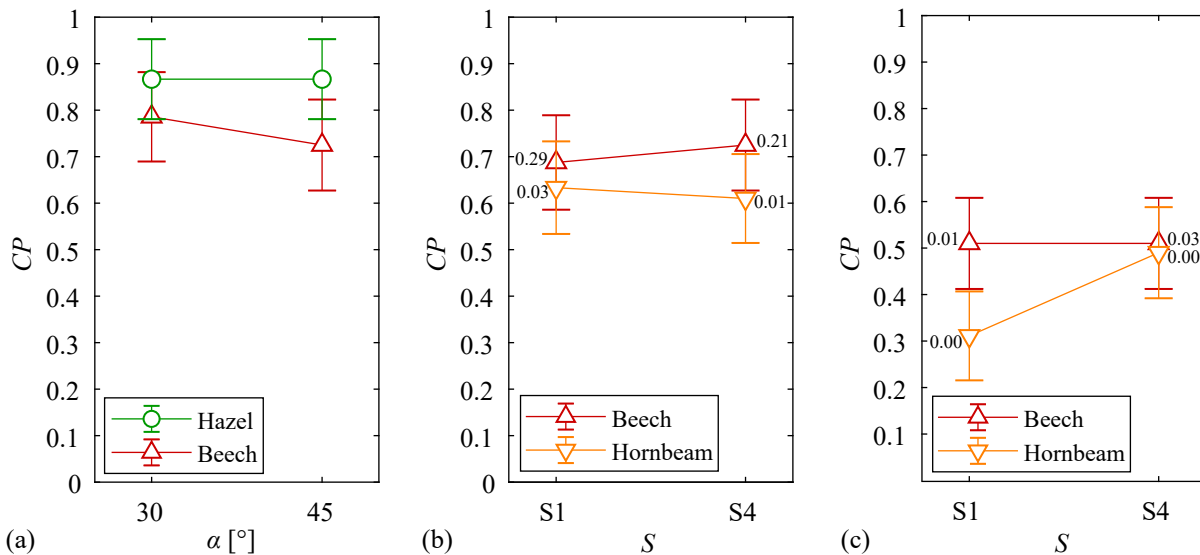
**Fig. 9.2:** (a) A picture series of a beech leaf approaching the HBR with S4-bars (foil-shaped),  $\alpha = 45^\circ$ ,  $s_b = 20$  mm, (b) foliage clogging at the same rack after a test series with ten beech leaves, and (c) clogging with leaves and branches at the HBR with S1-bars (rectangular),  $\alpha = 45^\circ$ , and  $s_b = 20$  mm (adapted from Meister *et al.*, 2018a)

Figure 9.3 shows  $CP$  as a function of the watering nights (Fig. 9.3a) and  $U_o$  (Fig. 9.3b), where the modified clogging probability  $CP_{2+}$  is indicated with small numbers beside the data points.  $CP_{2+}$  considers leaves which clogged across multiple bars only (cf. Section 4.4.5). The leaves were watered between one and nine nights, before they were used for the experiments. The number of watering nights did neither affect  $CP$  nor  $CP_{2+}$ , as the small variations in Fig. 9.3a lay within the confidence intervals. The average approach flow velocity had also no effect on  $CP$  within the range of  $U_o = 0.50$ – $0.75$  m/s (Fig. 9.3b). All further clogging experiments were therefore conducted with  $U_o = 0.50$  m/s. However, for beech leaves,  $CP_{2+}$  was larger for  $U_o = 0.50$  m/s than for  $U_o \geq 0.65$  m/s. Although hornbeam leaves hardly clogged at multiple bars, the same trend of  $CP_{2+}$  was observed. This means that the overall number of leaves which clogged at the HBR was independent of  $U_o$ , but a larger rack area was blocked for  $U_o = 0.5$  m/s than for  $U_o = 0.65$ – $0.75$  m/s, as leaves clogged more frequently across multiple bars.



**Fig. 9.3:** Effect of the (a) watering nights for  $U_o = 0.5$  m/s and (b)  $U_o$  on  $CP$  for the rack configuration S4,  $\alpha = 45^\circ$ , and  $s_b = 20$  mm; the numbers beside the data points show  $CP_{2+}$  (adapted from Ganzmann, 2019)

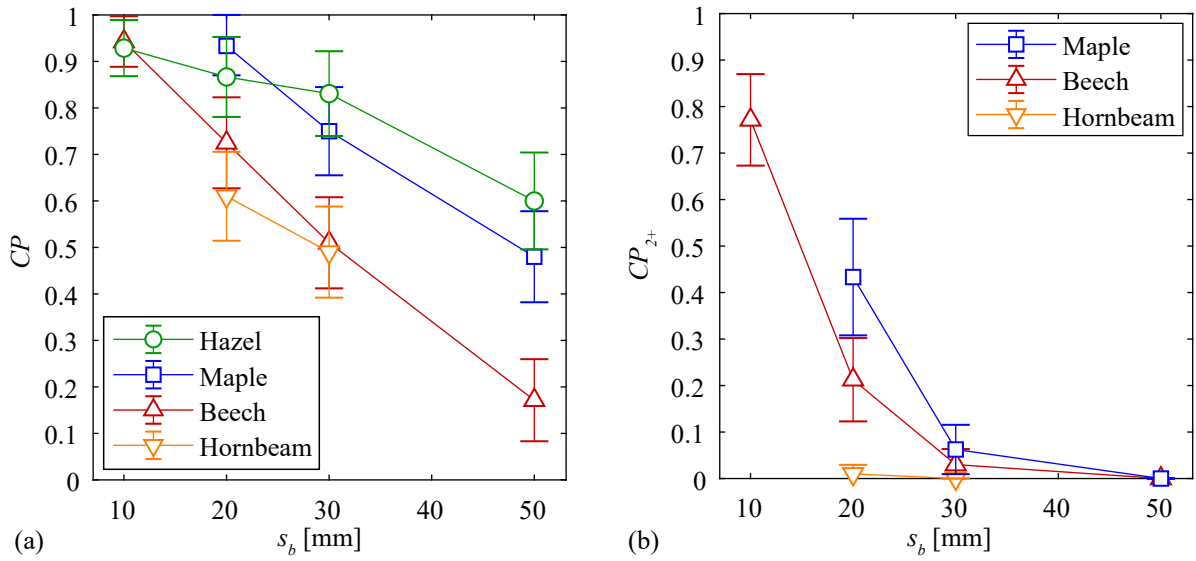
The effect of the horizontal approach flow angle  $\alpha$  was investigated for hazel and beech leaves, but no significant effect was observed in the range of  $\alpha = 30$ – $45^\circ$  (Fig. 9.4a). Likewise, no clear trend could be detected for the effect of the bar shape, where beech and hornbeam leaves were tested at an HBR with rectangular bars (S1) and at an HBR with foil-shaped bars (S4) for  $s_b = 20$  mm (Fig. 9.4b) and  $s_b = 30$  mm (Fig. 9.4c). The numbers beside the data points in Fig. 9.4b,c show  $CP_{2+}$ , which were very small for hornbeam leaves and for  $s_b = 30$  mm. However, for the considerably larger beech leaves (cf. Table 4.5) and  $s_b = 20$  mm,  $CP_{2+}$  was larger for rectangular bars (Fig. 9.4b).



**Fig. 9.4:** Effect of (a)  $\alpha$  on  $CP$  for S4-bars (foil-shaped) and  $s_b = 20$  mm, and the effect of the bar shape (S1: rectangular; S4: foil-shaped) on  $CP$  for (b)  $s_b = 20$  mm (c)  $s_b = 30$  mm with  $U_o = 0.5$  m/s; the numbers beside the data points show  $CP_{2+}$  (adapted from Ganzmann, 2019)

Figure 9.5 shows  $CP$  and  $CP_{2+}$  as a function of  $s_b$ . Note that the experiments with  $s_b = 10$  mm were conducted with slightly different-sized leaves, but the effect on  $CP$  is assumed to be small

(cf. Table 4.5). Compared to the other parameters discussed so far,  $s_b$  significantly affected  $CP$  in the range of  $s_b = 10$ –50 mm (Fig. 9.5a). The clogging probability  $CP$  decreased linearly with  $s_b$ , but the gradient and the absolute  $CP$  varied between leaf types (Fig. 9.5a). In general,  $CP$  increased with the leaf size from hornbeam ( $A = 18 \text{ cm}^2$ ), to beech ( $A = 28 \text{ cm}^2$ ), maple ( $A = 60 \text{ cm}^2$ ), and hazel leaves ( $A = 100 \text{ cm}^2$ ; cf. Fig. 9.5). In contrast to  $CP$ ,  $CP_{2+}$  decreased exponentially with  $s_b$  (Fig. 9.5b) and was very small for  $s_b \geq 30$  mm ( $CP_{2+} \leq 0.10$ ). The probability  $CP_{2+}$  very much depended on the leaf size and varied between 0.01 for hornbeam leaves ( $A = 18 \text{ cm}^2$ ) and 0.43 for maple leaves ( $A = 60 \text{ cm}^2$ ) and  $CP_{2+}$  disproportionately increased from  $s_b = 20$  mm to  $s_b = 10$  mm. The different correlations of  $CP$  and  $CP_{2+}$  with  $s_b$  is highlighted with the example of beech leaves. If an HBR with  $s_b = 20$  mm was replaced with an HBR with  $s_b = 10$  mm,  $CP$  would increase by 30% (from 0.73 to 0.94), while  $CP_{2+}$  would increase by 260% (from 0.21 to 0.77).



**Fig. 9.5:** Effect of  $s_b$  on (a)  $CP$  and (b)  $CP_{2+}$  for an HBR with S4-bars and  $\alpha = 45^\circ$  with  $U_o = 0.5$  m/s (adapted from Ganzmann, 2019)

## 9.3 Implications of clogging and remediation measures

### Implications on hydraulic losses

Foliage clogging can strongly increase the hydraulic losses of HBRs, especially if leaves clog at multiple bars such as in Fig. 9.1b and Fig. 9.2b, which occurs mainly for small  $s_b$ . However, practical examples showed that permanent clogging at HBR-BSs can be prevented even for  $s_b = 10$  mm (Ebel *et al.*, 2018). The floating debris load and especially the amount of transported leaves is very site-specific (Schälchli *et al.*, 1997). As an example, floating debris mainly consists of leaves in autumn at lower altitudes, whereas leaves play only a minor role in rivers at 700–900 m.a.s.l. (Schälchli *et al.*, 1997). The head losses due to partial clogging, can be accounted for with the overlay coefficient  $C_{Ov}$  (Eq. 6.7 in Section 6.2). If no site-specific information is available, it is recommended to assume partial clogging of 20% of the rack area as proposed by Turnpenny and O’Keeffe (2005) for the head loss estimation in autumn, that is,  $H_{Ov} = 0.2$  and  $C_{OL} = 0.9$  in Eq. (6.7).

### Implications on the velocity field and fish guidance

Foliage clogging does also affect the velocity field and potentially the fish behavior. If an HBR is partially clogged,  $V_n$  increases locally at the unclogged rack area, which might increase the rack passage and impingement risk. To avoid these negative effects, Turnpenny and O’Keeffe (2005) recommended to design racks with an over-capacity of at least 20%. Zaugg and Mendez (2018) observed that clogged leaves were in motion due to the flow, from which the authors hypothesized that fewer small fish passed the HBR at HPP Stroppel, as the partially clogged HBR did not only act as a physical but also as a behavioral barrier. In the present study, most leaves which clogged at the HBR were stable and hardly moved with the flow. It is also questionable if leaves which are in motion really increase the behavioral avoidance effect, as fish also passed through small-spaced vibrating cables in the experiments of Kammerlander *et al.* (2020) (Section 3.7.4). However, as it is very challenging to study the effect of partial clogging on the fish behavior especially in monitoring campaigns, few information exists, which makes further research indispensable.

### Remediation measures

The main parameters affecting HBR foliage clogging are the amount of floating debris, the leaf sizes, and  $s_b$ . It is often not possible to reduce the amount of floating debris and to increase  $s_b$  as it lowers FGE (cf. Section 7.2). It is also mostly not possible to fully prevent clogging at HBR-BSs, which is the main operational challenge. However, if HBR-BSs, including the RCMs, are designed according to common recommendations (cf. Section 3.4), the effect of partial clogging can be mitigated. The most important points are that the RCM is designed appropriately with a rake to remove clogged logs from between the vertical tie-bars and that an open channel bypass with a flushing gate is installed instead of a pressurized pipe bypass. From an operational point of view, it is recommended to use bars with a small constricted section at the bar tip and with a reduced width from tip to tail (such as Fig. 4.14b–d), as clogged logs can be removed more easily compared to rectangular bars; this was already pointed out by Kirschmer (1925) for traditional trash racks. Bottom and top overlays increase the ratio of the rack-parallel to rack-normal velocity component close to the bottom and the surface of HBRs, respectively, such that they can be installed to guide sediments and floating debris towards the bypass (cf. Fig. 5.5). If large sediment loads are expected, it is recommended to install a sediment flushing channel below the HBR (cf. Section 9.1). Apart from foliage clogging, sediments can cause operational challenges which require remediation measures as described in Section 3.5.

## 10 Design recommendations and engineering application

In this chapter, the most important design recommendations are summarized, and the head losses and survival rates are calculated on the basis of a practical example with the equations proposed within the present thesis. More background, references, and details about the equations can be found in the corresponding chapters of the present thesis.

### 10.1 Design recommendations

Designing efficient horizontal bar rack bypass systems (HBR-BSs) is very site-specific and many different aspects have to be considered. This section summarizes the most important recommendations for the design of HBR-BSs, which are based on the findings of the present study, including a detailed literature review, a survey involving hydropower plant (HPP) operators, an extensive hydraulic laboratory investigation (velocity fields, head losses, and foliage clogging), and live fish tests. These design recommendations were developed to account for fish protection, cost-efficiency, and sustainable operation of HBR-BSs and is based on the present state of knowledge. Table 10.1 briefly summarizes the key criteria to design horizontal bar racks (HBRs), which are explained in more detail in the following (Table 10.2). The typical parameter ranges in Tables 10.1 and 10.2 are reference values, which are targeting common European HPPs.

**Table 10.1:** Key criteria for designing HBR-BSs, where  $V_p$  and  $V_n$  are the velocity components parallel and normal to the rack, respectively,  $s_b$  is the clear bar spacing, and  $w_f$  the fish width

Criterion number	Criterion	Typical parameter range
1	$V_n < v_f^*$	0.20–0.50 m/s
2	$V_p/V_n > 1$	1.0–2.5
3	$s_b < w_f$	10–20 mm

\* Sustained swimming speed, typically for durations of  $t = 200 \text{ min} = 12\,000 \text{ s}$

The most important design parameters are the horizontal approach flow angle  $\alpha$ , which depends on the approach flow velocity  $U_o$  and the target fish swimming capabilities, and the clear bar spacing  $s_b$ , which depends on the fish dimensions. HBRs should be designed such that at design discharge,  $V_n$  does not exceed the sustained swimming speed of the smallest fish of the species with the weakest swimming performance, which should be protected. As an example, the sustained swimming speed of non-rheophilic species is  $v_f = 0.28 \text{ m/s}$ , given typical assumptions (Eq. 2.10 with a total length of  $TL = 0.1 \text{ m}$ , a duration of  $t = 12\,000 \text{ s}$ , and a water temperature of  $T = 5^\circ\text{C}$ ). With an approach flow velocity at design discharge of  $U_o = 0.6 \text{ m/s}$  at a diversion hydropower plant (HPP;  $V \approx 0 \text{ m/s}$ ), this would yield to  $\alpha = 28^\circ$  (from  $v_f = V_n$  and Eq. 3.1; neglecting partial clogging for simplicity). It has to be additionally ensured that  $V_p/V_n > 1$ ,

which means that  $\alpha$  should never be larger than  $45^\circ$ , ideally not larger than  $40^\circ$  to account for inhomogeneous velocity distributions. At diversion HPPs, where the HBR is installed across the entire headrace channel,  $V_p/V_n$  can be calculated as  $V_p/V_n = 1/\tan(\alpha) = \cot(\alpha)$ . For different HPP layouts, a numerical simulation is recommended to verify  $V_p/V_n > 1$  in a rack-parallel cross section upstream of the HBR for various load cases. If this criterion is not fulfilled, possible countermeasures are the installation of a dividing pier between turbine and weir or the reduction of the relative turbine discharge, for example through increased weir discharge. It is recommended to install a bottom overlay or a similar structure to enhance guidance of bottom-oriented fish and sediments. If surface-oriented fish or much floating debris at the water surface is expected, it is also suggested to install a top overlay, where water level fluctuations throughout the year have to be considered. Foil-shaped bars are recommended to reduce the hydraulic losses and to allow for an efficient cleaning with an automated rack cleaning machine (RCM), which should protrude at least 2 cm into the bar gaps. A flushing gate should be installed at the downstream rack end, which automatically opens when it is approached by the RCM. The clear bar spacing  $s_b$  is typically in the range of  $s_b = 10\text{--}20$  mm (Table 10.2). It should be designed to reach the required total survival rate, which is described in detail in Section 10.3. The bar thickness  $t_b$  is limited by structural considerations, and the relative bar depth should not exceed  $D_b = 7.5$  to reduce hydraulic head losses. Instead of strictly demanding a certain relative bypass discharge  $Q_{by,rel}$ , it is important to focus on the flow conditions at the bypass inlet. The mean flow velocities at the bypass inlet should be in the range of  $U_{by,in} = 0.30\text{--}1.50$  m/s (Ebel, 2016). The ratio of the mean flow velocity at the bypass inlet to the mean approach flow velocity is recommended to be  $VR = U_{by,in}/U_o \approx 1.2$ , and turbulences and pronounced flow accelerations should be avoided. Ideally, flow velocities slightly increase from the downstream rack end into the bypass. If feasible, a full depth open channel bypass is recommended to allow for downstream movements in all flow depths. Otherwise, parts of the flow depth can be obstructed, where the dimensions of the bypass openings have to be designed to account for the largest and most demanding fish species. Bypass openings are typically 0.40–0.60 m wide and 0.60–0.90 m high (Ebel, 2016). The bypass openings should be designed such that the bypass can be fully opened for flushing of floating debris and to prevent clogging of the bypass openings. If these criteria are fulfilled,  $Q_{by,rel}$  is typically larger than 2%. Curvatures in the bypass should be avoided and maximal flow velocities should be limited to 4.5 m/s, but 7–8 m/s are acceptable for overflowing water, if the tailwater depth exceeds one quarter of the differential head, but at least 0.90 m (details in Section 3.4.2).

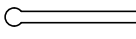
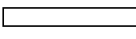
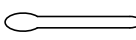
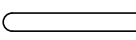
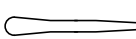

**Table 10.2:** Typical parameter range of HBRs based on different design criteria and considerations

Parameter	Design criteria	Typical parameter range
$\alpha$	Designed to fulfill criterion 1 and 2	$\alpha = 20\text{--}40^\circ$
$U_o$	Designed to fulfill criterion 1	$U_o = 0.40\text{--}0.80$ m/s
$s_b$	Designed to fulfill criterion 3	$s_b = 10\text{--}20$ mm
$t_b$	Structural considerations	$t_b = 8\text{--}10$ mm
$D_b$	Reduced hydraulic losses	$D_b = 5.5\text{--}7.5$
Bar shape	Reduced hydraulic losses	Foil-shaped

## 10.2 Head loss assessment

In Table 10.3, all important equations for the head loss assessment of HBRs are summarized, which were described in detail in Chapter 6. Their application is then explained with an example.

**Table 10.3:** Empirical equations for the head loss assessment of HBRs

	Hydrodynamic bars	Non-hydrodynamic bars
Blocking ratio	$BR = \frac{t_b + s_b n_v t_s / w_{ds}}{s_b + t_b}$	
Simplified blocking ratio <sup>1</sup>	$BR = 1.2 \frac{t_b}{s_b + t_b}$	
Blocking ratio coefficient	$C_{BR} = \frac{BR}{(1-BR)}$	$C_{BR} = \left(\frac{BR}{1-BR}\right)^{3/2}$
Approach flow angle coefficient	$C_\alpha = \sin(\alpha)^{2/3}$	$C_\alpha = \sin(\alpha)^{4/3}$
Bar shape coefficient	 $C_S = 0.83$	 $C_S = 2.33$
	 $C_S = 0.67$	 $C_S = 1.60$
	 $C_S = 0.64$	 $C_S = 1.72$
Bar depth coefficient	$C_{Db} = 0.04 (D_b - 7.5) \left( \frac{90^\circ - \alpha}{60^\circ} \right) + 1$	
Overlay layout coefficient	$C_{OL} = 1.0$ bottom <u>or</u> top overlay	
	$C_{OL} = 0.9$ bottom <u>and</u> top overlay	
Overlay coefficient	$C_{Ov} = 1 + C_{OL} \left( \frac{0.5}{BR^2} + \frac{7.4 \sin(\alpha)^2}{C_S^{0.8}} \right) \left( \frac{H_{Ov}}{1-H_{Ov}} \right)^{4/3}$	
Rack head loss coefficient	$\xi_R = C_{BR} C_\alpha C_S C_{Db} C_{Ov}$	
Rack head losses	$\Delta h_R = \xi_R \frac{U_{th}^2}{2g}$	
Contraction head loss coefficient <sup>2</sup>	$\xi_c = \frac{1}{2} \left( 1 - \frac{A_{ds}}{A_o} \right)^{3/4}$	
Contraction head losses	$\Delta h_c = \xi_c \frac{U_{th}^2}{2g}$	
Head losses (rack + contraction) <sup>2</sup>	$\Delta h = \Delta h_R + 1.7 \Delta h_c$	

<sup>1</sup> Assumes that the vertical tie-bars contribute to 20% of the blocking ratio of the horizontal bars; this equation is only recommended as an approximation, if the detailed design of the vertical tie-bars is unknown

<sup>2</sup> For a sharp contraction between the downstream rack end and the weir/flushing gate



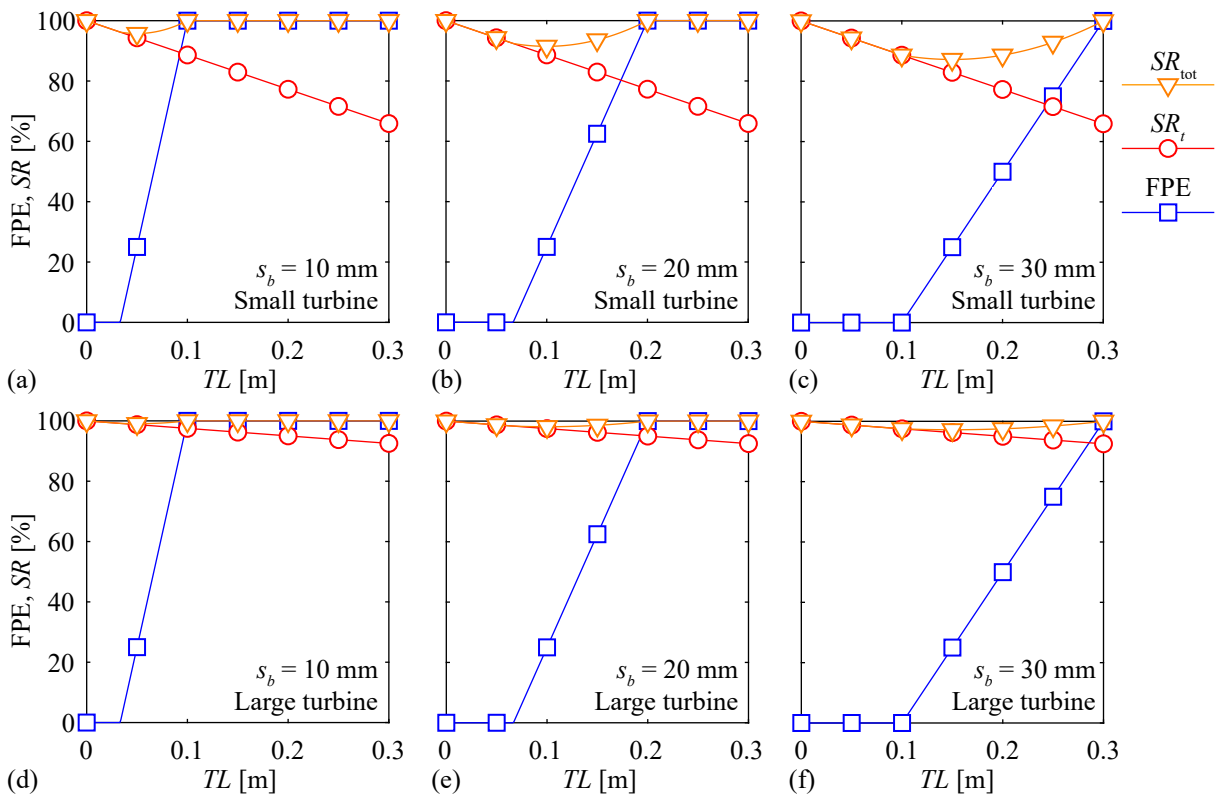
Slightly different equations were proposed for hydrodynamic and non-hydrodynamic bars to account for differences in the hydraulic processes. Hydrodynamic bars are characterized by a reduced thickness from tip to tail, whereas non-hydrodynamic bars have a nearly constant bar thickness. For the practical example, plausible input parameters were chosen, which fulfill all design criteria of Section 10.1. They are listed on the left side of Table 10.4. The rack length is determined from trigonometry as  $l_R = w_{ds} / \sin(\alpha) = 40$  m, which means that  $n_v = 40 \text{ m} / 0.6 \text{ m} \approx 67$  vertical tie-bars are required. The total relative overlay height determines to  $H_{Ov} = H_{Bo} + H_{To} = 0.2$ . At diversion HPPs, where the upstream and downstream channel width are equal ( $w_o = w_{ds}$ ), the theoretical average flow velocity corresponds to the approach flow velocity, that is,  $U_{th} = Q_i / (h_o w_{ds}) = 36 \text{ m}^3/\text{s} / (3 \text{ m} \times 20 \text{ m}) = 0.6 \text{ m/s}$ . The output parameters, calculated with the equations of Table 10.3, are summarized on the right side of Table 10.4. The total rack head losses of the unclogged HBR are  $\Delta h_R = 8.5$  mm (Table 10.4). The head losses of the partially clogged HBR can be estimated with an increased relative overlay height. If partial clogging of 20% of the rack area is assumed, the relative total overlay height increases from  $H_{Ov} = 0.2$  to  $H_{Ov} = 0.4$ , while the overlay layout coefficient reduces from  $C_{OL} = 1$  to  $C_{OL} = 0.9$ , as partial clogging is expected in different flow depth. This yields an overlay coefficient of  $C_{Ov} = 4.10$ , a rack head loss coefficient of  $\xi_R = 0.98$ , and rack head losses of  $\Delta h_R = 17.9$  mm. If a flushing gate is installed at the downstream rack end, the resulting contraction losses should be considered. Assuming a flushing gate width of 2 m ( $w_o = 22$  m,  $w_{ds} = 20$  m), the contraction losses for constant flow depth are  $\xi_c = 0.08$ , leading to contraction head losses of  $\Delta h_c = 1.5$  mm. The HBR increases the contraction losses by a factor of 1.7, such that the total head losses of the HBR-BS are expected to be  $\Delta h = \Delta h_R + 1.7\Delta h_c = 11.0$  mm for the unclogged HBR and  $\Delta h = 20.5$  mm for the partially clogged HBR.

**Table 10.4:** Input and output parameters of the practical example of the head loss assessment; the values represent the diversion HPP without clogging and without considering the contraction losses due to the flushing gate

Input parameters		Output parameters	
Average approach flow velocity	$U_o = 0.6 \text{ m/s}$	Blocking ratio	$BR = 0.39$
Horizontal approach flow angle	$\alpha = 30^\circ$	Blocking ratio coefficient	$C_{BR} = 0.64$
Clear bar spacing	$s_b = 15 \text{ mm}$	Approach flow angle coeff.	$C_\alpha = 0.63$
Bar thickness	$t_b = 8 \text{ mm}$	Bar shape coefficient	$C_S = 0.64$
Relative bar depth	$D_b = 5.5$	Bar depth coefficient	$C_{Db} = 0.92$
Relative bottom overlay height	$H_{Bo} = 0.2$	Overlay layout coefficient	$C_{OL} = 1.00$
Relative top overlay height	$H_{To} = 0$	Overlay coefficient	$C_{Ov} = 1.93$
Bar shape	Foil-shaped	Rack head loss coefficient	$\xi_R = 0.46$
HPP layout	Diversion	Rack head losses [mm]	$\Delta h_R = 8.5$
Downstream channel width	$w_{ds} = 20 \text{ m}$		
Spacer/vertical tie-bars thickness	$t_s = 20 \text{ mm}$		
Distance between vertical tie-bars	$0.6 \text{ m}$		
Approach flow depth	$h_o = 3 \text{ m}$		
Turbine discharges	$Q_t = 36 \text{ m}^3/\text{s}$		

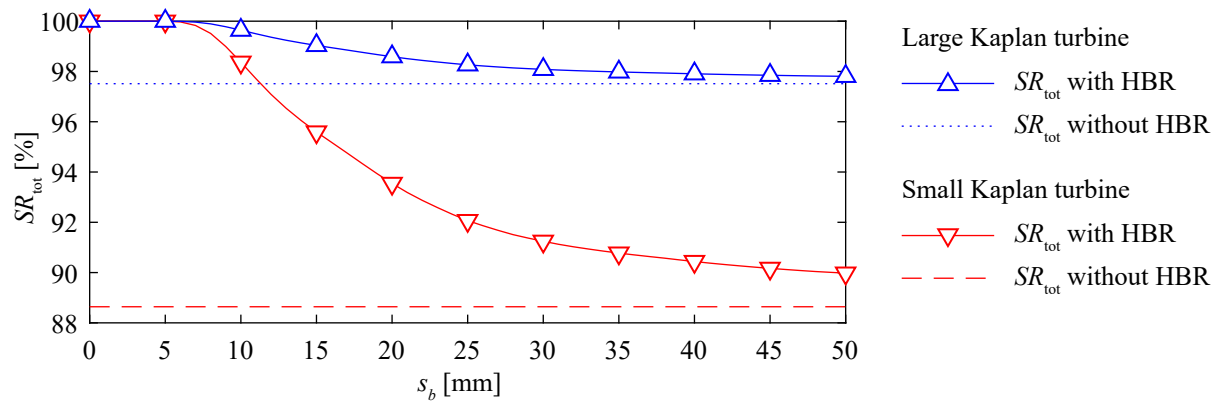
### 10.3 Fish protection, turbine survival rate, and total survival rate

One of the advantages of physical barriers is that larger fish are physically blocked by the barrier, while smaller fish, which have a larger probability to pass through the HBR, have a higher turbine survival rate. To properly account for this effect, it is necessary to calculate the total survival rate  $SR_{\text{tot}}$  for each size class independently, which is explained in the following. For this example, the fish protection efficiency FPE was calculated as  $FPE = 150w_f/s_b - 50$  (Eq. 7.2, details in Section 7.2.2) for a clear bar spacing of  $s_b = 10, 20, \text{ and } 30 \text{ mm}$  for a small and a large Kaplan turbine, assuming an average relative fish width of  $w_{f,\text{rel}} = 0.10$  (Fig. 10.1). The turbine survival rate  $SR_t$  was calculated as  $SR_t = 100 - 50TL/s_{\text{rel,mid}}$  (Eq. 2.13, details in Section 2.3.2) following Montén (1985) with  $s_{\text{rel,mid}} = 0.44 \text{ m}$ , which was determined for a small Kaplan turbine with six turbine blades, 214 rotations per minute, a minimal runner diameter of  $0.7 \text{ m}$ , a maximal runner diameter of  $2.9 \text{ m}$ , and a turbine discharge of  $Q_t = 60 \text{ m}^3/\text{s}$ . The same calculations were done for a large Kaplan turbine with  $s_{\text{rel,mid}} = 2.01 \text{ m}$ , where four turbine blades with 64 rotations per minute, a runner diameter of  $1.0\text{--}5.9 \text{ m}$ , and  $Q_t = 400 \text{ m}^3/\text{s}$  were assumed. If injuries from other downstream passage corridors such as the bypass and the spillways are negligible, the total survival rate determines to  $SR_{\text{tot}} = FPE + (100\% - FPE)SR_t$ .



**Fig. 10.1:** Turbine survival rate  $SR_t$ , fish protection efficiency FPE of an HBR, and total survival rate  $SR_{tot}$  as a function of total fish length  $TL$  for a small Kaplan turbine with clear bar spacing of (a)  $s_b = 10$  mm, (b)  $s_b = 20$  mm, and (c)  $s_b = 30$  mm and for a large Kaplan turbine with (d)  $s_b = 10$  mm, (e)  $s_b = 20$  mm, and (f)  $s_b = 30$  mm

With  $s_b = 10$  mm, all fish with  $TL \geq 0.1$  m are physically protected, while fish with  $TL = 0.05$  m have the lowest total survival rate of  $SR_{tot} = 96\%$  for the small Kaplan turbine (Fig. 10.1a). Very small fish ( $TL < 0.05$  m) have a higher  $SR_{tot}$  due to the high  $SR_t$ , while slightly larger fish ( $0.05 \text{ m} < TL < 0.1$  m) have a high  $SR_{tot}$  as they are protected by the HBR with a high probability. With  $s_b = 20$  mm and  $s_b = 30$  mm, the minimal survival rates with the small Kaplan turbine are  $SR_{tot} = 91\%$  with  $TL = 0.1$  m and  $SR_{tot} = 87\%$  for  $TL = 0.15$  m, respectively (Fig. 10.1b,c). In comparison, the minimal survival rates at the large Kaplan turbine are  $SR_{tot} = 99\%$ ,  $SR_{tot} = 98\%$ , and  $SR_{tot} = 97\%$  for  $s_b = 10$  mm,  $s_b = 20$  mm, and  $s_b = 30$  mm, respectively (Fig. 10.1d–f). If the size distribution of the fish passing through the turbines is known (e.g. from stow net catches),  $SR_{tot}$  can be weighted with the relative abundance per size class. Independent of its life stage, each individual is weighted equally in the following example. However, it is also possible to weight size classes differently, as one large individual is more valuable to the ecosystem than one small individual. In the example in Fig. 10.2, FPE,  $SR_t$ , and  $SR_{tot}$  were calculated as described above for each size class of barbels in the Limmat River from Fig. 2.5a with  $w_{f,rel} = 0.11$  (Table 2.2) for different  $s_b$ . Without any fish protection measure and the assumption that all fish swim through the turbines, the total survival rate is  $SR_{tot} = 88.6\%$  and  $SR_{tot} = 97.5\%$  for the small and large Kaplan turbine, respectively (dashed and dotted lines in Fig. 10.2). These percentages increase to  $SR_{tot} = 93.6\%$  and  $SR_{tot} = 98.6\%$  with an HBR with  $s_b = 20$  mm and to  $SR_{tot} = 98.4\%$  and  $SR_{tot} = 99.6\%$  with  $s_b = 10$  mm.



**Fig. 10.2:** Total estimated survival rate of barbels for the fish size distribution in Fig. 2.5a as a function of the clear bar spacing  $s_b$  for the small and large Kaplan turbine with  $w_{f,rel} = 0.11$  for barbels (cf. Table 2.2)

This practical example illustrates how the proposed equations can be applied to estimate the total survival at HPPs. However,  $SR_{tot}$  is very site-specific, such that Fig. 10.1 and 10.2 cannot be generalized. When  $SR_{tot}$  is interpreted, it is very important to know the underlying assumptions, such as the limitations described in Section 7.7 and the equation which was used to determine  $SR_t$ . To choose an appropriate  $s_b$ , which is one of the most critical design parameters of HBRs, it has to be defined to which extent small fish with  $TL < 10\text{--}20$  cm have to be protected, which typically make up the vast majority of individuals in a river system. After the construction of an HBR-BS, it is important to quantify the efficiency with a monitoring campaign. If the survival rate of very small fish ( $TL \leq 10$  cm) is of interest, it is strongly recommended to install stow nets at the turbine outlets (cf. Section 2.3.1), where the size-selectivity of the catching units has to be considered.



# 11 Conclusions and outlook

## 11.1 Conclusions

The overall goal of this doctoral thesis was to provide technical knowledge, such that horizontal bar rack bypass systems (HBR-BSs) can be designed as a compromise between fish protection, cost-efficiency, and sustainable operation. To reach this goal, an extensive laboratory study was carried out, where the velocity fields and head losses were measured for a wide parameter range of horizontal bar racks (HBRs). The fish guidance efficiency of HBR-BSs was then quantified for various fish species with and without the combination of a low-voltage electric field. Additional experiments were conducted to quantify the effect of different parameters on foliage clogging, which is one of the most important operational aspects of HBR-BSs. In the following, each of these chapters is very briefly summarized and the main findings are highlighted.

### Chapter 5: Velocity fields

The velocity fields at HBRs were presented for four different bar shapes, with approach flow angles  $\alpha = 30^\circ$ ,  $45^\circ$  and  $90^\circ$ , clear bar spacings  $s_b = 10, 20$ , and  $30$  mm, and various overlay configurations. The upstream velocity field was analyzed with respect to the guidance efficiency of fish, sediments, and floating debris, while the downstream velocity field was evaluated with respect to the turbine admission flow. Besides the diversion hydropower plant layout, a block-type layout was investigated (a) with an abrupt contraction, (b) with a short pier, (c) with a long pier, and (d) with a short pier and additional weir discharge. Different bypass configurations were analyzed in terms of their hydraulic characteristics for fish guidance. The analysis of the velocity fields led to the following key findings:

- I) The bar shape, approach flow angle  $\alpha$ , and the clear bar spacing  $s_b$  have a minor effect on the velocity field. The discharge difference between the left and right channel halves downstream of the HBR were smaller than 4.2% for all configurations without overlays. The effect of HBRs without overlays on the velocity field was largest for rectangular bars, large approach flow angles  $\alpha$ , and small clear bar spacing  $s_b$ .
- II) Bottom and top overlays at HBRs have a governing effect on the velocity fields upstream and downstream of the rack. The discharge difference between the left and right channel halves downstream of the HBR was up to 24.8%. Overlays potentially improve guidance of fish and floating debris, but they can negatively affect the turbine admission flow and thus reduce the turbine efficiency. This negative effect is particularly important if the rack is installed close to the turbines.
- III) For unclogged HBRs without overlays at a diversion hydropower plant, the ratio of the parallel to the normal flow velocity component ( $V_p/V_n$ ) mainly depends on the horizontal approach flow angle  $\alpha$  and can be calculated in good approximation as a cross-sectional

average to  $V_p/V_n = 1/\tan(\alpha) = \cot(\alpha)$ . For a horizontal approach flow angle of  $\alpha = 30^\circ$ , this ratio is  $V_p/V_n = 1.73$ , which is considered favorable for fish guidance.

- IV) The hydropower plant layout strongly affects the approach flow field to HBRs. For a block-type hydropower plant with an abrupt contraction and without weir discharge, the ratio  $V_p/V_n$  continuously decreased from 1.8 at the rack head to 0 at the bypass inlet, resulting in unfavorable flow conditions for fish guidance.
- V) To optimize the fish guidance of HBRs at block-type hydropower plants, the installation of a dividing pier or partial spillway operation are suitable measures. To maintain symmetrical turbine admission flow, the installation of a pier (block-type) or a flow-straightening wall downstream of the rack are effective measures.
- VI) The bypass affects the velocity field only locally. With the full depth open channel bypass, velocities increased locally at the bypass inlet and were constant further downstream. The spatial velocity gradient and the turbulent kinetic energy were small.
- VII) The cross section at the bypass inlet can be narrowed down with installations such as a restrictor or a pipe bypass to reduce the bypass discharge, while maintaining flow accelerations. However, they either lead to a velocity drop in front of the bypass or very large accelerations, which both is considered not optimal for fish guidance.

## Chapter 6: Head losses

The head losses of HBRs were investigated in a sectional laboratory model on a Froude scale of 1:1. Potential model effects were studied to ensure the transferability of the results to prototype situations. The parameter variation included different bar shapes (rectangular and three types of hydrodynamic bars), clear bar spacings  $s_b = 10, 20$ , and  $30$  mm, approach flow angles  $\alpha = 30^\circ, 45^\circ$ , and  $90^\circ$ , relative bar depths  $D_b = d_b/t_b = 3.5\text{--}15$ , and a wide range of overlay configurations. Additional experiments were conducted for a wider upstream channel to account for different hydropower plant layouts (diversion vs. block-type). The head losses of HBRs can be predicted using Eq. (6.1) and (6.6) for hydrodynamic and rectangular bars, respectively, thereby incorporating the following key findings:

- I) The hydraulic processes at racks with rectangular bars differ significantly from hydrodynamic bars. Therefore, separate head loss prediction equations are proposed.
- II) Head losses are significantly reduced by foil-shaped bars. On average, foil-shaped bars lead to more than 40% smaller losses compared to rectangular bars. This loss reduction is more pronounced for racks with large blocking ratios  $BR$ , large approach flow angles  $\alpha$ , and small relative overlay blocking ratios  $H_{Ov}$ .
- III) For practical applications at an HBR with an approach flow angle  $\alpha = 30^\circ$  and a relative bar depth of  $D_b = 5\text{--}10$ , the effect of  $D_b$  on  $\xi_R$  is small ( $\leq \pm 10\%$ ). However, if very short ( $D_b = 3.5$ ) or very deep bars ( $D_b = 15$ ) are used in combination with small clear



bar spacing ( $s_b = 10$  mm, blocking ratio  $BR \approx 0.49$ ),  $\xi_R$  can reduce by 16% or increase by 30%, respectively, in comparison to  $D_b = 7.5$ .

- IV) Overlays strongly increase head losses. For typical hydropower plants (approach flow angle  $\alpha = 30^\circ$ , clear bar spacing  $s_b = 20$  mm, blocking ratio  $BR \approx 0.35$ ), the application of bottom and top overlays with a height of 20% of the flow depth ( $H_{Bo} = H_{To} = 0.2$ ) increases the loss coefficient  $\xi_R$  by a factor of 4.0–4.5.
- V) The validation showed that measurement data from literature of HBRs with rectangular, cylindrical, and one-side rounded bars can be predicted with an accuracy of  $\pm 30\%$ .
- VI) In addition to diversion hydropower plants, the proposed equations can also be applied for block-type hydropower plants. HBRs installed at block-type hydropower plants with a sharp contraction increase the contraction losses by a factor of 1.7.
- VII) Depending on the exact blocking ratio, the rack head loss coefficient of an optimized HBR configuration without overlays is approximately equal to traditional trash racks and smaller than at most other fish guidance structures such as inclined racks or modified bar racks, given that substantial clogging can be prevented.

## Chapter 7: Live fish tests without electrification

A large number of live fish tests was conducted with spirlin, barbel, nase, trout, salmon parr, and eel for various flow conditions and different bypass configurations, which led to the following key findings:

- I) No fish impingements or injuries were observed at the HBR without electrification with average approach flow velocities of  $U_o = 0.5\text{--}0.7$  m/s and a clear bar spacing of  $s_b = 15\text{--}20$  mm.
- II) Fish aligned themselves with various angles  $\alpha_f$  to the normal flow velocity component  $V_n$ . Especially small individuals with limited swimming capabilities (spirlin, nase) did hardly position themselves directly against the flow. Instead, they approached the HBR almost with a parallel orientation ( $\alpha_f \approx 90^\circ$ ) and swam away from the HBR with  $\alpha_f \approx 0\text{--}45^\circ$ .
- III) A part of the fish of all tested species (except eel) rotated themselves to pass through HBRs. Hence, fish can only be fully protected with HBRs, if both the height  $h_f$  and width  $w_f$  are larger than the clear bar spacing  $s_b$ .
- IV) Besides this physical barrier effect, smaller fish of certain species were partially guided into the bypass, suggesting that HBRs act as behavioral barriers to a certain extent. This behavioral guidance effect was quantified as a function of the ratio of the fish width to the clear bar spacing  $w_f/s_b$ .

- V) Most fish, including eels, were protected and efficiently guided along the HBR to the downstream rack end. Exceptions were small individuals, which were not physically protected and often passed through the rack.
- VI) The fish protection and guidance efficiencies varied across species, which for the most part can be explained by the ratio of the fish width to the clear bar spacing  $w_f/s_b$  for nase, salmon, trout, barbel, and eel. Given identical  $w_f/s_b$ , spirlin were better protected than all other species.
- VII) Considering all fish species, the approach flow velocity  $U_o = 0.5\text{--}0.7$  m/s did neither affect the number of bypass passages nor rack passages, but it significantly increased the number of refusals. An increased ratio of the bypass inlet to mean approach flow velocity  $VR = 1.2\text{--}1.4$  led to significantly less bypass passages, but more rack passages and refusals. This is because many fish of some species hesitated to enter the bypass for larger  $VR$ , which increased the rack passage risk as they actively searched for an alternative downstream passage corridor. A suitable bypass at the downstream rack end is therefore essential to reduce the rack passage risk.
- VIII) Fish passed through the HBR primarily within the first few bars above the bottom in the flume with an approach flow depth of  $h_o = 0.90$  m. The transition from the HBR to the flume bottom is therefore crucial to avoid model effects in laboratory experiments with live fish.

## Chapter 8: Live fish tests with electrification

Live fish tests with spirlin and eels were conducted at a hybrid barrier, where the HBR was combined with an electric field. Different clear bar spacings were tested and compared to the results of the HBR without electrification, which led to the following key findings:

- I) The electric field strongly depends on the setup. As an example, the voltage gradients and equipotential lines were very different between output voltages of  $U_e = 38$  V and  $U_e = 80$  V.
- II) It is very difficult to find an electrification setup with small voltage gradients at the transition from the barrier to the bypass, at least at the experimental scale of the current laboratory setup.
- III) Most spirlin were protected well by the electrified HBR, although a few rack passages were observed, independent of the clear bar spacing in the range of  $s_b = 20\text{--}51$  mm. The majority of spirlin refused to enter the bypass, which was caused by the voltage gradient at the bypass inlet.
- IV) Eels could only be sufficiently protected with the electrified HBR for a clear bar spacing of  $s_b = 20$  mm, while multiple rack passages were observed for  $s_b = 51$  mm. Eels were well protected when they approached the rack almost perpendicular to the equipotential

lines. Rack passages were observed only for eels which were aligned parallel to the rack and therefore also parallel to the equipotential lines.

- V) The electrified HBR caused fish injuries even for output voltages of  $U_e = 38 \text{ V}$  and maximal voltage gradients of  $\approx 2.1 \text{ V/cm}$  between the anode and the cathode.

## Chapter 9: Operational aspects

A questionnaire was sent to multiple operators of HBR-BSs to assess operational challenges. Additionally, systematic laboratory experiments were conducted to better understand the clogging processes at HBRs, which led to the following key findings:

- I) Operational challenges can be reduced by following common design recommendations. Some of the most important aspects are to use a sufficiently strong designed rack cleaning machine with a rake, to use optimized bars, and to build an open channel bypass with a flushing gate instead of a pressurized pipe bypass.
- II) If HBR-BSs are designed according to common design recommendations, foliage clogging with leaves in autumn will likely be the main operational challenge. This can lead to large hydraulic losses and, in the worst case, to emergency shutdowns of the hydropower plant.
- III) The clogging probability of leaves mainly depends on the leaf size and the clear bar spacing  $s_b$ . The clogging probability of leaves decreases linearly with  $s_b$ , while the probability that leaves clog across multiple bars simultaneously ( $CP_{2+}$ ) decreases exponentially with  $s_b$ . Rack cleaning machines at HBRs with  $s_b = 10 \text{ mm}$  must therefore be much more efficient than at racks with  $s_b = 20 \text{ mm}$  to prevent increased hydraulic losses.
- IV) Only a small fraction of leaves will clog across multiple bars for a clear bar spacing of  $s_b \geq 30 \text{ mm}$  and an average approach flow velocity of  $U_o = 0.5 \text{ m/s}$ , which can considerably reduce operational challenges.
- V) Efficient rack cleaning machines in combination with a proper bypass and flushing system are key to reduce operational challenges. Remediation measures such as sediment removal plates, sediment flushing channels below the HBR, and bottom and top overlays are useful to mitigate operational challenges.
- VI) The implications of partially clogged racks on fish guidance and fish protection is largely unknown and should therefore be investigated in future studies.

## 11.2 Outlook

The present thesis contributes to the understanding of the hydraulics of HBR-BSs and to the knowledge of the fish swimming behavior at these structures, but it also identified further research gaps, which should be addressed in future research projects:

- I) An extensive monitoring campaign should be conducted at a modern HBR-BS, which fulfills all design criteria specified in Chapter 10. To reliably quantify the fish guidance efficiency for different species and size classes, all movement corridors should be sampled with stow nets simultaneously.
- II) Live fish tests with HBR-BSs should be carried out for a wider parameter range. The experiments should include very small approach flow velocities ( $U_o \approx 0.2$  m/s), night experiments, and different bar shapes. Besides rectangular and foil-shaped bars, it is also recommended to investigate other shapes (e.g. similar to a tilde), which would induce larger turbulences and flow deflections. This would likely trigger avoidance reactions of small fish and would thereby increase the behavioral protection effect, while it would most likely cause only marginally larger head losses if designed appropriately. It is also important to test different size classes of the same fish species to verify the findings of the present thesis.
- III) The fish behavior at different bypasses should be studied either in the field or in the laboratory, where the bypass is ideally built on a scale of 1:1. It is particularly important to study the acceptance at different velocity ratios of the bypass inlet to mean approach flow velocity for various fish species and size classes. It is also relevant to not only guide fish into the bypass, but to design the bypass such that the hydraulic head can be overcome and that fish cannot return to the upstream.
- IV) Live fish tests should be carried out at electrified HBR-BSs, where each bar is alternatively used as anode and cathode. It is important that the electric field is known prior to the experiments and that low voltage gradients are used to prevent fish injuries. In any case, fish injuries should be studied, even if they are not externally visible. It is also important to focus on fish which approach the electric barrier with negative rheotaxis, as they have less room for reaction than positively-oriented fish. If an electrified rack configuration works well for fish which can actively avoid it, it should also be tested with other life stages such as small juveniles and larvae, which may passively drift through the electric field.

# Abbreviations and list of symbols

## Abbreviations

ABR	Angled Bar Rack
ADV	Acoustic Doppler Velocimeter
AIC	Akaike Information Criterion
BIC	Bayesian Information Criterion
CBR	Curved-Bar Rack
FGC	Fish Guidance Capacity, $FGC = V_p/V_n$
FGE	Fish Guidance Efficiency
FPE	Fish Protection Efficiency
GLM	Generalized Linear Model
gpDC	Direct current gated bursts
HBR	Horizontal Bar Rack
HBR-BS	Horizontal Bar Rack Bypass System
HPP	HydroPower Plant
MBR	Modified Bar Rack
MID	Magnetic-Inductive flow meter
OC	Full depth open channel bypass
PIT	Passive Integrated Transponder
RCM	Rack Cleaning Machine
RE	Open channel bypass with inlet restrictor
RI	Rack Interaction
UDS	Ultrasonic Distance Sensor
WPA	Swiss Federal Act on the Protection of Waters

## Greek symbols

$\alpha$	Horizontal approach flow angle	[°]
$\alpha_f$	Angle between the fish axis and $V_n$	[°]
$\alpha_{\text{sig}}$	Significance level	[–]
$\beta$	Regression coefficient of the GLM	[–]
$\Delta h_c$	Contraction head loss	[m]
$\Delta h_f$	Friction head loss	[m]
$\Delta h_R$	Rack head loss, $\Delta h_R = \xi_R U_{th}^2 / (2g)$	[m]

$\Delta Q$	Discharge difference between left and right channel halves, $\Delta Q =  Q_l - Q_r $ [m <sup>3</sup> /s]	
$\Delta U_e$	Voltage gradient	[V/cm]
$\gamma$	Vertical inclination angle of inclined racks or flap gates	[°]
$\lambda$	Friction factor	[-]
$\mu$	Mean	[unit of the respective variable]
$\nu$	Kinematic viscosity	[m <sup>2</sup> /s]
$\sigma$	Standard deviation	[unit of the respective variable]
$\sigma_b = s_b/t_b$	Relative clear bar spacing	[-]
$\varepsilon$	Standard error	[-]
$\xi$	Head loss coefficient	[-]
$\xi_c$	Contraction head loss coefficient	[-]
$\xi_R$	Rack head loss coefficient	[-]

### Roman Symbols

$A_i$	Area of the sector $i$	[m <sup>2</sup> ]
$A_o$	Approach flow cross-sectional area, $A_o = h_o w_o$	[m <sup>2</sup> ]
$A_{\text{tot}}$	Total area of sectors 1–7	[m <sup>2</sup> ]
$A_{ch}$	Cross-sectional area of the flow	[m <sup>2</sup> ]
$A_{ds}$	Cross-sectional area downstream of the rack, $A_{ds} = h_{ds} w_{ds}$	[m <sup>2</sup> ]
$BR$	Total blocking ratio	[-]
$BR^*$	Approximate blocking ratio	[-]
$BR_b$	Blocking ratio of the horizontal bars	[-]
$BR_{bp}$	Blocking ratio of the bottom plate	[-]
$BR_s$	Blocking ratio of the spacers	[-]
$C_\alpha$	Approach flow angle coefficient	[-]
$c_D$	Drag coefficient	[-]
$C_S$	Bar shape coefficient	[-]
$C_{BR}$	Blocking ratio coefficient	[-]
$C_{Db, \text{red}}$	Reduction of $C_{Db}$	[%]
$C_{Db}$	Bar depth coefficient	[-]
$C_{OL}$	Overlay layout coefficient	[-]
$C_{Ov}$	Overlay coefficient	[-]
$CI$	Confidence interval	[-]
$CP$	Clogging probability, considering all leaves clogged at bars	[-]
$CP_{2+}$	Clogging probability, considering leaves which clogged at multiple bars only	[-]

$D$	Duty cycle	[%]
$D_b$	Relative bar depth, $D_b = d_b/t_b$	[-]
$d_b$	Bar depth	[m]
$F$	Froude number, $F = U_o/\sqrt{gL}$	[-]
FGE	Fish guidance efficiency (bypass passages with rack interaction only)	[%]
FGE*	Fish guidance efficiency (all bypass passages)	[%]
FPE	Fish protection efficiency (bypass passages with rack interaction only)	[%]
FPE*	Fish protection efficiency (all bypass passages)	[%]
$g$	Gravitational acceleration constant, $g = 9.81 \text{ m/s}^2$	[m/s <sup>2</sup> ]
$h$	Flow depth	[m]
$h_f$	Absolute fish height	[m]
$h_g$	Gross head	[m]
$h_o$	Approach flow depth (upstream)	[m]
$H_{Bo}$	Relative bottom overlay height, $H_{Bo} = h_{Bo}/h_o$	[-]
$h_{Bo}$	Bottom overlay height	[m]
$h_{ds}$	Downstream flow depth	[m]
$h_{f,rel}$	Relative fish height, $h_{f,rel} = h_f/TL$	[-]
$H_{Ov}$	Total relative overlay height, $H_{Ov} = H_{Bo} + H_{To}$	[-]
$H_{To}$	Relative top overlay height, $H_{To} = h_{To}/h_o$	[-]
$h_{To}$	Top overlay height	[m]
$k_s$	Equivalent sand roughness height	[m]
$L$	Characteristic length	[m]
$l_R$	Rack length, $l_R = w_{ds}/\sin(\alpha)$	[m]
$L_{gap}$	Gap length	[ms]
$L_{pulse}$	Pulse length	[ms]
$l_{ch}$	Channel length	[m]
$N$	Total number of fish	[-]
$n$	Number of active fish used in the analysis	[-]
$n_b$	Number of horizontal bars	[-]
$n_s$	Number of spacers per vertical tie-bar	[-]
$n_v$	Number of vertical tie-bars	[-]
$N_{by,all}$	Total number of fish entering the bypass	[-]
$N_{by,RI}$	Number of fish entering the bypass with rack interaction	[-]
$\bar{n}_{hes}$	Average number of hesitations per fish at the bypass inlet	[-]
$N_{pulse}$	Number of pulses within a pulse group	[-]



$N_{\text{rack}}$	Number of fish passing through the rack	[-]
$N_{\text{refusal}}$	Number of fish refusing the HBR-BS	[-]
$\bar{n}_{\text{ref}}$	Average number of bypass refusals per fish at the bypass inlet	[-]
$n_{\text{use}}$	Number of times a fish was used for an experiment	[-]
$OR$	Odds ratio, $OR = p(X)/(1 - p(X))$	[-]
$p(X)$	Probability of the parameter $X$ , $p(X) = OR/(1 + OR)$	[-]
$P_{ch}$	Wetted perimeter	[m]
$\overline{PE}$	Mean prediction error	[%]
$PE$	Prediction error	[%]
$PI$	Permeability index, $PI = s_b/w_f$	[-]
$Q$	Discharge	[m <sup>3</sup> /s]
$Q_d$	Design discharge	[m <sup>3</sup> /s]
$Q_l$	Discharge through the left channel half	[m <sup>3</sup> /s]
$Q_o$	Total approach flow discharge	[m <sup>3</sup> /s]
$Q_r$	Discharge through the right channel half	[m <sup>3</sup> /s]
$Q_t$	Turbine discharge	[m <sup>3</sup> /s]
$Q_w$	Weir discharge	[m <sup>3</sup> /s]
$Q_{by}$	Bypass discharge	[m <sup>3</sup> /s]
$R$	Reynolds number, $R = LU_o/\nu$	[-]
$R_b$	Bar Reynolds number, $R_b = t_b U_o/\nu$	[-]
$R_h$	Hydraulic radius, $R_h = A_{ch}/P_{ch}$	[m]
$R_{c,i}$	Residence coefficient of the sector $i$	[-]
$R_{c,i,\text{norm}}$	Normalized residence coefficient of the sector $i$	[-]
$S$	Bar shape	[-]
$s_{\text{rel,mid}}$	Relative blade spacing at the middle of the runner	[m]
$s_b$	Clear bar spacing	[m]
$s_{\text{abs,max}}$	Blade spacing at the maximal runner diameter	[m]
$SR_t$	Turbine survival rate	[%]
$SR_{\text{tot}}$	Total survival rate	[%]
$SVG_x$	Spatial velocity gradient in $x$ -direction	[m/s/m]
$T$	Water temperature	[°C]
$t$	Duration	[s]
$t_b$	Bar thickness at thickest point	[m]
$t_{\text{rep}}$	Repetition time	[ms]
$t_{b,m}$	Bar thickness at mid cross section	[m]

$t_{bp}$	Thickness of the bottom plate	[m]
$t_{i,j}$	Time the fish $j$ spent in sector $i$	[s]
$t_{j,tot}$	Total time the fish $j$ spent in any of the sectors 1–7	[s]
$t_{X=-4}$	Time a fish needed to cross the coordinate $X = -4$	[s]
TKE	Turbulent kinetic energy	[m <sup>2</sup> /s <sup>2</sup> ]
$TL$	Total fish length	[m]
$TL_{crit}$	Critical total length of a fish passing through a barrier with a certain $s_b$	[m]
$u', v', w'$	Local instantaneous flow velocity fluctuations in $x$ -, $y$ -, and $z$ -direction	[m/s]
$U, V, W$	Local time-averaged velocities in $x$ -, $y$ -, and $z$ -direction	[m/s]
$u, v, w$	Local instantaneous flow velocities in $x$ -, $y$ -, and $z$ -direction	[m/s]
$U_e$	Voltage	[V]
$U_f, V_f$	Streamwise and transversal fish swimming velocities	[m/s]
$U_g, V_g$	Streamwise and transversal fish ground velocities (velocities of tracks)	[m/s]
$U_o$	Mean approach flow velocity from continuity, $U_o = Q_o/(h_o w_o)$	[m/s]
$U_{th}$	Theoretical average flow velocity, $U_{th} = Q_t/(h_o w_{ds})$	[m/s]
$U_{by,in}$	Flow velocity at the bypass inlet	[m/s]
$u_{max}$	Maximal tangential velocity of the runner	[m/s]
$U_{ds}$	Mean downstream flow velocity from continuity	[m/s]
$v_f$	Absolute fish swimming speed	[m/s]
$V_n$	Flow velocity component normal to the rack	[m/s]
$V_p$	Flow velocity component parallel to the rack	[m/s]
$VR$	Ratio of bypass inlet to mean approach flow velocity, $VR = U_{by,in}/U_o$	[-]
$w_f$	Absolute fish width	[m]
$w_o$	Upstream channel width	[m]
$w_{by}$	Bypass width	[m]
$w_{ch}$	Constant channel width (diversion HPP)	[m]
$w_{ds}$	Downstream channel width	[m]
$w_{f,rel}$	Relative fish width, $w_{f,rel} = w_f/TL$	[-]
$x, y, z$	Coordinates in streamwise, transversal, and vertical direction	[m]
$X, Y, Z$	Normalized coordinates, $X = x/h_o$ , $Y = y/w_{ds}$ , and $Z = z/h_o$	[-]



## References

- Adam, B. (2018). Mit dem Frühwarnsystem Migromat abwandernde Aale schützen ('Protecting downstream migrating eels with the early warning system Migromat'). *zekHydro*, 15(03): 68–70 [in German].
- Adam, B.; Engler, O.; Schwevers, U. (2018). HDX-Monitoring Wupper: Projektendbericht ('HDX-monitoring Wupper: final project report'). *Technical report*, Institut für angewandte Ökologie, Kirtorf-Wahlen, Germany [in German].
- Adam, B.; Lehmann, B. (2011). Ethohydraulik — Grundlagen, Methoden und Erkenntnisse ('Ethohydraulic — Fundamentals, methods, and findings'). ISBN 9783642172090. *Springer*, Heidelberg, Germany. <http://dx.doi.org/10.1007/978-3-642-17210-6> [in German].
- Adam, B.; Schwevers, U. (1999). Neue Erkenntnisse zur Aalabwanderung ('New findings of downstream eel migration'). *Proc. 2<sup>nd</sup> Mainsymposium. Arbeitsgemeinschaft Main e.V.*: 72–95.
- Adam, B.; Schwevers, U.; Dumont, U. (1999). Beiträge zum Schutz abwandernder Fische — Verhaltensbeobachtungen in einem Modellgerinne ('Contribution to the protection of downstream migrating fish — Behavioral observations in a laboratory flume'). ISBN 3927889326. Bibliothek Natur & Wissenschaft Band 16. *VNW Verlag Natur & Wissenschaft*, Solingen, Germany [in German].
- Adam, B.; Schwevers, U.; Dumont, U. (2002). Rechen- und Bypassanordnungen zum Schutz abwandernder Aale (Bar Racks and Bypass Systems to protect Downstream Migrating Eels). *Wasserwirtschaft*, (4/5): 43–46 [in German].
- Agostinho, C.S.; Pelicice, F.M.; Marques, E.E.; Soares, A.B.; de Almeida, D.A.A. (2011). All that goes up must come down? Absence of downstream passage through a fish ladder in a large Amazonian river. *Hydrobiologia*, 675(1): 1–12. <http://dx.doi.org/10.1007/s10750-011-0787-0>.
- Albayrak, I.; Boes, R.M.; Kriewitz, C.R.; Peter, A.; Tullis, B.P. (2020). Fish guidance structures: hydraulic performance and fish guidance efficiencies. *Journal of Ecohydraulics*: 1–19. <http://dx.doi.org/10.1080/24705357.2019.1677181>.
- Albayrak, I.; Kriewitz, C.R.; Hager, W.H.; Boes, R.M. (2018). An experimental investigation on louvres and angled bar racks. *Journal of Hydraulic Research*, 56(1): 59–75. <http://dx.doi.org/10.1080/00221686.2017.1289265>.
- Albayrak, I.; Maager, F.; Boes, R.M. (2019). An experimental investigation on fish guidance structures with horizontal bars. *Journal of Hydraulic Research*, 52(3). <http://dx.doi.org/10.1080/00221686.2019.1625818>.
- Algera, D.A.; Rytwinski, T.; Taylor, J.J.; Bennett, J.R.; Smokorowski, K.E.; Harrison, P.M.; Clarke, K.D.; Enders, E.C.; Power, M.; Bevelhimer, M.S.; Cooke, S.J. (2020). What are

- the relative risks of mortality and injury for fish during downstream passage at hydroelectric dams in temperate regions? A systematic review. *Environmental Evidence*, 9(3). <http://dx.doi.org/10.1186/s13750-020-0184-0>.
- Baier, E. (2019). Machbarkeitsstudie zur Einführung eines Aal-Taxis am Hochrhein von Schaffhausen bis Iffezheim ('Feasibility study to implement an eel-taxi at the High Rhine from Schaffhausen to Iffezheim'). *Technical report*, Fischwanderung.ch, Zurich, Switzerland [in German].
- Balestra, A.; Scherngell, A. (2019). Konzessionserneuerung Laufwasserkraftwerk Dietikon an der Limmat (Concession renewal of the Dietikon hydropower plant on Limmat river). *Wasserwirtschaft*, 109(5): 110–113 [in German].
- Bammatter, L.; Baumgartner, M.; Greuter, L.; Haertel-Borer, S.; Huber Gysi, M.; Nitsche, M.; Thomas, G. (2015). Renaturierung der Schweizer Gewässer: Die Sanierungspläne der Kantone ab 2015 ('Renaturation of Swiss water bodies: remediation plans of the cantons from 2015 on'). *Technical report*, Federal Office for the Environment (FOEN), Ittigen, Switzerland [in German, French, and Italian].
- Bates, D.W.; Vinsonhaler, R. (1957). Use of Louvers for guiding fish. *Transactions of the American Fisheries Society*, 86(1): 38–57. [http://dx.doi.org/10.1577/1548-8659\(1956\)86\[38:UOLFGF\]2.0.CO;2](http://dx.doi.org/10.1577/1548-8659(1956)86[38:UOLFGF]2.0.CO;2).
- Bauer, C.; Hirschberg, S. (eds.); Bäuerle, Y.; Biollaz, S.; Calbry-Muzyka, A.; Cox, B.; Heck, T.; Lehnert, M.; Meier, A.; Prasser, H.-M.; Schenler, W.; Treyer, K.; Vogel, F.; Wieckert, H.C.; Zhang, X.; Zimmermann, M.; Burg, V.; Bowman, G.; Erni, M.; Saar, M.; Tran, M.Q. (2017). Potentials, costs and environmental assessment of electricity generation technologies. *Final report*, PSI, WSL, ETHZ, EPFL, Paul Scherrer Institut, Villigen PSI, Switzerland.
- Baumer (2018). Ultrasonic distance measuring sensors. *Datasheet UNAM 30I6103/S14*.
- Baumgartner, T. (2020). Schwimmverhalten von Fischen an Fischleitrechen-Bypasssystemen ('Fish swimming behavior at fish guidance rack bypass systems'). *Bachelor's thesis*, Laboratory of Hydraulics, Hydrology and Glaciology, ETH Zurich, Switzerland [unpublished, in German].
- Beach, M.H. (1978). The use of infra-red light and closed circuit TV to validate records from automatic fish counters\*. *Journal of Fish Biology*, 13(5): 639–644. <http://dx.doi.org/10.1111/j.1095-8649.1978.tb03478.x>.
- Beamish, F.W.H. (1979). Chap. Swimming capacity: 101–187. In: W.S. Hoar; D.J. Randall (eds.) *Fish physiology*. Academic Press, New York, USA.
- Beaumont, W.R.C. (2016). Electricity in fish research and management — Theory and practice. ISBN 9781118935583. 2<sup>nd</sup> edn. *John Wiley & Sons, Ltd*, Chichester, UK.
- Beck, C. (2020). Fish protection and fish guidance at water intakes using innovative curved-bar rack bypass systems. *VAW-Mitteilung* 257 (R.M. Boes, ed.). Laboratory of Hydraulics,

- Hydrology and Glaciology, ETH Zurich, Switzerland.
- Beck, C.; Albayrak, I.; Meister, J.; Boes, R.M. (2019a). Hydraulic performance of fish guidance structures with curved bars — Part 1: Head loss assessment. *Journal of Hydraulic Research*. <http://dx.doi.org/10.1080/00221686.2019.1671515>.
- Beck, C.; Albayrak, I.; Meister, J.; Boes, R.M. (2019b). Hydraulic performance of fish guidance structures with curved bars — Part 2: Flow fields. *Journal of Hydraulic Research*. <http://dx.doi.org/10.1080/00221686.2019.1671516>.
- Beck, C.; Albayrak, I.; Meister, J.; Peter, A.; Selz, O.M.; Leuch, C.; Vetsch, D.F.; Boes, R.M. (2020). Swimming behavior of downstream moving fish at innovative curved-bar rack bypass systems for fish protection at water intakes. *Water*, 12(11): 3244. <http://dx.doi.org/10.3390/w12113244>.
- Becker, B.; Notermanns, F.; Reuter, C.; Schüttrumpf, H. (2009). Entwicklung einer fischfreundlichen Turbinensteuerung für Laufwasserkraftwerke an der Mosel (Development of a fish-friendly turbine-operation mode in run-of-river hydropower plants on the River Mosel). *Hydrology and Water Resources Management*, 53(1): 4–12 [in German].
- Bell, M.C.; DeLacy, A.C.; Copp, H.D. (1972). A compendium on the survival of fish passing through spillways and conduits. *Technical report*, U.S. Army Engineers Division, North Pacific Corps of Engineers, Portland, USA.
- Berger, C. (2018). Rechenverluste und Auslegung von (elektrifizierten) Schrägrechen anhand ethohydraulischer Studien (Screen losses and design of inclined (and electrified) screens with horizontal bars on the basis of ethohydraulic studies). *PhD Thesis*, Institut für Wasserbau und Wasserwirtschaft, Technische Universität Darmstadt, Germany [in German].
- Bianchi, A.; Rovati, C. (2020). Fish activity in ethohydraulic experiments. *Project thesis*, Laboratory of Hydraulics, Hydrology and Glaciology, ETH Zurich, Switzerland [unpublished].
- Blevins, R.D. (1984). Chap. Fluid dynamic drag: 279–381. In: *Applied fluid dynamic handbook*. ISBN 0442212968. Van Nostrand Reinhold Company Inc., New York, USA.
- Boes, R.M.; Albayrak, I.; Kriewitz, C.R.; Peter, A. (2016). Fischschutz und Fischabstieg mittels vertikaler Leitreechen-Bypass-Systeme: Rechenverluste und Leiteffizienz (Fish protection and downstream fish migration by means of guidance systems with vertical bars: head loss and bypass efficiency). *Wasserwirtschaft*, 106(7/8): 29–35 [in German].
- Boller, L.; Dönni, W. (2011). Potentialabschätzungen und Massnahmen für die Rückkehr des Lachses in die Schweiz — Passierbarkeit der Wasserkraftwerke und Regulierwehre an Rhein, Aare, Limmat und Reuss (‘Potential assessment and measures for the return of the salmon to Switzerland — Passability of the hydropower plants and regulating weirs in the Rhine, Aare, Limmat, and Reuss’). *Technical report*, AquaPlus und Fischwerk, Zug and Kriens, Switzerland.
- Bollrich, G. (2007). Technische Hydromechanik 1 — Grundlagen (‘Technical hydromechanics

- 1 — Fundamentals'). ISBN 9783345009129. 6<sup>th</sup> edn. *Beuth*, Berlin, Germany [in German].
- Böttcher, H.; Gabl, R.; Aufleger, M. (2019a). Experimental hydraulic investigation of angled fish protection systems — Comparison of circular bars and cables. *Water*, 11(5): 1056. <http://dx.doi.org/10.3390/w11051056>.
- Böttcher, H.; Zeiringer, B.; Brinkmeier, B.; Aufleger, M. (2019b). Verhaltensuntersuchungen zum Fischeschutz und Fischabstieg am Seilrechen (Ethohydraulic experiments on the innovative fishprotection and guidance system Flexible Fish Fence). *Wasserwirtschaft*, 109(2–3): 29–35 [in German].
- Boys, C.A.; Pflugrath, B.D.; Mueller, M.; Pander, J.; Deng, Z.D.; Geist, J. (2018). Physical and hydraulic forces experienced by fish passing through three different low-head hydropower turbines. *Marine and Freshwater Research*, 69(12): 1934–1944. <http://dx.doi.org/10.1071/MF18100>.
- Breitenstein, M.; Kirchhofer, A.; Hoppler, L.; Bruppacher, L.; Flück, M. (2019). Erneuerung Kraftwerk Hagneck: Wirkungskontrolle Fischeaufstieg — Teil A: Nachweis der Funktionstüchtigkeit des Umgehungsgewässers als Fischeaufstiegshilfe und der Eignung als Lebensraum für Fische ('Modernization power station Hagneck: monitoring fish upstream migration — Part A: Proove of functional efficiency of the natural fishway for upstream movements and acceptability as a fish habitat'). *Technical report*, Wasser Fisch Natur AG (WFN), Bern, Switzerland [in German].
- Brinkmeier, B.; Boettcher, H.; Tutzer, R.; Aufleger, M. (2017). Fish protection using electric flexible fish fences. *Proc. Hydro 2017 Conference*. Sevilla, Spain.: paper no. 23.01.
- Brown, L.; Boubée, J.; Haro, A. (2007). Behaviour and fate of downstream migrating eels at hydroelectric power station Intakes. *Proc. 6<sup>th</sup> International Symposium on Ecohydraulics*. Christchurch, New Zealand.
- Brown, L.; Haro, A.; Castro-Santos, T. (2009). Chap. Three-dimensional movement of silver-phase American eels in the forebay of a small hydroelectric facility: 277–291. In: J.M. Casselman; D.K. Cairns (eds.) *Eels at the edge — Science, status, and conservation concerns*. ISBN 9781888569964. *American Fisheries Society*, Bethesda, USA.
- Brown, R.S.; Colotelo, A.H.; Pflugrath, B.D.; Boys, C.A.; Baumgartner, L.J.; Deng, Z.D.; Silva, L.G.M.; Brauner, C.J.; Mallen-Cooper, M.; Phonekhampeng, O.; Thorncraft, G.; Singhanouvong, D. (2014). Understanding barotrauma in fish passing hydro structures: a global strategy for sustainable development of water resources. *Fisheries*, 39(3): 108–122. <http://dx.doi.org/10.1080/03632415.2014.883570>.
- Čada, G.F. (2001). The development of advanced hydroelectric turbines to improve fish passage survival. *Fisheries*, 26(9): 14–23.
- Calles, O.; Karlsson, S.; Hebrand, M.; Comoglio, C. (2012). Evaluating technical improvements for downstream migrating diadromous fish at a hydroelectric plant. *Ecological Engineering*, 48: 30–37. <http://dx.doi.org/10.1016/j.ecoleng.2011.05.002>.

- Carlsson, N. (2019). Låglutande galler och betydelsen av spaltvidd för passageeffektivitet och beteende hos nedströmsvandrande Europeisk ål (*Anguilla anguilla*) (Low-sloping racks and the importance of bar spacing for passage efficiency and behavior of downstream migrating European eel (*Anguilla anguilla*)). *Master's Thesis*, Karlstad University, Sweden [in Swedish].
- Chatellier, L.; Wang, R.-W.; David, L.; Courret, D.; Larinier, M. (2011). Experimental characterization of the flow across fish-friendly angled trashrack models. *Proc. 34<sup>th</sup> IAHR Congress. International Association for Hydro-Environment Engineering and Research (IAHR)*, Brisbane, Australia: 2776–2783.
- Chow, V.T (1988). Open-channel hydraulics. ISBN 070107769. *McGraw-Hill Book Company, Inc.*, Bosten, USA.
- Clough, S.C.; Lee-Elliott, I.E.; Turnpenny, A.W.H.; Holden, S.D.J.; Hinks, C. (2004). Swimming speeds in fish: phase 2. *R&D technical report W2-049/TR1*, Environment Agency, Bristol, UK.
- Clough, S.C.; Turnpenny, A.W.H. (2001). Swimming speeds in fish: phase 1. *R&D technical report W2-026/TR1*, Environment Agency, Bristol, UK.
- Courret, D.; Larinier, M. (2008). Guide pour la conception de prises d'eau "ichthyocompatibles" pour les petites centrales hydroélectriques ('Design guidelines of fish-friendly water intakes for small hydropower plants'). *Technical report*, Agence de L'Environnement et de la Maîtrise de l'Energie (ADEME), France [in French].
- Davidson, J.; Svenning, M.-A.; Orell, P.; Yoccoz, N.; Dempson, J.B.; Niemelä, E.; Klemetsen, A.; Lamberg, A.; Erkinaro, J. (2005). Spatial and temporal migration of wild Atlantic salmon smolts determined from a video camera array in the sub-Arctic River Tana. *Fisheries Research*, 74(1): 210–222. <http://dx.doi.org/10.1016/j.fishres.2005.02.005>.
- de Bie, J. (2017). Quantification of the collective response of fish to hydrodynamics for improving downstream fish passage facilities. *PhD Thesis*, Faculty of engineering and the environment, University of Southampton, UK.
- de Bie, J.; Peirson, G.; Kemp, P.S. (2018). Effectiveness of horizontally and vertically oriented wedge-wire screens to guide downstream moving juvenile chub (*Squalius cephalus*). *Ecological Engineering*, 123: 127–134. <http://dx.doi.org/10.1016/j.ecoleng.2018.07.038>.
- Deleau, M.J.C.; White, P.R.; Peirson, G.; Leighton, T.G.; Kemp, P.S. (2019). Use of acoustics to enhance the efficiency of physical screens designed to protect downstream moving European eel (*Anguilla anguilla*). *Fisheries Management and Ecology*, 27(1): 1–9. <http://dx.doi.org/10.1111/fme.12362>.
- Dönni, W.; Spalinger, L.; Knutti, A. (2017). Erhaltung und Förderung der Wanderfische in der Schweiz — Zielarten, Einzugsgebiete, Aufgaben ('Conservation and support of migratory fish in Switzerland — Species of interest, catchments, tasks'). *Technical report*, Fischwerk, Lucerne, Switzerland [in German].



- Ducharme, L.J.A. (1972). An application of louver deflectors for guiding Atlantic salmon (*Salmo salar*) smolts from power turbines. *Journal of the Fisheries Research Board of Canada*, 29(10): 1397–1404. <http://dx.doi.org/10.1139/f72-217>.
- Dumont, U.; Anderer, P.; Schwevers, U. (2005). Handbuch Querbauwerke ('Handbook transverse structures'). *Technical report*, Ministry for Environment, Agriculture, Conservation and Consumer Protection of the State of North Rhine-Westphalia (MULNV), Düsseldorf, Germany [in German].
- Duncan, J.P.; Deng, Z.D.; Arnold, J.L.; Fu, T.; Trumbo, B.A.; Carlson, T.J.; Zhou, D. (2018). Physical and ecological evaluation of a fish-friendly surface spillway. *Ecological Engineering*, 110: 107–116. <http://dx.doi.org/10.1016/j.ecoleng.2017.10.012>.
- Duncan, R.E. (1956). Use of infrared radiation in the study of fish behavior. *Special Scientific Report Fisheries No. 170*, U.S. Fish and Wildlife Service, Washington, USA.
- Durif, C.; Elie, P.; Gosset, C.; Rives, J.; F., Travade (2003). Chap. Behavioral study of downstream migrating eels by radio-telemetry at a small hydroelectric power plant: 243–356. In: D.A. Dixon (ed.) *Biology, management, and protection of catadromous eels*. ISBN 1888569425. *American Fisheries Society*, Bethesda, USA.
- DWA (2004). Fischschutz- und Fischabstiegsanlagen — Bemessung, Gestaltung, Funktionskontrolle ('Fish protection technologies and downstream fishways — Design, dimensions, effectiveness inspection'). ISBN 3934063915. *German Association for Water, Wastewater and Waste (DWA, former ATV-DVWK)*, Hennef, Germany [in German].
- DWA (2014). Fischaufstiegsanlagen und fischpassierbare Bauwerke — Gestaltung, Bemessung, Qualitätssicherung ('Fish upstream passage facilities and fish traversable constructions — Layout, design, quality control'). *Merkblatt DWA-M 509*, German Association for Water, Wastewater and Waste (DWA), Hennef, Germany [in German].
- EAWAG; SAEFL (2004). Dem Fischrückgang auf der Spur — Schlussbericht des Projekts Netzwerk Fischrückgang Schweiz — "Fischnetz" ('Tracking the decline of fish populations — Final report of the project network fish decline Switzerland — "Fishing Net"'). *Technical report*, Swiss Federal Institute of Aquatic Science and Technology (EAWAG) and Swiss Agency for the Environment, Forests and Landscape (SAEFL), Dübendorf and Bern, Switzerland [in German and French].
- Ebel, G. (2008). Turbinenbedingte Schädigung des Aals (*Anguilla anguilla*) — Schädigungsraten an europäischen Wasserkraftanlagenstandorten und Möglichkeiten der Prognose ('Turbine induced injuries of eels (*Anguilla anguilla*) — Injury rates at European hydropower plants and possibilities for prediction'). ISBN 9783000254451. *Büro für Gewässerökologie und Fischereibiologie Dr. Ebel*, Halle (Saale), Germany [in German].
- Ebel, G. (2013). Fischschutz und Fischabstieg an Wasserkraftanlagen — Handbuch Rechen- und Bypasssysteme. Ingenieurbiologische Grundlagen, Modellierung und Prognose, Bemessung und Gestaltung (Fish protection and downstream passage at hydro power stations —

- Handbook of bar rack and bypass systems. Bioengineering principles, modelling and prediction, dimensioning and design). ISBN 9783000396861. 1<sup>st</sup> edn. *Büro für Gewässerökologie und Fischereibiologie Dr. Ebel*, Halle (Saale), Germany [in German].
- Ebel, G. (2016). Fischeschutz und Fischabstieg an Wasserkraftanlagen — Handbuch Rechen- und Bypasssysteme. Ingenieurbiologische Grundlagen, Modellierung und Prognose, Bemessung und Gestaltung (Fish protection and downstream passage at hydro power stations — Handbook of bar rack and bypass systems. Bioengineering principles, modelling and prediction, dimensioning and design). ISBN 9783000396861. 2<sup>nd</sup> edn. *Büro für Gewässerökologie und Fischereibiologie Dr. Ebel*, Halle (Saale), Germany [in German].
- Ebel, G.; Gluch, A.; Kehl, M. (2015). Einsatz des Leitrechen-Bypass-Systems nach Ebel, Gluch & Kehl an Wasserkraftanlagen — Grundlagen, Erfahrungen und Perspektiven (Application of the angled bar rack bypass system of Ebel, Gluch & Kehl at hydropower plants — Basic principles, experiences and prospects). *Wasserwirtschaft*, (7/8): 44–50 [in German].
- Ebel, G.; Kehl, M.; Gluch, A. (2018). Fortschritte beim Fischeschutz und Fischabstieg: Inbetriebnahme der Pilot-Wasserkraftanlagen Freyburg und Öblitz (Advances in fish protection and downstream passage at hydropower stations — startup of pilot plants at Freyburg and Öblitz). *Wasserwirtschaft*, 108(9): 54–62 [in German].
- Egg, L.; Mueller, M.; Pander, J.; Knott, J.; Geist, J. (2017). Improving European silver eel (*Anguilla anguilla*) downstream migration by undershot sluice gate management at a small-scale hydropower plant. *Ecological Engineering*, 106: 349–357. <http://dx.doi.org/10.1016/j.ecoleng.2017.05.054>.
- Egg, L.; Pander, J.; Mueller, M.; Geist, J. (2018a). Comparison of sonar-, camera- and net-based methods in detecting riverine fish-movement patterns. *Marine and Freshwater Research*, 69(12): 1905–1912. <http://dx.doi.org/10.1071/MF18068>.
- Egg, L.; Pander, J.; Mueller, M.; Geist, J. (2018b). Effectiveness of the electric fish fence as a behavioural barrier at a pumping station. *Marine and Freshwater Research*, 70(10): 1459–1464. <http://dx.doi.org/10.1071/MF18459>.
- Eichenberger, D.; Kirchhofer, A. (2013). Barben in der Limmat (‘Barbels in the Limmat River’). *Technical report*, Wasser Fisch Natur (WFN), Gümmenen, Switzerland [in German].
- Enders, E.C.; Gessel, M.H.; Anderson, J.J.; Williams, J.G. (2012). Effects of decelerating and accelerating flows on juvenile salmonid behavior. *Transactions of the American Fisheries Society*, 141(2): 357–364. <http://dx.doi.org/10.1080/00028487.2012.664604>.
- Engel, A.P.; Weber, E. (2003). Lochblechrechen — neue Anwendungen einer alten Technik (‘Perforated plates — New applications for an old technology’). *Wasserwirtschaft*, 93(6): 42–44 [in German].
- Engler, O.; Adam, B. (2014). HDX-Monitoring Wupper — Untersuchung der Wanderung von Fischen (Untersuchungszeitraum vom 31. Oktober 2013 bis 31. Mai 2014) (‘HDX-monitoring Wupper — Investigation of fish migration (study period 31<sup>st</sup> of October 2013 until 31<sup>st</sup> of

- May 2014)'). *Technical report*, Institut für angewandte Ökologie, Kirtorf-Wahlen, Germany [in German].
- Environment Agency (2009). Good practice guidelines annex to the environment agency hydropower handbook — The environmental assessment of proposed low head hydro power developments. *Technical report GEHO0310BSCT-E-E*, Bristol, UK.
- EPRI (2011). "Fish friendly" hydropower turbine development and deployment: Alden turbine preliminary engineering and model testing. *Technical report 1019890*, Electric Power Research Institute (EPRI), Palo Alto, USA.
- EPRI (2013). Fish protection at cooling water intake structures — A technical reference manual — 2012 update. *Technical report 3002000231*, Electric Power Research Institute (EPRI), Palo Alto, USA.
- EPRI; DML (2001). Evaluation of angled bar racks and Louvers for guiding fish at water intakes. *Technical report 1005193*, Electric Power Research Institute (EPRI) and Dominion Millstone Laboratories (DML), Palo Alto and Waterford, USA.
- Feigenwinter, L.; Vetsch, D.F.; Kammerer, S.; Kriewitz, C.R.; Boes, R.M. (2019). Conceptual approach for positioning of fish guidance structures using CFD and expert knowledge. *Sustainability*, 11(6): 1646. <http://dx.doi.org/10.3390/su11061646>.
- Ferguson, J.W.; Absolon, R.F.; Carlson, T.J.; Sandford, B.P. (2006). Evidence of delayed mortality on juvenile Pacific salmon passing through turbines at Columbia River dams. *Transactions of the American Fisheries Society*, 135(1): 139–150. <http://dx.doi.org/10.1577/T05-080.1>.
- Ferguson, J.W.; Poe, T.P.; Carlson, T.J. (1998). Chap. 22: Surface-oriented bypass systems for juvenile salmonids on the Columbia River, USA: 281–299. In: M. Jungwirth; S. Schmutz; S. Weiss (eds.) Fish migration and fish bypasses. ISBN 0852382537. *Fishing News Books*, Oxford, UK.
- Fiedler, K.; Göhl, C. (2006). Chap. Verhaltensweisen von Aalen vor den Einläufen in Wasserkraftanlagen und praxisorientierte Konzepte für ihren Schutz und ihre Abwanderung (Behaviour patterns of eels at hydropower intakes, practical concepts for their protection and downstream passage): 100–106. In: Durchgängigkeit von Gewässern für die aquatische Fauna (Free passage for aquatic fauna in rivers and other water bodies). ISBN 9783939057192. *German Association for Water, Wastewater and Waste (DWA)*, Hennef, Germany [in German].
- Flay, R.G.J. (2013). Chap. 3: Bluff body aerodynamics: 59–84. In: Y. Tamura; A. Kareem (eds.) Advanced structural wind engineering. ISBN 9784431543367. *Springer*, Tokyo, Japan.
- Flügel, D.; Bös, T.; Peter, A. (2015). Massnahmen zur Gewährleistung eines schonenden Fischabstiegs an grösseren mitteleuropäischen Flusskraftwerken — Ethohydraulische Untersuchungen zum Fischabstieg entlang eines vertikalen, schräg ausgerichteten Fischleitrechens ('Measures to implement safe fish downstream passage at larger central-European run-of-

- river hydropower plants — Ethohydraulic investigations of downstream moving fish along a vertical, angled fish guidance rack'). *Technical report*, EAWAG, Kastanienbaum, Switzerland [in German].
- Flury, N. (2019). Schwimmverhalten an Fischleitrechen für den Fischabstieg ('Swimming behavior of downstream moving fish at guidance racks'). *Bachelor's thesis*, Laboratory of Hydraulics, Hydrology and Glaciology, ETH Zurich, Switzerland [unpublished, in German].
- Füllner, G. (1997). Notwendigkeit der Begrenzung der lichten Stabrechenweite vor Turbinen von Wasserkraftanlagen auf 20 mm ('Necessity to reduce the clear bar spacing in front of hydropower plant turbines to 20 mm'). *Technical report*, Sächsische Landesanstalt für Landwirtschaft, Königswartha, Germany [in German].
- Ganzmann, M. (2019). Model investigation of flow conditions and foliage clogging at fish guidance structures. *Master's Thesis*, Laboratory of Hydraulics, Hydrology and Glaciology, ETH Zurich, Switzerland [unpublished].
- Gerhard (1893). Über Aalleitern und Aalpässe ('About eel ladders and eel passes'). *Zeitschrift für Fischerei und deren Hilfswissenschaften*, 1: 194–199 [in German].
- Giesecke, J.; Heimerl, S.; Mosonyi, E. (2014). Wasserkraftanlagen — Planung, Bau und Betrieb ('Hydroelectric power plants — Planning, construction and operation'). ISBN 9783642538704. 6<sup>th</sup> edn. *Springer*, Berlin, Germany. <http://dx.doi.org/10.1007/978-3-642-53871-1> [in German].
- Gluch, A. (2007). Kombiniertes Fisch- und Treibgutabweiser für Wasserkraftanlagen ('Combined fish and floating debris deflector for hydropower plants'). *Wasser und Abfall*, 7–8: 38–43 [in German].
- Godde, D. (1994). Experimentelle Untersuchungen zur Anströmung von Rohrturbinen — Ein Beitrag zur Optimierung des Turbineneinlaufes ('Experimental investigation of the bulb turbine approach flow — A contribution to optimize the turbine inlet'). *TUM-Mitteilung 75* (T. Strobl, ed.). Chair of Hydraulic and Water Resources Engineering, TU Munich, Germany [in German].
- Gomes, P.; Larinier, M. (2008). Dommages subis par les anguilles lors de leur passage au travers des turbines Kaplan — Etablissement de formules prédictives ('Injuries of eels passing through Kaplan turbines — Establishment of prediction equations'). *Technical report*, Pole Ecohydraulique, ONEMA, Toulouse, France [in French].
- Goring, D.G.; Nikora, V.I. (2002). Despiking acoustic Doppler velocimeter data. *Journal of Hydraulic Engineering*, 128(1): 117–126. [http://dx.doi.org/10.1061/\(ASCE\)0733-9429\(2002\)128:1\(117\)](http://dx.doi.org/10.1061/(ASCE)0733-9429(2002)128:1(117)).
- Gruber, R. (2018a). Italienisches Kraftwerk Jovencan setzt zur Stromgewinnung auf österreichische Technik ('Italian power plant Jovencan relies on Austrian technology for electricity production'). *zekHydro*, 16(3): 55–57 [in German].

- Gruber, R. (2018b). Oberösterreichischer Branchenspezialist stellt maximale Anlagenverfügbarkeit sicher ('Upper Austrian industry specialist ensures maximal operational availability'). *zekHydro*, 15(4): 60–61 [in German].
- Gruber, R. (2019a). Kraftwerk Schennerpolster an der Ischl punktet mit durchdachten Innovationen im Detail ('Power plant Schennerpolster at the Ischl River scores with sophisticated innovations in detail'). *zekHydro*, 17(6): 70–72 [in German].
- Gruber, R. (2019b). Traun-Kraftwerk Danzermühl nimmt planmässig den Betrieb auf ('The hydropower plant Danzermühl at Traun River starts operation on schedule'). *zekHydro*, 17(3): 22–27 [in German].
- Harby, A.; Charmasson, J.; Boavida, I.; Pinheiro, A.N.; Godinho, F.; Tuhtan, J.; Albayrak, I.; Detert, M.; Boes, R.M.; Schneider, M.; Pawels, I. (2020). Deliverable 3.2 Tools for fish behaviour assessment. *Technical report*, Fishfriendly Innovative Technologies for Hydropower (FIThydro).
- Haro, A.; Odeh, M.; Noreika, J.; Castro-Santos, T. (1998). Effect of water acceleration on downstream migratory behavior and passage of Atlantic salmon smolts and juvenile American shad at surface bypasses. *Transactions of the American Fisheries Society*, 127(1): 118–127. [http://dx.doi.org/10.1577/1548-8659\(1998\)127<0118:EOWAOD>2.0.CO;2](http://dx.doi.org/10.1577/1548-8659(1998)127<0118:EOWAOD>2.0.CO;2).
- Hassinger, R.; Hübner, D. (2009). Entwicklung eines neuartigen Aal-Abstiegssystems mithilfe von Laborversuchen (Development of innovative eel descent devices with the help of laboratory experiments). *Korrespondenz Wasserwirtschaft*, 2(5): 276–281 [in German].
- Havn, T.B; Sæther, S.A.; Thorstad, E.B; Teichert, M.A.K.; Heermann, L. and. Diserud, O.H; Borcharding, J.; Tambets, M.; Økland, F. (2017). Downstream migration of Atlantic salmon smolts past a low head hydropower station equipped with Archimedes screw and Francis turbines. *Ecological Engineering*, 105: 262–275. <http://dx.doi.org/10.1016/j.ecoleng.2017.04.043>.
- Hefti, D. (2012). Wiederherstellung der Fische auf- und -abwanderung bei Wasserkraftwerken ('Re-establishing up- and -downstream fish passage at hydropower plants'). *Best practice checklist UW-1210-D*, Federal Office for the Environment (FOEN), Bern, Switzerland [in German].
- Heisey, P.G.; Mathur, D.; Skalski, J.R.; McDonald, R.D.; Velazquez, G. (2008). Chap. Effects of spillway structural modifications on fish condition and survival: 165–179. In: S.V. Amaral; D. Mathur; E.P. Taft (eds.) *Advances in fisheries bioengineering*. ISBN 9781934874028. *American Fisheries Society*, Bethesda, USA.
- Henze, N. (2013). Stochastik für Einsteiger — Eine Einführung in die faszinierende Welt des Zufalls ('Stochastic for beginners — An introduction to the fascinating world of randomization'). ISBN 9783658030766. 10<sup>th</sup> edn. *Springer Spektrum*, Wiesbaden, Germany. <http://dx.doi.org/10.1007/978-3-658-03077-3> [in German].
- Hermann, F.; Hollenstein, R. (1998). Zur Entstehung von Rechenverlusten bei gerader

- und schräger Anströmung ('About the generation of rack losses at straight and angled approach flow conditions'). *Proc. Planung und Realisierung im Wasserbau — Vergleich von Zielvorstellungen mit den Ergebnissen ('Planning and realization in hydraulic engineering — Comparison of objectives and results')*. Technical University Munich, Germany: 69–78 [in German].
- Hermens, G.; Gubbels, R. (2017). Abstiegswege ausgewählter Fischarten an den Abstiegsanlagen der Wasserkraftanlage ECI (Results of the downstream monitoring at the hydropower plant ECI). *Wasserwirtschaft*, 107(2–3): 71–76 [in German].
- Hogan, T.W.; Čada, G.F.; Amaral, S.V. (2014). The status of environmentally enhanced hydropower turbines. *Fisheries*, 39(4): 164–172. <http://dx.doi.org/10.1080/03632415.2014.897195>.
- Holzner, M.; Blankenburg, D. (2007). Vorversuche zur Eignung horizontaler Rechenanlagen für den Schutz von Fischen an Kraftwerkseinläufen ('Preliminary experiments to assess the suitability of racks with horizontal bars for fish protection'). *Technical report*, Büro für Gewässerökologie und Fischbiologie, Freising, Germany [in German, unpublished].
- Holzner, M.; Blankenburg, D. (2008). Vorversuche zur Eignung horizontaler Rechenanlagen für den Schutz von Fischen an Kraftwerkseinläufen — Ergänzende Auswertungen ('Preliminary experiments to assess the suitability of racks with horizontal bars for fish protection — Additional analyses'). *Technical report*, Büro für Gewässerökologie und Fischbiologie, Mengkofen, Germany [in German, unpublished].
- Hütte, M. (2000). Ökologie und Wasserbau — Ökologische Grundlagen von Gewässerverbauung und Wasserkraftnutzung ('Ecology and hydraulic engineering — Ecological fundamentals of river obstruction and hydropower use'). ISBN 9783528025830. 1<sup>st</sup> edn. Vieweg+Teubner, Wiesbaden, Germany [in German].
- ICES (2019). European eel (*Anguilla anguilla*) throughout its natural range. *Technical report*, International Council for the Exploration of the Sea (ICES), Copenhagen, Denmark. <http://dx.doi.org/10.17895/ices.advice.4825>.
- Idelchik, I.E. (2008). Handbook of hydraulic resistance. ISBN 8179921182. 3<sup>rd</sup> edn. Jaico Publishing House, Mumbai, India.
- Jank, S. (2018). Jank-Horizontalrechenreiniger: Richtungsweisende Erfindung feiert 35 Jahre Jubiläum ('Horizontal rack cleaning machines of company Jank: trend-setting concept celebrates 35 year anniversary'). *zekHydro*, 15(4): 57–59 [in German].
- Jens, G. (1987). Plädoyer für den 20-mm-Turbinenrechen ('Plea for the 20 mm intake rack'). *das wassertriebwerk*, 36(12): 145–147 [in German].
- Kammerlander, H.; Schlosser, L.; Zeiringer, B.; Unfer, G.; Zeileis, A.; Aufleger, M. (2020). Downstream passage behavior of potamodromous fishes at the fish protection and guidance system "Flexible Fish Fence". *Ecological Engineering*, 143. <http://dx.doi.org/10.1016/j.ecoleng.2019.105698>.

- Katopodis, C.; Gervais, R. (2016). Fish swimming performance database and analyses. *Research Document 2016/002*. vi + 550 p, DFO Canadian Science Advisory Secretariat, Winnipeg, Canada.
- Katopodis, C.; Williams, J.G. (2011). The development of fish passage research in a historical context. *Ecological Engineering*, 48. <http://dx.doi.org/10.1016/j.ecoleng.2011.07.004>.
- Keenleyside, M.H.A. (1955). Chap. Some aspects of the schooling behaviour of fish: 183–247. In: *Behaviour*, 8(2/3). Brill, Leiden, The Netherlands. <http://dx.doi.org/10.1163/156853955X00229>.
- Kemp, P.S.; Gessel, M.H.; Sandford, B.P.; Williams, J.G. (2006). The behaviour of Pacific salmonid smolts during passage over two experimental weirs under light and dark conditions. *River Research and Applications*, 22(4): 429–440. <http://dx.doi.org/10.1002/rra.913>.
- Kemp, P.S.; Katopodis, C. (2016). Introducing the *Journal of Ecohydraulics*: fundamental and applied research on the road to transdisciplinarity. *Journal of Ecohydraulics*, 1(1–2): 1–4. <http://dx.doi.org/10.1080/24705357.2016.1259139>.
- Kemp, P.S.; Williams, J.G. (2009). Illumination influences the ability of migrating juvenile salmonids to pass a submerged experimental weir. *Ecology of Freshwater Fish*, 18(2): 297–304. <http://dx.doi.org/10.1111/j.1600-0633.2008.00347.x>.
- Kirchhofer, A.; Breitenstein, M.; Zaugg, B. (2007). Rote Liste Fische und Rundmäuler — Rote Liste der gefährdeten Arten der Schweiz ('Red list fish and cyclostomata — Red list of endangered species in Switzerland'). *Technical report UW-0734-D*, Federal Office for the Environment (FOEN) and Schweizer Zentrum für die Kartografie der Fauna (SZKF/CSCF), Bern and Neuenburg, Switzerland [in German, French, and Italian].
- Kirschmer, O. (1925). Untersuchungen über den Gefällsverlust an Rechen ('Investigation of head losses at racks'). *PhD Thesis*, Technical University of Munich, Germany [in German].
- Klopries, E.-M.; Kroll, L.; Jörgensen, L.; Teggers-Junge, S.; Schüttrumpf, H. (2016). 20 Jahre aktive Partnerschaft für den Aal an Mosel und Saar ('20 years of active partnership for eels at Mosel and Saar River'). *Technical report*, Aalschutz-Initiative Rheinland-Pfalz & innogy SE, Mainz, Germany [in German].
- Klopries, E.-M.; Wilmink, A.; Pummer, E.; Böckmann, I.; Hoffmann, A.; Schüttrumpf, H. (2020). Development and evaluation of an empirical equation for the screening effect of bar racks. *Journal of Ecohydraulics*: 1–14. <http://dx.doi.org/10.1080/24705357.2020.1770135>.
- Könitzer, C.; Wagner, T.; Mathys, L.; Zaugg, C.; Pedroli, J.-C. (2012). Wiederherstellung der Fischwanderung — Strategische Planung. Ein Modul der Vollzugshilfe Renaturierung der Gewässer ('Re-establishment of fish migration — Strategic planning. A module of the guideline renaturation watercourses'). *Technical report UV-1209-D*, Federal Office for the Environment (FOEN), Bern, Switzerland [in German and French].
- Kriewitz, C.R. (2015). Leitrechen an Fischabstiegsanlagen: Hydraulik und fischbiologische

- Effizienz ('Guidance screens at fish protection facilities: hydraulics and fish-biological efficiency'). *VAW-Mitteilung 230* (R.M. Boes, ed.). Laboratory of Hydraulics, Hydrology and Glaciology, ETH Zurich, Switzerland [in German].
- Larinier, M. (1998). Chap. 10: Upstream and downstream fish passage experience in France: 127–145. In: M. Jungwirth; S. Schmutz; S. Weiss (eds.) *Fish migration and fish bypasses*. ISBN 0852382537. *Fishing News Books*, Oxford, UK.
- Larinier, M. (2002). Location of fishways. *Bull. Fr. Pêche Piscic.*, (364): 39–53. <http://dx.doi.org/10.1051/kmae/2002106>.
- Larinier, M.; Dartiguelongue, J. (1989). La circulation des poissons migrateurs: le transit a travers les turbines des installations hydroélectriques. *Bull. Fr. Pêche Piscic.*, (312–313): 1–90. <http://dx.doi.org/10.1051/kmae:1989011>.
- Larinier, M.; Travade, F. (2002). Downstream migration: problems and facilities. *Bull. Fr. Pêche Piscic.*, (364 suppl.): 181–207. <http://dx.doi.org/10.1051/kmae/2002102>.
- Lehmann, B.; Adam, B.; Engler, O.; Hecht, V.; Schneider, K. (2016). Ethohydraulische Untersuchungen zur Verbesserung des Fischschutzes an Wasserkraftanlagen ('Ethohydraulic investigations to improve fish protection at hydropower plants'). ISBN 9783784340517. Naturschutz und Biologische Vielfalt, Heft 151. *Bundesamt für Naturschutz (BfN)*, Bonn, Germany. <http://dx.doi.org/10.19213/973151> [in German].
- Lemkecher, F.; Chatellier, L.; Courret, D.; David, L. (2020). Experimental study of fish-friendly angled trash racks with horizontal bars. *Journal of Hydraulic Research* [under review].
- Li, M.; Shi, X.; Jin, Z.; Ke, S.; Lin, C.; An, R.; Li, J.; Katopodis, C. (2020). Behaviour and ability of a cyprinid (*Schizopygopsis younghusbandi*) to cope with accelerating flows when migrating downstream. *River Research and Applications*: 1–12. <http://dx.doi.org/10.1002/rra.3686>.
- Lifa, I.; Schlegel, F.; Dosch, S. (2017). Optimierung der Coanda-Rechen für Schweizer Gewässer ('Optimizing Coanda screens for Swiss rivers'). *Final report BFE SI/501288-01*, Institute for Construction in Alpine Regions (IBAR), HTW Chur, Switzerland [in German].
- Lifa, I.; Witek, M.; Braun, S.; Krummenacher, B.; Boes, R.M.; Beck, C.; Peter, A. (2020). Optimierung von Coanda-Rechen für Wasserfassungen an alpinen Gewässern ('Optimization of Coanda screens for hydropower intakes in alpine rivers'). *Final report BFE SI/501288-01*, Institute for Construction in Alpine Regions (IBAR), HTW Chur, Switzerland [in German].
- Lindberg, J.; Hagman, S. (2018). CBA of environmental projects within hydropower. *Master's Thesis*, KTH Royal Institute of Technology, Stockholm, Sweden.
- Lowe, R.H. (1952). The influence of light and other factors on the seaward migration of the silver eel (*Anguilla anguilla* L.). *Journal of Animal Ecology*, 21(2): 275–309.
- LUBW (2016). Handreichung Fischschutz und Fischabstieg an Wasserkraftanlagen — Fachliche Grundlagen ('Guideline fish protection and fish downstream passage at hydropower



- plants — Technical fundamentals'). *Technical report*, Landesanstalt für Umwelt, Messungen und Naturschutz Baden-Württemberg, Karlsruhe, Germany [in German].
- Lucas, M.C.; Baras, E. (2001). Migration of freshwater fishes. ISBN 0632057548. *Blackwell Science*, Oxford, UK.
- Maager, F. (2016). Fischleitrechen mit horizontalen Stabelementen ('Fish guidance racks with horizontal bars'). *Master's Thesis*, Laboratory of Hydraulics, Hydrology and Glaciology, ETH Zurich, Switzerland [unpublished, in German].
- Meister, J.; Beck, C.; Roth, A.; Fuchs, H.; Albayrak, I.; Selz, O.; Boes, R.M. (2020a). EthoMoSt, Etho-hydraulische Modellversuche an elektrifizierten Fischleitrechen (EthoMoSt, Etho-hydraulic model study on electrified fish guidance structures). *Final report BFE SI/501758-01*, VAW, ETH Zurich, Zurich, Switzerland [in German].
- Meister, J.; Fuchs, H.; Albayrak, I.; Boes, R.M. (2019). Hydraulics of horizontal bar racks for fish downstream migration. *Proc. 38<sup>th</sup> IAHR World Congress. International Association for Hydro-Environment Engineering and Research (IAHR)*, Panama City, Panama: 2188–2194. <http://dx.doi.org/10.3850/38WC092019-0369>.
- Meister, J.; Fuchs, H.; Beck, C.; Albayrak, I.; Boes, R.M. (2020b). Head losses of horizontal bar racks as fish guidance structures. *Water*, 12(2): 475. <http://dx.doi.org/10.3390/w12020475>.
- Meister, J.; Fuchs, H.; Beck, C.; Albayrak, I.; Boes, R.M. (2020c). Velocity fields at horizontal bar racks as fish guidance structures. *Water*, 12(1): 280. <http://dx.doi.org/10.3390/w12010280>.
- Meister, J.; Fuchs, H.; Boes, R.M. (2018a). Hydraulische Laboruntersuchungen horizontaler Fischleitrechen ('Hydraulic laboratory investigations of horizontal fish guidance racks'). *zekHydro*, 15(2): 54–56. <http://dx.doi.org/10.3929/ethz-b-000295001> [in German].
- Meister, J.; Helge, F.; Albayrak, I.; Boes, R.M. (2018b). Horizontal bar rack bypass systems for fish downstream migration: State of knowledge, limitations, and gaps. *Proc. 12<sup>th</sup> International Symposium on Ecohydraulics*. Tokyo, Japan. <http://dx.doi.org/10.3929/ethz-b-000305990>.
- Mendez, R.; Zaugg, C. (2020). Wirkungskontrolle Fischabstieg am Horizontalrechen des Kraftwerks Stroppele ('Monitoring campaign of downstream moving fish at the horizontal bar rack of the power plant Stroppele'). *Wasser Energie Luft*, 112(1): 27–33 [in German].
- Meusburger, H. (2002). Energieverluste an Einlaufrechen von Flusskraftwerken ('Hydraulic losses at bar racks of run-of-river plants'). *VAW-Mitteilung 179* (H.-E. Minor, ed.). Laboratory of Hydraulics, Hydrology and Glaciology, ETH Zurich, Switzerland [in German].
- Meusburger, H.; Hermann, F.; Hollenstein, R. (1999). Comparison of numerical and experimental investigations of trashrack losses. *Proc. 28<sup>th</sup> IAHR Congress. International Association for Hydro-Environment Engineering and Research (IAHR)*, Graz, Austria.
- MIT (2008). Chap. 7: Velocity profiles and turbulence: 1–10. In: Transport processes in the

- environment. Boston, USA.
- Montén, E. (1985). Fish and turbines — Fish injuries during passage through power station turbines. ISBN 9171862471. *Vattenfall*, Stockholm, Schweden.
- Mori, N.; Suzuki, T.; Kakuno, S. (2007). Noise of acoustic Doppler velocimeter data in bubbly flows. *Journal of Engineering Mechanics*, 122(1): 122–125. [http://dx.doi.org/10.1061/\(ASCE\)0733-9399\(2007\)133:1\(122\)](http://dx.doi.org/10.1061/(ASCE)0733-9399(2007)133:1(122)).
- Mueller, M.; Bierschenk, A.M.; Bierschenk, B.M.; Pander, J.; Geist, J. (2020a). Effects of multiple stressors on the distribution of fish communities in 203 headwater streams of Rhine, Elbe and Danube. *Science of The Total Environment*, 703: 134523. <http://dx.doi.org/10.1016/j.scitotenv.2019.134523>.
- Mueller, M.; Knott, J.; Egg, L.; Suttor, C.; Pander, J.; Geist, J. (2020b). Fischökologisches Monitoring an innovativen Wasserkraftanlagen — Abschlussbericht Band 4: Lindesmühle an der Fränkischen Saale ('Fish ecological monitoring campaign at innovative hydropower plants — Final report volume 4: Lindesmühle at the Franconian Saale'). *Technical report*, Chair of Aquatic Systems Biology, Technical University of Munich, Germany [in German].
- Mueller, M.; Knott, J.; Pander, J.; Geist, J. (2020c). Fischökologisches Monitoring an innovativen Wasserkraftanlagen — Abschlussbericht Band 11: Standortübergreifende Verbesserungsmöglichkeiten für den Fischschutz und die Gewässerökologie (ohne Schachtkraftwerk) ('Fish ecological monitoring campaign at innovative hydropower plants — Final report volume 11: ways to improve fish protection and the aquatic ecology (without shaft power plant)'). *Technical report*, Chair of Aquatic Systems Biology, Technical University of Munich, Germany [in German].
- Mueller, M.; Pander, J.; Geist, J. (2017). Evaluation of external fish injury caused by hydropower plants based on a novel field-based protocol. *Fisheries Management and Ecology*, 24(3): 240–255. <http://dx.doi.org/10.1111/fme.12229>.
- Mulligan, K.B.; Towler, B.; Haro, A.; Ahlfeld, D.P. (2017). A computational fluid dynamics modeling study of guide walls for downstream fish passage. *Ecological Engineering*, 99: 324–332. <http://dx.doi.org/https://doi.org/10.1016/j.ecoleng.2016.11.025>.
- Mulligan, K.B.; Towler, B.; Haro, A.; Ahlfeld, D.P. (2018). Downstream fish passage guide walls: A hydraulic scale model analysis. *Ecological Engineering*, 115: 122–138. <http://dx.doi.org/https://doi.org/10.1016/j.ecoleng.2018.02.006>.
- Nestler, J.M.; Goodwin, R.A.; Smith, D.L.; Anderson, J.J.; Li, S. (2008). Optimum fish passage and guidance designs are based in the hydrogeomorphology of natural rivers. *River Research and Applications*, 24(2): 148–168. <http://dx.doi.org/10.1002/rra.1056>.
- Nezu, I.; Nakagawa, H. (1993). Turbulences in open-channel flows. ISBN 9054101180. A.A. Balkema, Rotterdam, The Netherlands.
- Nieland, J.L.; Sheehan, T.F.; Saunders, R. (2015). Assessing demographic effects of dams

- on diadromous fish: a case study for Atlantic salmon in the Penobscot River, Maine. *ICES Journal of Marine Science*, 72(8): 2423–2437. <http://dx.doi.org/10.1093/icesjms/fsv083>.
- NMFS (1997). Fish screening criteria for anadromous salmonids. *Technical report*, National Marine Fisheries Service (NMFS), Southwest Region, Santa Rosa, USA.
- NOAA Fisheries (2008). Biological opinion — consultation on remand for operation of the Federal Columbia River Power System, 11 Bureau of Reclamation projects in the Columbia Basin and ESA section 10(a)(1)(A) permit for juvenile fish transportation program. *Biological opinion*, National Marine Fisheries Service (NOAA Fisheries), Northwest Region, Seattle, USA.
- Norconsult (2017). Fortsatt utredning av fiskavledning vid Edsforsens kraftverk: Tekniska förutsättningar och konsekvensbedömning av 2 nya utförande alternativ ('Continued investigation of fish guidance at hydropower plant Edsforsen: technical requirements and impact assessment of 2 new alternative designs'). *Technical report*, Norconsult, Sweden [unpublished, in Swedish].
- Nordlund, B. (2008). Designing fish screens for fish protection at water diversions. *Technical report*, National Marine Fisheries Service, Lacey, USA.
- Normandeau Associates, Inc. (1995). Exclusion and guidance of Atlantic salmon smolts by a fish diversion structure at Bellows Falls hydroelectric station. *Normandeau Associates Project No. 15030.001*, Normandeau Associates, Brattleboro, USA.
- Normandeau Associates, Inc. (2009). An estimation of survival and injury of fish passed through the Hydro Green Energy hydrokinetic system, and a characterization of fish entrainment potential at the Mississippi lock and dam no. 2 hydroelectric project (P-4306) Hastings, Minnesota. *Normandeau Associates Project No. 21288.000*, Westmoreland, USA.
- Norrgård, J.R.; Greenberg, L.A.; Piccolo, J.J.; Schmitz, M.; Bergman, E. (2013). Multiplicative loss of landlocked Atlantic salmon *Salmo salar* L. smolts during downstream migration through multiple dams. *River Research and Applications*, 29(10): 1306–1317. <http://dx.doi.org/10.1002/rra.2616>.
- Nortek AS (2016). Vectrino — 3D water velocity sensor — Lab Probe. *Datasheet TS-060-en-06.2010*, Rud, Norway.
- Northcote, T.G. (1978). Chap. 13: Migratory strategies and production in freshwater fishes: 326–359. In: S.D. Gerking (ed.) *Ecology of freshwater fish production*. ISBN 0632002565. Blackwell, Oxford, UK.
- Northcote, T.G. (1998). Chap. 1: Migratory behaviour of fish and its significance to movement through riverine fish passage facilities: 3–18. In: M. Jungwirth; S. Schmutz; S. Weiss (eds.) *Fish migration and fish bypasses*. ISBN 0852382537. Fishing News Books, Oxford, UK.
- Nyqvist, D.; Elghagen, J.; Heiss, M.; Calles, O. (2018). An angled rack with a bypass and a nature-like fishway pass Atlantic salmon smolts downstream at a hydropower dam. *Marine*

- and Freshwater Research*, 69(12). <http://dx.doi.org/10.1071/MF18065>.
- Nyqvist, D.; McCormick, S.D.; Greenberg, L.; Ardren, W.R.; Bergman, E.; Calles, O.; Castro-Santos, T. (2017a). Downstream migration and multiple dam passage by Atlantic salmon smolts. *North American Journal of Fisheries Management*: 1–36. <http://dx.doi.org/10.1080/02755947.2017.1327900>.
- Nyqvist, D.; Nilsson, P.A.; Alenäs, I.; Elghagen, J.; Hebrand, M.; Karlsson, S.; Kläppe, S.; Calles, O. (2017b). Upstream and downstream passage of migrating adult Atlantic salmon: Remedial measures improve passage performance at a hydropower dam. *Ecological Engineering*, 102: 331–343. <http://dx.doi.org/10.1016/j.ecoleng.2017.02.055>.
- Odeh, M.; Orvis, C. (1998). Chap. 21: Downstream fish passage design considerations and developments at hydroelectric projects in the north-east USA: 267–280. In: M. Jungwirth; S. Schmutz; S. Weiss (eds.) Fish migration and fish bypasses. ISBN 0852382537. *Fishing News Books*, Oxford, UK.
- O’Farrell, M.; Burger, C.; Crump, R.; Smith, K. (2014). Blocking or guiding upstream-migrating fish: a commentary on the success of the graduated field electric fish barrier. *Proc. International fish screening techniques*. WIT Press, Southampton, UK: 165–175.
- Økland, F.; Teichert, M.A.K.; Havn, T.B.; Thorstad, E.B.; Heermann, L.; Sæther, S.A.; Tambets, M.; Borcharding, J. (2017). Downstream migration of European eel at three German hydropower stations. *NINA Report 1355*, University of Cologne and Norwegian Institute for Nature Research, Cologne and Trondheim, Germany and Norway.
- Økland, F.; Teichert, M.A.K.; Thorstad, E.B.; Havn, T.B.; Heermann, L.; Sæther, S.A.; Diserud, O.H.; Tambets, M.; Hedger, R.D.; Borcharding, J. (2016). Downstream migration of Atlantic salmon smolt at three German hydropower stations. *NINA Report 1203*, University of Cologne and Norwegian Institute for Nature Research, Cologne and Trondheim, Germany and Norway.
- Pander, J.; Mueller, M.; Knott, J.; Geist, J. (2018). Catch-related fish injury and catch efficiency of stow-net-based fish recovery installations for fish-monitoring at hydropower plants. *Fisheries Management and Ecology*, 25(1): 31–43. <http://dx.doi.org/10.1111/fme.12263>.
- Pavlov, D.S. (1989). Structures assisting the migrations of non-salmonid fish: USSR. *FAO Fisheries Technical Paper 308*, Food and Agriculture Organization of the United Nations (FAO), Fisheries Department, Rome, Italy.
- Pelicice, F.M.; Agostinho, C.S. (2012). Deficient downstream passage through fish ladders: the case of Peixe Angical Dam, Tocantins River, Brazil. *Neotropical Ichthyology*, 10(4): 705–713. <http://dx.doi.org/10.1590/S1679-62252012000400003>.
- Piper, A.T.; Rosewarne, P.J.; Wright, R.M.; Kemp, P.S. (2018). The impact of an Archimedes screw hydropower turbine on fish migration in a lowland river. *Ecological Engineering*, 118: 31–42. <http://dx.doi.org/https://doi.org/10.1016/j.ecoleng.2018.04.009>.

- Pracheil, B.M.; DeRolph, C.R.; Schramm, M.P.; Bevelhimer, M.S. (2016). A fish-eye view of riverine hydropower systems: the current understanding of the biological response to turbine passage. *Reviews in Fish Biology and Fisheries*, 26(2): 153–167. <http://dx.doi.org/10.1007/s11160-015-9416-8>.
- Radinger, J.; Wolter, C. (2014). Patterns and predictors of fish dispersal in rivers. *Fish and Fisheries*, 15(3): 456–473. <http://dx.doi.org/10.1111/faf.12028>.
- Rainey, W.S. (1985). Considerations in the design of juvenile bypass systems. *Proc. Symposium on small hydropower and fisheries*, F.W. Olson; R.G. White; R.H. Hamre (eds.). *The American Fisheries Society*, Aurora, USA: 261–268. ISBN 0913235377.
- Raymond, H.L. (1979). Effects of dams and impoundments on migrations of juvenile chinook salmon and steelhead from the Snake River, 1966 to 1975. *Transactions of the American Fisheries Society*, 108(6): 505–529. [http://dx.doi.org/10.1577/1548-8659\(1979\)108<505:EODAI0>2.0.CO;2](http://dx.doi.org/10.1577/1548-8659(1979)108<505:EODAI0>2.0.CO;2).
- Raynal, S.; Chatellier, L.; Courret, D.; Larinier, M.; David, L. (2013a). An experimental study on fish-friendly trashracks — Part 2. Angled trashracks. *Journal of Hydraulic Research*, 51(1): 67–75. <http://dx.doi.org/10.1080/00221686.2012.753647>.
- Raynal, S.; Courret, D.; Chatellier, L.; Larinier, M.; David, L. (2013b). An experimental study on fish-friendly trashracks — Part 1. Inclined trashracks. *Journal of Hydraulic Research*, 51(1): 56–66. <http://dx.doi.org/10.1080/00221686.2012.753646>.
- Richkus, W.A.; Dixon, D.A. (2003). Chap. Review of research and technologies on passage and protection of downstream migrating catadromous eels at hydroelectric facilities: 295–305. In: D.A. Dixon (ed.) *Biology, management, and protection of catadromous eels*. ISBN 1888569425. *American Fisheries Society*, Bethesda, USA.
- Richmond, M.C.; Serkowski, J.A.; Ebner, L.L.; Sick, M.; Brown, R.S.; Carlson, T.J. (2014). Quantifying barotrauma risk to juvenile fish during hydro-turbine passage. *Fisheries Research*, 154: 152–164. <http://dx.doi.org/10.1016/j.fishres.2014.01.007>.
- Rouvé, G. (1958). Der Krafthaustrennpfeiler — Strömungsverhältnisse an gekrümmten Wänden ('The dividing pier between the powerhouse and weir — Flow conditions at curved walls'). *Arbeit 145* (H. Wittmann, ed.). Theodor-Rehbock-Laboratorium, Karlsruhe Institute of Technology, Germany [in German].
- Ruggles, C.P.; Ryan, P. (1964). An investigation of Louvers as a method of guiding juvenile Pacific salmon. *The Canadian Fish Culturist*, 33: 1–68.
- Russon, I.J.; Kemp, P.S. (2011). Advancing provision of multi-species fish passage: Behaviour of adult European eel (*Anguilla anguilla*) and brown trout (*Salmo trutta*) in response to accelerating flow. *Ecological Engineering*, 37(12): 2018–2024. <http://dx.doi.org/10.1016/j.ecoleng.2011.08.005>.
- Russon, I.J.; Kemp, P.S.; Calles, O. (2010). Response of downstream migrating adult European

- eels (*Anguilla anguilla*) to bar racks under experimental conditions. *Ecology of Freshwater Fish*, 19(2): 197–205. <http://dx.doi.org/10.1111/j.1600-0633.2009.00404.x>.
- Sand, O.; Enger, P.S.; Karlsen, H.E.; Knudsen, F.; Kvernstuen, T. (2000). Avoidance responses to infrasound in downstream migrating European silver eels, *Anguilla anguilla*. *Environmental Biology of Fishes*, 57(3): 327–336. <http://dx.doi.org/10.1023/A:1007575426155>.
- Schälchli, U.; Baumgartner, A.; Baumann, P. (1997). Geschwemmsel bei Kleinwasserkraftwerken — Optimierung der Wasserfassung (‘Floating debris at small hydropower plants — Optimization of the water intake’). *Technical report*, Bundesamt für Energiewirtschaft (BEW), Bern, Switzerland [in German].
- Scharf, D. (2012). Der Sedimenttransport im Bereich von Fisch- und Treibgutableitern einer Kleinwasserkraftanlage (‘Sediment transport in front of a fish and floating debris guidance rack at a small hydropower plant’). *Master’s Thesis*, Universität der Bundeswehr München, Neubiberg, Germany [in German].
- Schlägel, U.E.; Grimm, V.; Blaum, N.; Colangeli, P.; Dammhahn, M.; Eccard, J.A.; Hausmann, S.L.; Herde, A.; Hofer, H.; Joshi, J.; Kramer-Schadt, S.; Litwin, M.; Lozada-Gobilard, S.D.; Müller, M.E.H.; Müller, T.; Nathan, R.; Petermann, J.S.; Pirhofer-Walzl, K.; Radchuk, V.; Rillig, M.C.; Roeleke, M.; Schäfer, M.; Scherer, C.; Schiro, G.; Scholz, C.; Teckentrup, L.; Tiedemann, R.; Ullmann, W.; Voigt, C.C.; Weithoff, G.; Jeltsch, F. (2020). Movement-mediated community assembly and coexistence. *Biological Reviews*, 95(4): 1073–1096. <http://dx.doi.org/10.1111/brev.12600>.
- Schleiss, A. (1985). Schwingungen von Einlaufrechen bei Wasserkraftanlagen — Ursachen, Bemessungsansätze und konstruktive Massnahmen (Trashrack vibrations in hydroelectric power plants — Causes of forcing frequencies, prevention of resonant response and fatigue failure, constructive measures). *Wasser Energie Luft*, 77(10): 299–303 [in German].
- Schleiss, A.; Fust, A. (1992). Schwingungsuntersuchungen bei den Einlaufrechen des Rheinkraftwerks Laufenburg (‘Investigation of trash rack vibrations at the Rhine river hydroelectric power plant Laufenburg’). *Proc. Betrieb, Unterhalt und Modernisierung von Wasserbauten (‘Operation, maintenance, and modernization of hydraulic structures’)*, T. Strobl (ed.). *Technical University of Munich*, Garmisch-Partenkirchen, Germany: 225–237 [in German].
- Schmalz, M. (2012). Optimierung von Bypässen für den Fischabstieg (‘Optimization of bypasses for fish downstream migration’). *Technical report Az 26632-24/0*, Bauhaus-Universität Weimar, Schleusingen, Germany [in German].
- Schmalz, W. (2010). Untersuchungen zum Fischabstieg und Kontrolle möglicher Fischschäden durch die Wasserkraftschnecke an der Wasserkraftanlage Walkmühle an der Werra in Meiningen (‘Investigation of fish downstream passage and monitoring of potential fish injuries due to the Archimedes screw turbine at the hydropower plant Walkmühle at the Werra River in Meiningen’). *Technical report*, Fischökologische & Limnologische Untersuchungsstelle

- Südthüringen (FLUSS), Breitenbach, Germany [in German].
- Schmassmann, W. (1928). Versuche über die Beschädigungen von Fischen durch Turbinen ('Experiments about fish injuries due to turbines'). *Schweizerische Fischerei-Zeitung*, 36(1): 347–353 [in German].
- Schoeneman, D.E.; Pressey, R.T.; Junge Jr., C.O. (1961). Mortalities of downstream migrant salmon at McNary Dam. *Transactions of the American Fisheries Society*, 90(1): 58–72. [http://dx.doi.org/10.1577/1548-8659\(1961\)90\[58:MODMSA\]2.0.CO;2](http://dx.doi.org/10.1577/1548-8659(1961)90[58:MODMSA]2.0.CO;2).
- Schölzel, N.; Wilmsmeier, L.; Peter, A. (2020). Schlussbericht PIT-Tagging am KW Schiffmühle und Aue an der Limmat 2017–2020 ('Final report PIT-tagging at HPP Schiffmühle and Aue at the Limmat River 2017–2020'). *Final report*, FishConsulting GmbH, Olten, Switzerland [in German].
- Schwevers, U.; Adam, B. (2019). Biometrie einheimischer Fischarten als Grundlage für die Bemessung von Fischwegen und Fischschutzanlagen ('Biometry of native fish species as a basis for designing fishways and fish protection facilities'). *Wasser und Abfall*, 1–2: 46–52 [in German].
- Schwevers, U.; Adam, B. (2020). Fish protection technologies and fish ways for downstream migration. ISBN 9783030192419. 1<sup>st</sup> edn. *Springer*, Cham, Switzerland. <http://dx.doi.org/10.1007/978-3-030-19242-6>.
- Schwevers, U.; Adam, B.; Engler, O. (2011). Befunde zur Aalabwanderung 2008/09 — Erarbeitung und Praxiserprobung eines Maßnahmenplans zur ökologisch verträglichen Wasserkraftnutzung an der Mittelweser ('Findings of eel downstream migration 2008/09 — Formulation and practical tests of an action plan for the environmentally compatible hydropower use at the central part of the Weser River'). *Technical report 75*, Institut für angewandte Ökologie, Kirtorf-Wahlen, Germany [in German].
- Sell, L.E. (1971). Hydroelectric power plant trashrack design. *Proc. American Society of Civil Engineers (ASCE). Journal of the Power Division*, New York, USA: 115–121.
- SFOE (2020). Schweizerische Elektrizitätsstatistik 2019 ('Swiss electricity statistics 2019'). *Technical report*, Swiss Federal Office of Energy (SFOE), Bern, Switzerland [in German and French].
- Shepherd, D.; Katopodis, C.; Rajaratnam, N. (2007). An experimental study of louvers for fish diversion. *Canadian Journal of Civil Engineering*, 34(6): 770–776. <http://dx.doi.org/10.1139/l06-118>.
- Sheridan, S.; Turnpenny, A.; Horsfield, R.; Solomon, D.; Bamford, D.; Bayliss, B.; Coates, S.; Dolben, I.; Frear, P.; Hazard, E.; Tavner, I.; Trudgill, N.; Wright, R.; Aprahamian, M. (2014). Chap. Screening at intakes and outfalls: measures to protect eel (*Anguilla anguilla*): 17–30. In: A.W.H. Turnpenny; R.A. Horsfield (eds.) *International fish screening techniques*. ISBN 9781845648497. *WIT Press*, Southampton, UK.

- Silva, A.T.; Bærum, K.M.; Hedger, R.D.; Baktoft, H.; Fjeldstad, H.-P.; Gjelland, K.Ø.; Økland, F.; Forseth, T. (2020). The effects of hydrodynamics on the three-dimensional downstream migratory movement of Atlantic salmon. *Science of The Total Environment*, 705: 135773. <http://dx.doi.org/10.1016/j.scitotenv.2019.135773>.
- Silva, A.T.; Katopodis, C.; Tachie, M.F.; Santos, J.M.; Ferreira, M.T. (2016). Downstream swimming behaviour of catadromous and potamodromous fish over spillways. *River Research and Applications*, 32(5): 935–945. <http://dx.doi.org/10.1002/rra.2904>.
- Silva, A.T.; Lucas, M.C.; Castro-Santos, T.; Katopodis, C.; Baumgartner, L.J.; Thiem, J.D.; Aarestrup, K.; Pompeu, P.S.; O'Brien, G.C.; Braun, D.C.; Burnett, N.J.; Zhu, D.Z.; Fjeldstad, H.-P.; Forseth, T.; Rajaratnam, N.; Williams, J.G.; Cooke, S.J. (2018). The future of fish passage science, engineering, and practice. *Fish and Fisheries*, 19(2): 340–362. <http://dx.doi.org/10.1111/faf.12258>.
- Skalski, J.R.; Mathur, D.; Heisey, P.G. (2002). Effects of turbine operating efficiency on smolt passage survival. *North American Journal of Fisheries Management*, 22(4): 1193–1200. [http://dx.doi.org/10.1577/1548-8675\(2002\)022<1193:EOTOEO>2.0.CO;2](http://dx.doi.org/10.1577/1548-8675(2002)022<1193:EOTOEO>2.0.CO;2).
- Snyder, D.E. (2003). Invited overview: conclusions from a review of electrofishing and its harmful effects on fish. *Reviews in Fish Biology and Fisheries*, 13: 445–453. <http://dx.doi.org/10.1007/s11160-004-1095-9>.
- Spalinger, L.; Dönni, W.; Guthruf, J. (2017). NAWA Trend Biologie — 2. Kampagne (2015) ('NAWA trend biology — 2<sup>nd</sup> campaign (2015)'). *Final report*, argeNOWA, Lucerne, Switzerland [in German and French].
- Steffen, B.; Hischier, D.; Schmidt, T.S. (2018). Current and future energy performance of power generation technologies in Switzerland. *Technical report*, ETH Zurich, Switzerland.
- Stewart, J.; Ferrell, D.J. (2002). Escape panels to reduce by-catch in the New South Wales demersal trap fishery. *Marine and Freshwater Research*, 53: 1179–1188. <http://dx.doi.org/10.1071/MF02062>.
- Svendsen, J.C.; Eskesen, A.O.; Aarestrup, K.; Koed, A.; Jordan, A.D. (2007). Evidence for non-random spatial positioning of migrating smolts (Salmonidae) in a small lowland stream. *Freshwater Biology*, 52(6): 1147–1158. <http://dx.doi.org/10.1111/j.1365-2427.2007.01743.x>.
- Szabo-Meszaros, M.; Navaratnam, C.U.; Aberle, J.; Silva, A.T.; Forseth, T.; Calles, O.; Fjeldstad, H.-P.; Alfredsen, K. (2018). Experimental hydraulics on fish-friendly trash-racks: an ecological approach. *Ecological Engineering*, 113: 11–20. <http://dx.doi.org/10.1016/j.ecoleng.2017.12.032>.
- Taft, E.P. (1986). Assessment of downstream migrant fish protection technologies for hydro-electric a pplication. *Technical report AP-4711*, Electric Power Research Institute (EPRI), Palo Alto, USA.



- Teitelbaum, C.S.; Mueller, T. (2019). Beyond migration: causes and consequences of nomadic animal movements. *Trends in Ecology & Evolution*, 34(6): 569–581. <http://dx.doi.org/10.1016/j.tree.2019.02.005>.
- Thorstad, E.B.; Rikardsen, A.H.; Alp, A.; Økland, F. (2013). The use of electronic tags in fish research — An overview of fish telemetry methods. *Turkish Journal of Fisheries and Aquatic Sciences*, 13: 881–896. [http://dx.doi.org/10.4194/1303-2712-v13\\_5\\_13](http://dx.doi.org/10.4194/1303-2712-v13_5_13).
- Thorstad, E.B.; Whoriskey, F.; Uglem, I.; Moore, A.; Rikardsen, A.H.; Finstad, B. (2012). A critical life stage of the Atlantic salmon *Salmo salar*: behaviour and survival during the smolt and initial post-smolt migration. *Journal of Fish Biology*, 81(2): 500–542. <http://dx.doi.org/10.1111/j.1095-8649.2012.03370.x>.
- Travade, F.; Larinier, M. (1992). La migration de dévalaison: problèmes et dispositifs ('Downstream migration: problems and facilities'). *Bull. Fr. Pêche Piscic.*, (326–327): 165–176. <http://dx.doi.org/10.1051/kmae:1992013> [in French].
- Travade, F.; Larinier, M. (2006). Chap. French experience in downstream migration devices: 91–99. In: Free passage for aquatic fauna in rivers and other water bodies. ISBN 9783939057192. *German Association for Water, Wastewater and Waste (DWA)*, Hennef, Germany.
- Tuhtan, J.A.; Fuentes-Perez, J.F. (2018). How do fish sense flow? *Proc. 12<sup>th</sup> International Symposium on Ecohydraulics*. Tokyo, Japan.
- Turnpenny, A.W.H. (1998). Chap. 23: Mechanisms of fish damage in low-head turbines: an experimental appraisal: 300–314. In: M. Jungwirth; S. Schmutz; S. Weiss (eds.) Fish migration and fish bypasses. ISBN 0852382537. *Fishing News Books*, Oxford, UK.
- Turnpenny, A.W.H.; Babbie, J.; Clough, S.C. (2006). Chap. Physiological abilities of migrating fish: 12–23. In: Free passage for aquatic fauna in rivers and other water bodies. ISBN 9783939057192. *German Association for Water, Wastewater and Waste (DWA)*, Hennef, Germany.
- Turnpenny, A.W.H.; Clough, S.; Hanson, K.P.; Ramsay, R.; McEwan, D. (2000). Risk assessment for fish passage through small, low-head turbines. *Technical report ETSU H/06/00054/REP*, Fawley Aquatic, Southampton, UK.
- Turnpenny, A.W.H.; O'Keeffe, N (2005). Screening for intake and outfalls: a best practice guide. *Technical report SC030231*, Environment Agency, Bristol, UK.
- Tutzer, R.; Brinkmeier, B.; Böttcher, H.; Aufleger, M. (2019a). Der Elektro-Seilrechen als integrales Fischschutzkonzept (The electric flexible fish fence – an integral fish protection measure). *Wasserwirtschaft*, 109(2–3): 36–40 [in German].
- Tutzer, R.; Brinkmeier, B.; Zeiringer, B.; Führer, S.; Unfer, G.; Aufleger, M. (2019b). The Fishprotector — An integral fish protection system. *Proc. 38<sup>th</sup> IAHR World Congress. International Association for Hydro-Environment Engineering and Research (IAHR)*, Panama

- City, Panama: 1692–1700. <http://dx.doi.org/10.3850/38WC092019-0230>.
- USBR (2006). Fish protection at water diversions — A guide for planning and designing fish exclusion facilities. *Water Resources Technical Publication*, U.S. Department of the Interior, Bureau of Reclamation, Denver, USA.
- USFWS (2017). Fish passage engineering design criteria. *Technical report*, U.S. Fish and Wildlife Service (USFWS), Northeast Region R5, Hadley, USA.
- Vigne-Lepage, V. (2020). Les grilles orientées à barreaux horizontaux arrivent en France ('Racks with horizontal bars reach France'). *Puissance Hydro*, (10): 16–18 [in French].
- Voith (2011). Environmentally-friendly turbine design. *Brochure*, Voith Hydro Inc., York, USA.
- Vollset, K.W.; Lennox, R.J.; Thorstad, E.B.; Auer, S.; Bär, K.; Larsen, M.H.; Mahlum, S.; Näslund, J.; Stryhn, H.; Dohoo, I. (2020). Systematic review and meta-analysis of PIT tagging effects on mortality and growth of juvenile salmonids. *Reviews in Fish Biology and Fisheries*, 30: 553–568. <http://dx.doi.org/10.1007/s11160-020-09611-1>.
- von Raben, K. (1957). Über Turbinen und ihre schädliche Wirkung auf Fische ('About turbines and their harmful effect on fish'). *Zeitschrift für Fischerei und deren Hilfswissenschaften*: 171–182 [in German].
- Vowles, A.S.; Anderson, J.J.; Gessel, M.H.; Williams, J.G.; Kemp, P.S. (2014). Effects of avoidance behaviour on downstream fish passage through areas of accelerating flow when light and dark. *Animal Behaviour*, 92: 101–109. <http://dx.doi.org/10.1016/j.anbehav.2014.03.006>.
- Vowles, A.S.; Eakins, L.R.; Piper, A.T.; Kerr, J.R.; Kemp, P. (2013). Chap. 8: Developing realistic fish passage criteria: an ecohydraulics approach: 143–156. In: I. Maddock; A. Harby; P. Kemp; P. Wood (eds.) *Ecohydraulics — An integrated approach*. ISBN 9780470976005. *John Wiley & Sons, Ltd*, Chichester, UK.
- Vowles, A.S.; Kemp, P.S. (2012). Effects of light on the behaviour of brown trout (*Salmo trutta*) encountering accelerating flow: Application to downstream fish passage. *Ecological Engineering*, 47: 247–253. <http://dx.doi.org/10.1016/j.ecoleng.2012.06.021>.
- Wagner, F. (2016). Vergleichende Analyse des Fischabstiegs an drei Wasserkraftanlagen einer Kraftwerkskette (Comparative analysis of the downstream movement of fish at three consecutive hydropower plants). *Wasserwirtschaft*, 106(2–3): 35–41 [in German].
- Wagner, F.; Körnig, J.; Warth, P.; Schmalz, W. (2019a). Ergebnisse der Methodenkombination bei Untersuchungen eines Fischschutzsystems an einer WKA (Combination of investigation methods to evaluate a fish protection system at a HPP). *Wasserwirtschaft*, 109(2–3): 23–28 [in German].
- Wagner, F.; Royan, M.; Mirza, J.; Schubert, A. (2013). Überprüfung der Fischschutz- und Fischabstiegseinrichtungen sowie der Fischschädigung an der WKA Wehlitz/Weiße Elster ('Monitoring of the fish protection and fish downstream passage facility and fish injuries at

- HPP Wehlitz/White Elster'). *Technical report*, Institut für Gewässerökologie und Fischereibiologie Jena [in German].
- Wagner, F.; Warth, P.; Schmalz, W. (2019b). Evaluierung von Fischschutz- und Fischabstiegsmaßnahmen an einem Wasserkraftstandort für die Umsetzung des WHG § 35 (Evaluation of fish protection- and downstream migration for the implementation of the WHG § 35). *Technical report*, Institut für Gewässerökologie und Fischereibiologie Jena and Fischökologische & Limnologische Untersuchungsstelle Südthüringen, Jena and Breitenbach, Germany [in German].
- Watene, E.M.; Boubée, J.A.T. (2005). Selective opening of hydroelectric dam spillway gates for downstream migrant eels in New Zealand. *Fisheries Management and Ecology*, 12(1): 69–75. <http://dx.doi.org/10.1111/j.1365-2400.2004.00422.x>.
- Weibel, U. (2016). Ergebnisse zum Fischabstieg durch elektrisches Scheuchen von Lachsen und Aalen ('Results of fish downstream migration through electrical shooping of salmon and eels'). *Proc. 27<sup>th</sup> SVK-Fischereitagung*. Künzell bei Fulda, Germany [in German].
- Whitney, R.R.; Calvin, L.D.; Erho, M.W.; Coutant, C.C. (1997). Downstream passage for salmon at hydroelectric projects in the Columbia River basin: development, installation, and evaluation. *Technical report*, Northwest Power Planning Council, Portland, USA.
- Wilke, T.; Gnaudschn, E.; Schneider, T.; Teggers-Junge, S.; Ingendahl, D.; Weimer, P. (2019). Abschlussbericht zum Projekt Fischschutz und Fischabstieg an der Pilotanlage Unkelmühle ('Final report of the project fish protection and fish downstream migration at the pilot plant Unkelmühle'). *Technical report*, Bezirksregierung Köln, innogy SE, and Ministry for Environment, Agriculture, Conservation and Consumer Protection of the State of North Rhine-Westphalia (MULNV), Düsseldorf, Köln, and Essen, Germany [in German].
- Yu, D.; Kareem, A. (1998). Parametric study of flow around rectangular prisms using LES. *Journal of Wind Engineering and Industrial Aerodynamics*, 77–78(Supplement C): 653–662. [http://dx.doi.org/10.1016/S0167-6105\(98\)00180-9](http://dx.doi.org/10.1016/S0167-6105(98)00180-9).
- Yuen, A.; Tackaberry, B.; Hartloper, C.; Wong, J.; Vertz, J.; Sessarego, M. (2010). VLH Turbine Project. *Fall Final Report Document*, University of Calgary, Canada.
- Zaugg, C.; Mendez, R. (2018). Kleinwasserkraftwerk Stroppel — Wirkungskontrolle Fischabstieg am Horizontalrechen mit Bypass ('Small hydropower plant Stroppel — Monitoring campaign of fish downstream passage at the horizontal bar rack bypass system'). *Technical report*, Axpo Power AG, Baden, Switzerland [in German].
- Zimmermann, J. (1969). Widerstand schräg angeströmter Rechengitter ('Resistance of racks caused by oblique inflow'). In *Mitteilung Nr. 157* (E. Mosonyi, ed.). Theodor-Rehbock-Flußbaulaboratorium, Universität Fridericiana Karlsruhe, Germany, 1–130 [in German].

# A Appendix

## A.1 Generalized linear models for the comparison with the curved-bar rack

In Section 7.8.1, the HBR was compared to the CBR with different GLMs. The main results of these GLMs are summarized in the following. Table A.1 lists the AICs/BICs of different GLMs, while the output of the main model is shown in Tables A.2–A.4.

**Table A.1:** Summary of the AICs and BICs of the main model and with models considering different interactions for the dependent variables bypass passage, rack passage, and refusal; \* indicates the smallest AIC/BIC for each column

Model	Bypass		Rack		Refusal	
	AIC	BIC	AIC	BIC	AIC	BIC
Main	847.375	874.134	734.096 *	760.855 *	370.835	397.595
Interaction $VR$ : rack type	838.001	869.221 *	734.729	765.948	363.703 *	394.922 *
Interaction $U_o$ : rack type	848.625	879.845	734.927	766.146	372.415	403.634
Interaction $VR$ : $U_o$	849.325	880.545	736.020	767.240	372.518	403.737
Interactions $U_o$ : rack type + $U_o$ : $VR$	850.598	886.278	736.773	772.452	374.089	409.769
Interactions $VR$ : rack type + $U_o$ : $VR$	839.618	875.297	736.602	772.281	365.382	401.061
Interactions $U_o$ : rack + $VR$ : rack type	839.090	874.769	735.718	771.397	365.489	401.168
All 2-way interactions	840.728	880.867	737.551	777.690	366.941	407.080
Full model with 3-way interaction	836.423 *	881.022	738.228	782.827	368.821	413.421

**Table A.2:** Summary of the GLM with all HBR (OC,  $s_b = 20$  mm) and CBR data (OC) with the **bypass passage** as the dependent variable; the reference categories are the HBR,  $U_o = 0.5$  m/s,  $VR = 1.2$ , and morning; \* denotes  $p < 0.05$ , \*\*  $p < 0.01$ , and \*\*\*  $p < 0.001$

	Intercept	Rack type: CBR	$U_o = 0.7$ m/s	$VR = 1.4$	Usage	Time: afternoon
Coefficient $\beta$	0.746 **	0.553 ***	−0.158	−0.327 *	−0.077	−0.539 **
Exp( $\beta$ )	2.108	1.738	0.854	0.721	0.926	0.583
Std. error $\varepsilon$	0.285	0.168	0.176	0.165	0.083	0.170
$N$	639					
Log-likelihood	−417.687					
AIC	847.375					
BIC	874.134					

**Table A.3:** Summary of the GLM with all HBR (OC,  $s_b = 20$  mm) and CBR data (OC) with the **rack passage** as the dependent variable; the reference categories are the HBR,  $U_o = 0.5$  m/s,  $VR = 1.2$ , and morning; \* denotes  $p < 0.05$ , \*\*  $p < 0.01$ , and \*\*\*  $p < 0.001$

	Intercept	Rack type: CBR	$U_o = 0.7$ m/s	$VR = 1.4$	Usage	Time: afternoon
Coefficient $\beta$	$-1.428^{***}$	$-0.834^{***}$	$-0.477^*$	$0.380^*$	$0.315^{***}$	0.223
$\text{Exp}(\beta)$	0.240	0.434	0.620	1.463	1.371	1.250
Std. error $\varepsilon$	0.319	0.187	0.201	0.182	0.091	0.189
$N$	639					
Log-likelihood	-361.048					
AIC	734.096					
BIC	760.855					

**Table A.4:** Summary of the GLM with all HBR (OC,  $s_b = 20$  mm) and CBR data (OC) with the **refusal** as the dependent variable; the reference categories are the HBR,  $U_o = 0.5$  m/s,  $VR = 1.2$ , and morning; \* denotes  $p < 0.05$ , \*\*  $p < 0.01$ , and \*\*\*  $p < 0.001$

	Intercept	Rack type: CBR	$U_o = 0.7$ m/s	$VR = 1.4$	Usage	Time: afternoon
Coefficient $\beta$	$-1.982^{***}$	$0.682^*$	$1.386^{***}$	0.145	$-0.831^{***}$	$1.085^{***}$
$\text{Exp}(\beta)$	0.138	1.978	4.000	1.156	0.436	2.960
Std. error $\varepsilon$	0.444	0.291	0.285	0.277	0.175	0.283
$N$	639					
Log-likelihood	-179.418					
AIC	370.835					
BIC	397.595					

## A.2 Fish injury reports



**Nationale Fischuntersuchungsstelle (NAFUS)**  
Laboratoire pour le diagnostic des maladies des poissons

**Zentrum für Fisch und Wildtiermedizin (FIWI)**

Länggassstrasse 122, Postfach, 3001 Bern  
Tel: 031 631 2465; Fax: 031 631 2611  
e-mail: nafus@vetsuisse.unibe.ch

Diagnostische  
Labors  
Vetsuisse  
Bern

**u<sup>b</sup>**

UNIVERSITÄT  
BERN

### Auftraggeber:

EAWAG  
z.H. Andreas Taverna  
Seestr. 79  
6047 Kastanienbaum

**PRÜFBERICHT F19\_4847\_422**

Bern, 20.11.2019

**Eingangsdatum:** 06.11.2019

Auftrag: angenommen vet. med. Melanie Rupp

**Art/Rasse:** Andere Fische Schneider  
**Material:** 1 ganzer Fisch  
**Länge in cm:** 11.4  
**Geschlecht:** weiblich  
**Nährzustand:** gut  
**Frischezustand:** lebend

**Herkunft:** Gewässer

### DIAGNOSE:

Haut: fokal Verfärbung der Haut

### BEURTEILUNG:

Es konnten keine Blutungen oder Nekrosen in der Muskulatur oder an der Wirbelsäule festgestellt werden. Ob die Dunkelfärbung der Haut mit der Stromeinwirkung im Zusammenhang steht, bleibt unklar. Histologisch wurden keine assoziierten Veränderungen im darunterliegenden Gewebe festgestellt.

1) 2) 3) 4) siehe Rückseite von Seite 1 / 1) 2) 3) 4) voir verso de la page 1  
Angaben über die Einsendung von Probenmaterial und über Untersuchungen können dem aktuellen Vademecum der NAFUS (<http://www.fiwi.vetsuisse.unibe.ch>) entnommen werden. Angaben zu den Analysen können im Labor erfragt werden. Die Resultate in diesem Bericht beziehen sich ausschliesslich auf das untersuchte Material. Dieser Bericht darf nicht auszugsweise kopiert werden, dagegen ist die Weiterverwendung einzelner Resultate unter Quellenangabe erlaubt.



F19\_4847\_422

Seite 1 von 2

**Fig. A.1:** Page 1 of the fish injury report of the Centre for Fish and Wildlife Health of the spiralin 1 (cf. Section 8.3)

**BEFUNDE:****Makroskopische Befunde:**

**Augen:** linkes Auge leicht blutig  
**Haut:** leichte schwarze Streifen auf linker Körperseite  
**Skelett:** im Bereich der schwarzen Streifen leichte Wirbelsäulenverkrümmung seitwärts

**Parasitologie (Direktnachweis, wenn keine andere Methode vermerkt)**

Parasitennachweis nativ: keine Parasitologie durchgeführt

**Histologische Befunde:**

**Skelett:** keine Skelettveränderungen sichtbar  
**Muskulatur:** fokal Trematode, enzystiert, umgeben von wenig Makrophagen und Lymphozyten  
 keine Blutungen oder Nekrose sichtbar

Auftrag ausgeführt durch:  
 Dr. med. vet. Dipl. ECVP Heike Schmidt Posthaus

**Medizinische Freigabe:**  
 Dr. med. vet. Dipl. ECVP Heike Schmidt Posthaus

*Heike Schmidt*  
 Nationale Fischuntersuchungsstelle  
 Zentrum für Fisch- und Wildtiermedizin  
 Universität Bern  
 Postfach  
 Länggassstrasse 122  
 CH-3001 Bern



Kopie an: Keine

Taxe exkl. MWST: Fr. 100.-

**Rechnung erfolgt separat**

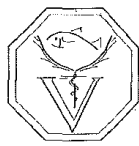
1) 2) 3) 4) siehe Rückseite von Seite 1 / 1) 2) 3) 4) voir verso de la page 1  
 Angaben über die Einsendung von Probematerial und über Untersuchungen können dem aktuellen Vademecum der NAFUS (<http://www.fwi.vetsuisse.unibe.ch>) entnommen werden. Angaben zu den Analysen können im Labor erfragt werden. Die Resultate in diesem Bericht beziehen sich ausschliesslich auf das untersuchte Material. Dieser Bericht darf nicht auszugsweise kopiert werden, dagegen ist die Weiterverwendung einzelner Resultate unter Quellenangabe erlaubt.



F19\_4847\_422

Seite 2 von 2

**Fig. A.2:** Page 2 of the fish injury report of the Centre for Fish and Wildlife Health of the spiralin 1 (cf. Section 8.3)



**Nationale Fischuntersuchungsstelle (NAFUS)**

Laboratoire pour le diagnostic des maladies des poissons

**Zentrum für Fisch und Wildtiermedizin (FIWI)**

Länggassstrasse 122, Postfach, 3001 Bern

Tel: 031 631 2465; Fax: 031 631 2611

e-mail: nafus@vetsuisse.unibe.ch

Diagnostische  
Labors  
Vetsuisse  
Bern

**u<sup>b</sup>**

**UNIVERSITÄT  
BERN**

**Auftraggeber:**

EAWAG z.H. Oliver Selz  
Seestrasse 79

6047 Kastanienbaum

**PRÜFBERICHT F19\_4875\_425**

Bern, 20.11.2019

**Eingangsdatum:** 08.11.2019

Auftrag: angenommen med. vet. Melchior Isler

**Art/Rasse:** Andere Fische Schneider  
**Material:** 1 ganzer Fisch  
**Länge in cm:** 9,3  
**Geschlecht:** weiblich  
**Nährzustand:** gut  
**Frischezustand:** lebend

**Herkunft:** Gewässer Zürich

**DIAGNOSE:**

Vereinzelte Myxozoa, Nematodenlarven

Bewegungsapparat: Wirbelsäulenbruch im Bereich des Spinalkanals mit assoziierten Blutungen in den Spinalkanal und in die umliegende Muskulatur. Einhergehend mit Kompression und Degeneration des Rückenmarks und Degeneration der Muskulatur

**BEURTEILUNG:**

Mit dem in Betracht ziehen des Vorberichts sind der festgestellte Wirbelsäulenbruch, die Blutungen sowie die Rückenmarks- und Muskeldegeneration mit grösster Wahrscheinlichkeit auf einen Stromschlag zurückzuführen.

Die nachgewiesenen Parasiten sind normal für wildlebende Fische.

1) 2) 3) 4) siehe Rückseite von Seite 1 / 1) 2) 3) 4) voir verso de la page 1

Angaben über die Einsendung von Probenmaterial und über Untersuchungen können dem aktuellen Vademecum der NAFUS (<http://www.fiwi.vetsuisse.unibe.ch>) entnommen werden. Angaben zu den Analysen können im Labor erfragt werden. Die Resultate in diesem Bericht beziehen sich ausschliesslich auf das untersuchte Material. Dieser Bericht darf nicht auszugsweise kopiert werden, dagegen ist die Weiterverwendung einzelner Resultate unter Quellenangabe erlaubt.

F19\_4875\_425

Seite 1 von 2



**Fig. A.3:** Page 1 of the fish injury report of the Centre for Fish and Wildlife Health of the spiralin 2 (cf. Section 8.3)



**BEFUNDE:****Makroskopische Befunde:**

**Haut:** Dorsal des Fisches ein 0.5cm breiter schwarzer Streifen auf Höhe 4cm cranial von Schwanzflossenende.

**Schwimmbase:** tympanisch

**Muskulatur:** 2cm lange Blutung links lateral an Wirbelsäule in der Muskulatur auf Höhe der Verletzung (rechte Seite wurde nicht aufgeschnitten um sie für Histologie komplett zu erhalten).

**Parasitologie (Direktnachweis, wenn keine andere Methode vermerkt)**

Parasitennachweis nativ: keine Parasitologie durchgeführt

**Histologische Befunde:**

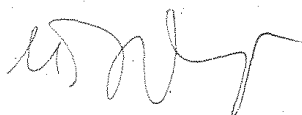
**ZNS:** Blutungen in den Spinalkanal mit Kompression und Verlagerung des Rückenmarks nach Dorsal.

**Skelett:** Rückenmark degeneriert mit Gliose, Malazie und Vakuolisierung. Bruch des Spinalkanals (auf Höhe der festgestellten Verlagerung des Rückenmarks) mit Blutung in der Muskulatur darum herum

**Muskulatur:** Blutungen um die Wirbelsäule und teilweise Muskeldegeneration. Einzelne Myxozoa-Zyste ohne Entzündungsreaktion darum herum.

**Übrige Organe:** Exokriner Pankreas: Nematodenlarve, abgekapselt durch granulomatoses Gewebe mit Makrophagen und mehrkernigen Riesenzellen.

Auftrag ausgeführt durch:  
med. vet. Melchior Isler



Kopie an: Keine

Taxe exkl. MWST: Fr. 115.-

**Medizinische Freigabe:**

Dr. med. vet. Dipl. ECVP Heike Schmidt Posthaus

*Heike Schmidt*

Nationale Fischuntersuchungsstelle  
Zentrum für Fisch- und Wildtiermedizin  
Universität Bern  
Postfach  
Länggassstrasse 122  
CH-3001 Bern



Rechnung erfolgt separat

1) 2) 3) 4) siehe Rückseite von Seite 1 / 1) 2) 3) 4) voir verso de la page 1

Angaben über die Einsendung von Probematerial und über Untersuchungen können dem aktuellen Vademecum der NAFUS (<http://www.fwi.vetsuisse.unibe.ch>) entnommen werden. Angaben zu den Analysen können im Labor erfragt werden. Die Resultate in diesem Bericht beziehen sich ausschliesslich auf das untersuchte Material. Dieser Bericht darf nicht auszugsweise kopiert werden, dagegen ist die Weiterverwendung einzelner Resultate unter Quellenangabe erlaubt.



F19\_4875\_425

Seite 2 von 2

**Fig. A.4:** Page 2 of the fish injury report of the Centre for Fish and Wildlife Health of the spiralin 2 (cf. Section 8.3)